

AD-A246 304



Ocean Engineering Studies

Compiled 1991

Volume VII:
Acrylic Windows—

Diverse Design Features
and Types of Service

J. D. Stachiw

NAVAL OCEAN SYSTEMS CENTER

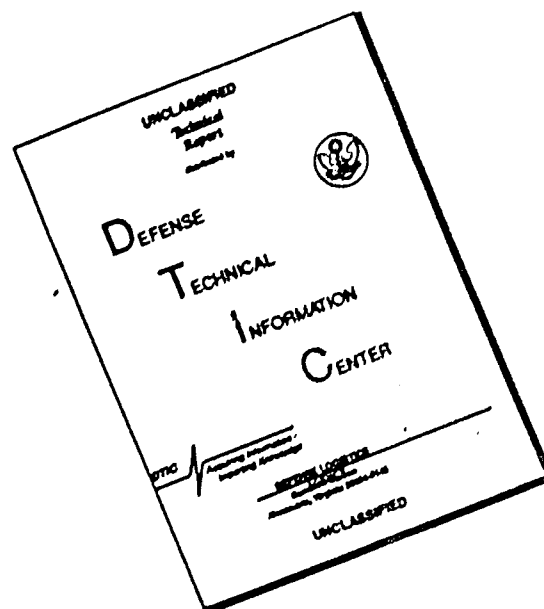
This document has been approved
for public release and sale;
distribution is unlimited.

92 2 17 015

92-04068



DISCLAIMER NOTICE



THIS DOCUMENT IS BEST QUALITY AVAILABLE. THE COPY FURNISHED TO DTIC CONTAINED A SIGNIFICANT NUMBER OF PAGES WHICH DO NOT REPRODUCE LEGIBLY.



Ocean Engineering Studies

Compiled 1991

Volume VII: Acrylic Windows— Diverse Design Features and Types of Service

Accession For	
NTIS CRA&I	<input checked="" type="checkbox"/>
DTIC TAB	<input type="checkbox"/>
Unannounced	<input type="checkbox"/>
Justification	
By	
Distribution	
Date	
A-1	



J. D. Stachiw

PUBLISHED BY
NAVAL OCEAN SYSTEMS CENTER
SAN DIEGO, CALIFORNIA

Foreword

For successful operation, all manned diving systems, submersibles, and hyperbaric chambers require pressure-resistant viewports. These viewports allow the personnel inside the diving bells and submersibles to observe the environment outside the pressure-resistant hulls. In addition, on land, operators of hyperbaric chambers can observe the behavior of patients or divers undergoing hyperbaric treatment inside the chambers.

Since the viewports form a part of the pressure-resistant envelope, they must meet or surpass the safety criteria used for designing either the metallic or plastic composite pressure envelope. The ASME Boiler and Pressure Vessel Code Section 8 provides such design criteria, and the chambers/pressure hulls designed on their basis have generated an unexcelled safety record.

The viewports, because of the unique structural properties of the acrylic plastic used in constructing the windows, could not be designed according to the same criteria as for the pressure envelope fabricated of metallic or plastic composite materials. To preclude potential catastrophic failures of windows designed on the basis of inadequate data, in 1965, the U.S. Navy initiated a window testing program at the Naval Civil Engineering Laboratory and the Naval Ocean Systems Center. Under this program, window testing was conducted until 1975.

The objective of the window testing program was to generate test data concerning the structural performance of acrylic-plastic windows fabricated in different shapes, sizes, and thicknesses. Candidates for investigation included the effect of major design parameters, like the thickness to diameter ratio, bevel angle of bearing surfaces, and the ratio of window diameter to seat-opening diameter on the structural performance of the windows; and empirical relationships were to be formulated between these variables and the critical pressures at which windows fail. To make the test results realistic, the test conditions were varied to simulate the in-service environment that the windows were to be subjected. Thus, during testing, the windows were subjected not only to short-term pressurization at room temperature, but also to long-term sustained and repeated pressurization at different ambient temperatures.

On the basis of these data, empirical relationships were formulated between design parameters and test conditions. Committees in the Pressure Technology Codes of the American Society of Mechanical Engineers subsequently incorporated these relationships into the Safety Standard for Pressure Vessels for Human Occupancy (ASME PVHO-1 Safety Standard). Since that time, this ASME Safety Standard has formed the basis — worldwide — for designing acrylic windows in pressure chambers for human occupancy. Their performance record is excellent; since the publication of the Safety Standard in 1977, no catastrophic failures have been recorded that resulted in personal injury.

The data generated by the Navy's window testing program were originally disseminated in technical reports of the Naval Civil Engineering Laboratory and the Naval Ocean Systems Center, and were made available to the general public through the Defense Technical Information Center. Some of the data were also presented in technical papers that subsequently were published in the Transactions of the American Society of Mechanical Engineers. To facilitate distribution of these data to users inside and outside of the Department of Defense, the technical reports have been collected and are being reissued as volumes of the U.S. Navy Ocean Engineering Studies.

Volume VII of the Ocean Engineering Series is a compilation of several technical reports and papers dealing with different aspects of the acrylic plastic window technology. The first report describes in detail the development of a fabrication technique for casting thick spherical shell windows in permanent metal molds to net dimensions and the subsequent experimental evaluation of their structural performance. The second report summarizes the results of a testing program that analyzed the fracture toughness of spherical shell windows under point impact generated by simulated collisions between submersibles equipped with spherical bow windows and massive obstacles, like ships, offshore platform, docks, and rocks.

The third report presents experimental data on the effect of bubble inclusions in acrylic castings on the mechanical properties of cast acrylic plastic. These data are particularly valuable for setting acceptance limits in quality assurance programs for fabricating large acrylic windows from (1) monolithic casting or (2) multiple segments joined by adhesive bonding.

The fourth report presents the designer with information on how weathering and long-term sustained loading degrade the structural properties of acrylic plastic. On the basis of such information, the designer can apply the appropriate safety factors to design stress values so the acrylic structure can, even after 10 or 20 years of service, safely carry the load for which it was designed. The data contained in this report are further augmented by technical papers on the same subject published in the Transactions of ASME.

The remainder of the technical papers deal with various design and fabrication aspects of acrylic windows and pressure hulls. Of particular interest is the paper on the design and performance of plane disc windows with twin conical bearing surfaces. These windows are installed in diving bells and personnel transfer capsules where the window is subjected to pressurizations from either side. Another paper covers the design and performance of hyperhemispherical windows that find application as observation domes on submersibles or nonpenetrating periscopes on submarines. There are also several papers of interest to designers of acrylic spherical hulls; one addresses the effect of multiple penetrations, another the incorporation of polycarbonate plastic inserts, and still another the increase of wall thickness on the structural performance of acrylic spherical hulls.

The pressure and duration of loading data summarized in the reports apply directly to windows of any size with an identical t/D_i ratio, while the displacements shown must be multiplied by a scale factor based on the ratio of minor diameters on the test and operational windows. To date, these test data have been used successfully in designing windows and pressure hulls in sizes up to 96 inches for tourist submarines.

J. D. Stachiw
Marine Materials Office
Ocean Engineering Division

TABLE OF CONTENTS: VOLUME VII

NUC TP 410	Development of a Precision Casting Process for Acrylic Plastic Spherical Shell Windows Applicable to High-Pressure Service
NUC TP 486	Acrylic Plastic Spherical Windows Under Point Impact Loading
NUC TP 305	Effect of Bubble Inclusions on the Mechanical Properties of Cast Polymethyl Methacrylate
NOSC TR 1303	Crazing and Degradation of Flexure Strength in Acrylic Plates as a Function of Time
Transactions ASME	Effect of Weathering and Submersion in Seawater on the Mechanical Properties in Acrylic Plastic
Transactions ASME	Effect of Weather, Age, and Cyclic Pressurizations on Structural Performance of Acrylic Plastic Spherical Shells Under External Pressure Loading
Transactions ASME	Polycarbonate Plastic Inserts for Spherical Acrylic Plastic Shells Under Hydrostatic Loading
Transactions ASME	Spherical Acrylic Pressure Hulls With Multiple Penetrations
Transactions ASME	Acrylic Plastic Spherical Pressure Hull for 2439 m (8000 ft) Design Depth: Phase I
Transactions ASME	Structural Performance of Acrylic Plastic Plane Disk Windows With Twin Conical Bearing Surfaces.
Transactions ASME	Hyperhemispherical Viewports for Undersea Applications
Transactions ASME	The Origins of Acrylic Plastic Submersibles



**DEVELOPMENT OF
A PRECISION CASTING PROCESS FOR
ACRYLIC PLASTIC SPHERICAL SHELL WINDOWS
APPLICABLE TO HIGH-PRESSURE SERVICE**

by

Jerry D. Stachiw

Ocean Technology Department

May 1974





NAVAL UNDERSEA CENTER, SAN DIEGO, CA. 92132

AN ACTIVITY OF THE NAVAL MATERIAL COMMAND

ROBERT H. GAUTIER, CAPT, USN

Commander

Wm. B. McLEAN, Ph.D.

Technical Director

ADMINISTRATIVE INFORMATION

The research described in this report covers the time period from June 1972 to December 1973. The research has been jointly supported by the Director of Naval Laboratories and the Naval Facilities Engineering Command, under NAVFAC project number 165869.

Acknowledgment

The precision casting process for acrylic plastic spherical shell windows was developed by Mr. Bruce Beasley at Polymer Products, Oakland, California. The hydrostatic testing of the cast window specimens was conducted at Southwest Research Institute, under the personal supervision of Mr. J. Jones, and at Naval Civil Engineering Laboratory by Mr. K. O. Gray. The molds were fabricated by Adroit Engineering, San Diego, California, according to specifications provided by NUC.

Under authority of
H. R. TALKINGTON, Head
Ocean Technology Department

UNCLASSIFIED

SECURITY CLASSIFICATION OF THIS PAGE (When Data Entered)

REPORT DOCUMENTATION PAGE		READ INSTRUCTIONS BEFORE COMPLETING FORM
1. REPORT NUMBER NUC TP 410	2. GOVT ACCESSION NO.	3. RECIPIENT'S CATALOG NUMBER
4. TITLE (and Subtitle) Development of a Precision Casting Process for Acrylic Plastic Spherical Shell Windows Applicable to High-Pressure Service		5. TYPE OF REPORT & PERIOD COVERED Research and Development June 72 to December 73
7. AUTHOR(s) Jerry D. Stachiw		8. CONTRACT OR GRANT NUMBER(s)
9. PERFORMING ORGANIZATION NAME AND ADDRESS Naval Undersea Center San Diego, California 92132		10. PROGRAM ELEMENT, PROJECT, TASK AREA & WORK UNIT NUMBERS NAVFAC Project Number 165869
11. CONTROLLING OFFICE NAME AND ADDRESS Naval Facilities Engineering Command, Wash., D.C. 20360 Director of Naval Laboratories, Wash., D.C. 20390		12. REPORT DATE May 1974
14. MONITORING AGENCY NAME & ADDRESS (if different from Controlling Office)		13. NUMBER OF PAGES 58
		15. SECURITY CLASS. (of this report) UNCLASSIFIED
		15a. DECLASSIFICATION/DOWNGRADING SCHEDULE
16. DISTRIBUTION STATEMENT (of this Report) Approved for public release; distribution unlimited.		
17. DISTRIBUTION STATEMENT (of the abstract entered in Block 20, if different from Report)		
18. SUPPLEMENTARY NOTES		
19. KEY WORDS (Continue on reverse side if necessary and identify by block number) Acrylic hulls pressure vessel windows undersea habitat windows Acrylic plastic submersible windows acrylic plastic castings viewports hyperbaric chamber windows pressure testing spherical shells		
20. ABSTRACT (Continue on reverse side if necessary and identify by block number) A casting technique was developed that allows casting of acrylic plastic spherical shell sector windows to curvature and thickness tolerances generally found only in machined windows. By means of this technique, 18-inch OD X 10-inch ID windows were made; after a minor polishing operation, they met the ASTM-D-702 specification for optical clarity. The mechanical and physical properties of the castings were in the same range as those of commercially available cast plates and sheets. (cont'd)		

DD FORM 1 JAN 73 1473 EDITION OF 1 NOV 65 IS OBSOLETE

UNCLASSIFIED

SECURITY CLASSIFICATION OF THIS PAGE (When Data Entered)

UNCLASSIFIED

SECURITY CLASSIFICATION OF THIS PAGE(When Data Entered)

20. (Continued)

The results obtained from long-term and cyclic pressure testing of nine cast hemispherical windows indicate that the windows with a t/R_i (thickness to inner radius) ratio of 0.8 are acceptable for service in manned installations with hydrostatic pressures to 5000 psi at temperatures equal to, or less than, 75°F.

The casting process is applicable to production of man-size spherical acrylic pressure hulls to decrease their cost.

UNCLASSIFIED

SECURITY CLASSIFICATION OF THIS PAGE(When Data Entered)

SUMMARY

PROBLEM

Spherical shell sector windows of cast acrylic plastic have been found to be better suited, structurally and optically, for high-pressure service than flat disc or conical frustum windows. To perform successfully, however, they require close dimensional tolerances that cannot be met by thermoforming techniques alone. To date, these tolerances have been met only by machining of cast, or cast and thermoformed, acrylic plastic stock. However, this method of fabrication of such windows, although otherwise very satisfactory, is prohibitively expensive for the larger sizes. A less expensive fabrication technique was sought so that the spherical shell sector windows would become attractive economically.

RESULTS

A technique of casting to finished dimensions was developed that allows the production of acrylic plastic spherical shell sector windows to curvature and thickness tolerances generally found only in machined windows.

Acrylic plastic spherical shell sector windows with 9-inch outside and 5-inch inside radii were cast to a radial tolerance of ± 0.05 -inch. The finish on the spherical surfaces was of such high quality that no machining or sanding of these surfaces was required. After a minor polishing operation the windows met the ASTM D-702 specification for optical clarity. Machining was required only on the bearing surface of the window.

The mechanical and physical properties of the casting were comparable to those of commercially available cast acrylic plastic plates (Plexiglas G, Swedlow 310, Acrylite).

RECOMMENDATION

The casting process can be used for fabrication of windows applicable to high-pressure service in manned and unmanned systems, provided that the dimensional and material quality controls used in this study are maintained.

Acrylic plastic spherical shell sector windows with $t/R_i = 0.8$ and included angle of 180° fabricated by casting can be operated in manned service, up to a 5000-psi hydrostatic pressure, provided: (1) the radii and thickness do not deviate more than 1 percent and 2 percent respectively from specified values; (2) the mechanical properties of cast materials are equal to or better than those found in the cast windows described in this report (table 2).

It is recommended that the casting process for acrylic plastic spherical shell sector windows developed in this study be applied to production of man-size spherical acrylic pressure hulls in order to decrease their high acquisition costs. Savings of 50% over the typical modular NEMO fabrication technique are projected for spherical hulls assembled from cast hemispheres.

CONTENTS

INTRODUCTION	3
BACKGROUND	3
FABRICATION	4
WINDOW SPECIMENS	5
TESTING OF WINDOWS	6
TEST OBSERVATIONS	7
FINDINGS	9
CONCLUSION	10
RECOMMENDATIONS	10
REFERENCES	11

INTRODUCTION

Acrylic plastic windows* have found wide application as viewports for high-pressure service at sea and on land (references 1-8, 15, 16). Several window configurations have been studied for their structural and optical properties. Of these only the conical frustum, flat disc, and spherical shell sector have found practical application. These windows have been made from cast acrylic plastic plates by machining. Although the three shapes can be made massive enough to withstand hydrostatic pressures to 20,000 psi, only the spherical shell sector** offers optimum optical and structural properties. However, the cost of its fabrication is an order of magnitude higher than that of the other two shapes, because precise machining is required on all surfaces of spherical windows to bring it within the necessary dimensional tolerances.

Only casting to finished dimensions promises to be a viable approach for the reduction of fabrication costs. Several casting techniques with potential for producing spherical windows to finished dimensions were studied. Two were developed to the final production stage. The process reported here is the precision casting process of windows to finished dimensions.***

BACKGROUND

The difficulty of casting acrylic plastic spherical windows to finished dimensions increases with the magnitude of the included spherical angle. The basic reason for this difficulty is the large shrinkage of acrylic plastic resin upon polymerization. Since casting to finished dimensions requires a set of male and female molds held in a fixed orientation, such shrinking is restrained by the rigidly held molds.

So long as the included spherical angle is $\leq 90^\circ$, the male mold exerts very little radial restraint on the shrinking resin and the resulting castings are relatively stress-free. However when the included spherical angle is 180° , the radial restraint at the equator of the hemisphere assumes the full value generated by the shrinking resin. If no special steps are taken to compensate for the 20% shrinkage of the acrylic resin (methyl methacrylate monomer resin), sufficiently high tensile stresses would be generated in the casting to produce tensile cracks. The presence of such cracks, besides trapped air bubbles, is the most common reason for rejection of castings.

Several approaches have been utilized to decrease tensile stresses in acrylic plastic resulting from shrinkage of resin during curing. The most common approach has been to add to the methyl methacrylate monomer resin some already polymerized acrylic plastic in the form of fine powder. Depending on the percentage of powder added, the shrinkage of the casting can be decreased to about 5%. Although this procedure is very beneficial in decreasing of shrinkage stresses, in most cases it is not sufficient enough to prevent a few tensile cracks.

*The production of acrylic plastic transparent pressure hulls (references 9-15), their technology being similar to that of windows, should benefit from the progress in casting reported here.

**For the sake of brevity, spherical shell sector windows will be referred to as "spherical windows."

***The other process is reported in reference 17.

The additional steps taken for the further reduction of tensile stresses in the casting address themselves to the reduction of radial restraint. This can be accomplished by making the male mold from a compliant material, so that it would compress radially under the action of shrinking acrylic plastic resin and prevent the buildup of tensile stresses in polymerized acrylic plastic to dangerous levels. The mold would have to have a thin wall and be constructed from a material with (1) a low modulus of elasticity, (2) a coefficient of thermal expansion matching that of acrylic plastic and (3) the ability to retain its structural properties at temperatures encountered in polymerization of acrylic plastic resin.

A material meeting most of those requirements is glass-fiber-reinforced epoxy plastic. With a male mold of this material, successful castings of acrylic plastic hemispherical windows have been produced.¹⁷

The major shortcoming of this approach has been that the cast hemisphere requires excessive amounts of hand sanding and polishing to make it optically acceptable. In addition, the dimensions deviate from those specified considerably in excess of those attainable through machining. Still, because this type of mold is inexpensive, this approach to casting of acrylic plastic spherical windows is economically attractive — provided that only one or two castings of given dimensions are required and the noticeable deviations from specified sphericity and thickness can be tolerated.

The approach described here to reduce tensile stresses in cast spherical windows avoids sacrifice of any quality of surface finish or dimensional tolerances typically associated with machined and subsequently polished acrylic plastic hemispheres.

The casting technique developed satisfied the requirement of economical mass production of precision-made, large, spherical acrylic windows applicable to high-pressure service. A low unit cost was achieved by eliminating the expensive and time-consuming machining and polishing of spherical surfaces commonly associated with the production of precision-made spherical windows. The only machining necessary was on the equatorial bearing surface of the spherical window.

FABRICATION

These goals were achieved by developing the proper tooling, casting mix, and polymerization process.

Tooling

The tooling consisted of mated male and female molds (figure 1) machined from 6061-T6 aluminum alloy forged billets (figure 2). The spherical surfaces on both molds were machined to a 32 rms finish and subsequently polished to a mirror-like finish. Through careful control of dimensional tolerances on the spherical radii of mold surfaces and location of indexing pins in the assembly components, the mold cavity was within ± 0.032 in. of the specified nominal curvature dimensions. This tolerance does not indicate the maximum attainable precision for this type of mold assembly. It was considered more than adequate for the window size chosen for test purposes.

Casting Mix

A batch of casting mix consisted of 1000 ml methyl methacrylate monomer (DuPont H324), 1500 g polymer (DuPont 4FNC99) passing No. 77 sieve, 2 g catalyst (DuPont Vazo 52), and 10 ml of methylene glycol methacrylate (Sartomer Resins Co.) for crosslinking. The materials were mixed with an electric rotary mixer and placed under 80 mm of vacuum. After several minutes the vacuum was released and the mix was stirred until it thickened to a creamy consistency. At that time the mix was poured into the mold assembly, which had been cleaned with methyl or ethyl alcohol (figure 3).

Casting

The mold assembly, filled with the casting mix, was placed into an autoclave, which was kept in the 70 to 80°F temperature range (figure 4). The autoclave door was closed and pressurization with compressed air was begun. When, after approximately six hours the internal pressure reached 150 psi, the thermal cycle was begun.

The thermal cycle consisted of the temperature of the pressurized autoclave being raised from 80° to 180°F in 3 hr and 30 min. The 180°F temperature was maintained for 18 hr. Then the pressurized autoclave was cooled to 120°F, which took 24 hr. When 120°F was reached the autoclave was depressurized and the door opened, and the male mold was removed from the assembly, leaving the casting undisturbed in the female mold. The autoclave was closed again and, remaining unpressurized, cooled down to 80°F.

When the interior of the autoclave reached 80°F the door was opened and the casting removed from the female mold (figure 5). Subsequently the molds were cleaned with methyl alcohol and were ready for another batch of casting mix.

It is important to note here that the removal of the male mold when the polymerized casting is at 120°F prevents the formation of tensile cracks in the finished casting. This temperature is quite critical: if the male mold is removed at higher temperatures, parts of the casting adhere to the male mold and are torn from the casting, while at lower temperatures cracks are already present in the casting.

WINDOW SPECIMENS

Shape

Two shapes were chosen for casting the test specimens (figures 6 and 7). One shape was that of a classical, thick-walled hemisphere, the other of a flanged, thick-walled hemisphere. The flangeless hemisphere was chosen to demonstrate the capability of the new casting process to produce true spherical windows with optically clear surfaces within tight dimensional tolerances. The flanged hemisphere was chosen to test the capability of the casting process to produce optically acceptable spherical castings with heavy equatorial flanges. A total of nine flangeless and three flanged hemispheres were cast in the machined aluminum molds to establish the feasibility of the precision casting process for spherical windows.

Dimensions

The dimensions of the windows were determined by the diameter of the available deep-ocean test simulator with a maximum hydrostatic working pressure of 20,000 psi. The thickness also was determined by this maximum pressure, which was suitable for the subsequent destructive testing. Through accommodating the window dimensions to the capacity of the available deep-ocean simulator, substantial economies were achieved in the testing. This permitted the testing of more specimens with greater detail than would otherwise have been feasible with the available funding.

Quality Control

The windows produced fully met the objectives of the study. The internal and external surfaces did not require any sanding or machining in order to meet the tolerances specified. Only machining of the equatorial bearing surfaces was required to convert the castings into a finished optical product (figures 8 and 9). The visibility through the windows more than surpassed the requirements of ASTM D-702 and no bubbles or cracks were noticeable.

The mechanical and physical properties of the cast material were established through testing of coupons cast from the same mix by means of the same polymerization process. The massiveness of the coupons (4 in. in diameter and 12 in. long), ensured similarity of the mechanical properties of the coupons with those of the window castings (figure 10).

The properties (table 1) were found to be comparable to those of commercially available cast acrylic plastic plate 4-in. thick commonly used as machining stock for small pressure-resistant windows. This indicates that the process described here produces high-quality window castings acceptable for high-pressure service in manned and unmanned systems, such as submersibles, habitats, hyperbaric chambers, water tunnels, and deep ocean simulators.

TESTING OF WINDOWS

Objective

The objective of the test program was to establish experimentally the safe operational pressure to which the flangeless spherical windows with $t/R_i = 0.8$ (figure 7) could be subjected in service. They were tested under three pressure conditions: short-term, long-term, and cyclic (table 2). The three cast flanged windows (figure 6) were not tested at this time.

The short-term test determined the pressure at which catastrophic failure of the flangeless spherical window would occur under accidental increase in service pressure (such as through loss of control over a diving submersible, or failure of the pressure regulator on the pressurization system for a hyperbaric chamber). In the short-term test the pressure was raised till either catastrophic failure took place or the operational limit of the pressure vessel was reached at 20,000 psi internal pressure.

The long-term test showed how much creep could be expected in the flangeless spherical window under sustained pressure loading, such as in a habitat submerged for weeks or even years. The duration of each test was 750 hr.

The cyclic test produced data for a cyclic fatigue curve, which would be used for predicting the fatigue life of windows. The duration of each cycle was 8 hr, of which 4 hr was sustained loading and 4 was relaxation. This pressure cycle regimen was considered representative of typical submersible service. Each window was subjected to 100 pressure cycles unless catastrophic failure occurred sooner.

Test Conditions

The tests were performed in a water-filled, deep ocean simulator maintained at 70-75°F temperature range. All tests but the short-term were performed with the hemispheres resting on a steel bulkhead with 63 rms machined finish (figure 11).

For the short-term test, two hemispheres were bonded together to form a sphere (figure 12) and were tested as a unit. This was done to avoid influencing the character of catastrophic failure by end conditions.

The pressurization was achieved through positive displacement pumps raising the pressure at 500 psi/min. The depressurization was accomplished at approximately the same rate.

The instrumentation consisted mainly of electric-resistance, 90°, strain-gage rosettes. In addition, for the short-term test, the water displacement technique was utilized (figure 12), as it was feared that the strain gages might fail before catastrophic failure occurred.

TEST OBSERVATIONS

Short-Term Test

Since the sphere composed of two hemispheric windows did not fail catastrophically at 20,000 psi, the maximum working pressure of the deep-ocean test simulator, it cannot be stated positively what is the short-term collapse pressure of the windows tested. However, judging by the recorded strains, displaced water, and radial displacements (figures 13, 14, 15), the short-term collapse pressure lies somewhere in the 22,000-to-24,000-psi range.

The maximum stresses reached were above the yield strength of the material and thus it can be predicted that the catastrophic failure would have the character of plastic instability. That considerable plastic flow occurred at 20,000 psi is evident by extensive fracturing having taken place at 2,000 psi during the depressurization of the deep-ocean simulator. All the cracks originated on the interior spherical and equatorial bearing surfaces (where the highest compressive stresses and the associated plastic flow occurred) and propagated through approximately 75% of the wall thickness (figures 16, 17, 18, 19).

Cyclic Fatigue Tests

The cyclic fatigue tests conducted on four windows at 13,500-, 10,000-, 7500- and 5000-psi pressure levels for 100 consecutive pressure cycles have shown that the spherical windows tested can probably withstand without catastrophic failure at least 10,000 pressure loadings of 4-hour duration at 5000 psi (figure 20).

This evaluation is based on the fact that 13 pressure cycles to 13,500 psi were required for a catastrophic failure to occur (figure 20), while even 100 pressure cycles to 7500 or 10,000 psi failed to damage the windows catastrophically (figures 21, 22, 23 and 24). The complete absence of cracks in the window cycled 100 times to 5000 psi, and only moderate cracking in the window cycled 100 times to 7500 psi, attest to the adequacy of the window for cyclic service at 5000 psi.

The strains (figures 25 and 26) recorded during pressure cycling also substantiate a phenomenon peculiar to cyclic pressure testing of spherical windows. This phenomenon, postulated before by researchers (reference 18) but never proven, is that the initiation of cracks on the interior surface of windows occurs during the relaxation and not the sustained loading phase of the pressure cycle.

The cracks are initiated by tensile strains in the plastically deformed interior surface. These strains are generated by expansion of the material still in elastic condition near the outer surface of the hemisphere when the hydrostatic pressure on the window is reduced to zero. The plastically compressed material cannot return to its original relaxed condition, although it is physically joined to the elastically expanding material, thus generating tensile stresses in the plastically compressed material.

The growth of tensile stresses during each relaxation phase is cumulative; the magnitude increases during each relaxation phase by approximately the same increment. So long as cycling continues, the magnitude increases until it surpasses the tensile strength of the acrylic plastic. At that time a tensile crack is initiated that rapidly propagates inward towards the elastic zone of material. As the strain records show (figures 25 and 26), this occurs when the magnitude of strains in the interior surface reaches +9000 microinches/inch. Since both the creep of material producing the plastically deformed zone and the subsequent tensile static fatigue are functions of duration of loading and relaxation periods, it is obvious that acrylic windows under cyclic loading are very sensitive to the duration of the pressure cycle. This substantiates the author's testing philosophy that the length of a test cycle should, whenever possible, correspond to the length of the operational cycle of the system in which the windows are to be incorporated.

The strain magnitude observed during the initiation of cracks on the interior surface of the spherical windows correlates rather well with the magnitude of positive strains in a biaxial stress field predicted (reference 19) for tensile failure of acrylic plastic.

The same explanation can be postulated for the initiation of the circumferential cracks in the bearing surface. They are also created during the relaxation phase of the cycle, by tensile radial strains generated through elastically expanding outer layers of window acting on the plastically compressed inner layer. This would also logically explain why the cracks are more frequent and are located at closer intervals near the inner surface of the window, where the maximum compressive stresses are found during hydrostatic loading of the window.

The repeated contraction and expansion of the window during pressure cycling also resulted in radial scoring of the bearing surface in contact with steel. Use of a gasket would have prevented this.*

*A concurrent study (reference 20) has shown that the use of a Fairprene 5722A or epoxy-impregnated KEVLAR 49 fabric gasket completely eliminates the scoring of the bearing surface on spherical acrylic windows with an included angle $> 120^\circ$.

Long-Term Tests

The 750 hr long sustained pressure loadings conducted on three windows at 15,000-, 10,000-, and 5000-psi pressure levels have shown that the windows tested can sustain with reasonable degree of confidence a pressure loading of 5000 psi for a period of time in excess of 1000 hr.

This evaluation is based both on the magnitude of creep (figure 27) recorded during sustained loadings at different pressure levels and on the severity of cracking observed after termination of tests at different pressure levels (figures 28, 29 and 30). Not only is the total creep at 5,000 psi less than 5,000 microinches/inch; also the creep rate approaches zero after the first 200 hr of sustained loading. In addition, while the cracks observed in windows after testing to 15,000 and 10,000 psi are severe, in the window tested to 5,000 psi they are absent completely.

The radial cracks observed on the interior surface and the circumferential cracks observed on the bearing surface are postulated to have occurred only after the pressure was released. In this case, the action of crack initiation is similar to that observed during fatigue cycling of other window specimens.

Since the total period of sustained loading during which creep could occur was near 750 hr, while during cycling fatigue tests it was only 400 hr (100 cycles with individual 4-hr sustained loading periods), it was to be expected that the number and depth of cracks would be greater in windows subjected to long-term sustained loading at the same pressure level as the cyclically fatigued windows.

Observation of window specimens 5 and 8 tested to 10,000 psi under cyclic and long-term conditions, respectively, bears this out. The cracks in specimen 8, subjected to uninterrupted 750 hr of sustained loading, were significantly deeper and more numerous than those in specimen 5, which experienced only 400 hr under sustained loading (figures 23, 29).

FINDINGS

A fabrication process was developed for precision casting of acrylic plastic spherical shell sector windows with a spherical included angle $\leq 180^\circ$, in a mold assembly of matched metallic male and female molds. Potential cracking of castings due to polymerization shrinkage is precluded by removal of the male mold from the casting, while it is cooling, when its temperature is at 120°F . Such spherical castings do not require machining or sanding of spherical surfaces.

The casting technique utilizes a polymerization process that produces acrylic plastic with mechanical and physical properties comparable to that of commercially available cast acrylic plates (Plexiglas G, Swedlow 310, Acrylite, etc.).

The windows, in the form of hemispheres with a thickness-to-inner-radius ratio of $t/R_i = 0.8$, were found to be safe for operational hydrostatic pressure of 5000 psi.

Cracking of the windows during cyclic pressure loading tests was found to originate on the equatorial bearing and internal spherical surfaces during the relaxation phase of the cycle, when the external pressure on the window is equal to zero.

Cracking of the windows during long-term sustained loading tests, when failure through general instability did not occur, was found to originate also on the equatorial bearing and internal spherical surfaces, but only during depressurization at the end of the test.

The short-term critical pressure of the hemispherical windows, having $t/R_i = 0.8$, was found to be in excess of 20,000 psi.

CONCLUSION

Massive spherical shell sector windows of acrylic plastic can be mass produced, economically and within tight dimensional tolerances, for high-pressure service in unmanned or manned systems. There appears to be no size limitations inherent in the casting process developed.

RECOMMENDATIONS

In general, the casting process described can be used for fabrication of acrylic plastic spherical shell sector windows applicable to high-pressure service in manned and unmanned systems – providing that the dimensional and material quality controls used in this study are maintained.

Cast spherical windows with $t/R_i = 0.8$ and included angle of 180° can be operated in manned service to 5000 psi, provided that: (1) the radii and thickness do not deviate more than 1% and 2% respectively from specified values and (2) the mechanical properties of the casting are equal to, or surpass, those specified in table 1.

For cast acrylic plastic spherical shell windows with different t/R_i ratios and included angles, the design specifications should be those developed in previous studies for spherical windows machined, or formed,¹⁴ from cast acrylic plates with the material properties shown in table 1.

The casting process developed also can be applied to production of man-size spherical acrylic pressure hulls in order to decrease their high acquisition costs. Savings of 50% should be feasible over the typical modular fabrication technique previously developed by the Navy for fabrication of the first acrylic plastic submersible NEMO.

REFERENCES

1. Naval Civil Engineering Laboratory. Technical Report R-512, Windows for External or Internal Hydrostatic Pressure Vessels; Part 1. Conical Acrylic Windows Under Short Term Pressure Application, by J. D. Stachiw, K. O. Gray. January 1967 (AD 646882).
2. ———. Technical Report R-527, Windows for External or Internal Hydrostatic Pressure Vessels; Part 2. Flat Acrylic Windows Under Short Term Pressure Application, by J. D. Stachiw, G. M. Dunn, K. O. Gray. May 1967 (AD 652343).
3. ———. Technical Report R-645, Windows for External or Internal Hydrostatic Pressure Vessels; Part 4. Conical Acrylic Windows Under Long Term Pressure Application of 20,000 psi, by J. D. Stachiw. October 1969 (AD 697272).
4. ———. Technical Report R-708, Windows for External or Internal Hydrostatic Pressure Vessels; Part 5. Conical Acrylic Windows Under Long Term Pressure Application of 10,000 psi, by J. D. Stachiw, W. A. Moody. January 1970 (AD 718812).
5. ———. Technical Report R-747, Windows for External or Internal Hydrostatic Pressure Vessels; Part 6. Conical Acrylic Windows Under Long Term Pressure Application of 5,000 psi, by J. D. Stachiw, K. O. Gray. June 1971 (AD 736594).
6. ———. Technical Report R-773, Windows for External or Internal Hydrostatic Pressure Vessels; Part 7. Effect of Temperature and Flange Configuration on Critical Pressure of 90 Degree Conical Acrylic Windows Under Short Term Loading, by J. D. Stachiw, J. R. McKay. August 1972 (AD 748583).
7. ———. Technical Report N-1127, Flat Disc Acrylic Plastic Windows for Man-Rated Hyperbaric Chambers of the U. S. N. Experimental Diving Unit, by J. D. Stachiw. November 1970 (AD 716751).
8. ———. Technical Report R-631, Windows for External or Internal Hydrostatic Pressure Vessels; Part 3. Critical Pressure of Acrylic Spherical Shell Windows Under Short Term Pressure Application, by J. D. Stachiw, F. W. Brier. June 1969 (AD 689789).
9. ———. Technical Report R-676, Development of a Spherical Acrylic Plastic Pressure Hull for Hydrospace Application, by J. D. Stachiw. April 1970 (AD 707363).
10. ———. Technical Note N-1113, The Spherical Acrylic Pressure Hull for Hydrospace Application; Part 2. Experimental Stress Evaluation of Prototype NEMO Capsule, by J. D. Stachiw, K. L. Mack. October 1970 (AD 715772).
11. ———. Technical Note N-1094, The Spherical Acrylic Pressure Hull for Hydrospace Application; Part 3. Comparison of Experimental and Analytical Stress Evaluations for Prototype NEMO Capsule, by H. Ottsen. March 1970 (AD 709914).

12. ———. Technical Note N-1134, The Spherical Acrylic Pressure Hull for Hydrospace Application; Part 4. Cyclic Fatigue of NEMO Capsule #3, by J. D. Stachiw. October 1970 (AD 715345).
13. Naval Undersea Center. NUC TP 315, Acrylic Plastic Hemispherical Shells for NUC Undersea Elevator, by J. D. Stachiw. September 1972 (AD 749029).
14. ———. NUC TP 355, Flanged Acrylic Plastic Hemispherical Shells for Undersea Systems, by J. D. Stachiw. August 1973 (AD 769213).
15. ———. NUC TP 305, Effect of Bubble Inclusions on the Mechanical Properties of Cast Polymethyl Methacrylate, by J. D. Stachiw. August 1972 (AD 746862).
16. ———. NUC TP 378, Recommended Practices for the Design, Fabrication, Proof-testing and Inspection of Windows in Man-rated Hyperbaric Chambers, by J. D. Stachiw. December 1973 (AD 773737).
17. ———. NUC TP 383, Cast Acrylic Dome for Undersea Applications, by J. D. Stachiw. January 1974.
18. J. D. Stachiw, J. J. Lones. Deep Submergence Windows for Optical Systems. Underwater Photo-Optical Instrumentation Applications Seminar, Volume 24, Proceedings of the Society of Photo-Optical Instrumentation Engineers, Honolulu, March 1971.
19. Redstone Arsenal. Technical Report No. RR-TR-64-15, Combined Stress Properties for Acrylic Tube Specimens, by R. E. Ely. 31 August 1964.
20. Naval Undersea Center. NUC TP 393. Glass or Ceramic Spherical Shell Window Assembly for 20,000-psi Operational Pressure, by J. D. Stachiw. May 1974.

**Table 1. Physical Properties of Cast Acrylic Plastic Hemispheres
and of Plexiglas G Sheets**

Property	ASTM method	Units	Hemisphere casting*	Plexiglas G sheets**
Specific gravity	D792	—	1.17	1.19 ± 0.01
Residual monomer	SPI	%	0.2	1.5 max.
Tension				
ultimate strength	D638	psi	9,750	9,000 min.
max. elongation	D638	%	3.64	2 min.
modulus	D639	psi	480,000	400,000 min.
Flexure				
ultimate strength	D790	psi	14,500	14,000 min.
modulus	D790	psi	490,000	420,000 min.
Compression				
yield	D695	psi	15,800	15,000 min.
modulus	D695	psi	400,000	400,000 min.
deformation (at 4000 psi & 120°F)	D621	%	0.72	1.0 max.
Shear				
ultimate strength	D732	psi	9,250	8,000 min.
Impact				
Izod notch	D256	ft lb/ in. of notch	0.22	0.3 min.
Heat distortion (temperature at 264 psi)	D648	°F	213	205 min.
Resistance to stress (critical crazing stress in presence of isopropyl alcohol)	MIL-P-8184	psi	2,000 psi minor crazing	1,500 min.

*Actual measured values of hemispheres fabricated by Polymer Products, Oakland, CA.

**Specified values for procurement of Plexiglas G material used in fabrication of pressure-resistant windows for man-rated submersibles and hyperbaric chambers (Reference 16).

Table 2. Hydrostatic Tests of Cast Acrylic Plastic Hemispheres

Test	Test parameters	Specimen no.	Results
Short-term	Pressurized to 20,000 psi and held for 1 hr	1, 2	Severe cracks appeared during depressurization.
Cyclic fatigue	Cycle regimen: 4 hr at 5,000 psi 4 hr at 0 psi	3	No cracks after 100 cycles.
	Cycle regimen: 4 hr at 7,500 psi 4 hr at 0 psi	4	Minor cracks after 100 cycles.
	Cycle regimen: 4 hr at 10,000 psi 4 hr at 0 psi	5	Severe cracking after 28 cycles. Survived 100 cycles without catastrophic failure, but failure imminent.
	Cycle regimen: 4 hr at 13,500 psi 4 hr at 0 psi	6	Catastrophic failure after 13 cycles.
Long-term	sustained 5,000 psi for 750 hr	7	No cracks after 750 hr of loading and depressurization.
	sustained 10,000 psi for 750 hr	8	Cracks after 750 hr of loading and depressurization.
	sustained 15,000 psi for 750 hr	9	Severe cracks after 750 hr of loading and depressurization.

All tests conducted in water at 70°-75°F range.
 All hemispheres have an 18-in. OD and 10-in. ID.
 Pressurization and depressurization rates are 500 psi/min.



Figure 2. Aluminum alloy (6061-T6) forgings used for fabrication of molds.

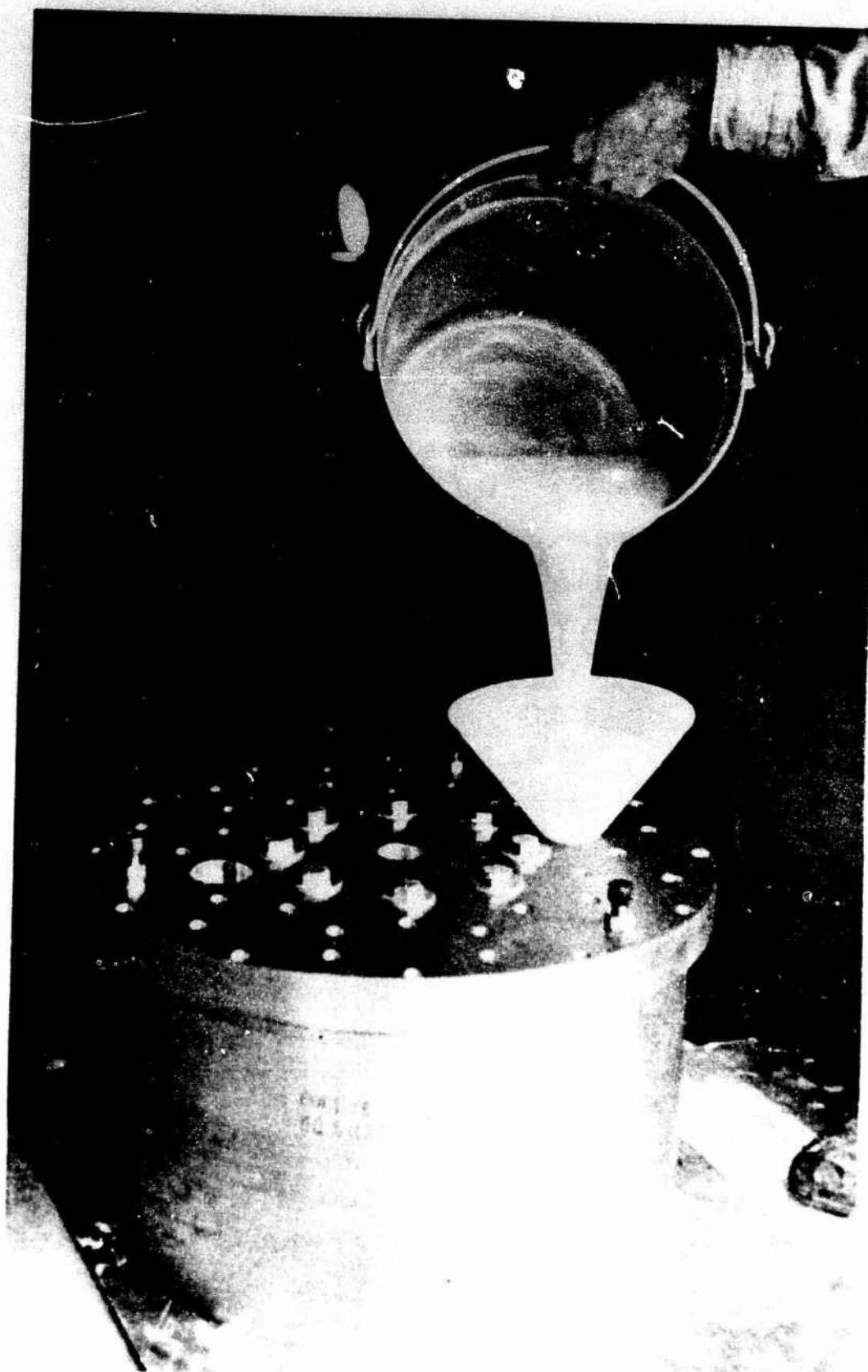


Figure 3. Acrylic plastic casting mix being poured into mold assembly.

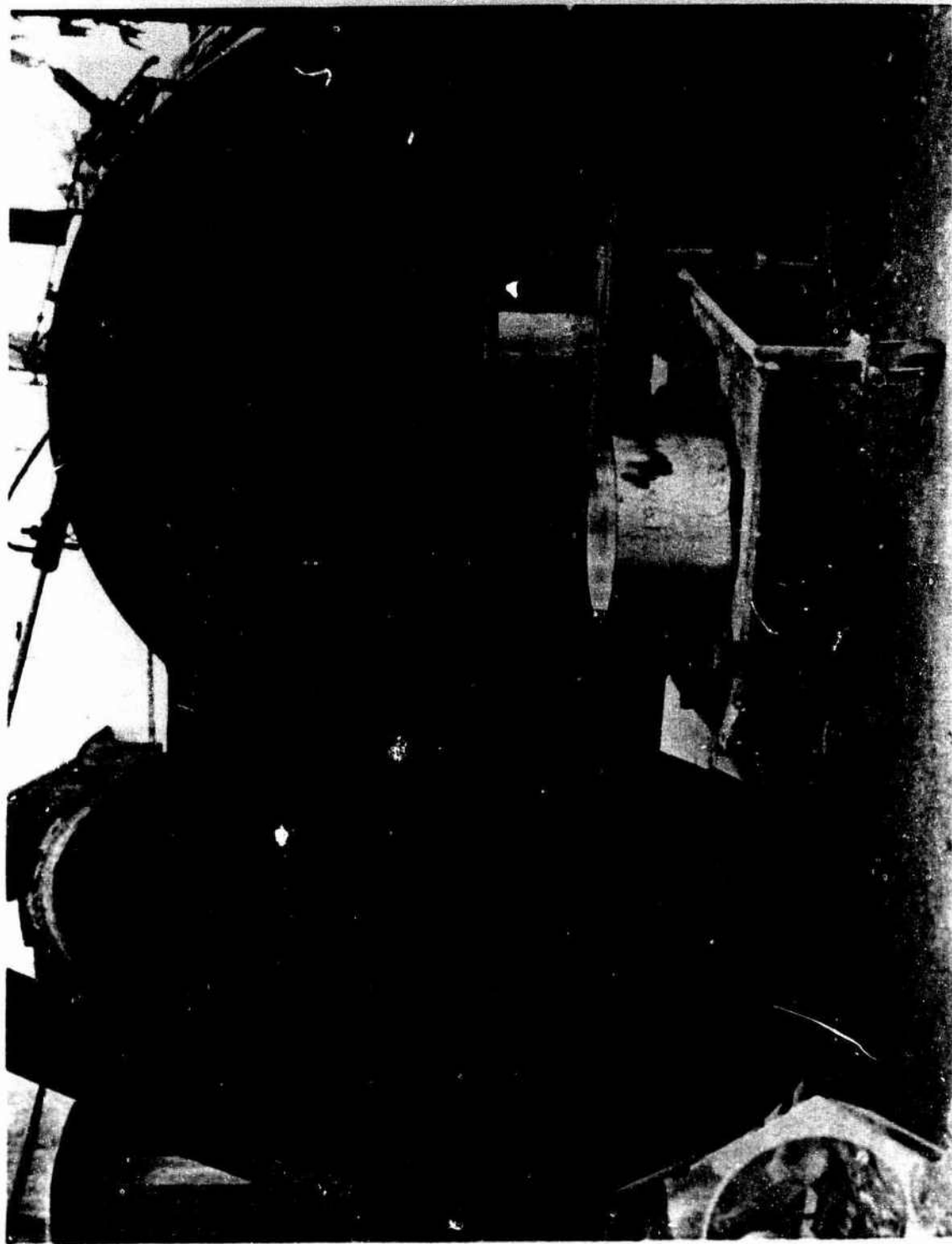


Figure 4. Autoclave used for polymerization of casting mix.



Figure 5. Casting after removal from the mold. Note that only equatorial surface is wrinkled and requires machining.

A. PRIOR TO MACHINING.

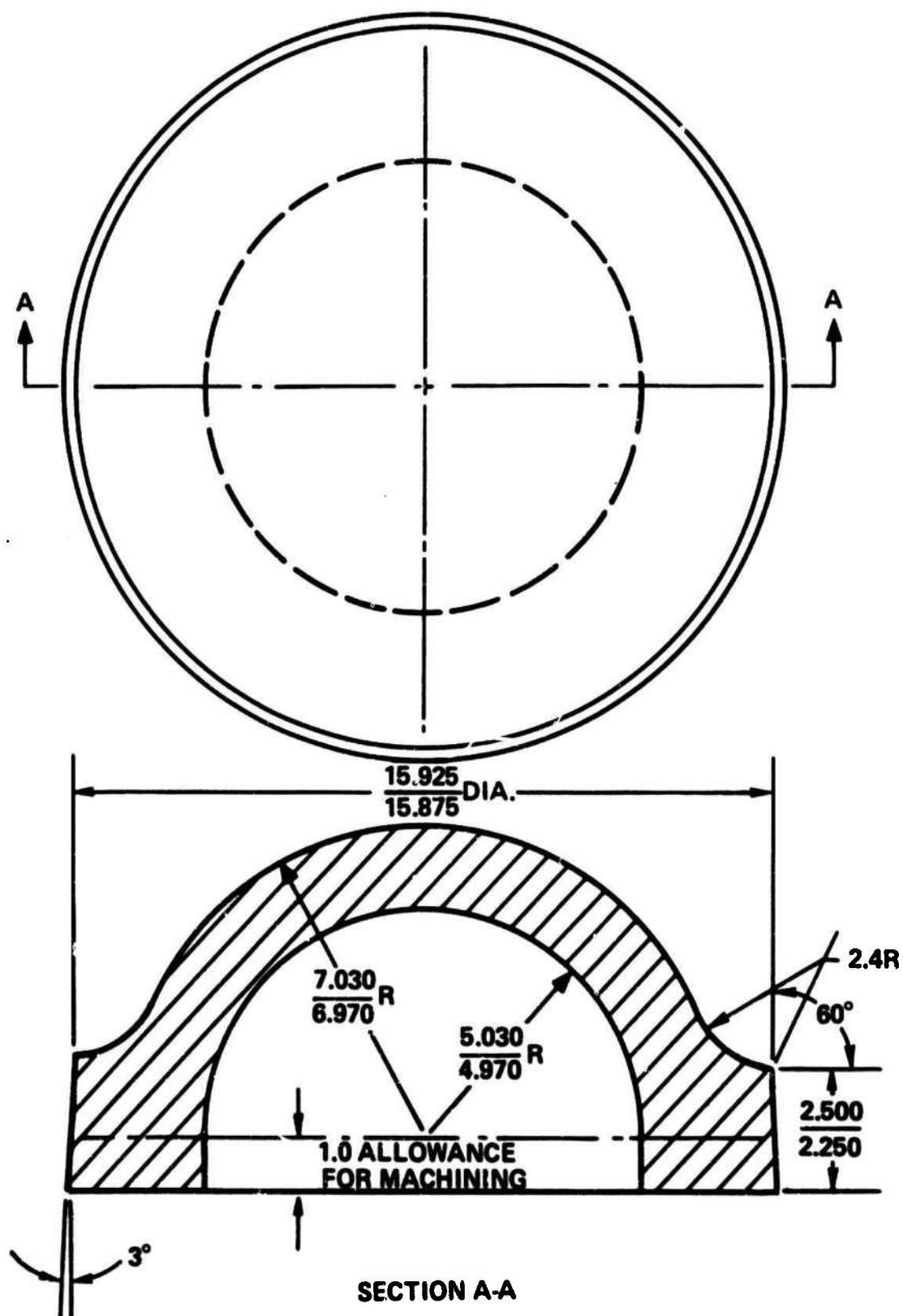
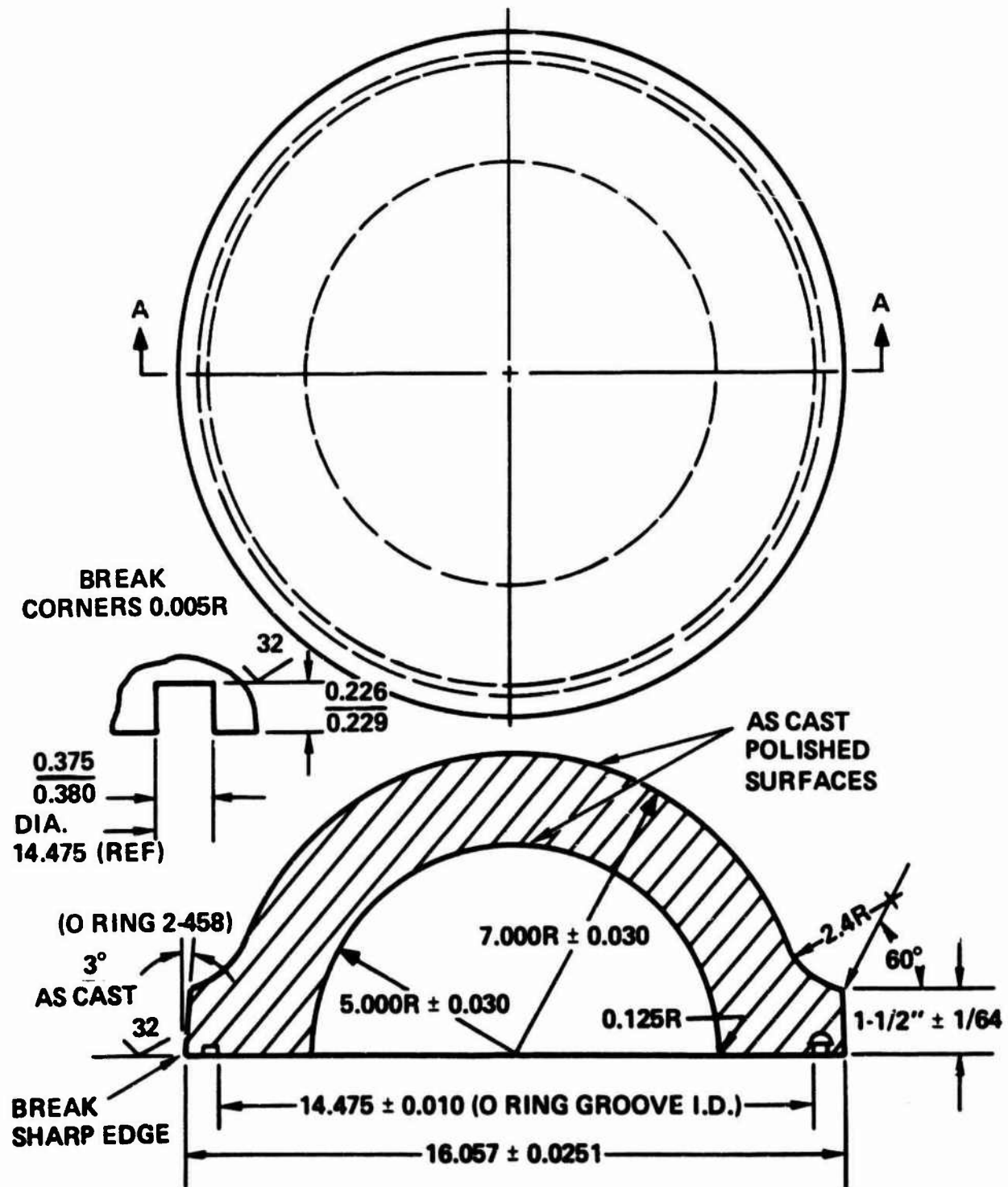


Figure 6. Dimensions of flanged spherical window casting.

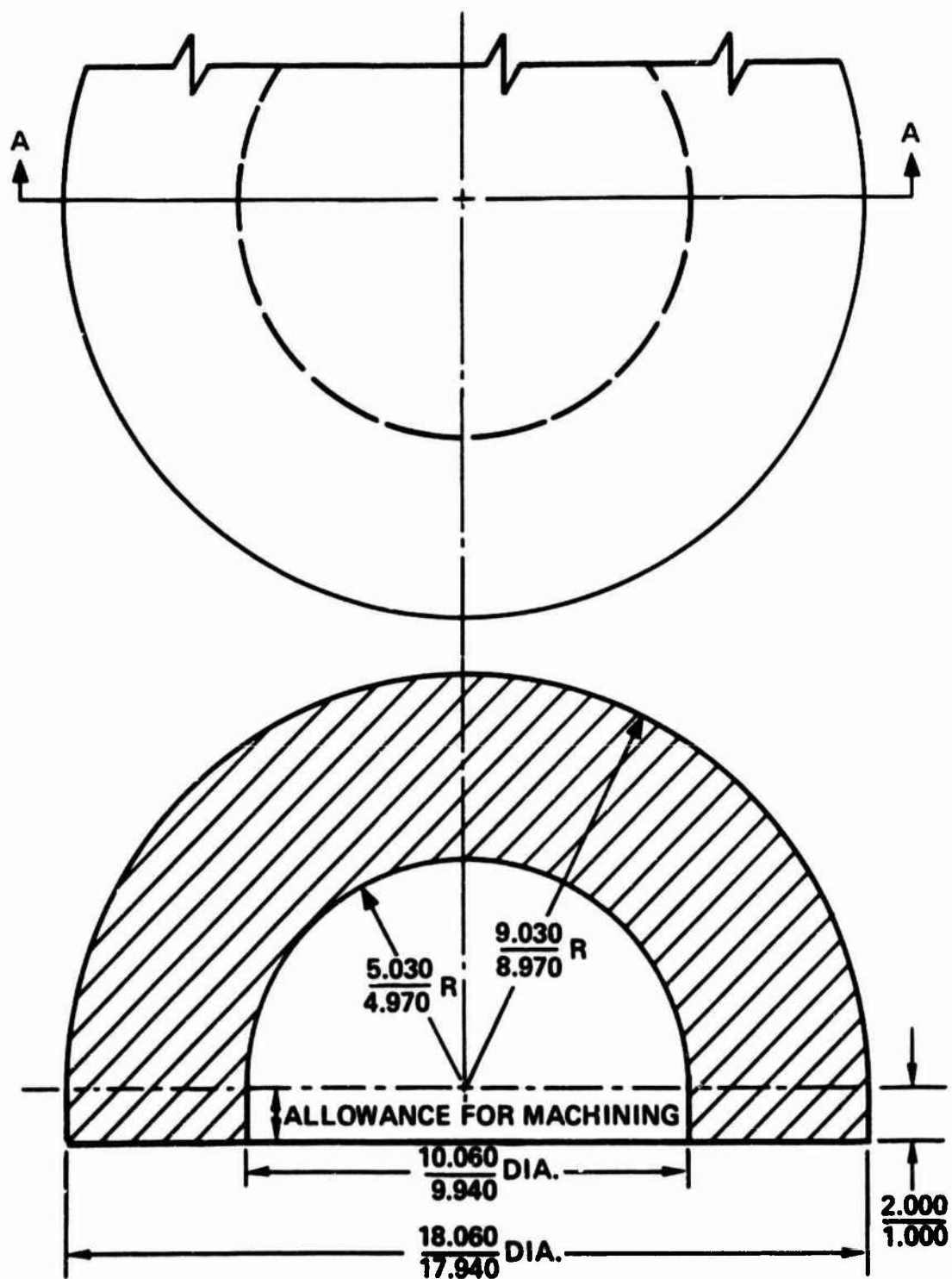
B. AFTER MACHINING.



SECTION A-A

Figure 6. (Continued).

A. PRIOR TO MACHINING.



SECTION A-A

Figure 7. Dimensions of spherical window casting.

A technical drawing of a semi-circular object. The object has a dashed inner circle and a stepped top edge. Section lines 'A' are shown on the right side, indicating a cross-section.

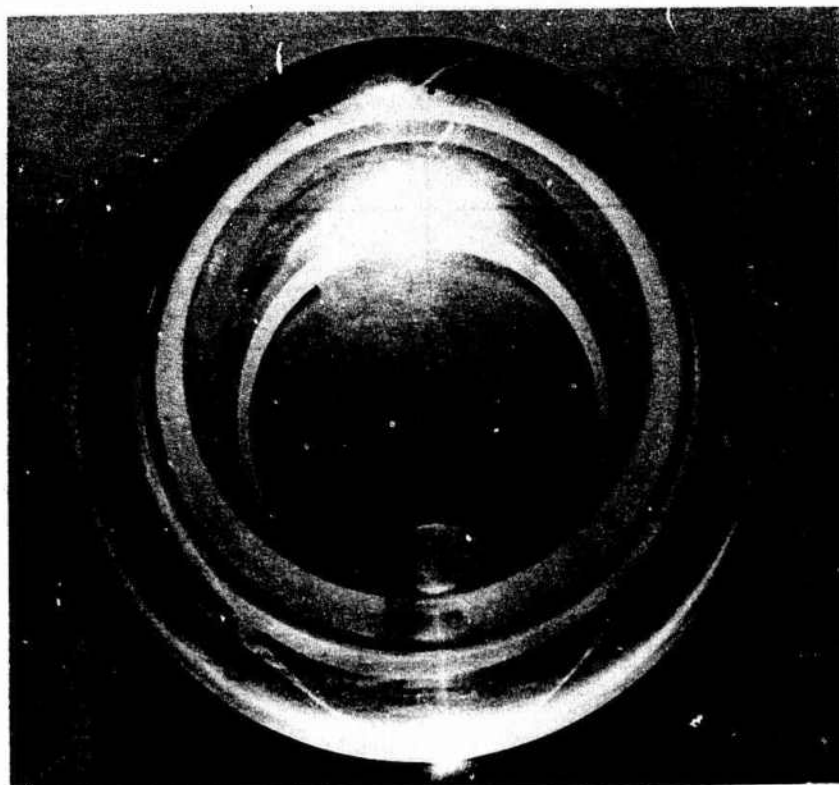
Technical drawing of a semi-circular cross-section of a pipe. The drawing shows a shaded outer semi-circle and an unshaded inner semi-circle. The following dimensions are provided:

- Outer radius: $\frac{9.030}{8.970}$
- Inner radius: $\frac{5.030}{4.970}$
- Outer diameter: $\frac{18.060}{17.940}$
- Inner diameter: $\frac{10.060}{9.940}$
- Wall thickness at the top: $\frac{9.030}{8.970}$
- Wall thickness at the bottom: $\frac{5.030}{4.970}$
- Angle at the bottom right: 32°

Labels include "SHARP EDGES" pointing to the corners of the inner semi-circle and "BREAK SHARP EDGES" pointing to the corners of the outer semi-circle.

Figure 7. (Continued).

A. TOP VIEW.



B. BOTTOM VIEW.

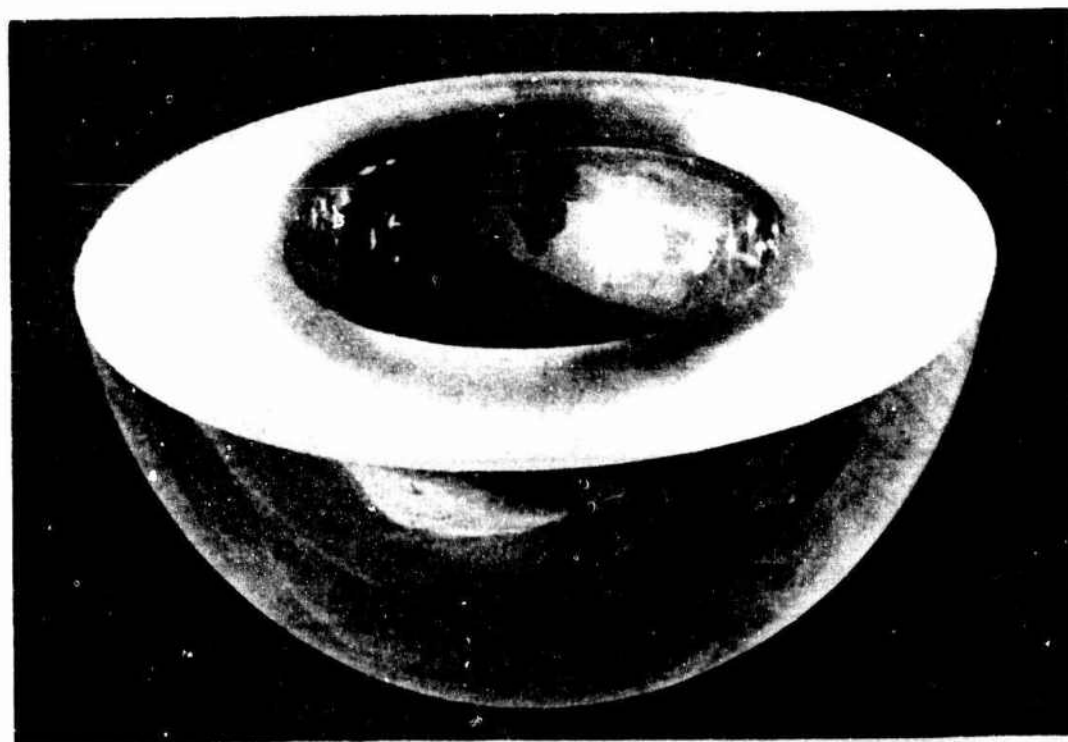
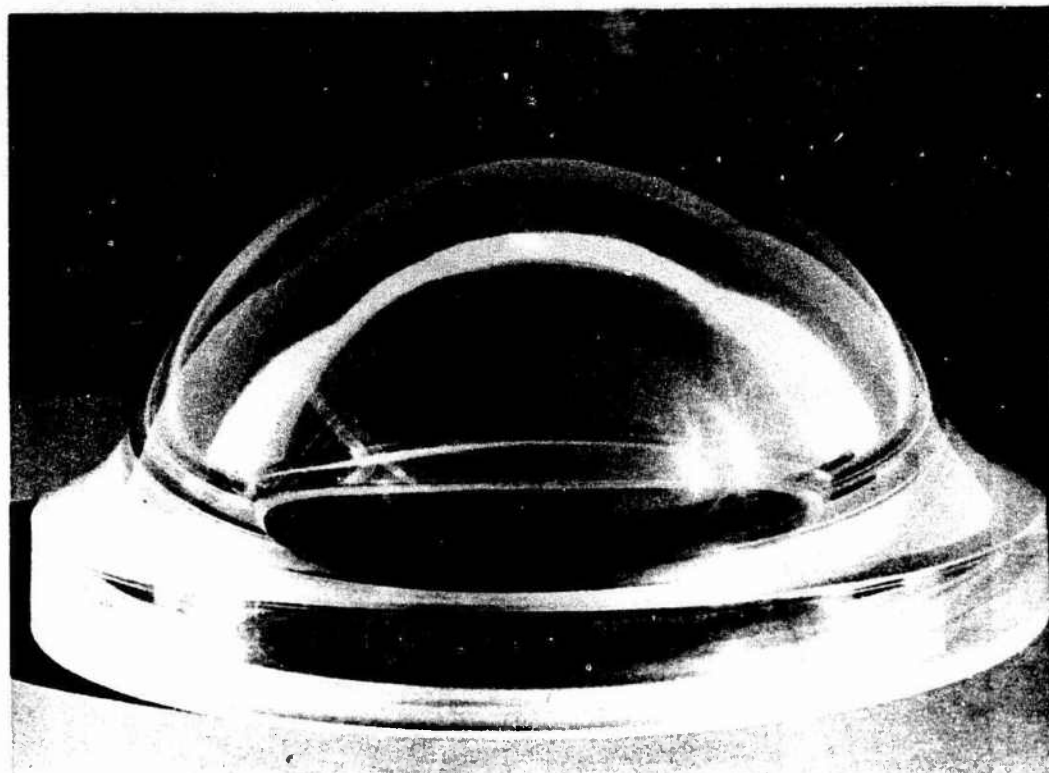


Figure 8. Finished 18-in. OD x 10-in. ID flangeless spherical window.

A. TOP VIEW.



B. BOTTOM VIEW.



Figure 9. Finished 14-in. OD x 10-in. ID flanged window.

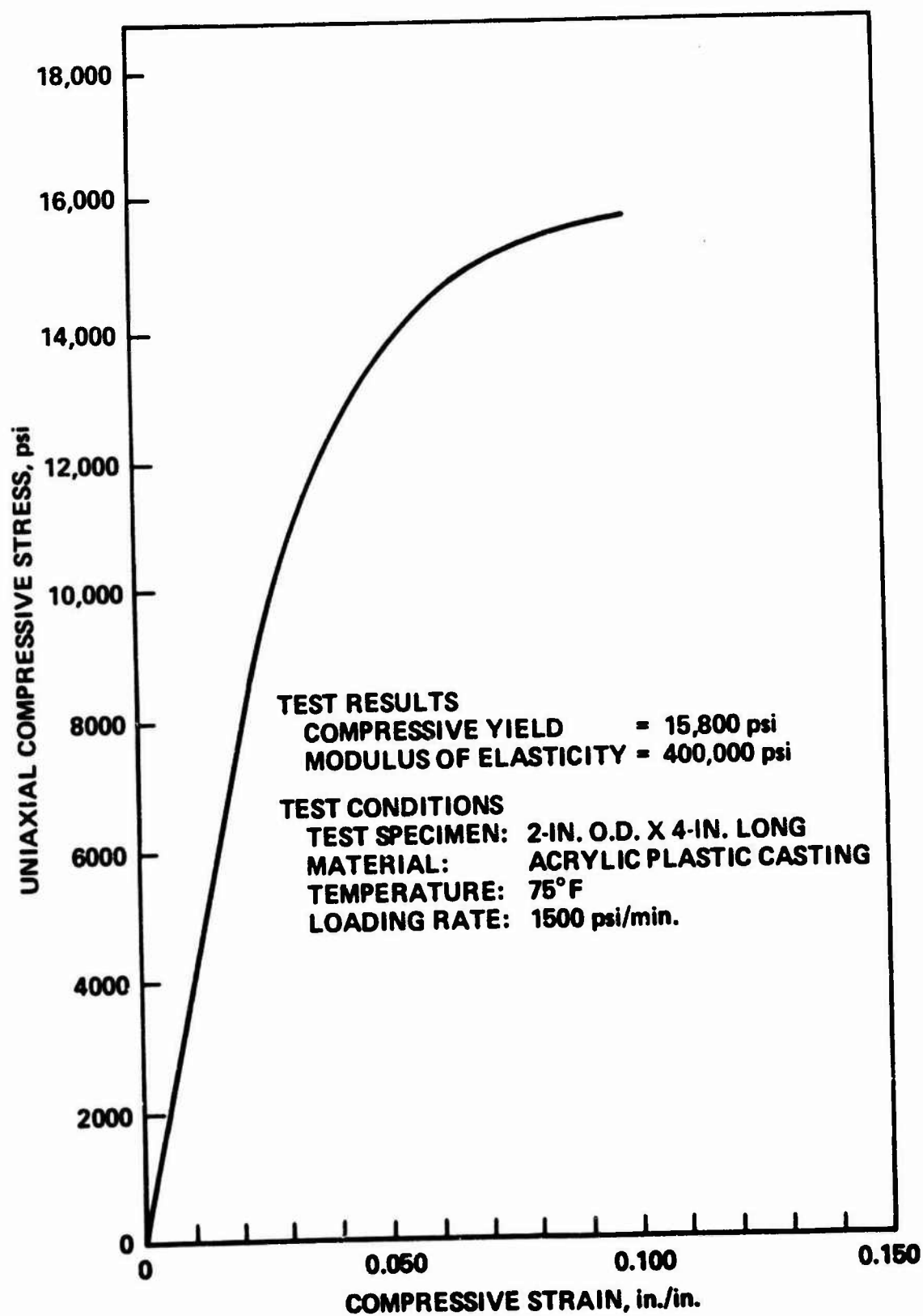


Figure 10. Compressive strength of acrylic plastic casting.

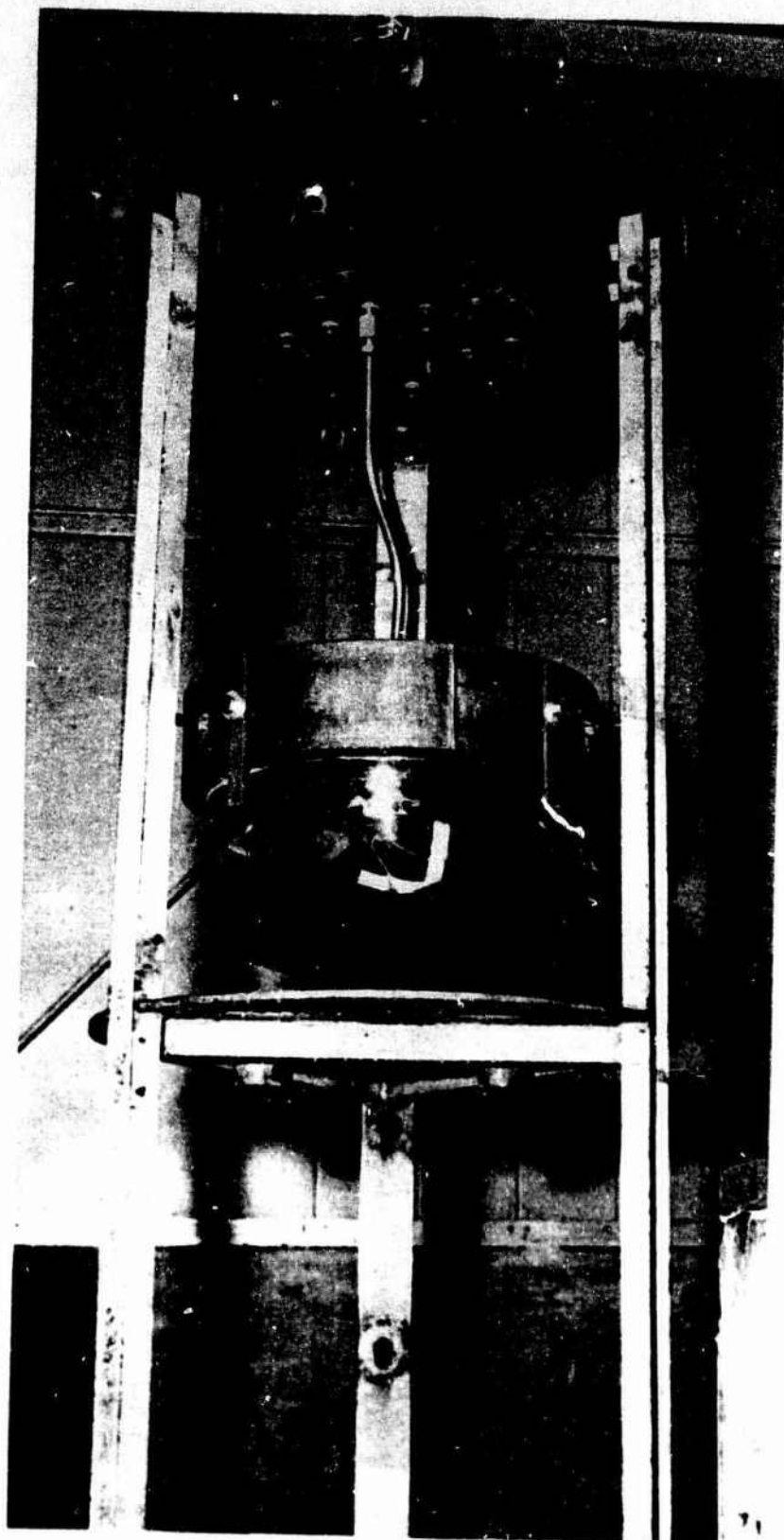


Figure 11. Test arrangement for long-term and cyclic-pressure testing of cast spherical windows. Note tube used for venting interior of hemisphere to ambient atmosphere outside the pressure vessel.

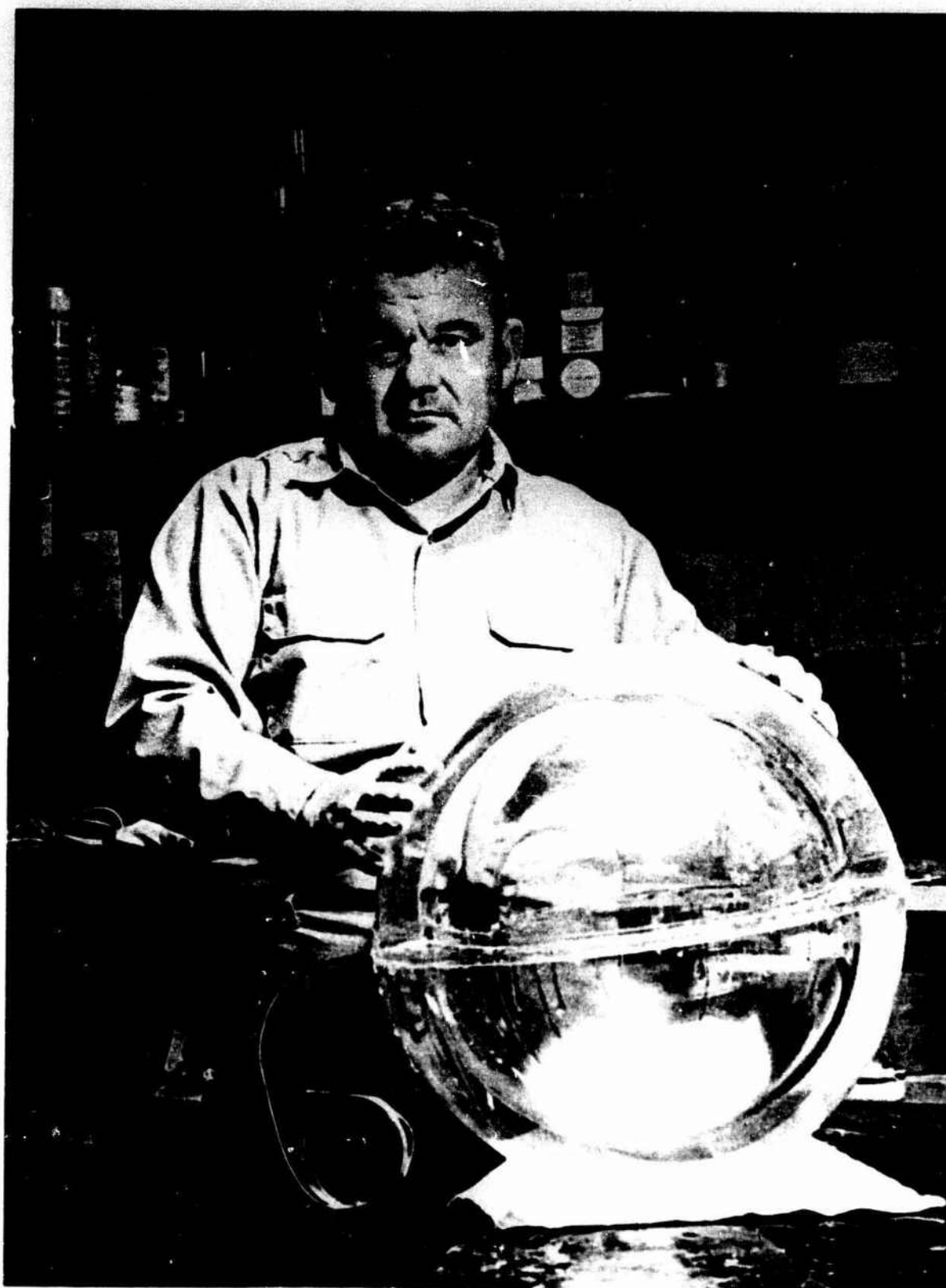


Figure 12. Test arrangement for short-term hydrostatic testing of cast acrylic spherical windows. Note tubing used for filling the interior of the sphere with water prior to hydrostatic testing. During the test displaced water from the interior of the sphere flows through the tubing to a graduated container located outside the pressure vessel.

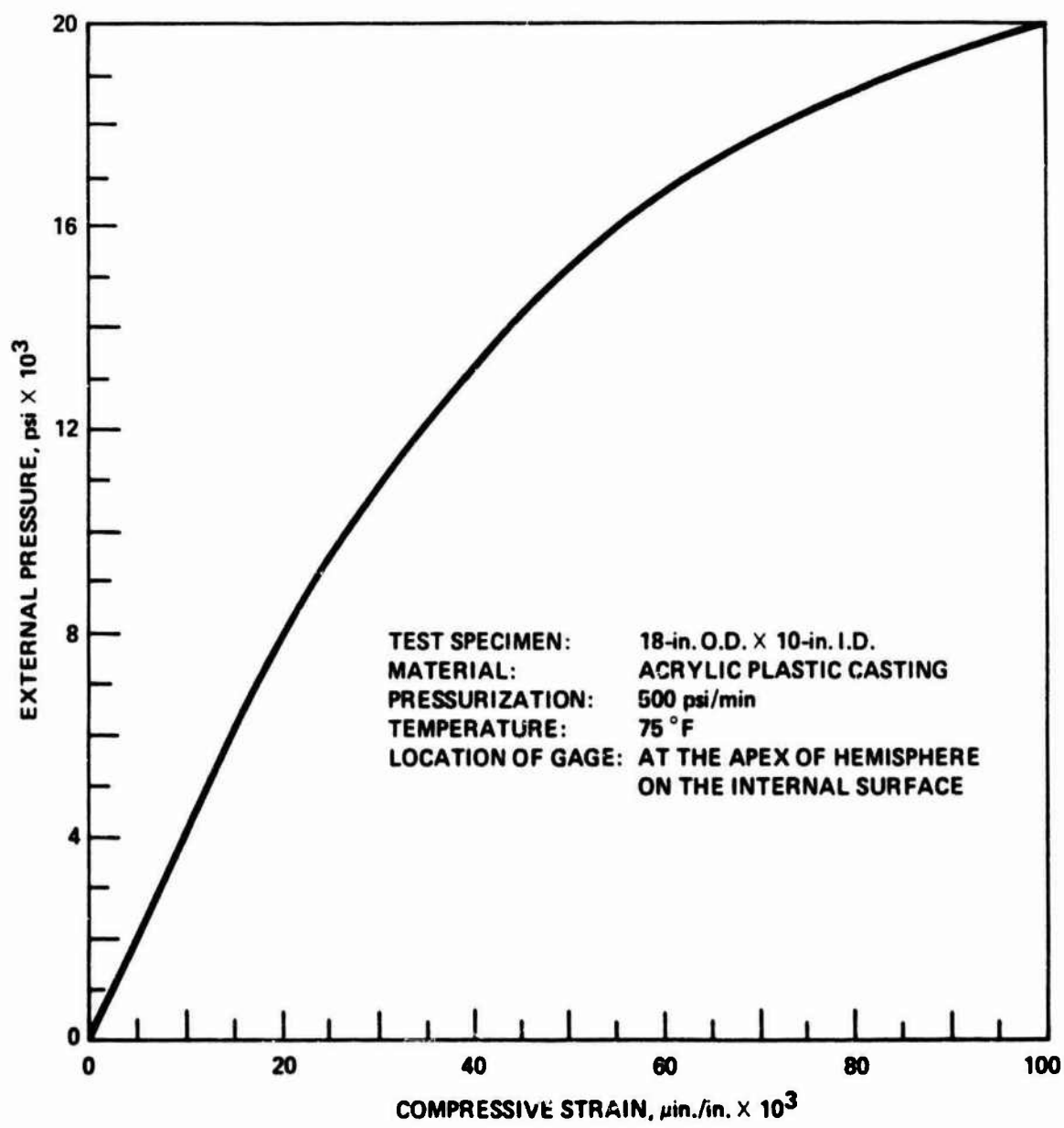


Figure 13. Strains on interior of sphere under short-term external hydrostatic loading.

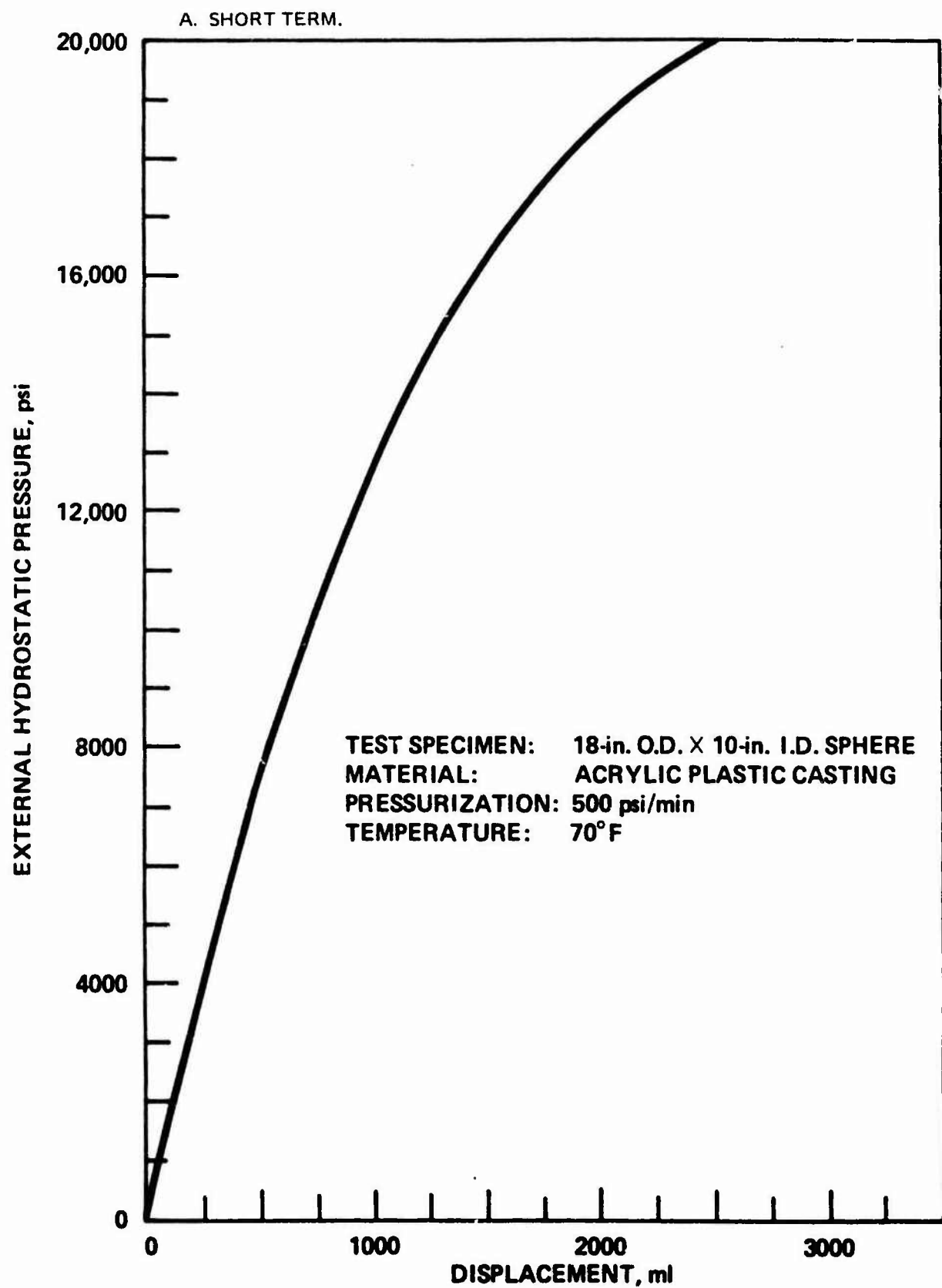


Figure 14. Decrease in internal volume of sphere under external hydrostatic loading.

B. LONG TERM.

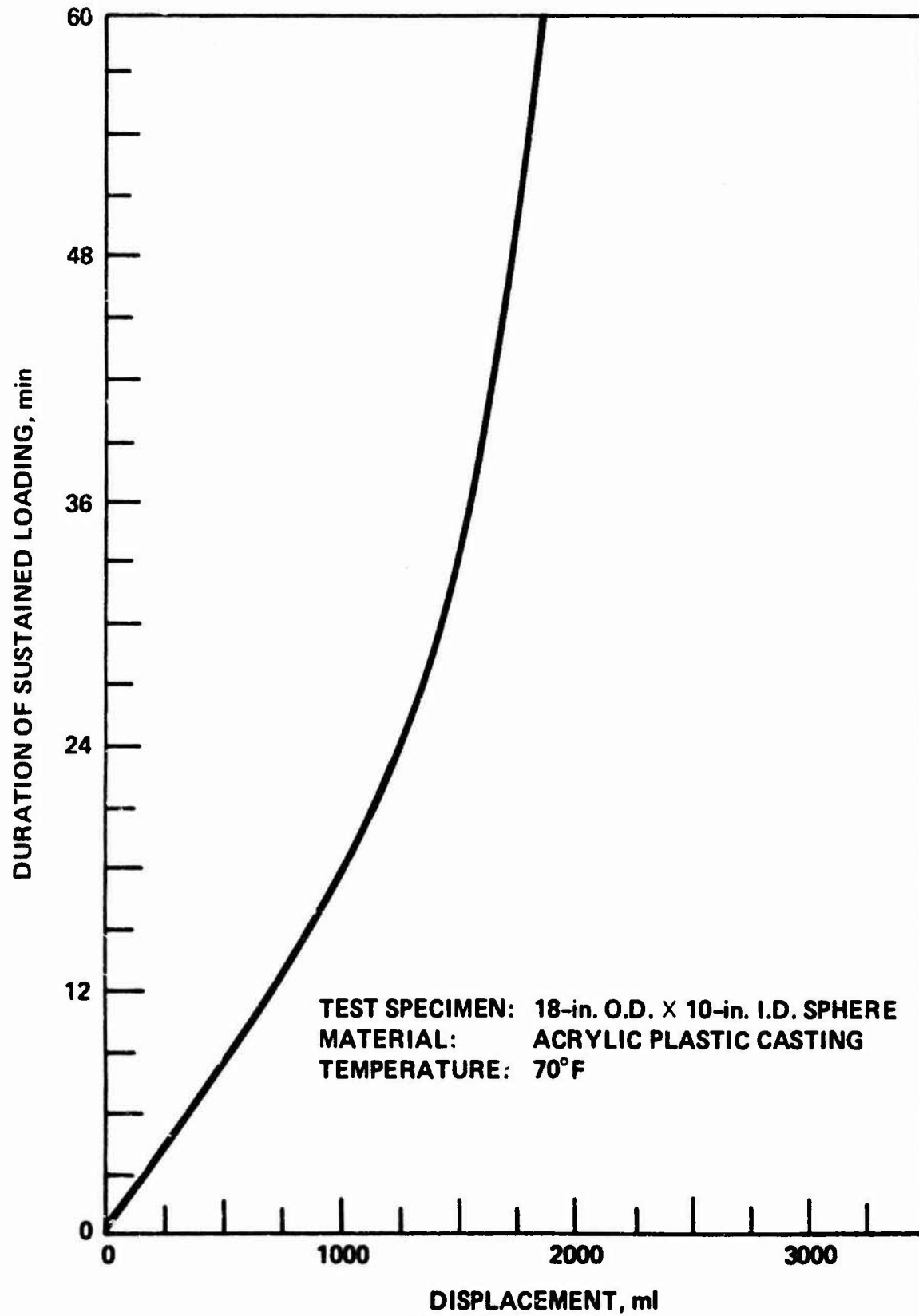


Figure 14. (Continued).

A. SHORT TERM.

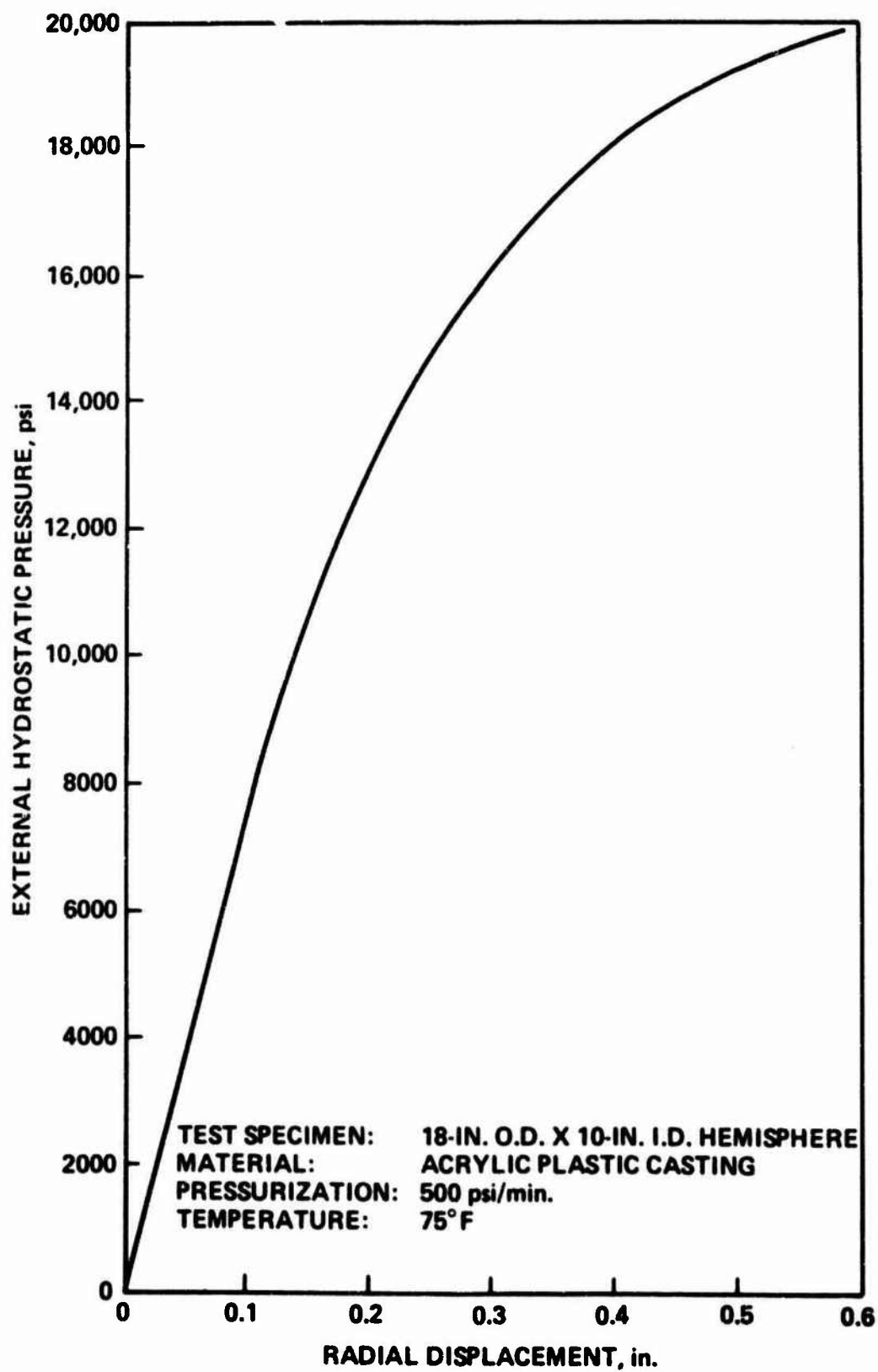


Figure 15. Radial displacement of sphere under external hydrostatic loading.

B. LONG TERM.

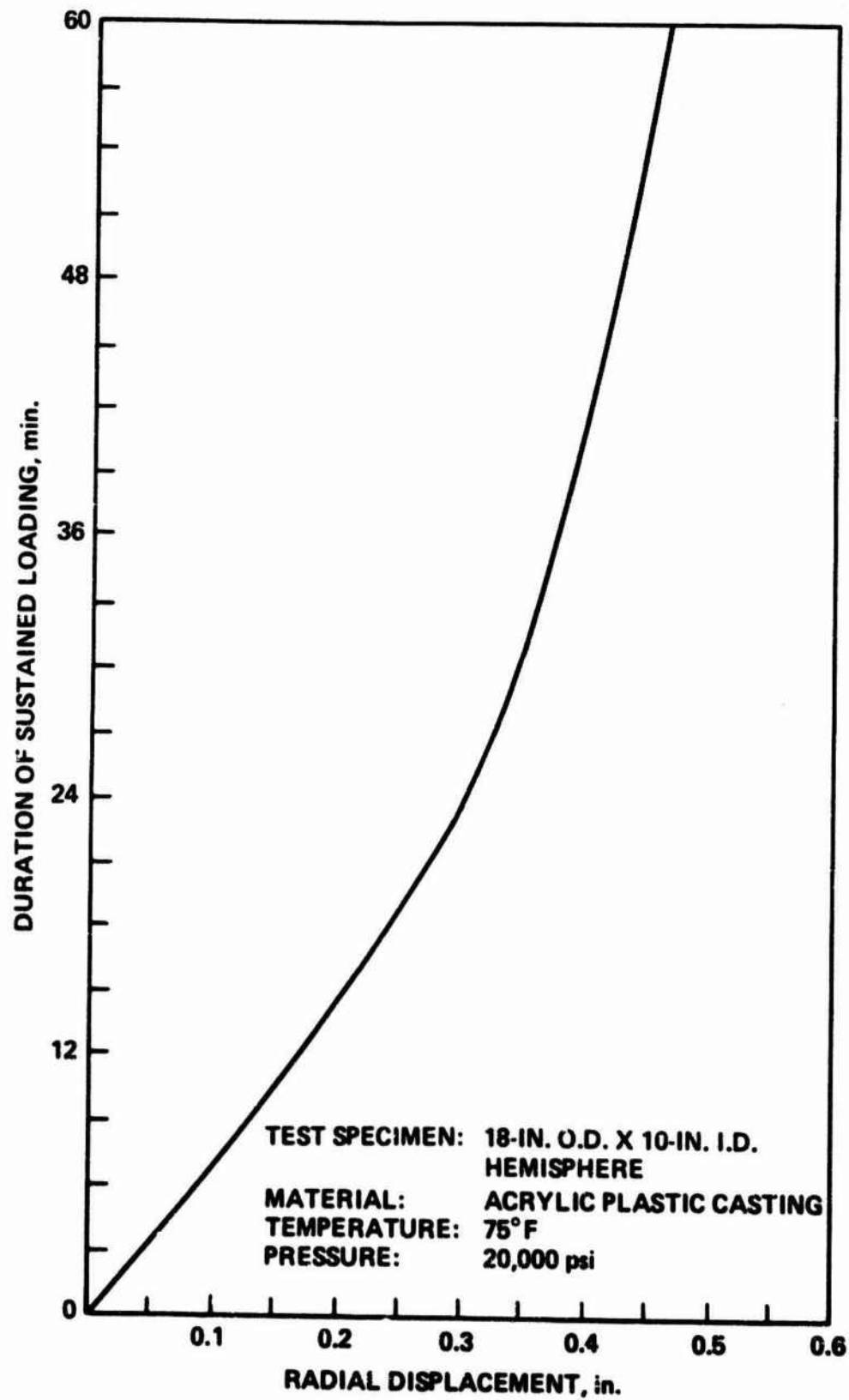


Figure 15. (Continued).



Figure 16. Fracturing in cast acrylic sphere after 20,000-psi external hydrostatic pressure for 1 hr. The cracks formed during depressurization. View of top hemisphere.



Figure 17. Fracturing in cast acrylic sphere after 20,000-psi external hydrostatic pressure for 1 hr. The cracks formed during depressurization. View of bottom hemisphere.

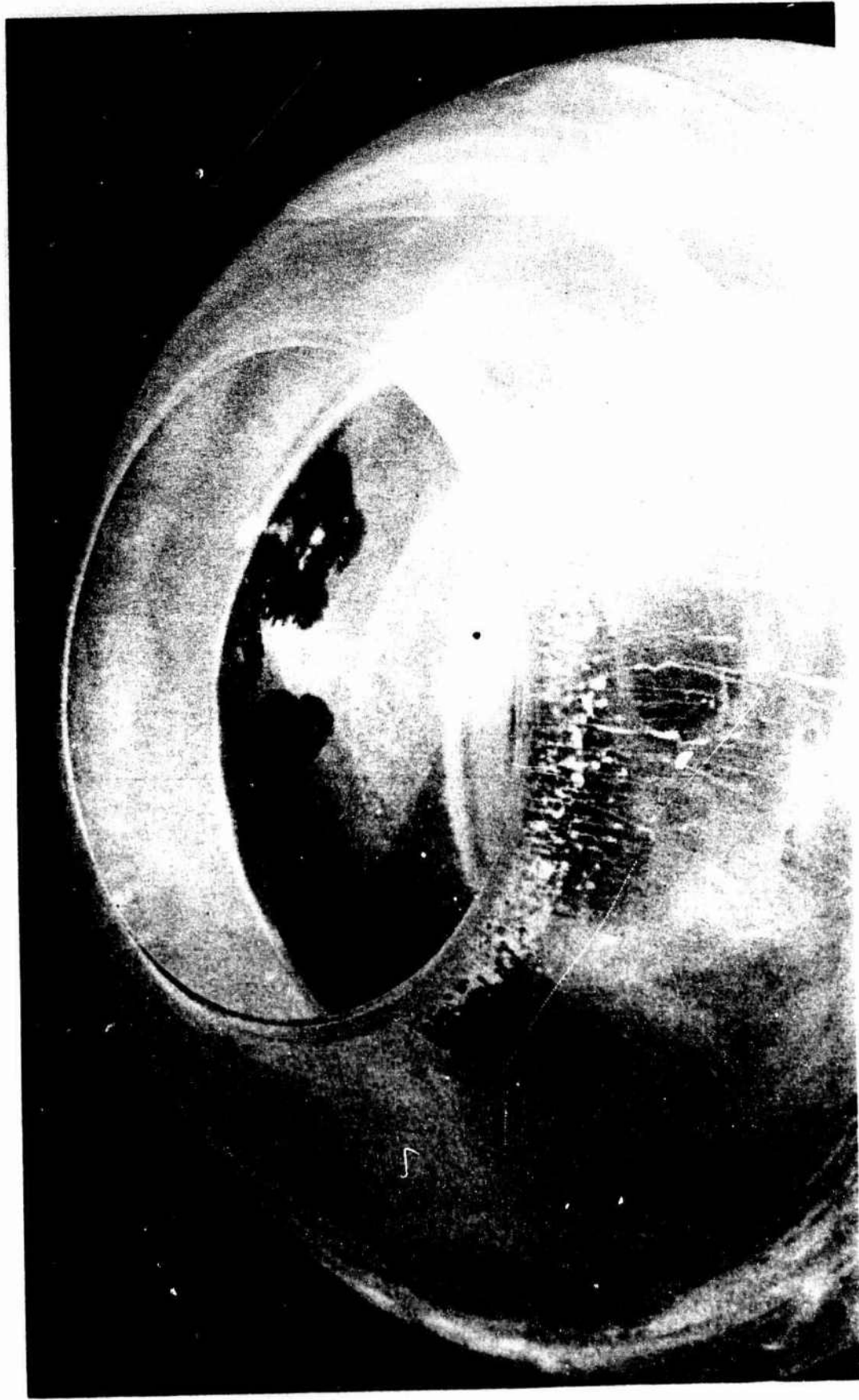


Figure 18. Fracturing in cast acrylic sphere after 20,000-psi external hydrostatic pressure for 1 hr. The cracks formed during depressurization. Detail of fracture surface on bottom hemisphere.

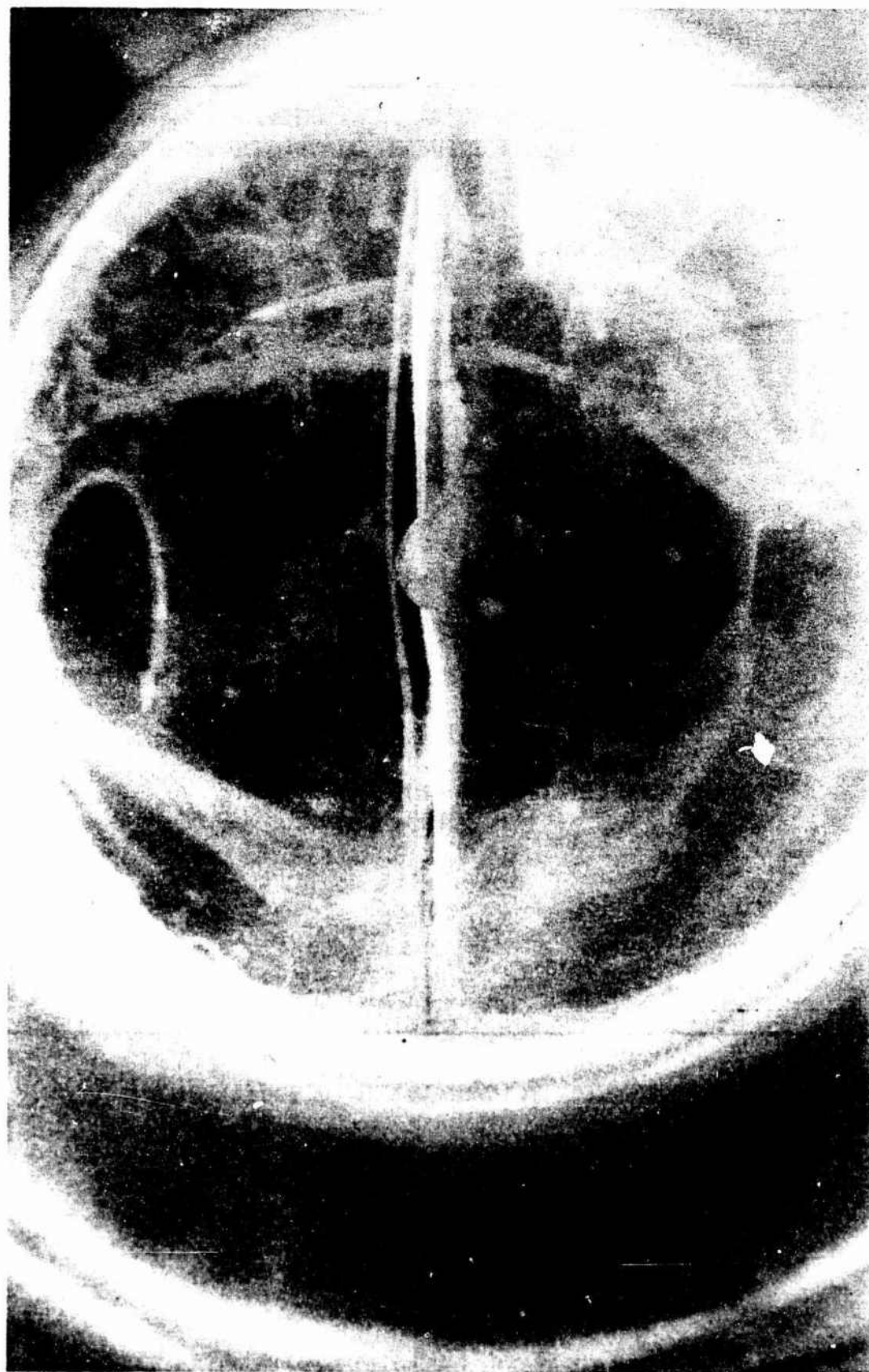


Figure 19. Fracturing in cast acrylic sphere after 20,000-psi external hydrostatic pressure for 1 hr. The cracks formed during depressurization. Detail of open fracture on interior pole of top hemisphere. The fracture width tapers down from interior surface towards exterior surface.

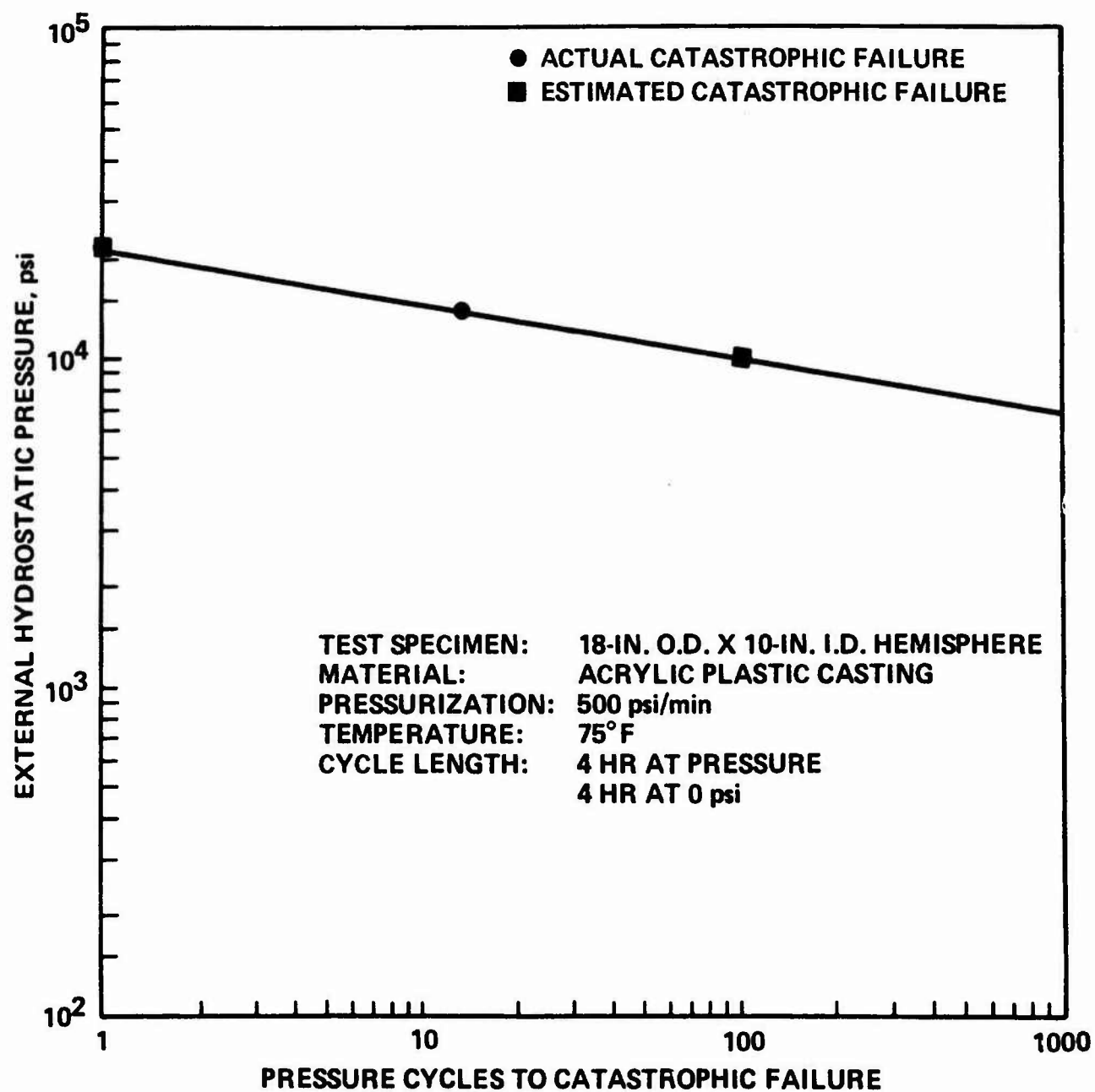


Figure 20. Cyclic fatigue curve for spherical cast acrylic windows with $t/R_1 = 0.8$.

A. TOP VIEW.



B. BOTTOM VIEW.

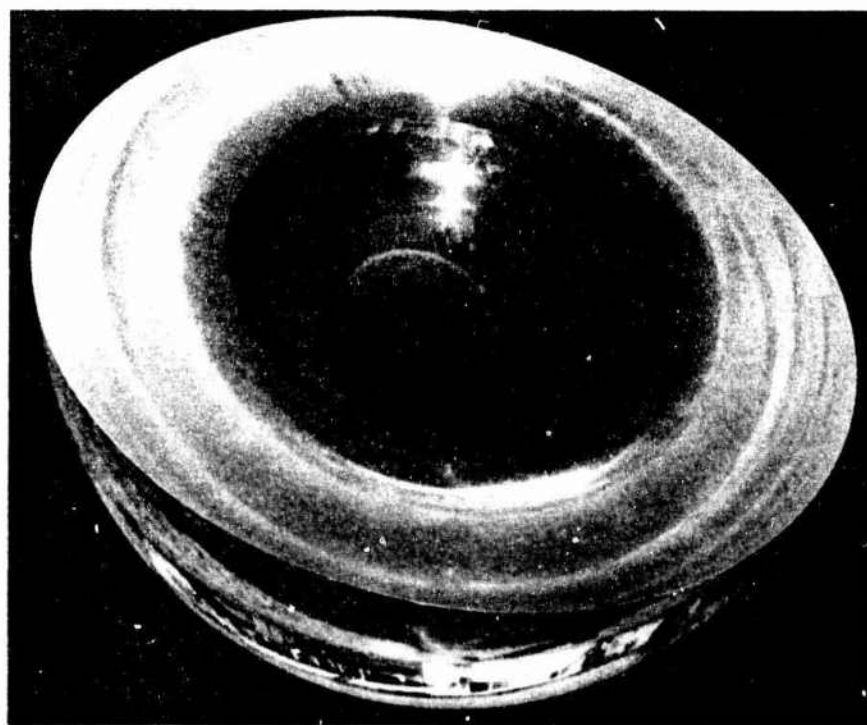


Figure 21. Spherical specimen 3 after 100 pressure cycles to 5000-psi hydrostatic pressure. Note complete absence of cracks.

A. TOP VIEW.

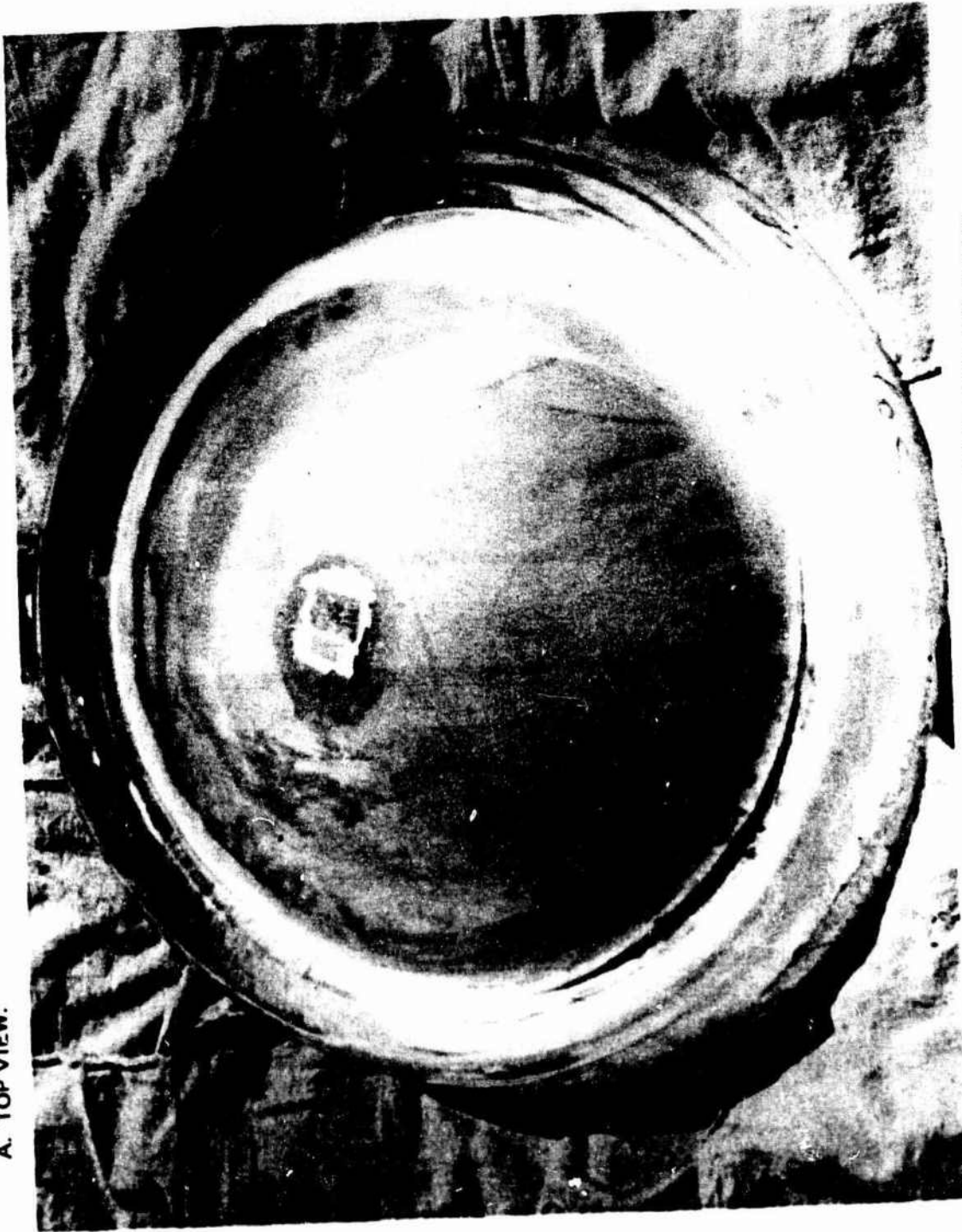


Figure 22. Spherical specimen 4 after 100 pressure cycles to 7500-psi hydrostatic pressure.

B. BOTTOM VIEW; NOTE FEW CIRCUMFERENTIAL CRACKS IN BEARING SURFACE NEAR INSIDE DIAMETER.



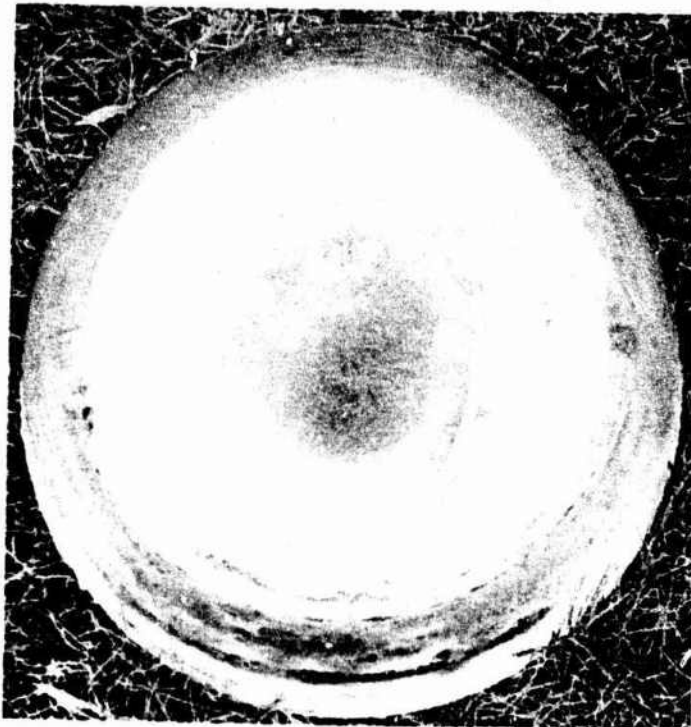
Figure 22. (Continued).

C. BEARING SURFACE, CLOSE-UP; NOTE SHORT RADIAL GOUGES ON BEARING SURFACE
CAUSED BY REPEATED CONTRACTION AND EXPANSION OF WINDOW ON STEEL
BULKHEAD UNDER CYCLIC PRESSURE LOADING.



Figure 22. (Continued).

A. TOP VIEW; NOTE MERIONAL CRACKS.



B. BOTTOM VIEW; NOTE MANY CIRCUMFERENTIAL CRACKS IN BEARING SURFACE NEAR INSIDE DIAMETER.



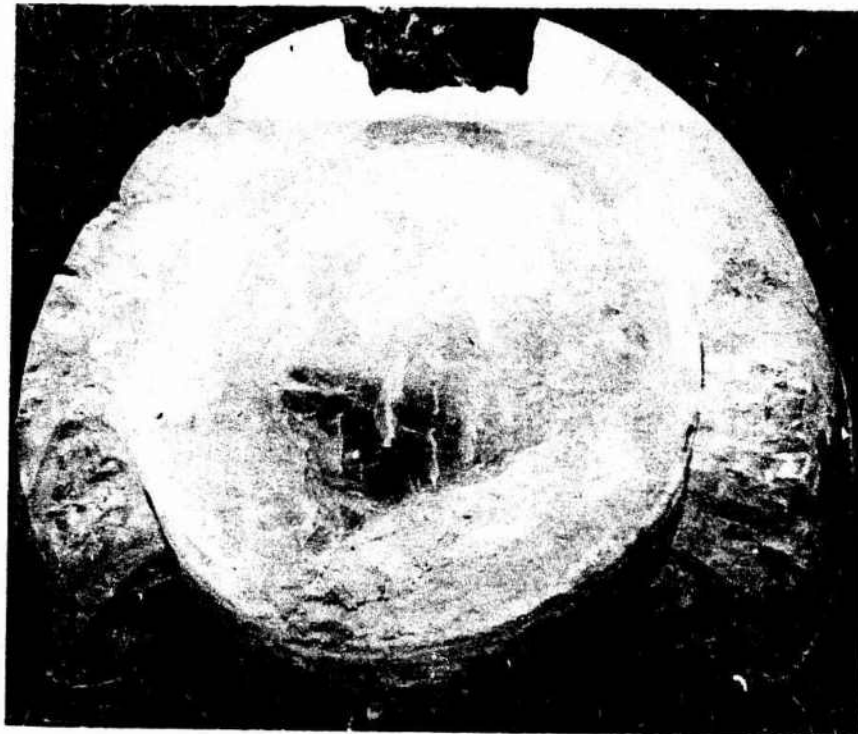
Figure 23. Spherical specimen 5 after 100 pressure cycles to 10,000-psi hydrostatic pressure.

C. BEARING SURFACE, CLOSE-UP; NOTE THE SHORT RADIAL GAUGES ON BEARING SURFACE
CAUSED BY REPEATED PRESSURE CYCLING.



Figure 23. (Continued).

A. TOP VIEW.



B. SIDE VIEW; NOTE THAT CENTER OF WINDOW SHEARED IN FORM OF \wedge PLUG.



Figure 24. Spherical specimen 6 after 13 pressure cycles to 13,500-psi hydrostatic pressure. The catastrophic failure took place midway through the pressure cycle.

C. BOTTOM VIEW; NOTE THAT SPHERICAL CAVITY HAS BEEN FILLED IN COMPLETELY BY PLASTIC FRAGMENTS.



Figure 24. (Continued).

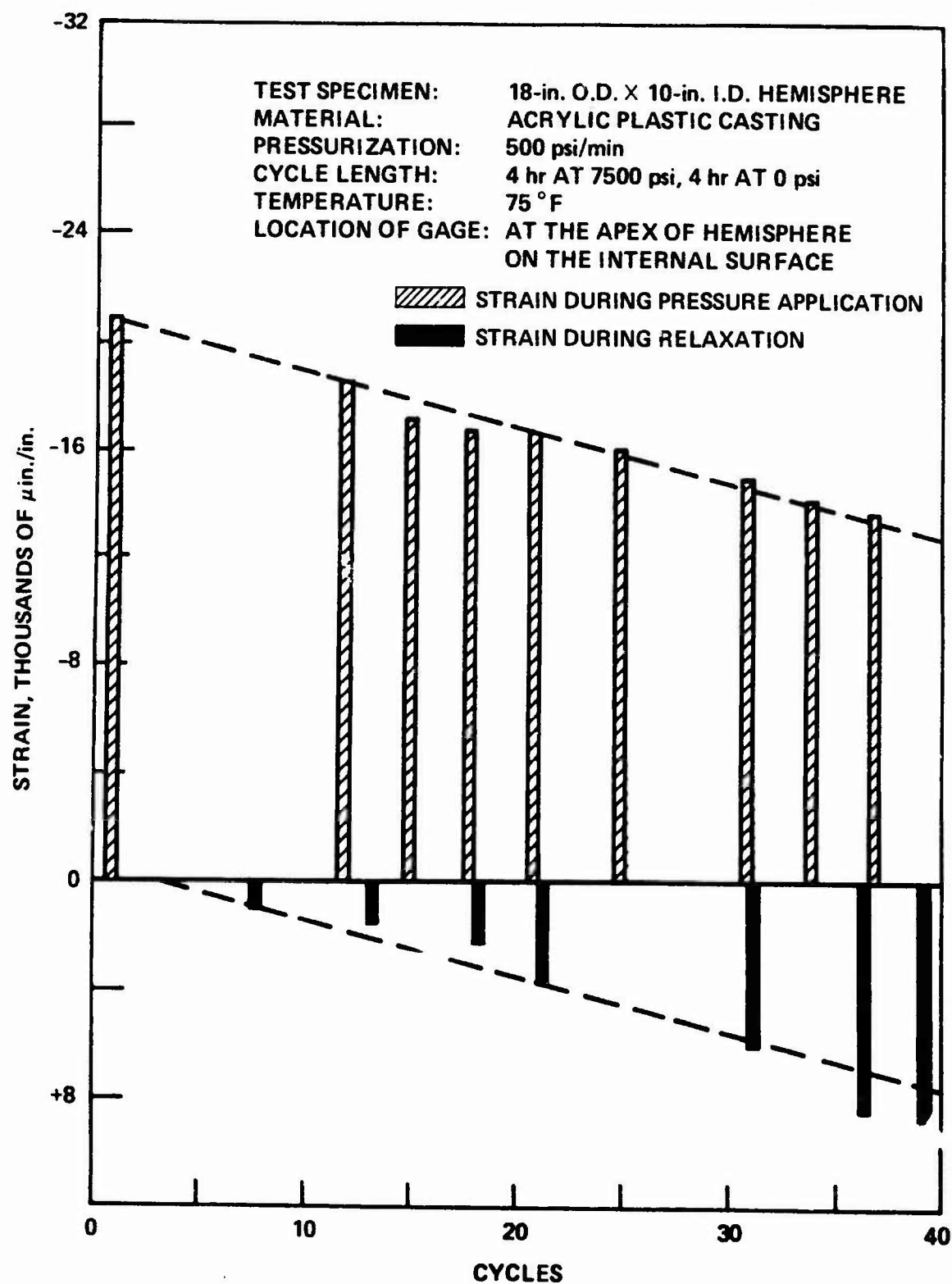


Figure 25. Strain on interior surface of spherical window during pressure cycling to 7500-psi hydrostatic pressure. Note that compressive strain decreased in magnitude with each succeeding pressure application, while tensile strain increased with each relaxation period between pressure cycles.

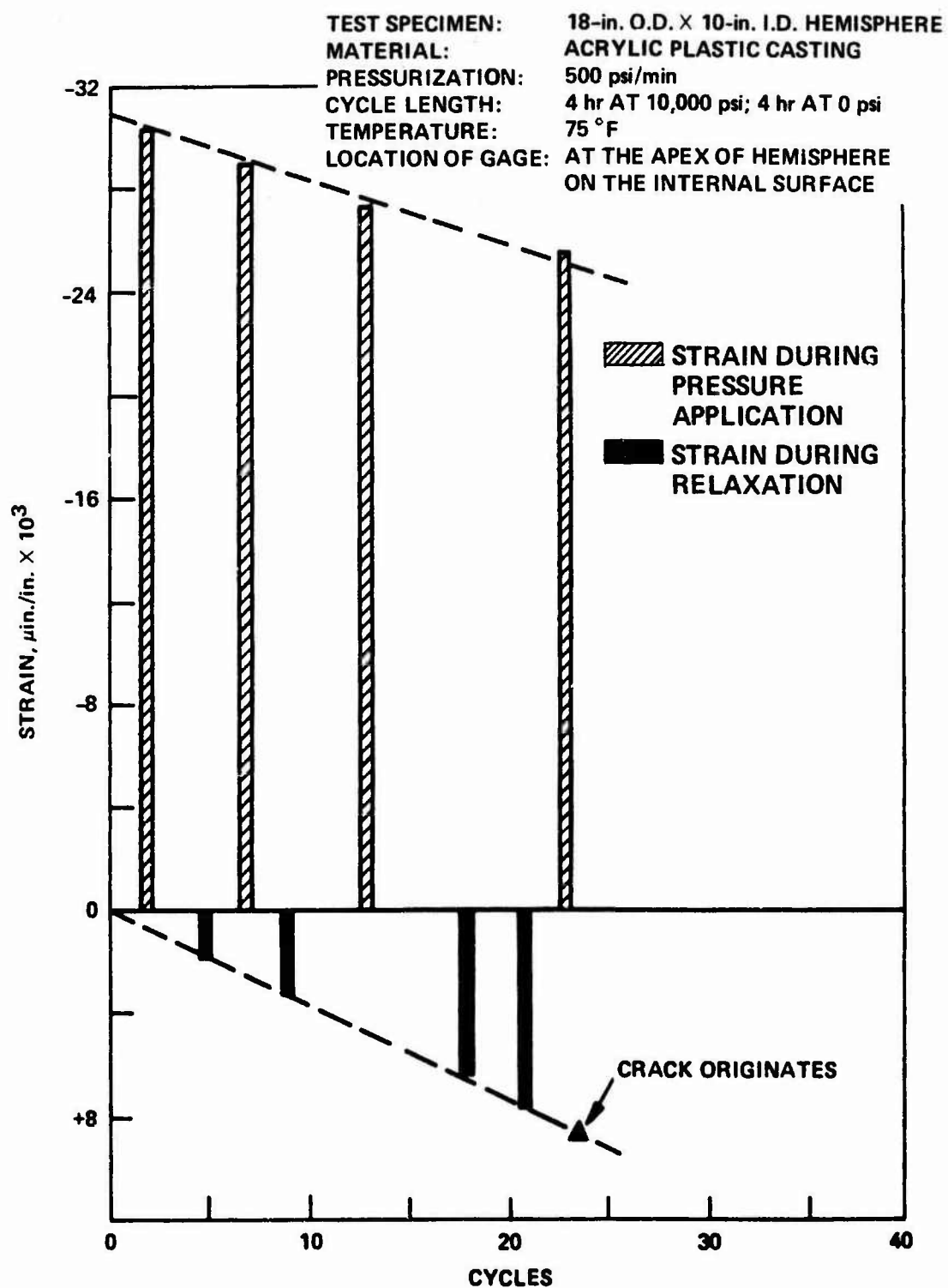


Figure 26. Strain on interior surface of spherical window during pressure cycling of the window to 10,000-psi hydrostatic pressure. Note again that compressive strain decreased in magnitude with each succeeding pressure application, while tensile strain increased with each succeeding relaxation period between pressure cycles.

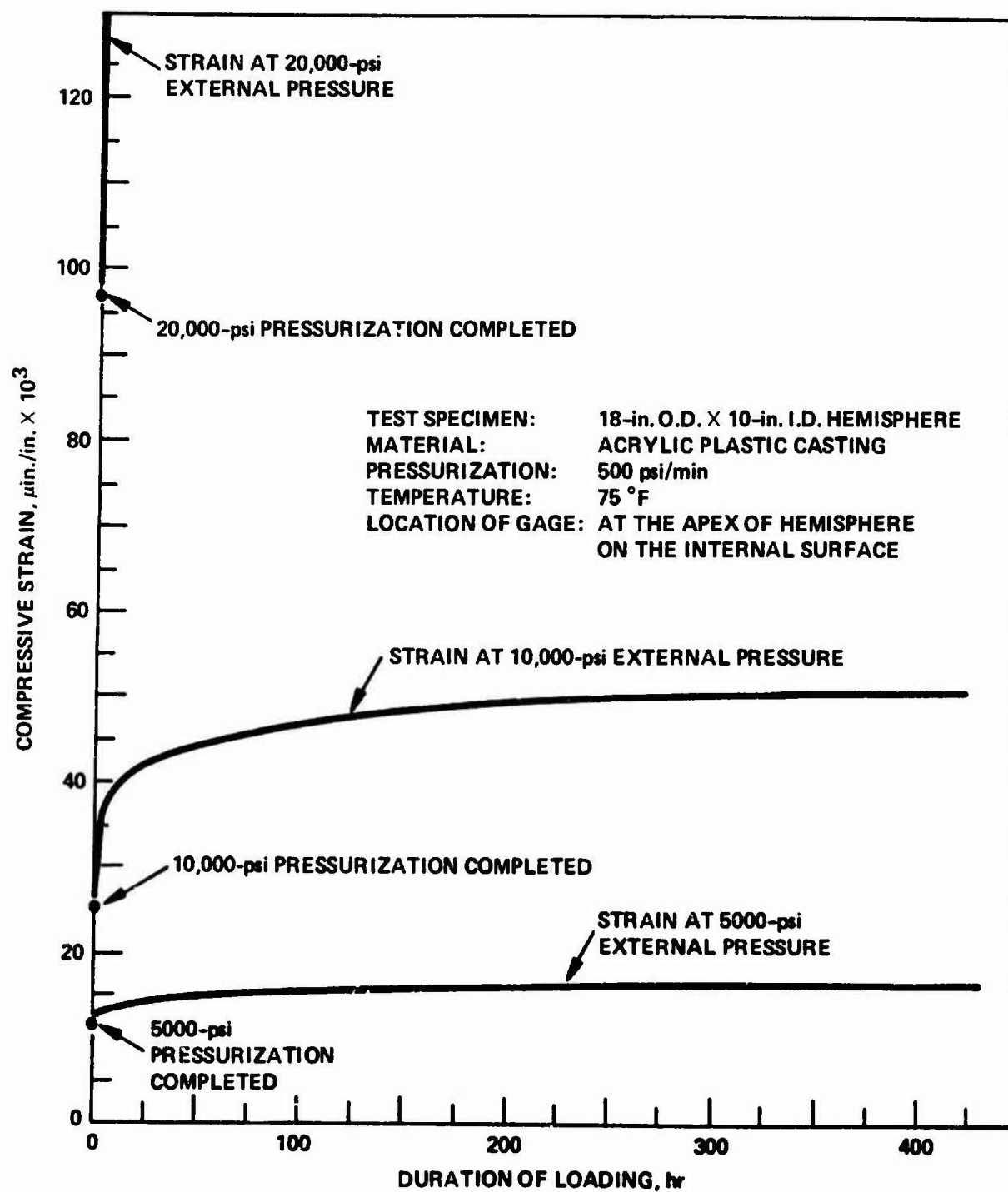


Figure 27. Strain on interior surface of spherical window during sustained pressure loading. Note that magnitude of time-dependent strain is very small at 5000 psi, while at 10,000 psi it is quite high. At 20,000 psi, time-dependent strain increases at catastrophic rate.

A. TOP VIEW



B. BOTTOM VIEW.



Figure 28. Spherical specimen 7 after 750 hr of sustained hydrostatic loading at 5000 psi. Note complete absence of cracks.

C. BEARING SURFACE, CLOSE-UP.



Figure 28. (Continued).

A. TOP VIEW; NOTE SEVERE MERIDIONAL CRACKS, AND FORMATION OF POLYGONAL SHEAR FRACTURE SURFACE.



B. BOTTOM VIEW; NOTE CIRCUMFERENTIAL CRACKS IN BEARING SURFACE.



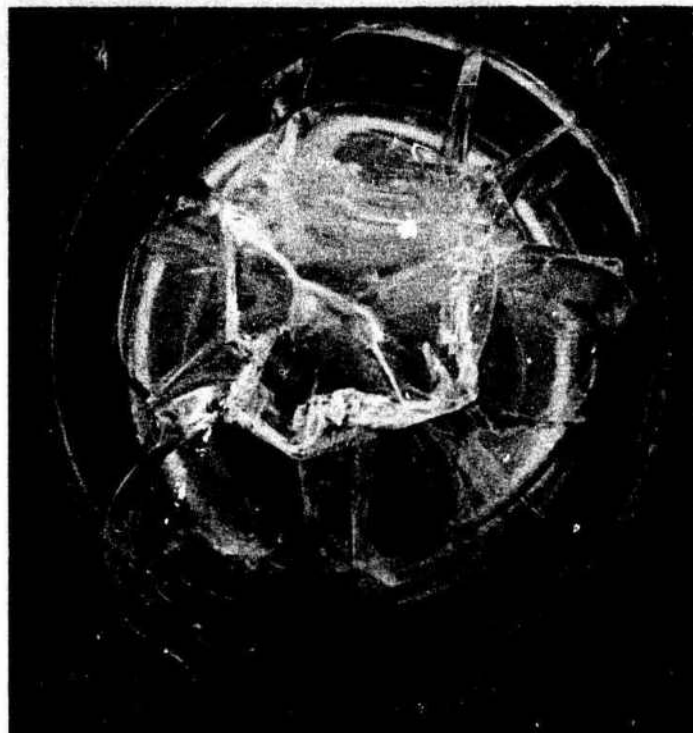
Figure 29. Spherical specimen 8 after 750 hr of sustained hydrostatic loading at 10,000 psi.

C. BEARING SURFACE, CLOSE-UP; NOTE ABSENCE OF GAUGES SO PREVALENT IN WINDOWS THAT HAVE BEEN PRESSURE-CYCLED.



Figure 29. (Continued).

- A. TOP VIEW; NOTE SEVERE MERIDIONAL CRACKS AND FORMATION OF POLYGONAL SHEAR FRACTURE SURFACE.



- B. BOTTOM VIEW; NOTE CIRCUMFERENTIAL CRACKS IN BEARING SURFACE, WHICH APPEAR TO BE DISTRIBUTED ACROSS WHOLE THICKNESS OF WINDOW.



Figure 30. Spherical specimen 9 after 750 hr of sustained hydrostatic loading at 15,000 psi.

C. BEARING SURFACE, CLOSE-UP; NOTE THE ABSENCE OF RADIAL GAUGES SO PREVALENT IN
WINDOWS SUBJECTED TO PRESSURE-CYCLING.

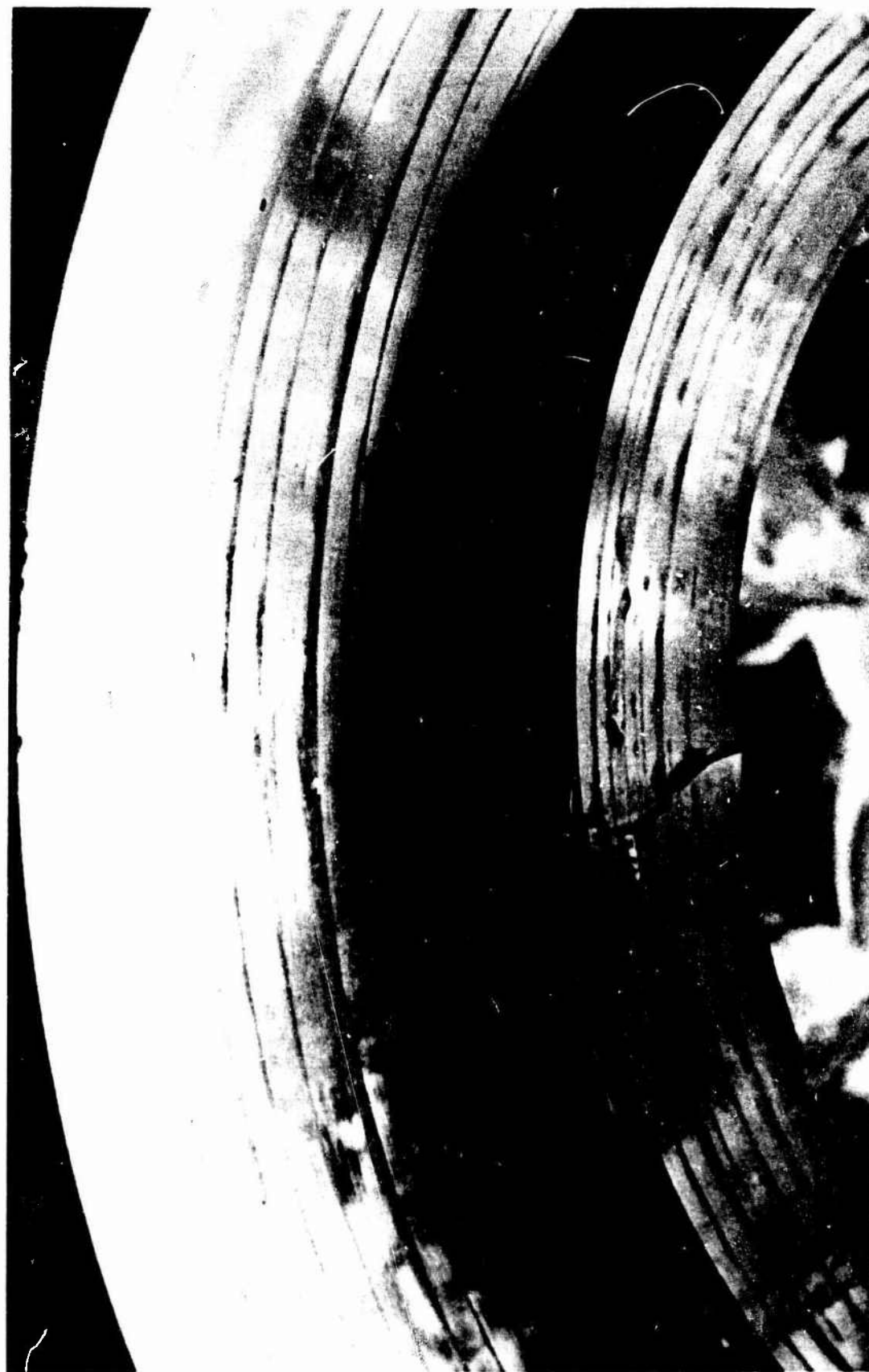


Figure 30. (Continued).



ACRYLIC PLASTIC SPHERICAL SHELL WINDOWS UNDER POINT IMPACT LOADING

by

J. D. Stachiw

Naval Undersea Center, San Diego, California

and

O. H. Burnside

Southwest Research Institute, San Antonio, Texas

July 1975





NAVAL UNDERSEA CENTER, SAN DIEGO, CA. 92132

AN ACTIVITY OF THE NAVAL MATERIAL COMMAND

R. B. GILCHRIST, CAPT, USN

Commander

HOWARD L. BLOOD, PhD

Technical Director

ADMINISTRATIVE STATEMENT

This report describes research performed by the Ocean Technology Department in the period of June 1971 to June 1974 as part of the investigation into man-rated submersibles with underwater panoramic visibility. The study was sponsored jointly by the Naval Undersea Center through the Independent Exploratory Development Program and the Harbor Branch Foundation of Fort Pierce, Florida. The work was performed under Subproject Task Area Number ZF61-412-001.

The study owes its successful completion to the administrative support of H. R. Talkington, Head, Ocean Technology Department; moral support of Dr. Wm. B. McLean, retired Technical Director, Naval Undersea Center; and financial support of E. A. Link, Director, Harbor Branch Foundation.

Released by
H. R. TALKINGTON, Head
Ocean Technology Department

UNCLASSIFIED

SECURITY CLASSIFICATION OF THIS PAGE (When Data Entered)

REPORT DOCUMENTATION PAGE		READ INSTRUCTIONS BEFORE COMPLETING FORM
1. REPORT NUMBER NUC TP 486	2. GOVT ACCESSION NO.	3. RECIPIENT'S CATALOG NUMBER
4. TITLE (and Subtitle) ACRYLIC PLASTIC SPHERICAL SHELL WINDOWS UNDER POINT IMPACT LOADING		5. TYPE OF REPORT & PERIOD COVERED Research and Development June 1971 to June 1974
7. AUTHOR(s) J. D. Stachiw O. H. Burnside		6. PERFORMING ORG. REPORT NUMBER
9. PERFORMING ORGANIZATION NAME AND ADDRESS Naval Undersea Center San Diego, CA 92132		8. CONTRACT OR GRANT NUMBER(s)
11. CONTROLLING OFFICE NAME AND ADDRESS Naval Undersea Center San Diego, CA 92132		10. PROGRAM ELEMENT, PROJECT, TASK AREA & WORK UNIT NUMBERS ZF61-412-001
14. MONITORING AGENCY NAME & ADDRESS (if different from Controlling Office)		12. REPORT DATE July 1975
		13. NUMBER OF PAGES 78
		15. SECURITY CLASS. (of this report) UNCLASSIFIED
		15a. DECLASSIFICATION DOWNGRADING SCHEDULE
16. DISTRIBUTION STATEMENT (of this Report) Approved for public release; distribution unlimited.		
17. DISTRIBUTION STATEMENT (of the abstract entered in Block 20, if different from Report)		
18. SUPPLEMENTARY NOTES		
19. KEY WORDS (Continue on reverse side if necessary and identify by block number) Viewports Acrylic plastic Submersible windows Impact testing Undersea habitat windows Finite Element Analyses		
20. ABSTRACT (Continue on reverse side if necessary and identify by block number) Acrylic plastic spherical sector windows have been subjected to point impact loading applied to the convex surface at the center of the window. The point impact loading simulated the velocities and kinetic energies encountered in a typical collision between an immovable underwater obstacle and a submersible equipped with a large panoramic bow window.		

DD FORM 1 JAN 73 1473 EDITION OF 1 NOV 65 IS OBSOLETE

UNCLASSIFIED

SECURITY CLASSIFICATION OF THIS PAGE (When Data Entered)

UNCLASSIFIED

SECURITY CLASSIFICATION OF THIS PAGE(When Data Entered)

20. Continued

Experimental results show that spherical sector windows with 117° included angle and $t/R_o = 0.094$ fracture during simulated underwater collisions where the kinetic energy of the impactor was at least 435 foot-pounds. For windows with $t/R_o = 0.166$ the required kinetic energy to generate fracture is 1750 foot-pounds. The kinetic energy of a submersible required for initiation of fracture in the bow window increased with depth, but only moderately.

Protective shields fabricated from 0.375-inch thick acrylic plastic did not provide any significant protection against impact generated fracture of spherical windows. Only a bumper appears to provide adequate protection for the bow window in a submersible colliding with a large underwater object.

UNCLASSIFIED

SECURITY CLASSIFICATION OF THIS PAGE(When Data Entered)

SUMMARY

PROBLEM

Manned submersibles for work and research require panoramic visibility for operational safety and performance of their missions. The presence of a large spherical panoramic window in the bow of a submersible, however, constitutes a potential hazard to the crew if the submersible were to collide head-on with a submerged object. If the impact parameters are known at which the failure of a spherical window takes place, steps can be taken to protect the window against damage under impact. These steps may take the form of design changes (such as the incorporation of impact shields and bumpers) and/or limitation on operational speeds of the submersible in the vicinity of obstacles.

RESULTS

Acrylic plastic spherical shell sector windows with 117° included angle and outside radius of 24-inches (610 millimeters), have been impacted at their center, with a 12,500-pound (5662-kilogram) weight, in a simulated ocean environment. Velocities of impacts ranged from 0.205 to 10.702 feet (0.06 to 3.26 meters) per second.

It has been found that window fracture is initiated by tensile stresses on the concave surface of the window, directly below the point of impact. Compressive stresses, generated by external hydrostatic pressure, decrease the destructive effect of tensile stresses introduced by point impact loading. For 2.25 and 4.0-inch (57 and 101 mm) thick windows the critical impact velocities were found to fall into the 1.5 to 3-foot (0.45 to 0.91 m) per second range, the exact value being a function of window thickness and external hydrostatic pressure.

A finite element analysis was found to agree rather well with the experimental results. This analysis can be employed to predict, with a reasonable degree of confidence, the critical impact velocities for acrylic plastic spherical windows in the bows of submersibles.

RECOMMENDATION

Submersibles equipped with panoramic windows either should be provided with bumpers, or should reduce their cruising speed in the vicinity of massive underwater obstacles to avoid the possibility of a window fracture generated by the collision with the obstacle.

CONTENTS

	Page
INTRODUCTION	3
STUDY PARAMETERS	3
EXPERIMENTAL PROCEDURE	4
Test Specimens	4
Test Arrangement	4
Instrumentation	6
EXPERIMENTAL TEST RESULTS	7
2.25-Inch Thick Windows	7
4.0-Inch Thick Windows	10
DISCUSSION OF EXPERIMENTAL TEST RESULTS	11
Critical Impact Velocity	11
Dynamic Strains	12
Fractures	12
ANALYTICAL CALCULATIONS	12
Background	12
Finite Element Model	13
Finite Element Mesh Verification	13
Acrylic Window Stress Solution with External Pressure Load	15
Acrylic Window Impacting the Rigid Wall	16
COMPARISON OF EXPERIMENTAL AND ANALYTICAL DATA	20
Location of Fracture	20
Shape of Fracture Plane	20
Critical Kinetic Energy	21
FINDINGS	21
CONCLUSION	22
Design	22
Operation	23
REFERENCES	24

INTRODUCTION

Acrylic plastic windows in submersibles and undersea habitats have earned a reputation over the years for reliability and safety even when subjected to operational conditions outside the stated performance specifications. Window failure has been avoided because of a circuitous combination of material properties, window shapes and window design philosophy. The high plasticity of the acrylic plastic, the small sizes of conical frustum windows and the high safety factors used in window design have made it possible for the windows to withstand impacts and dynamic pressure loadings not included by the designer in the operational scenario for the submersible or habitat.

The situation is somewhat different in the case of the large spherical shell sector windows^{1,2,3,4,5} and transparent pressure hulls^{6,7,8,9,10,11}. Although the spherical windows and pressure hulls are also fabricated from the proven acrylic plastic, their large size makes them significantly more susceptible to point impact damage in an underwater collision with a submerged obstacle. This can be seen readily from the comparison of the window areas in the bows of traditional submarines such as Soucoupe, for example, and modern submersibles such as the Aquarius, PC-8B, Johnson-Sea-Link and others (figures 1 and 2).

There is less than 10 percent probability of an object impacting the window in an old fashioned submersible during a head-on collision with an obstacle because the windows represent less than 10 percent of the bow frontal area. On the other hand, in a modern submersible with a panoramic bow window or transparent pilot capsule, the probability of impact during a head-on collision is over 90 percent. With the odds for a window impact approaching 100 percent certainty, steps must be taken to evaluate the potential damage to the transparent plastic bow in order to prevent catastrophic flooding of the pressure hull with its one atmosphere interior.

The Naval Undersea Center, San Diego, California, and the Harbor Branch Foundation, Vero Beach, Florida, jointly have initiated an exploratory study to evaluate the threat posed to panoramic visibility submersibles by head-on collisions with underwater obstacles. This report is a summary of the study.

STUDY PARAMETERS

The objective of the exploratory study was to determine the seriousness of the impact damage to spherical shell acrylic windows and to evaluate the performance of transparent impact shields for such windows.

The scope of the study was limited to spherical shell windows with 24.0-inch radius and 117° included spherical angle, thermoformed from 2.250- and 4.000-inch thick acrylic plastic plates (figure 3). The evaluation of impact shields was limited to the spherical shell type with 2-inch standoff, thermoformed from 0.375-inch thick acrylic plastic sheet. The impact generator configuration was limited to a 12,500-pound steel ram with a flat impactor

moving at velocities ranging from 0.2 to 11.0 feet/second. The depths at which the impacts were generated were 11, 224 and 1120 feet.

The approach chosen for obtaining of the required data from windows subjected to impact was experimental with a minimum of analytical calculations.

The results of the study were to be presented in the form of recommendations for the use of designers and operators of submersibles.

EXPERIMENTAL PROCEDURE

TEST SPECIMENS

Spherical shell windows fabricated from acrylic plastic sheets served as test specimens. Their material properties met the proposed U. S. Navy and ASME material specifications (table 1) for acrylic plastic windows in manned hyperbaric pressure vessels. The windows were vacuum thermoformed (figure 4) in a metallic mold with 24-inch radius from 2.250-inch and 4.000-inch acrylic plastic discs cut from standard 48- by 60-inch sheets. After thermoforming, the edges of the discs were machined to form an included spherical angle of 117° with a 63-root mean square finish on the machined bearing surface of the window (figure 5).

The impact shields were fabricated from 0.375-inch thick acrylic plastic. The 26-inch radius impact shield was thermoformed at 270°F by free blowing (figure 6) an acrylic sheet clamped to a plywood jig with steel retainer rings. Holes were drilled in the impact shield flange to complete fabrication of the shield (figure 7).

TEST ARRANGEMENT

The test arrangement was set up to simulate, as much as feasible, the forces encountered by a panoramic window during a head-on collision with an immovable obstacle such as a ship's hull, legs of a drill platform or surface of a cliff. Since the surfaces of those objects are either flat or have a very large radius of curvature, an impactor with a flat surface was chosen for simulating collisions with an immovable object.

Several test parameters appeared to influence the generation of a fracture in an impacted window. These parameters are (1) the kinetic energy, (2) momentum and (3) velocity of the impactor striking the window. Although the velocity of the impactor enters into the expression for momentum and kinetic energy, it also has a major effect of its own. It generates a compression wave in the material. Upon reflection from the free concave surface of the window, this compression wave changes into a tension wave. Through interference between the incident and reflected waves this will cause a tensile stress to be built up a short distance from the free surface. If the tensile stress reaches a sufficiently high value the window could form a Hopkinson fracture.

It was not known at what impact speed a compression wave impulse might form to result in scabbing of the acrylic plastic spherical window surfaces. Therefore, it was considered prudent to make the simulated collision as realistic as possible so that no uncertainties would appear in the design and engineering recommendations based on the experimental

Table 1. Specified Values of Physical Properties in Acrylic Plastic Sheets Used to Thermoform 2.25- and 4.0-inch Thick Spherical Shell Sector Windows

Property	ASTM Method	Units	Plexiglas G Sheets
Specific gravity	D792	—	1.19 ± 0.01
Residual monomer	SPI	%	1.5 maximum
Tension			
ultimate strength	D638	psi	9,000 minimum
maximum elongation	D638	%	2 minimum
modulus	D638	psi	400,000 minimum
Flexure			
ultimate strength	D790	psi	14,000 minimum
modulus	D790	psi	420,000 minimum
Compression			
yield	D695	psi	15,000 minimum
modulus	D695	psi	400,000 minimum
deformation	D621	%	1.0 maximum
Shear			
ultimate strength	D732	psi	8,000 minimum
Impact			
Izod notch	D256	ft lb/ in. of notch	0.3 minimum
Heat distortion (temperature at 264 psi)	D648	°F	205 minimum
Resistance to stress (critical crazing stress in presence of isopropyl alcohol)	MIL-P-8184	psi	1,500 minimum
Compressive deformation at 4000 psi loading and 122°F ambient temperature	D621	%	1.0 maximum

data. Thus, instead of selecting an experimental setup where the known kinetic energy of the impacting submersible is simulated by a small impactor (about 100 pounds) moving at a high velocity (50 to 100 feet), a test arrangement was considered more appropriate where the mass of the impactor is of the same magnitude as a small submersible and the velocity of impact is in the same range as operational speeds of typical work and research submersibles (figure 8).

Based on these premises, the mass of the impact generator was chosen to be 12,500 pounds, which approximates the weight of a small manned submersible in air. The velocities chosen for the experimental program were in the 0.2 to 11 feet per second range, which are typical for operational speeds of modern research and work submersibles. Obviously, there are and will be other submersibles that weigh more or less than the impact generator chosen and thus the experimental data will not be directly applicable to them. Since the difference in mass of the impactor and operational submersibles is less than an order of magnitude, it is acceptable to apply the experimental data to those submersibles. However, the difference in mass must be taken into account during calculations by compensating the difference in masses with increased or decreased impact velocities so that the kinetic energy of the impacting submersible is the same as that of the impact generator used in the test program.

The impact generator consisted of a vertical gravity actuated ram with 12,500-pound mass whose impact speed could be varied from 0.1 to 11 feet/second (figure 9). The window specimen was held in a steel flange with conical bearing surface directly below the impact ram (figure 10). When the ram latch was released the ram descended downwards until the flat impact surface of the ram contacted the apex of the window (figure 11).

INSTRUMENTATION

The instrumentation for the window impact tests consisted of a 90° strain gage rosette mounted on the concave window surface (figure 12) directly below the point of impact and a rotary potentiometer displacement indicator mounted on the frame of the ram (figure 13). Strains and ram displacement were recorded by a high frequency response oscillograph at 8- and 32-inch/second chart speeds (figure 14). Failed windows were photographed after the impact tests.

The window test specimen was placed into the previously well-greased window flange by means of a vacuum suction cup attached to the forks of a forklift (figure 15). After the window was aligned in the flange, a 0.25-inch thick rubber gasket was placed over the joint between the window and the flange to serve as the primary water seal for the window flange assembly (figure 16). A beveled 1-inch thick window retainer ring subsequently was placed on top of the gasket and fastened with bolts to the window flange (figures 17 and 18).

If the test setup called for an impact shield, a 2-inch thick steel spacer ring with 0.25-inch thick gaskets on both sides of the spacer was placed on top of the retainer ring (figure 19). The impact shield (figure 20) and shield retainer ring were placed on top of the spacer ring and secured to the window flange by means of bolts (figure 21). This completed the assembly of window and impact shield specimens inside the impact test jig (figure 22).

After the window and the impact shield were secured in the window flange the whole impact ram assembly was placed inside the Southwest Research Institute's 90-inch diameter pressure vessel (figure 23). If the simulated collision was conducted at 11-foot

depth, the pressure vessel cover was left off after filling the vessel with tap water. On the other hand, for tests at 224- and 1120-foot simulated depth, the pressure vessel cover was locked in place and the interior of the vessel pressurized to 100 or 500 psi, respectively (figure 24).

The ram inside the pressure vessel was released hydraulically, and the oscillograph recorder was actuated simultaneously. At the completion of each impact test the ram assembly was removed from the vessel, damage to the window was photographed (figure 25) and the ram was reset for another impact test. If there was no visible damage to the window, the same window was subjected to another, but more severe, impact test. The operation was repeated until the window showed damage.

EXPERIMENTAL TEST RESULTS

A total of 19 impact tests were performed on four windows with 2.250-inch thickness (table 2) and five impact tests, on windows with 4-inch thickness (table 3). The tests were conducted under simulated submergences of 11, 224 and 1120 feet. The impact velocities ranged from 0.202 to 10.702 feet/second.

2.25-INCH THICK WINDOWS

Strains were recorded on the internal surface of the window as its apex. The level of strain depended on the nature of the loading and the magnitude of the load. Static compressive strains generated by hydrostatic pressure applied to the window's exterior varied with the pressure at 8-microinches/inch psi rate. Static tensile strains, generated by statically supporting the submerged dead weight of the ram (about 11,500 pounds) on the window's apex, were in the +2000- to +2800-microinches/inch range.

Dynamic tensile strains generated by the impacting ram with 12,500-pound mass were significantly higher than the static tensile strains generated by supporting the ram statically (figure 26). Fracture was initiated on the low pressure face of the window at its apex when the tensile strains at that site passed the 8000-microinches/inch level.

An impact velocity of only 1.5 feet/second was required to generate the tensile strain of 8000 microinches/inch in a window submerged 11 feet below the water surface. At greater simulated depths the impact velocity had to be higher for the dynamic tensile strains to exceed the hydrostatically generated compressive static strains by at least 8000 microinches/inch. Thus, at 100 and 500 psi the ram had to strike the window with 1.7- and 2-feet/second velocities, respectively, for the resultant tensile strain to be equal to, or exceed 8000 microinches/inch. These impact velocity values are only approximated, extrapolated from widely scattered velocity data points.

The dynamic response of the window to the point impact was similar to a dampened spring with a 10-cycle/second frequency and maximum amplitude of 0.5 inches. The windows, as a rule, stored sufficient energy during the initial dynamically generated deflection to bounce the 12,500 pound ram clear of its surface between the first and second dynamic loading cycles (figure 27). The impact generated maximum dynamic strains during the initial deflection cycle. The succeeding cycles showed progressively lower dynamic strains until

Table 2. Impact Testing of Acrylic Plastic Spherical Shell Windows with 2.25-inch Thickness

Test Number	Window Specimen	Impact Velocity (feet/second)	Hydrostatic Pressure (psi)	Strain on Window Surface (Microinches/inch)		Visible Damage
				Static	Dynamic Resultant	
1A	A	0.205	5	0	+2500	No cracks
2A	A	0.589	5	0	+3600	No cracks
3A	A	1.576	5	0	+8000	Cracked
4A	B	0.376	100	-1000	+3200	No cracks
5A	B	0.960	100	-1000	+8000	No cracks
6A	B	1.913	100	-1200	+9600	Cracked
7A	C	0.545	500	-4400	+3200	No crack
8A	C	0.513	500	-4000	+2800	No crack
9A	C	1.026	500	-3900	+5200	No crack
10A	C	1.641	500	-4000	+11,200	No crack
11A	C	0.820	500	-4000	+3500	No crack
12A	C	0.820	500	-4000	+3600	No crack
13A	C	0.820	500	-4050	+3600	No crack
14A	C	0.410	500	-4100	+2100	No crack
15A	C	1.641	500	-3900	+9200	No crack
16A	C	0.202	500	-4000	+2000	No crack
17A	C	1.229	500	-4000	+5600	No crack
18A	C	10.335	500	-4000	+18,000	Cracked
19A	D*	9.895	500	-4000	+16,000	Cracked
					+12,000	

Notes: See notes on Table 3.

Table 3. Impact Testing of Acrylic Plastic Spherical Shell Windows with 4.00-inch Thickness

Test Number	Window Specimen	Impact Velocity (feet/second)	Hydrostatic Pressure (psi)	Strain on Window Surface (Microinches/inch)		Visible Damage
				Static	Dynamic Resultant	
1B	E	1.583	5	0	+4500	No cracks
2B	E	2.829	5	0	+6500	No cracks
3B	E	3.928	5	0	+13,500	Cracked
4B	F	10.702	500	-2000	+15,500	Cracked
5B	G*	5.350	500	-2000	+10,500	Cracked

Notes:

1. The spherical sector windows have an external radius of 24 inches and an included spherical angle of 117°.
2. All impacts were accomplished in water with a free falling mass of 12,500 pounds; the interior of the window cavity was dry and exposed to atmospheric pressure at all times.
3. The contact area on the free falling ram is a flat steel plate.
4. The electric resistance strainage rosette is located at the center of the window's low pressure face.
- 5.* Denotes a spherical sector window protected by a 0.375-inch thick acrylic plastic impact shield located 2 inches from the window surface.

the tenth cycle when the magnitude of the dynamic strains following it became essentially equal to the static strain generated by the 12,500 pound ram (about 11,500 pounds in water) resting on the window.

The fracture patterns were the same for all windows tested. The fracture pattern was in the shape of a cone whose apex was located at the middle of the shell thickness, while the base intersected the interior surface of the shell. The fracture plane was always initiated by a star-shaped crack whose edges would progressively coalesce into a conical fracture plane. During the impact test 3A on window A the kinetic energy of the ram was adequate to initiate the cracks but not sufficient to complete the formation of the fracture plane. Therefore, window A is an excellent illustration for the mechanism of fracture initiation (figure 28).

Close up study of the star-shaped crack in window A shows the leading edges of the crack beginning to curl along the conical plane whose apex is at the center of the star crack. If the impact velocity was 10 to 20 percent greater than the 1.576 feet/second that initiated the crack, the leading edges of the cracks would have joined, resulting in a cone-shaped fracture plane. Cone-shaped fracture planes were observed in fractured windows B, C and D (figure 29) where the kinetic energy of the ram was in excess of the energy required to initiate cracks.

All of the fractured windows retained their watertight integrity even though after the test they had to support the static weight of the ram. Since the external hydrostatic pressures varied from 5 to 500 psi during the impact tests, it is postulated that watertight integrity of the bow window in a submersible will be maintained over a wide range of external pressures after initiation of cracks in the window.

The impact shield, 0.375-inch thick acrylic plastic, has been found to provide very little, if any, practical protection against point impact by the 12,500 pound ram (figure 30). This is substantiated by tests 18A and 19A. There the impact velocities were roughly the same, except that in test 18A the window was bare while in test 19A the window was protected by a shield (figure 31). In both cases the damage to the window was in the form of a fracture cone. Each impact resulted in damage of equal severity (figure 32), even though one window was shielded and the other one was not. This does not imply, however, that at very low impact speeds the shield may not mean the difference between the presence or absence of a crack.

4.0-INCH THICK WINDOWS

The strains in the 4.0-inch windows were, as a rule, lower than in the 2.25-inch windows. The static tensile strain on the internal window surface directly below the point of ram contact was measured to be in the 1000- to 1500-microinches range. The static compressive strain on the internal window surface at the apex increased at 4-microinches/inch psi rate with the external hydrostatic pressure.

Under impact loading the dynamic strains rose quite rapidly, but it required an impact velocity of at least 3 feet/second before a dynamic tensile strain of 8000 microinches/inch would be generated on the internal window surface at the apex (figure 33). If the window was not externally pressurized, the impact velocity of 3 feet/second was sufficient to initiate fracture in the window. Slightly higher impact velocities were required to overcome the effect of negative static strains if the window was externally pressurized.

The dynamic strains measured at 5.35- and 10.702-feet/second impact velocities (tests 4B and 5B) were significantly lower than expected from the extrapolation of slower impact velocities data (tests 1B, 2B and 3B). It appears that once the tensile strain reaches the level required for initiation of fracture, it seldom increases beyond this value because the rapidly progressing conical fracture plane immediately relieves the peak stresses found on the inner surface of the window at the apex.

Dynamic response of the 4-inch thick windows was similar to that of the 2.25-inch thick windows except that the frequency of vibration was 8 cycles/second and the maximum amplitude about 0.25 inches (figure 34). There was sufficient energy stored in the initial dynamically generated deflection of the window to bounce the ram clear of the window's external surface immediately following the first dynamic loading cycle. Windows that fractured under the impact also vibrated and bounced off the impact ram after initial loading cycle.

The fracture patterns generated by impact loading in the 4-inch windows were similar to those observed in the 2.25-inch thick windows. Since in all cases the impact velocity of the ram was significantly higher than required for initiation of cracks on the inner surface of the window, the result was always a complete fracture cone (figures 35 and 36).

None of the fractured windows lost their watertight integrity even though the tests spanned the pressure range of 5 to 500 psi. On this basis it can be postulated that the windows will retain their watertight integrity, regardless of the depth at which the submersible window impacts an obstacle, if the impacting surface is flat and the impact velocity is only moderately higher than the critical velocity required for initiation of cracking.

The impact shield fabricated from 0.375-inch thick acrylic plastic was found to be just as ineffective in preventing fracture of 4-inch thick windows (figure 37) as it was for 2.25-inch thick windows. The strains plotted during the impact testing (test number 5B) of the shielding window showed no irregularities (like dips or steps) attributable to the protective action of the acrylic shield (figure 38).

DISCUSSION OF EXPERIMENTAL TEST RESULTS

CRITICAL IMPACT VELOCITY

Although the number of impact tests conducted was not adequate to establish accurately the critical impact velocities for the whole range of depths between 0 and 1120 feet, it was sufficient to predict the probable value of impact velocities. The evaluation of test results was complicated further by repeated impacts performed on the same window and fatigue had some effect on the window performance.

Additionally, the gravity operated impact ram generated an impact that was more severe than in an actual collision between a submersible and an underwater obstacle. In an actual collision the submersible bounces back from the obstacle after the initial impact because of the window's spring-like resilience. However, in the simulated collision the impact ram returned to impact the window several times in rapid succession until the oscillations of the window decayed to zero. Inasmuch as the test conditions were more severe

than actual submersible collisions, the extrapolated critical impact velocities are probably conservative.

Critical impact velocities for acrylic spheres with the same t/R_i ratios as the spherical sector window test specimens can be expected to be in the same range as the distribution of tensile stresses in the spheres under the point of impact is the same as in spherical sector windows. Shock mounting of acrylic spheres in the submersible structure could be utilized to absorb some of the kinetic energy and thus decrease the magnitude of dynamic tensile stresses under the point of impact.

DYNAMIC STRAINS

The dynamic strains, recorded on the spherical sector window during impacts where no cracking of window took place, are fairly accurate, although they are probably on the low side. This is caused by the inertia of oscillograph recording mechanism that does not allow the recording galvanometers to track the strains in real time. Thus, it can be postulated with reasonable certainty that the recorded dynamic strains under subcritical impact velocities are low by approximately 10 to 20 percent.

In tests where the impact velocity was supercritical, the recorded strains at moment of fracture are probably lower than actual values by 30 to 40 percent. The lower values here are the result not only of recording galvanometer inertia, but also of the rapidly progressing fracture in the acrylic which relieves the peak strains directly underneath the point of impact. Therefore, it is postulated that the resultant tensile strain measured on the concave surface of the window at the critical impact velocity is probably in the range of 9000 to 14,000 microinches/inch. It is prudent, however, in all the critical velocity predictions to use the more conservative value of +8000 microinches/inch actually recorded during the impact tests with supercritical velocities.

FRACTURES

All windows fractured by the same failure mechanism. The shape of the fracture, where the apex of the fracture cone is at midplane of the shell and the base of the cone on the inner shell surface, substantiates the postulate that the shells fail in flexure. In a typical flexure situation, the outer half of the shell is in compression and only the inner one is in tension. Because of this type of stress distribution the apex of the fracture cone cannot extend past the shell midplane and intersect the convex surface of the window. The compressive stresses located in the outer half of the shell prevent the propagation of the tensile fracture cone into the outer half of the shell thickness.

ANALYTICAL CALCULATIONS

BACKGROUND

The analytical calculations use the finite element method to numerically predict the collapse of a window as it impacts a rigid wall. The finite element results were then to be correlated with the experimental failure data presented in this report. If both theoretical

and experimental results were in sufficient agreement, the finite element method could supplement experimental testing in computing the structural integrity of the submersible windows.

FINITE ELEMENT MODEL

Mesh

The acrylic window and rigid wall were modeled as axisymmetric bodies (figure 39), using the general-purpose finite element program ANSYS.¹² The window had inside and outside radii of 24.00 and 21.75 inches, respectively. The element mesh was very fine in the area of the expected contact with the wall. There were five elements across the thickness and the angular spacing was increased away from the contact point at the window's apex. The wall which the window impacted was modeled as a series of stiff springs with initial gaps. The total model included:

- 205 isoparametric axisymmetric elements (STIF 42 in ANSYS)
- 19 axisymmetric gap elements (STIF 12 in ANSYS)
- 224 total elements

Physical Constants

The elastic constants of the acrylic window were taken as

Young's modulus: $E = 500,000$ psi

Poisson's ratio: $\nu = 0.35$

The linear springs which model the rigid wall were given a spring constant of

$$K_s = 1 \times \frac{10^{12} \text{ lb}}{\text{in-rad}}$$

Each spring was sufficiently stiff so that a compression of 0.0001 inches would store 2618 foot-pounds of energy. However, the ratio of spring stiffness to the stiffness of the elements in the shell is not large enough to cause ill-conditioning of the total stiffness matrix.

FINITE ELEMENT MESH VERIFICATION

One case to be examined was the window subjected only to external pressure. For a complete sphere, the elasticity solution has been determined by Lamé in closed form and is given as reference 13.

$$\sigma_{RR} = \frac{-P \left[1 - \left(\frac{a}{R} \right)^3 \right]}{1 - \left(\frac{a}{b} \right)^3} \quad (1)$$

$$\sigma_{\theta\theta} = \frac{\left[\frac{-P}{2} \left(\frac{a}{R} \right)^3 + 2 \right]}{1 - \left(\frac{a}{b} \right)^3} \quad (2)$$

$$U_r = \left[-\frac{1}{3\lambda + 2G} \frac{b^3}{b^3 - a^3} R - \frac{a^3 b^3}{4G R^2 (b^3 - a^3)} \right] P \quad (3)$$

where

σ_{RR} is the radial stress

$\sigma_{\theta\theta}$ is the hoop or meridional stress

a is the inside radius

b is the outside radius

R is the radius

$$\lambda = \frac{E}{(1 + \nu)(1 - 2\nu)}$$

$$G = \frac{E}{2(1 + \nu)}$$

P = the external pressure

For the finite element solution, only the first ten rows of elements were analyzed (figure 40). To model a portion of a complete sphere, the boundary conditions were taken as:

$$\delta_{\theta} = 0$$

at the nodes 1 to 6 and 61 to 66, where δ_{θ} is the displacement in the θ -direction. When the Lamé and finite element solutions for 1000 psi external pressure were compared, they were in very close agreement in both the displacement and stress solutions (table 4).

Table 4. Comparison of Lamé and Finite Element Solutions

	σ_{rr} (psi)	σ_{Hoop} (psi)	$\sigma_{Meridional}$ (psi)		U_r (in.)
Lamé Solution					
Inside Surface	0	-5866.	-5866.		-0.1659
Outside Surface	-1000.	-5366.	-5366.		-0.1506
Finite Element Solution					
Element 1 Surface Stress	0	-5831.	-5831.	Node 1	-0.1665
Element 5 Surface Stress	-1000.	-5424.	-5428.	Node 6	-0.1517
Element 46 Surface Stress	0	-5858.	-5891	Node 61	-0.1665
Element 50 Surface Stress	-1000.	-5366.	-5348.	Node 66	-0.1509

ACRYLIC WINDOW STRESS SOLUTION WITH EXTERNAL PRESSURE LOAD

A stress analysis of the full acrylic window was then conducted for an external pressure load. The results of this solution were used in the window-wall impact case to determine the effects of hydrostatic pressure on the critical impact velocities.

Since the window is considered fixed to the submarine, the boundary conditions taken along this interface were

$$\delta X = \delta Y = 0$$

at nodes 247 to 252, where δX and δY are displacements in the global X and Y directions. Nodes 1 to 6 on the Y-axis of symmetry were free to move in the Y direction but were constrained in the X-direction. This gave

$$\delta X = 0$$

at nodes 1 to 6.

The external pressure was taken as 1000 psi. The computer generated displacement plot shows the undeformed configuration in dashed outline (figure 41). The stress contour plots show distribution of σ_X , σ_Y , and σ_H (hoop) stresses, respectively (figures 42 through 44). On the exterior elements 1 and 5 the numerical values of the surface stresses and strains are

Element	Component	Strain (μ -in./in.)	Stress (psi)
1	Hoop	-7823.	-6018.
	Meridional	-7824.	-6018.
	Normal	8426.	0.
5	Hoop	-6755.	-5737.
	Meridional	-6765.	-5741.
	Normal	6034.	-1000.

ACRYLIC WINDOW IMPACTING THE RIGID WALL

The Method of Approach

The following discussion is based upon the assumption that window failure is dependent only upon the submarine's kinetic energy before impact. With this assumption, the work performed by the window-submarine boundary forces can be used to relate the change in kinetic energy of the submarine to the stress state in the window.

Let us assume during impact the only forces acting on the submarine are the submarine-window boundary forces F_X and F_Y (figure 45). The units of F_X and F_Y are in pounds per radian. If the submarine only moves in the Y direction, the force F_X does no work, and the work done by the force F_Y is equal to the change in kinetic energy of the submarine, i.e.,

$$\text{Work} = \int_{s_i}^{s_f} -F_Y(s)ds = \frac{1}{2} M (V_f^2 - V_i^2) \quad (4)$$

where M is the submarine mass, V_i and V_f are the initial and final velocities, and s is the boundary displacement.

The window can be considered sufficiently strong to withstand a given impact if the submarine velocity can be reduced to zero without the window failing. From equation 4 this gives

$$\int_{s_i}^{s_f} F_Y(s)ds = \frac{1}{2} M V_i^2. \quad (5)$$

The integral in equation 5 can be evaluated by displacing the submarine window boundary in small increments and computing the boundary force $F_Y(s)$ at each step. Assuming the window will fail when a given strain or stress state is reached, the boundary displacements can be increased until the failure criterion is satisfied and the initial kinetic energy can be computed from equation 5.

Numerical Calculations

When the submarine impacts the wall, there is initial contact only at the window's apex. As the impact process continues, the contact area increases. This phenomenon can be

modeled mathematically by displacing the boundary nodes 247 to 252 in the +Y direction. These displacements should be in small enough increments to allow the window to gradually contact the wall. During a displacement increment, if the gap distance between the wall and window is zero, the stiffness of the corresponding spring element is added to the total stiffness matrix of the structure. Since large deflections were expected, the stiffness matrix of the window, based upon the current geometry, was recomputed at each step. The relationship between boundary displacement and step numbers has been plotted for the convenience of the reader (figure 46).

A synopsis of the results from the finite element analysis is shown in table 5. F_{Yi} is the resultant boundary force in the Y direction at nodes 247 to 252 for the i th displacement step, i.e.,

$$F_{Yi} = \sum_{n=247}^{252} f_{Yn}.$$

The relationship between total boundary force and boundary displacements is shown in figure 26 and the work done by the boundary forces is given by

$$W = \int_{s=0}^{s=s_f} F_{Yi}(s) ds.$$

This integral is the area under the curve in figure 47 and may be evaluated numerically using the trapezoidal integration rule

$$\Delta KE_i = \frac{(s_i - s_{i-1})}{2} (F_{Yi} + F_{Yi-1})$$

This method should be very accurate since the force curve is almost a straight line. The finite element analysis was continued for twelve boundary displacement steps and the strain and stress results shown in table 4 indicate this loading is sufficient to cause failure in the acrylic window.

During displacement steps 9 to 12 spring number 4 (nodes 24 to 303), as well as springs 1 to 3, are in contact with the window. This indicates that the contact area between the rigid obstacle and the window has a circular shape whose area is equal to 4.95 inch².

The maximum spring force of 4055 pound/radian during displacement steps 1 to 12 occurred in spring 3 at step 12. This indicates the rigidity of the wall since maximum displacement of the nodes which model the rigid wall during impact was

$$\delta = \frac{F}{K} = 4.055 \times 10^{-9} \text{ in.}$$

Figures 48 to 51 show stress contour plots for the window at the final load step 12. The σ_x and hoop stress plots indicate that the regions in the vicinity of the inside and outside apexes are in tension and compression, respectively. If the acrylic window fails primarily in tension, then one would expect the failure to propagate generally along the tension contour lines in figures 48 and 50. The change in kinetic energy of the submarine versus boundary

Table 5. Synopsis of Calculated Strains and Stresses on the Apex of a Spherical Sector Window Mounted in the Bow of a Submersible Impacting a Rigid Wall; $R_0 = 24$ inches, $R_i = 21.75$ inches, $t = 2.25$ inches, and included angle of 117° .

Step Number	Displacement, Y_i , in.	ΔY_i , in.	$F Y_i$, lb/rad	$\Delta K E_i$, in.-lb/rad	$\Delta K E_i$, ft.-lb.	Total K., ft.-lb.	Step Number	Element Surface Strains, microinches/inch				Element Surface Stress, psi			
								Meridional		Hoop		Meridional		Hoop	
								Inside, Element 1	Outside, Element 5	Inside, Element 1	Outside, Element 5	Inside, Element 1	Outside, Element 5	Inside, Element 1	Outside, Element 5
0	.00000	0.000	0.0000	0.000	0.000	0.000	0	0.000	0.000	0.000	0.000	0.000	0.000	0.000	0.000
1	.00402	.00402	68.153	.136988	.071727	.071727	1	136.0	-257.2	136.5	-212.1	105	-189	105	-172
2	.01608	.01206	272.699	2.05534	1.0761	1.1479	2	545.0	-932.4	547.0	-858.9	420	-703	420	-675
3	.03618	.02010	1077.255	3.56705	7.1036	8.2515	3	2037.2	-3007.2	2044.5	-3112.3	1569	-2334	1571	-2373
4	.06431	.02813	1987.441	43.1049	22.5697	30.8212	4	3772.1	-5731.6	3784.5	-5731.7	2904	-4409	2909	-4409
5	.10045	.03614	3428.424	97.8646	51.2418	82.0631	5	6141.6	-8561.2	6159.6	-8561.3	4728	-6586	4735	-6586
6	.12500	.02455	4337.253	95.3236	49.9136	131.9767	6	7731.7	-10473.0	7751.2	-10473.1	5951	-8056	5959	-8056
7	.15000	.02500	5262.671	119.999	62.8313	194.8081	7	9352.0	-12455.3	9373.0	-12455.4	7198	-9581	7206	-9581
8	.17500	.02500	6274.556	142.965	74.8565	269.6646	8	10972.3	-14439.2	10994.0	-14439.3	8445	-11107	8453	-11107
9	.20000	.02500	7212.040	167.332	87.6151	357.2797	9	12391.0	-15943.1	12412.0	-15943.2	9536	-12264	9544	-12264
10	.22500	.02500	8198.747	192.6348	100.8634	458.1431	10	13848.0	-17511.8	13868.5	-17511.9	10656	-13471	10664	-13471
11	.25000	.02500	9171.024	217.1221	113.6848	571.8279	11	15306.4	-19083.9	15325.8	-19084.0	11778	-14680	11785	-14680
12	.27500	.02500	10127.946	241.2371	126.3115	698.1394	12	16764.5	-20649.9	16782.2	-20650.0	12899	-15885	12906	-15885

displacement curve is shown in figure 52 and the kinetic energy of the submarine required to induce a given maximum stress and strain in the acrylic window is shown in figures 53 and 54. The maximum tension and compression occurs in elements 1 and 5, and although the hoop and meridional surface stresses and strains are almost equal, the hoop values are slightly higher.

Figure 53 indicates, for example, if the window fails at 10,000 psi tension, a submarine with 400 foot-pounds of initial kinetic energy would induce failure. The value of the initial kinetic energy initiating fracture is, of course, dependent upon the choice of failure criterion.

The Effect of Depth on Window Failure

Let us assume that the failure prediction is based upon a maximum tensile hoop stress criterion. Since an external pressure causes compression in the vicinity of the window's apex, this pressure will strengthen the window by requiring the submarine to have a greater initial kinetic energy to induce tension on the internal surface of the window at its apex during impact. Further assume that the stress solution due to external pressure may be added to the previous boundary displacement solution, then

$$\sigma_{\text{total}} = \sigma_{\text{depth}} + \sigma_{\text{boundary displacement}}$$

where

$$\sigma_{\text{total}} = \text{total hoop stress component}$$

$$\sigma_{\text{depth}} = \text{hoop stress component due to depth}$$

$$\sigma_{\text{boundary displacement}} = \text{hoop stress component due to boundary displacement.}$$

In salt water the pressure P due to a depth h in feet is

$$P = \frac{64 \text{ lb}_f}{\text{ft}^3} \times h.$$

From uniform external pressure solution a 1000 psi external pressure (2250 foot depth) induces a -6018 psi hoop stress and, therefore, σ_{depth} may be taken as

$$\sigma_{\text{depth}} = \frac{-6018 \text{ psi}}{2250 \text{ ft}} \times h$$

and

$$\sigma_{\text{boundary displacement}} = \sigma_{\text{total}} + \frac{6018 \text{ psi}}{2250 \text{ ft}} \times h. \quad (6)$$

Once the value of σ_{total} to induce failure has been assumed, $\sigma_{\text{boundary displacement}}$ from equation 6 with figure 53 can be used to compute the corresponding initial kinetic energy required for window failure. Figures 55 to 57 show curves of constant kinetic energy for hoop stress tension failures at 8,000, 10,000 and 12,000 psi failure criterion at water depths

of 0, 225 and 1125 feet. These figures indicate, for a submarine of a given weight, that the impact velocity required to initiate window failure increases as the depth increases.

Although precise failure criterion would be difficult to establish, the finite element solution does provide a method to analytically predict ranges of critical impact velocities for a given submarine. These velocities can be used by the designer in determining the adequacy of a given submarine window. For example, if we assume the window in the numerical problem fails between

$$8000 \text{ psi} < \sigma_{\text{total}} < 12,000 \text{ psi} ,$$

then the critical impact velocities in foot/second for a 12,500 pound_m submarine are from figures 55 to 57

$$1.1 < V_1 < 1.7 \quad (h = 0 \text{ ft})$$

$$1.2 < V_2 < 1.8 \quad (h = 225 \text{ ft})$$

$$1.6 < V_3 < 2.3 \quad (h = 1125 \text{ ft}).$$

COMPARISON OF EXPERIMENTAL AND ANALYTICAL DATA

In general, it appears that the correlation between experimental and analytical data is quite good. As a matter of fact, the agreement between the experimental and analytical data is close enough to establish the validity of the analytical program for predicting the magnitude of kinetic energy required to initial fracture in an acrylic plastic spherical sector window or pressure hull during a collision between a submersible and an underwater obstacle.

LOCATION OF FRACTURE

The analytical program predicts that the fracture will originate on the concave side of the window directly underneath the point of impact because this is the location of maximum tensile stresses (figures 48 and 50).

Observation of all failed window test specimens shows that in every case the fracture originated on the concave side of the window directly below the point of impact (figures 28, 29, 31, 35, 36 and 37).

SHAPE OF FRACTURE PLANE

The analytical program predicts that the fracture plane will be in the shape of an inverted cone whose apex is located at the mid-thickness of acrylic shell. This prediction is based on the calculated distribution of stresses below the point of impact shown in figures 48 and 50. The shape of the planes of equal tensile stress intensity is an inverted cone whose apex contacts the plane of zero stress located in the vicinity of mid-thickness of the shell. Above the plane of zero stress there exists a field of biaxial compressive stresses that prevents the propagation of any tensile cracks.

After the fragments were removed from the failed test specimens, each cavity was found to have a shallow cone shape with a major diameter of about 8 inches and an apex located at the mid-thickness of the shell (figures 28, 29, 31, 35, 36 and 37).

CRITICAL KINETIC ENERGY

The analytical program predicts that the magnitude of the critical kinetic energy necessary to initiate fracture in the acrylic spherical window is a function of shell thickness, radius of curvature and external hydrostatic pressure. Windows with thick shells and short radius of curvature located in a high ambient hydrostatic pressure environment require higher kinetic energy to initiate fracture than thin shells with large radius of curvature in a low ambient pressure environment.

The analytical program also predicts that the numerical solution for critical kinetic energy in impacts on 2.25-inch thick spherical sector windows with 117° included angle can be used without further modification as an approximation of critical kinetic energy for windows with larger included angle, or even complete spheres.

Actual values of critical impact velocities have been calculated for 2.25-inch thick spherical window test specimens (figures 55, 56 and 57). They show that for an assumed biaxial stress failure criterion of 10,000 psi the critical impact velocity in 0 psi ambient pressure environment for the 2.25-inch thick windows is 1.4 feet/second. For 500 psi ambient pressure environment the critical velocity is predicted to increase to 1.9 feet/second.

Experimental test data shows that the critical impact velocity in 0 psi ambient pressure environment for 2.25-inch thick acrylic plastic spherical windows is 1.5 feet/second. In 500 psi ambient pressure environment the critical velocity increased to 2 feet/second.

FINDINGS

1. Spherical shell acrylic plastic windows with $t/R_i \leq 0.2$ found in the bows of modern submersibles fracture readily in simulated collisions between a submersible and an immovable object.
2. The magnitude of the critical impact velocity capable of initiating fracture in the spherical shell window is a function of vehicle mass, R_i , t/R_i , included angle of the window and the ambient hydrostatic pressure.
3. The fracture in acrylic originates on the low pressure face of the window directly underneath the point of impact when the dynamic biaxial tensile stresses exceed the static strength of acrylic plastic under biaxial tension.
4. The fracture in acrylic takes the form of a star-shaped crack whose leading edges coalesce into the shape of a cone with very low height-to-diameter ratio.
5. External hydrostatic pressure generates in the spherical shell static compressive stresses which, when combined with dynamic stresses, result in lower magnitude of tensile stresses on the convex surface of the spherical window. The net effect of external hydrostatic

pressure is to make the spherical shell windows more resistant to cracking under point impact loading.

6. The critical impact velocity for 2.25-inch and 4-inch thick spherical shell windows with 24-inch radius and 117° included angle, when mounted on a 12,500-pound submersible cruising on the surface, is approximately 1.5 and 3 feet/second, respectively. The critical impact velocities for these windows when the submersible is at 1120-foot depth are approximately 2 and 3.2 feet/second.

7. Catastrophic failure, resulting in the loss of a submersible does not occur in spherical shell windows even at impact velocities that are 100 percent higher than the critical velocity providing that the surface area of the underwater obstacle is flat.

8. Thin spherical shields of acrylic plastic do not appear to increase significantly the critical impact velocity for spherical shell acrylic windows.

9. The finite element computer program which substitutes a series of very stiff springs for the rigid surface of the impactor seems to predict reasonably well the critical impact velocity for an acrylic spherical shell window.

CONCLUSION

Acrylic plastic spherical shells, serving as panoramic visibility bow windows or personnel capsules on submersibles, can be fractured by colliding with an underwater obstacle. This can occur at typical cruising velocities of submersibles and because of this must be considered seriously in the design and operation of modern submersibles with panoramic visibility.

Through proper design or operational procedures or both, the large spherical shell acrylic plastic windows of panoramic visibility submersibles should be protected from catastrophic failure in underwater collision.

DESIGN

The fracture of acrylic plastic spherical shell windows can be eliminated by one of two design approaches. In one, the submersible can be provided with an adequate bow bumper designed to absorb the kinetic energy of the submersible at its top cruising speed. When properly positioned, such a bumper eliminates all the danger to the window resulting from a collision, while at the same time imposing only minor restrictions on the visibility through the window.

The other design approach concentrates on improving the impact resistance of the window to such a degree that the critical impact velocity surpasses the top cruising speed of the submersible. In practical terms this means that the thickness of the windows should be in the range of about 6 to 8 inches and protected with an additional 1-inch layer of transparent elastomeric material.

At the present time the use of 6 to 8-inch thick spherical shell bow windows appears to impose an unacceptable cost and payload penalty on submersibles operating in the 0 to

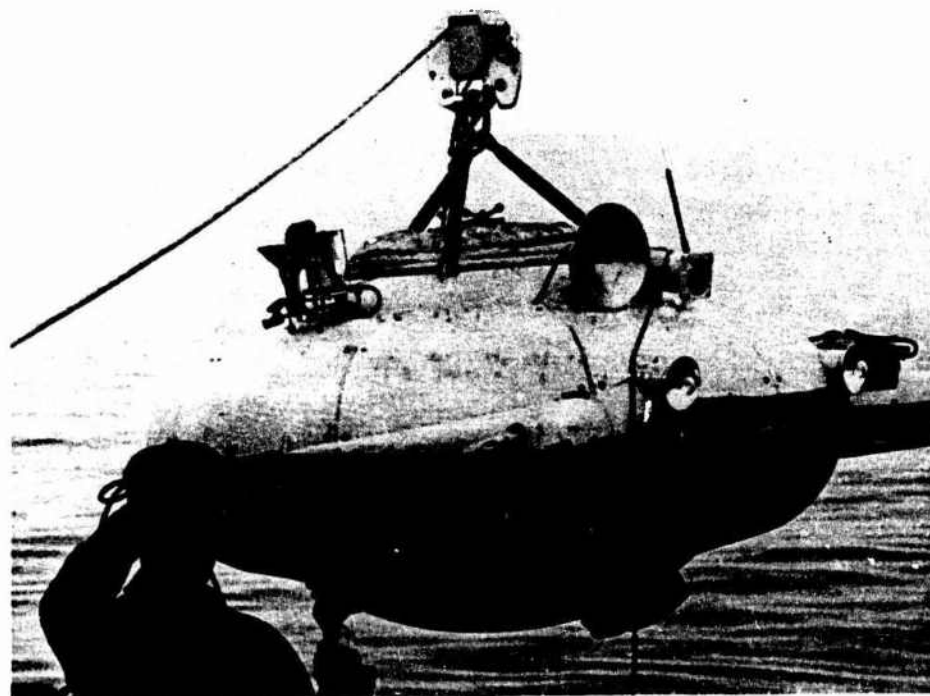
1200-foot depth range. In the near future, however, when the operational depth requirements for submersibles increase to 4000-foot depth, the thickness of spherical bow windows will be in the 6- to 8-inch range to satisfy hydrostatic load requirements. At that time the design approach utilizing a bumper will become less and the other approach more economically attractive.

OPERATION

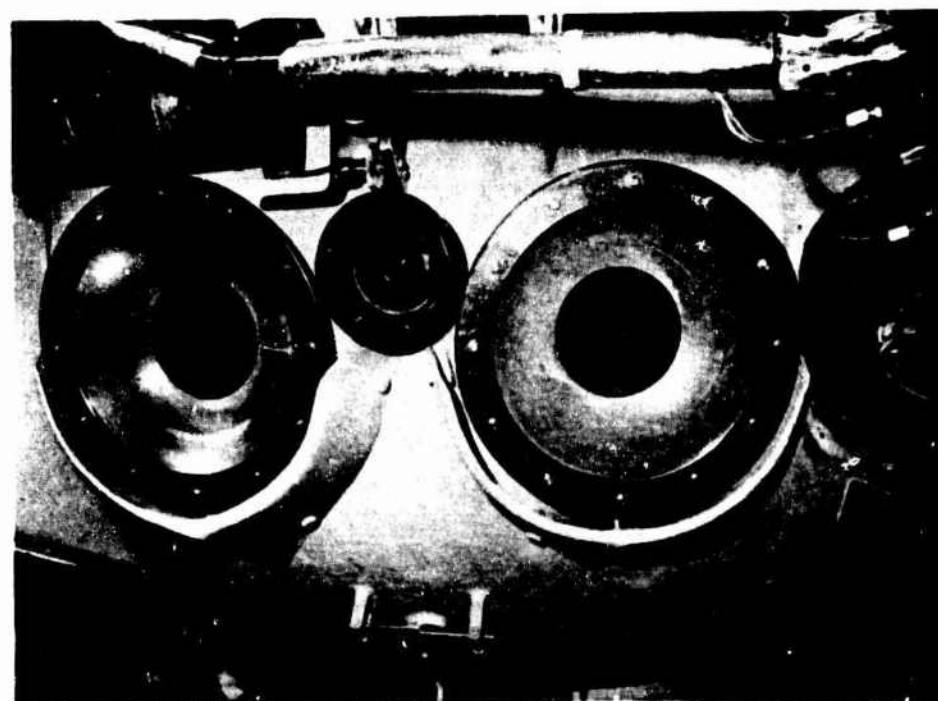
Two recommendations can be used to either substantially decrease, or even wholly eliminate, the collision hazard to spherical shell acrylic plastic windows. One, collision avoidance sonar can be installed in the submersible and, two, the operational speed of the submersible can be restricted to speeds ≤ 1 foot/second when operating in the immediate vicinity of massive underwater obstacles like wrecks, platforms or reefs. This approach is already practiced in other vehicles that have panoramic visibility windows; i.e., helicopters.

REFERENCES

1. Naval Civil Engineering Laboratory Technical Report R-631, Windows for External or Internal Hydrostatic Pressure Vessels; Part 3. Critical Pressure of Acrylic Spherical Shell Windows Under Short Term Pressure Application, by J. D. Stachiw, F. W. Brier. June 1969 (AD 689789).
2. Naval Undersea Center TP 355, Flanged Acrylic Plastic Hemispherical Shells for Undersea Systems, by J. D. Stachiw. August 1973 (AD 769213).
3. Naval Undersea Center TP 383, Cast Acrylic Dome for Undersea Applications, by J. D. Stachiw. January 1974 (AD 776587).
4. Naval Undersea Center TP 410, Development of a Precision Casting Process for Acrylic Plastic Spherical Shell Windows Applicable to High Pressure Service, by J. D. Stachiw, May 1974 (AD 782337).
5. Naval Undersea Center TP 453, Spherical Shell Sector Acrylic Plastic Windows with 12,000 ft. Operational Depth for Submersible ALVIN, by J. D. Stachiw, May 1975 (AD 011175).
6. Naval Civil Engineering Laboratory Technical Report R-676, Development of a Spherical Acrylic Plastic Pressure Hull for Hydrospace Application, by J. D. Stachiw, April 1970 (AD 707363).
7. Naval Civil Engineering Laboratory TN N-1113, The Spherical Acrylic Pressure Hull for Hydrospace Application; Part 2. Experimental Stress Evaluation of Prototype NEMO Capsule, by J. D. Stachiw, K. L. Mack. October 1970 (AD 715772).
8. Naval Civil Engineering Laboratory TN N-1134, The Spherical Acrylic Pressure Hull for Hydrospace Application; Part 3. Comparison of Experimental and Analytical Stress Evaluations for Prototype NEMO Capsule, by H. Ottsen. March 1970 (AD 709914).
9. Naval Civil Engineering Laboratory TN N-1134, The Spherical Acrylic Pressure Hull for Hydrospace Application; Part 4. Cyclic Fatigue of NEMO Capsule #3, by J. D. Stachiw. October 1970 (AD 715345).
10. Naval Undersea Center TP 315, Acrylic Plastic Hemispherical Shells for NUC Undersea Elevator, by J. D. Stachiw, September 1972 (AD 749029).
11. Naval Undersea Center TP 451, NEMO Model 2000 Acrylic Plastic Spherical Hull for Manned Submersible Operation at Depths of 3,000 feet by J. D. Stachiw, December 1974.
12. De Salvo, G., and Swanson, J., ANSYS: Engineering Analysis System User's Manual, Swanson Analysis Systems, Inc., Elizabeth, Pennsylvania, 1973.
13. Love, A. E. H., The Mathematical Theory of Elasticity, Dover Publications, New York, 1944.



a.



b.

Figure 1. Typical viewports found in the older generation of submersibles; Cousteau's Soucoupe submersible; (a) overall view, (b) detail view.

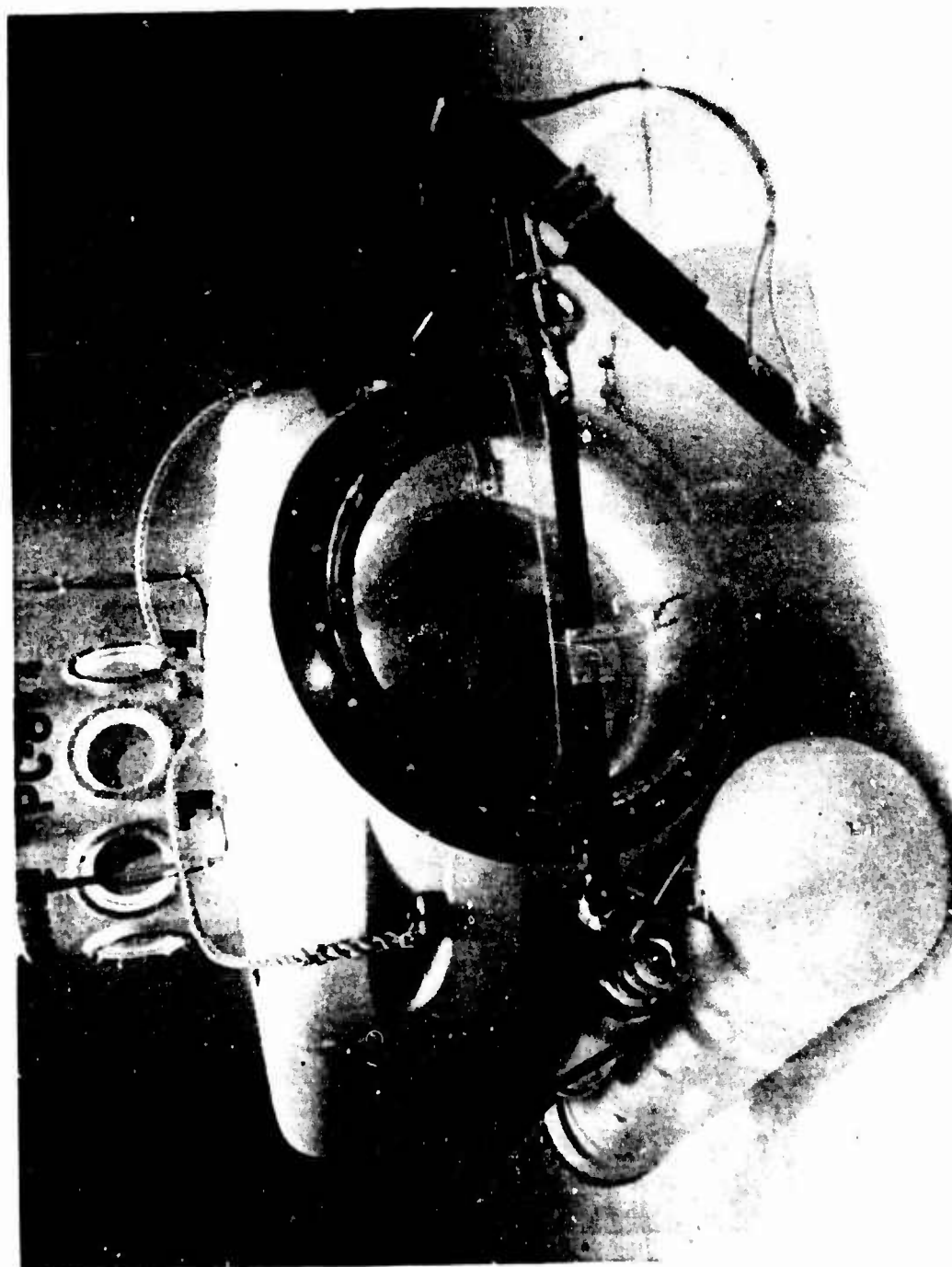


Figure 2. Typical bow viewport with panoramic visibility found in the younger generation of submarines; Perry's PC-8B submersible.

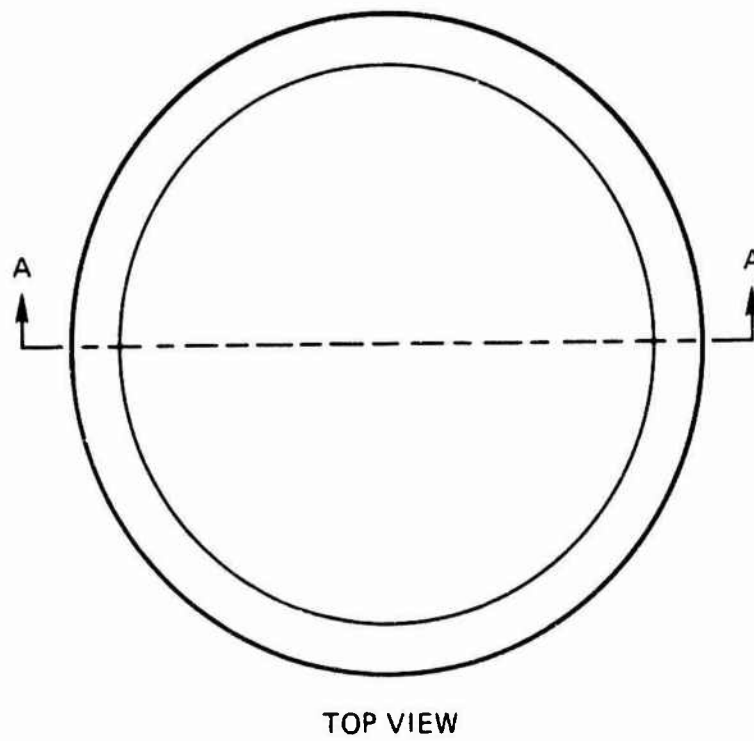
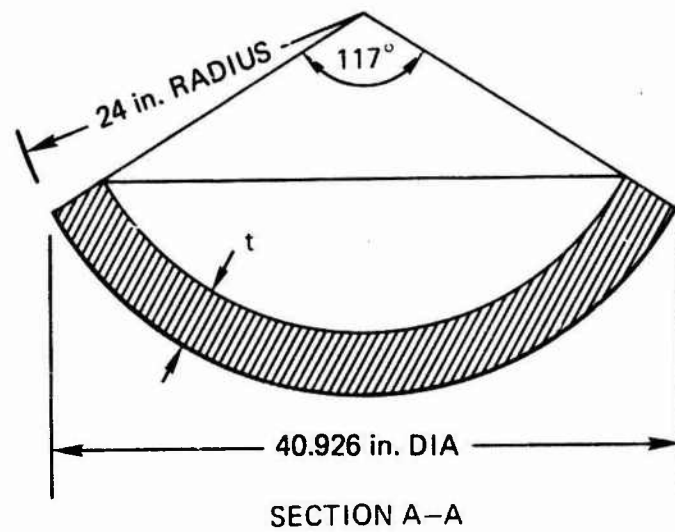


Figure 3. Dimensions of spherical shell sector windows used as test specimens in the point impact loading study.



Figure 4. Precision machined female mold with 24-inch radius used by the Southwest Research Institute for molding of spherical shell vector windows.

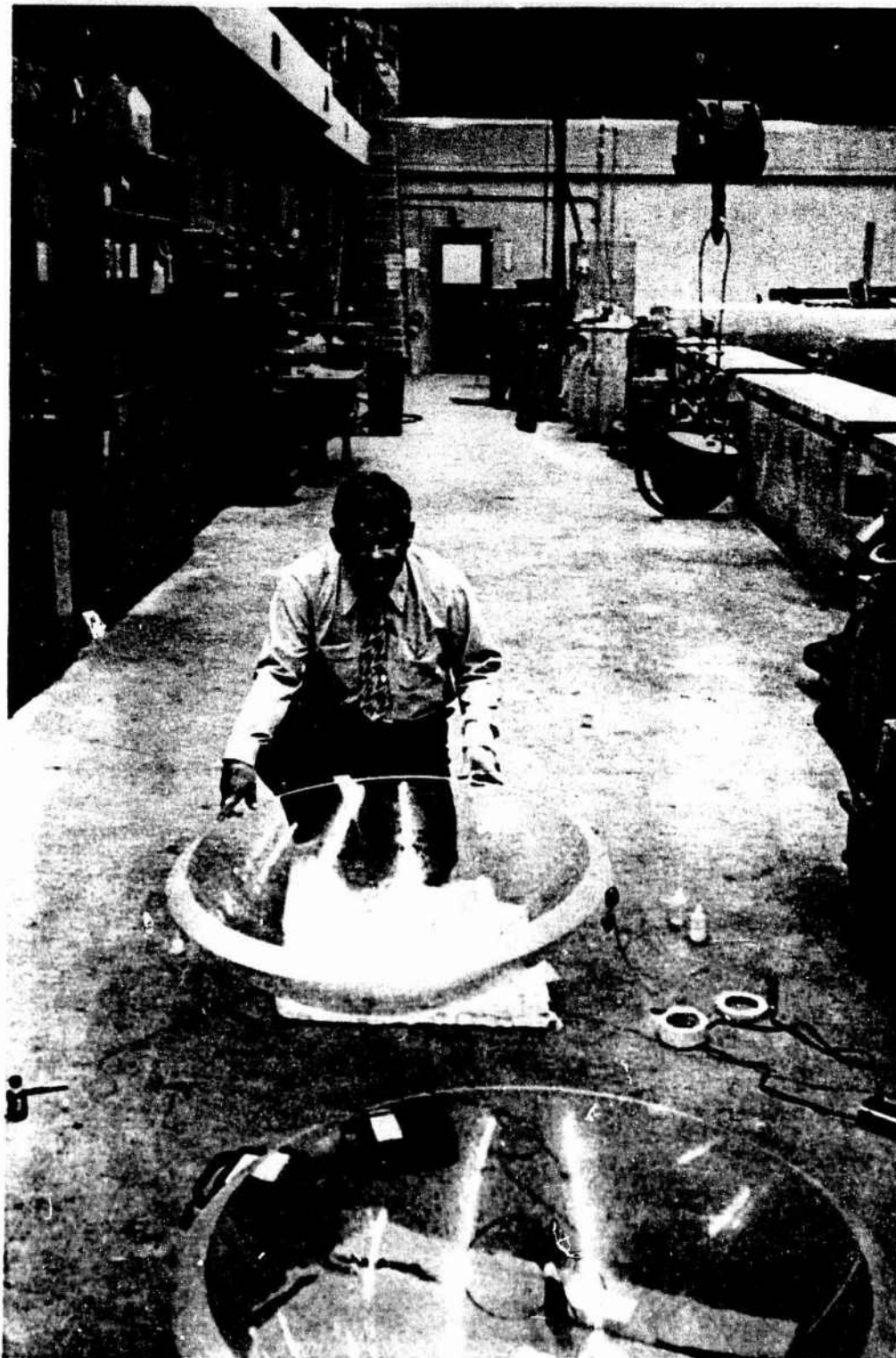


Figure 5. Typical acrylic plastic spherical sector window with $R_0 = 24$ inches, $t = 2.25$ inches and $\alpha = 117^\circ$ used as a test specimen in the impact loading study.



Figure 6. Jig for free blowing of acrylic plastic impact shields.



Figure 7. A acrylic plastic impact shield evaluated in the experimental program for its ability to protect spherical shell sector windows against point impacts.

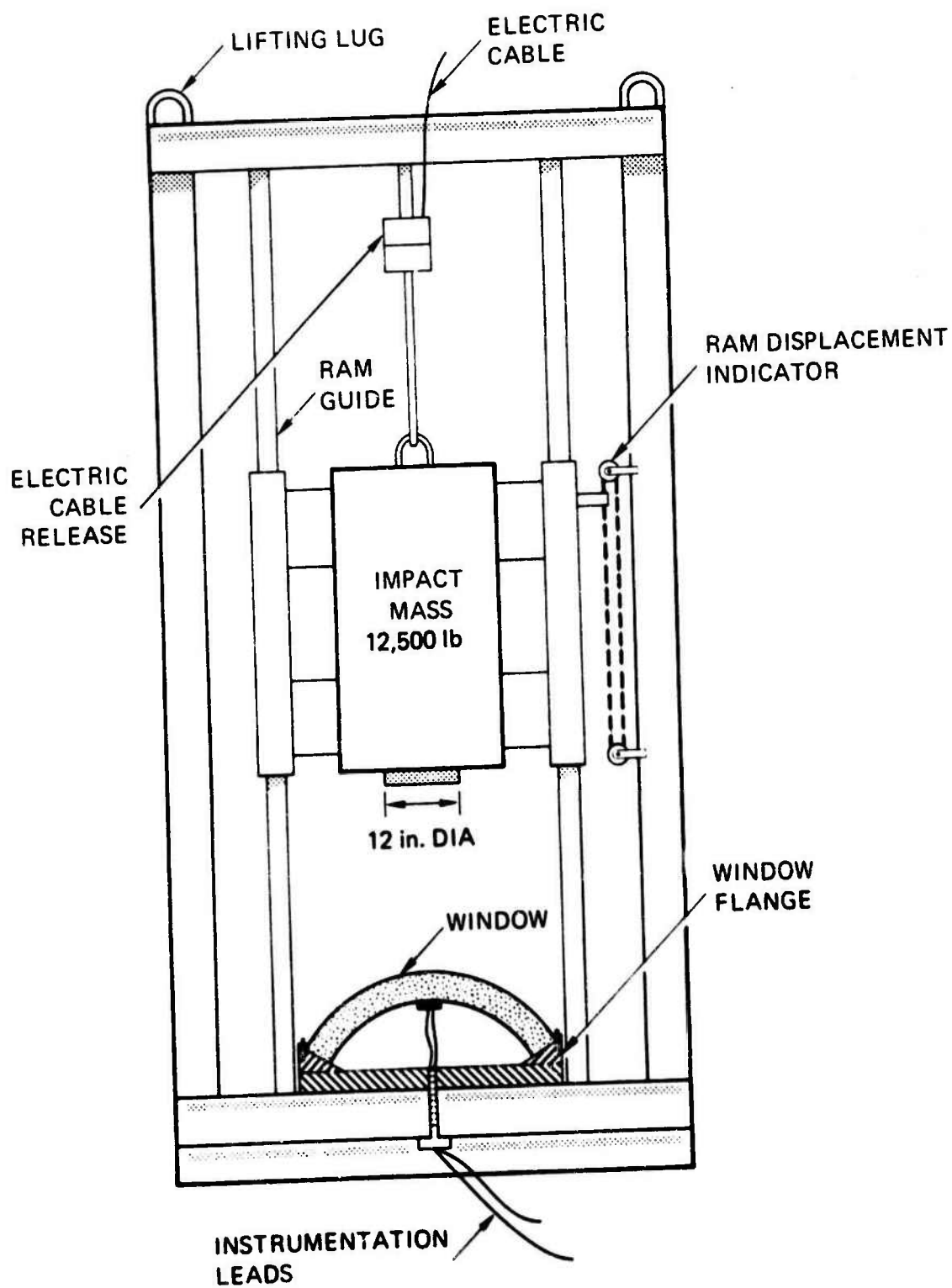


Figure 8. Schematic of the impact ram used to simulate underwater collisions between bow windows in submersibles and immovable obstacles.



Figure 9. Impact loading ram assembly prior to placement in the SWRI pressure vessel.

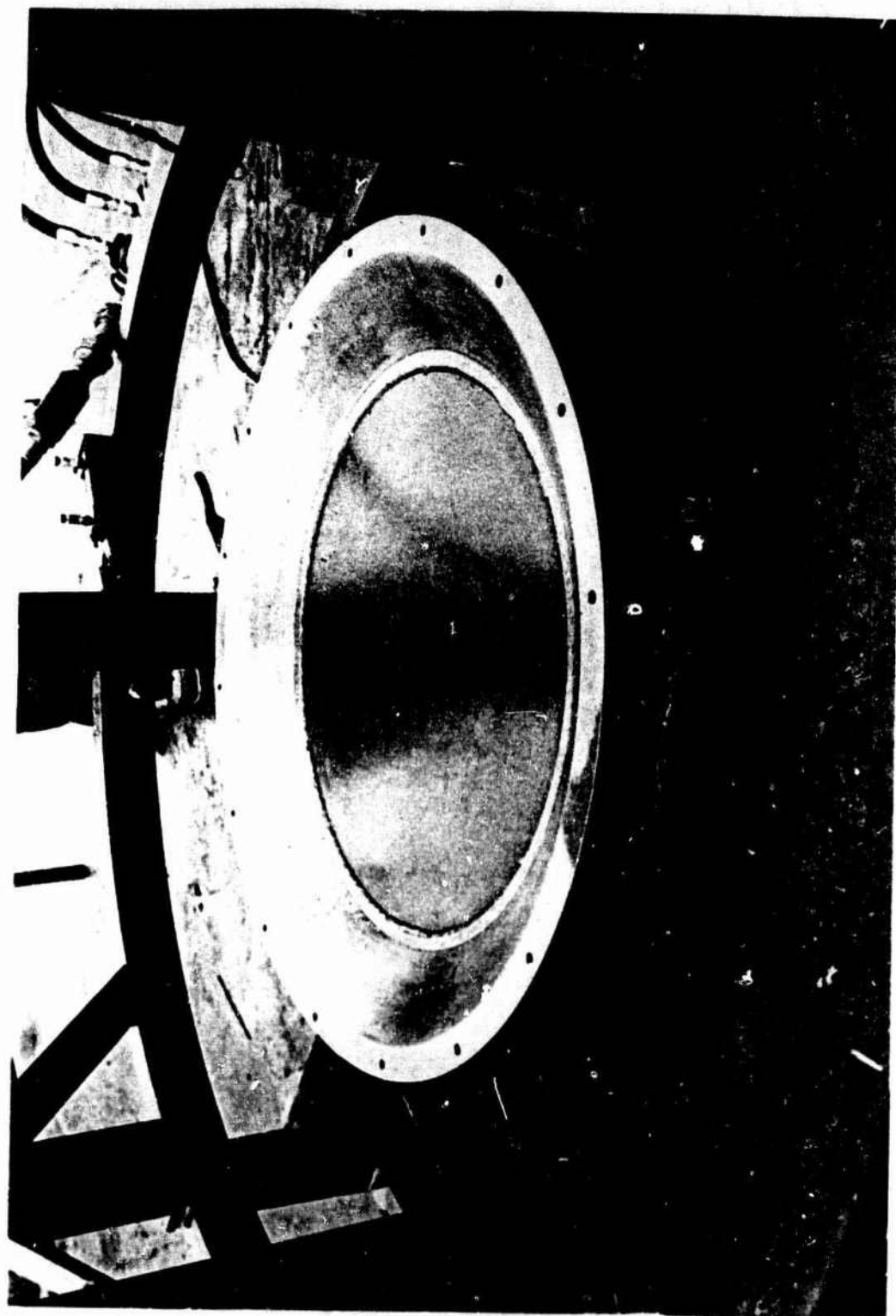


Figure 10. Steel flange for mounting the window test specimen in the impact loading ram assembly.



Figure 11. Position of ram at the instant of impacting the window test specimen.



Figure 12. Location of electric resistance strain gages on the concave surface of spherical shell sector windows.



Figure 13. Displacement indicator for real time measurement of impact ram location and rate of movement; a rotary potentiometer mechanically coupled to the ram served as displacement indicator.



Figure 14. Dynamic strains and ram displacement were recorded on paper moving at 32 inches/second.



Figure 15. Vacuum operated suction cup was used in the handling of spherical shell sector windows.

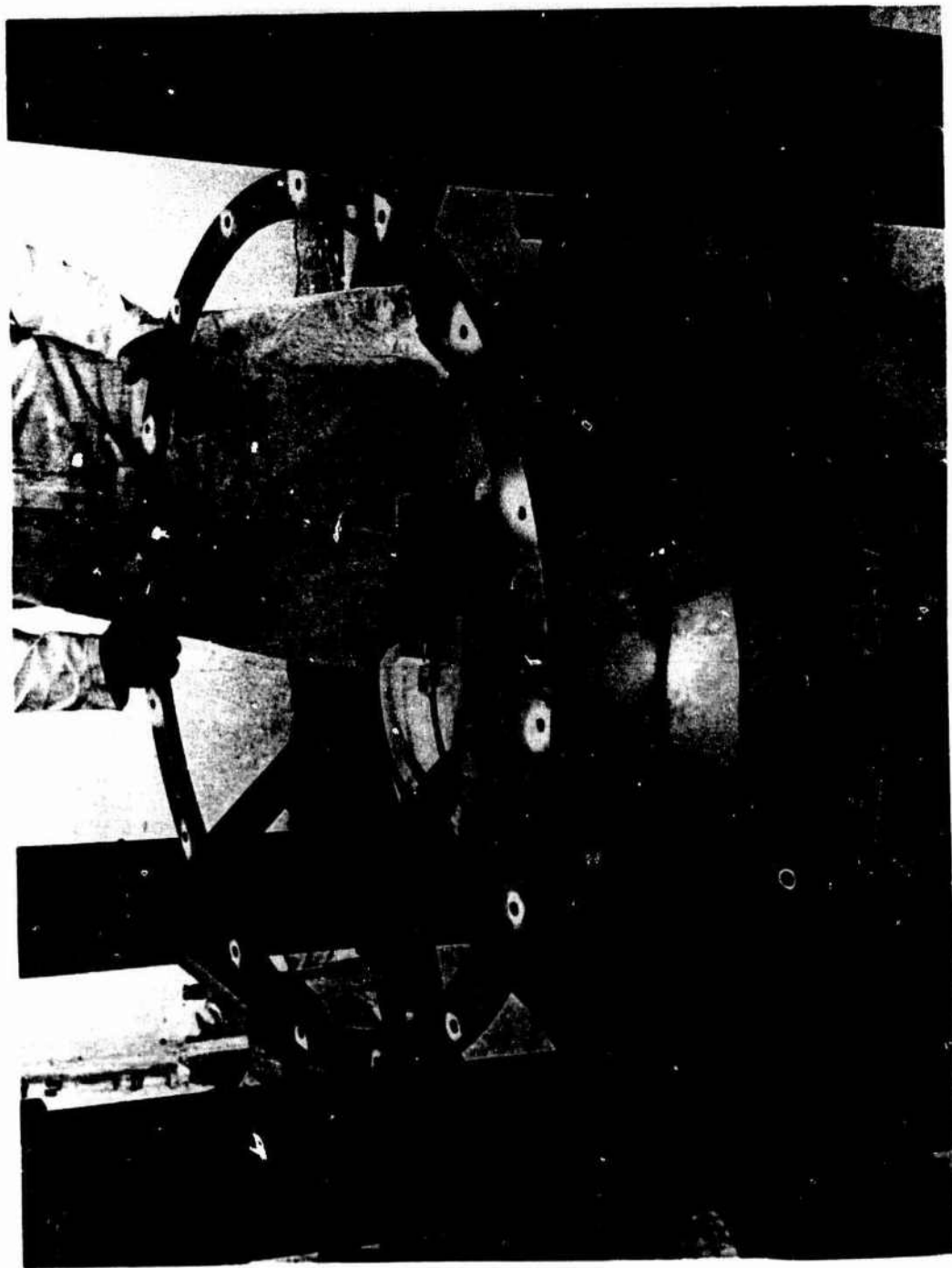


Figure 16. A 1-inch thick retaining ring was used to compress the 0.25-inch thick neoprene gasket.



Figure 17. 16 bolts, 0.5-inch diameter, held the retainer ring in place.

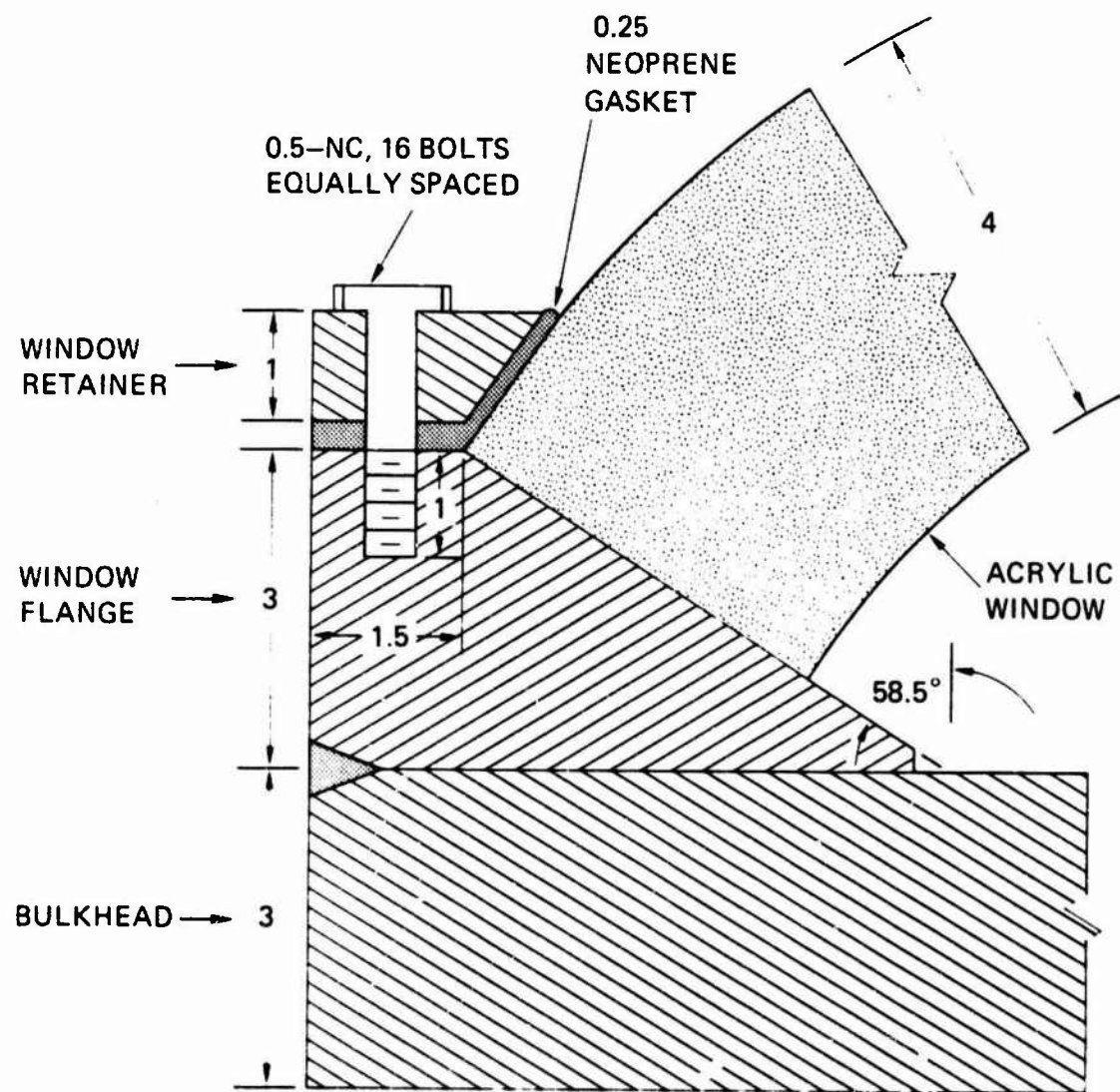


Figure 18. Schematic of the window installation under the impact ram. All dimensions are in inches.

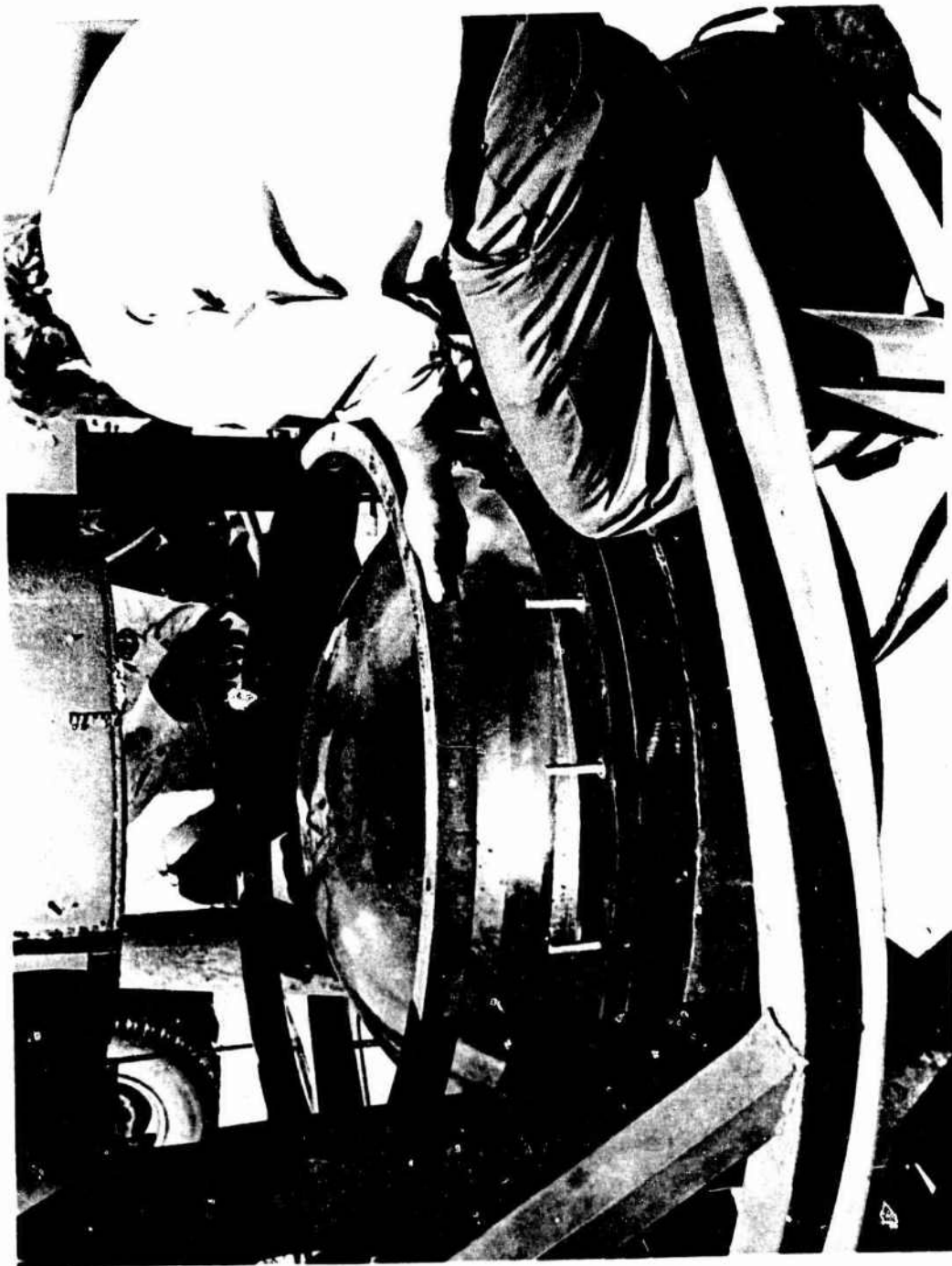


Figure 19. A 2-inch thick spacer ring was installed on top of the window retainer ring to give the impact shield a minimum 2-inch standoff.

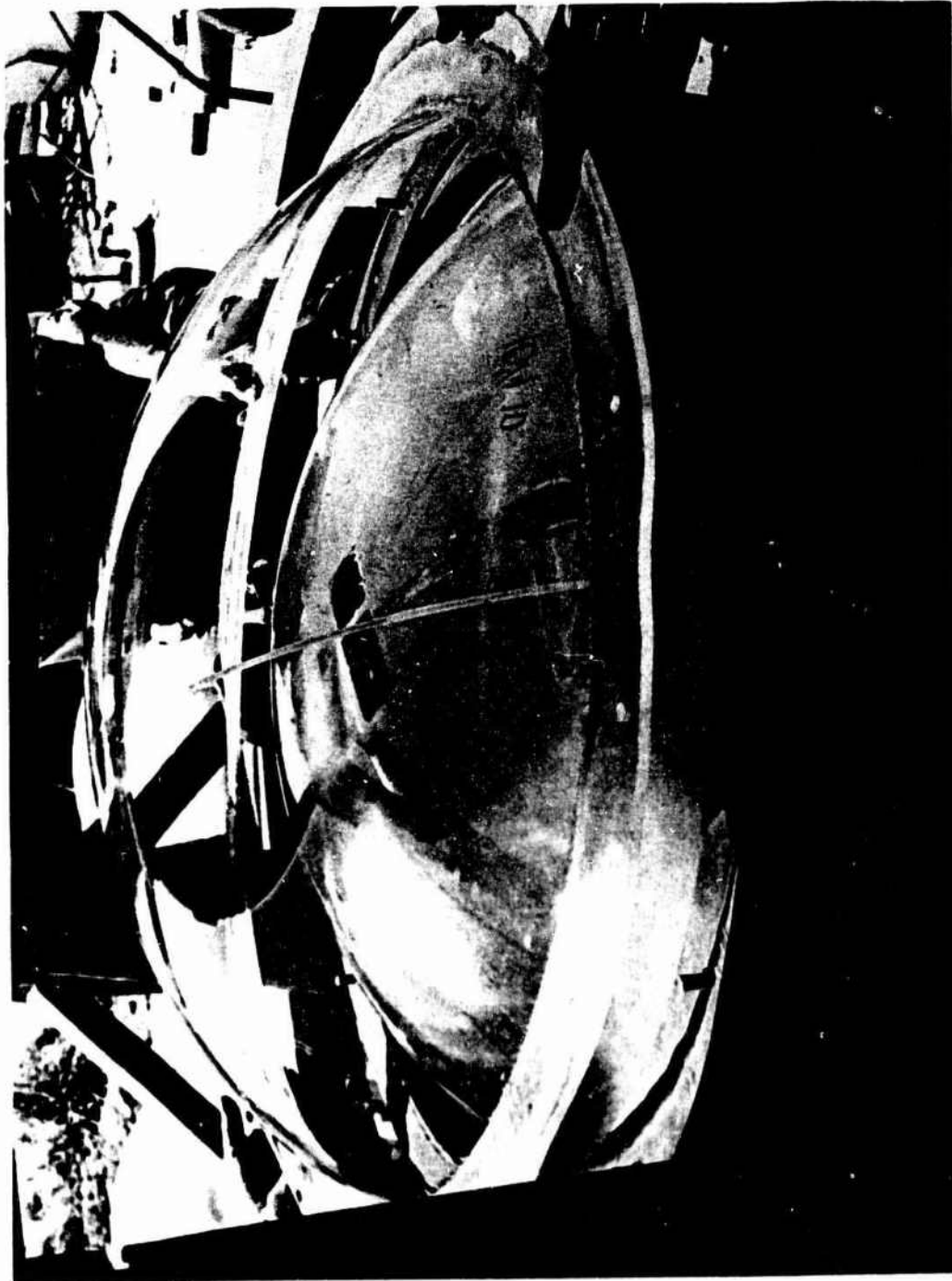


Figure 20. Placement of 0.375-inch thick impact shield on top of the spacer ring; plastic tubing was used to remove air trapped under the impact shield after the test assembly was placed into the water filled pressure vessel.



Figure 21. Completed window assembly with acrylic plastic shield.

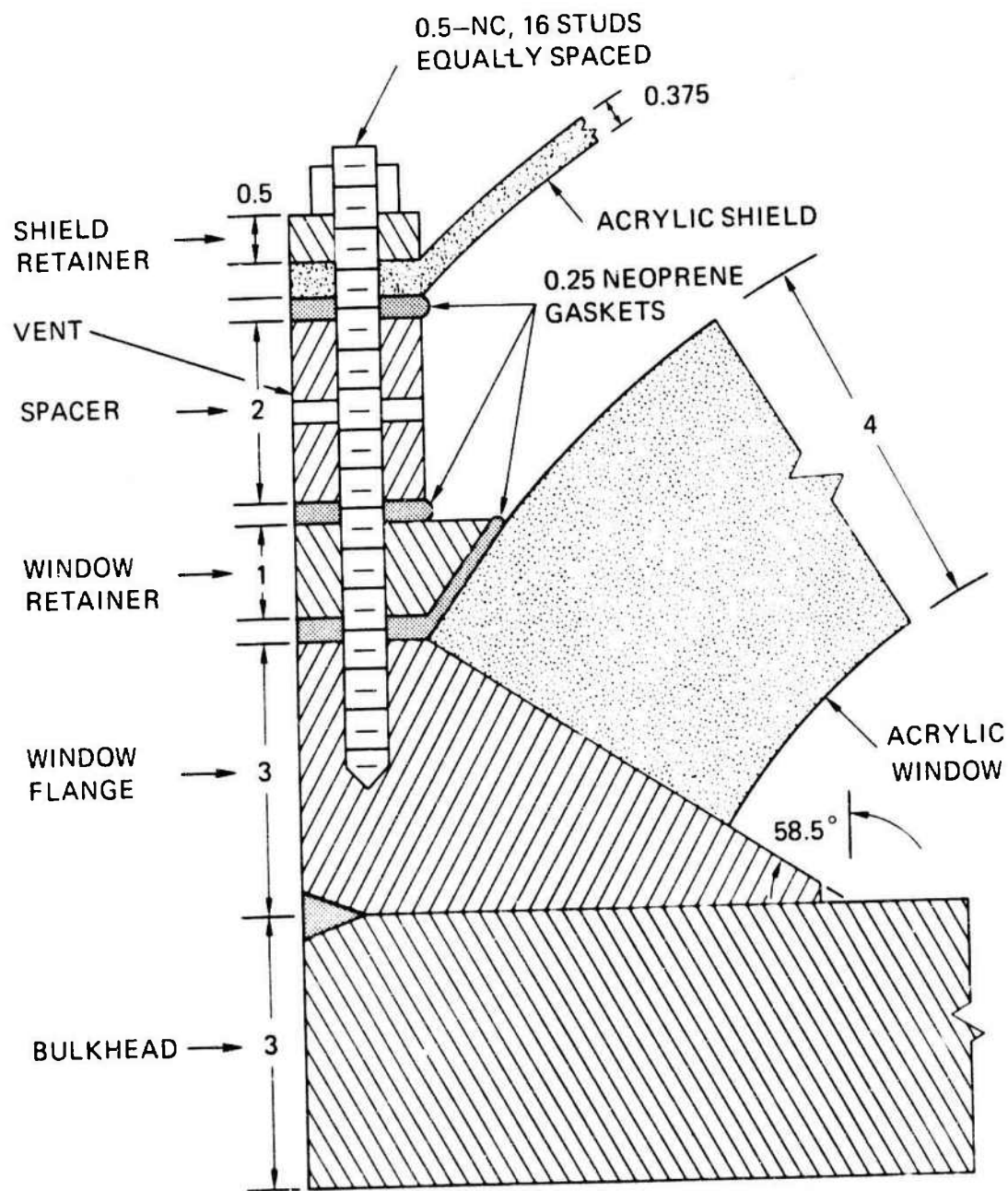


Figure 22. Schematic of the window assembly with acrylic plastic impact shield. All dimensions are in inches.

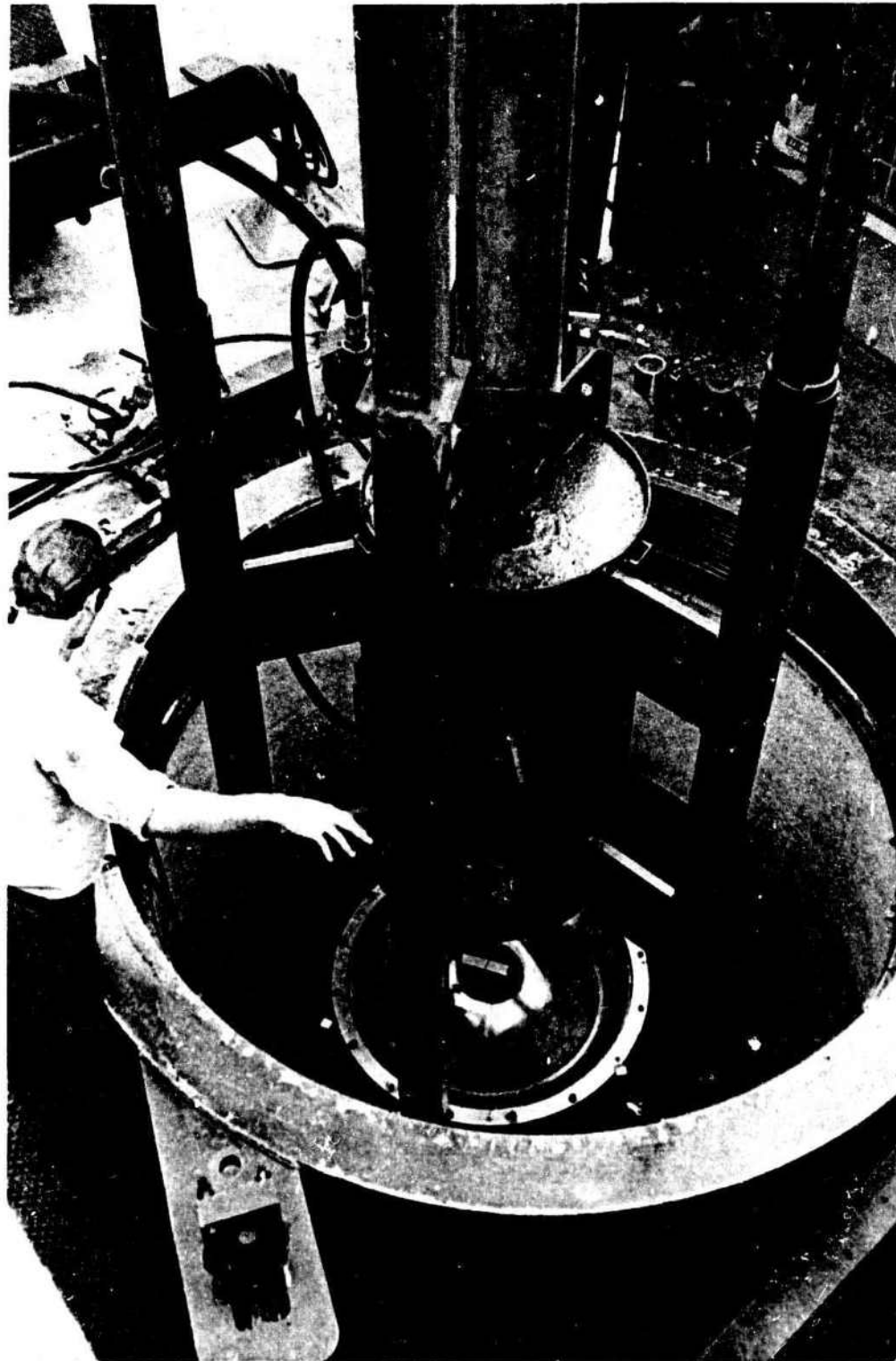


Figure 23. Placement of ram assembly into the 90-inch ID pressure vessel at SWRI.

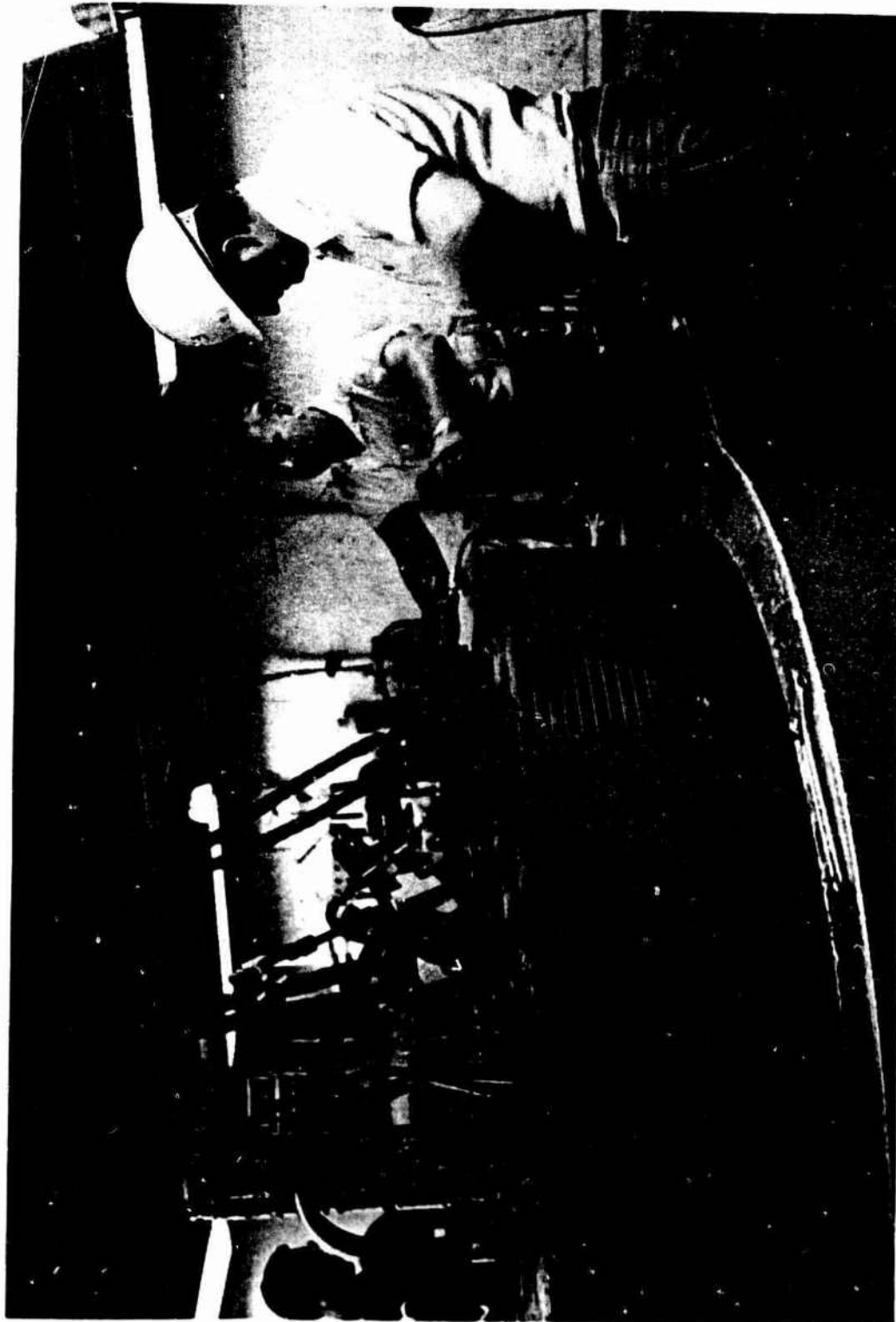


Figure 24. Placement of end closure on the pressure vessel for tests where depths greater than 10 feet were simulated.



Figure 25. Inspecting the window for cracks after an underwater collision was simulated inside the 90-inch ID pressure vessel.

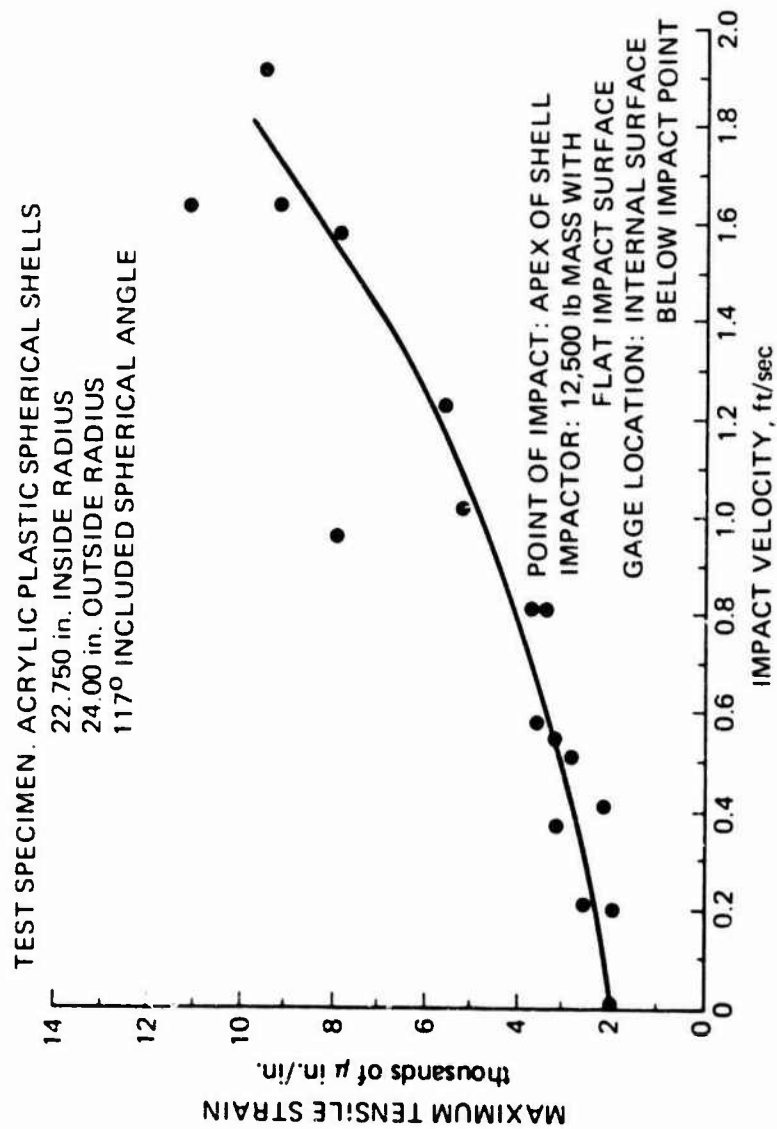


Figure 26. Dynamic tensile strains generated on the concave side of the 2.25-inch tensile windows directly under the point of impact with a 12,500 pound ram.

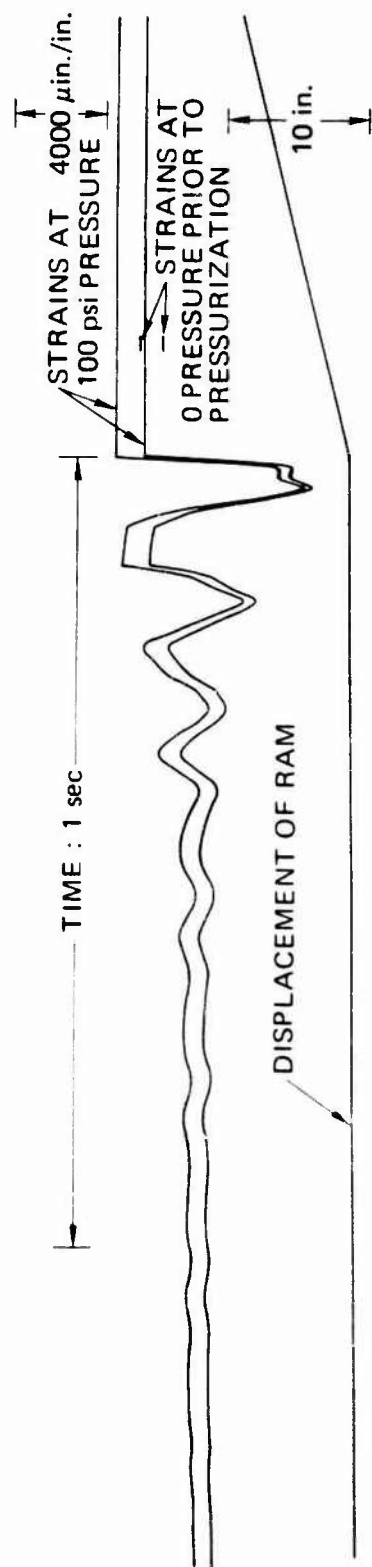


Figure 27a. Dynamic strains measured with a 90° strain gage rosette on the concave side of a 2.25-inch thick window directly under the point of impact with 0.960 foot/second velocity in a 100 psi ambient pressure environment.

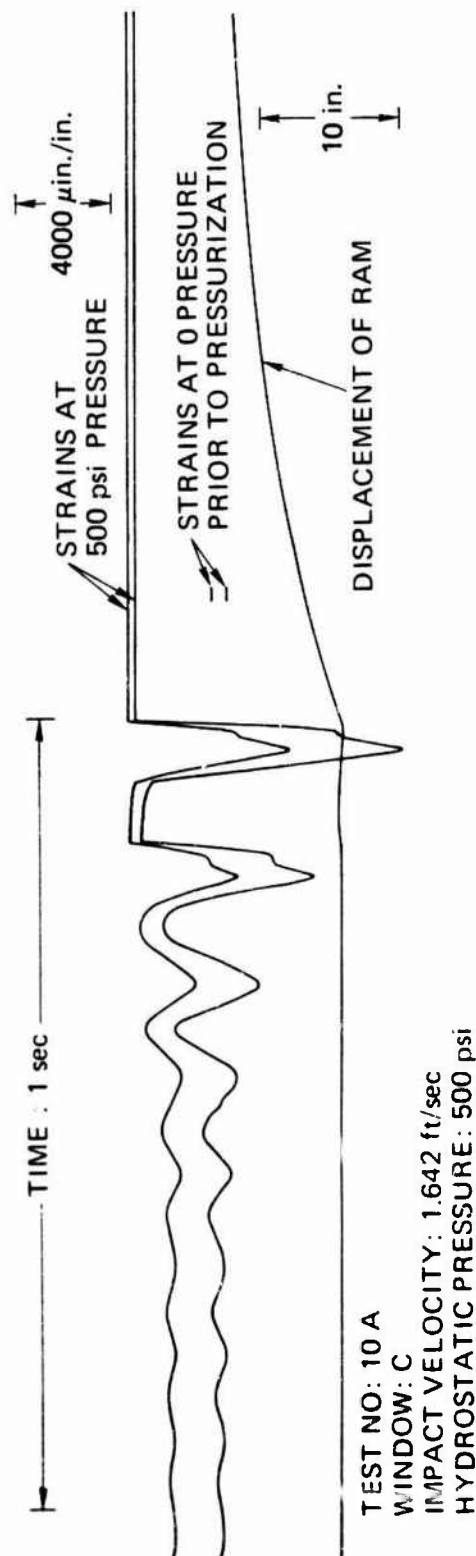


Figure 27b. Same test setup as in figure 27a, but at 1.642 feet/second impact velocity in a 500 psi ambient pressure environment.

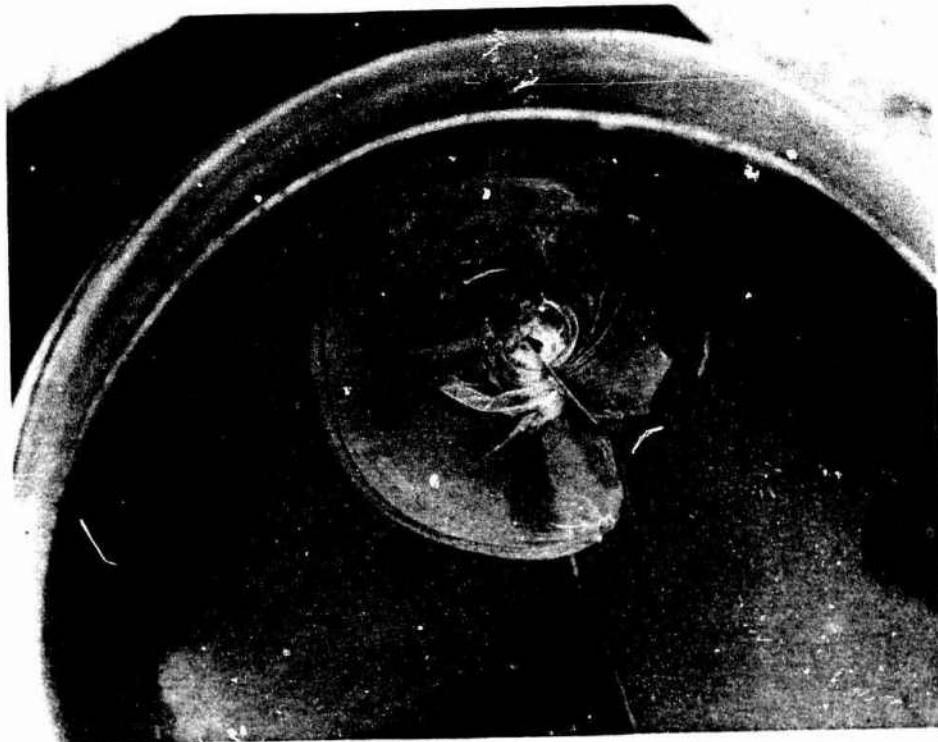


a.



b.

Figure 28. Star-shaped crack generated in a 2.25-inch thick window by 1,576 feet/second impact velocity in 5 psi ambient pressure environment; (a) Overall view, (b) Detail view.



a.

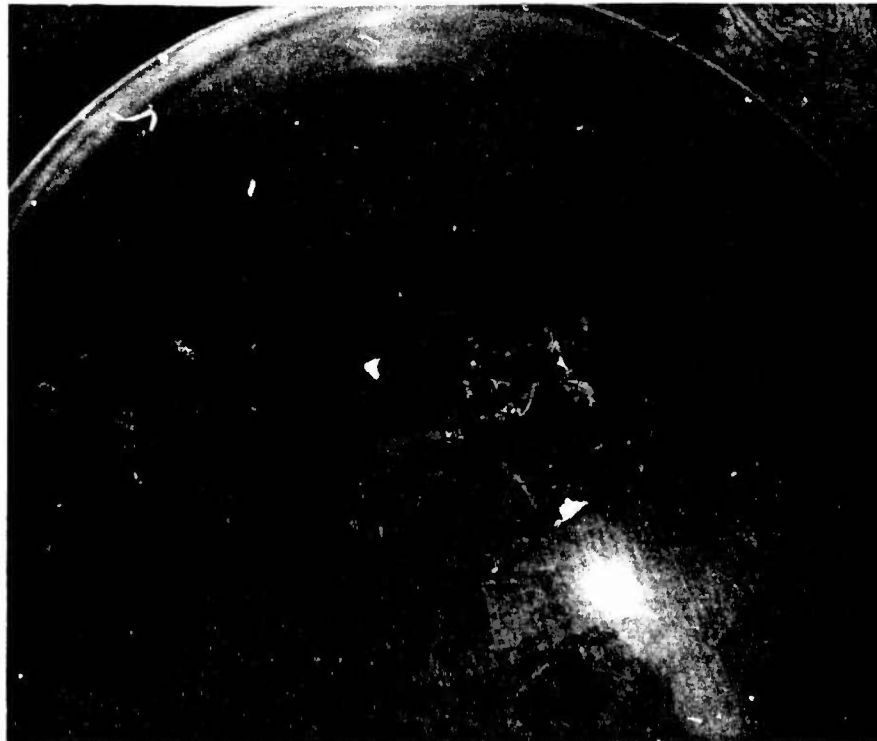


b.

Figure 29. Conical fracture plane generated in a 2.25-inch thick window by 1.913 feet/second impact velocity in 100 psi ambient pressure environment; (a) Overall view, (b) Detail view.



Figure 30. Fractured impact shield after the 9,895 feet/second impact with 12,500 pound ram.



a.



b.

Figure 31. 2.25-inch thick window after 9.85 feet/second impact with 12,500 pound ram;
(a) Overall view, (b) Close-up view.

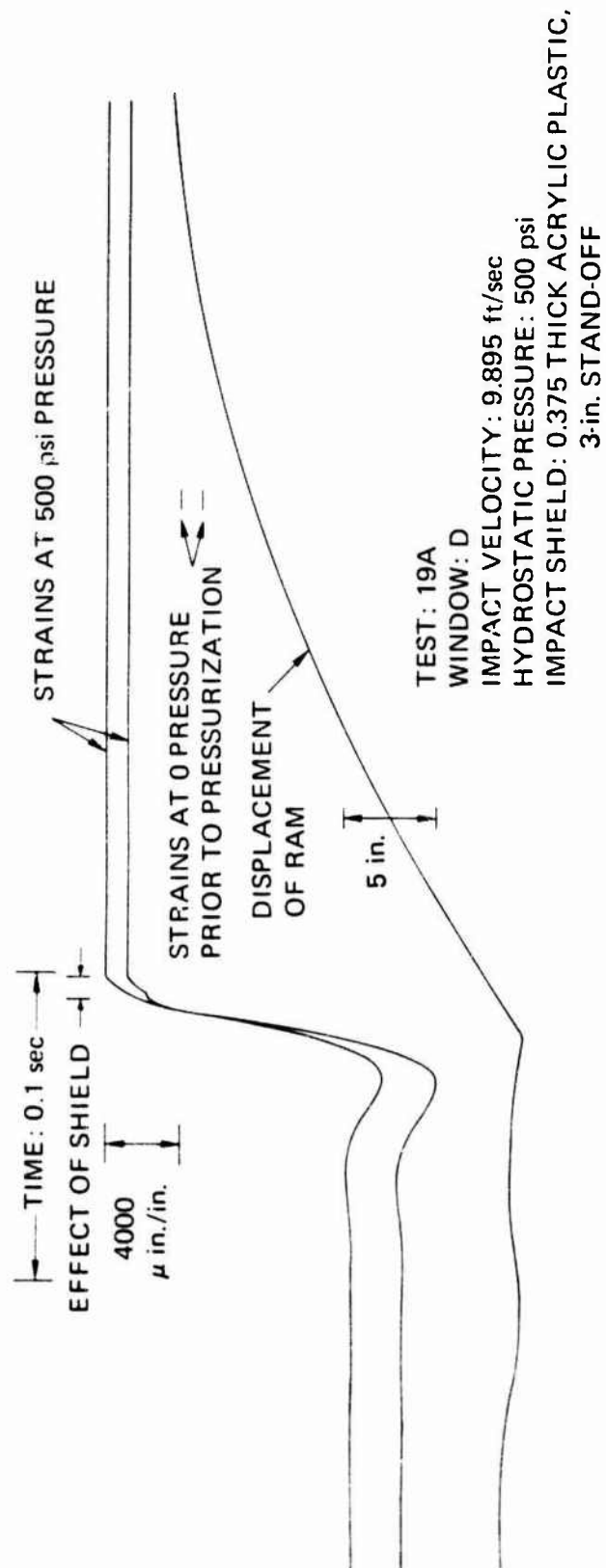


Figure 32. Dynamic strains measured with a 90° strain gage rosette on the concave side of a 2.25-inch thick window directly under the point of impact with 9.895 feet/second velocity in a 500 psi ambient environment; this window was protected with a 0.375-inch thick acrylic shield at 2-inch standoff.

TEST SPECIMEN: ACRYLIC PLASTIC SPHERICAL SHELLS

20.0 in. INSIDE RADIUS

24.0 in. OUTSIDE RADIUS

117° INCLUDED SPHERICAL ANGLE

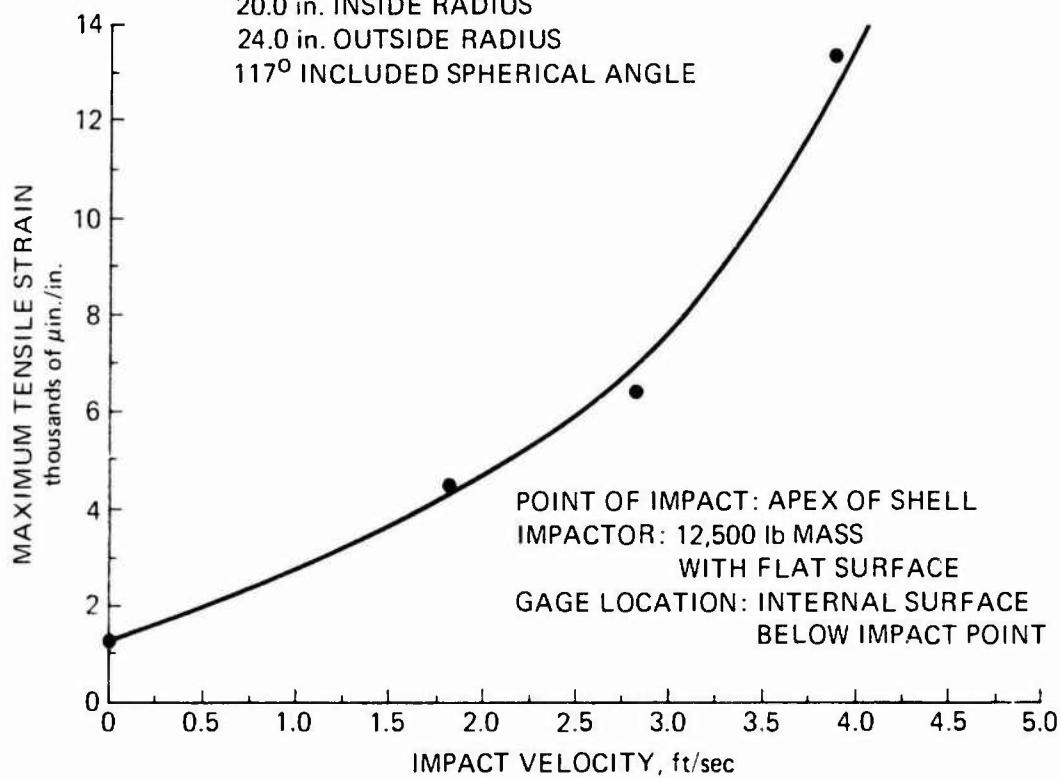


Figure 33. Dynamic tensile strains generated on the concave side of the 4.0-inch thick windows directly under the point of impact with 12,500 pound ram.

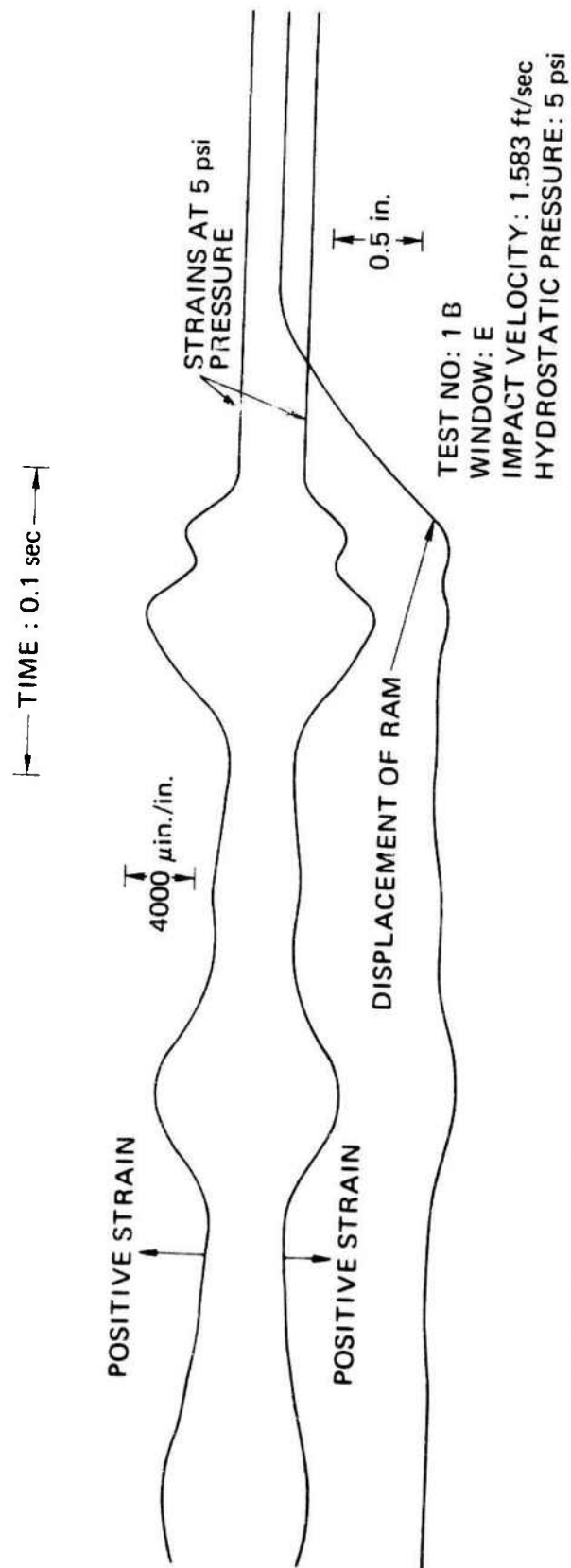


Figure 34a. Dynamic strains measured with a 90° strain gage rosette on the concave side of a 4.0-inch thick window directly under the point of impact with 1.583 feet/second velocity in 5 psi ambient pressure environment.

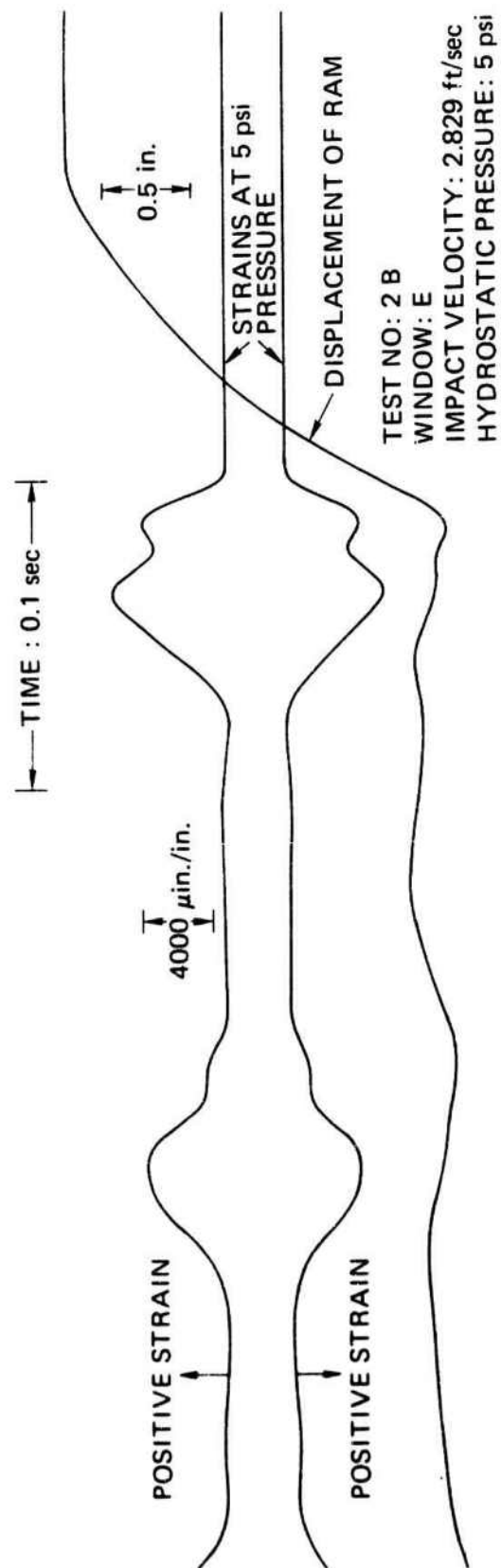


Figure 34b. Same test setup as in figure 14, but at 2.829 feet/second impact velocity.

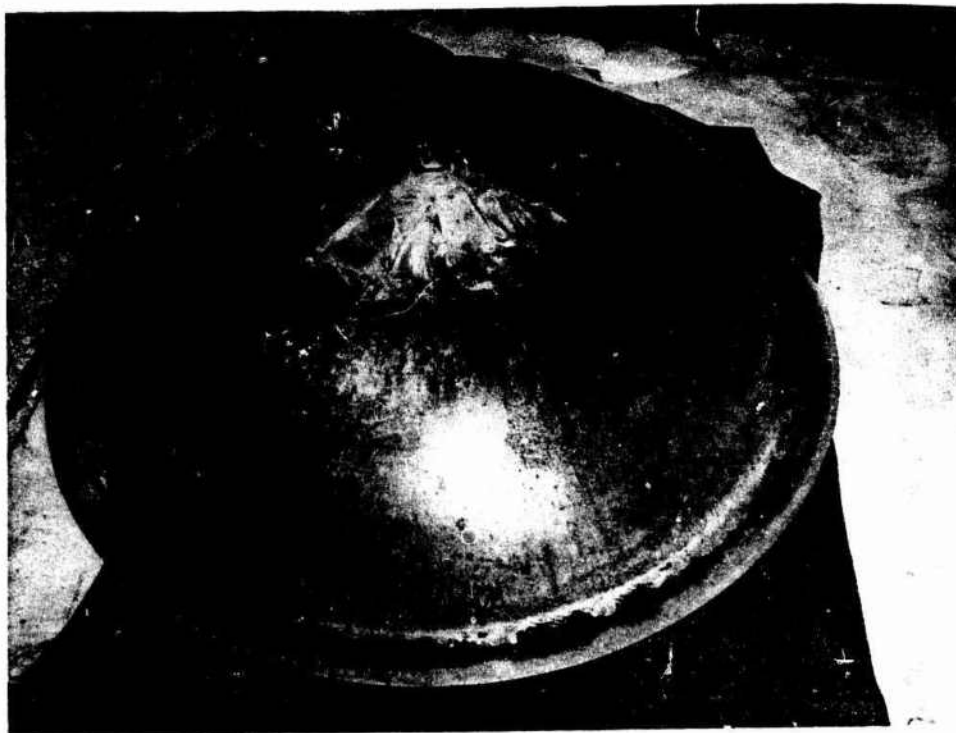


a.



b.

Figure 35. 4.0-inch thick window after 3.928 feet/second impact with the 12,500 pound ram;
 (a) Overall view, (b) Close up view.



a.

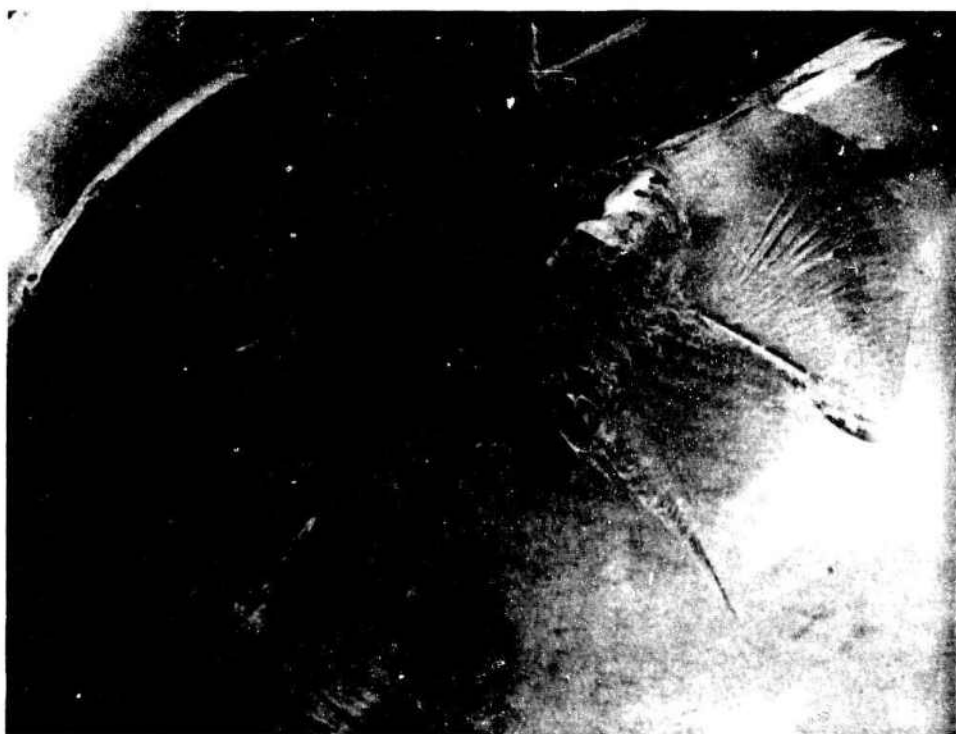


b.

Figure 36. Conical fracture plane generated in a 4.0-inch thick window by 10.702-feet/second impact velocity in 500 psi ambient pressure environment; (a) Overall view, (b) Detail view.



a.



b.

Figure 37. 4.0-inch thick window after 5,350 feet/second impact with the 12,500-pound ram.
(a) Overall view, (b) Close up view.

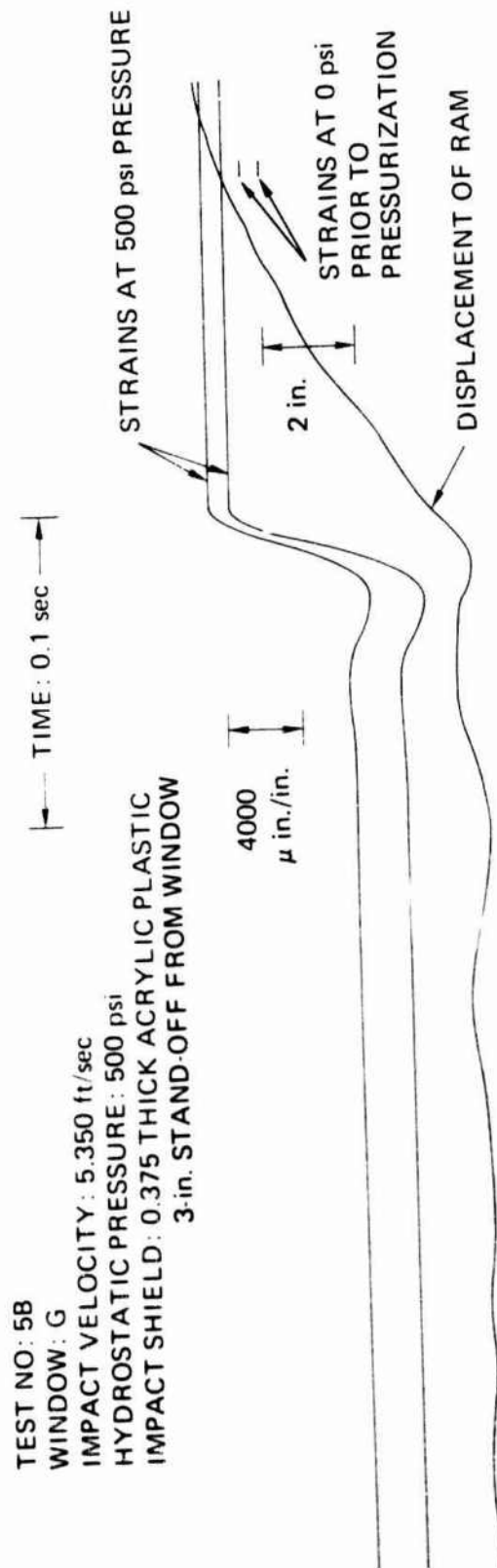


Figure 38. Dynamic strains measured with a 90° strain gage rosette on the concave side of a 2.25-inch thick window directly under the point of impact with 5,350-feet/second impact velocity in a 500 psi ambient pressure environment; this window was protected with a 0.375-inch thick acrylic shield at 2-inch standoff.

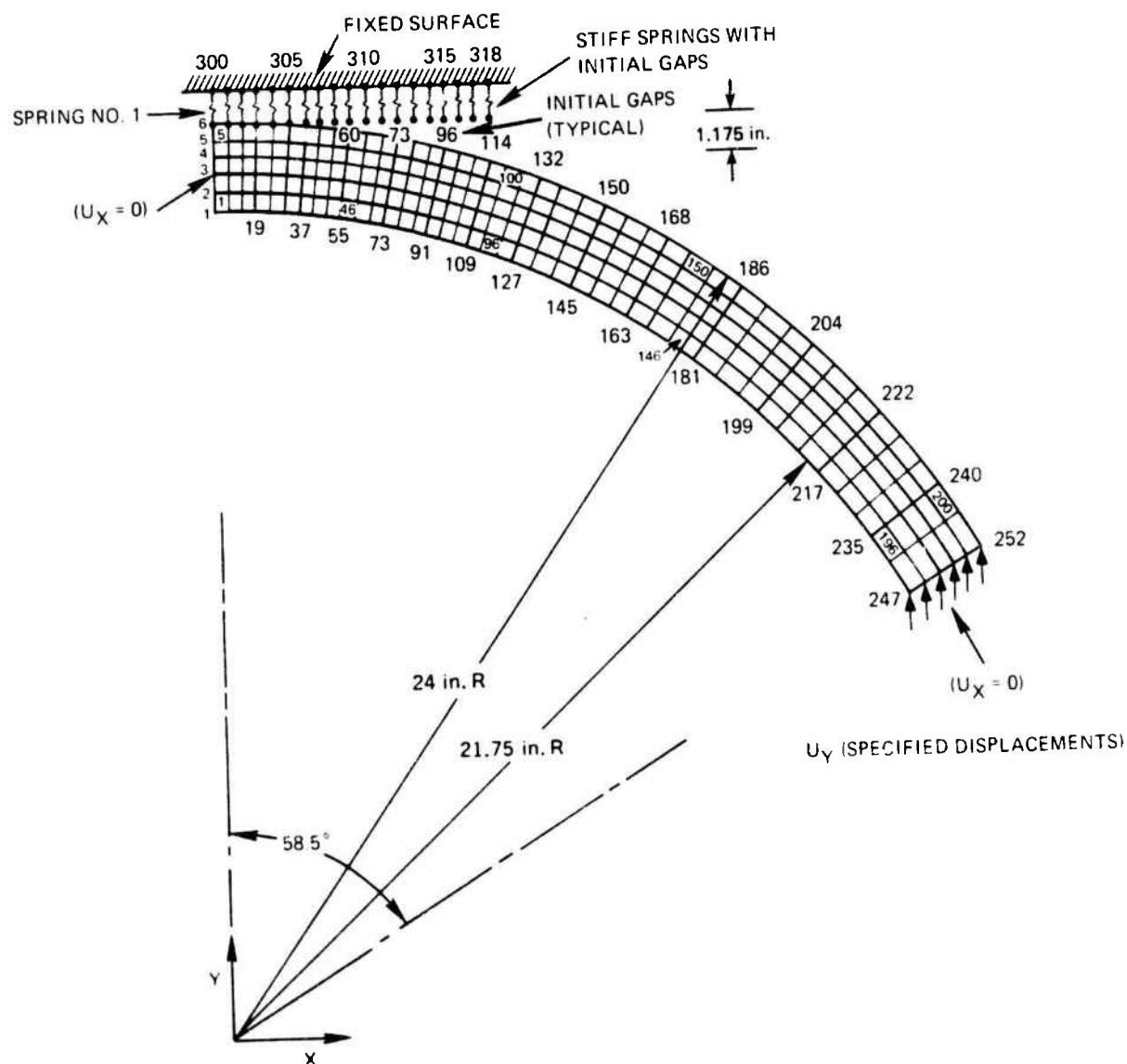


Figure 39. Finite element mesh representing a 2.25-inch thick spherical sector window with $R_0 = 24$ inches and $\alpha = 117^\circ$ impacting a rigid wall.

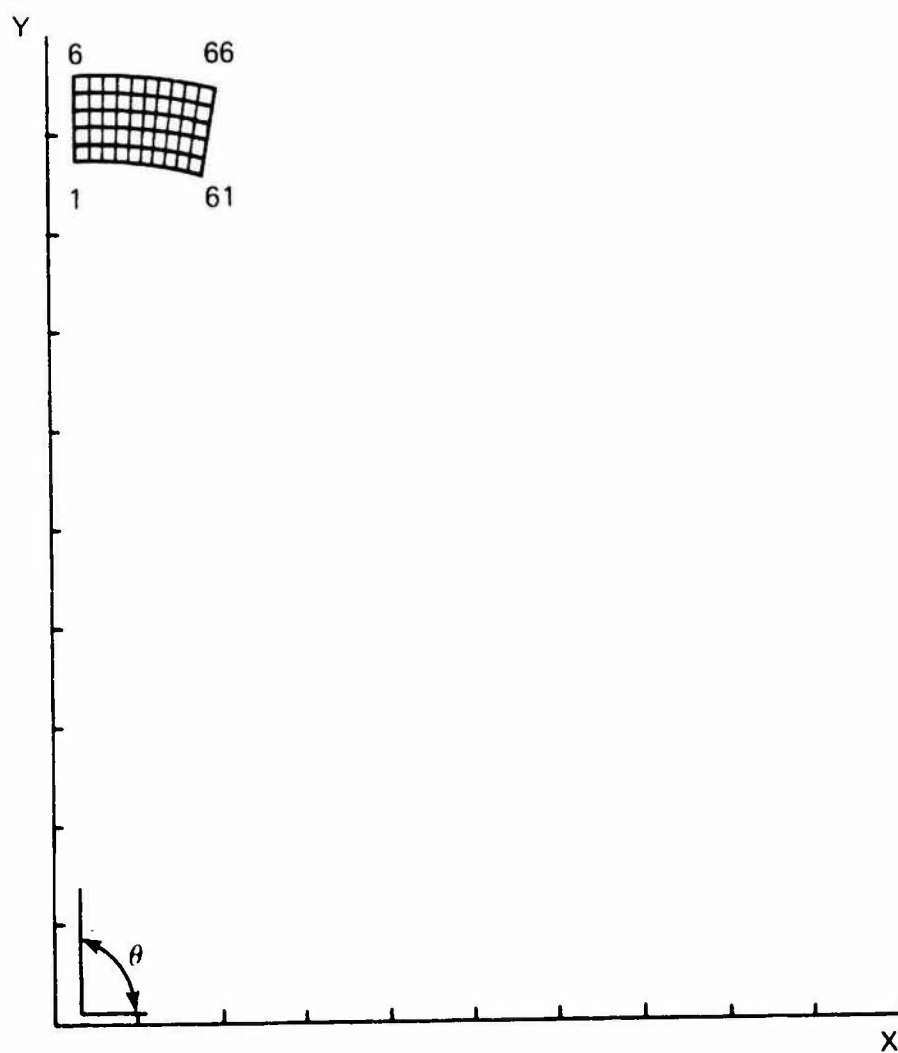
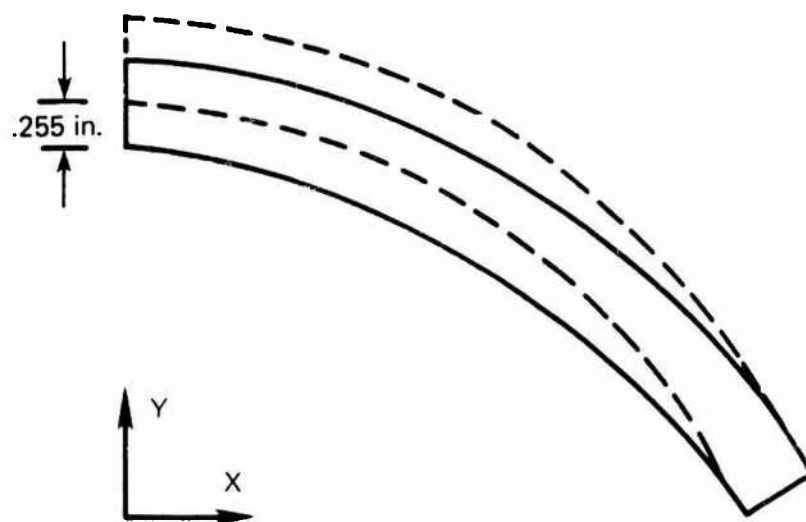


Figure 40. Finite element mesh used in the analysis of a complete sphere under external hydrostatic pressure.

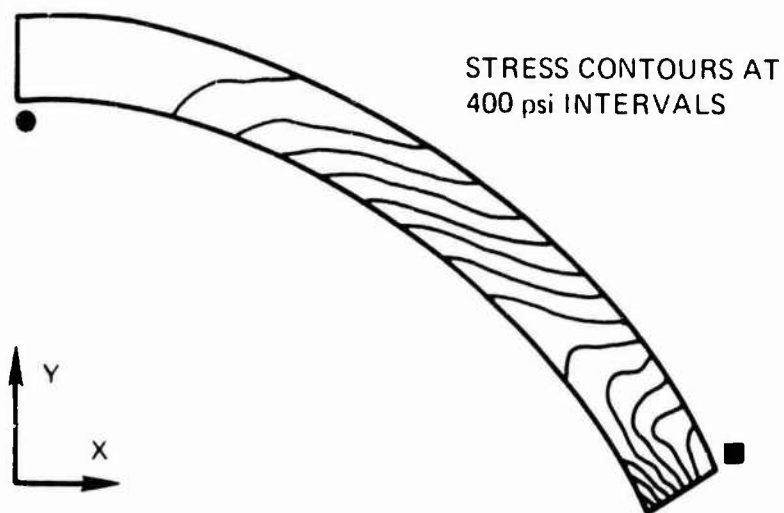


DISPLACEMENT AT 1000 psi EXTERNAL PRESSURE

Figure 41. Displacement plot of a 2.25-inch thick window under uniform 1000 psi external hydrostatic pressure.

MAX = -325 psi ■

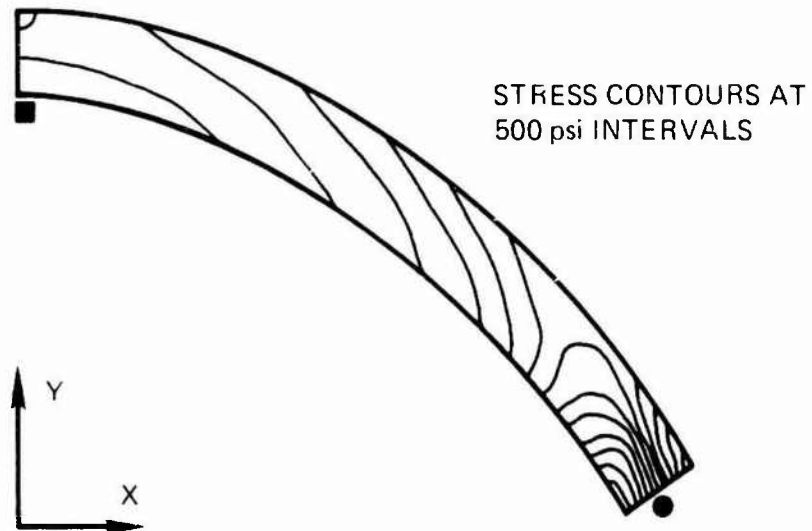
MIN = -5988 psi ●



σ_x STRESS AT 1000 psi EXTERNAL PRESSURE

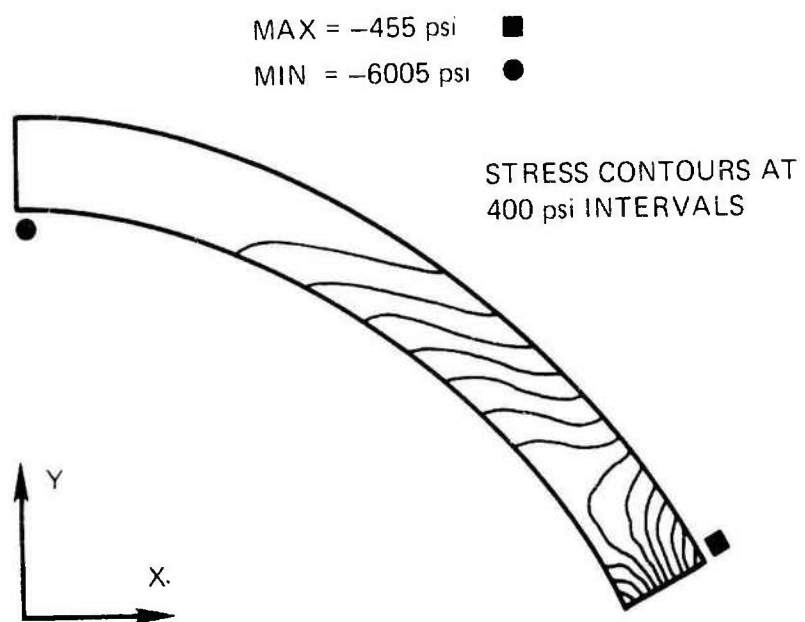
Figure 42. σ_x stress contour plot of 2.25-inch thick window under uniform external hydrostatic pressure.

MAX = -120 psi ■
MIN = -9253 psi ●



σ_y STRESS AT 1000 psi EXTERNAL PRESSURE

Figure 43. σ_y stress contour plot of 2.25-inch thick window under uniform 1000 psi external hydrostatic pressure.



HOOP STRESS AT 1000 psi EXTERNAL PRESSURE

Figure 44. σ_{Hoop} stress contour plot of 2.25-inch thick window under uniform 1000 psi external hydrostatic pressure.

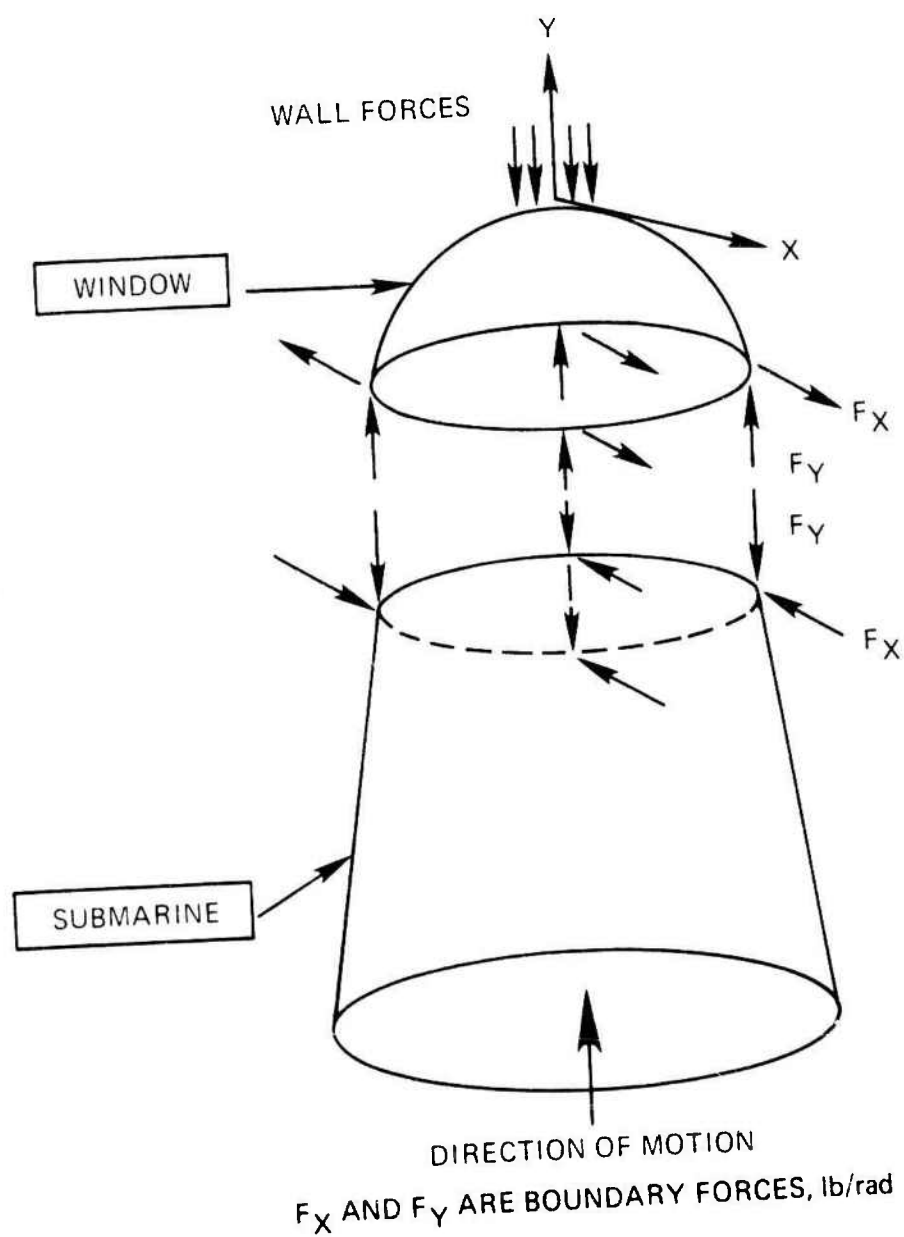


Figure 45. Free-body diagram of a spherical sector bow window in a submersible during impact.

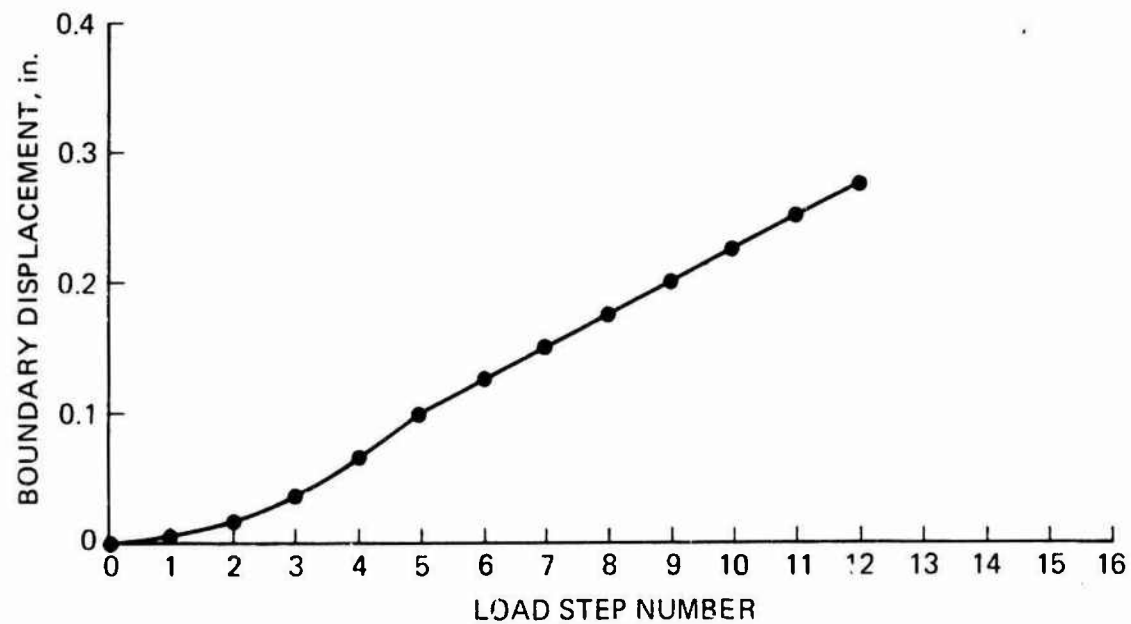


Figure 46. Window boundary (seat) displacement versus load step number.

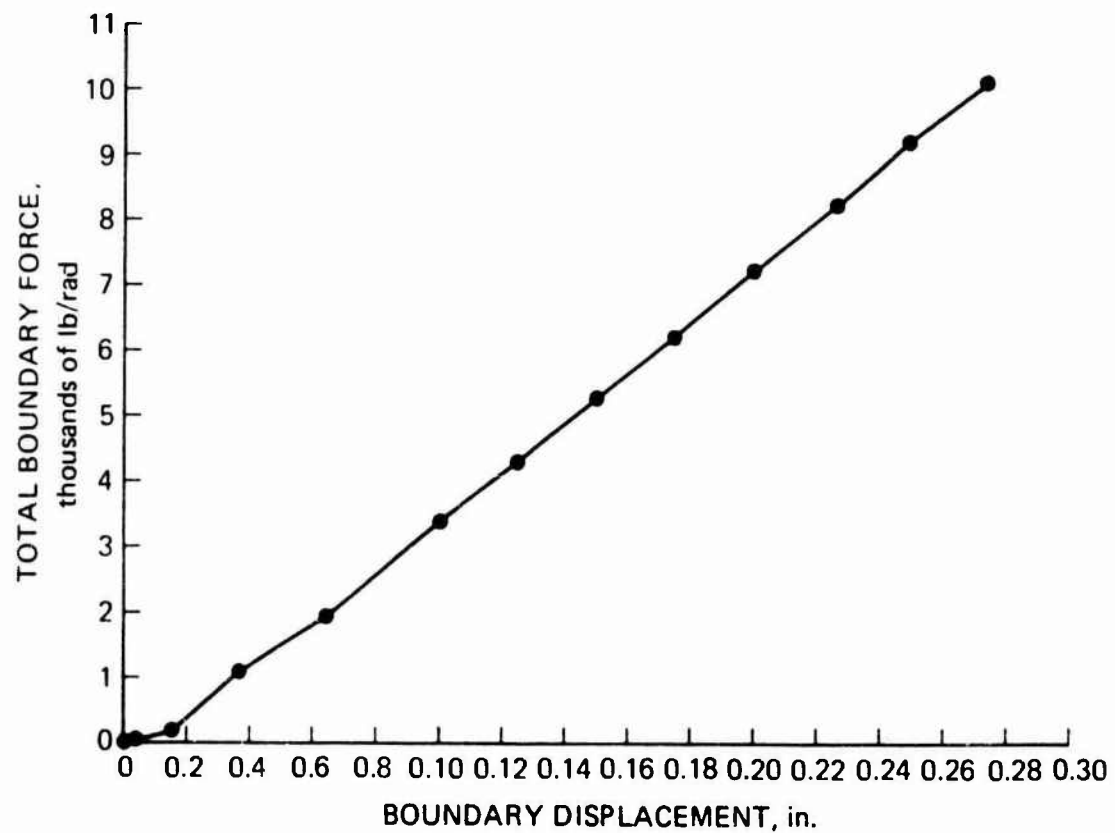
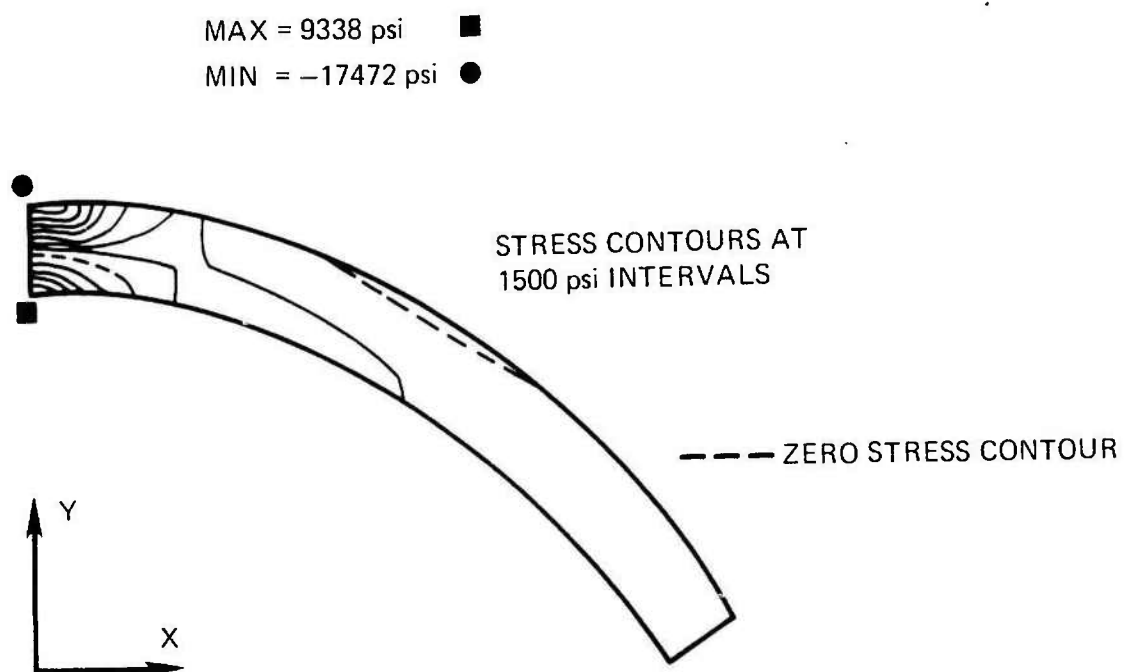
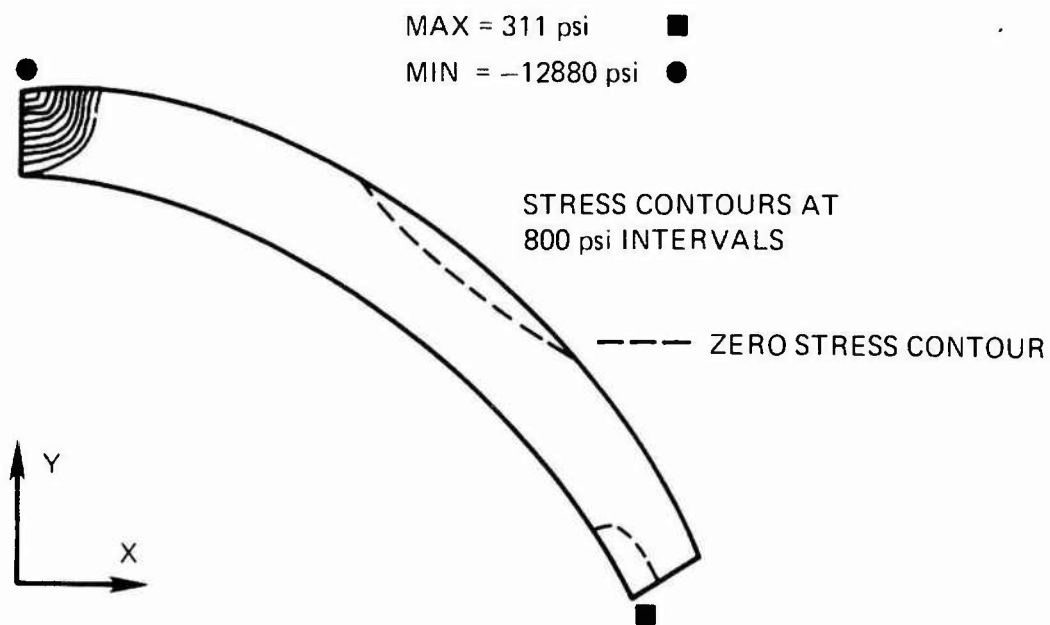


Figure 47. Total force acting on the boundary as a function of boundary displacement.



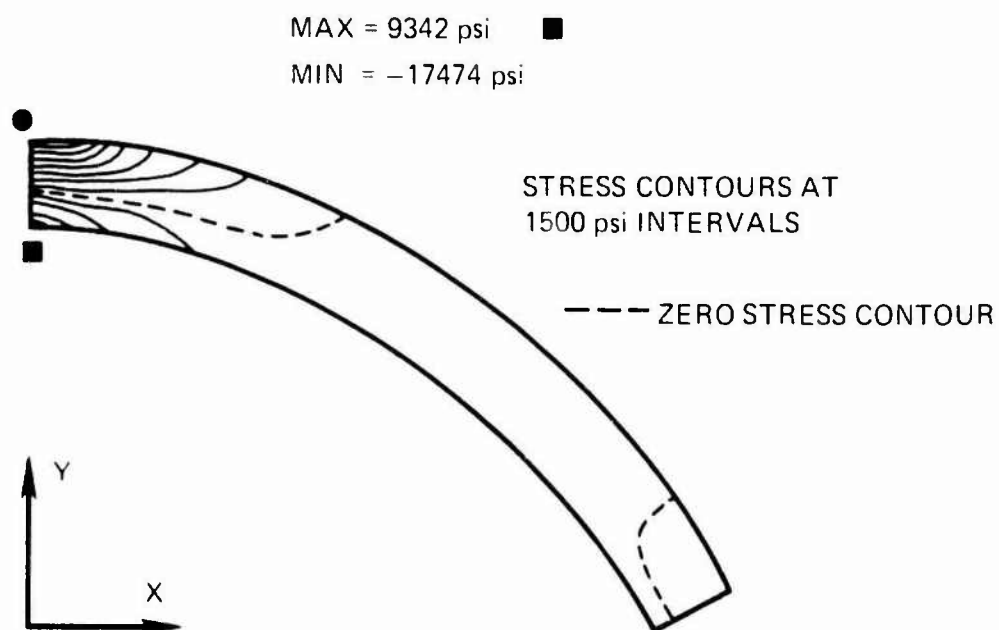
σ_x STRESS AT DISPLACEMENT STEP 12

Figure 48. σ_x stress contour plot of 2.25-inch thick window at displacement step 12 (where displacement = 0.275 inches).



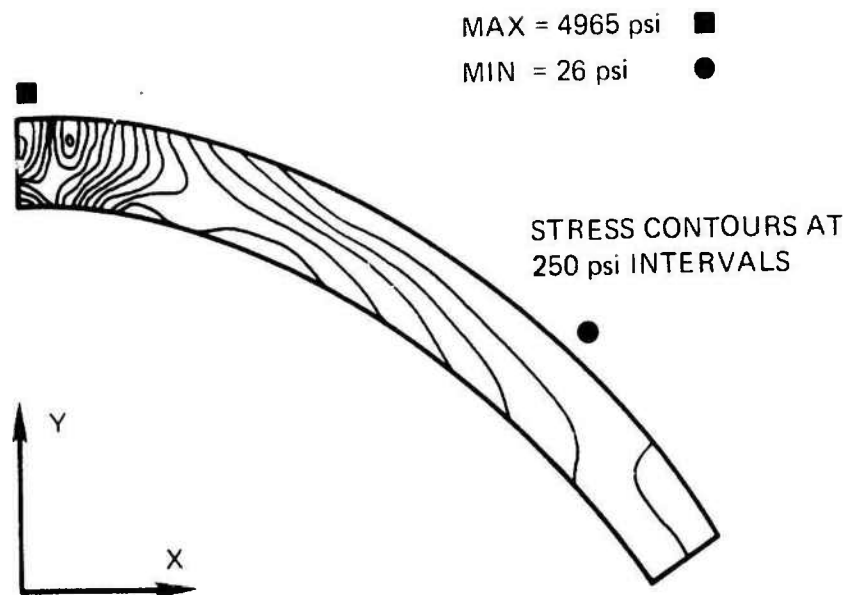
σ_Y STRESS AT DISPLACEMENT STEP 12

Figure 49. σ_Y stress contour plot of 2.25-inch thick window at displacement step 12 (0.275 inches).



HOOP STRESS AT DISPLACEMENT STEP 12

Figure 50. σ_{Hoop} stress contour plot of 2.25-inch thick window at displacement step 12 (0.275 inches).



MAXIMUM SHEAR STRESS AT DISPLACEMENT STEP 12

Figure 51. Maximum shear stress contour plot of 2.25-inch thick window at displacement step 12 (0.275 inches).

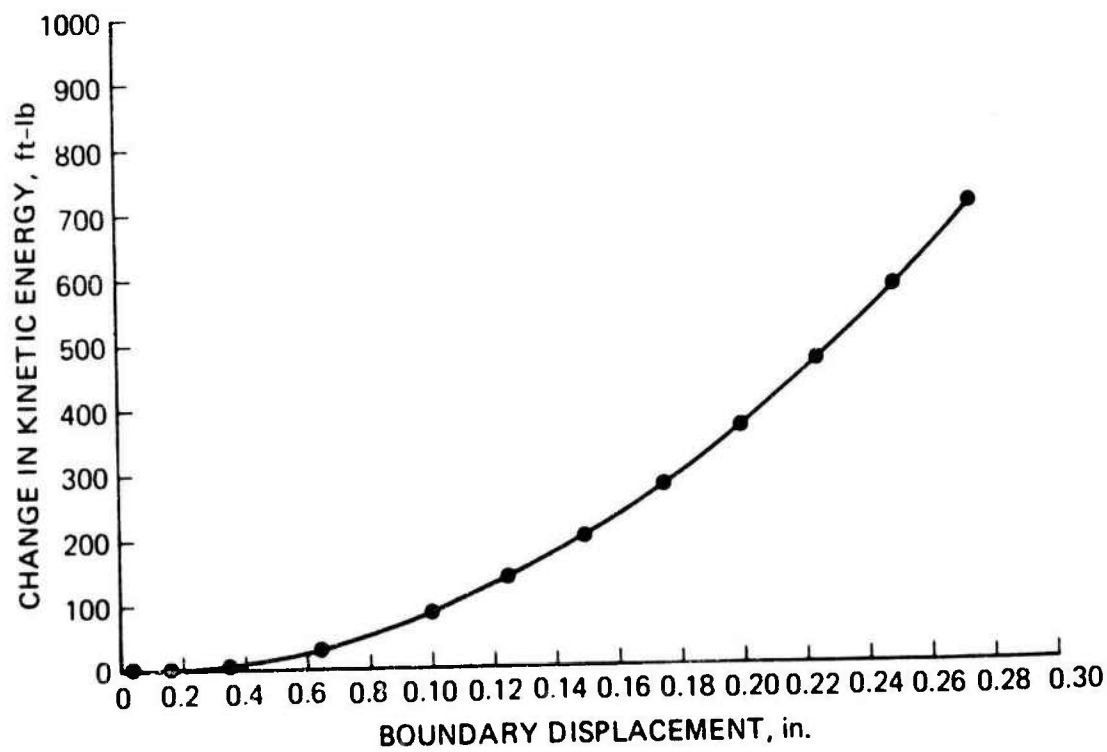


Figure 52. Change in kinetic energy of the submersible as a function of boundary displacement.

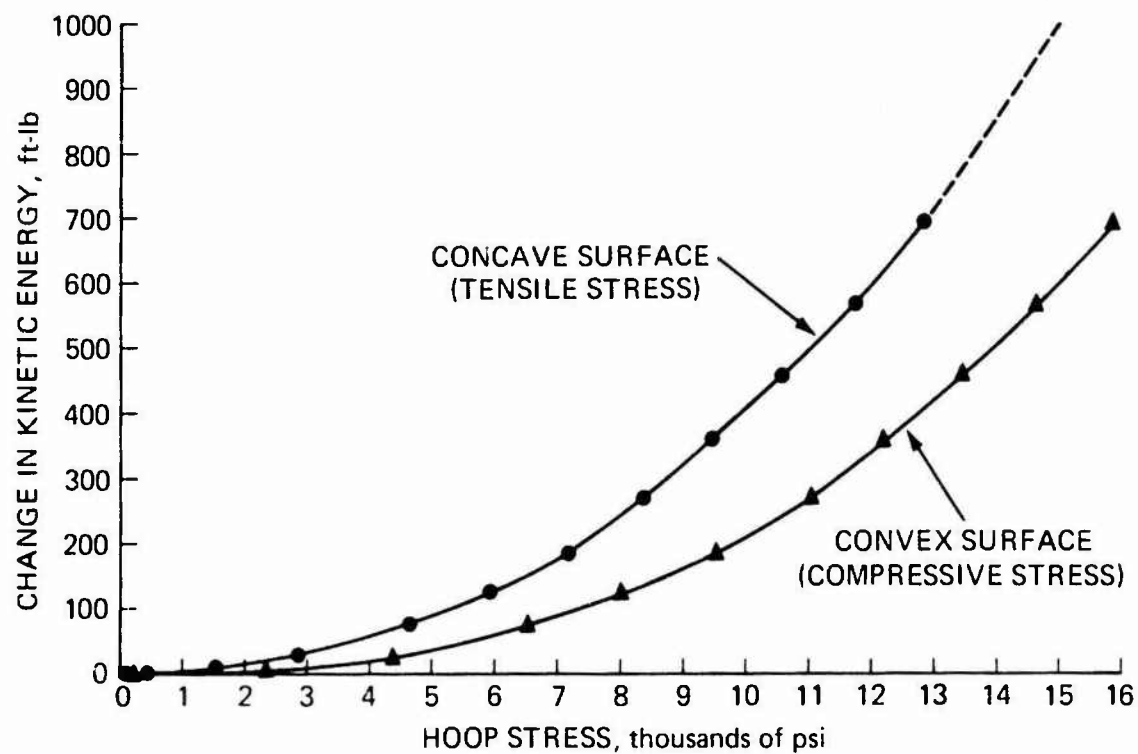


Figure 53. Hoop stresses at the apex of the 2.25-inch thick window as a function of change in kinetic energy of the submersible at impact with the rigid wall.

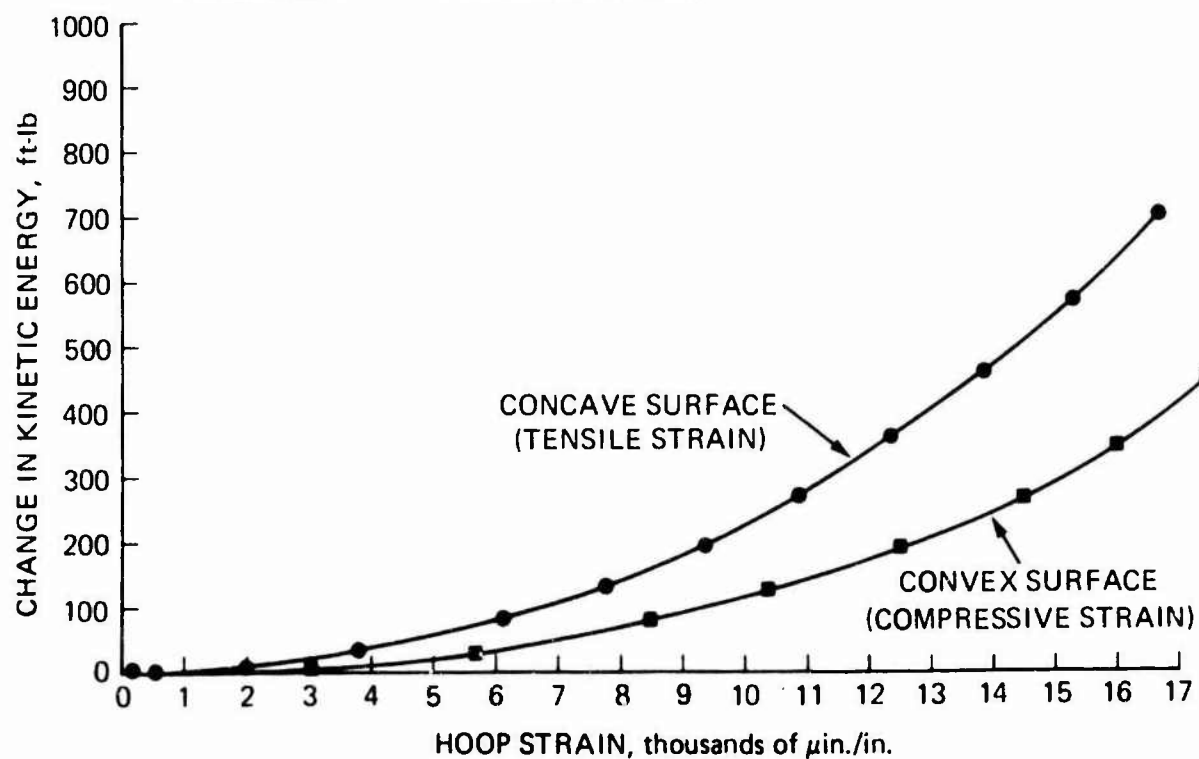


Figure 54. Hoop strains at the apex of the 2.25-inch thick window as a function of change in kinetic energy of the submersible at impact with the rigid wall.

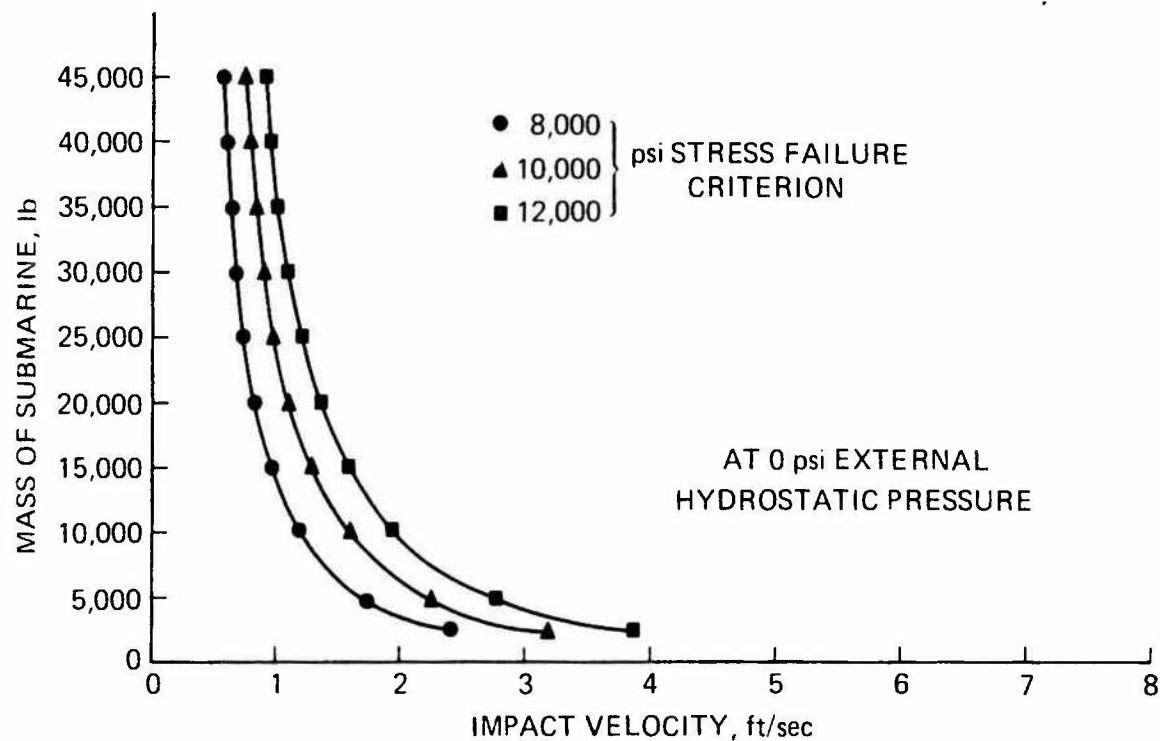


Figure 55. Critical impact velocities for 2.25-inch thick windows mounted on submersibles of different mass operating in 0 psi ambient pressure environment.

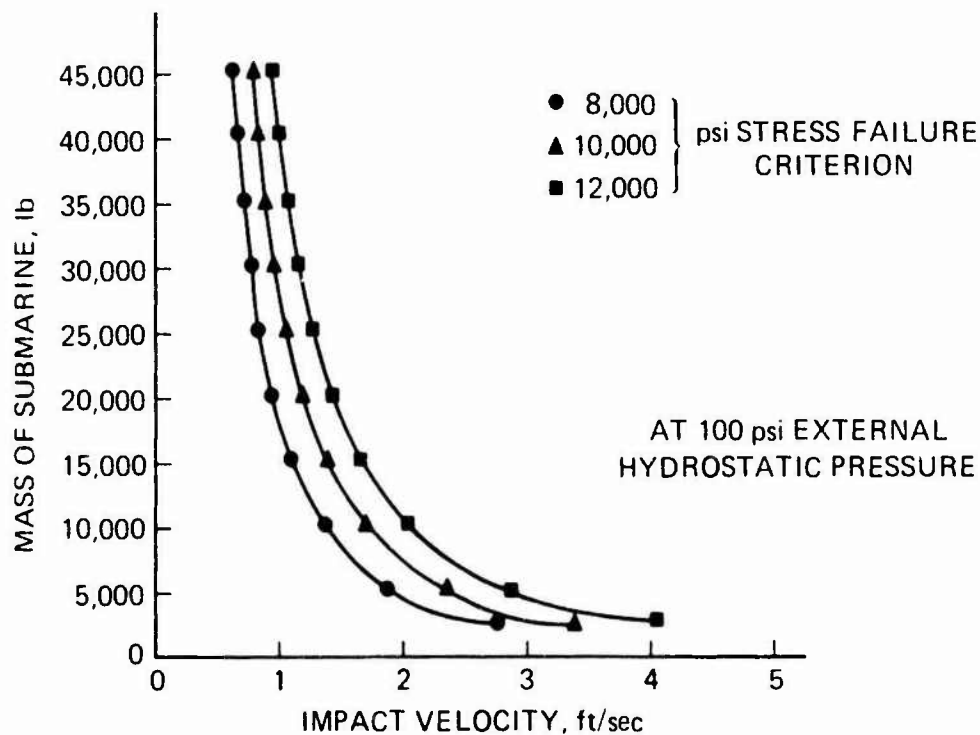


Figure 56. Critical impact velocities for 2.25-inch thick windows mounted on submersibles of different mass operating in 100 psi ambient pressure environment.

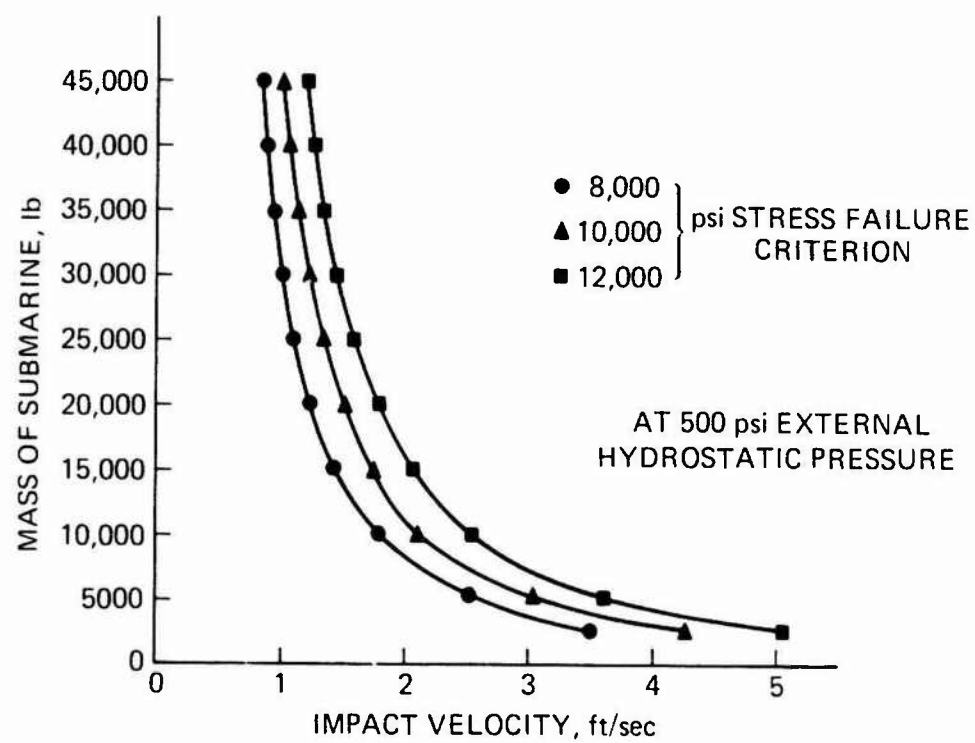


Figure 57. Critical impact velocities for 2.25-inch thick windows mounted on submersibles of different mass operating in 500 psi ambient pressure environment.



EFFECT OF BUBBLE INCLUSIONS ON THE MECHANICAL PROPERTIES OF CAST POLYMETHYL METHACRYLATE

by

J. D. Stachiw

Ocean Technology Department

August 1972



Approved for public release, distribution unlimited



NAVAL UNDERSEA CENTER, SAN DIEGO, CA. 92132

AN ACTIVITY OF THE NAVAL MATERIAL COMMAND

CHARLES B. BISHOP, Capt., USN

Commander

Wm. B. McLEAN, Ph.D.

Technical Director

ADMINISTRATIVE STATEMENT

This report summarizes work performed between January 1971 and January 1972 and related to the investigation of transparent structural materials for undersea application. The work was supported by the Director of Naval Laboratories through the Independent Exploratory Development Program.

Released by
H. R. TALKINGTON, Head
Ocean Technology Department

ACKNOWLEDGMENTS

The author is indebted to Mr. G. Devries for performing the material tests and to Mr. R. Krenik for photographing the test specimens.

SUMMARY

PROBLEM

Bubbles are often present in acrylic plastic castings purchased from commercial sources. Since they may lower the mechanical strength of the finished product machined from such a casting, it is necessary to define quantitatively their effect on mechanical properties.

RESULTS

The effect of bubbles on the mechanical properties of acrylic plastic was evaluated by testing of 120 specimens machined from castings with bubble inclusions. The specimens were tested under both uniaxial tension and compression.

The stress raiser effect of bubble inclusions caused the tensile specimens to fail at stress levels 7 to 30 percent lower than observed in control specimens without bubbles. The stresses at which yielding under uniaxial compression took place were found to be, however, the same as in control specimens without bubbles.

RECOMMENDATIONS

The allowable nominal tensile working stress in acrylic plastic with bubble inclusions should be 50 percent less than is generally allowed in acrylic plastic without bubbles.

The allowable nominal compressive working stress in acrylic plastic with bubble inclusions should be the same as in bubble-free acrylic plastic.

CONTENTS

INTRODUCTION	page 1
DISCUSSION	1
EXPERIMENTAL PROCEDURES	3
TEST OBSERVATIONS	5
Tensile Tests	5
Compressive Tests	5
CONCLUSIONS	7
RECOMMENDATIONS	10
REFERENCES	10

INTRODUCTION

The successful launching and certification for manned dives of acrylic plastic submersibles — NEMO by the Naval Civil Engineering Laboratory, *Johnson-Sea-Link* by the Smithsonian Institution, and MAKAKAI by the Naval Undersea Research and Development Center — have proven that acrylic plastic is a reliable structural material for fabrication of submersible hulls. Its low cost and optical transparency make it ideal for pressure-resistant hulls on any manned submersible operating in the 0- to 3000-foot depth range.

Although the mechanical properties of acrylic plastic are well known and described by Federal and ASTM material specifications, very little is known about its structural behavior when bubbles are present in it. Such bubbles are usually generated during casting or subsequent curing. When they are observed, the question of their stress raiser effect invariably arises. If the magnitude of this effect were known, the reduced ability of plastic with bubble inclusions to withstand stresses would be taken into consideration and the depth rating of an acrylic pressure hull fabricated from such plastic reduced accordingly. The current alternative to this approach is to reject any acrylic casting in which bubbles are present. This makes the procurement of massive acrylic plastic castings for ocean engineering applications a very costly process.

To alleviate the lack of this kind of data, a low-effort study was undertaken at the Naval Undersea Research and Development Center. The objective of the study was to provide some quantitative data on the ability of acrylic plastic to carry tensile and compressive stresses in the presence of stress raisers in the form of bubble inclusions. The experimental study was conducted on compressive and tensile test specimens machined from massive acrylic castings with a large quantity of bubbles. Specimens without any bubbles served as test controls.

DISCUSSION

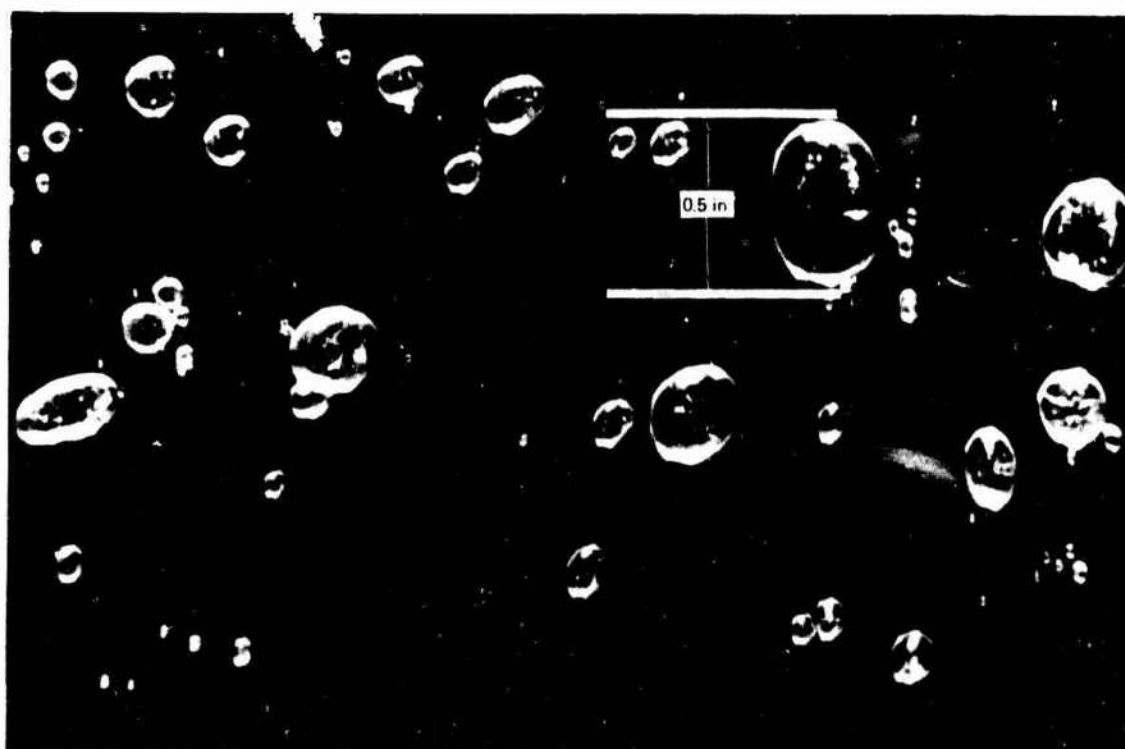
Bubbles can be found in almost any acrylic product when the process control has been less than perfect. Thus, one can find bubbles in cast sheets, massive custom castings, or cast joints in fabricated structures bonded together from many cast acrylic structural elements.

When bubbles are discovered in a piece of acrylic plastic, it is generally rejected because their presence is neither esthetically nor structurally beneficial. However, in cases involving large custom castings or complex fabricated structures, this either involves a severe economic penalty or makes the accomplishment of the technical objective impossible. Such is the case for (1) massive hemispherical castings used as pressure-resistant submersible windows and (2) cast-in-place joints bonding structural elements of acrylic pressure hulls for submersibles like NEMO, *Johnson-Sea-Link*, and MAKAKAI.

The presence of bubbles in the cast-in-place joints between individual spherical shell pentagons for NEMO-type modular hulls presented a difficult problem. (References 1–5.) Regardless of what precautions and casting procedures were used, some bubbles were found to be present in the cast acrylic plastic joints (Figure 1). Rejection of all hulls with imperfect joints would in effect have cancelled the program for building of transparent plastic



a. Overall view of typical joint.



b. Enlargement of joint section.

Figure 1. Typical bubbles in cast PS-18 joints on NEMO-type acrylic plastic hull.

submersibles, for no NEMO-type hull built to date has been found to have completely bubble-free cast-in-place joints.

Thus, early in the NEMO hull construction program, it was decided to accept cast joints with bubbles, providing the bubbles were small and few in number. This decision was considered to be acceptable from the safety viewpoint because (1) the stress levels in the hull at maximum depth were only at 15 percent of yield strength and (2) the cyclic fatigue cracks always originated at the hatch-hull interface rather than at bubbles in the bonded joint.

This, however, still did not answer the question at which compressive or tensile stress loading the bubbles would act as initiators of cracks. Without this information the working stress could not be raised above the level equal to 15 percent of yield strength, and thus, by the same token, the capability of the acrylic hulls would be always limited to continental shelf depths.

It was hoped that, by performing an exploratory experimental study on this subject, sufficient information would be generated to give a quantitative value to the stress level at which cracks begin to radiate from bubbles. Knowing the stress level at which this occurs, the design engineer would be able to specify a working stress for the hull that maximized its operational depth without initiation of cracks.

EXPERIMENTAL PROCEDURES

The effect of bubbles on the mechanical strength of cast acrylic plastic was experimentally studied by uniaxially testing acrylic specimens machined from massive castings with bubble inclusions. Since the relationship between the size of the test specimen and the bubbles could be an additional variable amplifying the effect of bubble size on machined strength, several sizes of test specimens were utilized in the study. In this manner the effect of bubbles on the strength of small test specimens could be compared to the effect of bubbles on the strength of large specimens. If no difference between these effects was found, the size of test specimens would be considered insignificant. Specimens without bubbles served as controls. They were cut from the same massive castings as were the specimens with bubbles.

For uniaxial compression testing the specimens had a constant length-to-diameter ratio of two, and the diameters were 0.50, 1.00, 2.00, and 4.00 inches. Some test specimens contained bubbles that penetrated their surface, while in other cases all of the bubbles were located in the interior of the test specimen (Figure 2).

For uniaxial tension testing the specimens had the following dimensions: 0.25-inch outside diameter by 2.0-inch length, 0.500-inch outside diameter by 5.0-inch length, and 1.00-inch outside diameter by 5.0-inch length. The location of the bubbles varied (Figure 3) as in the compressive specimens: In some cases all were contained in the interior of the specimen, while in others they penetrated the exterior surface. Each specimen had adequate extensions on the ends to permit secure gripping in the test machine.

The tensile specimens were loaded at a rate of approximately 1000 to 2000 psi per minute till failure took place. Compressive specimens were loaded at approximately the same rate till yielding took place or cracks appeared at the bubbles.

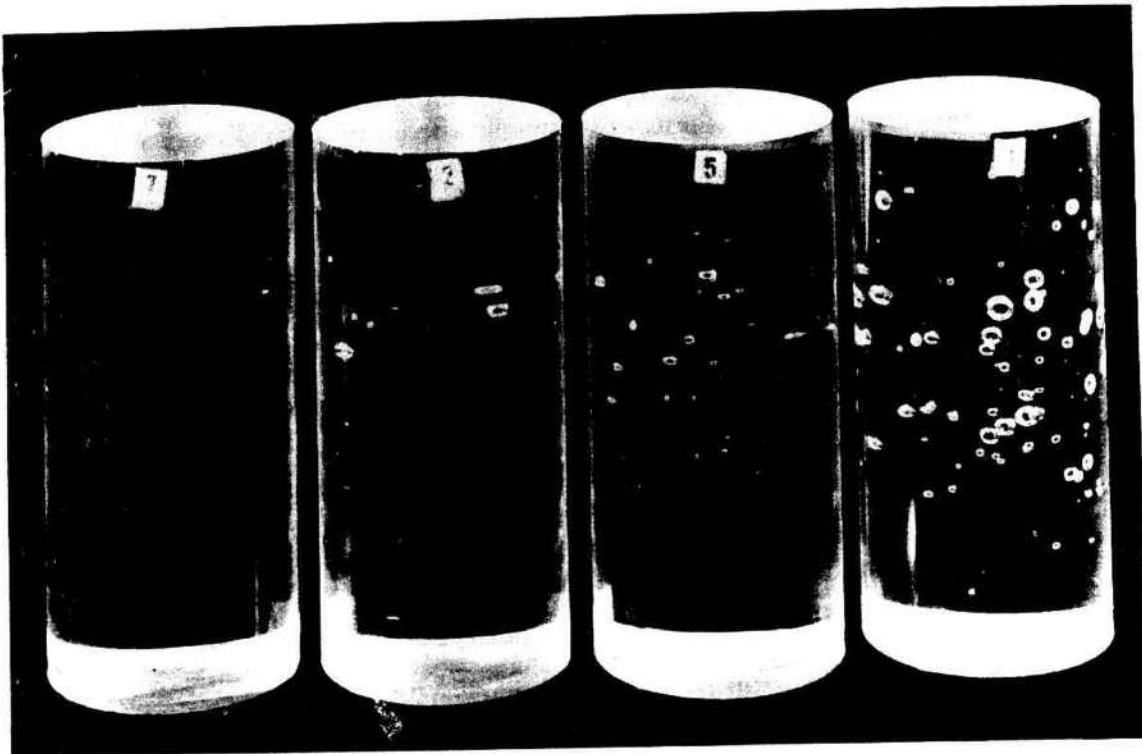


Figure 2. Compressive specimens machined from massive acrylic plastic casting containing bubbles; 2.000 inches in diameter by 4.000 inches long.

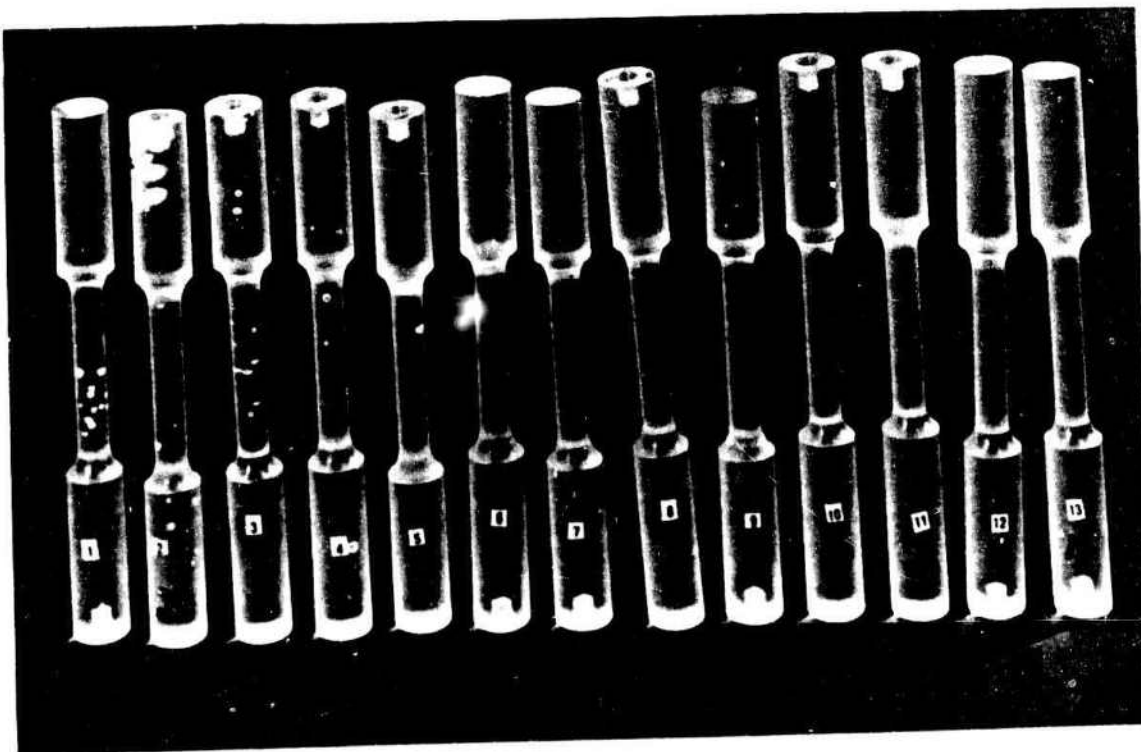


Figure 3. Tensile specimens machined from the same massive acrylic plastic casting; 0.500 inch in diameter by 5.000 inches long.

TEST OBSERVATIONS

TENSILE TESTS

Review of the experimental data indicates that the presence of bubbles decreased the tensile strength of acrylic plastic significantly. Furthermore, the decrease in strength was related to the number of bubbles in the test specimen. This can be readily seen by comparing average tensile strength values for test specimens categorized according to the number of bubbles they contained.

<u>Number of Bubbles in Specimen</u>	<u>Average Tensile Strength</u>
None	9154 psi
1	8515 psi
2	7695 psi
4-6	7453 psi
9-20	6420 psi

The location of bubbles (interior or exterior of specimen) appeared to have little influence on the stress level at which failure took place (Figure 4). Similarly no correlation was found between the size of the bubbles and the tensile strength so long as the bubbles ranged between 0.1 and 4.5 millimeters (0.004 and 0.18 inch). There appeared also to be no correlation between the tensile strength and the size of test specimen.

COMPRESSIVE TESTS

No significant correlation was found between the presence of bubbles and the compressive yield strength of acrylic plastic. The average strength was 10,072 psi for specimens without and 10,160 psi for specimens with bubbles. Thus it appears that bubbles have no effect on compressive yield strength, providing their total volume is less than 1 percent of the test specimen volume.

Although bubbles appeared to have no effect on the yield strength of the acrylic plastic (in less than 1 percent by volume concentration), they served as crack initiators when the uniaxial compression strain was in excess of 5 percent. The fracture planes always were oriented in the direction of the applied load and originated at the poles of bubbles in line with the load application axis (Figure 5). If the test specimens were compressed in excess of 10 percent, visually noticeable distortion of the bubbles took place. The originally spherical bubbles were transformed into slightly squashed spheroids (Figure 6).

The compressive strength of the massive castings from which the tensile and compressive test specimens were machined was somewhat less than for the Plexiglas G acrylic plastic sheets used for the fabrication of NEMO hulls (10,000 vs. 15,000 psi). If submersible hulls were to be machined from massive acrylic castings with lesser mechanical properties than Plexiglas G, the operational depth of such hulls would have to be reduced accordingly. The reasons the massive castings had a reduced compressive yield strength are not known.

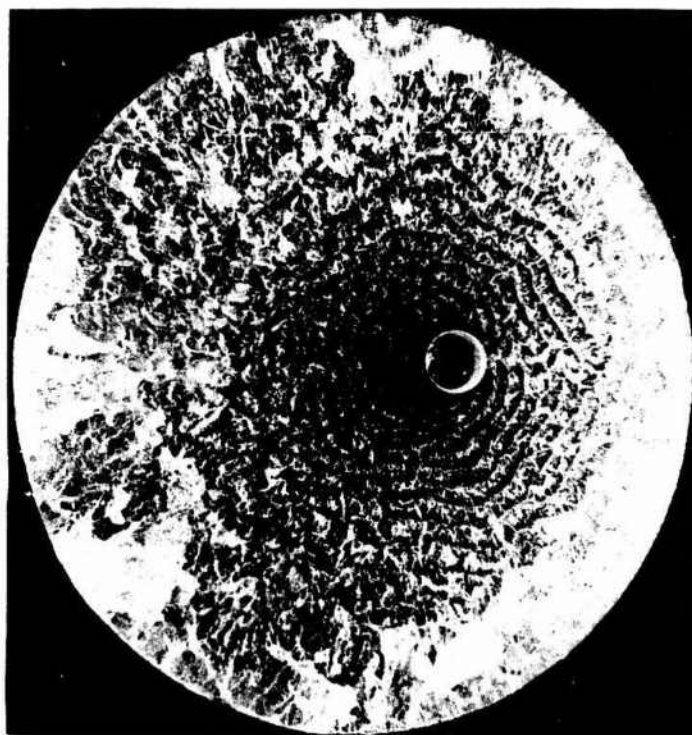


Figure 4. Typical fracture initiated by bubble in specimen under uniaxial tensile loading; test specimen diameter, 0.500 inch.

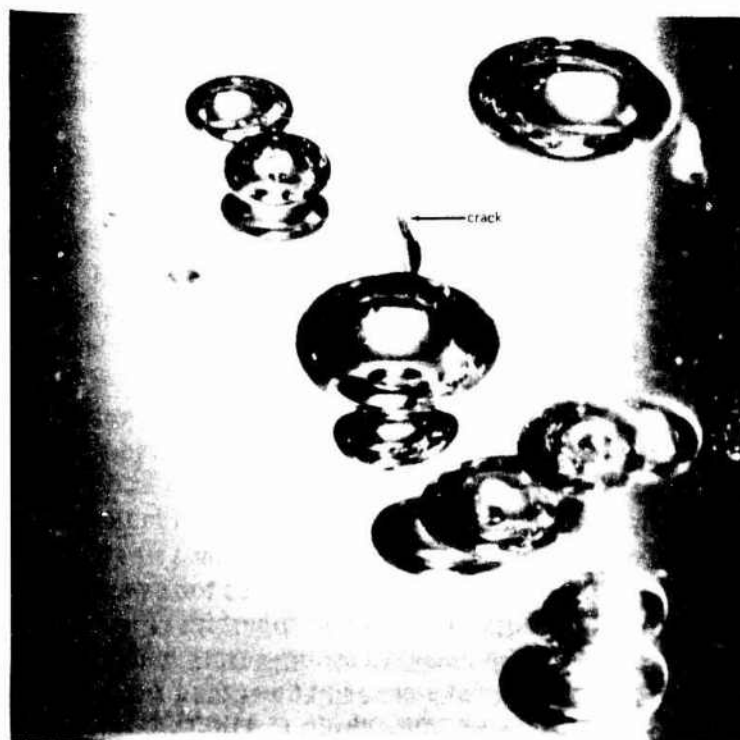


Figure 5. Typical fracture initiated by bubble in specimen under uniaxial compressive loading; the 0.200-inch-diameter bubble is located in a 2.000-inch-diameter specimen.

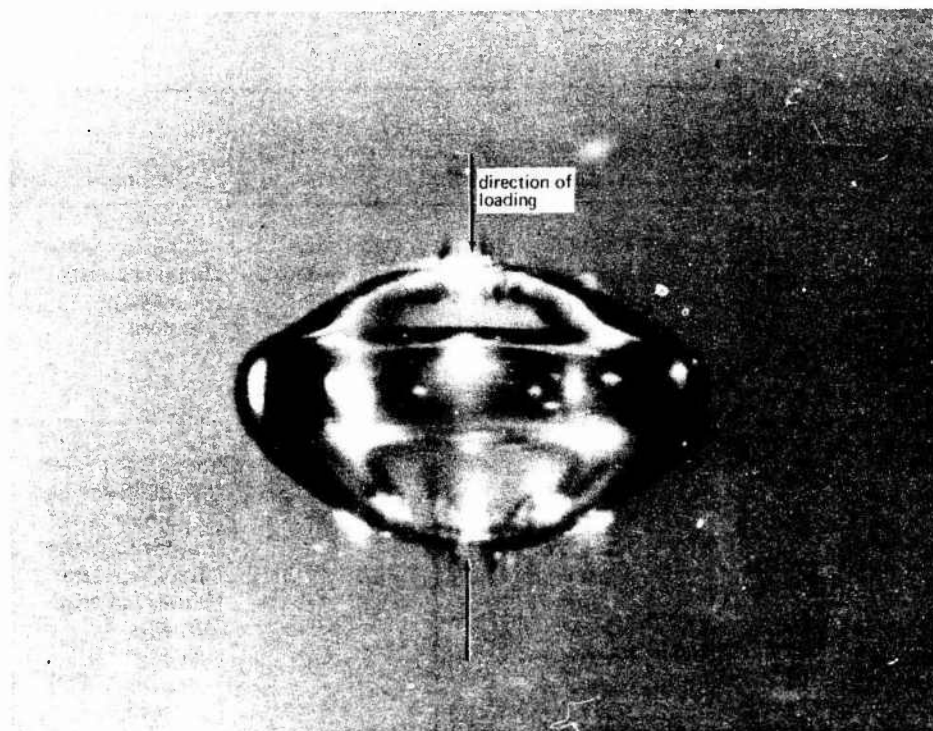


Figure 6. Typical spherical bubble in a specimen that has been subjected to approximately 10-percent uniaxial compressive strain; the 0.100-inch-diameter bubble is located in a 2.000-inch-diameter specimen.

CONCLUSIONS

The presence of bubbles in a massive acrylic plastic casting reduces significantly the ability of parts machined from the casting to carry tensile stresses. As a result the nominal working tensile stress of such parts should be lower than when a casting without bubbles is used.

Bubble inclusions do not affect the nominal compressive yield strength of acrylic plastic. However, they act as fracture sources when the plastic is uniaxially compressed more than 5 percent. Thus the magnitude of the nominal working compressive stress in castings with bubbles can be the same as in castings without bubbles. The magnitude of the peak working stress around stress raisers must be, however, lower than for bubble-free castings.

Table 1. Ultimate Tensile Strength of Specimens Machined from Massive Acrylic Plastic Castings.

Specimen	Diameter (in.)	Total Number of Bubbles	Number of Bubbles in Fracture Plane	Size of Bubbles in Fracture Plane (mm)	Initiation of Failure*	Ultimate Stress (psi)
1	0.25	1	1 inside	0.1 or less	Bubble in center	10200
2	0.25	1	1 at edge	0.1 or less	Bubble at edge	9200
3	0.25	0	None	—	At edge	10400
4	0.25	0	None	—	At edge	10000
5	0.25	0	None	—	At edge	9200
6	0.25	0	None	—	At edge	10000
7	0.25	0	None	—	At edge	9200
8	0.50	14	1 inside, 1 at edge	1.2; 3.2	L bubble at edge	5310
9	0.50	4	1 inside, 1 at edge	2.7; 1.8	L bubble at edge	6800
10	0.50	8	2 inside	1.6; 1.0	2 bubbles at edge	6820
11	0.50	2	1 inside	3.2	L bubble inside	6550
12	0.50	4	1 at edge	2.2	S bubble at edge	6300
13	0.50	1	1 inside	2.4	Bubble at edge	6300
14	0.50	1	1 inside	1.8	Bubble at edge	6350
15	0.50	0	None	—	At edge	7850
16	0.50	0	None	—	At edge	8250
17	0.50	0	None	—	At edge	8200
18	0.50	0	None	—	At edge	8210
19	0.50	0	None	—	In center	11000
20	0.50	1	1 inside	0.1	Bubble center	9200
21	0.50	1	None	—	At edge	8750
22	0.50	4	2 inside	2; 1.5	2 M bubbles at edge	7100
23	0.50	0	None	—	At edge	10250
24	0.50	5	1 inside	1.0	S bubble 1/4 way in	7620
25	0.50	2	None	—	At edge	7770
26	0.50	1	1 inside	0.4	At edge	7500
27	0.50	1	1 inside	1.0	Bubble at edge	7750
28	0.50	0	None	—	At edge	8200
29	0.50	1	1 inside	1.6	Bubble 2/3 way in	7670
30	0.50	4	1 inside	3.1	Bubble at edge	6950
31	0.50	0	None	—	At edge	8900
32	0.50	0	None	—	At edge	8500
33	1.00	13	1 inside	1.8	Bubble at center	7050
34	1.00	2	2 inside	3; 3.1	Bubble at edge	7850
35	1.00	14	1 inside	6.1	Bubble at edge	6050
36	1.00	10	1 inside	3.9	Bubble at edge	5850
37	1.00	5	1 inside	2.9	Bubble at edge	7700
38	1.00	2	1 inside	2.0	Bubble 1/4 way in	8050
39	1.00	0	1 inside	1.4	At edge	10200
40	1.00	20	1 inside	2.2	Bubble at center	7450
41	1.00	5	1 inside	2.6	Bubble 1/4 way in	8200
42	1.00	10	2 inside	1.0; 0.8	2 bubbles at center	6100
43	1.00	10	2 inside	3.5; 2.8	L bubbles at edge	6750
44	1.00	9	1 inside	2.0	Bubble at edge	6740
45	1.00	3	2 inside	3.8; 2.5	Bubble 1/4 way in	7250
46	1.00	6	2 at edge	4.5; 4.5	Bubble at edge	7300
47	1.00	5	1 inside	1.6	Bubble at edge	7500
48	1.00	3	1 inside	0.6	Bubble 2/3 way in	7300
49	1.00	4	1 at edge	0.1; 0.2	Bubble at edge	7500
50	1.00	2	2 inside	2.8; 1.7	At edge	8410

*T = tiny (approx. 0.1 mm); S = small (approx. 1.5-2.5 mm); M = medium (approx. 3 mm); L = large (approx. 4-5 mm).

Table 2. Compressive Yield Strength of Specimens Machined from Massive Acrylic Plastic Castings

Specimen	Diameter (in.)	Total Number of Bubbles	Size of Bubbles*	Yield Strength (psi)
1	0.500	6	LM	8900
2	0.500	6	LM	10350
3	0.500	2	L	8600
4	0.500	1	L	8900
5	0.500	4	SM	8800
6	0.500	0	—	9950
7	0.500	0	—	10100
8	0.500	0	—	11700
9	0.500	0	—	9850
10	0.500	0	—	10100
11	0.500	1	T	9670
12	0.500	0	—	10500
13	0.500	0	—	10500
14	0.500	1	M	8900
15	0.500	0	—	10200
16	0.500	0	—	9650
17	0.500	0	—	10300
18	0.500	0	—	10200
19	1.000	0	—	10200
20	1.000	0	—	10000
21	1.000	0	—	10700
22	1.000	0	—	10950
23	1.000	0	—	9450
24	1.000	0	—	10100
25	1.000	0	—	11000
26	1.000	0	—	9700
27	1.000	0	—	10200
28	1.000	0	—	9050
29	1.000	7	M	10700
30	1.000	9	M	10850
31	1.000	11	LM	10450
32	1.000	9	SML	11450
33	1.000	10	SML	10300
34	1.000	6	LM	10250
35	1.000	10	SML	10100
36	1.000	13	ML	9650
37	1.000	7	SM	10800
38	1.000	7	ML	10100
39	1.000	41	LS	9500
40	1.000	12	LS	9600
41	1.000	12	LS	9700
42	1.000	10	LS	10150
43	1.000	12	S	10200
44	1.000	6	M	10800
45	1.000	10	LS	9700
46	1.000	6	S	10600
47	1.000	8	M	10500
48	1.000	6	M	10200
49	1.000	2	S	10700
50	1.000	13	M	9700
51	1.000	0	—	10100
52	1.000	23	M	10700
53	1.000	30	ML	9250
54	1.000	18	M	9800
55	1.000	23	M	11450
56	1.000	—	—	—
57	1.000	7	M	10200
58	1.000	6	ML	9700
59	1.000	4	T	10600
60	1.000	1	S	10500
61	2.000	34	ML	10800
62	2.000	6	ML	10800
63	2.000	3	T	12100
64	2.000	0	—	10200
65	2.000	5	T	11500
66	2.000	0	—	12400
67	2.000	0	—	12800
68	2.000	30	TSM	9500
69	4.000	105	ML	10300
70	4.000	55	ML	9800

*T = tiny (approx. 0.1 mm), S = small (approx. 1.5-2.5 mm), M = medium (approx. 3 mm); L = large (approx. 4-5 mm).

RECOMMENDATIONS

In structures fabricated from acrylic plastic castings the *allowable nominal working tensile stress* should be 50 percent less when bubbles are present than when they are absent. (In bubble-free castings, the maximum allowable working tensile stress is 1500 psi. The 6-to-1 ratio between the 9000-psi short-term tensile strength of acrylic plastic and 1500-psi working stress takes into account the effects of static and cyclic fatigue, which will cause an acrylic casting to fail in service at a stress level below 9000 psi.)

The *allowable nominal working compressive stress* in an acrylic plastic casting with bubble inclusions should be the same as in bubble-free castings, except that local peak compressive strains should not exceed 3 percent. (In bubble-free acrylic plastic castings the allowable nominal working compressive stress is 5000 psi, providing local peak compressive strains at structural discontinuities do not exceed 6 percent.)

REFERENCES

1. J. D. Stachiw, "Development of a Spherical Acrylic Plastic Pressure Hull for Hydrospace Application," Naval Civil Engineering Laboratory, Port Hueneme, Calif., Technical Report R-676, April 1970.
2. J. D. Stachiw and K. L. Mack, "The Spherical Acrylic Pressure Hull for Hydrospace Application; Part II - Experimental Stress Evaluation of Prototype NEMO Capsule," Naval Civil Engineering Laboratory, Port Hueneme, Calif., Technical Note N-1113, October 1970.
3. H. Ottsen, "The Spherical Acrylic Pressure Hull for Hydrospace Application; Part III - Comparison of Experimental and Analytical Stress Evaluations for Prototype NEMO Capsule," Naval Civil Engineering Laboratory, Port Hueneme, Calif., Technical Note N-1094, March 1970.
4. J. D. Stachiw, "The Spherical Acrylic Pressure Hull for Hydrospace Application; Part IV -Cyclic Fatigue of NEMO Capsule No. 3," Naval Civil Engineering Laboratory, Port Hueneme, Calif., Technical Note N-1134, October 1970.
5. J. R. Maison and J. D. Stachiw, "Acrylic Pressure Hull for Johnson-Sea-Link Submersible," American Society of Mechanical Engineers, Annual Winter Conference, New York, 1971, Paper 71-WA/UnT-6.

UNCLASSIFIED
Security Classification

DOCUMENT CONTROL DATA - R & D		
(Security classification of title, body of abstract and indexing annotation must be entered when the overall report is classified)		
1 ORIGINATING ACTIVITY (Corporate author) Naval Undersea Center San Diego, California 92132		2a. REPORT SECURITY CLASSIFICATION UNCLASSIFIED
		2b. GROUP
3 REPORT TITLE EFFECT OF BUBBLE INCLUSIONS ON THE MECHANICAL PROPERTIES OF CAST POLYMETHYL METHACRYLATE		
4 DESCRIPTIVE NOTES (Type of report and inclusive dates) Research and Development January 1971 through January 1972		
5 AUTHOR(S) (First name, middle initial, last name) Jerry D. Stachiw		
6 REPORT DATE July 1972	7a. TOTAL NO. OF PAGES 13	7b. NO. OF REFS 5
8a. CONTRACT OR GRANT NO Independent Research and Exploratory Development b. PROJECT NO ZR031-02-01		9a. ORIGINATOR'S REPORT NUMBER(S) NUC TP 305
c. d.		9b. OTHER REPORT NO(S) (Any other numbers that may be assigned this report)
10 DISTRIBUTION STATEMENT Approved for public release; distribution unlimited.		
11 SUPPLEMENTARY NOTES		12 SPONSORING MILITARY ACTIVITY Chief of Naval Material Washington, D. C. 20360
13 ABSTRACT Bubbles are often present in acrylic plastic castings purchased from commercial sources. Since they may lower the strength of the finished product machined from such a casting, it is necessary to define quantitatively their effect on mechanical properties. The effect of bubbles on mechanical properties was evaluated by testing under uniaxial tension and compression 120 specimens machined from acrylic plastic castings. The tensile specimens failed at stress levels 7 to 30 percent lower than those observed in control specimens without bubbles. The stresses at which yielding under uniaxial compression took place were found to be the same as in the control specimens.		

Security Classification

14	KEY WORDS	LINK A		LINK B		LINK C	
		ROLE	WT	ROLE	WT	ROLE	WT
	Acrylic resins						
	Polymethyl methacrylate						
	Castings						
	Bubbles						
	Mechanical properties						
	Compressive strength						
	Tensile strength						

Technical Report 1303
June 1989

Crazing and Degradation of Flexure Strength in Acrylic Plates as a Function of Time

J. D. Stachiw
Naval Ocean Systems Center

J. L. Stachiw
San Diego School System

NAVAL OCEAN SYSTEMS CENTER

San Diego, California 92152-5000

E. G. SCHWEIZER, CAPT, USN
Commander

R. M. HILLYER
Technical Director

ADMINISTRATIVE INFORMATION

This work was accomplished by a member of the Marine Materials Technical Staff, Code 9402, Naval Ocean Systems Center, under an Independent Exploratory Development Program, OCNR-20T.

Released by
J. D. Stachiw, Head
Marine Materials
Technical Staff

Under authority of
N. B. Estabrook, Head
Ocean Engineering
Division

UNCLASSIFIED

SECURITY CLASSIFICATION OF THIS PAGE

REPORT DOCUMENTATION PAGE				
1a. REPORT SECURITY CLASSIFICATION UNCLASSIFIED		1b. RESTRICTIVE MARKINGS		
2a. SECURITY CLASSIFICATION AUTHORITY		3. DISTRIBUTION/AVAILABILITY OF REPORT Approved for public release; distribution is unlimited.		
2b. DECLASSIFICATION/DOWNGRADING SCHEDULE				
4. PERFORMING ORGANIZATION REPORT NUMBER(S) Technical Report 1303		5. MONITORING ORGANIZATION REPORT NUMBER(S)		
6a. NAME OF PERFORMING ORGANIZATION Naval Ocean Systems Center		6b. OFFICE SYMBOL (if applicable) Code 9402		7a. NAME OF MONITORING ORGANIZATION
6c. ADDRESS (City, State and ZIP Code) San Diego, CA 92152-5000		7b. ADDRESS (City, State and ZIP Code)		
8a. NAME OF FUNDING/SPONSORING ORGANIZATION Independent Exploratory Development Program (IED)		8b. OFFICE SYMBOL (if applicable) OCNR-20T		9. PROCUREMENT INSTRUMENT IDENTIFICATION NUMBER
8c. ADDRESS (City, State and ZIP Code) Arlington, VA 22217		10. SOURCE OF FUNDING NUMBERS		
		PROGRAM ELEMENT NO. 62936N	PROJECT NO. RV36121	TASK NO. ZE56 AGENCY ACCESSION NO. DN307 448
11. TITLE (Include Security Classification) CRAZING AND DEGRADATION OF FLEXURE STRENGTH IN ACRYLIC PLATES AS A FUNCTION OF TIME				
12. PERSONAL AUTHOR(S) J. D. Stachiw and J. L. Stachiw				
13a. TYPE OF REPORT Final		13b. TIME COVERED FROM 1977 TO 1988		14. DATE OF REPORT (Year, Month, Day) June 1989
15. PAGE COUNT 62				
16. SUPPLEMENTARY NOTATION				
17. COSATI CODES			18. SUBJECT TERMS (Continue on reverse if necessary and identify by block number)	
FIELD	GROUP	SUB-GROUP		
19. ABSTRACT (Continue on reverse if necessary and identify by block number) Thick acrylic plates in stressed and unstressed condition have been subjected to outdoor weathering for 10 years. The stressed specimens developed surface crazing whose extent and depth were a function of flexure stress to which they were continuously subjected. Continuously applied flexure stress of 2240 psi generated very deep crazing, which resulted in catastrophic failure of the test specimen after 9 years. On the other hand, the specimen subjected to only 810-psi flexure stress displayed no crazing. Based on our study, we conclude that for continuously stressed structural acrylic plastic components exposed to outdoor environment with 110°F maximum summer temperature, the maximum flexure design stress for a 10-year service life should not exceed 1000 psi; otherwise at the end of the service period, the remaining flexural strength of the weathered material will not provide the minimum required safety factor of 4. We also recommend that stressed acrylic plastic structures only be cleaned safely with water-based cleaners.				
20. DISTRIBUTION/AVAILABILITY OF ABSTRACT <input type="checkbox"/> UNCLASSIFIED/UNLIMITED <input checked="" type="checkbox"/> SAME AS RPT <input type="checkbox"/> DTIC USERS			21. ABSTRACT SECURITY CLASSIFICATION UNCLASSIFIED	
22a. NAME OF RESPONSIBLE PERSON J. D. Stachiw			22b. TELEPHONE (Include Area Code) (619) 553-1875	22c. OFFICE SYMBOL Code 9402

DD FORM 1473, 84 JAN

83 APR EDITION MAY BE USED UNTIL EXHAUSTED
ALL OTHER EDITIONS ARE OBSOLETEUNCLASSIFIED
SECURITY CLASSIFICATION OF THIS PAGE

UNCLASSIFIED

SECURITY CLASSIFICATION OF THIS PAGE (When Data Entered)

DD FORM 1473, 84 JAN

UNCLASSIFIED
SECURITY CLASSIFICATION OF THIS PAGE (When Data Entered)

SUMMARY

Thick acrylic plates in stressed and unstressed condition have been subjected to outdoor weathering for 10 years. The stressed specimens developed surface crazing whose extent and depth were a function of flexure stress to which they were continuously subjected. Continuously applied flexure stress of 2240 psi generated very deep crazing, which resulted in catastrophic failure of the test specimen after 9 years. On the other hand, the specimen subjected to only 810-psi flexure stress displayed no crazing.

The effect of weathering on the strength of acrylic plastic varies with distance from the weathered surface. In *unstressed* specimens 0.040 inch below the weathered surface there is no measurable decrease in flexure strength, while on the surface there is approximately a 50-percent decrease. This decrease in strength on the surface of the specimen was not accompanied by crazing. For this reason, the absence of crazing cannot be considered absolute proof that the structural properties of acrylic plastic have not been reduced by weathering below the safe limits specified by American National Standards Institute/American Society of Mechanical Engineers (ANSI/ASME) PVHO-1 Safety Standard for Pressure Vessels for Human Occupancy.

Based on this study, we conclude that for *continuously* stressed structural acrylic plastic components exposed to outdoor environment with 110° F maximum summer temperature, the maximum flexure design stress for a 10-year service life should not exceed 1000 psi; otherwise at the end of the service period, the remaining flexural strength of the weathered material will not provide the minimum required safety factor of 4. This finding supports the design stress levels specified for acrylic plastic by ANSI/ASME/PVHO-1.

Cleaning of stressed acrylic plastic structural components with organic solvents (i.e., alcohol, acetone, tylenol, methylethylketone, etc.) is to be avoided as their application may accelerate by many orders of magnitude the degradation of flexural strength and/or appearance of crazing, depending on the solvent used. Because of this phenomenon, only water-based cleaners can safely be used on acrylic plastic structures.

CONTENTS

INTRODUCTION	1
EXPERIMENTAL APPROACH.....	3
Phase 1	3
Phase 2	3
Phase 3	4
OBJECTIVES.....	5
Phase 1	5
Phase 2	5
Phase 3	5
TEST OBSERVATIONS.....	6
Phase 1	6
Phase 2	6
Phase 3	6
DISCUSSION	8
Effect of Weathering	8
Effects of Stress	9
Design Stress Selection	11
Deflections	12
FINDINGS	13
CONCLUSIONS	14
RECOMMENDATIONS	15
DEFINITIONS	52
REFERENCES	53

FIGURES

1.	Typical crazing on the exterior surface of a weathered, acrylic plastic structure	16
2.	Crazing on the exterior surface of an acrylic plastic plane disc window under sustained flexure stress of 2000 psi after 5 minutes of exposure to ethyl alcohol	17
3.	Thick weathering specimens cut from 2- and 4-inch-thick acrylic plastic plates after placement at test location in El Cajon, California	18
4.	Test fixture for application of bending moments to several 2- by 22- by 0.25-inch-thick acrylic strips	19
5.	Dimensions of test beams for flexure testing cut from 2-inch-thick acrylic plastic plate	20
6.	Anchoring of 4- by 48- by 2-inch-thick test beams in the outdoor weathering flexure test fixture	21
7.	Arrangement for application of bending moments to 4- by 48- by 2-inch-thick acrylic plastic test beams	22
8.	Completed installation of the flexure test beams at the Stachiw Associates' outdoor weathering test facility located in El Cajon	23
9.	The deflection of each 4- by 48- by 2-inch-thick beam was recorded periodically by placing a water level on the top surface of the beam at its base and measuring the distance between the tip of the deflected beam and the horizontal level	24
10.	Crazing of the upper surface on the 2- by 22- by 0.25-inch-thick flexure specimen after 20 minutes of sustained 2000-psi flexure stress and continuous wetting by ethyl alcohol	25
11.	Crazing on the upper surface of the 4- by 48- by 2-inch-thick test beam No. 1 after 4 years of sustained flexure loading as a cantilever beam; the flexure stress above the fulcrum is 2240 psi	26
12.	Crazing on the upper surface of the 4- by 48- by 2-inch-thick test beam No. 2 after 4 years of sustained flexure loading as a cantilever beam; the flexure stress above the fulcrum is 1960 psi	27
13.	Crazing on the upper surface of the 4- by 48- by 2-inch-thick test beam No. 3 after 4 years of sustained flexure loading as a cantilever beam; the flexure stress above the fulcrum is 1570 psi	28
14.	Crazing on the upper surface of the 4- by 48- by 2-inch-thick test beam No. 1 after 5 years of sustained flexure loading as a cantilever beam; the crazing was photographed from below the beam	29
15.	Crazing on the upper surface of the 4- by 48- by 2-inch-thick test beam No. 2 after 5 years of sustained flexure loading as a cantilever beam; the crazing was photographed from below the beam	30
16.	Crazing on the upper surface of the 4- by 48- by 2-inch-thick test beam No. 3 after 5 years of sustained flexure loading as a cantilever beam; the crazing was photographed from below the beam	31
17.	Note the absence of crazing on test beam No. 4 after 5 years of sustained flexure loading as a cantilever beam; the flexure stress above the fulcrum is 1200 psi. The beam was photographed from below	32
18.	The 4- by 48- by 2-inch-thick test beam under sustained 2240-psi flexure stress and outdoor weathering failed catastrophically after 9 years	33
19.	Crazing on test beam No. 1 after 9 years of sustained flexure loading as a cantilever beam. The stress above the fulcrum was 2240 psi	34

FIGURES (continued)

20.	Crazing on test beam No. 2 subjected to sustained flexure stress of 1960 psi for 10 years	35
21.	Crazing on test beam No. 3 subjected to sustained flexure stress of 1570 psi for 10 years	36
22.	Crazing on test beam No. 4 subjected to sustained flexure stress of 1200 psi for 10 years	37
23.	Crazing on test beam No. 5 subjected to sustained flexure stress of 970 psi for 10 years	38
24.	Crazing on test beam No. 6 subjected to sustained flexure stress of 810 psi for 10 years	39
25.	The 4- by 48- by 2-inch-thick test beam after 10 years of weathering and short-term flexure loading to catastrophic failure	40
26.	All of the 4- by 48- by 2-inch-thick test beams were, after 10 years of weathering, loaded to failure to determine the effective flexure strength of the weathered plastic. The highest effective strength was found in the <i>unstressed</i> specimen (No. 7), while the lowest one was found in the specimen subjected to the highest sustained flexure stress (No. 2)	41
27.	Deflections of the cantilevered test beams at their tips during sustained flexure loading in outdoor environment. The test beam under highest flexure loading failed in 9 years after extensive crazing	42
28.	Deflections of cantilevered test beams during short-term loading to destruction	43
29.	Decay of effective modulus of acrylic plastic (M) as a function of ambient test temperature	44

TABLES

1.	Physical properties of acrylic plastic prior to machining of test beams	45
2.	Effect of outdoor weathering on flexural strength of acrylic plastic plates	46
3.	Cantilever beams under long-term loading in outdoor environment	47
4.	Remaining strength of cantilever beams after 10 years' sustained loading in outdoor environment	48
5.	Physical and chemical properties of surface and subsurface layers in 2.5-inch Plexiglas G	49
6.	Flexural strength of 2.5-inch Plexiglas G—disc specimens	50
7.	Mechanical properties of 2.5-inch Plexiglas G—ASTM specimens	51

INTRODUCTION

For years, users and manufacturers of plastics have been aware of a phenomenon whereby glassy plastics develop what appears to be a multitude of cracks, which initiate at the surface of the material and grow perpendicularly to the direction of stress (figure 1).^{*} These discontinuities are not always cracks, however, and have been called "crazes" because they resemble, somewhat, the cracks found in glass and ceramics, particularly the glazes on pottery. Because many structures and structural components of pressure vessels subjected to hydrostatic pressures are made from glassy plastics (i.e., polystyrene, polymethyl methacrylate, and polycarbonate), the problems of crazing have become an important consideration in viewing the reliability and longevity of structural parts manufactured from these materials.

A craze, by definition, is a lens-shaped damage zone containing induced microvoids within a highly oriented polymer chain.⁽¹⁾ Within the crazed zone, voids comprise 40 to 60 percent of the area's volume.⁽²⁾ These voids allow an increase in material cross section without lateral contraction because the lateral contraction is prohibited, at least in thick specimens, by the elastic constraint of the surrounding or adjacent undeformed polymer.⁽²⁾

The craze propagates transversely to the principal stress vector, thereby maximizing the spreading stress at the tip of the craze.⁽³⁾ Crazes contain material which has a lower refractive index and density than the bulk of the resin.⁽⁴⁾ They are characterized as being quite narrow and are often difficult to see. In laminated transparencies, premature crazing is a particularly serious problem because the crazes tend to form on the outer surface of the acrylic ply.

But what causes crazing? Studies have shown that there are at least four factors which may cause glassy plastics to craze: (1) tensile stress, (2) temperature differential across thickness of acrylic member, (3) weathering, and (4) contact with organic solvents. Crazes are initiated and propagated only when the tensile stress on the material surface exceeds some critical value. This critical stress value changes, however, as a function of ambient temperature and humidity, duration of stress loading, duration and intensity of solar or x-ray, irradiation, and duration of contact with organic solvents.^(2,4)

Test results indicate that crazing will initiate when a specimen is exposed briefly to a stress level of approximately one-third of the failure stress,⁽⁵⁾ and that the crazing will spread as the load duration increases.⁽⁶⁾ However, crazing is also time dependent, and molded components may craze, with time, even when the magnitude of molded-in-strains are quite low.⁽⁷⁾ In a comparison between polystyrene and acrylic, it was found that polystyrene is intrinsically stronger, but because polystyrene has a greater tendency to craze than acrylic, the observed ultimate strength of normal uncracked samples of acrylic was higher.⁽⁴⁾

In the case of crazing caused by weathering, casual observation of everyday glassy plastics shows innumerable examples of such crazing. However, the tests performed show that weathering, itself, is a surface effect and that the removal of weather-caused crazes returns the material to its approximate former state chemically and mechanically. However, if the material has been thoroughly exposed to high temperature (i.e., used in solar collector covers), or X-ray radiation (i.e., hyperbaric chamber viewports) degradation does occur through the hull thickness of the plastic.⁽⁸⁾ Therefore, in such cases it is temperature and X-ray radiation that cause the material to degrade and not weathering, as such.

^{*}All figures and tables are placed at the end of the text.

Chemically induced crazing has been observed for many years. Most users of glassy plastics know they must not use organic solvents to clean the materials, particularly if they contain residual stresses or are subjected to tensile or flexure loadings (figure 2). Cleaners and disinfectants in a water solution attack acrylic, for example, less than the same cleaners and disinfectants in an alcohol solution.⁽⁹⁾ Water, itself, even seawater immersion for as long as 5 years, does not cause any significant chemical change in acrylic.⁽¹⁰⁾ Absorbed moisture gradient, however, can cause crazing as it generates a high surface tensile stress when the surface of a specimen has a high moisture content and is rapidly dried.⁽²⁾ It is the stress, then, that causes the crazing and not the moisture, per se.

Even though most crazes are not true cracks, crazes are still believed to initiate failure of a structure or of a structural member when the crazing becomes extensive and the depth of crazing exceeds some critical value. In the critical flaw theories, it is assumed that the strength of a brittle material is limited by the presence of flaws in the sample, as these discontinuities distort the stress field and cause the initiation of the failure process by rapid extension of the largest, properly oriented flaw when a critical tensile stress is attained.⁽¹¹⁾

Any one of the factors which cause crazing may be acting at any one time; however, usually more than one factor is present. There are probably synergistic effects between these factors. Little research with quantitative findings has been done on the magnitude of synergistic effects. The present study was conceived in an attempt to shed some light on major questions concerning the relationship between crazing, weathering, long-term application of flexure stresses, and structural performance of acrylic plastic structures made from thick plates.

The questions under investigation were as follows:

1. Does weathering decrease the flexure strength of thick acrylic plastic plates even without the presence of crazing?
2. Is the presence of sustained flexure stress required to initiate, maintain, and expand crazing in thick acrylic plastic plates exposed to weathering?
3. Does crazing significantly decrease the load carrying ability of thick acrylic plates loaded in tension or flexure?
4. Does sustained flexure stress accelerate the decrease of flexure strength in thick acrylic plates exposed to weathering?
5. Does the use of cleaners and disinfectants significantly accelerate formation of crazing on acrylic plastic under sustained tensile stress?
6. Is the absence of crazing a reliable indication that the acrylic plastic has not been affected by weathering?

The data generated by this study will be augmented to findings of other studies (12,13,14,15) which focused primarily on deterioration of tensile, compressive, and shear strengths due to weathering and immersion in seawater. The data generated by testing of coupons cut from the weathered 2.5-inch-thick spherical acrylic hull of submersible NEMO⁽¹⁵⁾ is of particular interest as the hull was subjected during its lifetime primarily only to compressive stresses that have shown to have no effect upon material deterioration rate (tables 5, 6, 7).

EXPERIMENTAL APPROACH

To provide answers to the above questions, the test program was divided into three phases.

PHASE 1

In this phase of the test program, emphasis was placed on weathering of unstressed acrylic blocks for 10 years. The blocks were cut from 2- and 4-inch-thick Plexiglas G (table 1). From data provided in previous studies, it was known that hot, tropical climates tend to have the most effect in lowering the strength of their acrylic samples.^(12,13,&14) Therefore, one set of specimens was placed at the Harbor Branch Oceanographic Institution in Linkport, Florida. Also airborne pollutants were suspected as possible sources of crazing in weathering samples, so some blocks were placed in Houston, Texas, at the Hahn and Clay facilities where they were exposed to a high level of hydrocarbon pollution. The third set of specimens was placed in El Cajon, California, in a hot, dry environment with more than 300 days per year of direct sunlight (figure 3). All of the blocks used in this phase of the study were plates with 12- by 12- by 4-inch and 12- by 12- by 2-inch dimensions. These samples differ radically from all previous weathered samples in that these samples were on an order of magnitude thicker (i.e., 4 or 2 inches versus .025 inch). If weathering is truly only a surface effect, thick specimens would exhibit this effect. None of the plate specimens were subjected to loading during the years they were exposed to the various environments. The specimens were placed in metal frames that kept them about 6 inches above the surfaces on which they were placed. The same face of the specimen was always facing towards the sun. Test coupons were periodically cut from weathered plates and tested for flexural strength (table 2).

PHASE 2

In this phase of the test program, 2- by 22- by 0.25-inch-thick strips of Plexiglas G were subjected to both stress and chemical solvents—a combination which causes rapid crazing that culminates in failure. While under a constant 2000-psi flexure stress, various organic solvents were applied to the area of maximum stress on the acrylic strips, resulting in rapid crazing (figure 4). By holding the stress level constant, the effects of different chemon initiation and progress of crazing could be observed. The 2000-psi flexure stress was selected as the test stress level because this magnitude of stress is the industry-wide accepted standard for detecting the onset of chemically induced crazing.

Some of the test specimens were immersed in organic solvents and dried off prior to placing them in the test fixture and applying the bending moment for generation of 2000-psi flexure stress. This was done to determine whether contact with organic solvents prior to stress application sensitized the acrylic plastic to craze initiation as severely as contact with the same organic solvents during stress application.

Data that were generated in this phase of testing were (1) the time to initiation of crazing on the surface of specimen, (2) the depth of the crazing, and (3) the time to catastrophic failure of the flexure specimen.⁽⁹⁾

PHASE 3

In this phase of test program, six acrylic beams of 48- by 4- by 2-inch dimensions were mounted in an outdoor bending load fixture and subjected to six different stress levels. Seven beams were cut from a single sheet of 2-inch-thick Plexiglas G plate (figure 5). They were sawed, sanded, and polished at the edges. Approximately 2 inches from each end, 3/4-inch diameter holes were drilled without any visible cracks in the material. After all the machining drilling and polishing was accomplished, the beams were annealed at 190°F for 24 hours. Material coupons were also machined at this time from the top, middle, and bottom of the Plexiglas G plate to determine whether there was a significant difference in the mechanical properties of the material at these locations prior to outdoor weathering.

One end of each beam was attached to the mounting plate set in concrete by a threaded rod through the hole in the beam, and a steel nut was screwed down tightly on the beam (figure 6). A threaded eye bolt was then attached to the other end of the cantilever beam. After securing the eye bolt to the beam, a specified weight was suspended from the eye bolt by a wire placing the beam under a continuous sustained flexure stress loading (figure 7). A control beam was placed beside this test fixture on the rock outcrop. This beam was allowed to weather unstressed. All the beams were installed in the test fixture on 25 June 1977 at the test site in El Cajon (figure 8). Deflection readings were taken frequently to determine the rate of creep in test beams under different levels of sustained flexure stress (figure 9). The test was terminated on 31 January 1988 by removing weights from all the six test beams and recording the snap-back of the bent test beams (table 3).

After 24 hours of relaxation, the six test beams were loaded individually until fracture occurred. Maximum deflection and load at moment of failure were recorded (table 4). For comparison purposes an identical test beam No. 7 that was exposed to 10 years of weathering but not sustained flexure loading, was also mounted in the outdoor bending load fixture and was loaded to failure. The maximum load and deflection at failure were also recorded (table 4).

OBJECTIVES

PHASE 1

Determine the effect of climate on the weathering of thick, unstressed acrylic plates.

Determine whether the change in material properties due to weathering is only a surface effect, or whether it extends through the whole thickness of acrylic plates.

Determine whether in unstressed acrylic plates a significant change in material properties is always accompanied by crazing of surfaces.

PHASE 2

Determine whether contact with organic solvents degrades the structural properties of acrylic plastic as much in unstressed specimens as it does in stressed specimens.

Determine the synergistic effect of sustained flexure stress on static fatigue of acrylic plastic in contact with organic solvents.

Determine whether contact with organic solvents generates crazing in unstressed acrylic specimens.

Determine whether prior contact by unstressed acrylic with an organic solvent will initiate rapid crazing in the material after application of sustained flexure stress.

PHASE 3

Determine the relationship between the magnitude of sustained flexure stress and the rate of crazing on surfaces of acrylic plastic subjected to weathering.

Determine whether the reduction in flexure strength of weathered acrylic plastic specimens under long-term flexure loading is solely a function of weathering, or also of sustained stress level.

Determine the magnitude of *maximum* flexure stress that can be continuously applied to an acrylic structural component in an outdoor environment with a 110°F peak daytime temperature without the occurrence of catastrophic failure in less than 10 years.

Determine the magnitude of *maximum* flexure stress that can be continuously applied to an acrylic structural component in an outdoor environment with a 110°F peak daytime temperature without the appearance of crazing in less than 10 years.

TEST OBSERVATIONS

PHASE 1

There was no visible crazing on the surfaces of unstressed test plates subjected to outdoor weathering in El Cajon, Linkport, or Houston. There was observed, however, a dulling of surfaces that reduced the light transmittance in the visible spectrum by 10 percent. Weathering affects the physical properties of acrylic plastic only in a thin layer below the surfaces of the specimen, as shown by the large difference in tensile strength and molecular weight of coupons sliced both from the surface and either of the test plates (table 2).

PHASE 2

Wetting with organic solvents of surfaces on acrylic strips subjected to sustained flexure stress of 2,000 psi rapidly initiated crazing. Some solvents (i.e., benzene, xylene, acetone, and methylethylketone) initiated crazing instantaneously, while others (i.e., methyl, ethyl, and isopropyl alcohols) required several minutes to initiate crazing (figure 10). Prolonged exposure ultimately produced catastrophic failure of the flexure specimen due to transformation of the crazing into deep cracks.

Reducing the flexure stress level in the flexure specimens prior to wetting them with organic solvents increases the time required for initiation of crazing. While at sustained flexure stress of 2,000 psi, it required approximately 20 minutes for development of *severe crazing* while wetted by ethyl alcohol, at 1,000 psi the time interval increased to 200 minutes, and at 500 psi it was in excess of 1000 minutes. Thus, it appears that crazing will take place *at any stress level*, providing that wetting with the solvent is *continued indefinitely*.

Wetting followed by drying off of surfaces on unstressed specimens that were subsequently subjected to 2,000-psi flexure stress did not appear to have the same effect as wetting of stressed specimens. While wetting with ethyl alcohol of specimens under sustained 2,000-psi flexure stress *initiated crazing* in approximately 1 minute and resulted in catastrophic failure in about 30 minutes, wetting and drying of unstressed specimens followed by application of 2,000-psi flexure stress did not initiate crazing even after 1,000 minutes of sustained loading.

PHASE 3

Test beams *did not craze significantly* even after 10 years of weathering if the maximum tensile flexure stress on the beam's surface was less than 810 psi. In the highly stressed beam No. 1 crazing became very noticeable in one year, in beam No. 2 after 2 years, and in beam No. 3 after 4 years, and in beam No. 4 only after 5 years (figures 11 through 17). Whenever present, the crazing was limited to a small area on the top surface above the cantilever beam fulcrum, where the tensile flexure stress was the highest. The extent and depth of crazing decreased rapidly with distance from the beam fulcrum until, at some distance, it disappeared totally. In beam No. 1, the crazing was observed only within 6 inches of the fulcrum. In that beam, the stress level at 6 inches from the fulcrum was calculated to be 1900 psi.

The catastrophic failure of the test beam No. 1, subjected to 2,240-psi sustained flexure stress for 9 years, indicates that all test beams under sustained loading will ultimately fail; the duration of loading required for failure will vary, however, inversely with the magnitude of sustained stress level (figure 18).

Application of sustained flexure stress to acrylic plastic can have a larger effect on its effective (residual) flexural strength than weathering; however, there is no doubt weathering significantly accelerates the effect of static fatigue (table 4). For example, test beam No. 7, which was subjected to weathering but not to sustained flexure stress for 10 years, had an effective flexural strength of 9,300 psi (i.e., lost 45 percent of original strengths) while beam No. 1, which in addition to weathering was also subjected to sustained flexure stress of 2,240 psi, lost 100 percent of its effective strength after 9 years (i.e., it failed). At low sustained stress levels, the effect of weathering exceeds the effect of static fatigue on effective strength. For example, beam No. 6 subjected to a sustained low stress level of 810 lost 45 percent of its original strength due to weathering and only 25 percent due to static fatigue. After 10 years of weathering, the crazing was *very severe* on test beams No. 1 and 2 (figures 19 and 20), *moderately severe* on test beam No. 3 (figure 21), *barely noticeable* on test beams Nos. 4 and 5 (figures 22 and 23), *incipient* on test beam No. 6 (figure 24), and *totally absent* on unstressed test beam No. 7 (figure 25). The extent and depth of crazing did not increase during the short-term flexure test to destruction conducted at the conclusion of the 10-year-long sustained flexure loading test program (figure 26).

The deflections of the test beams after 10 years of sustained flexure loading were proportional to the magnitude of flexure loading to which they were subjected (figure 27). Most of the deflection took place within 1 day after application of sustained flexure loading; the rate of creep decreased significantly thereafter.

The deflection of test beam No. 1 at catastrophic failure after 9 years of sustained flexure loading (figure 27) was significantly less than of test beam No. 7 during short-term destructive testing (figure 28). This was also true of test beams Nos. 2, 3, 4, 5, and 6 (tables 3 and 4).

The effective strength of test beams 2, 3, 4, 5, and 6 was, after 10 years of sustained flexure loading, found to *be significantly less* than that of test beam No. 7 not subjected to sustained flexure loading (figure 3).

DISCUSSION

EFFECT OF WEATHERING

The data generated in this study, as well as in previous studies conducted by the authors⁽¹⁵⁾ on the effect of weathering on the physical properties of acrylic plastic with ultraviolet absorber, very strongly support the following findings:

1. *Weathering degrades the physical properties of acrylic plastic.* The molecular weight and flexural strength decreases, while the material becomes more brittle (tables 2, 4, 5, 6, and 7).
2. *The effect of weathering does not penetrate deeply below the surface;* 0.06 inch below the surface the physical properties of the material remain unchanged (table 5).
3. *The physical properties most affected by weathering are the flexure strength, tensile strength, and tensile elongation at failure.* Shear strength is affected very little and the compressive strength almost none at all (table 7).

The flexure strength is the most affected by weathering because during bending the highest tensile component of the flexure stress is generated at the surface of the material where the effect of weathering is the greatest. The cracks, which originate during flexure loading in the weak, brittle surface layer, penetrate readily into the body of the unweathered material causing it to fail catastrophically.

The scenarios are quite different for acrylic plastic specimens under tensile or shear loading, where the stresses are uniformly distributed across the thickness of the specimen. Because of the uniform stress distribution across the thickness of the material, the layers of degraded material contribute very little to the overall reduction of strength in the 0.25-inch-thick test coupons. In structural components several inches thick, the effect of a weathered surface layer on the performance of the components loaded in tension is not significant.

Compressive strength of acrylic plastic structural components is totally unaffected by weathering as the stresses are uniformly distributed across the thickness of the components and, furthermore, the compressive strains prevent the initiation of cracks in the external weathered surfaces.

Based on the above discussion, we can postulate that *thick* structural members subjected to bending movements (for example, plane windows in pressure chambers) are as much affected by weathering as *thin* components, since the maximum tensile strain generated by flexure stress is always located on the surfaces most affected by weathering. For this reason, *the structural performance of new thick plane windows must be discounted for future deterioration due to weathering by the same percentage as the structural performance of new thin plane windows.*

Thus for a projected operational life of 10 years, the original flexure strength of acrylic plastic materials used in a structure must be discounted by *at least 35* and preferably *50 percent*. If the structure is subjected for 10 years to the maximum sustained flexure stress recommended by ANSI/ASME PVHO⁽¹⁶⁾ for a 125°F peak temperature, the static fatigue further reduces the effective flexure strength, so the original flexural strength must be discounted instead by *75 percent*. Data are not available for prediction of flexural strength in acrylic plastic that in addition to weathering is also subjected to cyclic flexure loading; for example, frequently pressurized plane windows in pressure chambers. A conservative assumption can be made, however, that weathering and cyclic application of flexure stresses *does not* decrease the flexural strength more than a sustained application of the same flexure stress.

Since the compressive strength of a structural member is not affected significantly by weathering (less than 2 percent) the structural performance of acrylic plastic structures loaded in compression need not be discounted for the effects of weathering, as is the case for structures subjected to flexure loading (table 7). Because of this observation it is desirable that, whenever feasible, acrylic plastic structures be designed for compressive, rather than flexure or tensile, loads. Thus, it is always preferable that viewports be curved rather than plane, even though the fabrication process for curved viewports is more expensive than for plane ones.

The effect of weathering on the tensile strength of acrylic plastic structures is significantly less than on the flexure strength, mostly because the tensile stress in a structural member under pure tension is distributed evenly across its thickness. This holds also true for the 0.25-inch-thick test specimens used for the determination of tensile strength in weathered thick plates. If the thickness of the tensile test specimens could be somehow reduced to 0.020 inch, the tensile strength of the weathered acrylic would be found to be the same as the flexure strength determined by 0.25-inch-thick flexure test specimens cut from the thick weathered plates.

Since this study did not address testing for tensile strength, data will be used from previous studies⁽¹⁵⁾ to determine by how much the tensile strength should be discounted for the effect of weathering. Data from previous studies show that the tensile strength of acrylic plastic members of a structure can be expected to decrease after 10 years of weathering by approximately 20 percent (table 7). Thus, it appears that tensile loading is less desirable than compressive loading, but certainly more desirable than flexure loading.

The shear strength appears to be even less affected by weathering than tensile strength (table 7). This is probably due to the fact that the test specimens for testing of shear strength are 0.5 inch thick and the distribution of shear stress across the specimen is fairly uniform. The reduction of strength due to weathering based on data from previous studies appears to be about 10 percent. Thus weathering affects the shear strength of acrylic plastic, as determined by standard test specimens, less than the flexure or tensile strength.

EFFECTS OF STRESS

Since most acrylic plastic structures or structural components subjected to weathering are also stressed either continuously or intermittently, the effect of stress on the effective strength of acrylic plastic must also be considered. As continuously applied stress is known from the published literature to affect the strength of an acrylic structure more than infrequent stress application, it was chosen for this study. The type of loading selected was flexure loading, as it would affect the flexural strength of materials shown to be the most sensitive to effects of weathering.

The range of stresses to which the flexure test beams were subjected was rather wide; the highest stress level chosen (2,240 psi) was to produce catastrophic failure in less than 10 years, while the lowest stress (810 psi) was not to initiate any significant crazing in 10 years. The test results confirmed this; test beam No. 1 under sustained flexure stress of 2,240 psi failed catastrophically after 9 years, while test beam No. 6 under sustained flexure loading of 810 psi did not exhibit any significant crazing.

The catastrophic failure of test beam No. 1 and the effective strengths of test beam Nos. 2 through 6 at the end of the 10-year-long test program (table 3) that were lower than the original strength of the material (table 1) confirm the existence of static fatigue, which was well documented by other investigators in technical literature. What this study added to the already published body of data is the contribution that weathering makes to the reduction in original flexure strength of thick beams under sustained flexure loading.

The reduction in strength due to static fatigue *alone* can be estimated by comparing the effective strengths (as denoted by maximum flexure stress during short-term testing to failure) of weathered test beams subjected to sustained flexure loading (test beams Nos. 1, 2, 3, 4, 5, & 6) with the remaining strength of the test beam that was weathered, but not subjected to sustained flexure loading (test beam No. 7). In this particular case, the effect of weathering by itself reduced the original strength of test beam No. 7 from 17,000 to 9,300 psi or to approximately 55 percent of original strength (table 4).

The additional reduction in strength due to static fatigue of the material was very significant, and the magnitude of this reduction in strength varied with the level of sustained stress to which the test beam was subjected. The static fatigue together with 10 years of weathering reduced the effective strength of flexure test beams to the following percent of original strength:

- Test beam No. 1 — 0 percent
- Test beam No. 2 — 19 percent
- Test beam No. 3 — 22 percent
- Test beam No. 4 — 24 percent
- Test beam No. 5 — 25 percent
- Test beam No. 6 — 30 percent

Since weathering alone appears to have reduced the flexure strength to 55 percent of original strength, the contribution of static fatigue to reduction of strength can be estimated. It is estimated that fatigued flexure beams would have retained the following percent of original strength if the effects of weathering were discounted:

- Test beam No. 1 — 45 percent
- Test beam No. 2 — 64 percent
- Test beam No. 3 — 67 percent
- Test beam No. 4 — 69 percent
- Test beam No. 5 — 70 percent
- Test beam No. 6 — 74 percent

A brief inspection of the estimated strengths that would remain in the flexure test beams if, during the sustained flexure loading they were not exposed to weathering, leads us to the opinion that at sustained stress levels below 2,000 psi weathering contributes more to reduction of original strength than static fatigue by itself.

Since the study did not address itself to intermittent stress application, there are no data on which to form an opinion on the contribution of cyclic stress fatigue to the reduction of original strength in weathered structures. A conservative opinion, however, can be formulated which states that the reduction of materials strength in an acrylic structure subjected to both weathering and intermittent flexure stress does not exceed the reduction in strength measured on flexure test beams subjected to both weathering and continuous sustained loading.

DESIGN STRESS SELECTION

Since both weathering and application of flexure stress reduce the effective strength of acrylic plastic, the reduction in effective strength after 10 years of service must be taken into account in the selection of design stress for any acrylic plastic structure or structural components that are subjected to flexure loading (i.e., plane windows under pressure loading, horizontal panels, and beams under gravity loading, etc.). Obviously, the *lower the value of design stress the higher the effective safety factor*, and the *lower the extent of crazing* will be after 10 years of operational service in outdoor environment.

Economic considerations, on the other hand, dictate that the design stress should be as high as possible without undue increase in risk of catastrophic failure. The highest design stress level that meets both safety and economic considerations is based on the premise that at no time during the operational life of the acrylic plastic shall the *effective safety factor* decrease below the value of 2. Flexure test beam No. 3 met this criteria after 10 years of sustained flexure loading at the 1570-psi maximum stress level. It still could withstand a *short-term* flexure stress of 3,800-psi magnitude prior to failure during short-term destructive testing in 65° F ambient air environment. The maximum safe design stress experimentally validated by flexure test beam No. 3 also meets the maximum design stress criteria of ANSI/ASME PVHO-1 for maximum ambient air environment temperature in the 100 to 125° F range. The minimum conversion factor (short-term critical stress divided by long-term design stress) specified by ANSI/ASME PVHO-1 for the 100 to 125° F temperature range is 10, which is readily converted into minimum design stress range of 1400 to 1700 psi magnitude (the exact value depending on the short-term flexural strength of acrylic plastic used in the construction of the structure).

Although a design stress of approximately 1500 psi will provide a minimum safety factor of at least 2, even at the end of the 10-year life operational period, it will not prevent the appearance of crazing that detracts from the appearance of the acrylic structure after about 5 years in an outdoor environment. To prevent the appearance of crazing during the 10-year operational life period calls for a maximum design stress of less than 810 psi. Flexure test beam No. 6 stressed to this sustained stress level did develop only barely noticeable crazing during the 10-year test period in outdoor environment. This design stress level for avoidance of significant crazing during a 10-year operational life translates into a minimum conversion factor of approximately 20. At this design stress level, the minimum effective safety factor at the end of 10-year service period is calculated to be 6.

From this discussion, it appears that the minimum conversion factor of 10 specified by ANSI/ASME PVHO-1 represents from the safety viewpoint the *maximum acceptable value of design stress* for an acrylic pressure-resistant window with a 10-year operational life in an outdoor environment with peak temperatures in 100 to 125° F range. At this design stress level, there will be, however, very noticeable crazing that may prompt the replacement of the pressure resistant window in less than 10 years. It would appear, therefore, cost effective to select for large, expensive plane windows, as in underwater observatories, a lower design stress preferably in the 500- to 800-psi range (conversion factors 30 to 20) to insure absence of crazing for 10 years.

DEFLECTIONS

The deflection of the cantilever test beams followed the classical strain theory for acrylic plastic (table 4). The *instantaneous deflection* after hanging of the dead weight from the tip of the beam was large, and its magnitude could be predicted on the basis of classical theory for bending of cantilever beams fabricated from totally elastic isotropic material with modulus of elasticity in the 450,000- to 500,000-psi range. The deflection continued to increase rapidly during the first hour after load application; the rate of creep, however, immediately began to decrease exponentially and continued to do so at this rate for approximately 24 hours.

After 24 hours, the creep rate stabilized into a logarithmic relationship between time and strain. Because of this logarithmic creep rate, the magnitude of beam deflection could be predicted for any time in the future using a mathematical formula and two deflection measurements.

$$M = \frac{\log \frac{d_2}{d_1}}{\log (T_2 - T_1)}$$

where

M = slope constant for a straight line expressing effective modulus elasticity decay on log coordinates.

d_1 = deflection at time T_1

d_2 = deflection at time T_2

T_1, T_2 = time, usually 1 to 10 days (a later reading may be substantiated for the 10-day reading).

The 0.057 value of M was calculated on the basis of 3.04- and 3.50-inch displacements recorded 1 day and 13 days after load application to test beam No. 2. Using $M = 0.057$, the deflection of test beam No. 2 was predicted to increase to 4.83 inches in 10 years; this value compares rather well with the measured deflection of 5.0 inches. The calculated value of M compares also well with published value of M in technical literature for MIL-P-5425 polymethyl methacrylate in 70°F environment (figure 29). The good agreement between experimentally measured displacement after 10 years and the calculated displacement was not expected, as the ambient temperature during this time period fluctuated for 45 to 110°F. The only possible explanation for this good agreement between the experimental and calculated data is that during the first 13 days of load application, when deflection d_1 and d_2 were measured for the determination of M , the ambient temperatures were in the upper half of the 45 to 110°F temperature range experienced during the following 10 years. This is a reasonable explanation, as during the typical year in El Cajon, the ambient temperature remains above 70° more than 70 percent of the time.

Also note that the deflections of the test beams after 10 years of sustained loading are approximately twice as large as instantaneous deflection upon load applications (table 2). Thus, a rule of thumb can be formulated which states that to predict the deflection of an acrylic structure after 10 years of sustained load application, measure the instantaneous deflection after application of the load and multiply it by a factor of 2.

FINDINGS

1. The effective flexural strength of acrylic plastic decreases with duration of exposure to outdoor weathering. After 10 years of weathering, the effective strength is only approximately 55 percent of original strength.

2. Sustained flexural stress decreases the effective strength further; at the 1500-psi maximum design stress level specified by ANSI/ASME PVHO for the peak ambient temperature range of 100 to 125°F, the total effective strength after 10 years of weathering is approximately only 3800 psi providing an effective safety factor of only 2.

3. The maximum design stress for avoidance of crazing during 10 years of sustained flexure loading and weathering appears to be <810 psi. Using the crazing avoidance design stress provides, at the end of 10-year-long service period, a strength of 30 percent and an effective safety factor of 6.

4. Weathering affects only the first 0.060 inch of thickness in acrylic plastic (MIL-P-5425); the remainder of the material retains its original strength even after 10 years of weathering.

5. The compressive strength of acrylic plastic structures appears not to be affected at all by weathering.

6. The deflection of acrylic structures during a 10-year-long period while under sustained flexure loading can be predicted on the basis of deflection measurements taken on the first and tenth day after the application of sustained loading.

7. The deflection after 10 years of sustained flexure loading appears to be 100 percent greater than the deflection immediately after application of sustained load.

8. Cleaning with organic solvents of acrylic plastic surfaces under tensile strain produced by flexure or tensile stresses accelerates the crazing process. Alcohol contained by most disinfectants and window cleaners will initiate crazing in several minutes on acrylic plastic surfaces that are under tensile stresses of 2000 psi and in several hours on surfaces that are under stresses of 1000 psi.

9. Cleaning with organic solvents prior to application of stress *does not* initiate crazing in realtime after load application.

10. Degradation of physical properties in acrylic plastic due to weathering appears to correlate well with the decrease of molecular weight in the material affected by weathering.

* These findings have been experimentally validated only for non-cross-linked polymethyl methacrylate plastic with ultraviolet filter additive meeting the requirements ANSI/ASME PVHO, section 2, table 2.1-1, and or MIL-P-5425.

CONCLUSION

1. Weathering affects only a thin surface layer on acrylic plastic with ultraviolet absorber; the affected material becomes more brittle and less able to withstand tensile strains.
2. The effective load-carrying capacity of thick acrylic plastic structural members under flexure loading (i.e., pressure proof windows, beams, roof paneling, etc.) is determined by the reduced mechanical properties of the thin weathered surface layer subjected to peak flexure stresses.
3. The flexure design stress of 1500-psi magnitude (i.e., conversion factor of 10) specified by ANSI/ASME PVHO-1 for plane pressure proof windows subjected to weathering and a biaxial tensile stress field in ambient environment with peak temperatures in the 100 to 125°F range provides an adequate effective safety factor of 2 at the end of the 10-year service period.
4. Crazeing of acrylic structures subjected to weathering and sustained flexure loading can be avoided over a 10-year period by specifying maximum flexure design stress ≤ 800 psi (i.e., conversion factor ≥ 20).
5. Cleaning of acrylic surfaces under applied, or residual, tensile strain with organic solvents (alcohol, methylethylketone, trichloroethylene, benzene, etc.) will accelerate the formation of crazeing by several orders of magnitude, leading in some cases to immediate catastrophic failure.
6. The experimental data are insufficient to allow prediction of effective strength in flexure loaded acrylic plastic structure after 20 years of weathering; it is certain, however, that the design stresses (i.e., conversion factors) specified by ANSI/ASME - PVHO for windows under flexure loading will not provide an adequate effective safety factor after 10 years of sustained loading in an outdoor environment.
7. It is preferable to design acrylic plastic structural components for compression rather than flexure or tensile loading, as weathering and sustained loading do not decrease significantly the compressed strength of acrylic plastic even after 10 years of exposure.
8. The most sensitive analytical tool for detecting the effect of weathering on acrylic plastic and its depth of penetration into the material is the measurement of molecular weight performed on thin coupons of material sliced from the surface of weathered material.
9. The most feasible approach to eliminating the effect of weathering on the effective strength of acrylic plastic structural members under flexure loading is to de-couple the weathered layer from the body of the structural member, so that a crack initiated in the weathered layer does not propagate into the body of the material, causing it to fail catastrophically. This can be accomplished by laminating a thin sheet of acrylic plastic with elastomeric adhesive to the thick structural member; a crack originating in the weathered layer would not propagate across the elastomeric adhesive interlayer into the body of the structural member.

RECOMMENDATIONS

1. The 1500-psi maximum design stress value specified by ANSI/ASME PVHO-1 (i.e., conversion factor of 10) for plane windows in chambers for human occupancy operating in ambient environment with peak temperatures in the 100 to 125°F range should not, for any reason, be increased to a higher value, as this will decrease the effective safety factor of the window after 10 years of service to less than 2.
2. To eliminate the appearance of unsightly crazing for a period of 10 years on the weathered surfaces of plane acrylic plastic windows in chambers for human occupancy, the design stress should not exceed 800 psi (i.e., conversion factor of 20).
3. Installed acrylic plastic windows should not be cleaned with anything but water and mild detergents approved for washing of dishes.
4. Brand new acrylic plastic windows of any shape (plane, spherical, and cylindrical) should, prior to installation in chamber viewports, be inspected under polarized light for the presence of residual stresses, as residual stresses in excess of 800 psi will produce crazing in less than 10 years.⁽¹⁷⁾

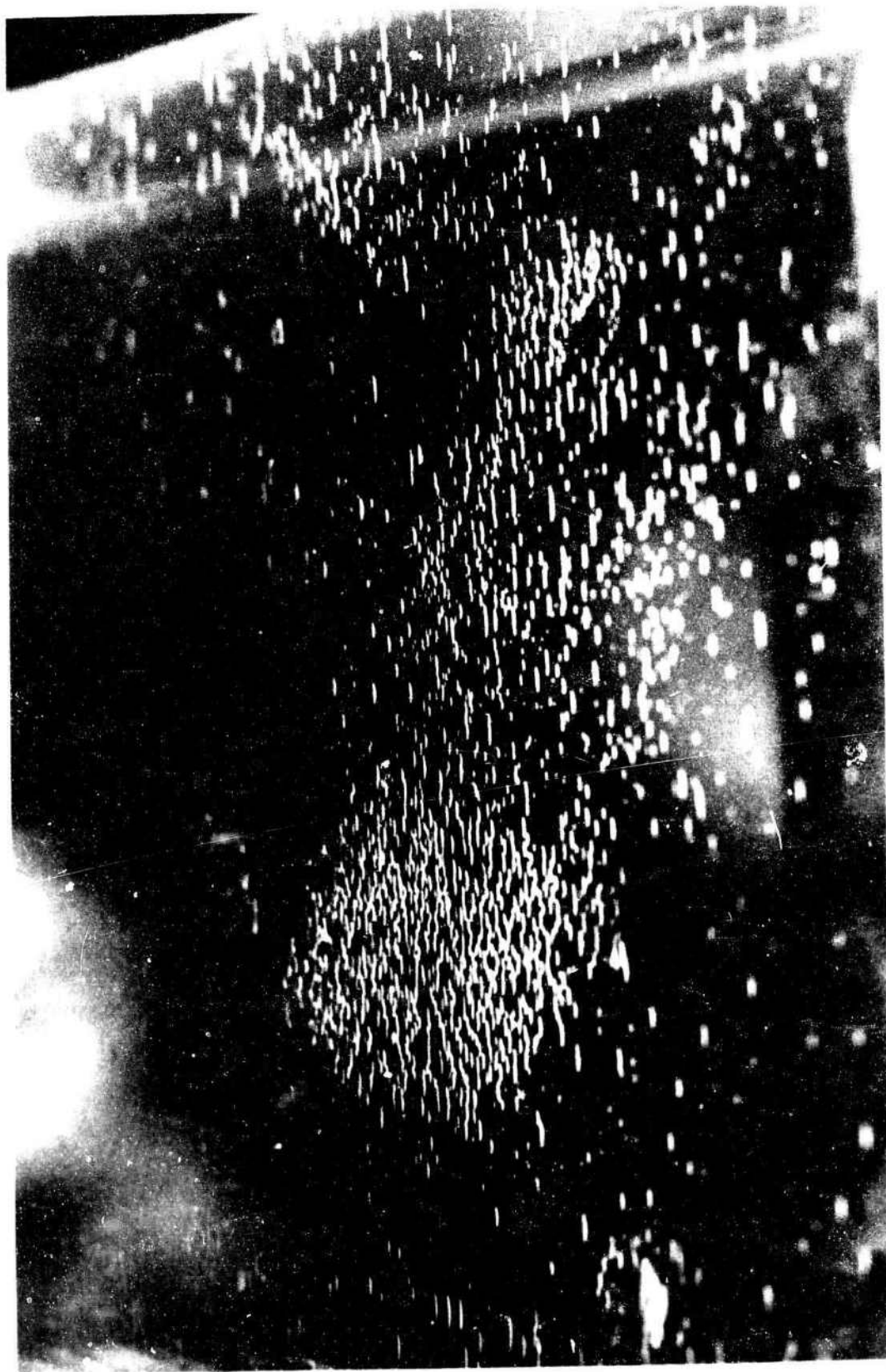


Figure 1. Typical crazing on the exterior surface of a weathered, acrylic plastic structure.

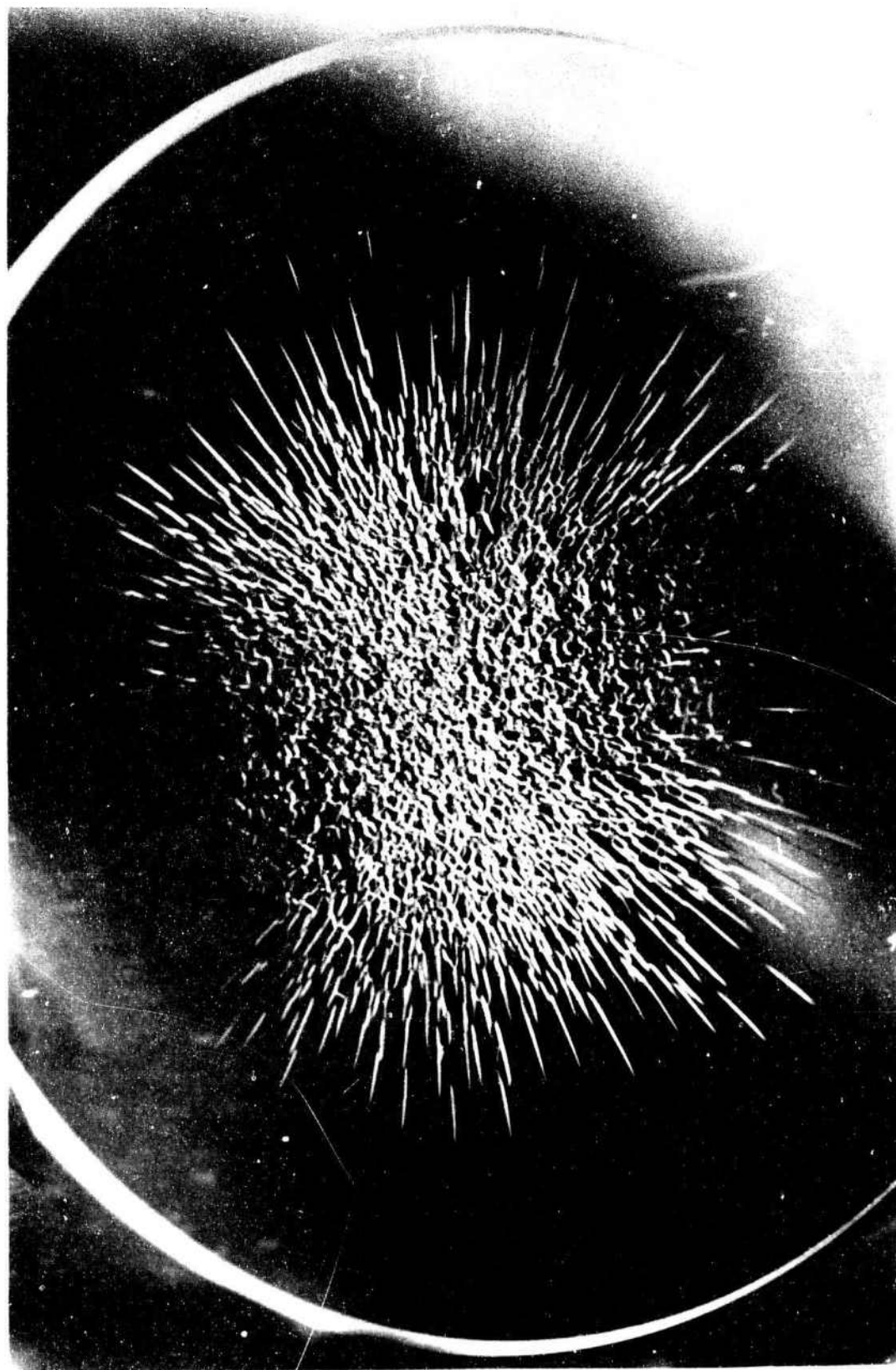


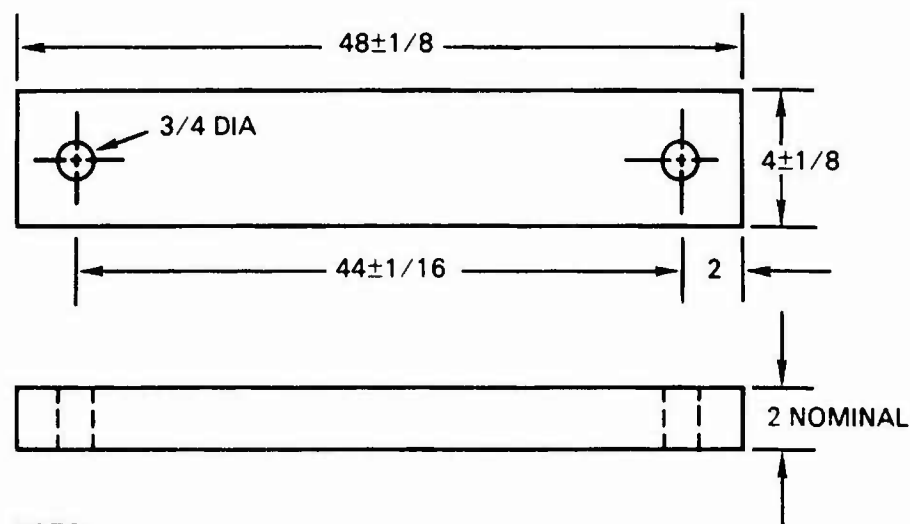
Figure 2. Crazing on the exterior surface of an acrylic plastic plane disc window under sustained flexure stress of 2000 psi after 5 minutes of exposure to ethyl alcohol.



Figure 3. Thick weathering specimens cut from 2- and 4-inch-thick acrylic plastic plates after placement at test location in El Cajon, California.



Figure 4. Test fixture for application of bending moments to several 2- by 22- by 0.25-inch-thick acrylic strips. Note that Dr. Stachiw is wetting the top surface of test specimens stressed to 2000 psi with ethyl alcohol.



NOTE:

1. All the test bars to be cut from a single sheet of 2 inch-thick Plexiglas G
2. The edges of the test bars to be saw cut, sanded smooth, and polished
3. After polishing, anneal the test bars at 190°F for 24 hours

Figure 5. Dimensions of test beams for flexure testing cut from 2-inch-thick acrylic plastic plate.



Figure 6. Anchoring of 4- by 48- by 2-inch-thick test beams in the outdoor weathering flexure test fixture.

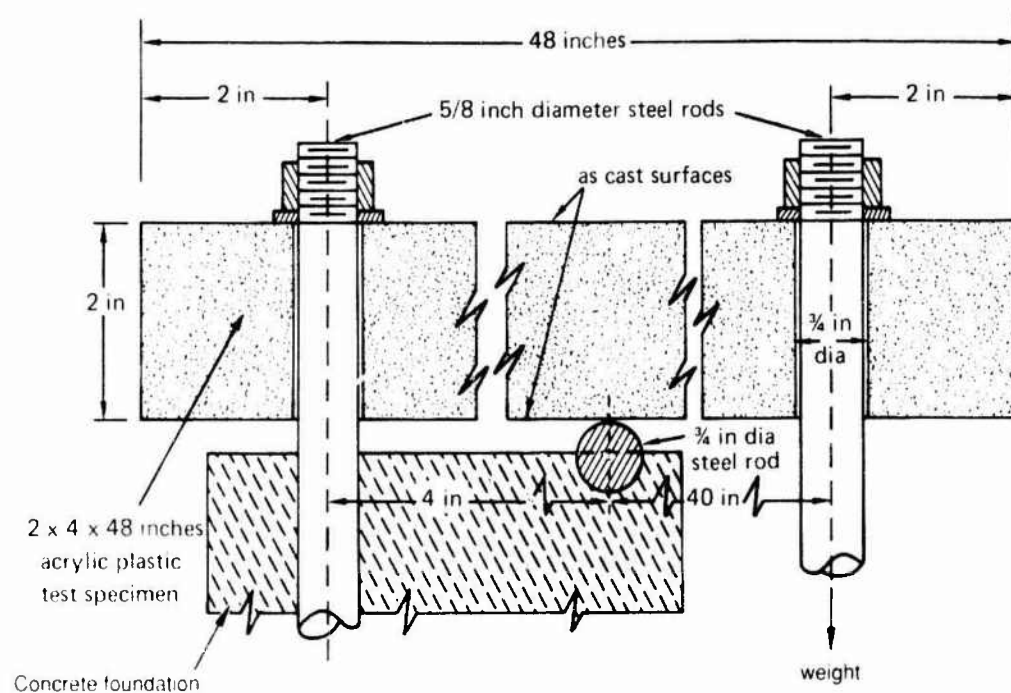


Figure 7. Arrangement for application of bending moments to 4- by 48-by 2-inch-thick acrylic plastic test beams.

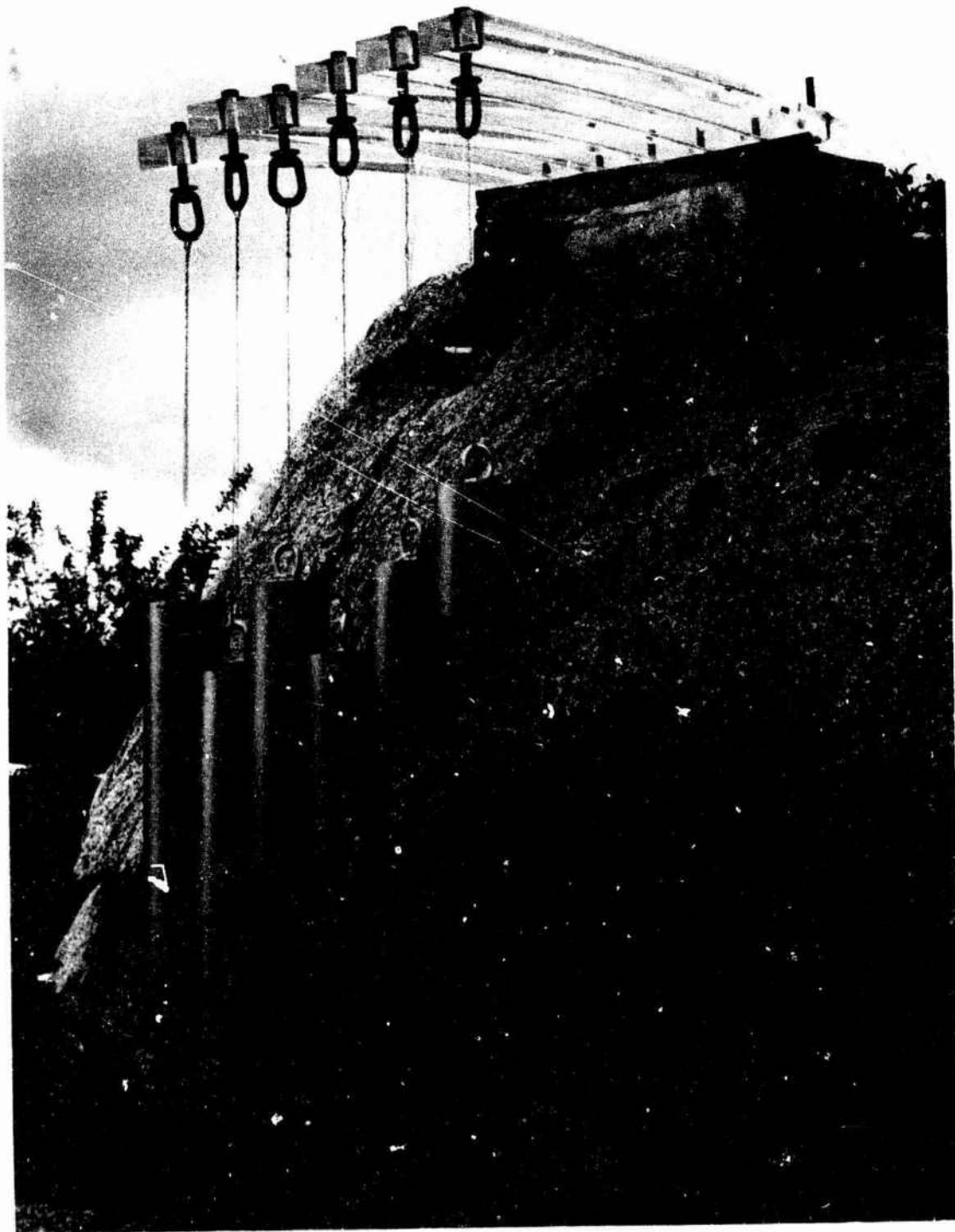


Figure 8. Completed Installation of the flexure test beams at the Stachiw Associates' outdoor weathering test facility located in El Cajon. Note that each of the cantilever beams is subjected to a different size of dead load.



Figure 9. The deflection of each 4- by 48- by 2-inch-thick beam was recorded periodically by placing a water level on the top surface of the beam at its base and measuring the distance between the tip of the deflected beam and the horizontal level.



Figure 10. Crazeing of the upper surface on the 2- by 22- by 0.25-inch-thick flexure specimen after 20 minutes of sustained 2000-psi flexure stress and continuous wetting by ethyl alcohol. Note that the crazeing is oriented at right angles to the direction of principal flexure stress.



Figure 11. Crazing on the upper surface of the 4- by 48- by 2-inch-thick test beam No. 1 after 4 years of sustained flexure loading as a cantilever beam; the flexure stress above the fulcrum is 2240 psi.

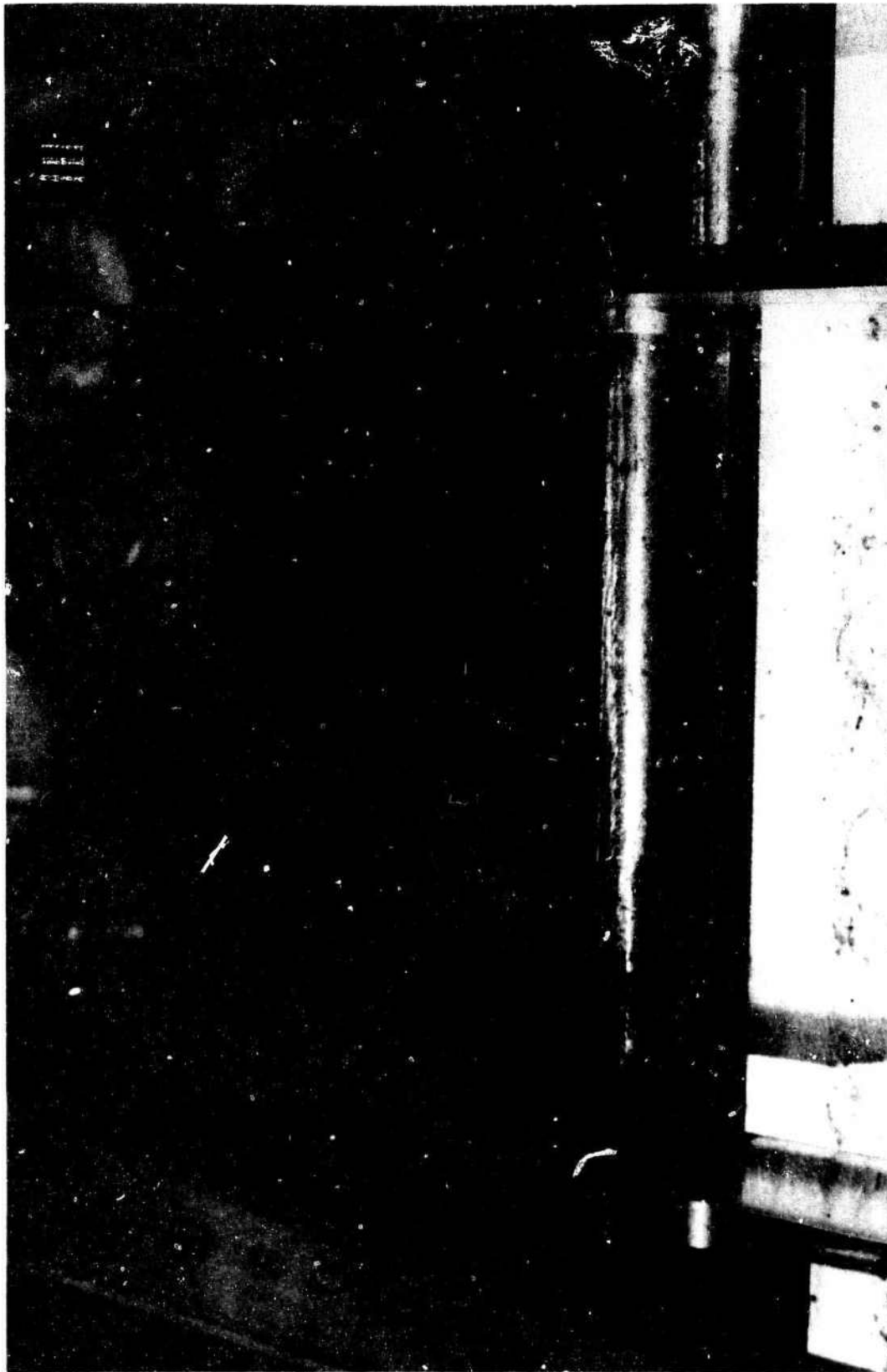


Figure 12. Crazing on the upper surfaces of the 4- by 48- by 2-inch-thick test beam No. 2 after 4 years of sustained flexure loading as a cantilever beam; the flexure stress above the fulcrum is 1960 psi.

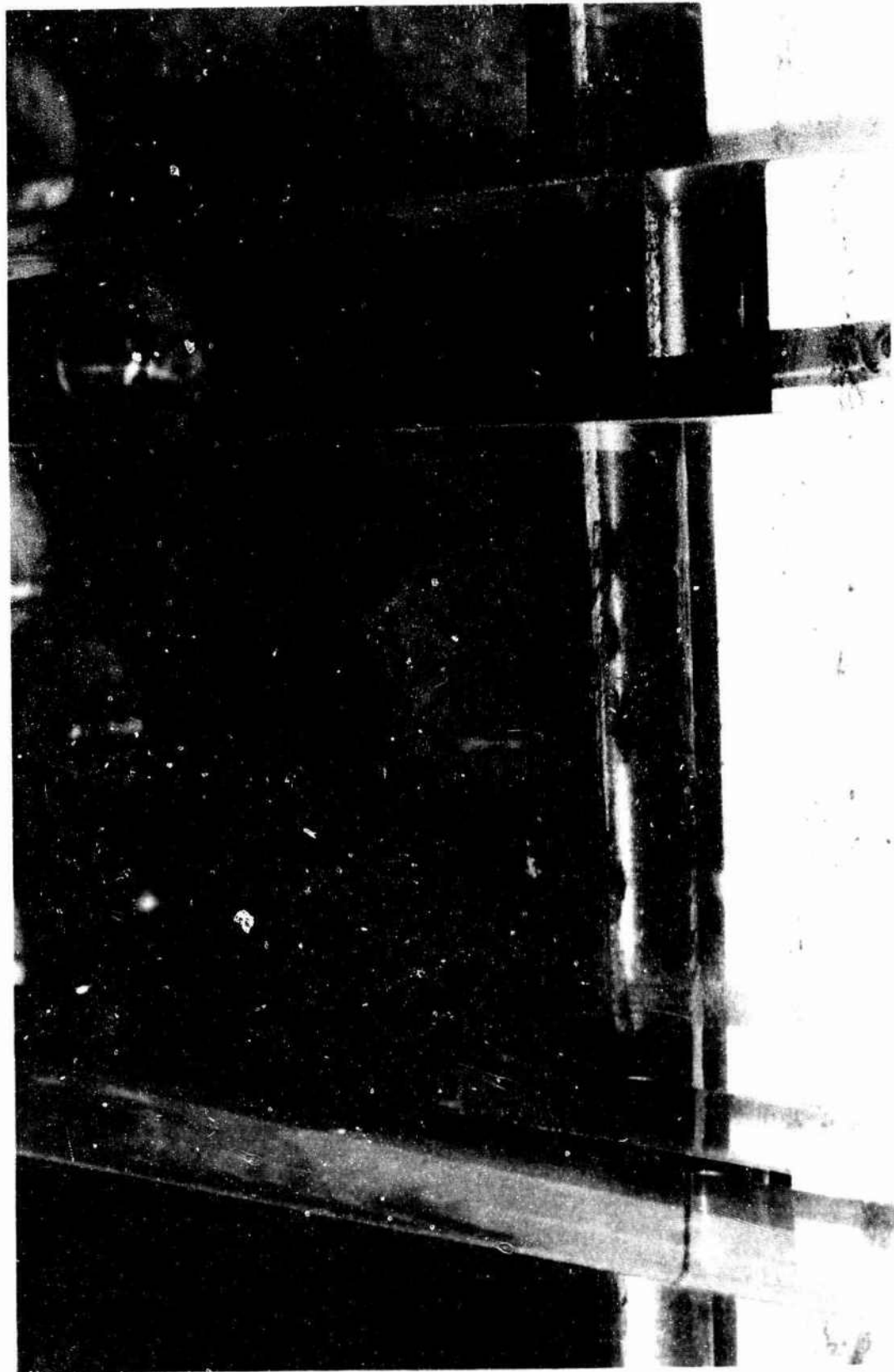


Figure 13. Crazing on the upper surface of the 4- by 48- by 2-inch-thick test beam No. 3 after 4 years of sustained flexure loading as a cantilever beam; the flexure stress above the fulcrum is 1570 psi.



Figure 14. Crazing on the upper surface of the 4- by 18- by 2-inch-thick test beam No. 1 after 5 years of sustained flexure loading as a cantilever beam; the crazing was photographed from below the beam.

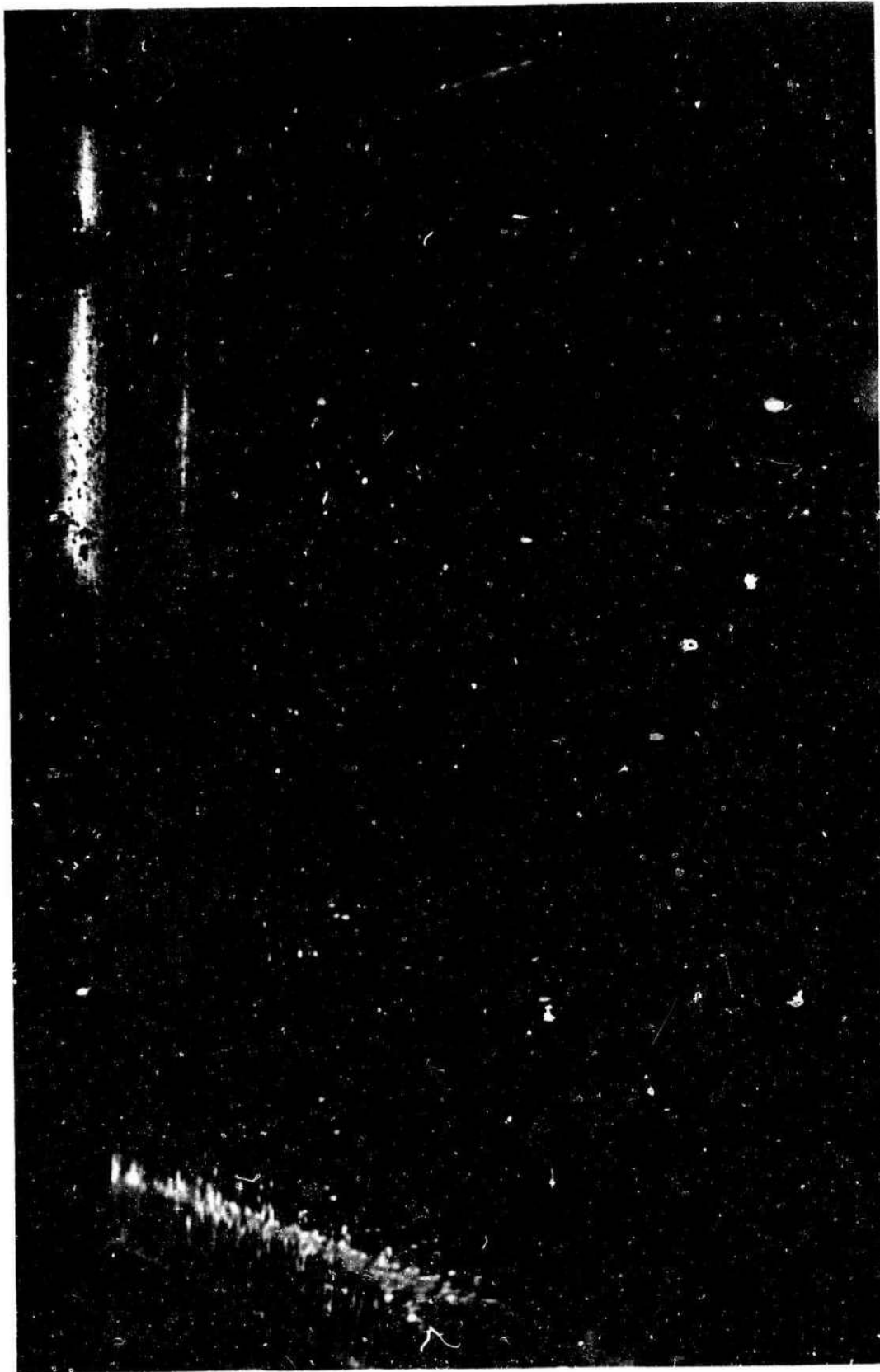


Figure 15. Crazeing on the upper surface of the 4- by 48- by 2-inch-thick test beam No. 2 after 5 years of sustained flexure loading as a cantilever beam; the crazeing was photographed from below the beam.

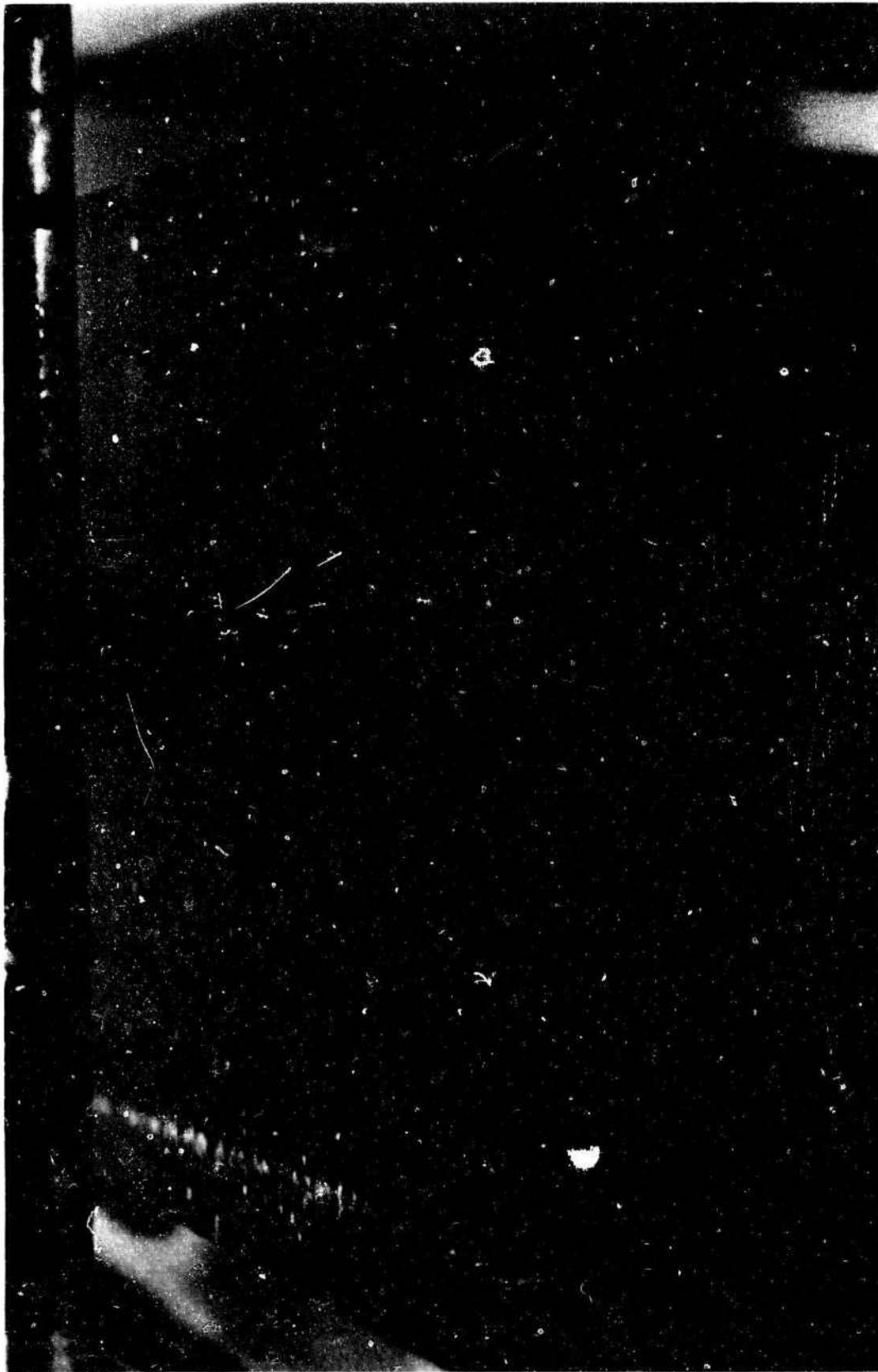


Figure 16. Crazing on the upper surface of the 48- by 2-inch-thick test beam No. 3 after 5 years of sustained flexure loading as a cantilever beam; the crazing was photographed from below the beam.



Figure 17. Note the absence of crazing on test beam No. 4 after 5 years of sustained flexure loading as a cantilever beam; the flexure stress above the fulcrum is 1200 psi. The beam was photographed from below.



Figure 18. The 4- by 48- by 2-inch-thick test beam under sustained 2240-psi flexure stress and outdoor weathering failed catastrophically after 9 years.



Figure 19. Crazing on test beam No. 1 after 9 years of sustained flexure loading as a cantilever beam. The stress above the fulcrum was 2240 psi.

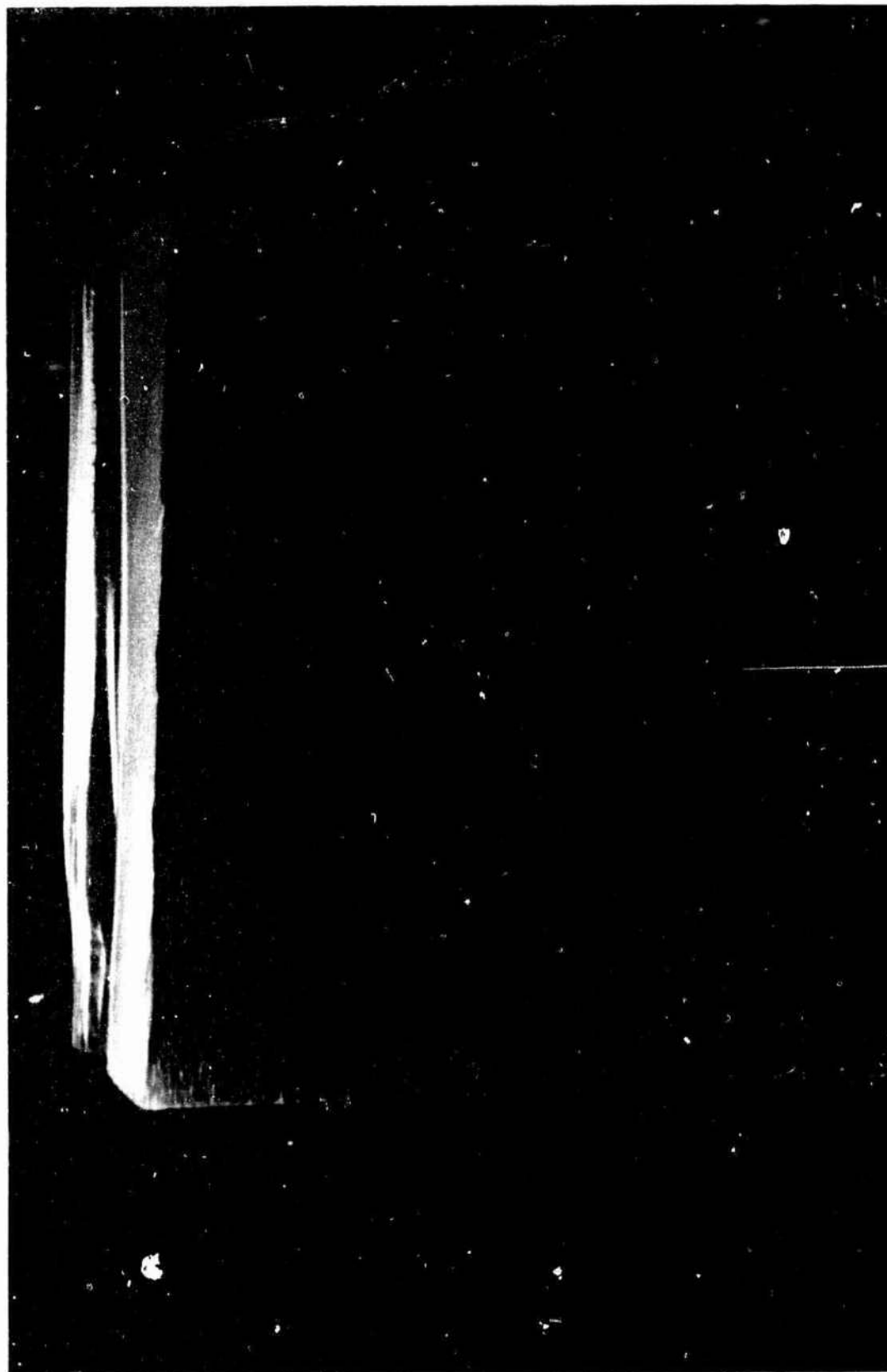


Figure 20. Crazing on test beam No. 2 subjected to sustained flexure stress of 1960 psi for 10 years.



Figure 21. Crazeing on test beam No. 3 subjected to sustained flexure stress of 1570 psi for 10 years.

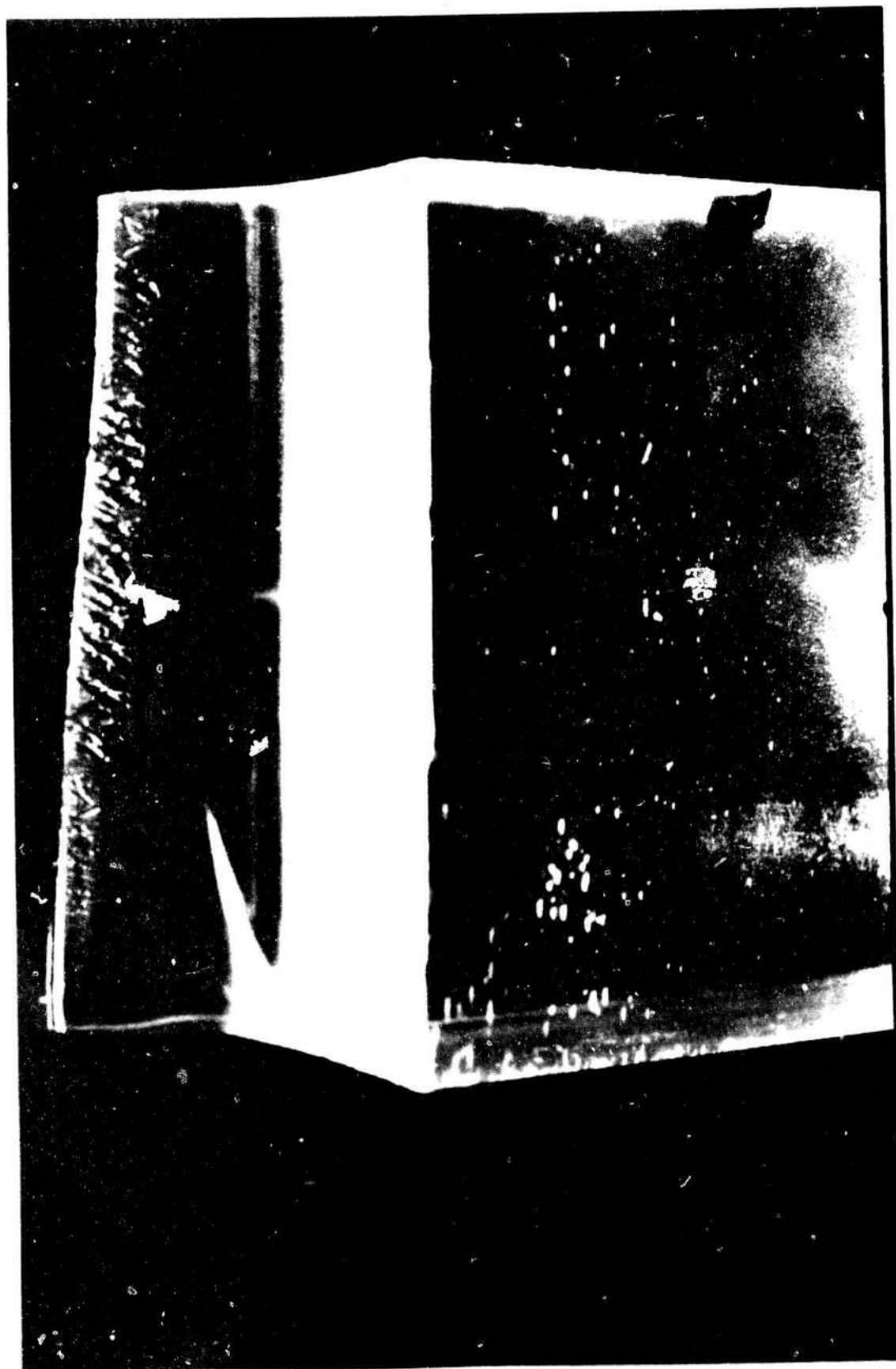


Figure 22. Crazing on test beam No. 4 subjected to sustained flexure stress of 1200 psi for 10 years.



Figure 23. Crazing on test beam No. 5 subjected to sustained flexure stress of 970 psi for 10 years.

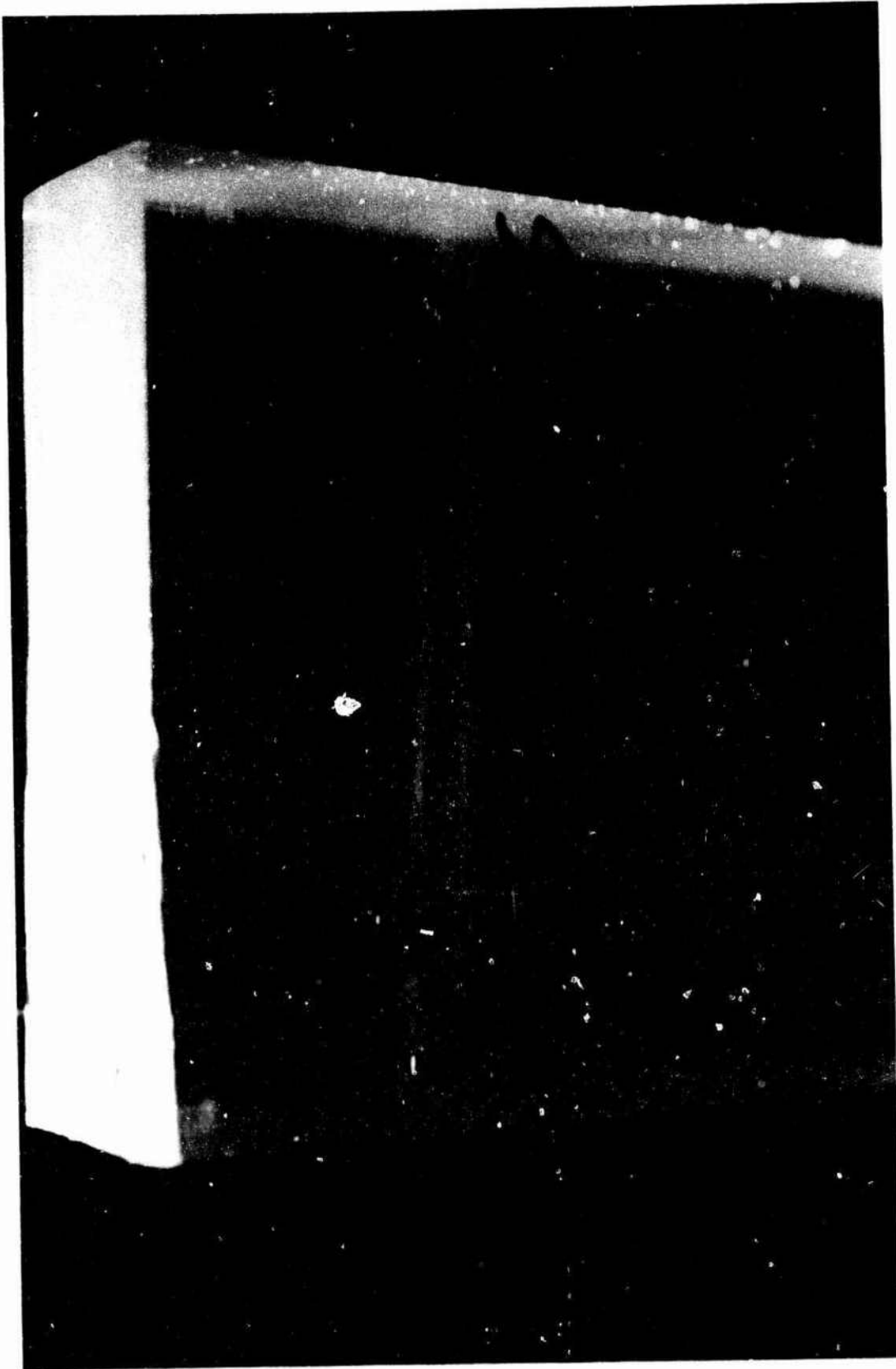


Figure 24. Crazing on test beam No. 6 subjected to sustained flexure stress of 810 psi for 10 years.



Figure 25. The 4- by 2-inch-thick test beam after 10 years of weathering and short-term flexure loading to catastrophic failure. Note the total absence of crazing on the surfaces of the beam.



Figure 26. All of the 4- by 48- by 2-inch-thick test beams were, after 10 years of weathering, loaded to failure to determine the effective flexure strength of the weathered plastic. The highest effective strength was found on *unstressed* specimen (No. 7), while the lowest one was found in the specimen subjected to the highest sustained flexure stress (No. 2).

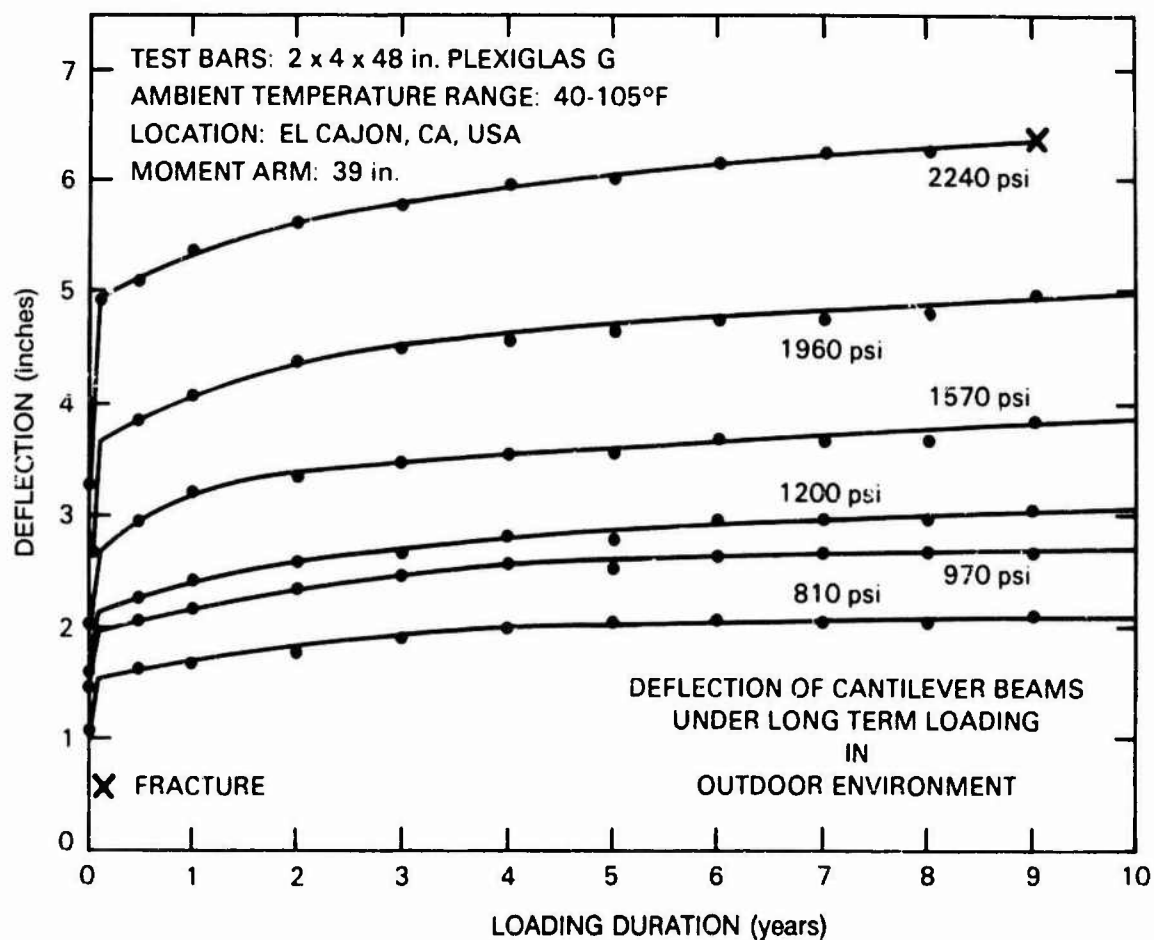


Figure 27. Deflections of the cantilevered test beams at their tips during sustained flexure loading in outdoor environment. The test beam under highest flexure loading failed in 9 years after extensive crazing.

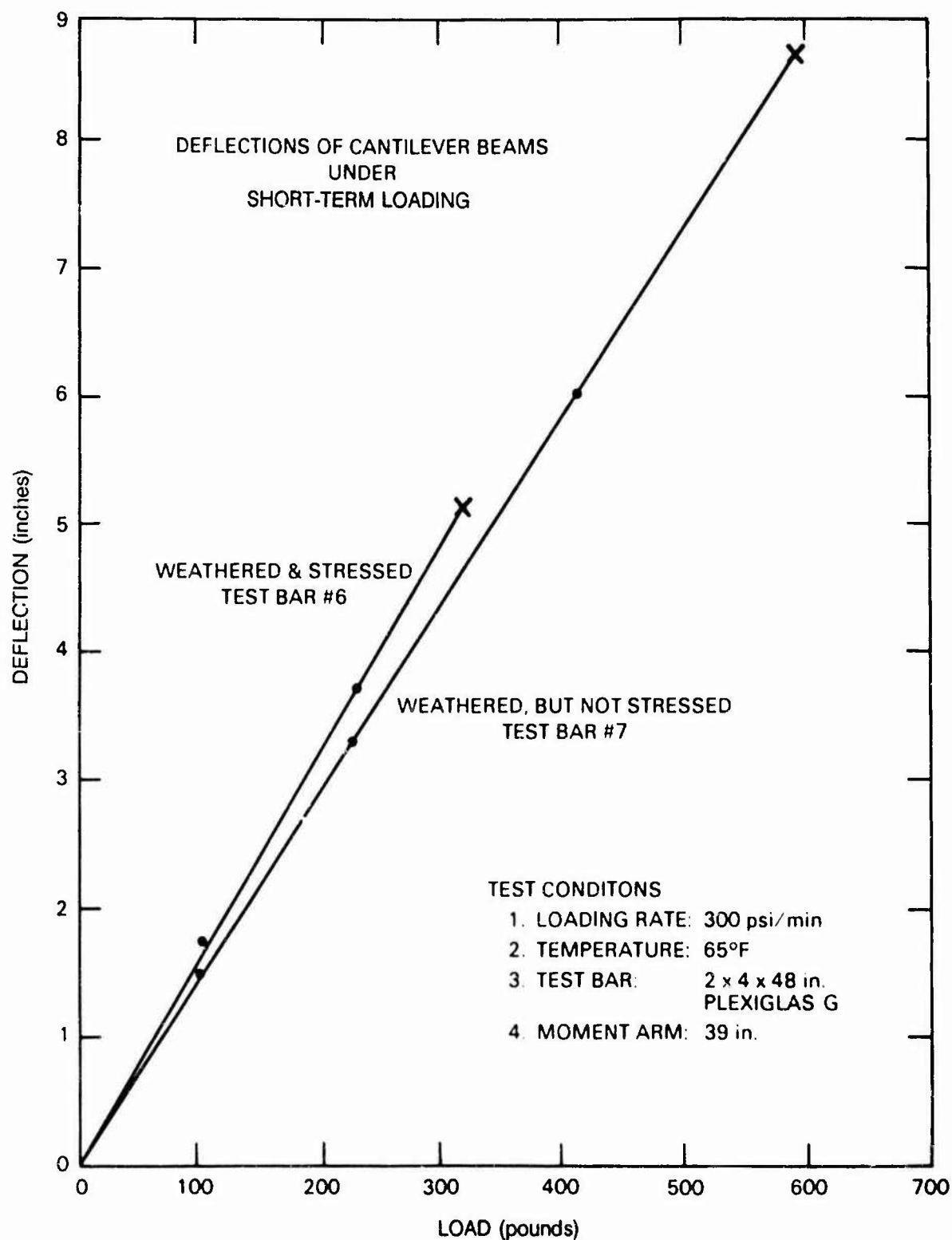


Figure 28. Deflections of cantilevered test beams during short-term loading to destruction. Note the significant difference in effective strength between the two weathered, crazing free beams: one unstressed and the other one under sustained flexure stress of 810 psi for 10 years.

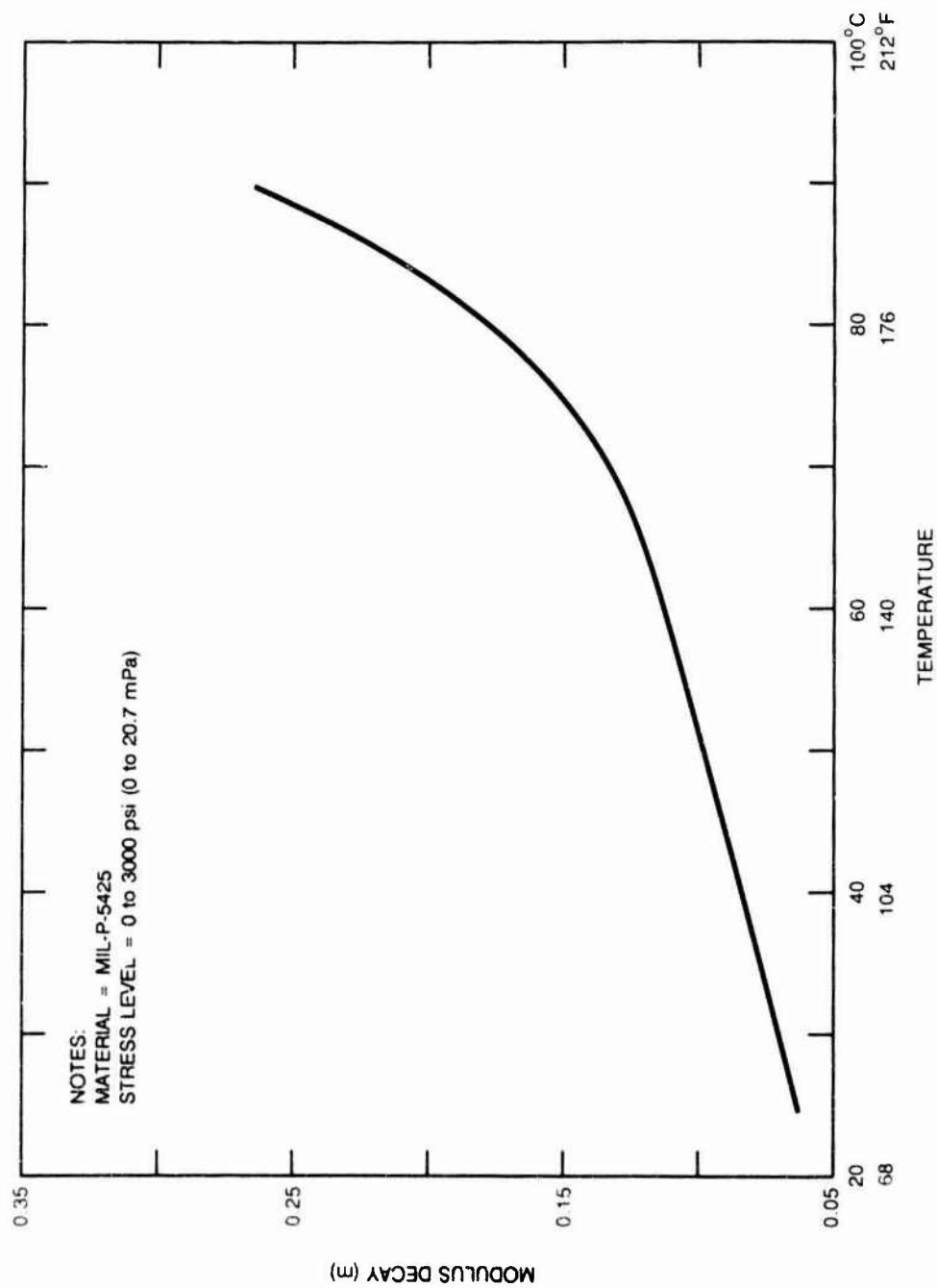


Figure 29. Decay of effective modulus of acrylic plastic (M) as a function of ambient test temperature.

Table 1. Physical properties of acrylic plastic prior to machining of test beams

Physical Property	Location						
	Top Surface	0.005 Below Top Surface	0.020 Below Top Surface	Mid-thickness	0.020 Above Bottom Surface	0.005 Above Bottom Surface	Bottom Surface
ASTM Tensile D-638 Strength (psi)	10,400	---	---	10,500	---	---	10,600
ASTM Flexure D-790 Strength (psi)	17,200	---	---	17,400	---	---	17,300
ASTM Compressive D-695 Yield (psi)	17,200	---	---	17,100	---	---	17,000
ASTM Shear D-732 Strength (psi)	10,200	---	---	10,300	---	---	10,300
ASTM Deformation Under Load D-621 24 hrs at 122°F and 400 psi	0.46	---	---	0.47	---	---	0.48
ASTM Izod D-256 Impact	0.37	---	---	0.38	---	---	0.36

Material: Plexiglas G 4 in. and 2 in. thick plates
 Weathering Specimens: 12 x 12 x 4 and 12 x 12 x 2 in.
 Test Specimens: ASTM

Table 2. Effect of outdoor weathering on flexural strength of acrylic plastic plates.

Length of Exposure	Location					
	Top Surface	0.005 Below Top Surface	0.020 Below Top Surface	Mid-thickness	0.020 Above Bottom Surface	0.005 Above Bottom Surface
0 year	17,000	17,300	17,300	17,400	17,300	17,200
5 year	15,600 ^E	16,800 ^E	16,200 ^E	17,400 ^E	16,900 ^E	17,100 ^E
10 year	E	---	---	---	---	---
	10,600 ^H	---	---	17,800 ^H	---	---
	5,900 ^L	---	---	17,200 ^L	---	---
	11,500 ^S	14,700 ^S	16,800 ^S	17,000 ^S	16,700 ^S	15,800 ^S
						15,000 ^H
						11,000 ^L
						15,400 ^S

Material: Plexiglas G
 Weathering Specimens: 12 x 12 x 4 in.
 Test Location: E - El Cajon
 L - Linkport
 H - Houston
 S - San Diego

Test Position: Horizontal
 Flexure Test: The indicated surfaces were flexed in tension
 Flexure Strength: psi, per ASTM D-790

Table 3. Cantilever beams under long-term loading in outdoor environment.

Test Bar	Maximum Flexure Stress (psi)	Deflection Upon Loading (inches)	Deflection After 1 hr (inches)	Deflection After 24 hrs (inches)	Deflection After 10 yrs (inches)	Deflection Upon Unloading (inches)	Deflection 1 hr After Unloading (inches)	Deflection 24 hrs After Unloading (inches)
#1	2240	3.250	3.82	4.00	6.25	---	---	---
#2	1960	2.625	2.85	3.04	5.00	2.68	2.375	2.06
#3	1570	1.908	2.095	2.22	3.875	2.00	1.700	1.50
#4	1200	1.408	1.533	1.72	3.09	1.625	1.370	1.125
#5	970	1.375	1.600	1.625	2.82	1.680	1.500	1.187
#6	810	0.97	1.200	1.220	2.125	1.125	1.00	0.810
#7	000	0.00	0.00	0.00	0.00	0.00	0.00	0.00

Test Conditions

Test Bars: 2 x 4 x 48 in.

Material: Plexiglas G

Moment Arm: 39 in

Temperature: 40-105°F range

Test Location: Outdoors, exposed to direct sunshine, El Cajon, CA

Table 4. Remaining strength of cantilever beams after 10 years' sustained loading in outdoor environment.

Test Bar	Maximum Flexure Stress Sustained for 10 yrs (psi)	Maximum Flexure Stress at Short Term Fracture (psi)	Maximum Deflection at Fracture (in.)
#1	2240	---	---
#2	1960	3300	3.37
#3	1570	3800	3.94
#4	1200	4130	3.80
#5	970	4230	3.90
#6	810	5020	5.06
#7	000	9300	8.50

Test Conditions

Test Bars 2 x 4 x 48 in. Plexiglas G

Moment Arm 39 in

Temperature 40-105°F range during long term testing
65°F during short term testing

Location Outdoors, exposed to direct sunshine, El Cajon, CA

Table 5. Physical and chemical properties of surface and subsurface layers in 2.5-inch Plexiglas G.

Location of Positively Stressed Specimen Surface	Flexure Test ASTM D-790			Type of Failure		Molecular Weight		Free Monomer Percent
	Strength, psi	Modulus, psi				Number Average	Weight Average	
Outward weathered surface	11,500	480,000		Brittle		378,800	665,100	0.57
0.005 inches removed from outward weathered surface	14,700	490,000		Ductile				
0.02 inches removed from outward weathered surface	15,800	480,060		Ductile		760,100	1,314,000	
0.04 inches removed from outward weathered surface	16,000	490,000		Ductile		12,140,000	1,675,000	
0.06 inches removed from outward weathered surface	16,200	490,000		Ductile		1,808,000	2,336,000	
0.08 inches removed from outward weathered surface	16,200	490,000		Ductile				
0.10 inches removed from outward weathered surface	16,100	480,000		Ductile				
Interior of the 2.5-inch thick Plexiglas G pentagon	15,800	490,000		Ductile		1,863,000	2,329,000	0.25
0.06 inches removed from inward unweathered surface	15,900	490,000		Ductile		1,514,000	1,963,000	
0.04 inches removed from inward unweathered surface	15,500	470,000		Ductile		1,096,000	1,632,000	
0.02 inches removed from inward unweathered surface	15,600	480,000		Ductile		578,000	870,900	
0.05 inches removed from inward unweathered surface	15,800	480,000		Ductile				
Inward unweathered	15,400	480,000		Brittle		437,000	683,900	0.31

NOTES:

1. The specimens were approximately 0.25 inches thick.
2. The specimens were cut from the 2.5-in thick spherical pressure hull of NEMO submersible. The submersible was commissioned in 1970 and decommissioned in 1980. The submersible was stored outdoors from 1975 to 1981.
3. Outward surface – convex exterior of NEMO hull, exposed to seawater and weathering.
Inward surface – concave interior of NEMO hull, exposed to condensation and interior atmosphere pollutants.
Interior – from midthickness of the hull.
4. Samples from outward layer were tested with outward surface in tension.
5. Samples from inward layer were tested with inward surface in tension.

Table 6. Flexural strength of 2.5-inch Plexiglas G—disc specimens.

MATERIAL	BIAXIAL FLEXURE STRENGTH	
	ARRANGEMENT A	ARRANGEMENT B
Interior of 10-year old weathered Plexiglas G	16,483 psi, mean 2,460 psi, standard deviation 6 specimens	17,583 psi, mean 2,456 psi, standard deviation 6 specimens
Outward layer 10-year old weathered Plexiglas G	8,500 psi, mean 2,236 psi, standard deviation 6 specimens	16,240 psi, mean 2,043 psi, standard deviation 6 specimens
Inward layer 10-year old weathered Plexiglas G	10,816 psi, mean 2,616 psi, standard deviation 6 specimens	14,460 psi, mean 1,751 psi, standard deviation 6 specimens
Interior of 1-year old unweathered Plexiglas G	16,750 psi, mean 995 psi, standard deviation 6 specimens	16,250 psi, mean 910 psi, standard deviation 6 specimens

NOTES

- 1 The dimensions of disc specimens were: 5 inches diameter x 0.5 inch thickness.
- 2 The specimens were taken from the following locations in the 2.5 inch thick spherical pentagon, cut out from the 10-year old, weathered pressure hull of submersible NEMO:
 - Outward Layer — The exterior surface of the sphere served as one surface of the disc specimen.
 - Interior Body — The disc specimen was cut from the mid thickness of the casting; both surfaces of the specimen were machined, sanded and polished.
 - Inward Layer — The interior surface of the sphere served as one surface of the disc specimen.
- 3 Arrangement A — The discs from outward and inward layers are tested with original hull surfaces in tension. Discs from the interior of the casting with both machined surfaces have the tension surface selected at random.
- Arrangement B — The discs from outward and inward layers are tested with original hull surfaces in compression. Discs from the interior of the casting with both machined surfaces have the compression surface selected at random.
- 4 The disc specimens were machined from the same spherical pentagon as ASTM specimens.

58

Table 7. Mechanical properties of 2.5-inch Plexiglas-G—ASTM specimens.

Type of Material	TENSION ASTM-D-638		Elongation percent	COMPRESSION ASTM-D-695		SHEAR ASTM-D-732	FLEXURE* ASTM-D-790		FLEXURE** ASTM-D-790		COMPRESSION ASTM-D-621 percent	IMPACT STRENGTH ASTM-D-256 Izod Notch ft lbs/in
	Strength psi	Modulus psi		Yield psi	Modulus psi		Strength psi	Modulus psi	Strength psi	Modulus psi		
Interior of 10-year old weathered Plexiglas G	11,300	440,000	5.9	16,300	490,000	12,300	16,800	490,000	16,800	470,000	0.65	0.38
	11,200	450,000	6.0	16,400	500,000	12,000	16,900	500,000	16,600	480,000	0.55	0.37
	11,300	490,000	5.2	16,300	490,000	12,500	16,900	500,000	16,900	500,000	0.58	0.27
Outward layer of 10-year old weathered Plexiglas G	11,100	520,000	4.3	16,400	500,000	12,500	17,000	490,000	16,700	490,000	0.54	0.39
	9,460	460,000	3.1	15,900	500,000	11,400	9,520	510,000	18,100	480,000	0.66	0.31
	10,000	480,000	3.5	16,100	490,000	10,800	10,100	500,000	16,500	510,000	0.66	0.34
Inward layer of 10-year old weathered Plexiglas G	7,180	450,000	2.6	16,100	500,000	11,200	12,000	500,000	16,600	490,000	0.66	0.38
	10,400	450,000	4.1	16,300	500,000	11,700	12,800	480,000	16,700	480,000	0.48	0.35
	9,410	510,000	3.0	15,700	490,000	11,900	15,800	490,000	16,600	450,000	0.67	0.37
Interior of 1-year old unweathered Plexiglas G	9,290	520,000	2.9	15,700	470,000	12,300	15,600	480,000	15,800	460,000	0.64	0.36
	9,870	480,000	3.6	15,700	480,000	12,100	15,700	480,000	16,700	450,000	0.88	0.29
	8,910	530,000	2.7	15,500	480,000	11,100	14,300	470,000	16,000	420,000	0.74	0.36
Interior of 1-year old unweathered Plexiglas G	10,100	440,000	3.8	16,500	480,000	11,200	16,600	480,000	17,000	500,000	0.7	0.4
	10,600	440,000	6.3	16,700	470,000	11,900	16,500	460,000	16,800	180,000	0.7	0.38
	10,600	440,000	4.9	16,900	480,000	12,300	16,200	480,000	16,700	460,000	0.8	0.39
	10,290	440,000	4.9	16,400	480,000	10,500	16,900	480,000	16,600	470,000	0.8	0.40

NOTE:

1. The specimens were approximately 0.25 inches thick, except for compression, deformation under load, and impact strength specimens which were 0.5 inches thick.
2. The weathered material was removed from NEMO pressure hull, commissioned in Bahamas during 1970 and decommissioned in San Antonio, Texas during 1981. From 1975 to 1981 the submersible was stored outdoors in San Antonio, Texas with the hatch closed.
3. *flexure - the original hull surface is placed in tension; orientation of specimens from interior is at random.
**flexure - the original hull surface is placed in compression; orientation of specimens from interior is at random.
4. Outward layer - layer from the exterior of the pressure hull, exposed to seawater and weathering.
Inward layer - layer from the interior of the pressure hull, exposed to condensation and interior atmosphere of submersible.
Interior - layer from the mid thickness of the pressure hull.

DEFINITIONS

Flexural strength — maximum calculated flexure stress in a specimen under four-point loading per ASTM D 790 at the moment of fracture initiation.

Compressive strength — nominal calculated compressive stress in a specimen under normal compression loading per ASTM D 695 at the initiation of yielding.

Tensile strength — nominal calculated tensile stress in a tensile specimen under uniaxial tensile loading per ASTM D 638 at the initiation of fracture.

Shear strength — nominal calculated shear stress in a shear specimen under shear punch loading per ASTM D 732 at the initiation of fracture.

Effective strength — (same as residual or remaining strength) strength of material after being subjected to weathering or service loading.

Degradation of material — difference between strengths of material *prior to* and *after* placement in service or environmental test program.

Short-term loading — continuous increase in load until yielding or fracture occurs.

Sustained loading — constant loading which, once applied, is not varied in magnitude until termination of test program.

Creep — time-dependent increase in strain under constant magnitude of loading.

Modulus of elasticity — stress-to-strain ratio of material under short-term loading, (slope of the stress-strain graph on linear coordinates).

Effective modulus — stress to *total* strain ratio of material after a selected time duration of sustained loading (total strain is the *sum* of elastic and time dependent strains). The effective modulus is always less than the modulus of elasticity.

Creep rate — the rate at which the magnitude of creep increases with duration of sustained loading (i.e., microinches per inch per unit of time).

Modulus decay — the rate at which the effective modulus decreases with duration of sustained loading.

Short-term critical pressure (STCP) — hydrostatic pressure causing a pressure-resistant window to fail catastrophically under short-term loading.

Working pressure (WP) — maximum pressure for which the window is rated.

Design pressure (DP) — magnitude of pressure used in structural calculations for windows. As a rule, P equals or exceeds WP.

Conversion factor (CF) — ratio of short-term critical pressure for a brand new window to the working pressure specified by ANSI/ASME PVHO-safety standard.

Safety factor — ratio of *effective material strength* after placement of acrylic structure in service to the design stress for that structure.

REFERENCES

1. Hertzberg, Richard W. 1973. "Fatigue Crack Propagation Characteristics in Polymeric Materials" *Closed Loop*, p. 12.
2. Technical Report No. 82-1 Swedlow submitted to Ralph Speelman, A7WAL/FiEA January 1982.
3. Sternstein, S.S., L. Ongchin, and A. Silverman. 1968. "Inhomogeneous Deformation and Yielding of Glasslike High Polymers" *Applied Polymer Symposia* No. 7, 175-199.
4. Berry, J.P. "Fracture Processes in Polymeric Materials. II. The Tensile Strength of Polystyrene." *Journal, Polymer Science*. Vol. L, p. 313-321.
5. Bodey, C.E. April 22, 1965. "Pressure Effects on Plexiglas Circular Disc." *Letter Report Autonetics*.
6. Winter, R., and J. Pozerycki. 1968. *Tests of Acrylic Deep Submergence Windows Under Simulated Operational Conditions*. Allied Research Associates, Inc. Concord, MA 1968.
7. Ogorkiewicz, R.M. 1970. *Engineering Properties of Thermoplastics*. Wiley-Interscience, New York.
8. Cheng, H., and R.B. Bannerot. 1981. *On the Weathering of Thin Plastic Films*. ASME Paper 81-WA, Winter Annual Meeting.
9. Stachiw, J.D. August 9, 1982. Letter to Colonel Paul Sheffield, USAF, "Tests on Cleaners/Disinfectants - Effect on Acrylic Crazing."
10. "Perspex" *Bulletin on Machining*, 1966. Imperial Chemical Industries Limited.
11. Rosen, Bernard, editor. 1964. *Fracture Processes in Polymeric Solids*, Interscience Publishers, N.Y.
12. Yustein, S.E., Winans R.R., and H.J. Stark. 1951. "Outdoor Weathering of Plastics under Various Climatological Conditions." *American Society For Testing Materials, Bulletin* No. 173.
13. Yustein, S.E., Winans R.R., and H.J. Stark. 1954. "Three Year's Outdoor Weather Aging of Plastics Under Various Climatological Conditions." *American Society For Testing Materials Bulletin*.
14. Stachiw, J.L., and J.D. Stachiw. 1977. "Effects of Weathering and Submersion In Seawater on the Mechanical Properties of Acrylic Plastic," ASME paper 77-WA/OCE-5 Winter Annual Meeting, ASME.
15. Stachiw, J.D., and R.B. Dolan. 1982. "Effects of Weather, Age, and Cyclic Pressurizations on Structural Performance of Acrylic Plastic Spherical Shells Under External Pressure Loading," *American Society of Mechanical Engineer's Proceedings/Journal of Engineering For Industry*, Vol. 103, No. 2.
16. American Society of Mechanical Engineers, Safety Codes Committee on Pressure Vessels For Human Occupancy. 1987. "ANSI/ASME PVHO-1 Safety Standards For Pressure Vessels For Human Occupancy," ASME, New York.
17. Stachiw, J.D. 1982. "Acrylic Plastic Viewports; Ocean Engineering and Other Hyperbasic Applications," Marcel Dekker, New York.



an ASME
publication

**\$3.00 PER COPY
1.50 TO ASME MEMBERS**

The Society shall not be responsible for statements or opinions advanced in papers or in discussion at meetings of the Society or of its Divisions or Sections, or printed in its publications. *Discussion is printed only if the paper is published in an ASME journal or Proceedings.* Released for general publication upon presentation. Full credit should be given to ASME, the Technical Division, and the author(s).

Effect of Weathering and Submersion in Seawater on the Mechanical Properties of Acrylic Plastic

J. L. STACHIW

San Diego Unified Schools,
San Diego, Calif.

J. D. STACHIW

Naval Ocean Systems Center,
San Diego, Calif.
Mem. ASME

Both weathering and submersion in seawater affect the optical and physical properties of cast methyl methacrylate plastic used for fabrication of pressure resistant viewports and pressure hulls in ocean engineering structures. Weathering has a more significant effect on deterioration of physical properties than long term submersion. Exposure to sunlight in humid tropical climate has the most significant effect, while dry arctic exposure has the least effect. It is now known, however, at the present time how much the thickness of the test specimen affects the rate of deterioration in physical properties. In lieu of definitive long-term weathering data on thick acrylic, a 10-year life limit has been temporarily set for such structures by ANSI/ASME PVHO-1 Safety Standard. Submersion appears to have no significant effect on material properties. Its effect on optical properties is, on the other hand, very detrimental; in less than 10 days the visibility is lost due to biological fouling. Chemical and mechanical techniques are available, however, for preserving visibility through submerged acrylic windows for an indefinite period of time. To satisfy the need for data on weathering of thick acrylic plastic, an exploratory test program has been initiated that, with cooperation of interested parties in ocean engineering community, may expand into a program with worldwide coverage of weathering conditions.

Contributed by the Ocean Engineering Division of The American Society of Mechanical Engineers for presentation at the Winter Annual Meeting, Atlanta, Georgia, November 27-December 2, 1977. Manuscript received at ASME Headquarters July 26, 1977.

Copies will be available until August 1, 1978.

Effect of Weathering and Submersion in Seawater on the Mechanical Properties of Acrylic Plastic

J. L. STACHIW

J. D. STACHIW

INTRODUCTION

When using acrylic as an engineering material, it is imperative that the characteristics of the material, as well as its resistance to ambient environment, be well known. In the case of fouling, effects of long term submergence, and weathering, extensive data are not present. Because we do not know how acrylic deteriorates, we have to severely limit the proposed life of an acrylic structure. This approach is clearly seen in the ANSI/ASME PVHO-1 Safety Standard.

In general, there are two prerequisites to being able to predict safe operational life of any structure. The first of these is to have an accurate prediction of what the loads will be to which the structure is subjected both under static and dynamic loading. To a major extent we can satisfy this prerequisite because we can predict the loads by controlling the use of the structure. In the second prerequisite, we must have an accurate schedule of material deterioration under the influence of environment if we are to accurately predict safe operational life. Because we do not have sufficient data, ANSI/ASME PVHO-1 Safety Standard has incorporated the use of conversion factors into the Safety Standard which do take into account some deterioration. But even with the conversion factors, we think at the present time that 10 yr is the maximum life for acrylic structures.

This 10-yr life is based on the experimental data that do exist in the areas of fouling, effects of long term submergence, and weathering.

FOULING

Marine microorganisms attach themselves to all submerged surfaces and create, first of all, a marine slime layer of bacteria, algae and other microorganisms (2).¹ On this primary layer which acts as an inducement, the barnacle

population begins to grow along with the hydroids and other marine plants and animals. These organisms multiply at a rate up to 1,000,000 times faster when attached than when free floating (2). There are, however, some natural deterrents to the accumulation of fouling. Cold, excessive heat, salinity, pressure, pollution and water movement all act to inhibit the growth of marine organisms (6). Fouling organisms decrease in variety and abundance with increased depth to about 100 ft and below 100 ft the fouling increases the closer the object is to the bottom (6). For information on what happens at greater depths, the work of James S. Muraoka of the Civil Engineering Laboratory, Port Hueneme, California, is very valuable.

Over a period of years, a large number of test specimens of various materials were lowered into the ocean to a maximum depth of 6800 ft and left for periods of up to 5 yr. When retrieved from the ocean, Muraoka found that most of the fouling on the acrylic panels consisted of mud tubes made by tubeworms and growth of various species of bryozoa, hydroids, barnacles, anomiae and colonial tunicates (7-11). It was also discovered that numerous deep to shallow grooves were present in the acrylic (12). These had been created when the acrylic was placed in contact with untreated wood and the borers had eaten through the wood and into the acrylic. In extruded acrylic, however, only a small number of borers penetrated into the plastic at all (8). It seems reasonable to assume that while acrylic is probably not susceptible to biological deterioration in the deep ocean, it must not be placed in direct contact with untreated wood as it will be damaged to some extent by wood borers attached to wood (9).

While the agents of fouling do not actually damage the acrylic in a way that would

¹ Numbers in parentheses designate References at end of paper.



Fig. 1 Untreated sample of 2.5-in. thick acrylic plastic after continuous submersion for two weeks, 9 ft below sea surface in 33 ft deep water off Pt. Mugu, Calif.

cause structural failure, they do cause the acrylic to cease to be useful because these agents reduce or destroy visibility. Dr. C. V. Metzler of the Naval Missile Center, Point Mugu, California, conducted a series of experiments to determine the rate of loss of visibility of acrylic in shallow water at the end of a pier. He found that after 8 hr, there was no loss of visibility and no fouling; after 1 wk a slight loss of visibility and fouling by algae; after 18 days, a complete loss of visibility and fouling by many different organisms (6), (Fig. 1). Muraoka conducted a similar experiment but this was in the open ocean at a depth of 120 ft. He found after 12 months exposure, visibility through a clear acrylic panel was only fair and fouling consisted of hydroid growth; in 18 months, the visibility was very poor (12). There were several factors apparently involved in the wide variation of results in these two tests. First, the difference in depth. Metzler's specimens were at times as close as 15 ft to the surface. Second, Muraoka's tests were conducted in the open ocean while Metzler's were from a pier located in calm water. In addition, there were differences in the temperature ranges, water movement and pollutants present. Therefore, the best that can be generalized from these studies is that fouling does occur and, in a relative short period of time, an acrylic panel can become so fouled as to be virtually opaque.

This loss of visibility, of course, makes



Fig. 2 Untreated sample of 2.5-in. thick acrylic plastic after 2 weeks cumulative submersion, 18 ft below sea surface in 33 ft deep water off Pt. Mugu, Calif. Sample was removed each day during the first week and bathed briefly in fresh water. During the second week the sample was left undisturbed.

an acrylic window useless once extensive fouling has set in. In the case of a submersible which may be in the water for only 4 to 6 hr a day and then rinsed off topside with fresh water, the windows will never become fouled. Fig. 2 illustrates this very clearly. The specimen was placed in the ocean but removed once a day and rinsed off with fresh water for a period of one week. Then the specimen was continually submerged for one week. As can be seen, visibility is still quite good (6). When instead of rinsing with fresh water, sea water was used, visibility was destroyed within the two week period (Fig. 3). If the windows are to be subjected to prolonged continuous exposure, however, some other method must be found to keep fouling organisms from attaching themselves to the windows.

Over the years various substances have been used in an attempt to provide an anti-fouling coating. Any anti-fouling material must be highly toxic to the fouling organisms, easily applied, have a long toxic life, and must be a clear material so that it will not affect the transparency of the acrylic (14). In addition, the substance must not attack the acrylic. Most anti-fouling "paints," whether those used on ship bottoms or windows, wear off in from 12 to 20 months (2). In some cases a bacterial film may form a protective layer over

SEPTEMBER 1967



Fig. 3 Untreated sample of 2.5 in. thick acrylic plastic after 2 weeks cumulative submersion 18 ft below sea surface in 33 ft deep water off Pt. Magu, Calif. Sample was removed each day during the first week and bathed briefly in sea water. During the second week the sample was left undisturbed.

the anti-fouling coating normally toxic to fouling animals, thereby affording a foothold for growth for those animals (13).

The Organo-tin compound known as bis (tri-N-butyltin) oxide or simply TBTO appeared to be the most promising of all the anti-fouling coatings as it met all the criteria for desirability (1, 6, 14). Ames found that in his tests the best protection was afforded by using Farboil 207-2 to which 3 to 5 percent of TBTO was added (1). After 60 days of immersion, Ames found no fouling organisms but there was a slight slime detritus film over the windows (1). However, visibility and transparency were still fair to good, and the windows could easily be cleaned by simply wiping with a soft cloth (1) (Fig. 4).

Metzler, in his shallow water tests, coated his windows with TBTO straight from the bottle and found that there was no fouling for at least two weeks (6) (Fig. 5).

Dyckman and others decided, after some inconclusive tests with anti-fouling agents, that the only way the anti-fouling agents would work for prolonged periods of time would be if the agent were introduced directly into the surface of the acrylic (6) or were bound within a resinous polymer matrix (2). Muraoka experimented with impregnating acrylic with a concentrated TBTO solution by placing the test



Fig. 4 Acrylic plastic samples after continuous submersion for 2 months in Charlestown Pond, R. I. Window on the left was coated with Farboil 207-2 (3 percent TBTO), while the one on the right was left untreated. The coated window was fouled only with algae film.

specimens under hydrostatic pressure and so attempting to force the TBTO inside the acrylic (14). In his experiment, Muraoka had four series of panels. One set was untreated and was the control set. A second set was simply dip-treated in a TBTO solution and allowed to dry in air. A third set was put in a concentrated solution of TBTO and subjected to 3000-psi hydrostatic pressure for 30 min. The fourth set was put in a concentrated solution of TBTO, and subjected to 10,000 psi for 5 hr. Both sets 3 and 4 were drip dried. This left a sticky coating which did distort visual images. Therefore, some of the 3000-psi treated windows were cleaned with alcohol to remove the sticky coating. All the sets were put in the ocean in approximately 20 ft of water about 5 ft off the bottom. After 9 days, the uncleaned 3000-psi treated panels showed very little growth, with good visibility. After 29 days, these windows were completely covered and no visibility. The average temperature during this test was 60 F (14). For the 10,000-psi treated and the dip treated panels the results were slightly different. After 6 days, these windows were free of biological growth but there was a slight reduction in visibility. After 18 days, there was no significant growth and visibility was very good. After 35 days the panels were covered with a fine film which significantly reduced visibility. The water temperature during

SEPTEMBER 1967

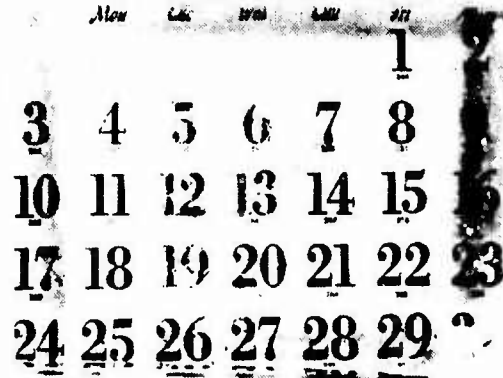


Fig. 5 Sample of 2.5-in. thick acrylic plastic treated with TBTO after continuous submersion for 2 weeks, 11 ft below sea surface in 33 ft deep sea water off Pt. Mugu, Calif.

this test averaged 64 F (14). While these tests are certainly not conclusive, it would seem reasonable to conclude that TBTO, no matter how applied, protects the acrylic only during the early stages of exposure and for only a limited time (14). In fact, some experiments indicate that no anti-fouling agent for acrylic windows has been truly successful for more than 20 days (3).

This same conclusion appears to hold true for the strippable films which can be applied directly to the window. Metzler found that N. F. Cardarelli of B. F. Goodrich Company has developed a transparent polyvinyl chloride film impregnated with TBTO (6). The film, like TBTO applied any other way, has a rather short life but does have the advantage of easy replacement. This strippable film was used on the PX-15 when it floated for 3 months in the Gulf Stream in 1968. Muraoka found that a plastic film of PTFE tested for 5 yr at 120 ft, while covered with growth, could easily be stripped away and underneath, the window was as clean as when first placed in the ocean (12). No cleaning of the window was necessary and therefore, there may be certain advantages of the strippable film over painted-on anti-fouling coatings.

It is apparent, however, that if an acrylic window is to be submerged for any appreciable period of time, for example in a submerged habitat, then some other anti-fouling measures besides the presently available anti-fouling coatings must be employed. If the

window is placed at diver depth, it is possible that a combination of painted-on TBTO, strip-pable film, and wiping could keep the window clean. At the greater depths, these approaches simply will not suffice.

When the Civil Engineering Laboratory at Port Hueneme, California, decided to build a concrete experimental habitat to test materials construction and deployment techniques at a depth of 600 ft a large spherical sector window of acrylic plastic was incorporated into the structure even though the habitat was never to be manned. After submersion of the habitat the window would allow manned submersibles and unmanned robots not only to inspect the interior of the habitat for leakage but also photographically record some data prominently displayed on instrumentation panels inside the habitat.

While SEACON I, the name given to this habitat, was still in the planning stages, it became apparent that some new approach must be tried if the window were to remain useful for the full 10 ¹/₂ months SEACON I was to be on the ocean floor, therefore, a special external fouling prevention system was designed, installed, and made operational. This system was composed of a window cover, a wiper brush assembly, a lift bag attached to the window cover and wiper assembly, a solenoid valve to activate air for the lift bag, a 1/10 hp d-c motor to rotate the brushes and a chemical dispenser of TBTO installed in the window cover (3). The window cover provided a stagnant area around the window exterior where TBTO was to be continually leached from the chemical dispenser. When the inspection party inside a submersible wished to use the window for viewing, the solenoid valve was activated and air at 10-psi above ambient pressure filled the bag. This caused the cover to rise, brought the brushes out of contact with the window and gave the inspection party an unobstructed view through the window. When set on automatic, the d-c motor rotated the wiper brushes for 2 min. every 3 hr, or, if on manual, for any desired time. It was planned that whenever the window cover was reclosed the dispenser would introduce TBTO into the stagnant area around the window until equilibrium of the TBTO solution was reached. However, the dispenser fell off while the habitat was being launched to the ocean floor and thus no chemical was used in the window anti-fouling system. The wiper assembly was set on automatic and operated successfully throughout the entire 10 ¹/₂ months SEACON I was down. The cover assembly

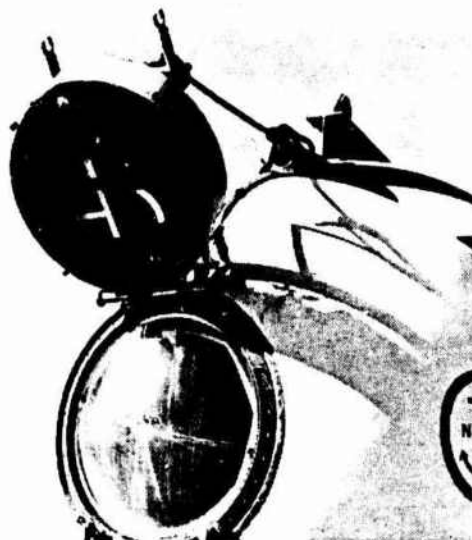


Fig. 6 Viewport assembly of SEACON I habitat showing protective cover and wiper brushes for cleaning of window. The cover is raised only for brief periods of time when observations are performed through the window.

was raised and lowered by inspection parties 10 times during this same period (3). The wiper brushes performed beyond expectations. On the perimeter of the window where the wipers did not reach, there were hydroids and primary slime but the action of the wipers apparently prevented the spread of the hydroids and a slime buildup (3). As Metzler had found previously, disturbing the environment appeared to reduce the rate of fouling markedly (6). A picture of this assembly is found in Fig. 6.

It is obvious from this rather brief discussion that at the present time there is no easy method that can be readily employed to counteract fouling. However, it must be remembered that fouling does not structurally affect an acrylic window. It causes the window to become useless for its designed purpose, but once cleaned of the fouling agents, it can usually be reused. The worst case of fouling occurs when the window is to be submerged for extended periods of time, as in a habitat. It is recommended that more experimental approaches be investigated for preventing fouling of windows in stationary habitats if their functional value is to be preserved over the projected operational life of the habitat.

EFFECTS OF SUBMERGENCE

For specimens that were submerged for varying lengths of time, data are much more

comprehensive than for fouling. It can be found that specimens immersed in water for a period as long as five years have undergone no significant chemical change (18). Schwartz found after investigating windows from the TRIESTE II submersible that there was no deterioration in the material's mechanical properties and no indication of degradation of the viewing characteristics or viewing quality (19). Willoughby states emphatically that Plexiglas simply does not deteriorate with age (19).

Acrylic, like other permeable materials, does absorb some water when subjected to prolonged exposure in the ocean. The results are varied, however. In one test, 1/16-in. thick specimens were placed in a 100 percent humidity environment and the water absorption was measured at 2 percent (18). Another experiment with 1/4-in. thick specimens that were immersed for 250 days lead to a 2.2 percent absorption of water (18). Muraoka found that his specimens which were left at 2370 ft, in the open ocean, for one year, absorbed about 0.44 percent moisture if the specimen were of extruded acrylic and 0.46 percent if made of cast acrylic (11). If the specimen were one year at 6800 ft, the extruded acrylic absorbed only 0.35 percent and the cast acrylic, 0.40 percent (9). In the tests conducted for two years at 5640 ft, Muraoka found moisture absorption for extruded acrylic to be 0.23 percent and cast acrylic, 0.51 percent (10). In general, it can be concluded that the maximum water absorption found was 2.2 percent for extended immersion of thin specimens. It should be emphasized, however, that all of the test specimens were extremely thin in comparison to actual windows or acrylic structures. How much effect this thickness difference makes is unknown. It is believed that the thicker windows would probably absorb less than the values recorded because only one face of the window would be exposed to the water and then only a small proportion of the total volume of the window would be wetted.

These same general conclusions can be made regarding the hardness tests that were conducted with acrylic before submergence and after. One series of tests showed the hardness test of acrylic before exposure reading 90.0 on the Durometer and 88.0 after five months at 600 ft (3). Another showed a dry reading of 90.0 for cast acrylic and 82.0 after being exposed two years at 5640 ft (10). Whether this change in hardness can be attributed to the absorption of water, effects of pressure, or slight changes in mechanical properties is un-

Table 1 Effects of Weathering in Various Climates on Acrylic Plastic -- A Three-Year Study on 1/8-In.-Thick Test Specimen (21)

	PAWAH	NEW MEXICO	NEW YORK	CANADA	ALASKA
Tensile Strength	down slightly with period of exposure	down slightly after most exposure	down slightly	cyclical	cyclical
Flexural Strength	down slightly with period of exposure	no change	no change of any significance	down slightly	down slightly after long exposure
Light Transmission	up	no change	down slightly	no change	no change
Haze	up	up	up to 65	up slightly	up slightly
Surface Appearance	yellowed some	yellowed some	no change	no change	no change

clear. The fact remains that while some slight changes do occur they are not significant and can be theoretically disregarded when designing with acrylic.

In the area of other physical properties, acrylic test specimens of 1/4 and 1/8-in. thickness were placed at 2300 ft in the open ocean for 6 1/2 months in both a flexed and relaxed position. The results showed an insignificant increase in E, flexural modulus and decrease in tensile and compressive strength (4). However, all changes were less than 10 percent. In another experiment with 1/4 and 1/8-in. thick specimens placed in 6780 ft of water for 403 days the same basic results were obtained (5). It would seem reasonable to conclude, therefore, that the physical properties of acrylic do not change rapidly even when subjected to long term loading in the greater depths of the ocean. However, again it must be realized that all test specimens were very thin and the results may not be completely applicable to acrylic structures or thick acrylic windows.

WEATHERING

Tests with weathering have produced only limited data over the years. In a study done by Yustein, Winans and Stark, it was found that of transparent materials subjected to weathering in various climatic locations, methyl methacrylate showed the least reduction in mechanical strength properties after three years exposure and no serious impairment of the serviceability of the material (20-21). The test specimens for this long term weathering experiment were from cast acrylic sheets with 1/8-in. nominal thickness and were subjected to weathering in five different locations which were selected to typify a hot, wet climate; a hot, dry climate; a temperate climate; a sub-arctic climate; and an arctic climate (20-21). Table 1 shows

Table 2 Effect of 2.5 to 3 Years' Outdoor Weathering and Storage on the Tensile Properties of MIL-P5415 Materials (15)

Tensile strength, 10 ³ psi	
Original	11.2
After 3 years' storage	10.4
After exposure to:	
3 years of temperate climate	10.5
3 years of subarctic climate	9.2
2.5 years of dry, hot climate	9.6
2.5 years of tropical climate	7.5
Strain at failure, percent:	
Original	5.8
After three years' storage	5.8
After exposure to:	
3 years of temperate climate	5.0
3 years of subarctic climate	3.9
2.5 years of dry, hot climate	3.6
2.5 years of tropical climate	2.2
Modulus of elasticity, 10 ⁵ psi	
Original	4.4
After three years' storage	4.1
After exposure to:	
3 years of temperate climate	4.4
3 years of subarctic climate	4.6
2.5 years of dry, hot climate	4.4
2.5 years of tropical climate	4.4

the results of this test over a three year period.

In another three year study published by the Armed Forces Supply Support Center similar results were obtained. Table 2 shows the results of this weathering experiment whose objective was to compare the changes in physical properties between materials exposed to various climates and those stored indoors. As can be seen, three years of indoor storage seems to have almost as much effect on the mechanical properties of acrylic as does weathering in a temperate climate for the same time span. Only in tropical climate was the deterioration of properties significant, on the order of 10 percent/year. In 1974, the results of a very interesting weathering study were released by Rainhart and Schimmel (16). They gained access to a 4 in. x 12 in. x 1/8 in. piece of Plexiglas which had been mounted for 17 yr and 8 months in a static test frame outside Albuquerque, New Mexico. The weathered panel was then subjected to a series of tests and compared to results obtained from unweathered acrylic.

The study shows that there is a significant increase in brittleness of the material. Furthermore, in the areas of flexural strength and maximum strain the study bears out Yustein, Winans and Stark's data by showing that losses in these areas are a continuous and not a step function of time. The degree of embrittlement after 18 yr in a desert climate is shown by a 65 percent decrease in strain at rupture and a 51 percent decrease in flexural strength. In addition, as in the study published by the Armed Forces Supply Center, there is a small

but steady increase in the tangent modulus of elasticity over time. Thus after 18 yr of exposure to a desert climate the modulus of elasticity had increased by 7 percent. Of all the properties measured, the optical transmission decreased the least. After the surface of the pitted acrylic specimen was repolished its transmissivity was the same as of an unweathered specimen.

Summarizing existing weathering data it can be stated that although acrylic plastic weathers, it is a slow process which decreases the tensile strength, flexural strength, and ductility by a few percent/per year. It needs to be pointed out, however, that all of the test specimens used in these experiments were extremely thin. Many authorities hypothesize that weathering is a surface effect. If this be true, then the action of ultra-violet rays, chemical attacks by pollutants such as ozone, abrasion by dust particles, rain and snow would have a marked effect on the results obtained when using thin specimens as test samples. These results then would not actually be applicable to windows or massive acrylic structures which are 10 to 40 times thicker than the test specimens. Therefore, the effects generated by the weathering tests may very well represent insignificant changes when applied to anything except 1/8-in. thick specimens.

Still, until data based on weathered 1 to 4-in. thick acrylic specimen becomes available, it is conservative to assume that the published data from thin specimen studies are also applicable to thick sheets used for construction of windows in hyperbaric chambers.

The lack of tensile and flexural strength data from thick weathered acrylic is, however, a minor inconvenience as compared to the lack of data on the change in compressive strength of weathered specimen. It could decrease a little, a lot, or none at all. It could even conceivably increase with exposure because weathered acrylic is known to be more brittle than unweathered acrylic. Since all spherical, as well as many conical frustum windows, see only compressive stresses in service this information would be of great value.

There is yet another area of ignorance about the properties of weathered acrylic plastic. It deals with the synergistic effect between stresses and weathering. Sufficient exploratory data exist to indicate that the presence of tensile or flexural stresses in material exposed to weather accelerates its deterioration dramatically. The data are not

present, however, that would permit quantifying of this synergistic effect over a period of ten to twenty years. It would be of great practical value in particular to find out what is the effect of compressive stress field on the rate of weathering as many hyperbaric windows in service are in compression when pressurized. It is very doubtful, however, whether such data will become soon available as the number of variables needing elucidation is very great. For example, the effect of different principal stresses in a stress field and also the effect of their magnitudes on the rate of weathering still has not been quantitatively established. When one adds to this, finally, the variables represented by cyclic and sustained loading conditions the true complexity of the problem facing the investigators of weathering becomes apparent.

Because of the complexity of the problem and lack of definitive data on which to formulate quantified relationships between deterioration of physical properties in weathered acrylic, length of exposure, magnitude of stresses and type of loading an empirical rule of thumb has been adopted by ASME (22) for predicting the useful life of acrylic viewports in service. This rule of thumb states that the useful life of acrylic viewports in pressure vessels for human occupancy is 10 yr based on the conservative assumption that in that length of time even stressed acrylic in a tropical climate will retain more than 50 percent of its original load carrying ability. Thus at the end of 10 yr the effective safety factor of acrylic viewports even in tropical service will decrease only from the original 3-4 range to 1.5-2 range, still a marginally adequate value for manned service. When appropriate data from thick acrylic specimen become available, the service life of acrylic viewports may be extended to 15 or 20 yr, saving the industry significant sums of money.

A LONG TERM WEATHERING PROGRAM FOR THICK ACRYLIC SPECIMENS

Because of the paucity of data on the weathering of acrylic, particular thick acrylic, the co-authors of this paper in conjunction with the Harbor Branch Foundation have begun a 10 yr testing program which will provide data in some much needed areas. Two primary climates were selected for use in this study -- a hot, dry desert climate with over 200 days of annual sun (represented by El Cajon CA) and a hot, humid, subtropical climate

(represented by Linkport FL).

There are two objectives to this weathering test program:

1 To test the effect of weathering on the physical properties of thick unstressed acrylic plates. Data will be collected on tensile and compressive strengths, hardness, impact resistance, and deformation under compressive loading both before and after weathering.

2 To test the effect of weathering on flexure strength in stressed and unstressed thick acrylic plates.

All test specimens were machined from heat resistant cast poly (methyl methacrylate) which is general purpose unplasticized ultra-violet absorbing acrylic. The 4 in. thick specimens are from Acrylite and the 2 in. thick ones of Plexiglas G. Both these satisfy the material requirements set forth by ANSI/ASME PVHO-1 Safety Standard and MIL-P-5425. In addition, these were chosen for use in this study because they are the material from which the windows for hyperbaric chambers are made.

It is known that modified (cross-linked) MIL-P-8184 and crack propagation resistant (stretched) MIL-P-25690 are both more weathering resistant than the acrylic selected for this test. However, neither of these acrylics are cast in thick enough plates for use in windows for hyperbaric chambers nor are they economical enough to be used by the underwater community.

The test specimens for meeting objective number (1) consist of the following:

- (a) Unstressed, exposed in El Cajon CA
 - 1 specimen 12 in. x 15 in. x 4 in.
 - 1 specimen 12 in. x 15 in. x 2 in.
- (b) Unstressed, exposed in Linkport FL
 - 1 specimen 12 in. x 15 in. x 4 in.
 - 1 specimen 12 in. x 15 in. x 2 in.
- (c) Unstressed, stored unexposed in El Cajon CA
 - 1 specimen 12 in. x 15 in. x 4 in.
 - 1 specimen 12 in. x 15 in. x 2 in.

The physical properties of these specimens were established prior to the weathering test being commenced and these same properties will be tested again after 10 yr weathering.

It is expected that the test results will make it possible to determine what properties changed, where the greatest changes

occurred (El Cajon, Linkport or in storage), and how the changes compare with the changes that have been noted for thin acrylic sheets.

In addition, negotiations are in progress for the Norwegian classification society Det Norske Veritas to place in numerous locations around the world unstressed specimens with the same properties and dimensions as those in El Cajon and Linkport. It is believed that if a large number of specimens can be exposed to world-wide climate conditions and polluting agents that definitive data will ensue upon which accurate knowledge of weathering of thick unstressed acrylic plates can be obtained. These tests, like the ones in El Cajon and Linkport, are for a projected span of 10 yr.

The second objective, the effect of weathering on flexure strength in stressed and unstressed thick acrylic plates, is a somewhat more complicated test. The specimens consist of six 4 in. x 48 in. x 2 in. pieces of acrylic plate. The flexure strength of these specimens was established prior to weathering by testing one of the specimens to failure in flexure. Using a simple cantilever test jig (Figs. 7 and 8), the specimens are being placed in flexure stress.

Specimen 1 -- 1800 psi flexure stress
Specimen 2 -- 1500 psi flexure stress
Specimen 3 -- 1125 psi flexure stress
Specimen 4 -- 900 psi flexure stress
Specimen 5 -- 0 psi flexure stress

All of these specimens are being exposed in El Cajon.

These magnitudes of flexure stresses were chosen because they correspond to the conversion factors established by ANSI/ASME PVHO-1 Safety Standard. It was felt that by using the conversion factors as a guide to the flexure stress levels, more applicable data would be forthcoming.

After 10 yr of weathering, loading will be increased until fracture takes place. At that time, fracture stresses will be compared and a relationship established between sustained stress level and remaining short term fracture strength.

These tests, though basic and much needed, will not, however, answer all the questions surrounding the weathering of thick acrylic plates. They will provide substantial data for comparing what happens to thin acrylic sheets versus thick acrylic plates. They will provide insight into the conservatism of the

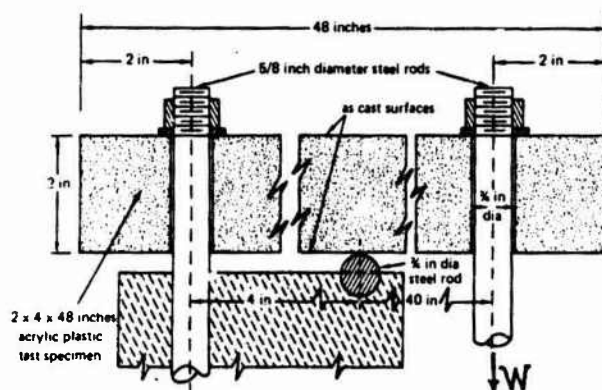


Fig. 7 Sketch of flexure test procedure

ANSI/ASME PVHO-1 Safety Standard conversion factors and they will allow the designer of windows which are to be in compression to maximize his design for extended life. In all, these tests will fill a void which now exists and will lay to rest numerous questions concerning the nature of weathering.

REFERENCES

- 1 Ames, W. L., "Final Report, NR-1 Ships Systems Developmental Test (NA-STS-02)-Viewpoint Marine Growth," General Dynamics, Electric Boat Division, Groton, Conn., Oct. 1968.
- 2 Dyckman, E. J., and Montemarano, J. A., "new Concepts in Antifouling Technology-Organometallic Polymers," American Paint Journal, Aug. 20, 1973.
- 3 Kretschmer, T. R., et al., "Seafloor Construction Experiment, SEACON I," Civil Engineering Laboratory, Port Hueneme, Calif., Technical Report R-817, Feb. 1975.
- 4 Lee, H. J., "Oceanographic Effects on Plastic Engineering Materials and Elastomeric Materials," U. S. Naval Air Engineering Center, Philadelphia, Pa., Jan. 1966, Report No. NAEC AML R-2260-C1, parts A and B.
- 5 Lee, H. J., "Oceanographic Effects on Plastic Engineering Materials," U. S. Naval Air Engineering Center, Philadelphia, Pa., Jan. 1966, Report No. NAEC AML R-2350 C-1.
- 6 Metzler, Dr. C. V., "Biological Fouling of Transparent Plastics," Naval Missile Center, Point Mugu, Calif., Technical Memorandum TM-68-9.
- 7 Muraoka, J. S., "Deep Ocean Biodeterioration of Materials -- Part I. Four Months at 5,640 feet," Naval Civil Engineering Laboratory, Port Hueneme, Calif., Technical Report R-329, Nov. 1964.
- 8 Muraoka, J. S., "Deep Ocean Biodeterioration of Materials -- Part II. Six Months at 2,340 feet," Naval Civil Engineering Laboratory, Port Hueneme, Calif., Technical Report R-393, Aug. 1965.
- 9 Muraoka, J. S., "Deep Ocean Biodeterioration of Materials -- Part IV. One Year at 6,800 feet," Naval Civil Engineering Laboratory, Port Hueneme, Calif., Technical Report R-456, June 1966.
- 10 Muraoka, J. S., "Deep Ocean Biodeterioration of Materials -- Part V. Two years at 5,640 feet," Naval Civil Engineering Laboratory, Port Hueneme, Calif., Technical Report R-495, Nov. 1966.
- 11 Muraoka, J. S., "Deep Ocean Biodeterioration of Materials -- Part VI. One Year at 2,370 feet," Naval Civil Engineering Laboratory, Port Hueneme, Calif., Technical Report R-525, May 1967.
- 12 Muraoka, J. S., "Biodeterioration and Fouling of Materials -- Five Years at Depth of 120 feet," Civil Engineering Laboratory, Port Hueneme, Calif., Technical Report R-810, May 1974.
- 13 Muraoka, J. S., "The Effects of Marine Organisms on Engineering Materials for Deep Ocean Use," Naval Civil Engineering Laboratory, Port Hueneme, Calif., Technical Report R-182, March 1962.
- 14 Muraoka, J. S., "Marine Fouling of Acrylic Plastics Pressure Treated with C-gano-Tin Compound," Naval Civil Engineering Laboratory, Port Hueneme, Calif., Technical Note N-1020, Feb. 1969.
- 15 "Plastics for Flight Vehicles -- Part



Fig. 8 Simple cantilever test assembly for flexure tests of weathering acrylic specimens

II, Transparent Glazing Materials," Military Handbook, Armed Forces Supply Support Center, Washington, D. C., MIL-HDBK-17, approval date Aug. 14, 1961.

16 Rainhart, L. G., and Schimmel, W. P., Jr., "Effect of Outdoor Aging on Acrylic Sheet," Sandia Laboratories, Sept. 1974.

17 Schwartz, F. M., "Material Characterization Studies of a TRIESTE II (DSV-1) Sphere Window After Deep Submergence Service," Naval Ship Research and Development Center, Bethesda, Md., May 1972.

18 "The Properties of 'Perspex' Acrylic Materials," Imperial Chemicals Industries Limited, Plastics Division, Welwyn Garden City, Herts, England.

19 Willoughby, T. E., Letter to Mr. A. I.

Snyder, Supervising Engineer, Pressure Vessel Department of Industrial Relations. Subject: Request for Permission to Use Non-Code Pressure Vessel of the Vickers Oxygen Chamber.

20 Yustein, S. E., Winans, R. R., and Stark, H. J., "Outdoor Weather Aging of Plastics Under Various Climatological Conditions," American Society for Testing Materials Bulletin, April 1951, pp. 31-43.

21 Yustein, S. E., Winans, R. R., and Stark, H. J., "Three Years' Outdoor Weather Aging of Plastics Under Various Climatological Conditions," American Society for Testing Materials Bulletin, Feb. 1954, pp. 29-29.

22 ASME/ANSI PVHO-1 Safety Standard for Pressure Vessels for Human Occupancy, 1977.

Effect of Weather, Age, and Cyclic Pressurizations on Structural Performance of Acrylic Plastic Spherical Shells Under External Pressure Loading

J. D. Stachiw

Naval Ocean Systems Center,
San Diego, Calif. 92152

R. B. Dolan

Harbor Branch Foundation Inc.,
Fort Pierce, Fla. 33450

Weathering, aging, and cyclic application of stresses to acrylic plastic degrades its physical properties. The rate of degradation must be known if the useful life of load-carrying acrylic structures is to be predicted with accuracy. Physical and chemical tests conducted by the authors on thick spherical shells indicate that the weathering affects only a thin surface layer of material, which after 10 years is still less than 0.020 in. thick. Similarly, pollutants in the ambient atmosphere of the pressure chamber affect the surface layer of the spherical shell facing the interior of the chamber. The physical and chemical properties of the thin surface layer affected by weathering differed significantly from those in the middle of 2.5-in.-thick Plexiglas G plate; the decrease in properties was: 40 percent in tensile elongation, 34 percent in flexure strength, 21 percent in tensile strength, and 79 percent in molecular weight. Since the interior body of the thick plastic shell is not affected by weathering or chemical attack and the affected surface layers are very thin, the ability of the shell to carry compressive loads is not significantly diminished after 10 years of service. Only an 11 percent decrease of critical pressure was observed in spherical shells with thickness of 1 in. subjected to 10 years of weathering and 2000 pressure cycles of 8 hour duration each to 30 percent of its original critical pressure. Based on the preceding data it appears safe to extend the operational life from 10 to 20 years of all acrylic plastic spherical shells with bearing surfaces normal to spherical surface designed on the basis of ANSI/ASME PVHO-1 Safety Standard for external pressure service.

Introduction

Acrylic plastic serve as the primary structural material for viewports in pressure vessels utilized by the offshore industry for exploration and exploitation of the oceans [1]. Because of its low cost, ease of fabrication in diverse shapes, and excellent physical properties it has almost totally replaced glass in all man-rated pressure vessels. Certification authorities such as Det Norske Veritas, American Bureau of Shipping, Germanischer Lloyd, Lloyds Register of Shipping, and U.S. Navy specify the acrylic plastic for structural components in submersibles, diving bells, personnel transfer capsules, deck decompression chambers, and diver recompression chambers under their cognizance [1].

As a basis for design of acrylic plastic viewports serve the experimental data generated for the U.S. Navy by the engineers at the Naval Civil Engineering Laboratory, Naval

Ocean Systems Center, and the Naval Ship Research and Development Center. These data have been reviewed, distilled, and summarized in the Safety Standard for Pressure Vessels for Human Occupancy [2] published jointly by the American Society of Mechanical Engineers and the American National Standards Institute. Acrylic plastic viewports and pressure vessels designed on the basis of the ANSI/ASME PVHO-1 Safety Standard have an outstanding safety record; to date no one has been seriously injured, or lost their life in an accident involving acrylic plastic viewports or pressure vessels.

When the Safety Standard was first formulated in 1970, certain restrictions were imposed on the use of acrylic plastic viewports and pressure vessels to preclude failure of these components in service. Some of these restrictions, such as the allowable cyclic fatigue life, exposure to X-rays, and nuclear radiation are based on fairly extensive data. This is not the case with the 10-year restriction on chronological service life. The 10-year chronological life restriction was formulated on the basis of data generated with 0.062 and 0.125-in.-thick

Contributed by the Ocean Engineering Division of THE AMERICAN SOCIETY OF MECHANICAL ENGINEERS, and presented at the Winter Annual Meeting, Washington, D.C., November 15-20, 1981. Manuscript received at ASME Headquarters, February 24, 1982.

specimens subjected to weathering at representative locations in the continental United States [3-5]. These data showed that after 10 years of outdoor exposure to weathering the tensile and flexural strength decreased significantly—25-50 percent depending on environmental factors. There was no information available on the effect of weathering on compressive yield strength, as there was neither the interest in compressive properties of acrylic plastic nor did the thin specimens lend themselves to standard compression testing.

It was obvious to the ASME/PVHO Safety Standards Committee that the data were not adequate for formulation of chronological life restriction on viewports and pressure vessels fabricated from thick plastic, or for viewport and pressure vessel configurations that were subjected only to compressive stresses. Still, in absence of any better data they were selected as the basis for formulation of the chronological age limit. A chronological life of 10 years was selected, as it was felt that a loss in excess of 25 percent in tensile or flexural strength would reduce the built-in safety margin of viewports designed according to ANSI/ASME PVHO to such an extent that they would become a potential hazard. The 10-year chronological life restriction was applied across the board to all viewport and vessel shapes regardless of their service location, thickness, or type of stress distribution even though it was surmised at that time that the chronological life of some of the viewport shapes exceeded the 10-year limit by at least a factor of two.

Over 10 years have passed since the formulation of the 10-year chronological life in 1970. Not only are there viewports and pressure vessels of acrylic plastic in service with chronological ages exceeding 10 years, but also some data have been generated by testing of specimens machined from 10-year old, weathered, thick plastic shapes. In some cases whole viewports or pressure vessels with 10-year chronological age were tested to destruction and their performance compared with identical viewports with zero chronological age. The data generated by those tests indicate that (a) weathering affects the optical and mechanical properties only of a thin layer of the surface exposed to weathering; (b) the ultimate load-carrying capability of a thick, weathered acrylic plastic structural member subjected to flexural stress is determined by the mechanical properties of the thin weathered surface layer; and (c) performance of thick, acrylic plastic under biaxial compressive loading is not significantly affected by the thin weathered surface layer.

Based on these findings, it appears feasible to modify the chronological life restriction on viewports and pressure vessels subjected to compressive stresses so that their costly replacement can be postponed to a chronological age where their structural performance deteriorates by at least 25 percent. This paper summarizes the study conducted by the authors with the express purpose of determining the effect of weathering and chronological age on the structural performance of acrylic plastic spherical shells under compressive stresses generated by external pressure loading.

Background Discussion

Acrylic plastic is one of the most weather-resistant plastics available to the structural engineer. However, like most other plastics, it is attacked by ultraviolet radiation present in the sunlight. The negative effect of ultraviolet radiation is augmented by the presence of high ambient temperature and humidity. Thus, one finds that acrylic plastic specimens exposed to weathering in the tropics deteriorate at a faster rate than those located in temperate climates. Specimens stored indoors exhibit insignificant degradation of physical properties even after 10 years, since they are protected from the sun, precipitation, air pollutants, and excessive heat.

The rate of deterioration is also accelerated by the presence

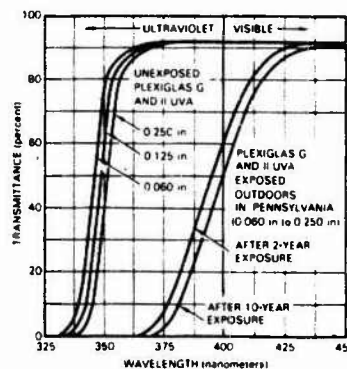


Fig. 1 Effect of weathering on the optical properties of acrylic plastic with ultraviolet light absorber (Rohm and Haas Publication PL-53i)

of unpolymerized methyl methacrylate and ethyl acrylate monomers in the body of the plastic. If the unpolymerized monomers exceed 2 percent, the plastic crazes rapidly, sometimes in less than two years. For this reason, ANSI/ASME PVHO-1 Safety Standard restricts the amount of residual monomer in acrylic plastic to less than 1.6 percent. Similarly the absence of ultraviolet absorbers in the acrylic plastic allows ultraviolet radiation to penetrate the full thickness of the plastic, thus affecting all of the material, instead of just the surface layer.

Addition of the absorber converts acrylic plastic into a filter for ultraviolet radiation that absorbs over 95 percent of incident ultraviolet radiation with wavelength less than 335 nm. Even with the addition of the ultraviolet radiation absorber the plastic still deteriorates in sunlight, but now only in a thin layer at the exposed surface. As a result of this arrangement, the body of the plastic is protected from deleterious effects of the ultraviolet radiation at the expense of accelerated localized surface deterioration.

The physical deterioration of the surface is preceded by changes in the optical properties of the surface layer. Under the action of ultraviolet radiation the absorber in the surface layer of the plastic yellows, thus increasing its effectiveness as an ultraviolet filter. This ultraviolet radiation-activated absorber layer forms rapidly; after 2 years of exposure to strong sunlight its thickness extends about 0.005 in. and its performance as a filter with 5 percent cutoff shifts from 335 to 375 nm (Fig. 1). Because the activated absorber in the surface layer absorbs most of the ultraviolet radiation, the activation of an absorber in the remainder of the plastic is delayed. The practical consequence of the rapid formation of this activated filter is that the rate of activated filter layer growth decreases exponentially with duration of exposure, such that even after 10 years, its thickness probably does not exceed 0.010 in. Since the rate of physical deterioration of plastic is a function of ultraviolet radiation intensity, most of the deterioration takes place in the activated absorber layer. Thus the thickness of the physically deteriorated material probably does not significantly exceed the thickness of the activated absorber acting as an optical ultraviolet filter. As a result, one can expect that even after 10 years of exposure, the weathered layer does not exceed 0.010 in. in thickness.

Because of the presence of the absorber, which protects the body of plastic from harmful effects of ultraviolet radiation at the expense of accelerated surface deterioration, weathering data generated with 0.062 and 0.125 in.-thick specimens are really not applicable to thick acrylic structures. In sheets of 0.125-in. thickness, the effect of the thin deteriorated layer on the overall tensile strength of the specimen is significant, whereas for a thick structure with a complex stress field, it may or may not be significant.

depending on the character and magnitude of tensile stresses on the weathered surface.

If the thin weathered layer on a thick plate is in uniaxial or biaxial tension, it will crack at a lower tensile stress level than the unweathered material below (i.e., the decreased ductility of weathered material will initiate a crack at lower strain). Once the crack originates in the weathered layer it will propagate into the unweathered body of the plate causing it to also fail at a lower tensile stress level.

A different case presents itself when the thin weathered layer on a thick plate is in uniaxial or biaxial compression. Since the weathered material is in compression, the decreased tensile ductility of weathered material will not initiate a crack under load and thus will not lead to a premature failure of the whole plate. Even if the weathered material has a lower compressive yield point than the unweathered material below it, this will not affect the structural performance of the whole plate significantly because the thickness of the weathered material is only a small fraction of the whole plate, and localized compressive yielding does not initiate fracture in the plastic that is under compression.

There is a possibility that a crack may originate in the weathered surface of a thick structural member during the relaxation phase after long-term application of high compressive stress. Its rate of propagation, however, will be very slow because during the subsequent application of compressive stress, the crack will close and will remain closed until the next relaxation phase. As stress cycling continues, the crack may propagate, but only in small discrete steps during each relaxation phase. The slow growth of the crack does not present any immediate danger to the structure and the structure can be retired from service when the inspection of the crack determines that its size makes the structure unacceptable for further service at the design stress level. Thus the presence of incipient cracks in a plastic structure under compressive stress should not serve as a source for immediate concern to the operators of the diving system.

If the foregoing postulates are applied to typical window shapes (Fig. 2), it is found that the only shapes with tensile stresses on the surfaces exposed to weathering are: (1) plane windows with plane bearing surfaces; (2) plane windows with single beveled bearing surface and t/D , less than 0.5; (3) plane windows with twin beveled surfaces and t/D , less than 0.5; and (4) spherical sector windows with square bearing surfaces. Window shapes that experience only compressive stresses on the surfaces exposed to weathering are: (1) spheres; (2) spheres with conical penetrations; (3) hyperhemispheres with conical bearing surface; (4) hemispheres; (5) spherical sector windows with conical bearing surface; (6) plane windows with single conical surface and t/D , larger than 0.5; and (7) plane windows with twin conical surfaces and t/D , larger than 0.5. Because of their large size, most of the spherical windows and pressure hulls in service represent a sizeable investment. Thus they are the prime candidates for extension of chronological life limit if the theoretical considerations previously discussed could be substantiated with experimental data. This paper summarizes some of the tests conducted by the authors in support of the postulate that the structural performance of thick spherical shells and sectors with beveled bearing surface is not significantly affected after 10 years of service and weathering.

Experimental Investigation

The objective of the experimental investigation was to show that the structural performance of thick, acrylic plastic spherical shells after 10 years of weathering in service does not significantly differ from that of unweathered spherical shells.

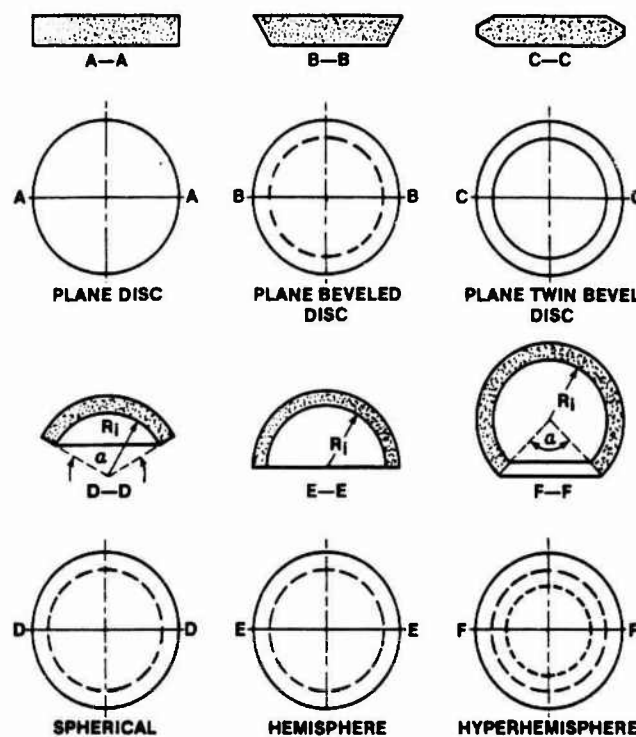


Fig. 2 Typical shapes of windows for pressure-resistant viewports



Fig. 3 Removal of polar pentagon from the 10-year-old, weathered NEMO Model #37 for determination of its physical properties

The scope of the investigation was limited to spherical shells with $0.036 \leq t/D, \leq 0.076$ fabricated from acrylic plastic, meeting the requirements of ANSI/ASME PVHO-1.

As test specimens served: (1) 15-in. OD \times 13-in. ID NEMO Model #37; (2) 1-in.-thick material coupons cut from the NEMO Model #37; (3) 1-in.-thick material coupons cut from

acrylic plate held in storage; (4) 2.5-in.-thick material coupons cut from the full size NEMO (DSV #4) submersible [6]; and (5) 2.5-in.-thick material coupons from commercially available Plexiglas G plates. Both the NEMO Model #37 and the full size NEMO submersible were 10 years old and were exposed during that time for at least 50 percent of the time to outdoor weathering between 30–40 deg. of northern latitude.

The test procedure was configured to provide the authors with information on both the condition of the 10-year-old weathered material and the performance of the pressure hull. The test results would be subsequently compared with data in the literature pertaining to performance of weathered and unweathered acrylic plastic.

Test Schedule

Spherical Shell. As test specimen served the 15-in. OD \times 13-in. ID NEMO Model #37. Since its fabrication in 1970 by the Technical Support Group at the Pacific Missile Range, it has served as a test specimen in several experimental investigations. Immediately after fabrication it was pressure cycled 1000 times from 0–1500 psi hydrostatic pressure with a typical pressure cycle of 8 hours duration (4 hours under pressure, generating an average compressive membrane stress of 5600 psi, followed by 4 hours of relaxation) at the Civil Engineering Laboratory, Port Hueneme, California [7]. After completion of the cycling program in 1973, it was placed outside to weather in El Cajon, California. In 1976 NEMO Model #37 was subjected to an explosive peak pressure of 1453 psi magnitude while submerged at 10-ft depth in the water tank at the Southwest Research Institute [8]. The damage consisted of a radial crack in one of the polar pentagons containing a hatch and several small cracks in one of the equatorial pentagons. After this test the NEMO Model #37 was again placed outside to weather in El Cajon, California until 1980 when it was chosen as a test specimen for this study.

To make the Model #37 watertight for this study the damaged polar and equatorial pentagons were removed by cutting out with a saw (Fig. 3) and replaced with new ones, fabricated for this purpose, from 1-in.-thick Plexiglas G meeting the requirements of ANSI/ASME PVHO-1. The new pentagons were bonded in place with CADCO PS-30 self-polymerizing acrylic adhesive. The completed spherical shell was then annealed for 24 hours at 175°F.

The instrumentation of NEMO Model #37 consisted of six rectangular electrical strainage rosettes (Micromasurement, EA-13-125TM-120). The gages were bonded to: (1) the center of the new equatorial pentagon; (2) the center of the old equatorial pentagon; (3 and 4) the edge of penetration in the old polar pentagon; and (5 and 6) the edge of penetration in the new polar pentagon. After installation of the gages, two titanium hatches (Fig. 4) were inserted into the polar penetrations and sealed against leakage with room vulcanizing silicone rubber squirted into the space between the flanges of the hatches and the convex surface of the spherical shell (Fig. 5).

The replacement of the two old damaged pentagons with two new ones did not change the response of remaining old pentagons to compressive stress under external pressure loading. Furthermore, the critical pressure of the repaired NEMO Model #37 would still be governed by the remaining 10 old pentagons, since the initiation of fracture in any of the old pentagons covered with extensive crazing (Fig. 6) would trigger the implosion of the whole shell.

The testing of the repaired NEMO Model #37 took place in two steps. First it was placed in a pressure vessel at Stachiw Associates and pressure cycled 1000 times from 0 to 1400–1500 psi range with pressure cycles of random duration,

DWG NO: SK6514-C-0140

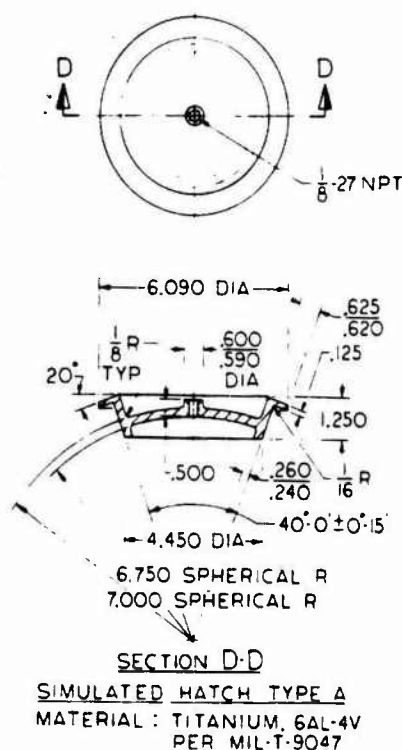


Fig. 4 Titanium hatches for NEMO Model #37

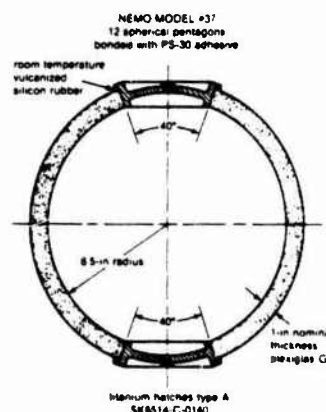


Fig. 5 NEMO Model #37 assembly, imploded at 4200 psi under short-term loading

simulating typical operational scenarios. Strains were read from the gages during the first pressure cycle. The length of the individual pressurizations during pressure cycling varied from 0.25–64.0 hours, averaging 3.93 hours, while the duration of relaxations varied from 0.1–220.9 hours, averaging 3.56 hours. The ambient temperature of the pressurizing medium varied from 58–89°F, averaging 73.44°F. At the conclusion of the pressure cycling program, the titanium hatches were removed from the NEMO Model #37 and the beveled seat surfaces in the penetrations through the polar pentagons were inspected for crazing and incipient cracks.

After inspection of the acrylic seat surfaces, the hatches were placed back in the polar openings of NEMO Model #37, the joints were resealed, and the whole sphere assembly was pressurized to destruction at 100 psi/min rate at Southwest Research Institute, San Antonio, Texas, utilizing tap water at 72°F.



Fig. 6 Crazing, typical of the weathered surface on the 10-year-old NEMO Model #37

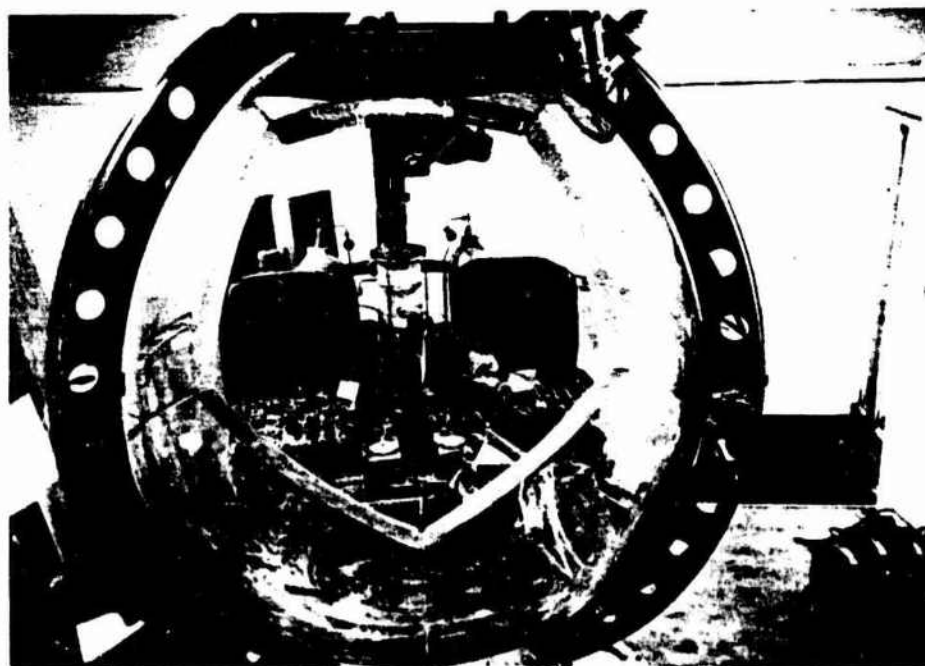


Fig. 7 DSV NEMO after removal of one of its 2.5-in. thick pentagons for determination of its physical properties

Material Test Coupons. As *test specimens* served coupons of acrylic plastic machined from the: (1) 1-in.-thick, *weathered*, 10-year-old spherical pentagon sawed out from NEMO Model #37; (2) 1-in.-thick, *unweathered*, 10-year-old spherical pentagon left over from the original construction program of NEMO Model #37; (3) 1-in.-thick, *unweathered*, 1-year-old masked sheet of Plexiglas G; (4) 2.5-in.-thick, *weathered*, 10-year-old spherical pentagon sawed out from submersible NEMO (Fig. 7); and (5) 2.5-in.-thick, *unweathered* 1-year-old plate of Plexiglas G. The NEMO submersible was subjected during its lifetime to 650 dives and was, for most of the time, exposed to outdoor weathering [9], either in Southern California or Southern Texas.

The *objective* of the tests was to determine the mechanical properties of the: (1) surface layer on the *weathered*, 10-year-old acrylic plastic; (2) subsurface material in *weathered*, 10-year-old acrylic plastic; and (3) surface layer on *unweathered*, 10-year-old acrylic plastic.

The *test procedures* for determining the mechanical properties of the surface layer consisted of slicing a layer from the top surface of the plastic plate and machining all of the ASTM test specimens from that layer. In this manner the properties of the *weathered* surface layer would affect the test results more significantly than if the test specimens were cut from the full thickness of the plate. In the flexure test, the load was applied to the test specimen in such a manner that

the weathered surface was placed in tension. Thus, the value of the ultimate flexural stress recorded in this test would represent the *actual* flexure strength of the weathered layer, and not the average of the weathered and unweathered layers as is the case with all the other ASTM tests.

To determine the depth of the weathered layer, slices of different thicknesses were removed from the surfaces of selected test specimens. By making those slices very thin and subjecting the surface on the test specimens facing the weathered surface of the plate to tensile flexure stresses, the extent of the deteriorated material below the original plate surface could be determined. Since the weathered layer was expected to be less than 0.1-in.-thick, the thickness of slices removed from the original plate surface was increased in increments of 0.005, 0.020, 0.040, 0.060, 0.080, and 0.100 in.

The mechanical properties of the subsurface layer were determined by cutting all the 0.25-in.-thick ASTM test specimens from the material only after the top 0.25-in. layer

was first removed from the material. The test specimens were subjected to the following tests: ASTM-D-638, ASTM-D-695, ASTM-D-732, ASTM-D-621, ASTM-D-256, and ASTM-D-790. Only three test specimens were used to establish the average value of mechanical property for each material condition and test.

In addition to ASTM test specimens, 5-in.-diameter \times 0.50-in.-thick disks were also machined from the surface and subsurface layers of the 2.5-in.-thick spherical pentagon cut out from NEMO submersible. These disks were subsequently tested to destruction by subjecting them individually to hydrostatic loading in a special fixture that provided simple support to the edge of the disk. The ratio of the outside disk diameter to the diameter of the opening in the fixture was 1.25. The objective of these tests was the same as of ASTM-D-790, to detect any difference among the flexural strengths of specimens from weathered surface, unweathered surface, and subsurface layers. Since flexing of the disk under hydrostatic loading subjects a larger surface of the specimen to tensile stresses than flexing of the bar specimen under three or four-point loading, the weather-induced flaws in the form of crazing scattered over the surface of the specimen and the deteriorated tensile strength of the weathered layer will initiate a crack sooner in a disk than in a bar, thus making the disk specimen a more sensitive detector of surface deterioration than a bar specimen.

For purposes of comparison, disks were also cut from the surface of 2.5-in.-Plexiglas G plate only 1 year old. Comparison of maximum flexure stresses at failure from these specimens with those cut from the interior of 2.5-in.-thick, weathered, Plexiglas G will show whether weathering affects the mechanical properties in the interior of thick acrylic plastic plates.

Test Results

Spherical Shell. *Strains* recorded during the first pressure cycle to 1500 psi of NEMO Model #37 show (Table 1) that the weathered, 10-year-old spherical pentagons deform elastically at approximately the same rate as the unweathered, new spherical pentagons. At the conclusion of the pressure cycle both the old and the new pentagons showed the same amount of permanent deformation. The same phenomenon was observed during pressurization of NEMO Model #37 to implosion (Table 1).

Cracks were not observed on the bearing surfaces of old or

Table 1 Structural performance of 15-in. OD \times 13-in. ID acrylic plastic spheres

AGE (years after fabrication)	Strains on Internal Surface At Equator				Implosion Pressure (at 75°F)
	1500 psi pressure Long	1500 psi pressure Circ.	3000 psi pressure Long	3000 psi pressure Circ.	
MODEL #34 All pentagons 1 yr old Prior cycling: 2 cycles, 8 hrs each to 1350 psi	-8.500	-8.600	-20.750	-21.200	4732 psi
MODEL #22 All pentagons 1 yr old No prior cycling	-8.550	-8.700	-20.850	-21.700	4700 psi
MODEL #36 All pentagons 6 yr old Prior cycling: 1000 cycles, 8 hrs each to 1050 psi	-8.600	-8.500	-20.800	-20.600	4350 psi
MODEL #37 10 pentagons 10 yr old prior cycling: 2000 cycles, 8 hrs each to 1500 psi	-8.390	-9.100	-18.950	-20.300	4200 psi
2 pentagons 1 yr old Prior cycling: 1000 cycles, 8 hrs each to 1500 psi	-8.950	-8.650	-18.920	-19.410	

NOTES

- All spheres were equipped with metallic hatches located in opposite polar pentagons.
- The pressurization was conducted at 100 psi/minute rate at 60 to 90°F ambient temperature.
- All strains were measured in microinches per inch.
- All spheres were fabricated by bonding with PS-30 adhesive of 12 spherical pentagons machined from thermoformed 1.0 inch thick Plexiglas G.
- NEMO Model #36 was immersed in tap water for 2 years and subsequently exposed to Southern California weather for 6 years.
- NEMO Model #37 was immersed in tap water for 2 years, exposed to Southern California weather for 7 years, and again immersed in tap water for 1 year.

Table 2 Mechanical properties of 1-in.-thick plexiglas G—ASTM specimens

Type of Material	Tension			Compression		Shear ASTM D-732 Strength psi	Flexure		Compressive Deformation ASTM D-621 Deformation percent	Impact Strength ASTM D-256 12ed Notch ft lbs/inch
	ASTM Strength psi	D-638 Modulus psi	Elongation percent	ASTM Yield psi	D-695 Modulus psi		ASTM Strength psi	D-790 Modulus psi		
Interior of 10 year old unweathered Plexiglas G	10,900	450,000	5.9	15,600	440,000	9,240	14,700	450,000	1.04	0.34
	11,000	440,000	5.7	16,000	450,000	9,260	15,000	440,000	1.15	0.38
	11,000	460,000	5.6	15,700	450,000	9,530	14,900	450,000	1.25	0.35
Interior of 10 year old weathered Plexiglas G	11,100	450,000	6.2	16,000	500,000	9,650	15,000	460,000	1.47	0.33
	11,100	450,000	9.0	15,800	510,000	9,710	14,800	440,000	1.58	0.38
	11,090	450,000	6.0	15,900	500,000	9,610	14,900	450,000	1.22	0.36
Interior of 1 year old masked Plexiglas G	11,200	460,000	4.2	18,000	460,000	9,800	16,500	475,000	0.81	0.40
	10,500	450,000	4.9	17,900	450,000	9,600	16,000	450,000	0.60	0.39
	10,970	465,000	5.3	18,400	520,000	10,000	17,700	460,000	0.70	0.41

Notes:

- All specimens were machined from midthickness of the 1 inch thick plate.
- The specimens were approximately 0.25 inches thick, except for compression, deformation under load, and impact strength specimens which were 0.5 inches thick.
- The weathered material was exposed to the elements from 1973 to 1980 in Southern California, the rest of the time it was submerged in tap water inside a pressure vessel.
- The unweathered material was stored inside a dark shed where it was exposed to diurnal and seasonal temperature variations in 32 to 110°F range.

Table 3 Mechanical properties of 2.5-in. plexiglas G—ASTM specimens

TYPE OF MATERIAL	TENSION ASTM-D-638			COMPRESSION ASTM-D-495		SHEAR ASTM-D-732	FLEXURE* ASTM-D-790		FLEXURE** ASTM-D-790		COMPRESSION DEFORMATION ASTM-D-621	IMPACT STRENGTH ASTM-D-256 1200 ft-lb/in
	Strength psi	Modulus psi	Elongation percent	Yield psi	Modulus psi		Strength psi	Modulus psi	Strength psi	Modulus psi		
Interior of 10-year old unweathered Plexiglas G	11,300	440,000	5.9	16,300	490,000	12,300	16,800	490,000	16,800	470,000	0.65	0.38
	11,200	450,000	6.0	16,400	500,000	12,000	16,900	500,000	16,600	480,000	0.55	0.37
	11,300	490,000	6.2	16,300	490,000	12,500	16,900	480,000	16,500	500,000	0.58	0.27
	11,100	520,000	4.3	16,400	500,000	12,500	17,000	490,000	16,700	490,000	0.54	0.39
Outward layer 10-year old unweathered Plexiglas G	9,660	460,000	1.1	15,900	500,000	11,400	9,520	510,000	19,100	480,000	0.66	0.31
	10,000	480,000	3.5	16,100	490,000	10,500	10,100	500,000	16,500	510,000	0.66	0.34
	7,180	480,000	2.0	16,100	500,000	11,200	12,000	500,000	16,600	490,000	0.66	0.36
	10,400	480,000	4.1	16,300	500,000	11,700	12,800	480,000	16,700	480,000	0.48	0.35
Inward layer 10-year old unweathered Plexiglas G	9,410	510,000	3.0	15,700	490,000	11,900	15,800	490,000	16,600	450,000	0.67	0.37
	9,290	520,000	2.9	15,700	470,000	12,300	15,500	480,000	15,900	460,000	0.64	0.36
	9,870	480,000	3.6	15,700	480,000	12,100	15,700	480,000	16,700	450,000	0.88	0.29
	8,910	530,000	2.7	15,500	480,000	11,100	14,300	470,000	16,000	420,000	0.74	0.36
Interior of 1-year old unweathered Plexiglas G	10,100	440,000	3.8	16,500	480,000	11,700	16,600	480,000	17,000	500,000	0.7	0.4
	10,600	440,000	6.3	16,700	470,000	11,900	16,500	460,000	16,800	480,000	0.7	0.38
	10,600	440,000	4.9	16,900	480,000	12,300	16,700	480,000	16,700	460,000	0.9	0.29
	10,200	440,000	4.9	16,400	480,000	10,500	16,900	450,000	16,400	470,000	0.8	0.40

NOTES:

- The specimens were approximately 0.25 inches thick, except for compression, deformation under load, and impact strength specimens which were 0.5 inches thick.
- The weathered material was removed from NEMO pressure hull, commissioned in Bahamas during 1970 and decommissioned in San Antonio, Texas during 1981. From 1975 to 1981 the submersible was stored outdoors in San Antonio, Texas with the hatch closed.
- *Flexure - the original hull surface is placed in tension; orientation of specimens from interior is at random.
**Flexure - the original hull surface is placed in compression; orientation of specimens from interior is at random.
- Outward layer - layer from the exterior of the pressure hull, exposed to seawater and weathering.
Inward layer - layer from the interior of the pressure hull, exposed to condensation and interior atmosphere of submersible.
Interior - layer from the mid thickness of the pressure hull.

Table 4 Flexural strength of 2.5-in. plexiglas G—disk specimens

Type of Material	Biaxial Flexure Strength	
	Arrangement A	Arrangement B
Interior of 10-year old unweathered Plexiglas G	16,983 psi, mean 2,460 psi, standard deviation 9 specimens	17,983 psi, mean 2,456 psi, standard deviation 9 specimens
Outward layer 10-year old unweathered Plexiglas G	8,500 psi mean 2,236 psi, standard deviation 6 specimens	19,240 psi mean 2,043 psi, mean 8 specimens
Inward layer 10-year old unweathered Plexiglas G	10,816 psi, mean 2,616 psi, standard deviation 6 specimens	14,660 psi, mean 1,781 psi, standard deviation 6 specimens
Interior of 1-year old unweathered Plexiglas G	18,788 psi, mean 995 psi, standard deviation 6 specimens	19,250 psi, mean 910 psi, standard deviation 6 specimens

NOTES:

- The dimensions of disk specimens were: 5 inches diameter x 0.9 inch thickness.
- The specimens were taken from the following locations to the 2.5 inch thick spherical pentagon.
Outward layer - The exterior surface of the sphere served as one surface of the disk specimen.
Inward layer - The disk specimen was cut from the mid thickness of the casting, both surfaces of the specimen were machined, sanded and polished.
Inward layer - The interior surface of the sphere served as one surface of the disk specimen.
- Arrangement A - The discs from outward and inward layers are tested with original hull surfaces in tension. Discs from the interior of the casting with both machined surfaces have the tension surface selected at random.
Arrangement B - The discs from outward and inward layers are tested with original hull surfaces in compression. Discs from the interior of the casting with both machined surfaces have the compression surface selected at random.
- The disk specimens were machined from the same spherical pentagon as specimens whose properties are shown on Tables 3 and 5.

new polar pentagons in NEMO Model #37 after application of an additional 1000 pressure cycles from 0-1500 psi, which generated a maximum compressive stress in the range of 8000-10,000 psi on the inner lip of the bearing surface. Cracks were also not observed on the inner (concave) or outer (convex) surfaces of old or new pentagons, even though the outer surfaces of old pentagons were heavily crazed by weathering prior to the beginning of the pressure cycling program.

The critical pressure of NEMO Model #37 was 4200 psi at 72°F ambient temperature. The implosion was of a general nature, resulting in total destruction of the NEMO Model #37. The magnitude of strains recorded during the implosion test showed that yielding of the acrylic shell probably began at 3000 psi, and that the extrapolated average compressive strain at moment of implosion was 35,000 $\mu\text{in./in.}$

Material Test Coupons

1. The mechanical properties of ASTM coupons cut out from a layer at least 0.25 in. below the weathered surface of the 1 and 2.5-in.-thick old, *weathered* NEMO pentagons were

identical to those cut from the interior of: (1) 1-in.-thick, 10-year-old, *unweathered* Plexiglas G; (2) 1.0-in.-thick 1-year-old Plexiglas G; and (3) 2.5-in.-thick, 1-year-old Plexiglas G (Tables 2-3).

2. Some of the mechanical properties of 0.25-in.-thick ASTM coupons cut out from the *weathered* surface of the 2.5-in.-thick 10-year-old, NEMO pentagon were significantly lower than those recorded for specimens cut from below the surface (Table 3). The properties that seemed to be affected most by weathering, when listed in order of their magnitude were:

Tensile elongation, percent	40 percent decrease
Flexure strength, psi	34 percent decrease
Tensile strength, psi	21 percent decrease
Shear strength, psi	9 percent decrease
Compressive yield, psi	1.5 percent decrease
Deformation under long term compressive loading	1 percent decrease

3. The flexural strength of 0.25-in-thick ASTM coupons and 0.5-in.-thick disk coupons cut from the weathered surfaces of 10-year-old, 2.5-in.-thick NEMO pentagon and flexure tested with the weathered surface in compression differed significantly from the flexure strength of coupons cut from identical location but flexure tested with the weathered surface in tension. The difference in values for the disk surfaces under biaxial flexure was: 18,240 psi for weathered surface in compression, and 8500 psi for weathered surface in tension (Table 4). For the ASTM coupons under uniaxial flexure the difference in values was 16,975 psi versus 11,105 psi (Table 3).

4. The mechanical properties of the 0.25-in.-thick coupons cut out from the *unweathered* surface of the 2.5-in.-thick 10-year-old NEMO pentagon also differed from those recorded for specimens cut out from below the surface (Table 3). The major difference was again in flexure strength when the flexure specimens were tested with the original, unweathered surface in tension. These findings were confirmed by testing of the 0.5-in.-thick disk coupons cut from the 10-year-old unweathered surface. The flexural strength of disks with the original unweathered surface in tension was 10,816 psi, and with it in compression was 14,466 psi (Table 4).

5. The flexural strength of ASTM coupons from NEMO whose weathered surface was sliced away at 0.020-in. intervals varied with the thickness of the removed weathered

Table 5 Physical and chemical properties of surface and subsurface layers in 2.5-in. plexiglas G

Location of Positively Stressed Specimen Surface	Tensile Test ASTM D-790			Molecular Weight		Free Monomer Percent
	Strength, psi	Modulus, psi	Type of Failure	Number Average	Weight Average	
Outward weathered surface	11,500	480,000	Brittle	378,800	665,100	0.57
0.005 inches removed from outward weathered surface	14,700	490,000	Ductile			
0.02 inches removed from outward weathered surface	15,800	480,000	Ductile	760,100	1,314,000	
0.04 inches removed from outward weathered surface	16,000	490,000	Ductile	1,140,000	1,675,000	
0.06 inches removed from outward weathered surface	16,200	490,000	Ductile	1,808,000	2,336,000	
0.08 inches removed from outward weathered surface	16,200	490,000	Ductile			
0.10 inches removed from outward weathered surface	16,100	480,000	Ductile			
Interior of the 2.5-inch thick Plexiglas G pentagon	15,800	490,000	Ductile	1,868,000	2,329,000	0.25
0.06 inches removed from inward unweathered surface	15,900	490,000	Ductile	1,514,000	1,963,000	
0.04 inches removed from inward unweathered surface	15,500	470,000	Ductile	1,096,000	1,632,000	
0.02 inches removed from inward unweathered surface	15,600	480,000	Ductile	578,000	870,900	
0.05 inches removed from inward unweathered surface	15,800	480,000	Ductile			
Inward unweathered surface	15,400	480,000	Brittle	437,000	683,900	0.31

NOTES:

1. The specimens were approximately 0.25 inches thick.
2. The specimens were cut from the 2.5 inches thick spherical pressure hull of NEMO submersible. The submersible was commissioned in 1970 and decommissioned in 1980. The submersible was stored outdoors from 1975 to 1981.
3. Outward surface - convex exterior of NEMO hull, exposed to seawater and weathering.
4. Inward surface - concave interior of NEMO hull, exposed to condensation and interior atmosphere pollutants.
5. Interior - from midthickness of the hull.
6. Samples from outward layer were tested with outward surface in tension.
7. Samples from inward layer were tested with inward surface in tension.

layer. When the surface of the test specimens facing the original weathered surface was subjected to tensile flexural stress, the maximum stress at fracture reached the value of unaged and unweathered plastic only after the thickness of layer removed from the weathered surface reached 0.020 in. (Table 5).

6. The molecular weight of acrylic plastic from *weathered* surface of NEMO was significantly lower than that of the plastic in the interior (378,000 versus 1,868,000) of the thick shell (Table 5). The molecular weight from the *unweathered* surface was also lower than that of the plastic in the interior of the shell (437,000 versus 1,868,000) (Table 5).

7. The percentage of free monomer in the *weathered* surface of NEMO was significantly higher than in the interior of the thick shell (0.57 versus 0.25 percent). The percentage of free monomer in the *unweathered* surface was also somewhat higher than in the thick shell (0.31 versus 0.25 percent) (Table 5).

Discussion

Spherical Shell. The test results generated by the pressure cycling and implosion testing of the spherical shell indicate beyond a shadow of a doubt that the structural performance under external hydrostatic loading of 10-year-old, weathered, extensively repaired, acrylic plastic spherical shells with 1-in. thickness does not differ significantly from performance of brand new shells. This postulate is based on the following findings:

1. The *critical pressure* of 10-year-old, weathered, 1-in.-thick NEMO Model #37, which was subjected to additional 1000 pressure cycles from 0-1500 psi, is only 11 percent less (Table 1) than of brand new NEMO Models #34 and #22 (4700 and 4732 psi) tested in other programs [8, 9]. The critical pressure of NEMO Model #37 is also only 3.5 percent less than that of the 6-year-old, weathered 1-in.-thick NEMO Model #36 tested in a previous study [10]. That model imploded under short term pressurization at 4350 psi. The fact that the critical pressures of the 6-year-old NEMO Model #36 and 10-year-old NEMO Model #37 were 7.4 and 11 percent,

respectively, less than those of 1-year-old NEMO Model #34 indicates that the decrease in critical pressure of the 1-in.-thick acrylic sphere is not a linear function of weathering duration. For conservative predictions of critical pressures, one may use a linear extrapolation based on 1.25 percent/year critical pressure decrease rate.

2. The small decrease in critical pressure changes the original conversion factor of 4.00 (10,600 ft implosion/2650 ft design depth) to 3.55. This decrease is acceptable because the minimum allowable conversion factor for spherical sector is three. This value is based on the consideration that at ambient temperatures below 50°F found at typical design depths, the conversion factor of three endows the spherical shell with an experimentally proven crack-free cyclic fatigue life in excess of 1000 dives with 4 hours duration at design depth [11]. The decrease of critical pressure due to age and weathering would have to exceed 25 percent of its original value before the spheres with 1-in. wall thickness were considered unacceptable for their rated depth of 2650 ft. Based on the conservative linear extrapolation rate of 1.25 percent/year, the 1-in.-thick sphere must be exposed to outdoor weathering for 20 years before it becomes unsafe for service at the original design depth of 2650 ft. After 20 years, the sphere must be retired from service, or its original design depth rating decreased by 50 percent.

3. The *strains* measured on 10-year-old, weathered parts of NEMO Model #37 during pressure cycling from 0-1400 psi were identical to those measured on brand new parts of NEMO Model #37 (Table 1). The magnitudes of residual strains measured on the 10-year-old, weathered and brand new parts were also the same. These findings are supported by strains measured on 6-year-old, weathered, NEMO #36 that had a portion of its old shell replaced with a brand new acrylic plastic patch in the shape of a 27 deg spherical sector [10]. This spherical sector patch was like the spherical pentagons in NEMO Model #37 bonded to the 10-year-old shell with CADCO PS 30 self-polymerizing cement (Fig. 8). It would thus appear that spherical shells that have been repaired by replacing damaged shell sections with new, bonded in place shell sections perform structurally in the same manner as



Fig. 8 Plug repair on NEMO Model #36. The removed material sample was used for determination of physical properties.

undamaged shells. They perform in an analogous way to a steel shell that had a damaged section cut out and replaced by a new section welded in place to the undamaged portion of the shell. The hole created in the 10-year-old NEMO submersible hull by removal of one of the spherical pentagons for material testing (Fig. 7) has been also repaired by bonding in place of a new spherical pentagon with CADCO PS 30 cement (Fig. 9).

4. The surfaces of acrylic seats under metallic hatches on 10-year-old, weathered, and brand new polar unweathered pentagons were in the same condition after 1000 pressure cycles from 0-1500 psi to which they were subjected in this study, even though the old and weathered polar pentagon was already once before subjected to 1000 pressure cycles from 0-1500 psi immediately after fabrication of NEMO Model #37 in 1971. Since ANSI/ASME PVHO-I Safety Standard limits the design depth of acrylic shells at $\leq 50^\circ\text{F}$ ambient temperature to only $0.25 \times$ critical pressure, the ability of the bearing surface on the 10-year-old, weathered acrylic plastic to withstand 1000 pressure cycles to $0.3 \times$ original critical pressure at 73.4°F average ambient temperature range without initiation of cracks, indicate that the age and weathering have not significantly lowered the cyclic fatigue life of the spherical shell structure.

Material Test Coupons. The test data generated by subjecting material coupons from selected structural components to standard ASTM tests (Tables 2 and 3) and hydrostatic testing of disk specimens (Table 4) indicate that the mechanical properties of material *below* the surface of acrylic sheets and plates have not significantly changed after a 10-year-long exposure to weathering, whereas those of the material *on the surface* of the same sheets and plates had significantly deteriorated. The thickness of the weathered layer extends less than 0.020-in. deep into the body of the material. These postulates are based on the following findings.



Fig. 9 DSV NEMO after repair. A new pentagon was bonded in place of removed old pentagon.

1. The tensile strength, elongation tensile modulus, shear strength, compressive yield strength, impact strength, and flexural strength of specimens removed from the *interior* of 1

and 2.5-in.-thick, 10-year-old, weathered acrylic plates do not differ significantly from values measured on brand new acrylic plates (Tables 2 and 3). There was some small difference in compressive deformations under load, but the small increase noted in old and weathered material is not considered structurally significant.

2. The flexural strength, shear strength, tensile strength, and elongation of specimens removed from the surface of 2.5-in.-thick 10-year-old, weathered plate differ significantly from values measured on specimens removed from the interior of the same plate; these values were identical to those measured on specimens taken from a brand new unweathered plate (Tables 2, 3 and 4). The largest difference in flexural strength was noted when the surface specimens were flexure tested with the weathered surface in tension, and the smallest difference was noted when the surface specimens were flexure tested with the weathered surface in compression. Since the thickness of flexural specimens was approximately 0.25 in., the effect of weathering was postulated to extend significantly less than 0.25-in. deep; only by removing progressively thicker slices from the exterior of weathered plate could the actual thickness be determined more accurately.

3. The actual thickness of the weathered layer was found to be less than 0.020 in. This finding is based on the significant increase in maximum flexural strength of test samples taken from the weathered surface when 0.020 in. were removed from weathered surface of flexure specimens (Table 5). This finding is further substantiated by (1) the significant increase in molecular weight of plastic and (2) the significant decrease of free monomer content with distance from the weathered surface.

Since the effect of weathering extends less than 0.020-in. deep into the body of the acrylic plates, the structural performance of thick shells under compression is not significantly influenced by it. This is true only in cases where both surfaces of the shell are under compression. As soon as the weathered surface is placed locally under tension, the decreased tensile strength of that surface may lead to initiation of cracks, and ultimately failures. Since the resultant stress on both concave and convex surfaces is compressive on spherical shells and sectors with conical seats, the thin weathered layer on the external surface has no significant effect on the structural performance of shells, providing that their overall thickness significantly exceeds the thickness of the weathered layer. In the case of NEMO Model #37 the overall thickness of the shell exceeded the thickness of the weathered exterior and interior layers by a factor of 25, and for the full scale NEMO submersible, by a factor of 62. The 11 percent decrease of NEMO Model #37 and 7.5 percent decrease of NEMO Model #36 implosion pressures (Table 1) indicates that the decrease in implosion pressure probably would be greater for shells with an overall thickness/weathered layer ratio less than 25 and smaller for shells with an overall thickness/weathered layer ratio larger than 25. As the 11 percent decrease in critical pressure between a brand new and 10-year-old, weathered shell is considered acceptable, it can be postulated that shells with an overall thickness/weathered layer ratio equal to or larger than 25 are not significantly affected by 10 years of weathering. Based on the conservative assumption that the thickness of the weathered layer is 0.020 in., the minimum thickness of the shell whose structural performance is not significantly affected by 10 years of weathering is 1 in.

Since 10 years of weathering decreased the critical pressure of acrylic spheres with 1 in. shell only about 11 percent, and 25 percent decrease is considered the limit for structural performance deterioration requiring the recall of acrylic submersibles from manned service, it appears safe to

postulate that it will require an additional 10 years of weathering before the decrease in critical pressure of 1-in.-thick acrylic plastic spheres reaches this limit. For shells thicker than 1 in. it may require several decades before the 25 percent limit of structural deterioration under external pressure loading is reached. Still, in order to be conservative and on the safe side, the 20-year age limit should apply equally well to all acrylic spherical shells with thickness in excess of 1 in., designed on the basis of ANSI/ASME PVHO-1 Safety Standard.

One of the unexpected findings in this study was the discovery that the interior, unweathered surface of the 2.5-in.-thick NEMO hull also exhibited lower physical properties (Tables 3-5). Since the interior of the NEMO hull was not exposed to ultraviolet radiation, it must be assumed that the deterioration of the interior surface is the result of pollutants in the ambient atmosphere inside the closed hull. These pollutants are vaporized plasticizers from vinyl seat covers and polyvinyl chloride insulation on electric wires, as well as vapors of hydraulic fluids that leaked from hydraulic control valves and fittings. The condensation of these pollutants on the interior surface of the hull would attack the plastic resulting in deterioration of physical properties similar to that found in weathering.

Conclusions

1. The exterior surface of acrylic plastic hull deteriorated significantly after 10 years of outdoor weathering. The decrease in tensile and flexural strengths as well as elongation under tensile loading is in the range of 30-40 percent. The depth of weathered surface layer is less than 0.020 in.

2. The interior surface of acrylic plastic pressure hulls on submersible NEMO also deteriorated. It was exposed during the 10-year storage period to pollutants in the enclosed ambient atmosphere inside the submersible at temperatures in the 60-150°F range. The decrease in physical properties as well as the depth of affected surface layer is similar to that found in weathered exterior surfaces.

3. Since weathering and/or atmospheric pollutants affect only the surface layers of thick acrylic plastic meeting the requirements of ANSI/ASME PVHO-1, the structural performance of windows that see only compressive strains in service is not significantly degraded after 10 years of weathering in service. This may not be the case with windows that see tensile strains in service, such as plane disks, conical frustums with t/D , less than 0.5, and cylinders under internal pressure.

4. Spherical pressure hulls and spherical sector windows with thickness in excess of 1 in. that see only compressive strains under hydrostatic loading retain at least 90 percent of their original strength (as defined by critical pressure) after 10 years of weathering in service. Spherical pressure hulls and spherical sector windows with thickness less than 1 in. are postulated to retain less than 90 percent of their original strength after the same length of weathering in service, because the affected surface layers constitute a larger fraction of the shell thickness; by the same token, shells with thickness in excess of 1 in. probably retain more than 90 percent of their original strength.

5. It appears that it requires at least an additional 10 years of weathering (i.e., 20 years total) before the critical pressure of spherical pressure hulls and spherical sector windows with thickness equal to or thicker than 1 in. will decrease to 75 percent of its original value, the limit for acceptable structural deterioration in acrylic plastic windows designed on the basis of ANSI/ASME PVHO-1 Safety Standard for Pressure Vessels for Human Occupancy.

6. Spherical pressure hulls and spherical sector windows can be repaired by removal of damaged sections and bonding in place of patches with the same sphericity and thickness as the removed sections. If the edges of the openings in the shell and of the patches are cut at right angles to the spherical surfaces and if they are mated together and held in place with CADCO PS-30 self-polymerizing cement, the structural performance of the shell under external hydrostatic loading will be identical to that of the brand new shells.

Recommendations

1. The general, 10-year chronological age limitation imposed by ANSI/ASME PVHO-1 on all acrylic plastic windows and pressure vessels should be revised to exclude 1-in. or thicker spherical pressure vessels and spherical sector windows with conical bearing surfaces under external pressure loading, since the 11 percent decrease in critical pressure after 10 years of weathering in service does not warrant, from a safety viewpoint, their removal from service.

2. The chronological age limitation for acrylic plastic windows in shape of spherical sectors and spherical pressure vessels under external pressure loading should be extended from 10 to 20 years by ANSI/ASME PVHO-1. At that time test coupons should be again taken from the cross section of the 20-year-old weathered thick acrylic plates to determine whether enough strength is remaining in the material to warrant the extension of chronological age limit past 20 years for these acrylic plastic structures.

3. The use of vinyl and polyvinyl chloride plastics inside pressure chambers for human occupancy should be avoided because the vapors of plasticizers contained in these plastics attack the surface of acrylic plastic causing it to deteriorate similarly to weathering.

4. Repairing damaged acrylic plastic spherical shells and spherical sector windows by removal of damaged sections and bonding in place of new sections is an acceptable practice, providing that the repair meets the following criteria:

- a The acrylic plastic used as a patch must meet the criteria of ANSI/ASME PVHO-1 Appendix A, Tables 1 and 2.
- b The thickness and curvature of the patch must match those of the shell being repaired.
- c The dimensions of the patch must be within plus 0 minus 0.125 in. of the opening in the shell.

d The edges of the patch and of the opening in the shell must be within 1 deg of the vertical to the surface of curvature.

e The edges must be finished smooth, the surface quality exceeding 125 rms.

f Both the patch and the edges of the opening should be annealed for 24 hours at 175°F.

g The patch must be bonded in place with self-polymerizing cement, CADCO PS-30, or equal.

h The bonded joint must be annealed for 24 hours at 175°F.

i The repaired shell must be hydrostatically or pneumatically tested to 1.25 of its design depth according to ANSI/ASME PVHO-1, Appendix A, paragraph J.8 prior to being placed in service.

References

- 1 Stachiw, J. D., "Acrylic Plastic Viewports for Ocean Engineering Applications," Naval Undersea Center, Technical Publication 562, Vol. 1 and 2, Feb. 1977.
- 2 American Society of Mechanical Engineers, Safety Codes Committee on Pressure Vessels for Human Occupancy, "ANSI/ASME PVHO-1 Safety Standard for Pressure Vessels for Human Occupancy," American Society of Mechanical Engineers, Oct. 1981.
- 3 Yustein, S. E., Winans, R. R., and Stark, H. J., "Outdoor Weathering of Plastics under Various Climatological Conditions," *American Society of Testing Materials Bulletin*, Apr. 1951, pp. 31-43.
- 4 Yustein, S. E., and Winans, R. R., and Stark, H. J., "Three Years' Outdoor Weather Aging of Plastics under Various Climatological Conditions," *American Society for Testing Materials Bulletin*, Feb. 1954, p. 29.
- 5 Armed Forces Supply Support Center, Military Handbook 17A, "Plastics for Flight Vehicles—Part II, Transparent Glazing Windows," June 1977.
- 6 Stachiw, J. D., "Development of a Spherical Acrylic Plastic Pressure Hull for Hydrospace Applications," Naval Civil Engineering Laboratory, Technical Report R-676, Apr. 1970 (AD 707363)/ASME JOURNAL OF ENGINEERING FOR INDUSTRY, Vol. 93, No. 2, 1971.
- 7 Stachiw, J. D., "NEMO Model 2000 Acrylic Plastic Spherical Hull for Manned Submersible Operation at Depths to 3000 Feet," Naval Undersea Center, Technical Publication 451, Dec. 1974/ASME JOURNAL OF ENGINEERING FOR INDUSTRY, Vol. 98, No. 2, 1976.
- 8 Stachiw, J. D., "Spherical Acrylic Plastic Hulls Under External Explosive Loading," Naval Undersea Center Technical Publication TP 505, Mar. 1976/ASME JOURNAL OF ENGINEERING FOR INDUSTRY, Vol. 99, No. 2, 1977.
- 9 Stachiw, J. D., "Acrylic Pressure Hull for Submersible NEMO," ASM Paper 71-UN-T-2, Winter Annual Meeting, ASM, 1971.
- 10 Stachiw, J. D., Dolan, R. B., and Clayton, D. L., "Polycarbonate Plastic Inserts for Spherical Acrylic Plastic Shells Under Hydrostatic Loading," ASME JOURNAL OF ENGINEERING FOR INDUSTRY, Vol. 103, No. 1, 1981.
- 11 Stachiw, J. D., *Acrylic Plastic Viewports: Ocean Engineering and Other Hyperbaric Applications*, Marcel Dekker, New York, 1982.

DISCUSSION

E. Briggs¹. The author needs to be commended for this paper, as it represents a significant contribution to our knowledge of the effect of weathering on the mechanical properties of acrylic plastic. It would be very desirable however to have the author compare the data based on material specimens from submersible NEMO (Tables 3, 4, and 5) with data from viewports on other submersibles. Did weathering affect the acrylic plastic viewports in other submersibles as severely as the acrylic plastic pressure hull of NEMO?

¹ Southwest Research Institute, San Antonio, Texas

Authors' Closure

The question posed by Mr. Briggs is very germane to the topic of our paper; i.e., is the deterioration of surfaces on NEMO acrylic plastic after 10 years of service unique, or typical of all acrylic plastic viewports in marine environment? Unfortunately, there are not enough data on hand to answer this question adequately. There are some indications, however, that the data based on testing of specimens from DSV NEMO are representative of surface deterioration found in acrylic plastic viewports on other submersibles.

The mechanical properties of 10-year old acrylic viewports removed from DSV TURTLE and DSRV AVALON (Tables 6 and 7) appear to support the data from DSV NEMO. Both the exterior and interior surfaces show some deterioration, the

Table 6 Physical properties of surface and subsurface layers in 3.4 in. Plexiglas G

Location of Positively Stressed Specimen Surface	Flexure Test ASTM D-790			Source of Specimens
	Strength, psi	Modulus, psi	Type of Failure	
Outward weathered surface	12,500	4.8	Brittle	Viewport SN 02
0.005 inches removed from outward weathered surface	16,600	4.8	Ductile	" "
0.02 inches removed from outward weathered surface	16,600	4.8	Ductile	" "
0.04 inches removed from outward weathered surface	16,600	4.8	Ductile	" "
0.06 inches removed from outward weathered surface	16,500	4.8	Ductile	" "
0.08 inches removed from outward weathered surface	16,200	4.7	Ductile	" "
0.10 inches removed from outward weathered surface	16,800	4.8	Ductile	" "
Interior of the 2.5 inch thick Plexiglas G pentagon	17,100	5.0	Ductile	Viewport SN 01
0.06 inches removed from inward unweathered surface	17,200	5.0	Ductile	" "
0.04 inches removed from inward unweathered surface	17,400	5.0	Ductile	" "
0.02 inches removed from inward unweathered surface	17,700	5.0	Ductile	" "
0.5 inches removed from inward unweathered surface	17,800	5.0	Ductile	" "
Inward unweathered surface	12,900	5.0	Brittle	" "

NOTES:

1. The specimens were approximately 0.25 inches thick; four specimens were taken from each location; the values shown above are averages of these specimens.
2. The specimens were cut from the 3.4 inches thick, viewports from DSV Turtle which were in service continuously for 10 years.

Table 7 Physical properties of surface and subsurface layers in 2.0 in. Plexiglas G

Location of Positively Stressed Specimen Surface	Flexure Test ASTM D-790			Source of Specimens
	Strength, psi	Modulus, psi	Type of Failure	
Outward weathered surface	14,700	4.8	Brittle	Viewport SN 02
0.005 inches removed from outward weathered surface	15,300	4.8	Brittle	" "
0.02 inches removed from outward weathered surface	15,100	4.9	Brittle	" "
0.04 inches removed from outward weathered surface	15,500	4.9	Brittle	" "
0.06 inches removed from outward weathered surface	15,600	4.8	Brittle	" "
0.08 inches removed from outward weathered surface	15,300	4.8	Brittle	" "
0.10 inches removed from outward weathered surface	15,300	4.9	Tensile	" "
Interior of the 2.5 inch thick Plexiglas G pentagon	15,200	4.8	Brittle	" "
0.06 inches removed from inward unweathered surface	15,700	4.8	Brittle	Viewport SN 01
0.04 inches removed from inward unweathered surface	15,800	4.9	Brittle	" "
0.02 inches removed from inward unweathered surface	15,700	4.8	Brittle	" "
0.05 inches removed from inward unweathered surface	15,900	4.9	Brittle	" "
Inward unweathered surface	14,600	4.7	Brittle	" "

Notes:

1. The specimens were approximately 0.25 inches thick; four specimens were taken from each location; the values shown above are averages of these specimens.
2. The specimens were cut from the 2.0 inches thick viewports in DSRV which were continuously in service for 10 years.
3. Outward surface-interior surface of submersible, exposed to seawater and weathering. Inward surface-interior surface of submersible, exposed to condensation and interior atmosphere pollution. Interior-from midthickness of viewport.
4. Samples from outward layer were tested with outward surface in tension.
5. Samples from inward layer were tested with inward surface in tension.

deterioration of surfaces on the viewport from DSV TURTLE being more significant (Table 6) than on the viewports from DSRV AVALON (Table 7). One possible explanation for the lesser deterioration of viewport surfaces on DSRV AVALON

is that DSV TURTLE has seen more ocean service than DSRV AVALON (i.e., it has been exposed more often to weathering on deck of ships during transit to dive areas than the other vehicle during the 10-year period).

J. D. Stachiw

Staff Scientist for Materials,
Naval Ocean Systems Center,
San Diego, CA 92152
Mem. ASME

R. B. Dolan

Senior Staff Engineer,
Harbor Branch Foundation Inc.,
Fort Pierce, Fla. 33450

D. L. Clayton

Manager, R&D,
Harbor Branch Foundation Inc.,
Fort Pierce, FL 33450

Polycarbonate Plastic Inserts for Spherical Acrylic Plastic Shells Under Hydrostatic Loading

An acrylic plastic spherical pressure hull incorporating polycarbonate inserts for mounting of penetrators has been built and pressure tested. The transparent hull will serve as one atmosphere cockpit in Johnson-Sea-Link #3 submersible for 2500 ft. service. Tests have been conducted with model scale polycarbonate inserts in acrylic plastic spherical pressure hulls and windows to evaluate the structural integrity and cyclic fatigue life of polycarbonate plastic inserts and acrylic shells in which they are mounted under repeated hydrostatic pressurizations. Test results indicate that the short term, long term and cyclic fatigue life of a polycarbonate insert, serving as a bulkhead for electric or hydraulic penetrators in spherical acrylic plastic pressure hulls or windows, exceeds that of the acrylic plastic shell in which it is mounted. Structural parameters of polycarbonate inserts are discussed and design criteria formulated for their utilization in manned submersibles and pressure vessels for human occupancy. Particular emphasis is placed on selection of material, seal configuration, and retainment design.

Introduction

Acrylic plastic windows in opaque pressure vessels and acrylic plastic hulls in submersibles provide panoramic visibility for their occupants. Since the introduction of acrylic plastic by Professor A. Piccard in 1947 as material for windows in submersibles, no fatal accident can be credited to the catastrophic failure of acrylic plastic. This remarkable safety record is due to a fortuitous combination of physical properties in acrylic plastic, a decade of research into the structural performance criteria of acrylic plastic windows by U.S. Navy laboratories, and formulation of safety standard by ASME in 1977.

The ANSI/ASME PVHO Safety Standard, in particular, because of its scope and focus on design details, has made it feasible for the designer to vary the shape, seat design, and bearing surface configuration of a window without departing beyond the boundaries of the Safety Standard. Extensive as the Safety Standard may be, it does not provide at the present time any guidance on the incorporation of electrical or hydraulic penetrators in acrylic plastic windows or pressure hulls. If penetrators are to be incorporated into the body of the acrylic plastic structure, an experimental study would have to be conducted first to establish the structural adequacy of the chosen materials and design parameters.

The first acrylic plastic pressure hulls for undersea exploration were spheres, assembled from two flanged hemispheres which were sealed at the equator by an equatorial joint fabricated from steel or aluminum. This clam shell design, however, not only made it impossible to board, or escape from a surfaced submersible at sea, but also obstructed the field of view for the two occupants of the submersible. In this type of acrylic plastic pressure hull, any penetrations for electrical, hydraulic, or mechanical penetrators were located in the metallic rings of the equatorial joint. The metallic ring themselves were seated on elastomeric gaskets, and mechanical attachments to the

flanged acrylic hemispheres by means of bolted-on retaining rings. Besides the operational shortcomings of an equatorial joint, the flanges on the hemispheres introduced serious bending moments into the hull with resulting high tensile stresses.

To overcome the shortcomings of the clam shell design, Dr. Stachiw introduced in 1965 the NEMO-type spherical hull in which the ingress and egress from the sphere was by means of a circular hatch located at the top of the sphere, while all the electrical and hydraulic penetrators were centralized in a metallic bulkhead located at the bottom of the sphere [1]. With this arrangement boarding or escape from a surface submersible was feasible, while the polar locations of the metallic hatch and bulkhead allowed the occupants to view their environment without any obstructions. Furthermore, the use of conical penetrations in the hull with matching conical hatches and bulkheads totally eliminated tensile stresses in the acrylic spherical hull while increasing the local compressive stresses near the seat only by approximately 100 percent. Several submersibles utilizing this type of penetrations have been successfully built and operated (i.e., NEMO, MAKAKA!, JOHNSON SEA-LINK #1 and #2, CHECK MATE and other) [2, 3].

To date, the design of the circular hatch located at the top and the bulkhead at the bottom of the acrylic plastic sphere has satisfactorily met all the structural and operational requirements of the submersibles, and for this reason has been incorporated into the ANSI/ASME PVHO Safety Standard. In addition, to provide the designer with more flexibility in design of submersibles, experimental studies have been conducted on the structural performance of acrylic plastic spherical hulls with multiple hatches and metallic bulkheads [4], and the results also incorporated into the ANSI/ASME PVHO Safety Standard.

Still, even though the designer has at his disposal proven design options for multiple metallic hatches and bulkheads in spherical hulls, there still remains a pressing need for smaller, less expensive, plastic inserts that serve as bulkheads for mounting of electro-hydraulic penetrators, or mechanical attachments to the hull. The smaller, in-



Fig. 1 Model scale polycarbonate plastic insert tested in the 15 X 13-inch NEMO Model #36 (Figure 2) and spherical sector test fixture (Fig. 4)

expensive plastic inserts would allow the designer to locate the penetrators and attachments at locations on the hull where they would minimize the length of cables and hoses and thus decrease the complexity and weight of the control, propulsion and life support subsystems.

This paper summarizes the experimental investigation into the design parameters and structural performance results of small plastic inserts serving as bulkheads for penetrators and attachments in acrylic plastic spherical hulls and windows. The experimental study was conducted wholly with model scale structural components to minimize expenses. This was considered to be acceptable as past studies have unequivocally shown that the test data generated with model scale acrylic plastic hulls and windows under hydrostatic pressure applies directly to their full scale counterparts.

Experimental Study

Test Parameters

The objective of the experimental study was to (1) validate major criteria governing the design of small plastic inserts in acrylic plastic spheres and (2) evaluate the structural performance of acrylic plastic spheres with plastic inserts containing penetrators.

The scope of the study was limited to a single insert configuration for 2500 ft. and 50°F design depth and temperature, respectively.

As test specimens served (1) two identical polycarbonate plastic inserts with 26°41' included spherical angle, containing nine smooth holes with 0.312 inch diameter and eight threaded holes with 0.125 inch diameter (Fig. 1), and (2) single acrylic plastic plug with the same dimensions as the polycarbonate plastic insert, but without any holes for penetrators. The acrylic plastic insert served as the basis of comparison during the evaluation of stress risers in the acrylic hull at the edges of penetrations. The polycarbonate plastic inserts were fabricated from premium UV stabilized polycarbonate plastic (Table 1) and their dimensions were chosen to represent in 1:4.4 scale, a typical insert with holes for functional electric or hydraulic feedthroughs.

There were several reasons for selecting polycarbonated plastic and the conical seat design for the insert with penetrators. The conical seat was chosen because it (1) minimized shear and bending moments at the interface between the insert and the hull and (2) it was self-sealing at higher pressures [1]. The choice of polycarbonate material was dictated by (1) compressive modulus and strength that closely matched those of acrylic plastic, and (2) excellent crack propagation resistance. Because of these properties, there would be a minimum of membrane stress increase at the insert/hull interface and the crack growth from the threaded holes in the insert would be arrested.

Two test setups were used. Test Setup A consisted of placing the polycarbonate plastic insert (Fig. 1) and the acrylic plastic plug into a 15-inch X 13-inch acrylic plastic scale model of NEMO acrylic plastic hull¹ (Figs. 2 and 3). The Test Setup B consisted of placing the polycarbonate plastic into an acrylic plastic spherical sector with 57°38' included angle, which in turn was mounted in a steel flange with matching conical angle (Figs. 4 and 5).

Instrumentation was used only on Test Setup A. It consisted of electrical resistance straingages placed at the edges of all penetrations and at the equator of the acrylic plastic sphere (Fig. 3).

The test procedures differed between Test Setup A and B. The acrylic plastic NEMO Model #36 (Setup A) was placed inside a deep ocean simulator and pressurized with tap water to destruction at a rate of 100 psi/minute in 75°F ambient environment. Strains were read at 500 psi intervals.

The acrylic plastic spherical shell sector in the steel mounting (Setup B) was mated with the flange of a pressure vessel and locked in place in such a manner that the pressurized tap water inside the vessel applied pressure to the convex surface of the spherical shell

Table 1 Specified Values of Physical Properties for Polycarbonate Plastic (to be verified by testing of specimen from each plate that serves as machining stock for inserts)

Test Procedures	Physical Property	Specified Values	
		Metric Units	Engineering Units
ASTM-D-638*	tensile ultimate strength	≥ 6.3 kg/mm ²	≥ 9000 psi
	elongation at break	≥ 20 percent	≥ 20 percent
	modulus of elasticity	≥ 280 kg/mm ²	≥ 300,000 psi
ASTM-D-695*	Compressive yield strength	≥ 10.5 kg/mm ²	≥ 12,000 psi
	modulus of elasticity	≥ 210 kg/mm ²	≥ 300,000 psi
ASTM-D-621*	Compressive deformation at 4000 psi and 122°F, 24 hours	≤ 2 percent	≤ 2 percent
ASTM-D-732*	Shear, Ultimate strength	≥ 6.3 kg/mm ²	≥ 9000 psi
ASTM-E-308	Ultraviolet transmittance (for 0.5 inch thickness)	≤ 5 percent	≤ 5 percent

NOTE 1. Tests marked with an asterisk (*) require testing of a minimum of two specimens. For others, test a minimum of one specimen.

NOTE 2. Where two specimens are required in the test procedure, the average of the test values will be used to meet the requirements of the minimum physical properties of Table 1.

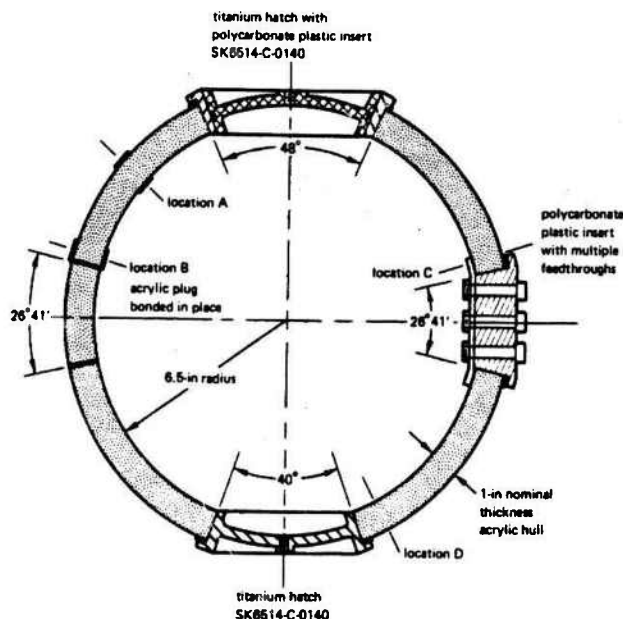


Fig. 2 Dimensions of model scale polycarbonate insert shown in Fig. 1

sector. The pressure inside the vessel was cycled at random, 1000 times, the average magnitude of sustained pressures, duration of sustained pressurizations and relaxation periods were 1361 psi, 7.55 hours and 7.99 hours, respectively. The ambient temperature was allowed to vary between 28° and 92°F, however, the average value of the ambient temperature was 60.36°F. The range of random and average values of pressure, duration of cycle phases, and ambient temperature were selected on the basis of operational scenarios for submersibles. (Peak pressures 400 to 1700 psi, duration of sustained loading 1 to 180 hours, duration of relaxation 2 to 257 hours.)

Test Results

Test Setup A. The acrylic sphere test assembly imploded at 4350 psi. Inspection of the failed assembly disclosed that the polycarbonate insert with penetrators and the metallic hatches were still intact, while the acrylic sphere was broken up into many irregular fragments. Strains at the interfaces between the polycarbonate insert and the acrylic hull (Location C) as well as between the acrylic plug and the acrylic hull (Location B) were the same as at a location midway between penetrations (Location A), while those at the interface between the metallic inserts and the acrylic hull (Location D) were significantly different, indicating the presence of a stress raiser (Table 2). The highest compressive strain at the interface between metallic insert and acrylic hull was measured along a meridian on the concave acrylic surface (Location D) and its magnitude was approximately 100% higher than the compressive strains on the concave surface of the hull midway between penetrations (Location A).

Both the 100% increase in compressive strain near metallic inserts and the 4350 psi critical pressure of the whole acrylic sphere are similar to results previously obtained during implosion testing of 15- \times 13-inch ID NEMO Models #34 and #22, which included metallic inserts only [1, 2].

Test Setup B. Detailed inspection of polycarbonate insert at conclusion of 1000 pressure cycles did not discover any damage to the polycarbonate insert or the seat in the acrylic shell. There was a total absence of cracks or crazing on the conical bearing surface of the polycarbonate plastic insert and mating seat in acrylic plastic shell. There were some minor cracks in the surfaces of drilled and tapped holes in the polycarbonate insert, but they were introduced there prior to pressure cycling by machining procedures. Pressure cycling generated some crazing and three shear cracks in the conical bearing surface of the acrylic spherical sector which contacted the conical seat

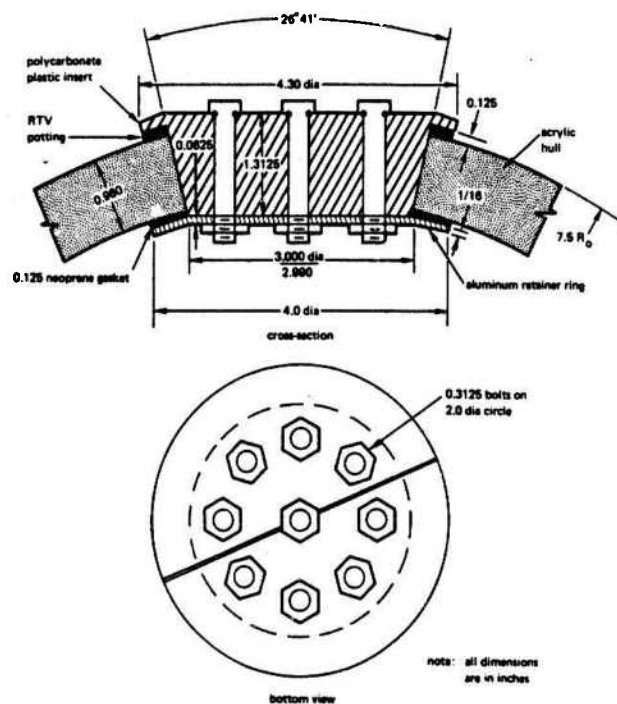


Fig. 3 15 \times 13-inch NEMO Model #36, imploded at 4350 psi under short term pressurization with tap water at 75°F

in the metallic flange. The interesting feature of these shear cracks in the acrylic spherical sector is that they appeared after 300 pressure cycles, but their rate of propagation was so slow that at 1000 pressure cycles their depth and width had only increased to approximately 0.5 inches. The surface of the conical seat on the steel flange was found to be badly corroded and pitted after 300 pressure cycles, which probably was a major factor in the initiation of crazing and cracks on the acrylic bearing surface.

Analysis of Test Results

The polycarbonate plastic insert and acrylic plug tested do not (1) act as stress risers in the acrylic plastic shell, (2) generate fatigue cracks on the mating seat in acrylic plastic shell, and (3) do not decrease the critical pressure of the acrylic plastic spherical shell containing inserts. Furthermore, the polycarbonate plastic insert itself does not show any fatigue cracking on its bearing surface, or around drilled and tapped holes in its body. In contrast the metallic inserts

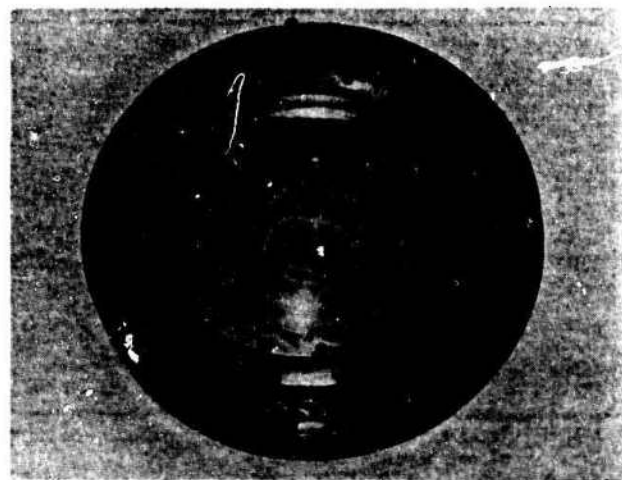


Fig. 4 Spherical sector test fixture for pressure cycling to 1500 psig the model scale polycarbonate insert shown in Fig. 1



Pressure	OUTSIDE								INSIDE							
	A		B		C		D		A		B		C		D	
	HOOP	LONG	HOOP	LONG	HOOP	LONG	HOOP	LONG	HOOP	LONG	HOOP	LONG	HOOP	LONG	HOOP	LONG
	<u>Negative Strain, microinches/inch</u>															
500 psi	2000	2100	2200	2200	2200	2400	550	2750	2700	2800	3100	2700	3300	2300	1850	5000
1000 psi	4200	4200	4300	4200	4100	4900	1600	5450	5500	5600	6300	5300	6200	5200	3850	11050
1500 psi	6600	6500	6500	6400	5100	7700	2150	8000	8500	8600	9800	7700	9100	8200	5150	16800
2000 psi	9100	9000	9100	8800	8200	10700	2700	10750	11800	12000	13500	10500	12500	11700	7500	24000
2500 psi	12000	11800	12000	11500	10500	13900	3400	13500	15800	16000	17900	13600	16300	15600	10500	31000
	<u>Compress. Stress, psi</u>															
500 psi	1402	1435	1523	1523	1558	1625	775	1509	1887	1920	2078	1940	2105	1771	1845	2895
1000 psi	2907	2907	2958	2925	2981	3248	1798	3081	3825	3858	4181	3848	4112	3779	3956	6356
1500 psi	4557	4517	4481	4448	4510	5043	2537	4487	5902	5935	6407	5707	6651	5838	5655	9537
2000 psi	6281	6248	6245	6145	6125	6958	3313	5996	8204	8271	8807	7807	8509	8243	8151	13650
2500 psi	8271	8204	8217	8050	7879	9012	4165	7531	10973	11040	11620	10186	11158	10925	10946	17778

Notes: 1. Failed at 4350 psi in 78° ambient environment.
2. Metallic hatches and polycarbonate plug were undamaged.

in the form of hatch covers or penetrator bulkheads, although they do not decrease the critical pressure of the spherical hull, act as stress risers in the acrylic plastic shell [1], and because of it, generate fatigue cracks in acrylic plastic after fewer pressure cycles than the polycarbonate plastic insert [2].

The formation of shear cracks on the conical bearing surface of the acrylic spherical sector in contact with the steel mounting confirms the findings of a previous study [2] which showed that the relative displacement between mating acrylic plastic and metallic bearing surfaces will generate shear cracks in the acrylic plastic surface sooner than if the bearing surface in contact with acrylic plastic was made of polycarbonate plastic. In the current study, the cracks appeared in the acrylic surface bearing against metal mounting after approximately 300 pressure cycles while there was still no sign of cracking or crazing in the acrylic surface bearing against the polycarbonate plastic after 1000 pressure cycles of average 0.2 STCP¹ magnitude and 7.5 hours duration at 60°F ambient pressure.

Discussion

The polycarbonate plastic insert evaluated in this study appears to be the ideal engineering solution for providing in the spherical acrylic shell a secure but demountable foundation on which electrical or hydraulic bulkhead penetrators may be mounted. The physical properties of the polycarbonate plastic match those of acrylic plastic so closely that the acrylic plastic shell does not react to the insert as a foreign structural body. Because of it, there is no increase in strains at the insert to acrylic shell interface, or relative displacement between the mating surfaces. Furthermore, the low notch sensitivity of the polycarbonate plastic allows drilling and tapping of holes in the insert for electric hydraulic penetrators without particular concern for crack propagation in the insert.

Even though polycarbonate plastic appears to be the proper material for inserts in acrylic plastic spherical shells metal is also acceptable, providing that the disadvantages associated with its use are understood and compensated for. Past tests have shown that although they serve as hard spots in the shell and increase compressive strains at the insert/shell interface by at least 100 percent, the overall effect on the critical pressure of the acrylic shell is negligible.² The only serious drawback of metallic inserts is that they significantly lower the fatigue life of the acrylic surface in contact with the metallic bearing surface. Thus, fatigue cracks may appear in the acrylic surface in contact with a metallic insert after approximately 500 pressure cycles of 0.3 STCP magnitude and an 8-hour duration at 70°F ambient temperature. This is not the case with the acrylic surface in contact with a polycarbonate insert, where after an identical cyclic loading history there is a total absence of any shear cracks.

There is a way, however, to utilize the beneficial effect of polycarbonate plastic for improving the fatigue life of seats in spherical acrylic plastic shells containing metallic inserts. This is accomplished by interposing a polycarbonate plastic gasket between the conical bearing surface on the metallic insert and the conical seat in the acrylic shell. Data from a past study [2] indicates that the presence of the polycarbonate gasket extends the cyclic fatigue life of the conical seat in an acrylic shell beyond 1000 pressure cycles of 0.3 STCP magnitude and an 8-hour duration at 70°F ambient temperature.

Polycarbonate plastic, or metallic inserts besides serving as bulkheads for mounting of the penetrators may also serve as foundations for attachments of small equipment to the acrylic plastic spherical windows and pressure hulls. Thus, many devices needed for safe operation of the diving system may be attached directly to the acrylic hull instead of the metallic hull or some external framework. As the

examples can serve here externally located cameras, lights, depth gages and direction finders. What makes this approach to mounting of external equipment so particularly attractive to the designer of the diving system is that an electric switch, or mechanical linkage used in the operation of this equipment can be mounted on the interior surface of the same insert within easy reach of the pilot.

The direct result of this design philosophy is substantial reduction in number and length of cables through the metallic hull, which directly translates into a lower cost and weight of the diving system. A less tangible, but nevertheless real gain associated with this design philosophy is an increase in safety due to the decrease in number and length of cables customarily used for control of externally located equipment. The savings in cost and weight associated with mounting of internal equipment to the acrylic plastic spherical shells are not as significant as for externally located equipment, but wherever they are used, the result is simplification and reduction of clutter in the pilot's compartment.

In summary, the experimentally proven ability to incorporate inserts into acrylic plastic spherical shells without significantly decreasing their short term, long term, or cyclic fatigue strength presents the engineer with a whole new field of design options previously not available to him. Such inserts have already been incorporated into the acrylic hull of JOHNSON-SEA-LINK #3. Since this is the first diving system to utilize polycarbonate plastic inserts as foundations for inserts and attachments in its acrylic plastic hull, its design, construction, and evaluation are described in the following section in some detail.

Acrylic Hull of Johnson-Sea-Link III

Hull Description

JOHNSON-SEA-LINK III is the third acrylic plastic submersible to be designed and built by the Harbor Branch Foundation, Inc. for service in support of their ocean science program. The submersibles No. I and II are identical in all respects. They feature an all acrylic 66- x 58-inches pilot's sphere and an aluminum lockout chamber. The interior of the acrylic sphere is maintained at atmospheric pressure so that the pilot and the scientific observer need not undergo decompression at the termination of the dive. The pressure inside the aluminum chamber can be adjusted to match the outside hydrostatic pressure within the operational depth range of the submersible. At the conclusion of the dive the divers may transfer under pressure to the deck decompression chamber aboard RV JOHNSON by mating the lockout hatch on the submersible with the lockout hatch on the deck decompression chamber [4].

The JOHNSON-SEA-LINK I and II are ideal for placement of divers outside the submersible for close-up investigation and collection of aquatic materials under the direction of the scientist inside the acrylic sphere. They are, however, less than ideal for exploration of sea bottom by large parties of scientists since there is room for only one scientist in the acrylic sphere, the other two must ride in the opaque diver chamber and view the sea bottom only through two small viewports with narrow field of view. Recognizing the limitations of the first two JOHNSON-SEA-LINK, namely, one scientist in the pilot's sphere with a panoramic view, Mr. Edwin A. Link, Vice-President of Harbor Branch Foundation, decided to embark on a third JOHNSON-SEA-LINK which would provide three scientists with a panoramic view on each dive at the expense of eliminating the compartment for divers.

JOHNSON-SEA-LINK III, therefore, is to be outfitted with two acrylic spheres in a tandem arrangement (Fig. 6).

The forward acrylic hull contains the typical top hatch and bottom penetrator plate, 180° apart. The aft acrylic hull, however, differs in that the penetrations are made through two smaller polycarbonate plugs approximately 10" in diameter (Figs. 7 and 8). At the bottom apex, a stainless pin for centering the hull in the framework is installed using a polycarbonate insert to interface with the acrylic hull. With this novel arrangement the aft acrylic sphere is lighter and provides better opportunity for the two scientists inside the sphere to observe the sea bottom directly below the submersible. Since reliable data did

¹ STCP—short term critical pressure, established by pressurizing the acrylic plastic sphere to implosion at 100 psi/minute rate in 70°F ambient environment.

² The 15- x 13-inch NEMO Model #36 was fabricated in 1971 by the Naval Missile Center, Point Mugu, California and was subjected, prior to this study, to (1) 1000 pressure cycles of 1000 psi magnitude and eight hour duration, (2) three dynamic pressurizations with maximum 6170 psi peak overpressure at 900 psi ambient pressure, and (3) four years of weathering in Southern California.

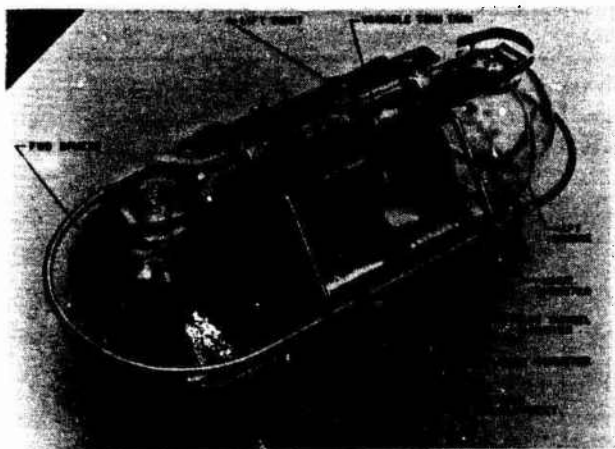


Fig. 6 Model of proposed JOHNSON-SEA-LINK III submersible with 2500 ft. design depth. For clarity of construction the ballast tanks on the model are made from acrylic, rather than aluminum

not exist on the performance of polycarbonate plastic inserts in acrylic hulls under short term, long term and cyclic pressure loading, an experimental design validation study was initiated by the Harbor Branch Foundation.³

The design validation study was conducted in two phases: The

objective of the first phase was to establish the structural performance limits of polycarbonate plastic inserts in spherical acrylic shells. This was accomplished by pressure testing model scale inserts, spheres, and spherical sectors until they imploded, or showed signs of structural fatigue. The results of the model scale tests have been already described in the preceding section of this paper and need no further discussion.

Design Validation

The second phase of the design validation study conducted on the full scale JOHNSON-SEA-LINK III acrylic sphere served to confirm the results generated in the first phase of the study with model scale inserts and sphere. The design of JOHNSON-SEA-LINK III acrylic sphere (Fig. 7) differed from the model scale sphere in the number and diameter of penetrations (Fig. 2). The 66- x 58-inch acrylic sphere was provided with a 48°30' penetration at the top, a 14° penetration at the bottom, and two 18° penetrations located 52° below the equator. An aluminum hatch resting on polycarbonate gasket filled the top penetration, a stainless steel centering pin inside a polycarbonate insert filled the bottom penetration, and two polycarbonate inserts (Fig. 8) containing eight penetrators each filled the two openings below the equator. The difference in designs of inserts between the model scale and full scale spheres was not considered significant enough to invalidate the comparison of strains between the 36 and 15-inch diameter spheres.

The scope of the tests performed on the full scale sphere was very limited as the full scale sphere could not be subjected to tests which

³ Harbor Branch Foundation Contribution #177.



Fig. 7 66 x 58-inch acrylic sphere for JOHNSON-SEA-LINK III after successful hydrotesting to 3500 ft. (1700 psig) at the Southwest Research Institute, San Antonio, Texas

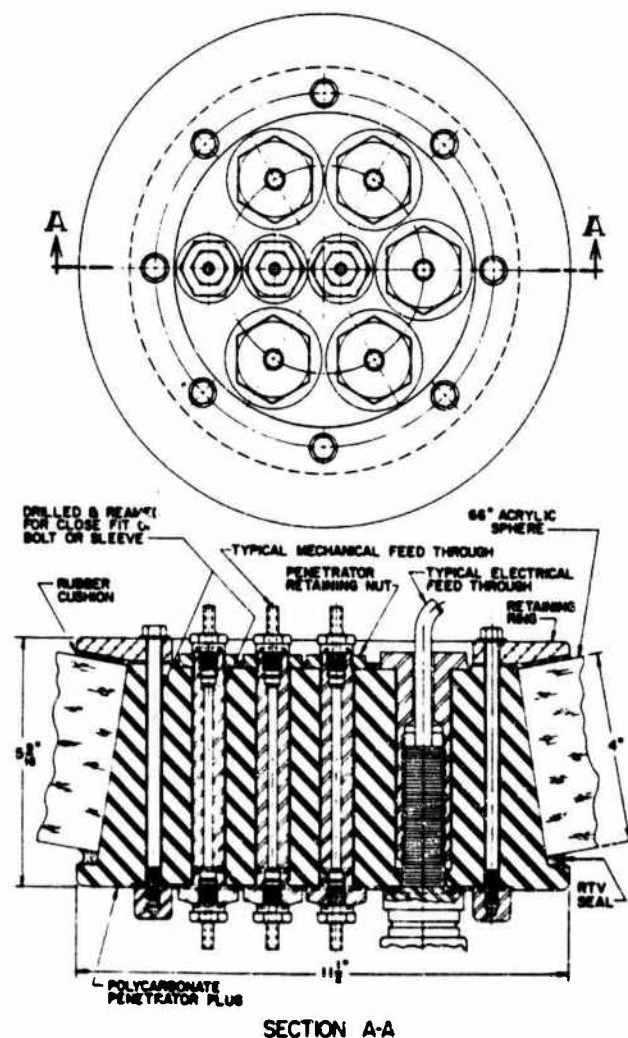


Fig. 8 Dimensions of the polycarbonate inserts in the 66 x 58-inch acrylic sphere shown in Fig. 7

Table 3 Strains and Stresses on 66 X 58-inch Sphere under Hydrostatic Loading

Pressure	OUTSIDE								INSIDE							
	A		B		C		O		A		B		C		O	
	HOOP	LONG	HOOP	LONG	HOOP	LONG	HOOP	LONG	HOOP	LONG	HOOP	LONG	HOOP	LONG	HOOP	LONG
	Negative Strain, microinches/inch															
400	1900	1960	1900	1840	1740	2240	960	1840	2440	2540	2420	2200	2160	2520	1660	3920
1000	4840	4800	4800	4460	3920	5480	1620	4380	6280	6380	6100	5840	5520	6900	4140	9400
1400	6860	6800	6920	6320	5500	7780	2000	6540	8980	9160	8680	8460	7820	10120	5940	13220
1700	6560	8480	9580	7980	6780	9640	2300	8300	11180	11400	10760	10520	9840	12760	7440	15920
1700*	9500	9380	9580	8500	7140	10420	8340	7420	12540	12720	11820	11800	10500	14340	10560	6560
0**	340	340	540	120	520	400	1260	900	380	360	460	640	540	560	620	560
	Compressive Stress, psi															
400	1179	1197	1160	1142	1151	1299	731	992	1517	1547	1454	1389	1387	1493	1382	2052
1000	2972	2960	2900	2799	2661	3123	1432	2255	3881	3910	3712	3635	3617	4026	3387	4945
1400	4212	4194	4163	3985	3748	4424	1955	3300	5555	5608	5306	5241	5179	5861	4817	6974
1700	5255	5231	5168	4961	4629	5476	2373	4150	6915	6980	6583	6512	6521	7386	5931	8440
1700*	5827	5791	5723	5403	5917	5889	4986	4713	7746	7799	7271	7265	7074	8212	7456	9234
0**	209	209	265	141	301	265	431	209	231	225	312	365	335	341	372	356

Locations: A - Equator

B - Midway between penetrations with polycarbonate inserts

C - Edge of penetration with polycarbonate insert

O - Edge of penetration with aluminum hatch

Notes: 1. The sphere was pressurized at 100 psi/minute rate to 1700 psi, held at that pressure for 4 hours then depressurized to 0 psi at the same rate.

2. * After 4 hours of sustained loading

**After 12 hours of relaxation at 0 psi

would destroy it, or severely shorten its fatigue life. Thus the full size acrylic sphere for JOHNSON-SEA-LINK III was subjected only to a single four-hour long pressurization to 1700 psi at ambient room temperature while the strains at critical locations were recorded.

Test Results from Hydrotesting of JOHNSON-SEA-LINK III Sphere

The magnitude and orientation of strains measured on the full scale sphere during short term pressurization (Table 3) compared rather well with the strain values measured on the 15-inch diameter sphere (Table 2) during its short term pressurization to implosion. Prior to comparing the strains one must, however, multiply the strain data from the 15-inch sphere by a factor of 1.09 in order to take into account that the t/D ratios of the two spheres are not identical (i.e., 0.0666 vs. 0.0606 for the 15 and 66 inch diameter spheres, respectively).

It is interesting to note that the creep measured on the acrylic sphere at the edge of the polycarbonate inserts (Location C) was not significantly higher than the creep measured at the equator (Location A) or midway between penetrations (Location B). This indicates that the polycarbonate plastic in the insert creeps at approximately the same rate as the acrylic plastic under biaxial compression.

Since the magnitude of residual strain on the acrylic sphere near the polycarbonate insert after depressurization and relaxation period is the same as at the equator or midway between penetrations it can be concluded that the polycarbonate plastic insert relaxes at the same rate as acrylic plastic sphere. Furthermore, the low value of residual strains on the acrylic sphere near penetrations indicates that (1) the stresses introduced into the acrylic sphere by metallic and plastic inserts during hydrotest to 1700 psi are below the yield point of acrylic plastic and that (2) hydrotesting of the JOHNSON-SEA-LINK III acrylic sphere to 50 percent above its design depth of 2500 feet (1116 psig) is structurally an acceptable procedure.

Conclusion

Conical inserts of polycarbonate plastic may be incorporated into the spherical shell of acrylic plastic windows and pressure hulls without significantly decreasing their short term critical pressure, or static and cyclic fatigue life under hydrostatic loading. These inserts can serve as foundations for penetrators or attachments to the acrylic shell.

Conical metallic inserts may be also incorporated into the spherical shell of acrylic plastic windows and pressure hulls without decreasing their short term critical pressure or static fatigue. There is, however, some decrease in the cyclic fatigue life of the acrylic shell surface in contact with the insert. This effect can be eliminated by interposing a polycarbonate plastic gasket between the metallic insert and the acrylic shell. This arrangement does not eliminate the metallic insert as a hardspot in the soft acrylic shell, but it allows the peak compressive and shear stresses to be born by the tough polycarbonate plastic gasket instead of the brittle acrylic plastic shell and thus prevents appearance of premature fatigue shear cracks in the acrylic plastic bearing surface.

Acrylic spheres and spherical sectors equipped with polycarbonate inserts or metallic inserts with polycarbonate gaskets can be safely operated to 0.25 STCP if the ambient environment does not exceed 50°F.

Design Recommendations

To insure safe performance of polycarbonate plastic or metallic inserts in acrylic plastic shells guidelines have been developed for their design and fabrication. These guidelines can be broken down into minor headings of material, shape, structural considerations, sealing, fastening, location and size.

Materials. Polycarbonate plastic satisfying the requirements of Table 1, and corrosion resistant metals with compressive yield \geq 25,000 psi are acceptable materials for inserts.

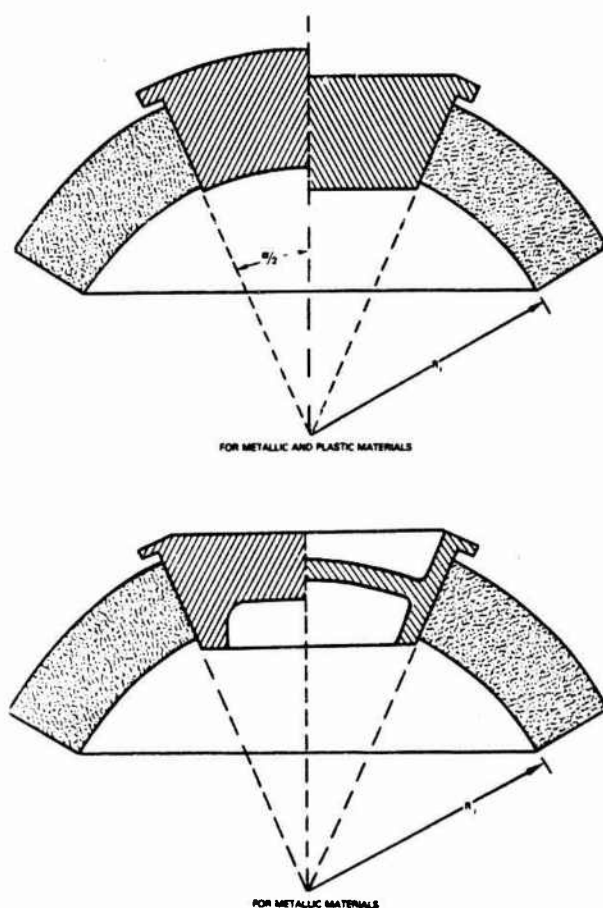


Fig. 9 Typical shapes of inserts

Shape. The insert must be circular, with a bearing surface that forms the inclined surface of a truncated cone whose imaginary apexes at the center of curvature for the concave surface of the acrylic shell. The included conical angle of the seat in acrylic shell must match the included conical angle of the insert within 30 minutes. The bearing surface of the insert must extend past the edges of the seat in the acrylic shell to insure adequate support to the shell.

Structural considerations. The external and internal surfaces of the insert may be plane or spherical. Regardless of surface configuration used on the insert, its thickness must reflect a safety factor of at least four based upon both yielding of the material and buckling design pressure.

Holes may be drilled and tapped in the inserts providing that the spacing between the edges of holes in polycarbonate plastic exceeds the diameter of the larger adjacent hole, and in metal exceeds the radius of the larger adjacent hole. The same relationship holds for the spacing between the edges of the holes and the edge of the insert. The holes in polycarbonate inserts must be sized for the penetrators to support the edges of the holes when the window assembly is subjected to design pressure.

Seal. Although the contact between the mating conical surfaces of the insert and the seat acts as a high pressure seal, a low pressure seal must also be incorporated into the insert. As a low pressure seal can serve an O-ring, gasket, or RTV silicon rubber potting compound axially compressed between a flange on the insert and the convex surface of the acrylic shell. The thickness of the flange and the clearance between the edge of the flange and the convex acrylic surface must be adequate to prevent shearing off of the flange during axial displacement of the insert under design pressure.

Fastening. Any mechanical fastening design is acceptable providing that it is adequate to (1) compress the seal, (2) retain the insert

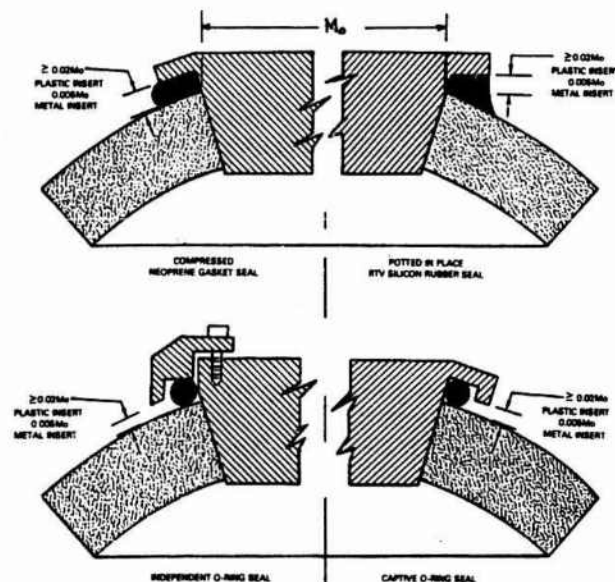


Fig. 10 Typical sealing arrangements for inserts

against forces encountered during typical diving operation. The forces that must be considered are accidental internal pressurization of pilot's compartment, wave slap, hydrodynamic drag, and any other static or dynamic load tending to pull the insert from its seat. Metallic clips, nuts and internal retaining rings bolted to the insert have been found to provide adequate restraint providing that an elastomeric gasket is interposed between the retainers and the concave surface of the acrylic shell.

Location. In spherical shells and sectors with conical bearing surfaces, the inserts may be located anywhere on the shell providing that the spacing between the edges of conical penetrations in the shell exceeds the radius of the larger adjacent hole and the spacing between the edge of the penetrations and the edge of the spherical sector exceeds the diameter of the penetration.

Size. There are three limitations imposed on the size of inserts. The diameter of a single penetration in the shell should not subtend

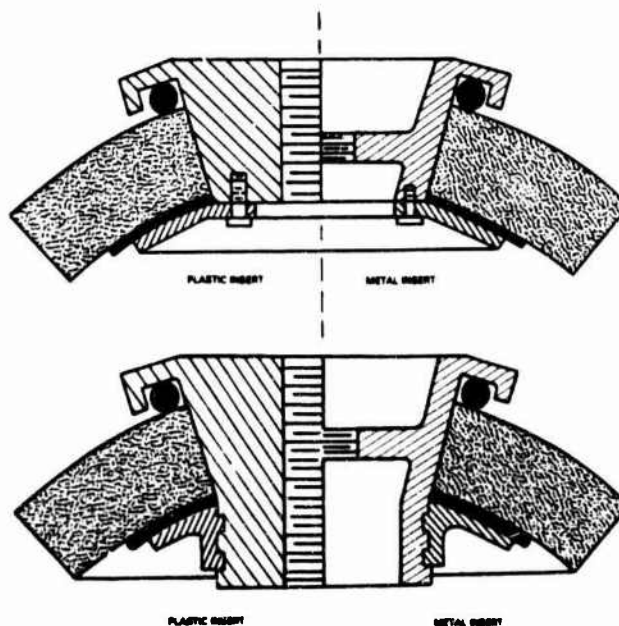


Fig. 11 Typical restraints for inserts

a larger spherical angle than 50°, while its area should not exceed 15% of the acrylic surface prior to machining of the penetration. In addition, the area of all the penetrations in the spherical shell sector should be limited to 30 percent of the shell area.

Service Restrictions. The polycarbonate plastic inserts may be exposed in service only to (1) temperatures which are below the design temperature of the window in which they are mounted, and (2) fluids and gases compatible with polycarbonate plastic. For this reason, the designer must critically review the construction and function of all penetrators prior to placement in the insert as their failure may expose the polycarbonate plastic to excessively high temperature and/or corrosive fluids.

Electrical penetrators. When shorted out, electrical penetrators can readily generate temperatures in excess of the window's design temperature, causing the polycarbonate plastic to deform plastically, and ultimately to fail catastrophically. This can be avoided either by selecting only circuits with low power inputs, or by incorporating circuit breakers which will sense the surge of current initiated by a short and interrupt the circuit before the penetrator can heat up significantly.

Hydraulic penetrators. Unless absolutely leaktight, hydraulic penetrators may bring corrosive hydraulic fluid in contact with the plastic insert causing it to crack and ultimately to fail catastrophically. This can be avoided by selecting only hydraulic fluids compatible with polycarbonate and acrylic plastics, and/or by utilization of leak proof penetrators.

References

- 1 Stachiw, J. D., "Spherical Acrylic Pressure Hulls for Undersea Exploration," ASME, *Journal of Engineering for Industry*, May 1971, Vol. 93.
- 2 Stachiw, J. D., "NEMO-Type Acrylic Plastic Spherical Hull for Manned Operation to 3000 Ft. Depth," ASME, *Journal of Engineering for Industry*, May 1976, Vol. 98.
- 3 Stachiw, J. D. and Lonea, J. J., "Development of Economical Casting Process for NEMO-Type Acrylic Submersible Hulls," ASME, *Journal of Engineering for Industry*, May 1977, Vol. 99.
- 4 Stachiw, J. D. and Dolan, R. B., "Spherical Acrylic Pressure Hulls with Multiple Penetrations," ASME, *Journal of Engineering for Industry*, May 1978, Vol. 100.
- 5 Maisson, J. R., and Stachiw, J. D., "Acrylic Pressure Hull for JOHNSON-SEA-LINK Submersible," ASME Paper No. 71-WA/Unt-6, 1971.

J. D. Stachiw

Naval Ocean Systems Center
San Diego, Calif.

R. B. Dolan

Harbor Branch Foundation, Inc.
Fort Pierce, Fla.

Spherical Acrylic Pressure Hulls With Multiple Penetrations

An experimental program has been conducted to determine the effect of multiple penetrations on the performance of spherical acrylic plastic hulls under external hydrostatic pressure. As test specimens served 15-in. OD \times 14-in. ID model scale NEMO spheres. The distribution of strains and the magnitudes of short term critical pressures indicate that the structural response of acrylic spheres with multiple penetrations to external hydrostatic pressure is identical to spheres with only one penetration equipped with a metallic closure providing that the included angles of the penetrations are ≤ 46 deg and the edges of the penetrations are at least one penetration radius apart. Based on these findings it is feasible to incorporate three or more large penetrations into the spherical hulls of acrylic submersibles without decreasing their operational depth rating that has been based on the experimentally proven structural performance of spheres with only one penetration, or two penetrations 180 deg center to center apart.

Introduction

Spherical hulls fabricated from acrylic plastic provide unrestricted underwater visibility for exploration of hydrospace. In addition, acrylic plastic provides excellent resistance to corrosion as well as insulation against heat loss. Since their introduction in 1969 acrylic plastic submersibles have performed reliably and have shown no sign of corrosion or structural deterioration. As a result of this outstanding performance, ship classification societies, like the American Bureau of Shipping and Det Norske Veritas, as well as the U. S. Navy, have accepted them for manned service without any reservations.

One of the reasons for the unqualified acceptance of acrylic submersibles by the users and classification societies is the wealth of experimental and analytical data on which their design is based [1-23].¹ The data were generated primarily by the Naval Civil Engineering Laboratory in support of the Navy's development of NEMO, the first all-acrylic plastic hull manned submersible [12]. Before NEMO was certified by the Navy for manned operations, 33 model scale and two full scale NEMO hulls with $0.071 \leq t/R_i \leq 0.073$ and 40 deg polar penetrations were built and tested to destruction under short term, long term, and cyclic pressure loadings. Since that time seven more model scale and two full scale hulls with $0.138 \leq t/R_i \leq 0.154$ and 46 deg polar penetrations have been built and tested by the

Naval Undersea Center to generate data that would complement findings from the prior test programs and extend the operational depth of acrylic plastic submersibles from 600 to 3000 ft depth [16] without increasing the cost [18] of the hulls (Fig. 1).

Still, although a total of 40 model scale and four full scale acrylic hulls were tested in the Navy's acrylic hull research program prior to this study, all of the data applied only to spheres with a single or two penetrations located at opposite poles of the sphere. The reason for the two polar penetrations was that this was the configuration of the hulls in Navy's NEMO and MAKAKAI submersibles [20] requiring experimental proof of their structural adequacy. The Navy's acrylic hull research program had only two major objectives: (1) discover the structural parameters that control the depth rating of an acrylic sphere under diverse operational conditions and (2) determine if there is any degradation of structural properties due to incorporation into the sphere of one or two polar penetrations. These objectives were met.

The findings of the Navy's acrylic hull research program were: (1) the safe operational depth of a spherical acrylic pressure hull must not exceed 30 percent of its short term critical pressure² if a crack-free cyclic fatigue life of 1000 dives (4 hour average duration) or static fatigue life of 4000 hours at operational depth is to be guaranteed, and (2) the presence of one or two penetrations equipped with polycarbonate inserts and metallic closures does not decrease the short term critical pressure of operational depth rating of an acrylic hull, providing that the spherical angle of the closure does not exceed 46 deg and that the centers of penetrations are located 180 deg apart. If the polycarbonate inserts between the metallic closures and acrylic

¹ Numbers in brackets designate References at end of paper.

Contributed by the Ocean Engineering Division for presentation at the Winter Annual Meeting, Atlanta, Ga., November 27-December 2, 1977 of THE AMERICAN SOCIETY OF MECHANICAL ENGINEERS. Manuscript received at ASME Headquarters Aug. 1, 1977. Paper No. 77-WA/Oce-2.

² Short term critical pressure (STCP), pressure at which implosion takes place when pressurized at 650 psi/min rate at 75°F ambient temperature.

(Fig. 5). This is quite feasible as the new submersible does not depend upon mechanical linkages for maneuvering in the water. Relocating the penetration plate from the lowest point in the sphere will prevent shorting out of electrical feedthroughs either by condensate running down the sides of the sphere or by seawater splashed in through the open hatch. In one of the acrylic spheres on Johnson-Sea-Link III the

bottom penetration plate will be probably completely omitted as that sphere will be occupied only by scientists not charged with the operational control of the submersible. Omission of the bottom penetration plate will provide also an additional operational bonus to the scientists for it provides unobstructed viewing and photographing of the ocean floor through the bottom of the sphere.

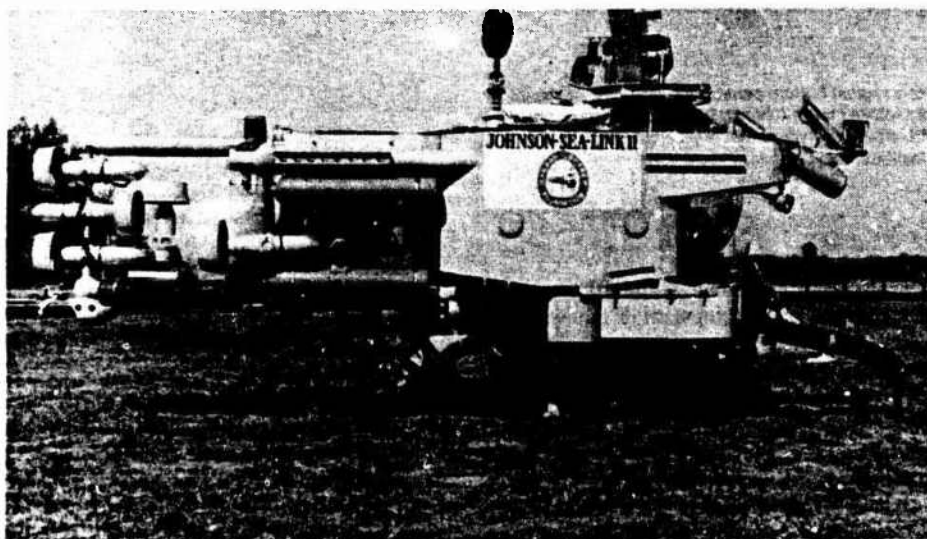


Fig. 2 Johnson-Sea-Link II incorporating a NEMO Model 2000 acrylic plastic sphere

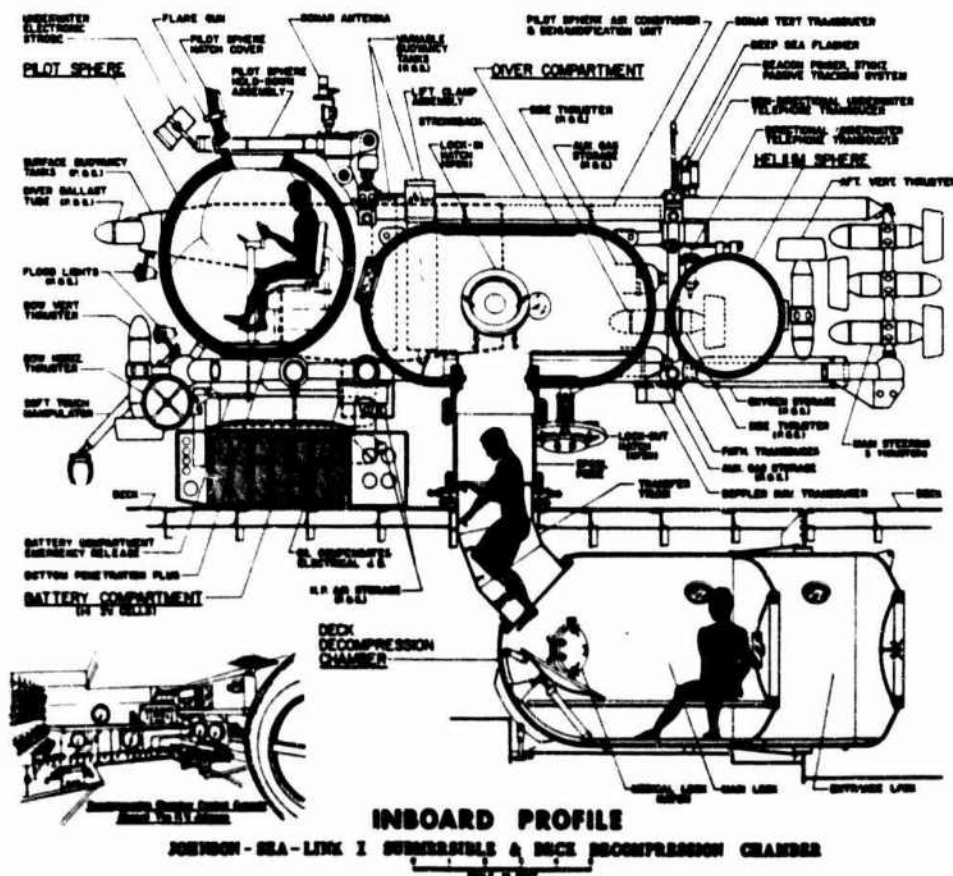


Fig. 3 Major components of Johnson-Sea-Link I submersible and the associated decompression chamber aboard the mother ship R. V. Johnson

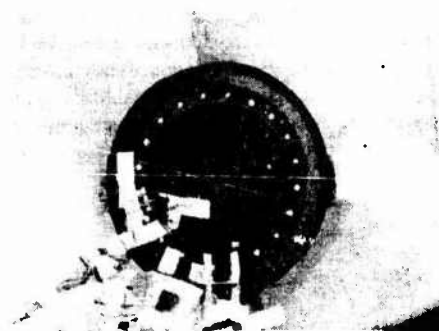


Fig. 4 Interior view of a typical bottom penetration plate inside the 66 in. outside diameter acrylic sphere for the Johnson-Sea-Link submersible series. The photograph was taken during hydrostatic pressurization to 1500 psi at Southwest Research Institute, San Antonio, Texas

But even with the revolutionary Johnson-Sea-Link III already on the engineering drafting boards, the development of Johnson-Sea-Link series of submersibles will not terminate with that vehicle. Other concepts of new submersible systems are already being formulated by the Harbor Branch Foundation. Short range excursion vehicles, towable or self-propelled in situ observatories, and rescue capsules for submersibles and habitats are being here seriously considered (Figs. 6(a), (b), (c), (d)). The common feature of all these concepts in addition to acrylic spheres with hatches and penetration plates are personnel tunnels that interconnect several acrylic spheres, or connect a single acrylic sphere to another chamber. If the current study on multiple penetrations in acrylic spheres proves the feasibility of multiple penetrations through the walls of the spheres, any one, or all, of these concepts may become reality in the near future.

The main purpose in presenting these concepts beyond Johnson-Sea-Link III was to speculate about the far future and prepare constructively for the next generation of submersibles equipped with multipenetrations spheres. Once the current test program has been completed and the critical design limits of multiple penetrations defined, the avenue to acrylic sphere design will have been significantly broadened beyond the standard proven Navy NEMO sphere design with twin penetrations.

Experimental Test Program

An experimental test program was initiated by the Harbor Branch Foundation Inc.³ to generate data that would support the conceptual designs being proposed by Mr. E. Link for the second generation of acrylic plastic submersibles utilized in scientific exploration of the sea. Since the conceptual designs were subject to change from day to day in response to new ideas and projected operational scenarios, the experimental test program had to be general enough to cover most projected hull designs and yet be sufficiently brief to fit a small budget.

Test Program Philosophy. The basic philosophy underlying the test program was to design the experiments in such a manner that the results would complement and extend wherever possible the body of existing data on standard NEMO acrylic hulls.⁴ In this manner, if the test results were shown to be similar to the existing standard NEMO hull data the whole existing standard NEMO hull data population could be used in support of the new hull designs. This objective could be achieved only if the test specimens used in the test program possessed the same general structural characteristics as the model scale

³ A portion of the work described in this report represents a contribution No. 68 from the Harbor Branch Foundation Inc.

⁴ Standard NEMO hull—acrylic sphere fabricated by bonding of 12 spherical pentagons, subsequently machined to receive two metallic hatches located 180 deg center to center apart. The hatches subtend spherical angles in the 40–46 deg range.

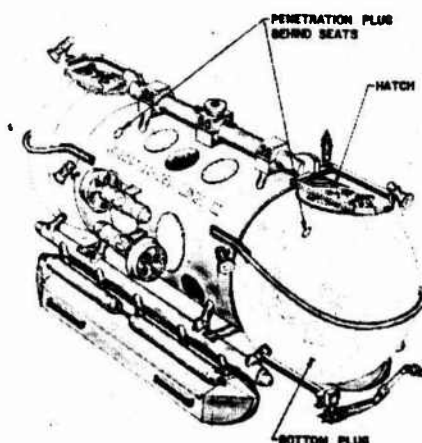


Fig. 5 Conceptual drawing of Johnson-Sea-Link III submersible incorporating two 66 in. outside diameter acrylic plastic spheres

and full scale standard NEMO hulls used exclusively in the prior Navy test programs.

This was achieved in this study by using as test specimen model scale spheres fabricated like NEMO hulls from 12 bonded spherical pentagons and equipped with penetrations and metallic closures of the same size and design as those utilized in the standard model scale NEMO hull [1, 9]. The only significant departure from standard model scale NEMO hulls consisted in the number and location of penetrations. Where in the standard model scale NEMO hulls there were only two penetrations equipped with metallic closures located at opposite poles of the sphere in the current test specimens, the location and number of the penetrations varied. There were enough variations in the location and number of 40 deg penetrations to allow the formulation of a general design rule on the effect of penetrations on the structural performance of spherical acrylic plastic hulls. Although 40 deg penetrations were used it was known from the Navy's test program that their effect on the structural performance of the hull is the same as of penetrations up to 46 deg in size.

If the strains measured on the nonstandard model scale NEMO hull test specimens were of the same magnitude as the strains on standard NEMO hulls with the same t/R , ratio and sizes of penetrations, and if the short term critical pressures of those test specimens were also of the same magnitude as standard model scale NEMO hulls, it could be then safely assumed that all other structural attributes of the test specimen were the same as of the standard model NEMO hulls. Thus, by only showing the magnitudes of strains and short term implosion pressures of the nonstandard model scale NEMO test specimens to be the same as of standard model scale NEMO hulls with the same t/R , ratios and sizes of openings, other structural performance characteristics, like the static and cyclic fatigue lives, could be postulated to be the same also.

Since the majority of existing test data was generated by standard NEMO hulls with t/R , = 0.071 and 40 deg penetrations, the test specimen chosen for this study had to have the same t/R , ratio and penetrations even though the hulls of submersibles under design by the Harbor Branch Foundation have t/R , ratios and penetrations in the 0.138–0.150 and 40–46 deg ranges, respectively. The difference in t/D , ratios between test specimens and full scale hulls under design by the Harbor Branch Foundation was not considered to be a barrier to extrapolating the findings from the test specimen with t/R , = 0.071 to the full scale hulls with t/R , = 0.150 as both are known to implode by elastic buckling. This postulate is based on the experimentally substantiated observation that if the hulls under design have a higher t/R , ratio than the test specimen, any experimental findings based on the critical pressure of test specimen with lower t/R , ratio can be applied with confidence to the design of the hulls with higher t/R , ratios.

This observation has been explained by the fact that hulls with

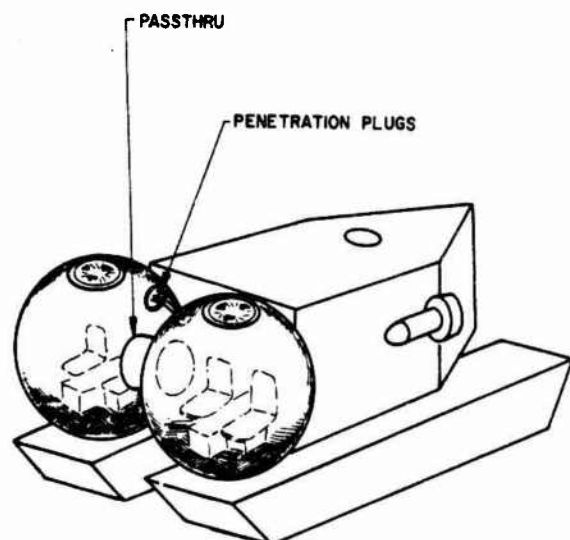


Fig. 6(a) Artist's concept of a short range excursion vehicle incorporating two interconnected acrylic spheres

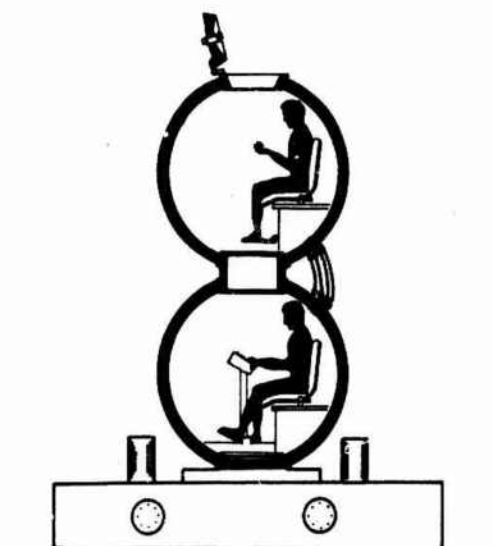


Fig. 6(c) Artist's concept of a portable observatory for in situ study of the ocean bottom

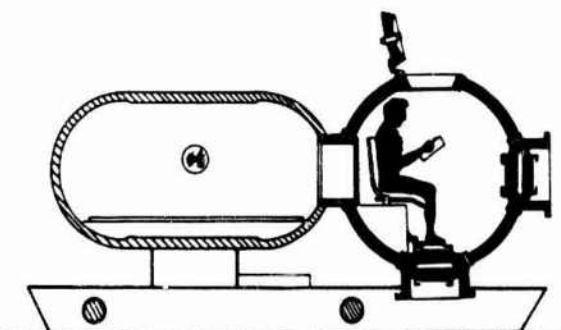


Fig. 6(b) Artist's concept of a rescue vehicle incorporating a single acrylic sphere connected to an aluminum personnel compartment

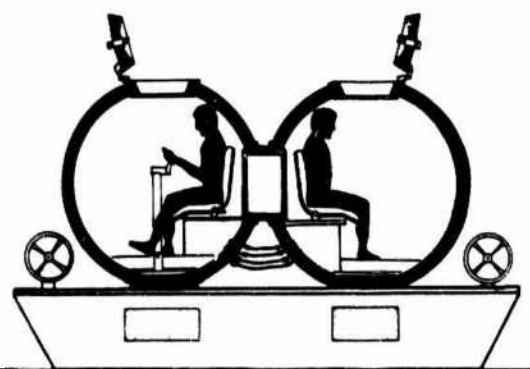


Fig. 6(d) Artist's concept of a self-propelled observatory for in situ study of the ocean bottom

lower t/R ratios are more susceptible to elastic buckling than hulls with higher t/R ratios. Since metallic closures act as hard spots in the hulls of plastic spheres, close proximity of several closures would be apt to trigger elastic buckling sooner in a shell with low t/R ratio than in one with a higher ratio. Thus, there was no doubt that if the close proximity of metallic closures in test specimen with $t/R = 0.071$ did not decrease the critical pressure or increase the magnitude of strains established previously in the Navy's test program by 33 standard model scale NEMO hulls with $t/R = 0.071$, it also would not affect the critical pressure or magnitude of strains on standard NEMO hulls with $t/R = 0.150$ established previously with only 9 model scale and two full scale NEMO hulls.

Test Specimen. As test specimen served acrylic spheres with 15-in. outside and 14-in. inside diameters fabricated by bonding of thermoformed Plexiglas G spherical pentagons (Fig. 7). Both the material and the construction method were identical to those used in the fabrication of standard model scale NEMO hulls in the Navy's test program on which the certification of NEMO, MAKAKAI, and Johnson-Sea-link I and II submersibles was based. Penetrations were machined in the test specimen to receive the same stainless steel hatches that were used in the standard model scale NEMO hulls (Figs. 8 and 9). A total of four test specimens was fabricated.

The number and location of hatches varied from one test specimen to another (Table 1 and Fig. 10). In test specimen numbers 41, 42, and 45, the penetrations were located in the center of spherical pentagons, as is typical in the construction of standard NEMO hulls. In test

specimen #44 the center of one penetration was located at the juncture of three spherical pentagons so that the circumference of the penetration intersected three bonded joints. The intersection of the penetration's edge by three bonded joints was considered to be an important design variation whose effect on the critical pressure and distribution of strains in the hull was worth investigating.

Instrumentation. Instrumentation consisted of 0.125 and 0.25 in. electric resistance strain gages arranged in the form of rectangular rosettes. The strain gages were positioned primarily at three locations: (1) near the edges of penetrations, (2) midway between penetrations, and (3) on the equator far removed from any penetration. Location #1 was known to be the area of maximum stresses in standard NEMO hulls, location #2 was postulated to be the area of probable stress increase due to close proximity of penetrations, and location #3, where membrane stresses predominate, would serve as a check on physical properties of acrylic material from which the model scale hulls were made. Water proofing of gages with Gagecotes #2 and #5 completed the installations of gages (Fig. 11).

Test Arrangement. Hydrostatic testing of test specimens was conducted in the 30-in. diameter deep ocean pressure simulator at the Southwest Research Institute, San Antonio, Texas. The test specimen was placed in a plastic bucket to retain fragments after implosion and the instrumentation wires were fed through a stuffing

Test Procedure. Pressurization of test specimens was conducted at 100 psi/min rate. Strains were read periodically at 200 psi intervals. The pressure was increased until implosion of the test specimen took place.⁵

⁵ The testing of test specimen #45 was terminated at 1400 psi to prevent hatches from being damaged in the implosion as they were needed for pressurization of test specimen #44.

Strains were found to be highest in meridional direction at the interior edges of penetrations (Figs. 12-15). Their magnitude was for all test specimens approximately 50-75 percent higher than on interior locations far removed from penetrations. Strains were lowest in circumferential direction at the exterior edges of penetrations. Their magnitude was approximately 25-50 percent less than on exterior locations far removed from penetrations. Strains midway between penetrations were of the same magnitude as on locations far removed from penetrations except in the test specimens with penetrations 63 deg center to center (i.e., 23 deg edge to edge) apart. In that case the longitudinal strain on the exterior surface was 25 percent higher than on exterior surface far removed from the edges of penetration indicating superposition of flexure strains on the negative membrane strain (Fig. 16). But even in that case the longitudinal strain on the interior surface at the edges of penetrations was higher and thus was the controlling factor in assigning the operational depth rating to this type of design.

Stresses at failure were in the 8000–15,000 psi range, depending



Fig. 7 Model scale NEMO sphere with standard polar location of penetrations



Fig. 8 Model scale NEMO sphere #42 with penetrations 83 deg apart (center to center) prior to installation of strain gages

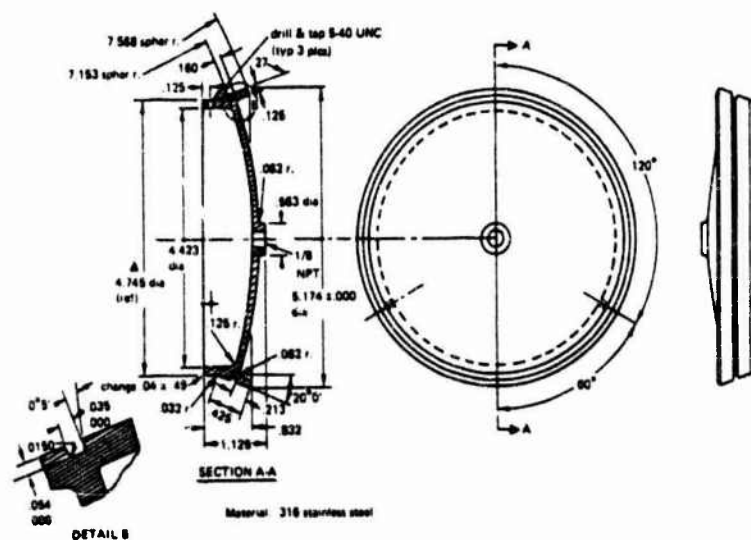


Fig. 8 Typical penetration closure for model scale NEMO spheres with 18 in. outside and 14 in. inside diameters

Table 1 Characteristics of test specimens

Specimen Description	Model #41	Model #42	Model #45	Model #44
Size of Penetrations	40 deg	40 deg	40 deg	40 deg
Number of Penetrations	2	2	3	3
Spacing of Penetrations	117 deg/243 deg	63 deg/297 deg	63 deg/117 deg/180 deg	90 deg/90 deg/180 deg
Closure Material	316 SS	316 SS	316 SS	316 SS
Hull Material	Plexiglas G	Plexiglas G	Plexiglas G	Plexiglas G
Joint Bonding	PS-30	PS-30	PS-30	PS-30
Construction of Hull	12 spherical pentagons	12 spherical pentagons	12 spherical pentagons	12 spherical pentagons
Outside Diameter	15 in.	15 in.	15 in.	15 in.
Inside Diameter	14 in.	14 in.	14 in.	14 in.
Sphericity	± 0.030 in.	± 0.030 in.	± 0.030 in.	± 0.030 in.
Width of Joints	0.1 in.	0.1 in.	0.1 in.	0.1 in.

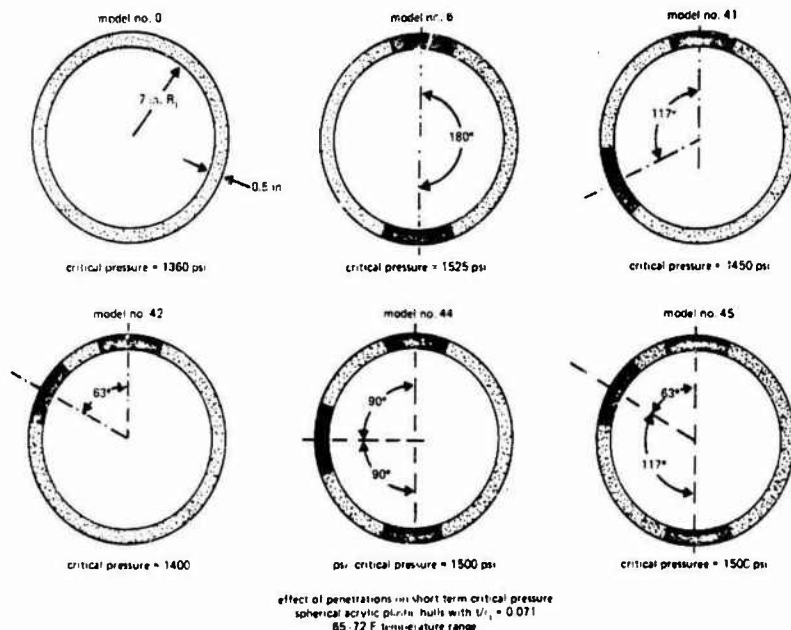


Fig. 10 Effect of penetrations on short term critical pressure of model scale NEMO spheres with 15 in. outside and 14 in. inside diameters

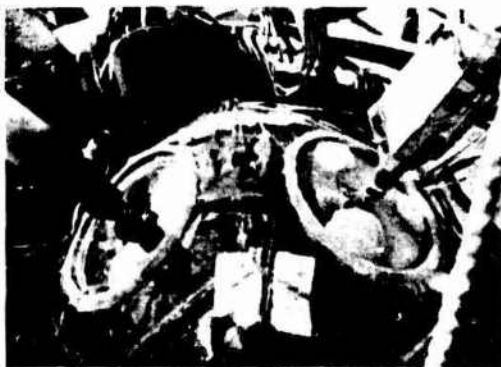


Fig. 11 Instrumented model scale NEMO sphere # 42 prior to hydrostatic testing to destruction at Southwest Research under 1400 psi external hydrostatic loading

on the location on the test specimen (Table 2). For all test specimens the highest stresses were on the interior near the edges of penetrations in longitudinal direction.

Discussion of Test Results. Critical pressures of test specimens # 41, 42, 44, and 45 were in the 1400-1500 psi range. This compares favorably with standard model scale NEMO test specimen # 0, 5, 6, 15 which failed during the Navy's test program in the 1360-1625 psi

range when tested at 65-72°F ambient temperature. As a matter of fact, the average critical pressure of current test specimen series was 1462 psi, while that of the Navy's test series was 1507 psi. This difference is statistically insignificant, indicating that the design variations from standard NEMO design incorporated in test specimens 41, 42, 44, and 45 have no detrimental effect on the short term critical pressure of the acrylic hulls with $t/R_i = 0.071$.

The strains measured on test specimens # 41, 42, 44, and 45 showed no radical departure in magnitude or pattern established previously on standard model scale NEMO hulls with the same t/R_i ratios. As in standard NEMO hulls, the maximum strains were found on the interior surface at the edges of penetration along meridional direction and their magnitude was approximately 50 percent higher than the membrane strain on the interior surface far removed from the penetration. Only on specimens # 42 and 45 was there a slight departure from strain distributions found on standard model scale NEMO hulls with $t/R_i = 0.071$. In these test specimens the magnitude of strains midway between penetrations 63 deg center to center apart was found to be approximately 20 percent higher on the exterior surface and 20 percent lower on the interior surface in meridional direction than the membrane strains on the same surfaces far removed from penetrations.

The increase in external and decrease in internal meridional strains midway between penetrations 63 deg center to center apart indicates that there is some bending taking place in the shell between penetrations. Since this increase in strain is less in magnitude than the maximum strain found in meridional direction on the interior edges

Table 2 Results of test program

Data Description	Model #41	Model #42	Model #44	Model #45
Critical Pressure ^a	1450 psi	1400 psi	1500 psi	1500 psi ^b
Mode of Failure	Elastic Instability	Elastic Instability	Elastic Instability	Elastic Instability
<i>Strain, inches/inch at 600 psi Pressure</i>				
<i>Near the edge of closure</i>				
Hoop, exterior	-3,300	-4,400	-2,000	-2,000
Hoop, interior	-5,200	-5,500	-5,200	-2,500
Meridional, exterior	-4,600	-6,800	-4,600	-5,000
Meridional, interior	-7,300	-7,300	-9,100	-10,400
<i>Midway between closures with edges 23 deg apart</i>				
Hoop, exterior		-4,500		-3,500
Hoop, interior		-8,600		-5,300
Meridional, exterior		-6,300		-6,200
Meridional, interior		-2,700		-2,500
<i>Midway between closures with edges 50 deg apart</i>				
Hoop, exterior			-6,200	
Hoop, interior			-6,200	
Meridional, exterior			-6,700	
Meridional, interior			-5,500	
<i>Midway between closures with edges 77 deg apart</i>				
Hoop, exterior	-6,000			-4,600
Hoop, interior	-6,500			-7,500
Meridional, exterior	-6,100			-4,800
Meridional, interior	-5,700			-5,000
<i>Midway between closures with edges >140 deg apart</i>				
Hoop, exterior	-6,500	-5,600	-4,000	-5,400
Hoop, interior	-6,000	-6,000	-6,200	-6,000
Meridional, exterior	-6,100	-5,500	-3,800	-5,600
Meridional, interior	-5,700	-6,000	-7,300	-5,200

^a Pressurization was at 100 psi minute rate in 65-72°F ambient temperature.

^b Estimated value, test was terminated at 1400 psi without failure.

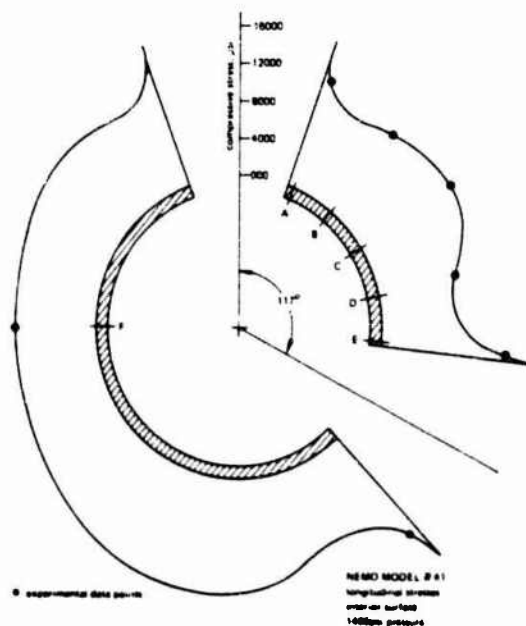


Fig. 12 Distribution of longitudinal stresses on the exterior surface of model scale NEMO sphere #41. Note that the highest stresses are at the edges of penetrations. Magnitude of hydrostatic loading was 1400 psi

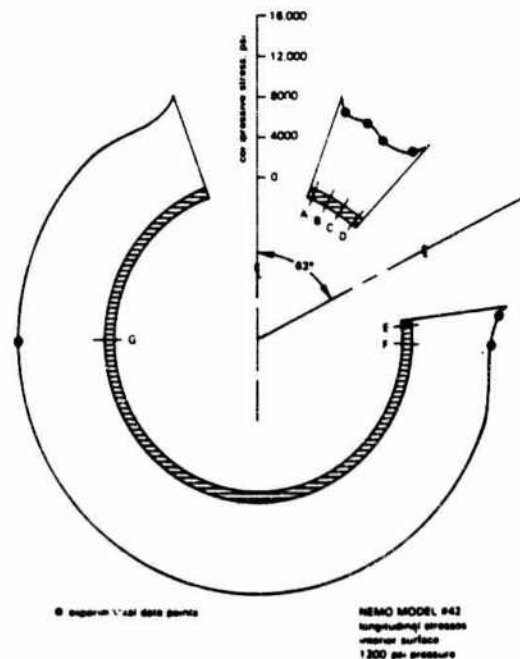


Fig. 13 Distribution of longitudinal stresses on the interior surface of model scale NEMO sphere #42 under 1200 psi external hydrostatic loading. Note that the highest stresses are at the edges of penetrations

of penetrations, it can be safely disregarded in setting of the operational depths for these hull configurations.

It cannot, however, be disregarded in the formulation of a general design rule of acrylic hulls with multiple penetrations. What the presence of increase in strains midway between penetrations 63 deg

center to center apart and the absence of increase in strains midway between penetrations 90, 117, and 180 deg center to center apart indicate is that at center to center spacings ≥ 90 deg apart there is no detectable flexure of the shell between penetrations, while at spacings ≤ 63 deg apart there is some.

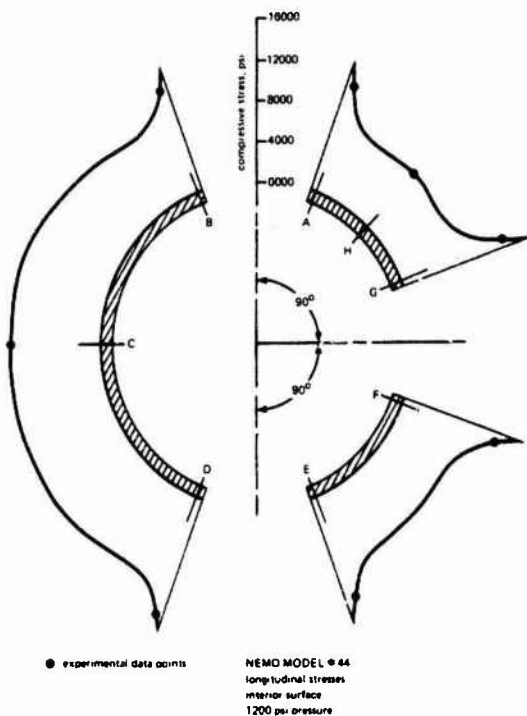


Fig. 14 Distribution of longitudinal stresses on the interior surface of model scale NEMO sphere #44 under 1200 psi external hydrostatic loading. Note that the highest stresses are at the edges of penetrations

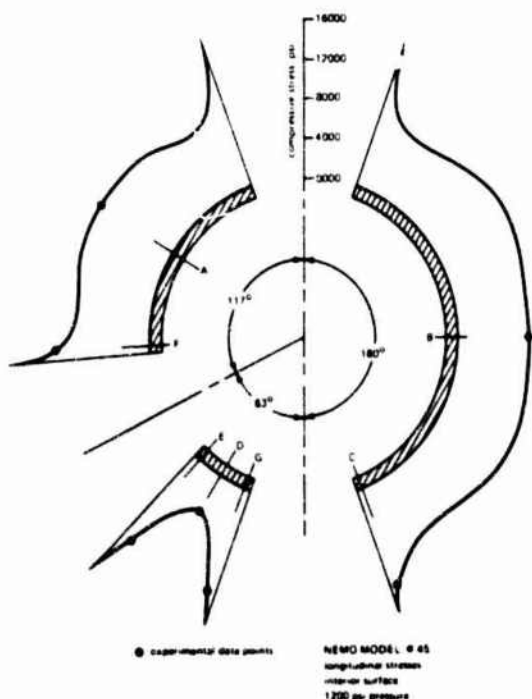


Fig. 15 Distribution of longitudinal stresses on the interior surface of model scale NEMO sphere #45 under 1200 psi external hydrostatic loading. Note that the highest stresses are at the edges of penetrations

Findings

1 The short term critical pressure of a spherical hull with $t/R_i = 0.071$ is not decreased by the presence of 1, 2, or 3 penetrations with metallic closures providing that the angular distance between the edges of closures is equal to or larger than the external radius of adjoining penetrations (i.e., >20 deg).

2 The maximum strain in an acrylic sphere with single or multiple metallic hatches is found at the interior edge of the penetration measured in longitudinal direction. Its magnitude is approximately 50-100 percent (depending on the distance of the strain gage from the edge) higher than the membrane strain on interior surface measured at a location far removed from the edge of penetration.

3 The edge of the penetration can intersect wide (0.09-0.125 in. wide) joints between spherical pentagons filled with polymerized PS-30 cement without affecting the critical pressure or distributions of strains in the hull.

Conclusions

Spherical acrylic hulls designed with two or more penetrations fitted with metallic closures can be certified for manned service on the basis of existing criteria developed by the Navy for standard NEMO hulls providing that the angular edge to edge distance between adjacent metallic closures equals or exceeds the external radius of adjoining penetrations.

References

- 1 Stachiw, J. D., "Development of a Spherical Acrylic Plastic Pressure Hull for Hydrospace Application," U. S. Naval Civil Engineering Laboratory Report R-676, April 1970.
- 2 Stachiw, J. D., and Mack, V. L., "The Spherical Acrylic Pressure Hull for Hydrospace Application; Part II—Experimental Stress Evaluation of Prototype NEMO Capsule," U. S. Naval Civil Engineering Laboratory Technical Note N-1113, Oct. 1970.
- 3 Ottsen, H., "The Spherical Acrylic Pressure Hull for Hydrospace Application; Part III—Comparison of Experimental and Analytical Stress Evaluations for Prototype NEMO Capsule," U. S. Naval Civil Engineering Laboratory Technical Note N-1094, March 1970.
- 4 Stachiw, J. D., "The Spherical Acrylic Pressure Hull for Hydrospace Application; Part IV—Cyclic Fatigue of NEMO Capsule #3," U. S. Naval Civil Engineering Laboratory Technical Note N-1134, Oct. 1970.
- 5 Stachiw, J. D., "NEMO Model 2000 Acrylic Plastic Spherical Hull for Manned Submersible Operation at Depths to 3000 Feet," Naval Undersea Center Technical Publication TP 451, Dec. 1974.
- 6 Stachiw, J. D., "Improved Fabrication Process for Spherical Acrylic Plastic Submersible Hulls," Naval Undersea Center Technical Publication TP 493, Dec. 1975.
- 7 Stachiw, J. D., "Spherical Acrylic Plastic Hulls Under External Explosive Loading," Naval Undersea Center Technical Publication TP 505, March 1976.

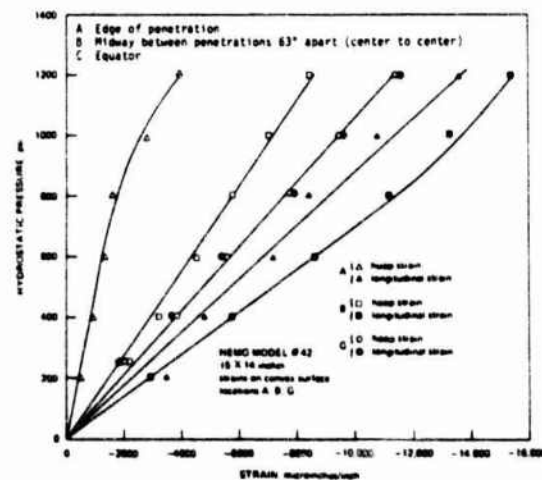


Fig. 16 Distribution of strains on the exterior surface of model scale NEMO sphere #42. Note that the longitudinal strain midway between penetrations 63 deg center to center apart (Location #B) is significantly higher than the membrane strain at the equator (Location #C) indicating some flexure between closely spaced penetrations

- 8 Stachiw, J. D., et al, "The Design, Fabrication and Testing of Acrylic Pressure Hulls for Manned Vehicles," ASME Paper No. 65-WA/UNT-10, Chicago, Nov. 1970.
- 9 Stachiw, J. D., "Spherical Acrylic Pressure Hulls for Undersea Exploration," JOURNAL OF ENGINEERING FOR INDUSTRY, TRANS. ASME, Series B, Vol. 93, No. 2, May 1971.
- 10 Tsuji, K., and Bates, R., "Fabrication of NEMO Type Submersible," ASME Paper No. 70-WA/UNT-4, New York City, Nov. 1970.
- 11 Maison, J. R., and Ottsen, H., "Stress Analysis of NEMO Type Submersible," ASME Paper No. 70-WA/UNT-8, New York City, Nov. 1970.
- 12 Snoey, M. R., and Briggs, E., "The NEMO Submersible," ASME Paper No. 70-UNT-C, Dec. 1970.
- 13 Snoey, M. R., and Katona, M. G., "Stress Analysis of a Spherical Acrylic Pressure Hull," ASME Paper No. 70-UNT-B, Dec. 1970.
- 14 Stachiw, J. D., "Acrylic Pressure Hull for Submersible NEMO," ASME Paper No. 71-UNT-2, Houston, Sept. 1971.
- 15 Stachiw, J. D., *Failure Modes of Spherical Acrylic Shells Under External Hydraulic Loading*, Edited by R. Szilard, The University Press of Hawaii, Library of Congress Catalog No. 72-93559, 1973.
- 16 Stachiw, J. D., "NEMO Type Acrylic Plastic Spherical Hull for Manned Operation to 3000 ft Depth," JOURNAL OF ENGINEERING FOR INDUSTRY, TRANS. ASME, Series B, Vol. 98, No. 2, May 1976.
- 17 Stachiw, J. D., "Spherical Acrylic Plastic Hulls Under External Explosive Loading," JOURNAL OF ENGINEERING FOR INDUSTRY, TRANS. ASME, Series B, Vol. 98, No. 4, Dec. 1976.
- 18 Stachiw, J. D., and Lones, J. J., "Development of Economical Casting Process for NEMO-Type Acrylic Submersible Hulls," JOURNAL OF ENGINEERING FOR INDUSTRY, TRANS. ASME, Series B, Vol. 98, No. 4, Dec. 1976.
- 19 Trowbridge, T., "Optical Properties of a Spherical Plastic Underwater Observatory NEMO," ASME Paper No. 70-UNT-A, Dec. 1970.
- 20 Talkington, H. R., and Murphy, D. W., "Transparent Hull Submersibles and the MAKAKAI," Naval Undersea Center Technical Publication TP 283, Feb. 1972.
- 21 Kelsey, R. A., "The JOHNSON-SEA-LINK," ASME Paper 70-WA/UNT-6, New York City, Nov. 1970.
- 22 Stachiw, J. D., and Maison, J., "Acrylic Pressure Hull for JOHNSON-SEA-LINK Submersible," ASME Paper 71-WA/UNT-6, Washington, Nov. 1971.
- 23 Stachiw, J. D., "Window in the Sea," Smithsonian Institution Library of Congress Catalog No. 0-87474-119-X, Smithsonian Institution Press, 1971.

Appendix

Design Recommendations

Acrylic plastic utilized in the construction of pressure hulls for human occupancy must meet the physical properties specified in ANSI/ASME PVHO-1 Safety Standard for Pressure Vessels for Human Occupancy, Appendix A. If the compressive yield of the material is in the 15,000-15,500 psi range (typical strength of premium custom castings) the pressure hull can be designed on the basis of short term critical pressures experimentally established in the Navy's acrylic hull research program with standard model scale NEMO hulls (Fig. 7) providing that the operational pressure is $\leq 0.25 \times \text{STCP}$.⁶ If the compressive yield of the material is in the 16,500-18,000 psi range (typical strength of sheets and plates, like Plexiglas G, Acrylite, Swedcast 310 and 320), the hulls can be designed with an operational pressure $\leq 0.3 \times \text{STCP}$.

Penetrations in the hull should not exceed 50 deg in size, and a polycarbonate insert should be used between the metallic closure and the bearing surface on the acrylic hull. Absence of polycarbonate insert will probably decrease the crack-free cyclic fatigue life to about 1000 dives at maximum operational depth. In either case, the included angle of the bearing surface on the edge of penetration must be equal to the spherical angle subtended by the penetration at the center of the hull. O-ring grooves in contact with the acrylic surface should be avoided as their presence will require the reduction of operational pressure to $\leq 0.2 \times \text{STCP}$ in order to maintain the 1000 cycle crack-free fatigue life of acrylic hull. To inhibit the initiation of fatigue cracks in the acrylic bearing surface around the penetrations, a surface finish $\leq 32 \text{ rms}$ is required on the bearing surfaces.

Penetration closures must be designed to fail at a pressure $\geq \text{STCP}$

⁶ STCP—short term critical pressure calculated on the basis of experimentally derived curves in ANSI/ASME PVHO-1 Safety Standard.

of the acrylic hull. The included angle of the bearing surface on the closure must match the included angle of the polycarbonate insert within ± 0.5 deg, and preferably within ± 0.25 deg. The outer edge of the bearing surface on the metallic closure must extend at least $0.01 R_i$ past the outer surface and $0.001 R_i$ past the inner surface of the acrylic hull. The closure must be configured so that the membrane stresses in the hull pass with the minimum of disturbance through the closure. For this reason it is desirable that the mean spherical radius of the closure coincide with the mean radius of the hull. It is acceptable to use an O-ring seal between the metallic closure and the polycarbonate insert as the polycarbonate plastic can tolerate the presence of stress risers like O-ring grooves.

The preferred material for penetration closures is 6061-T6 aluminum, as it is inexpensive, possesses adequate strength, does not corrode, is a good conductor of heat, and has low modulus of elasticity. This combination of physical properties results in a closure that is inexpensive, light, maintenance free, prevents the occupants of the submersible from cooking alive in case of air conditioning failure, and minimizes the effect of the closure as a hard spot in an otherwise compliant hull. In-service experience with aluminum closures in Johnson-Sea-Link I and II confirms these claims.

Where minimum weight is an absolute necessity Ti-6Al-4V alloy is recommended. However, it possesses the drawbacks of higher cost and less heat transfer. Still, for service in the ≥ 1350 psi range, it is a better choice for closures from the weight viewpoint than even aluminum. Cadmium plated 4130 steel in annealed condition has been found to be cost-effective and operationally acceptable for operational pressures < 500 psi where the low weight-to-displacement ratio of acrylic hull in this pressure range more than compensates for the weight penalty imposed by the heavy steel closures.

Penetration inserts are required between the metallic closures and the acrylic hull. Because they are located in areas of highest compressive strain found on the acrylic hull they must be made from crack-resistant material whose modulus of elasticity matches that of acrylic plastic. To date only ultraviolet ray absorbing polycarbonate plastic has been experimentally evaluated and found to be acceptable for intended service (Table 3). Test data and service observations show that cracks are absent in both the insert and the acrylic hull after 1000 pressure cycles of 8-hour duration (four hours under sustained loading followed by four hours of relaxation) at $0.3 \times \text{STCP}$ hydrostatic pressure loading. Other, less expensive, materials (like for example acrylic plastic) could probably perform just as satisfactorily but until an insert fabricated from a substitute material has been experimentally evaluated and found to be acceptable it cannot be

Table 3 Physical properties of polycarbonate plastic penetration inserts

Physical Property	Minimum Required Values	Typical Values
ASTM D-638		
Ultimate tensile strength, psi	5,000	7,000
Elongation, percent	≥ 2	2.5
Modulus of elasticity, psi	300,000	320,000
ASTM D-790		
Ultimate flexural, psi	10,000	12,000
ASTM D-732		
Ultimate shear strength, psi	9,000	10,000
ASTM D-695		
Compressive yield, psi	10,000	12,500
Compressive modulus, psi	350,000	370,000
ASTM D-621		
Deformation under load, percent 4000 psi, 122°F for 24 hours	≤ 0.15	0.13
ASTM D-256		
Izod impact strength	≥ 0.5	0.76
ASTM D-570		
Water absorption, percent 24 hours	< 0.2	0.15

utilized in manned submersibles. The experimental evaluation of an insert made from a different material must conclusively show that it has a minimum crack-free fatigue life of at least 1000 pressure cycles (8 hours' duration) to maximum operational pressure.

An insert must be dimensioned properly and fabricated within tight dimensional tolerances to insure close angular and diametrical fit with both the metallic closure and the acrylic hull. As the seal between the insert and the metallic closure serves a radially compressed O-ring in the closure. The sealing between the insert and the hull, on the other hand, is generally accomplished by placing a bead of RTV silicon rubber into the annular cavity formed by the outer surface of the hull and the flange on the insert. Care must be taken *not* to let the silicon rubber potting compound flow between the mating bearing surfaces of the hull and the insert. Bearing surfaces covered by RTV silicon potting compound will develop fatigue cracks sooner than they would otherwise.

Certification of spherical acrylic pressure hulls can be accomplished readily by having one of the classification societies review the design criteria, check the material properties, and witness the hydrostatic test to specified overpressure. If ANSI/ASME PVHO-1 Safety Standard is used as a basis of depth rating the maximum operational pressure cannot exceed $0.25 \times \text{STCP}$. The same applies to the classification by the Det Norske Veritas which is based also on the recommendations of Dr. Jerry Stachiw, Chairman of ANSI/ASME PVHO-1 Subcommittee on Viewports. Only the U.S. Navy and the American Bureau of Shipping possess sufficient flexibility in their classification rules to rate the acrylic hull to $0.3 \times \text{STCP}$ if the pressure hull complies with all the material, design, and performance requirements specified for manned application by NUC TP 451 [16]. Unless the extra depth capability is mandated by operational scenarios, it is highly recommended that the maximum operational pressure does not exceed $0.25 \times \text{STCP}$, as this depth rating allows the acrylic pressure hull to be accepted by all certifying and classification agencies. The more conservative depth rating also provides the hull with greater cyclic and static fatigue lives, assets with great economical value.

DISCUSSION

J. L. Atkerson⁷

The authors are to be commended for the current contribution to the store of knowledge on the behavior of spherical acrylic pressure shells under external hydrostatic loading. Since the publication of Dr. Stachiw's pioneering paper on "Spherical Acrylic Pressure Hulls for Undersea Exploration" in 1970 (reference [1]) the design of acrylic hulls for submersibles (NEMO, MAKAKAI, Johnson-Sea-Link 1 and 2) did not deviate from the structural criteria laid down in that paper. Due to lack of any other proven design criteria all acrylic spherical hulls built to date are equipped with two metallic hatches located at opposite poles of the sphere.

Recently some designers of acrylic submersibles were anxious to modify this basic design by changing the number or location of hatches, but since experimental data supporting their ideas were lacking it was considered too risky to depart from the proven design. The data presented in the paper makes it feasible to do just that.

The data presented in the paper shows clearly that up to four hatches of identical size can be incorporated into the acrylic spherical hull providing that (1) the spacing between edges of adjacent openings exceeds, or is at least equal to the radius of the opening, and (2) the centers of all openings lie on the same meridian. This finding can be extrapolated with confidence to a case where the sizes of adjacent penetrations differ significantly. In such a case the spacing between



Fig. 17 15 × 14 in. acrylic sphere with four penetrations closed with aluminum hatches; note that the penetrations are not located on a single meridian

the adjacent openings must exceed, or at least equal the radius of the larger opening.

As a result of these findings the design options available to the builder of an acrylic submersible increased from two (single penetration, or twin penetrations 180 deg apart) to at least six, or probably even more. But there still remained one unknown that tended somewhat to restrict the options available to the designer. This unknown was the effect on critical pressure and magnitude of maximum strain by 3 or more metallic hatches in penetrations that do not lie on a common meridian. If this unknown could be elucidated the designer would have at his disposal an almost infinite number of options where to locate the penetrations.

An experimental study has just been completed at Southwest Research Institute shedding light on this problem area. This particular study was unfortunately completed just after the authors have already submitted their paper to ASME for publication. Because of this the results of my study could not be discussed in their paper. Since the findings of that study complement the findings of the paper they will be summarized here.

As a test specimen for this study served also a 15 in × 14 in acrylic sphere equipped with 4 penetrations of 40 deg size. Three of those penetrations were on a single meridian spaced 63, 117 and 180 deg center to center apart, while the fourth penetration was situated on another meridian in such a manner that the spacing between it and the centers of the other three penetrations was 63, 63 and 117 deg (Fig. 17). Instrumentation consisted of 0.25 in strain gages located at edges and midway between penetrations. The crucial delta rosettes were located on the convex and concave surfaces of the sphere midway between the three adjoining penetrations.

Testing consisted of subjecting the sphere to external pressurization at 100 psi/minute rate in 75 F environment till implosion took place at 1400 psi. This collapse pressure was of the same magnitude as the collapse pressures of acrylic spheres described in the paper (Fig. 10). The strains measured midway between three adjacent 40 deg openings 63 deg center to center apart were found to indicate some bending

⁷ P.O. Box 2343; El Cajon, Calif.

since the exterior strains were significantly higher than those on the interior (Table 4).

Still, the maximum meridional strain at this location at the moment of implosion was found to be less (-18,825 microinches/inch) than the meridional strain on the interior surface at the edge of penetration (-22,500 microinches/inch), the typical location of maximum compressive strains for acrylic spherical hulls with metallic hatches. Thus, even in acrylic spherical hulls with three adjacent openings the maximum strain is found at the same location and is of the same magnitude as in spherical hulls with a single, or twin penetrations providing that the t/R_i ratio is the same.

As a result of data generated by this brief study the conclusions of the authors' presented in the paper can be safely expanded also to acrylic spheres with multiple penetrations that are not located on the same meridian.

Author's Closure

The discussion presented by J. L. Atkerson proves to be very valuable as it allows the authors to generalize the findings presented in the paper. Based on the experimental data presented in Table 4 of the discussion Finding #1 in the paper can be modified to read as follows:

The short term critical pressure of a spherical hull with $t/R_i = 0.071$ is not decreased by the presence of any number of penetrations with metallic closures providing that the angular distances between the

Table 4 Stresses in 15 X 14 in. acrylic sphere under 1200 psi hydrostatic loading at 75 F

LOCATION	STRESSES, psi			
	Hoop		Longitudinal	
	Inside	Outside	Inside	Outside
On Equator, far removed from any penetration	-8279	-8716	-7712	-8832
At edge of solitary penetration 117° center to center apart from the next penetration	-6674	-1430	-10,840*	-2480
Midway between three adjacent penetrations 63° center to center apart	-8604	-9002	-6071	-9135
At edges of three adjacent penetrations 63° center to center apart	-8377	-3973	-10,852*	-7466

NOTES:

1. All penetrations subtend 40° spherical angle.
2. * Highest stresses are at edges of penetrations, whether solitary or in clusters of three.

edges of penetrations are equal to, or exceed the external radius of adjoining penetrations (i.e., ≥ 20 deg).

The authors deeply appreciate the contribution made to the paper by the experimental data presented in the discussion by J. L. Atkerson.

Acrylic Plastic Spherical Pressure Hull for 2439 m (8000 ft) Design Depth: Phase I

J. D. Stachiw

A. Clark

C. B. Brenn

Harbor Branch Oceanographic
Institution, Inc.,
Ft. Pierce, Fla. 33450

A program has been initiated to provide the oceanographic community with a manned submersible with panoramic visibility for 2439 m (8000 ft) design depth. The first phase of the program is to validate the design of the acrylic plastic pressure hull utilizing model scale spheres with different diameters and thickness to inside diameter (t/D_i) ratios. This paper summarizes 1) the criteria used in the design of the acrylic plastic hull for 2439 m (8000 ft) depth, 2) the experimental test plan for validation of the hull design, and 3) the fabrication, and short-term pressurization to destruction of the first scale model with an aluminum hatch. The 457-mm (18-in.) o.d. acrylic sphere with t/D_i ratio of 0.2 successfully withstood 1-hr long pressurizations from 0 to 6.9, 13.8, 20.7, 27.6, 34.4 and 41.3 MPa (1000, 2000, 3000, 4000, 5000, and 6000 psi) followed by 1-hr long relaxation periods after each pressurization prior to imploding at 110.2 MPa (16,000 psi) under 4.5 MPa/min (650 psi/min) pressurization. The selected t/D_i ratio 0.2 appears to exceed the design depth requirement for 2439 m (8000 ft).

Introduction

Exploration of hydrospace requires utilization of transparent structural materials for the fabrication of viewports in the pressure hulls of underwater vehicles through which the crew, or electro-optical systems can observe hydrospace outside the vehicle. To date only three classes of materials have been utilized for this application: plastics, glasses, and ceramics. Of these three classes of material, plastics have been found to be the most economical, and readily available in large sizes and great thicknesses.

The plastic which has been most widely used for this purpose is polymethyl methacrylate, or for short, acrylic plastic. Because of its excellent performance record in the field it has been accepted by ASME, American Bureau of Shipping, and others as the standard construction material for pressure resistant structural components of pressure vessels for human occupancy (ANSI/ASME 1984). Viewports with 101 mm (4 in.) diameter have been built to date for 137.8 MPa (20,000 psi) service, and with 1067 mm (42 in.) diameter for 457 MPa (1500 psi) service.

Acrylic plastic has also been used for construction of spherical pressure vessels that serve as one atmosphere cockpits on manned submersibles. Acrylic plastic pressure hulls for submersibles represent an ideal engineering solution for the construction of such hulls. Acrylic plastic pressure hulls are economical, light, corrosion resistant, nonmagnetic, and transparent, thus providing the crew with a panoramic

view of hydrospace. The first submersible incorporating an acrylic pressure hull was NEMO with 305 m (1000 ft) design depth, launched in 1970, and operated successfully until 1980 as U.S. Navy DSV4 (Stachiw, 1971a, 1971b; Trowbridge, 1970; Snoey and Katona, 1970; Snoey and Briggs, 1970).

Since that time several other submersibles have been built with acrylic pressure hulls; JOHNSON-SEA-LINK I, JOHNSON-SEA-LINK II, CHECKMATE, and DEEP ROVER (Maison and Stachiw, 1971; Stachiw, 1976; Stachiw, 1977). The design depth has steadily increased also, and presently the record for deepest diving acrylic submersible is held by DEEP ROVER with 1000 m (3200 ft) (Hawkes 1983). Since the physical depth limit for acrylic plastic spherical pressure hull has not been conclusively established, plans are underway in many quarters for submersibles with design depths in excess of 1000 m (3200 ft).

One of the organizations contemplating the construction of an acrylic plastic submersible with increased depth capability is Harbor Branch Oceanographic Institution (HBOI). To satisfy the operational requirement for biological studies on continental shelf around Florida, HBOI is proposing the construction of a submersible with acrylic plastic pressure hull capable of transporting a crew of three to the design depth of 2439 m (8000 ft). As the first step towards achieving this goal, the Institution has commissioned the authors to study the factors impinging on the design of the acrylic plastic hull for such a depth, select the smallest acceptable t/D_i ratio for the spheric hull, lay out an experimental design validation plan, supply model scale pressure hull specimens, and test to destruction under short-term pressurization the first one of the model scale hulls.

Contributed by the Ocean Engineering Division and presented at the ETCE, February 15-20, 1985, Dallas, Texas, of THE AMERICAN SOCIETY OF MECHANICAL ENGINEERS. Manuscript received by the Ocean Engineering Division, September 1, 1984; revised manuscript received December 28, 1986.

Structural Considerations in Pressure Hull Design

The principal physical characteristics that differentiate the structural response of acrylic plastic from steel are:

- 1 The magnitude of strain under stress is not only a function of stress magnitude, but also of the ambient temperature and duration of loading.
- 2 The rate of strain increase under constant stress (i.e., creep) varies nonlinearly with stress magnitude, temperature, and time.
- 3 The rate of strain decrease after unloading (i.e., relaxation) varies nonlinearly with temperature, magnitude of strain prior to unloading, and time.
- 4 The magnitude of permanent deformation varies nonlinearly with stress magnitude, temperature and duration of sustained loading.
- 5 Implosion of the hull is initiated when the membrane compressive strain exceeds a certain threshold value. Elastic, plastic, and creep deformations contribute to the magnitude of strain.

Because of these unusual physical characteristics, the spherical acrylic hull in a submersible may fail in more ways than a steel hull. The known mechanisms of failure under external hydrostatic loading are:

- 1 General elastic instability (i.e., elastic buckling) due to elastic deformation of plastic under short-term loading, (i.e., rapid dive) of a thin-walled sphere to implosion.
- 2 General plastic instability (i.e., plastic buckling) due to plastic deformation (i.e., yielding) of plastic under short-term loading (i.e., rapid dive) of a thick-walled sphere to implosion.
- 3 General creep instability due to excessive strain generated by long-term loading, i.e., submersible exceeding the duration of a planned dive due to entanglement with a wreck on the ocean floor.
- 4 Local elastic, plastic, or creep instability due to local deviations in sphericity, aggravated by nonuniform strain rates across the surface of the sphere.
- 5 Material fracture on the concave surface of the sphere due to excessive tensile membrane stresses generated by the difference in relaxation rates across the wall thickness of the sphere following rapid depressurization of the hull after a long dive.

Thus, acrylic plastic spherical shells with t/D_i ratios less than 0.05 tend to fail primarily by general, or local elastic instability, and for this reason the design focuses on prevention of this type of failure. Medium thick shells with t/D_i ratios in the 0.05 to 0.1 range are prone mostly to general, or local plastic instabilities. Since both the thin and medium thick shells fail due to general or local instabilities the design depth of these spheres is, by and large, based on analytically derived (Stachiw 1971a) and empirically validated graphs relating implosion depth under short-term loading to t/D_i ratio at ambient room temperature.

The safe design depth is, as a rule, considered to be in the 25 to 50 percent range of the short-term imposition depth. To guarantee the submersible at least a 1) cyclic fatigue life of 10,000 dives to design depth at 10°C (50°F) ambient temperature, and 2) static fatigue life of 40,000 hr at design depth of 10°C (50°F) ambient temperature the ASME PVHO-1 Safety Standard (ANSI/ASME 1984) sets the design depth of acrylic pressure hulls at 25 percent of short-term implosion depth. The acrylic plastic submersibles with spherical pressure hulls in the $0.035 \leq t/D_i \leq 0.076$ range built to date according to this standard have performed individually more than 1000 dives without any initiation of cracks. The successful performance of these submersibles indicates that the

one-to-four (1:4) ratio of design to implosion depth recommended by the Standard is a conservative design criterion for acrylic spheres with implosion depth <3048 m (10,000 ft). This ratio also provides an adequate safety margin for avoidance of general creep instability due to entrapment of submersible at design depth (Stachiw, 1971a).

A different case presents itself for thick ($0.076 < t/D_i < 0.2$) and very thick ($t/D_i \geq 0.2$) spherical acrylic plastic shells. Although these spheres may also implode due to plastic, or creep instability the primary concern of the designer focuses on the potential for material fracture initiated by tensile strains during rapid depressurization of the sphere from design depth. Pressure testing of thick spheres has shown that the magnitude of maximum tensile strain on the concave surface during depressurization is caused by the difference in strain relaxation rates across shell thickness. The magnitude of tensile strain is a function of the 1) sphere's t/D_i ratio, 2) magnitude of average membrane compressive stress generated by pressurization, 3) duration of external, sustained pressurization, and 4) number of repeat pressurizations (Stachiw and Beasley, 1974; Stachiw and Sletten, 1978).

The underlying reason for the presence of tensile strain on the concave surface of thick spheres during rapid depressurization is that the external and internal surfaces of a thick sphere have crept at different rates (i.e., concave surface crept faster) during pressurization when they were subjected to compressive stresses of different magnitudes. During depressurization these surfaces relax also at different rates; the outside surface at higher rate than in the inside one. The difference in strain relaxation rates across the wall thickness of the sphere generates stresses in the sphere, tensile on the concave surface, and compressive on the convex surface.

If the difference in relaxation rates across the wall thickness is large the resulting tensile stress on the concave surface may exceed the tensile strength of the acrylic plastic and initiate a crack on that surface, which subsequently proceeds toward the exterior of the sphere. Depending on the rate of depressurization and the difference in relaxation rates between the exterior and interior surfaces the crack may penetrate the whole wall thickness. Thick spheres, which were subjected to high compressive stresses and were depressurized rapidly did, as a rule, disintegrate due to total penetration of the wall by cracks.

When the average compressive membrane stress generated by external pressurization exceeded 172.3 MPa (25,000 psi) a thick sphere with a $t/D_i = 0.4$ ratio did, after a single pressurization of 1-hr duration, disintegrate during depressurization when the external pressure decreased below 6.9 MPa (1000 psi) (Stachiw and Beasley, 1974). When the maximum compressive membrane stress generated in another sphere during pressurization was 137.8 MPa (20,000 psi), 13 consecutive pressure cycles of 8-hr duration were required to initiate fracture on the concave surface. Another sphere which was stressed during pressurizations to 75.8 MPa (11,000 psi) did not exhibit any internal cracks even after 100 consecutive pressure cycles of 8 hr each. This would seem to indicate that if the maximum compressive membrane stress could be reduced by the designer to some low value the cyclic fatigue life of the concave surface would increase beyond 1000 pressure cycles of 8-hr duration (i.e., 4 hr of sustained loading followed by 4 hr of relaxation at zero pressure).

Based on these tests it appears that for spheres with $t/D_i = 0.4$ the average compressive membrane stress at design depth must be kept below 51.7 MPa (7500 psi) to insure crack free cyclic fatigue life for the sphere in excess of 1000 dives. There is no experimental cyclic fatigue data for acrylic plastic spheres with $0.1 < t/D_i < 0.4$. It can be postulated, however, with reasonable confidence that to provide a cyclic fatigue life in excess of 1000 dives the average compressive membrane stress at design depth should not exceed 51.7 MPa (7500 psi), unless experimental data becomes available which shows that

Table 1 Model scale acrylic plastic spheres

Specimen description	Outside diameter, mm (in.)	Inside diameter, mm (in.)	t/D_i	No. of penetrations	Bearing gasket materials	Hatch materials
AA	457 (18)	326 (12.85)	0.2	1	Extruded polycarbonate	Aluminum
BB	381 (15)	272 (10.70)	0.2	1	Extruded polycarbonate	Aluminum
CC	381 (15)	272 (10.70)	0.2	5	Cast polycarbonate	Aluminum
					Cast epoxy	Aluminum
					Cast polyurethane	Aluminum
					Cast acrylic	Aluminum
					Cast nylon	Aluminum
1	52 (6)	127 (5.00)	0.10	1	None	Acrylic
2	52 (6)	122 (4.80)	0.125	1	None	Acrylic
3	52 (6)	117 (4.62)	0.149	1	None	Acrylic
4	52 (6)	112 (4.40)	0.175	1	None	Acrylic
5	52 (6)	110 (4.34)	0.191	1	None	Acrylic
6	52 (6)	109 (4.28)	0.20	1	None	Acrylic
7	52 (6)	107 (4.22)	0.21	1	None	Acrylic
8	52 (6)	105 (4.14)	0.225	1	None	Acrylic

- NOTES: 1. All penetrations are conical, subtending a spherical included angle of 48 deg, with the apex of the cone coinciding with the center of the sphere.
2. The outside of the bearing gaskets mates snugly with the conical surface of the penetrations. The inside of the bearing gaskets subtends a spherical conical angle of 44 deg.

higher average compressive stress levels can be tolerated without lowering the cyclic fatigue life to less than 1000 dives.

The presence of penetrations does not decrease the implosion pressure of acrylic plastic spheres, providing that:

- 1 the spacing between edges of penetrations exceeds the radius of the larger of two adjoining penetrations (Stachiw and Dolan, 1978);
- 2 the beveled edge of penetration lies on a conical surface whose apex lies at the center of the sphere;
- 3 the penetration is sealed off with a tight-fitting hatch whose conical bearing surface matches that of the opening;
- 4 the membrane stiffness and compressive strength of the hatch are equal to, or exceed, those of acrylic plastic sphere (Stachiw, 1971a; Stachiw et al., 1981).

Design of the Spherical Pressure Hull for 2439-m (8000-ft) Depth

The acrylic plastic spherical pressure hull was designed on the basis of the following parameters:

- 1 Implosion depth under short-term pressurization must be equal to, or exceed four times the design depth.
- 2 The average compressive membrane stress in the sphere must not exceed 51.7 MPa (7500 psi) at design depth.
- 3 The t/D_i ratio selected for the sphere must represent the minimum value compatible with parameter nos. 1 and 2.

It was found that all three design parameters could be met by a sphere with $t/D_i = 0.2$. Empirically generated curves for hemispherical acrylic plastic windows (Stachiw, 1969) were predicting for $t/D_i = 0.2$ ratio, an implosion at 107.9 MPa (15,660 psi); a pressure which exceeds the 98.1 MPa (14,241 psi) implosion pressure requirement, based on the design pressure of 24.5 MPa (3560 psi) multiplied by four. The average compressive membrane stress at design pressure of 25.1 MPa (3650 psi) was calculated to be 50 MPa (7254 psi) based on pressure cycling of thick spheres (Stachiw and Beasley, 1974). The weight to displacement ratio of the sphere with $t/D_i = 0.2$ was estimated to be 0.74, a rather high value for a hull that serves as the main source of buoyancy for the submersible.

The access to the interior of the sphere was provided by conical penetrations developed, and experimentally proven during the Navy's NEMO program (Stachiw, 1971a; Stachiw, 1971b; Snoey and Briggs, 1970). The conical penetrations were sealed with removable aluminum hatches fabricated from 6061-T6 alloy. The conical acrylic bearing surfaces of penetrations were to be protected (from scoring by the relative movement between the hard metallic hatch and the soft acrylic plastic) with plastic bearing gaskets. The 48-deg included angle of the penetration was selected to provide easy access to the interior of any full-sized sphere, even for the largest crew members.

Experimental Validation of Sphere Design

Objectives. Since the selected ratio of $t/D_i = 0.2$ was based to a large extent on the extrapolation of data from model scale hemispheres with radically different t/D_i ratios, an experimental program was required to validate the chosen t/D_i ratio. The experimental program was planned to answer the following questions about acrylic plastic spheres with a ratio of $t/D_i = 0.2$:

- 1 Does the short-term implosion pressure actually exceed the specified implosion pressure at 98.1 MPa (14,241 psi)?
- 2 Does the cyclic fatigue life meet, or exceed, the specified 1000 pressurizations to design pressure, without crack initiation on the concave surface of the sphere, or conical surfaces of penetrations in the sphere?
- 3 Which of the plastic bearing materials are capable to survive 1000 pressure cycles to design depth without extruding out, or disintegrating?

Approach. To provide answers for the foregoing questions a total of eleven model scale spheres were designed and fabricated from acrylic plastic castings (Table 1).

Model AA was to be tested to implosion and the recorded implosion pressure compared with the specified critical pressure of 98.1 MPa (14,241 psi). If the model fails at lesser pressure, the t/D_i ratio would have to be increased from 0.2 to some larger value.

Model BB and CC were, after instrumentation with ten strain gages each, to be pressure cycled together from 0 to 24.5 MPa (0 to 3560 psi) at ambient room temperature. Ap-

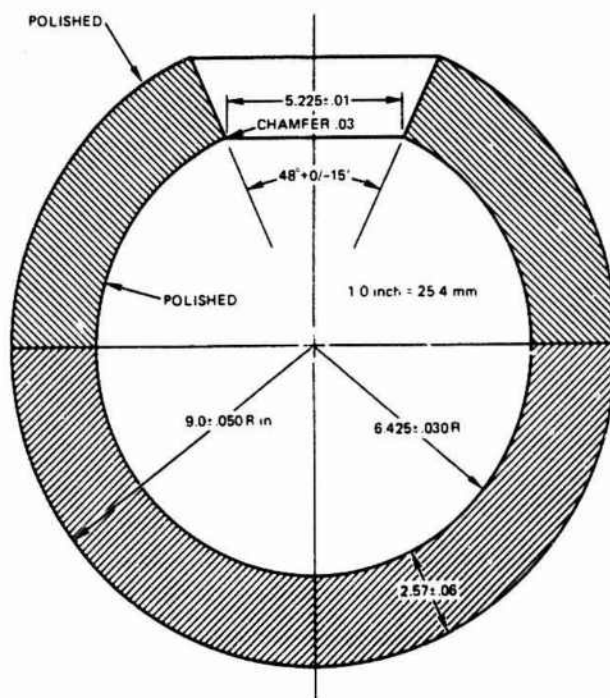


Fig. 1 Acrylic plastic Model AA tested to implosion

pearance of cracks on concave surface of acrylic plastic in less than 1000 pressure cycles would require that the t/D_i ratio be increased from 0.2 to some larger, yet unspecified value.

The typical pressure cycle was to consist of 4 hr sustained pressure at 24.5 MPa (3560 psi), followed by 4 hr of relaxation at 0 MPa (0 psi) in 18 to 24°C (65 to 75°F) ambient temperature environment. The strains were to be recorded during the first, second and tenth pressure cycle, and the condition of all sphere components inspected at 250 cycle intervals. If any of the bearing gaskets on Model CC permanently deformed or cracked they were to be removed, and replaced with polycarbonate plastic gaskets whose satisfactory performance in this application has been already established in previous test programs (Stachiw, 1976; Stachiw, 1977; Stachiw and Dolan, 1978; Stachiw et al., 1981).

Models 1 through 8 were to be pressure cycled together in the same manner as Models BB and CC, but in a separate pressure vessel. Because of widely different t/D_i ratios ($0.1 \leq t/D_i \leq 0.225$) a few of the spheres would implode, and some only crack prior to completion of 1000 cycles. Plotting the number of cycles at which individual spheres cracked, and subsequently imploded, versus their t/D_i ratio will generate a family of cyclic fatigue curves for repeated pressurizations to 24.5 MPa (3560 psi). These empirically derived curves will aid in determining the minimum t/D_i ratio which gives the acrylic plastic sphere a fatigue life of 1000 cycles to 24.5 MPa (3560 psi) design depth without crack initiation, and 10,000 cycles without catastrophic failure. If the extrapolated t/D_i ratio is less than 0.2 then the t/D_i ratio of the proposed acrylic plastic submersible hull may be reduced to improve its weight to displacement without reducing its specified fatigue life.

Model Scale Spheres

The model scale spheres shown in Table I were fabricated by slush casting, then by machining the rough, hemispherical acrylic plastic casting. They were subsequently joined together by bonding with self-polymerizing acrylic cement. The model scale spheres were annealed twice; prior to, and after bonding. The quality of the bonded equatorial joints in Models AA and CC was excellent, while in the other models it was barely acceptable. The joints in the 152-mm- (6-in-) dia spheres (Models

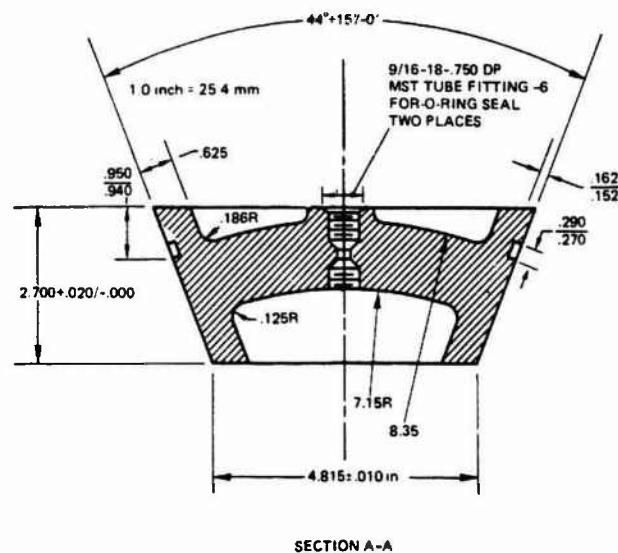


Fig. 2 Aluminum alloy 6061-T6 hatch for Model AA

I thru 8) incorporated an undesirable quantity of voids, but the spheres were accepted for testing, as attempts at recasting these joints failed to improve their quality due to inaccessibility of the spheres' interior to the fabricator's hand.

Models AA (Fig. 1) and BB were each provided with a simple penetration, closed off with an aluminum hatch (Fig. 2) resting on extruded polycarbonate plastic bearing gaskets (Fig. 3). Model CC was provided with five penetrations to allow simultaneous evaluation of five different gasket bearing materials under cyclic pressurization. The materials chosen for evaluation as potential replacements for extruded polycarbonate plastic were selected because they could be cast in large sections economically (Table 2). The search for a suitable replacement was motivated by the very high cost and unavailability of extruded polycarbonate in thick plates.

This constitutes a marked departure from past acrylic submersible construction programs where extruded polycarbonate plate was used exclusively as the construction material for bearing gaskets around hatches. The qualification of a castable, instead of an extrudable plastic for this application would significantly decrease the cost and lead time for construction of any acrylic plastic submersible with a design depth in excess of 762 m (2500 ft).

The most promising candidate material serving as a bearing gasket in Model CC appears to be castable polycarbonate plastic, since its physical properties are similar to those of extruded polycarbonate plastic. The less promising bearing

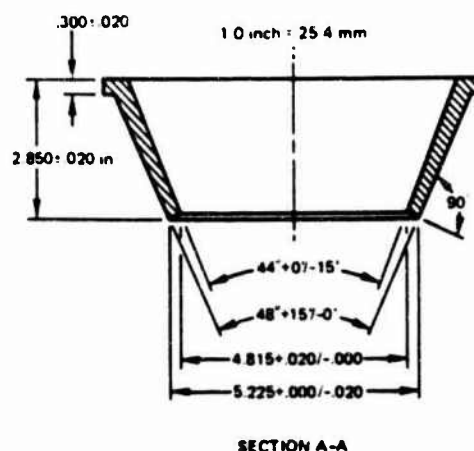


Fig. 3 Polycarbonate plastic bearing gasket for Model AA

Table 2 Physical properties of bearing gasket materials

Material	Tensile strength, MPa (psi)	Tensile modulus, MPa (psi)	Tensile elongation percent	Compressive yield, MPa (psi)	Compression modulus, MPa (psi)
Extruded polycarbonate	49.3 (7160)	2205 (3.2×10^5)	2.6	88.2 (12,800)	2549 (3.7×10^5)
Cast polycarbonate	51.3 (7440)	2482 (3.6×10^5)	2.5	84.9 (12,325)	2205 (3.2×10^5)
Cast nylon	63.1 (9160)	2687 (3.9×10^5)	28	63.0 (9145)	2177 (3.16×10^5)
Cast epoxy	72.1 (10,460)	1943 (2.82×10^5)		99.3 (14,410)	2412 (3.5×10^5)
Cast polyurethane	50.3 (7,300)	2225 (3.23×10^5)	12	65.4 (9,490)	2108 (3.06×10^5)
Cast acrylic	71.7 (10,400)	3100 (4.5×10^5)	4.9	121.3 (17,600)	3100 (4.5×10^5)
Material	Flexural strength, MPa (psi)	Flexural modulus, MPa (psi)	Compressive deformation, percent ^(a)	Shear MPa (psi)	Izod Notched J/mm (FT LB/IN)
Extruded polycarbonate	82.0 (11,900)	2205 (3.2×10^5)	0.12	71.1 (10,400)	40.6 (0.76)
Cast polycarbonate	96.0 (13,930)	2232 (3.24×10^5)	0.14	56.8 (8240)	48.0 (0.9)
Cast nylon	86.3 (12,530)	2680 (3.89×10^5)	1.25		48.0 (0.9)
Cast epoxy	113.8 (16,520)	2494 (3.62×10^5)	0.02		39.0 (0.73)
Cast polyurethane	93.8 (13,610)	3541 (5.14×10^5)	0.96		55.1 (1.03)
Cast acrylic	109.6 (15,900)	3100 (4.5×10^5)	0.16	61.3 (8,900)	21.3 (0.4)

^(a) 27.6 MPa (4000 psi) for 24 hr at 24°C (75°F)

gasket materials in Model CC were epoxy, polyurethane, nylon and acrylic. Bearing gaskets machined from 76 mm (3 in.) thick extruded polycarbonate plastic were incorporated into Models AA and BB to serve as a standard of comparison for the other bearing gasket materials.

Models 1 through 8 were not equipped with bearing gaskets, as conical acrylic plugs were used there instead of aluminum hatches. Since there was no relative motion between the plugs and the penetrations, bearing gaskets were not required between the conical mating surfaces of the plugs and of the penetrations. Aluminum hatches were not used in these models as the objective of their construction was to minimize the presence, and thus the effect, of any discontinuities on the cyclic fatigue of spheres with different t/D ratios (Stachiw et al., 1981; Stachiw and Dolan, 1982).

The aluminum plugs and hatches for Models AA (Fig. 2), BB and CC do not represent structurally optimized designs of metallic hatches and instrumentation bulkheads. The dimensions of these components were selected to give them the same strength as the acrylic sphere (i.e., fail at external pressure in the 96.5 to 103 MPa [14,000 to 15,000 psi] range). This was done to prevent them from acting as potential initiators of buckling failure when the model scale spheres are tested to implosion at completion of the pressure cycling program.

Testing of Model Scale Sphere AA

Test Schedule. Acrylic sphere Model AA was tested first, since the experimental confirmation of the predicted implosion depth for the proposed pressure hull with $t/D = 0.2$ ratio would provide reassurance that the planned time-consuming pressure cycling of other scale models with the $t/D = 0.2$ ratio will conclude without cyclic fatigue failure.

Pressurization to implosion was preceded by pressure cycling of Model AA in the 0 to 41.3 MPa (0 to 6,000 psi) range. The pressure cycling consisted of six pressure cycles:

- First: 0-06.9-0 MPa (0-1000-0 psi)
- Second: 0-13.8-0 MPa (0-2000-0 psi)
- Third: 0-20.7-0 MPa (0-3000-0 psi)
- Fourth: 0-27.6-0 MPa (0-4000-0 psi)
- Fifth: 0-34.5-0 MPa (0-5000-0 psi)
- Sixth: 0-41.3-0 MPa (0-6000-0 psi)

Each pressure cycle consisted of pressurization at 4.5 MPa/minute (650 psi/min) rate, sustained pressure loading of 60-min duration, depressurization at 4.5 MPa/min (650 psi/min) rate, and relaxation at 0 MPa (0 psi) for a minimum of 60 min. Strains were read at 6.89 MPa (1000 psi) pressure and 5-min time intervals, respectively.

Instrumentation. Model AA was instrumented on the concave surface with two rectangular strain gage rosettes, type CEA-06-125WT-120. Gages 1 and 2 were located at the bottom of the sphere, while gages 3 and 4 were located at the top of the sphere near the edge of penetration. Gages 3 and 4 were to provide peak strain readings on the concave surface near hatch penetration. Models BB and CC were instrumented on the concave surface with five rosettes each.

Test Arrangement. The test arrangement for Model AA consisted of attaching the sphere assembly to the pressure vessel end closure with a 9.5-mm (3/8-in.) pipe. The pipe was threaded on both ends; one end was screwed into the threaded opening of an adaptor plug designed to fit the central penetration in the pressure vessel end closure.

The instrumentation wires from the straingages were fed from inside the sphere to the exterior of the pressure vessel end closure through the interior of the pipe. This arrangement provided a dry and secure conduit for the instrumentation leads at any external pressure to which the sphere may be subjected during implosion testing.

Test Procedure. Testing was conducted inside a 457-mm-

Table 3 Strains on concave surface of model AA during pressure cycling

Pressure cycle no.	At beginning of sustained pressurization period	At conclusion of sustained pressurization period	Creep during sustained pressurization period	At beginning of relaxation period	At conclusion of relaxation period
0-6.9 MPa (0-1000 psi)	-3200	-3300	-100	-60	0
0-13.8 MPa (0-2000 psi)	-6300	-6800	-500	-290	-90
0-20.7 MPa (0-3000 psi)	-9400	-10300	-900	-400	-40
0-27.6 MPa (0-4000 psi)	-12700	-14600	-1900	-500	-40
0-34.5 MPa (0-5000 psi)	-16300	-19500	-3200	-650	+80
0-41.3 MPa (0-6000 psi)	-20300	-25400	-5100	-700	+150

NOTES: 1. The hoop and meridional strains were the same at the pole of the sphere opposite from the penetration.
2. All strains were in 10^{-6} units (microin./in.).
3. The strain recorder was re-zeroed at conclusion of each pressure cycle.

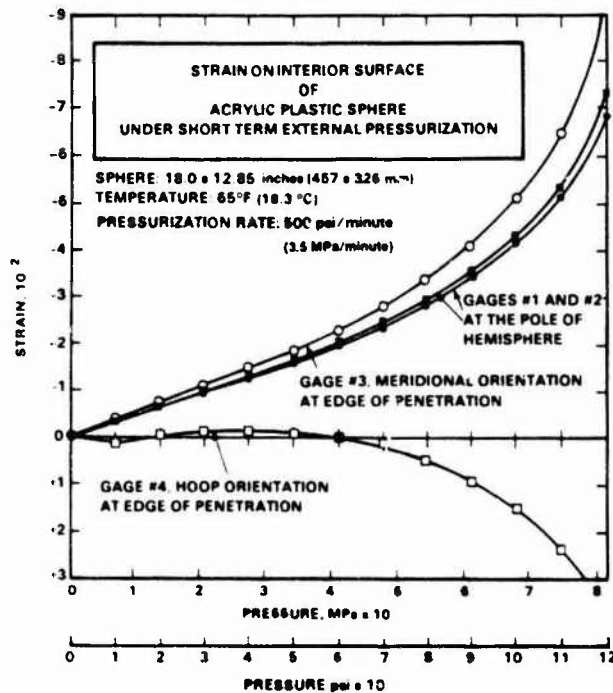


Fig. 4 Distribution of strains on the concave surface of Model AA under short-term pressurization

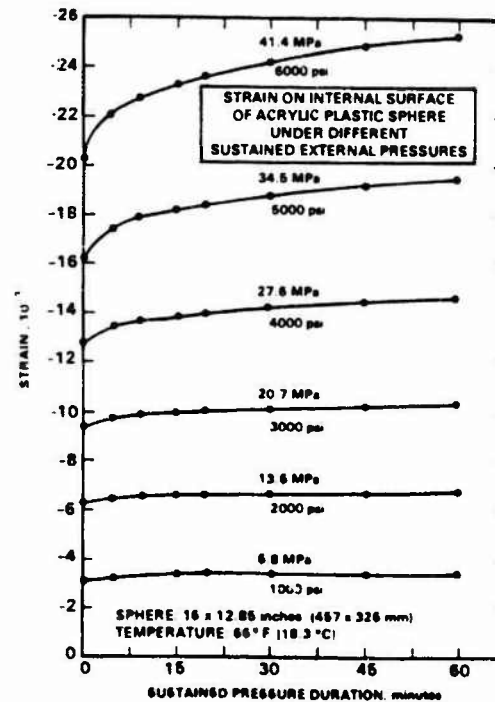


Fig. 5 Cumulative strains on the concave surface of Model AA under sustained pressure loading

(18-in) dia pressure vessel rated 137.8 MPa (20,000 psi). The pressurization was accomplished by means of air-operated positive displacement pump. The ambient water temperature during testing of Model AA varied only plus or minus one degree from 18°C (65°F). Because of this small temperature variation all the strains generated during the pressure testing of Model AA could be compared with each other directly without any adjustments for temperature variation.

During the final pressurization to implosion considerable difficulties were encountered in trying to maintain the 4.5 MPa/min (650 psi/min) pressurization rate at pressure above 41.3 MPa (6000 psi).

To remedy this situation a large, gasoline engine driven compressor was connected to the pump. After installation of the portable compressor, the pumping rate was increased and the pump maintained this rate to 110.2 MPa (16,000 psi) at which implosion took place with a loud noise.

Findings

Pressure Cycling. The hoop and meridional strains

recorded by gages 1 and 2 (at the pole of the lower hemisphere without penetration) did not differ from each other, indicating a uniform biaxial stress field on the concave surface of the sphere (Fig. 4). The meridional strain recorded by gage 3 at the penetration in the upper hemisphere was, however, approximately 20 percent higher, and the hoop strain recorded by gage 4 at the same location approximately 80 percent lower than the strains at gages 1 and 2.

This distribution of strains is considered typical for acrylic plastic spheres with a conical penetration sealed by a metallic hatch. Testing of acrylic spheres with t/D ratios in the 0.036 to 0.076 range during the previous test programs had produced similar results (Stachiw, 1971a, 1971b; Snoey and Katona, 1970; Snoey and Briggs, 1970; Stachiw and Dolan, 1978).

The basic difference between the effect of penetrations on the magnitude of strains in the spheres with $0.036 \leq t/D \leq 0.76$, and Model AA with a t/D of 0.2 is that the relative increase in strain magnitude at the penetration was larger for the thin spheres. Thus for $t/D = 0.036$ the strain increase on the concave surface in meridional direction at the

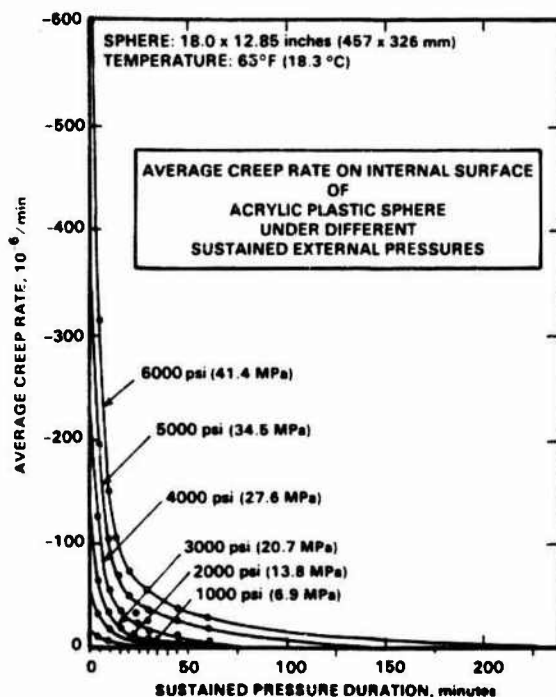


Fig. 6 Creep (time-dependent strain rate) on the concave surface of Model AA under sustained pressure loading

penetration was in excess of 50 percent, while for $t/D_i = 0.069$ the increase was only about 33 percent. Also, stiff hatch plugs have been shown to generate higher strains at the penetrations than compliant hatch plugs (Stachiw et al., 1981).

The magnitude of membrane strains at the pole of the lower hemisphere increased linearly with pressure during pressurization in the first pressure cycles (Table 3); the strains became nonlinear during the sixth pressure cycle (Fig. 5) at pressures above 34.5 MPa (5000 psi). This would seem to indicate that during short-term pressurization the sphere with $t/D_i = 0.2$ compressed elastically in the 0 to 77.1-MPa (0 to 11,235-psi) range.

The creep rate (Figs. 5 and 6) and cumulative creep increased exponentially with pressure. For example, at 6.99 MPa (1000 psi) sustained pressurization the average creep rate during the first 5 min was $10 \times 10^{-6}/\text{min}$ (10 microin./in./min), while at 41.3 MPa (6000 psi) it became $330 \times 10^{-6}/\text{min}$ (330 microin./in./min). The creep rate decreased exponentially with time; after 60 min of sustained pressurization at 6.9 MPa (1000 psi), it became less than

$1 \times 10^{-6}/\text{min}$ (1 microin./in./min) and at 41.3 MPa (6000 psi) it became $35 \times 10^{-6}/\text{min}$ (35 microin./in./min).

As a result of the great variation in creep rates at different pressure loadings there was also a great variation in the magnitude of cumulative creep (Fig. 7). Thus, at the conclusion of one-hour-long sustained pressurization the cumulative creep in the 6.9 MPa (1000 psi) cycle was only 100×10^{-6} (100 microin./in.), while in the 41.3 MPa (6000 psi) cycle it was observed to be 5100×10^{-6} (5100 microin./in.) (Table 3).

The large cumulative creep resulted in an operationally significant decrease of sphere's buoyancy. The buoyancy of the 457-mm- (18-in-) dia Model AA acrylic sphere decreased by approximately 7 percent after 60 min of sustained pressurization at 27.6 MPa (4000 psi).

During relaxation periods between individual pressurization cycles the acrylic plastic attempted to return to its unstrained state. The 60-min long relaxation periods appeared to be of adequate duration for the compressive membrane strains to return almost to zero after 60-min long pressurization periods at 6.9, 13.8, 20.7, and 27.6 MPa (1000, 2000, 3000 and 4000 psi). After sustained pressurization at 34.5 MPa (5000 psi) the 60-min-long relaxation period generated tensile membrane strains on the concave surface (Table 3). Tensile membrane strains were again observed after sustained pressurization to 41.3 MPa (6000 psi), except that they were larger than during the relaxation period after sustained pressurization at 34.5 MPa (5000 psi) (80 versus 150×10^{-6} [80 versus 150 microin./in.] after 60 min of relaxation).

The appearance of tensile strains during a relaxation period indicates that some of the cumulative creep which took place on the concave surface during pressurization was in the nature of permanent compressive deformation. Since the cumulative creep on the convex surface during sustained pressurization is less due to lower membrane stresses on this surface, permanent compressive deformation can also be expected to be less there than on the concave surface. As a result of this difference in magnitude of residual compressive strains on these surfaces, the interior surface of the sphere may at some time during relaxation period be placed in tension and the exterior surface in compression. The higher the pressure during sustained loading, the sooner the tensile strains will appear during the relaxation. If the pressure during sustained loading is high enough, fractures may appear immediately after, or even during, depressurization to zero.

The absence of tensile strains during the relaxation period after 27.6 MPa (4000 psi) pressure cycle; and their appearance after the following pressure cycle to 34.5 MPa (5000 psi) indicates that permanent compressive deformation (i.e., yielding) will appear on the concave surface during 60-min-

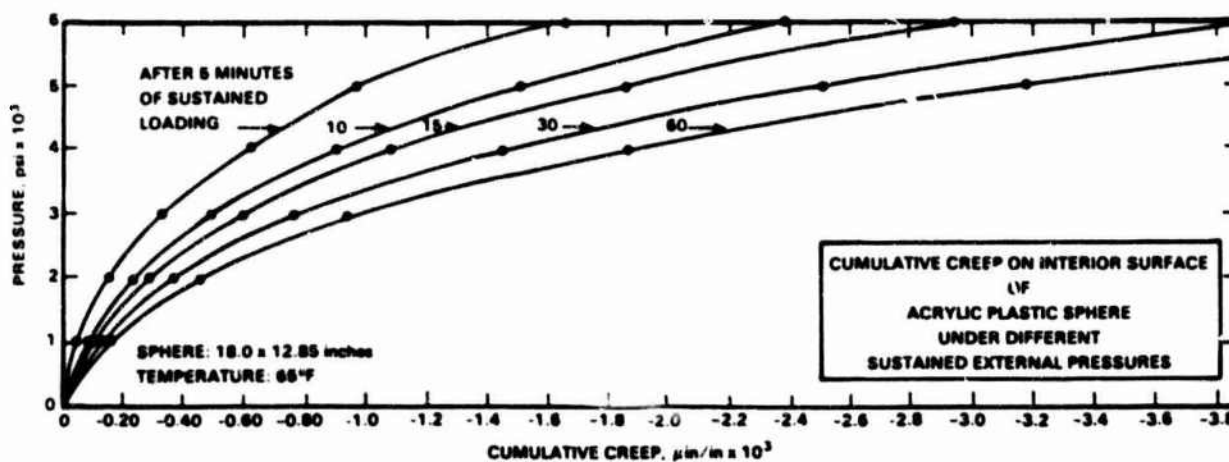


Fig. 7 Cumulative creep as a function of pressure and sustained loading duration

long sustained pressure loading in 16°C (60°F) ambient environment at some pressure level in the 27.6 to 34.5 MPa (4000 to 5000 psi) range. At sustained pressure loadings in excess of 60-min duration permanent compressive deformation may take place at pressure levels less than 27.6 MPa (4000 psi). At low ambient temperatures encountered in deep ocean, on the other hand, the permanent compressive deformation may only appear at pressure in excess of 34.5 MPa (5000 psi).

Previous discussion, based on the strain data from six pressure cycles to which Model AA was subjected, does not allow one to predict with certainty whether tensile strains will appear and subsequently increase to dangerous levels during 1000 pressure cycles of 8-hr duration (4 hr sustained pressure loading followed by 4 hr of relaxation) at 24.5 MPa (3560 psi) to which Models BB and CC will be subjected. One can postulate, however, that the chances for Models BB and CC successfully completing the 1000 pressure cycles at design pressure without crack initiation on the concave surface are excellent if the ambient temperature during the pressure cycling does not exceed 18°C (65°F).

Implosion Testing. Implosion of Model AA took place at 110.2 MPa (16,000 psi) in 18°C (65°F) ambient temperature environment. Since the ambient temperature at design depth and beyond is in the -2 to 1°C (28 to 34°F) range the actual implosion depth of the acrylic submersible would be in excess of 10961 m (110.2 MPa \times 99m/MPa) 35,952 ft [16,000 psi \times 2.247 ft/psi]. The actual implosion depth can be fairly accurately predicted on the basis of data generated during the Navy's NEMO test program (Stachiw, 1971). In that program acrylic spheres with $t/D_i = 0.036$ were tested to implosion under different ambient temperatures and the experimentally obtained implosion pressures plotted versus ambient temperature. The relationship between critical pressure and ambient temperature appeared to be linear in the 0 to 38°C (32 to 100°F) temperature range.

Utilizing that data, one can postulate that the implosion depth of the acrylic submersible with $t/D_i = 0.2$ ratio at 0°C (32°F) under short-term loading will be approximately 25 percent greater. Utilizing this information as the basis for predicting the short-term implosion depth it is calculated to be 137.8 MPa (20,000 psi), well in excess of greatest ocean depth.

Data from NEMO test program enables one also to predict with reasonable certainty the implosion depth under long-term entrapment on the ocean floor. For entrapment of 150-hr duration (typical duration of life support) the implosion depth is predicted to occur at 50 percent of short-term implosion depth. Thus, in order for an acrylic submersible with $t/D_i = 0.2$ ratio to implode during 150 hr of entrapment, or disablement on the ocean floor at 0°C (32°F) ambient temperature, the depth of the ocean floor must exceed 6098 m (20,000 ft).

Spherical sector hatch of 6061-T6 aluminum and bearing gasket of extruded polycarbonate plastic performed well in the 0 to 41.3 MPa (0 to 6000 psi) pressure range (0 to 4104 m [0 to 13,482 ft] depth range). Both the aluminum and polycarbonate plastic yielded during the short term pressurization to 110.2 MPa (16,000 psi). There was observed extensive shear cracking on the hatch skirt and bearing gasket. It can be postulated that the structural performance of the aluminum hatch in Model AA matches that of the acrylic sphere, which failed also by yielding of material.

Conclusions

1 The short-term implosion depth of acrylic spheres with $t/D_i = 0.2$ and equipped with metallic hatches in the shape of spherical sectors with included angle of under 44 deg is 10,961 m at 18°C (35,952 ft at 65°F) ambient temperature.

2 Tensile strains appear on the concave surface of acrylic sphere with $t/D_i = 0.2$ during the relaxation period following a 60-min dive at 18°C (65°F) ambient temperature, if the dive depth exceeds 2139 m (8988 ft). At depths under 2739 m (8988 ft) strains appear to return to zero after a relaxation period equal to, or exceeding the duration to the dive.

3 The hatch bearing gasket fabricated from extruded polycarbonate plastic performs satisfactorily in the acrylic sphere with $t/D_i = 0.2$ during six dives in the 0 to 4104 m (0 to 13,462 ft) depth range. There is extensive permanent deformation of the bearing gasket after short-term dive to 10961 m (35,952 ft).

4 The spherical sector hatch with 44-deg included angle, when fabricated from 6061-T6 aluminum alloy performs satisfactorily during repeated dives in the 0 to 4104 m (0 to 13,482 ft) depth range. Yielding of the material occurs, and a shear fracture is initiated in the hatch skirt during a short-term dive to 10961 m (35,952 ft).

Recommendations

1 Cast acrylic plastic spheres with 0.2 thickness to internal diameter ratio, and equipped with aluminum spherical sector hatches that subtend a 44-deg included angle should be seriously considered for service as pressure hulls in manned submersibles operating in the 0 to 2439 m (0 to 8000 ft) depth range.

Acknowledgment

The research has been sponsored by the Harbor Branch Oceanographic Institution, Ft. Pierce, Florida. This paper represents Contribution No. 551 of the Institution.

References

- Hawkes, G. S., 1977, "Development of Economical Casting Process for NEMO Type Acrylic Submersible Hulls," *ASME Journal of Engineering for Industry*, Vol. 99.
- Maison, J. R., and Stachiw, J. F., 1971, "Acrylic Pressure Hull for JOHNSON-SEA-LINK Submersible," ASME Paper No. 71-WA/Unt-6.
- "Safety Standard for Pressure Vessels for Human Occupancy," 1984, ASNI/ASME PVHO-1-1984.
- Snoey, M. R., and Katona, M. G., 1970, "Stress Analysis of a Spherical Acrylic Pressure Hull," ASME Paper 70-Unt-B.
- Snoey, M. R., and Briggs, E. M., 1970, "The NEMO Submersible," ASME Paper 70-Unt-C.
- Stachiw, J. D., 1969, "Critical Pressure of Spherical Shell Acrylic Windows Under Short-Term Pressure Loading," *ASME Journal of Engineering for Industry*, Vol. 91.
- Stachiw, J. D., 1971a, "Spherical Acrylic Pressure Hulls for Undersea Exploration," *ASME Journal of Engineering for Industry*, Vol. 93.
- Stachiw, J. D., 1971b, "Acrylic Pressure Hull for Submersible NEMO," ASME Paper 71-Unt-2.
- Stachiw, J. D., and Beasley, B., 1974, "Precision Casting Process for Acrylic Plastic Spherical Windows in High Pressure Service," ASME Paper 74-WA/Oct-70, Winter Annual Conference, November 17-22, 1974, New York, New York.
- Stachiw, J. D., 1976, "NEMO Type Acrylic Plastic Spherical Hull for Manned Operation to 3000 ft Depth," *ASME Journal of Engineering for Industry*, Vol. 98.
- Stachiw, J. D., 1977, "Development of Economical Casting Process for NEMO Type Acrylic Submersible Hulls," *ASME Journal of Engineering for Industry*, Vol. 99.
- Stachiw, J. D., and Sletten, R., 1978a, "Flanged Acrylic Plastic Hemispherical Shells for Undersea Systems: Part II - Static and Cyclic Fatigue Life Under Hydrostatic Loading," *ASME Journal of Engineering for Industry*, Vol. 100.
- Stachiw, J. D., and Dolan, R. B., 1978b, "Spherical Acrylic Pressure Hulls with Multiple Penetrations," *ASME Journal of Engineering for Industry*, Vol. 100.
- Stachiw, J. D., Dolan, R. B., and Clayton, D. L., 1981, "Polycarbonate Plastic Inserts for Spherical Acrylic Plastic Shells under Hydrostatic Loading," *ASME Journal of Engineering for Industry*, Vol. 103.
- Stachiw, J. D., and Dolan, R. B., 1982, "Effects of Weather, Age and Cyclic Pressurizations on Structural Performance of Acrylic Plastic Spherical Shells under External Pressure Loading," *ASME Journal of Engineering for Industry*, Vol. 104.
- Trowbridge, T., 1970, "Optical Properties of a Spherical Plastic Underwater Observatory, NEMO," ASME Paper 70-Unt-A.

J. D. Stachiw

Naval Ocean Systems Center,
San Diego, Calif.

N. E. Smith

Sub Sea International,
New Orleans, La.

O. H. Burnside

Southwest Research Institute,
San Antonio, Tex.

Structural Performance of Acrylic Plastic Plane Disk Windows With Twin Conical Bearing Surfaces

Exploratory investigation into the structural performance of acrylic plastic plane disk windows with twin conical bearing surfaces has shown that such windows behave under hydrostatic loading similarly to plane disk windows with a single conical bearing surface. This conclusion is based both on experimental data from a test program and on findings from a finite element stress analysis. The test program encompassed short term and cyclic pressure testing of plane disk windows with twin conical bearing surfaces in the $0.21 \leq t/D_i \leq 0.423$ and $60 \text{ deg} \leq \alpha \leq 120 \text{ deg}$ ranges. The finite element stress analysis addressed itself only to plane disk windows with 90 deg twin conical bearing surfaces in the $0.23 \leq t/D_i \leq 1$ range. On the basis of findings reached in this investigation it is recommended that the existing criteria (ANSI/ASME PVHO-1) for the design of plane disk windows with a single bearing surface be applied also in the design of plane disk windows with twin conical bearing surfaces since their structural performance under external hydrostatic loading appears to be very similar.

Introduction

Acrylic plastic viewports have since their introduction by Professor Piccard several decades ago proven themselves to be reliable structural components of pressure hulls in submersibles, habitats, diving bells, and hyperbaric chambers [1].¹

The two most significant contributions to achieving the accident free service record of acrylic windows were the Navy's² research program on the performance of acrylic plastic structures under hydrostatic loading and ASME's³ development of the Safety Standard for the design, fabrication, and acceptance testing of viewports in pressure vessels for human occupancy. By standardizing the specifications for acrylic plastic configurations of windows and safety factors for different configurations and operational temperature ranges the

ANSI/ASME PVHO-1 Safety Standard insured predictable performance of all viewports in manned pressure vessels [2].

Because the Safety Standard is based on the empirical relationship between the short term critical pressure and the safe maximum operational pressure (also often referred to as design pressure) of acrylic windows, both must be experimentally defined for a given window shape, t/D_i ratio, included angle, and temperature. The short term critical pressure (STCP) has been defined as the pressure at which catastrophic failure occurs at room temperature under 650 psi/min pressurization rate. By testing a multitude (over 2000 specimens) of full scale and scale model windows to destruction and plotting the resulting short term critical pressures versus t/D_i ratios, a series of graphs has been derived for common window shapes relating their STCP to t/D_i ratio.

The safe maximum operational pressure has been, on the other hand, experimentally defined by subjecting windows to cyclic and static fatigue tests and observing the condition of the window at frequent intervals. On the basis of such observations a definition of safe maximum operational pressure has been formulated. The safe maximum operational pressure (DP) for a given window design has been defined as that hydrostatic pressure loading which at a given ambient temperature will (1) not initiate cracks in the acrylic window prior to completion of at least 1000 standard pressure cycles,⁴ or 4000 hours

¹ Numbers in brackets designate References at end of paper.

² Research sponsored by the Navy at the Naval Civil Engineering Laboratory (Naval Facilities Engineering Command), Naval Ship Research and Development Center (Naval Ship Systems Command), and the Naval Undersea Center (Naval Material Command).

³ ASME/ANSI PVHO-1 Safety Standard for Pressure Vessels for Human Occupancy developed under the auspices of the American Society of Mechanical Engineers by the Committee on Pressure Vessels for Human Occupancy.

Contributed by the Ocean Engineering Division and presented at the Winter Annual Meeting, Atlanta, Ga., November 27-December 2, 1977 of THE AMERICAN SOCIETY OF MECHANICAL ENGINEERS. Manuscript received at ASME Headquarters Aug. 1, 1977. Paper No. 77-WA/Oce-3.

⁴ A typical pressure cycle consists of four hours of sustained loading followed by four hours of relaxation at zero pressure.

of continuous pressure loading, and will (2) not cause catastrophic failure prior to completion of additional 9000 standard pressure cycles, or 36,000 hours of continuous pressure loading.

The relationship between the short term critical pressure at ambient room temperature (70–75°F) and the safe maximum operational pressure at some specified maximum design temperature has been defined as a conversion factor ratio (CF). The magnitude of conversion factors varies with the window configuration, maximum design temperature, and operational pressure range. To date, conversion factors have been postulated for plane disk with plane bearing surface, plane disk with conical bearing surface, spherical sectors with conical bearing surface, spherical sectors with plane bearing surface, hemispheres with equatorial flanges, cylinders, and hyperhemispheres with conical bearing surface. The windows designed on the basis of these conversion factors have accumulated to date an admirable safety and service record. This service record leaves no doubt that the magnitudes of conversion factors specified by ANSI/ASME PVHO-1 for different window configurations and temperature ranges are appropriate for the intended service.

There is, however, one distinct disadvantage in relating the STCP to DP; it is a very expensive and time consuming process to develop sufficient experimental data that would allow plotting of STCP curves and selection of CF ratios that cover the whole range of t/D_i ratios and temperatures for a new window configuration. The conservative estimate is that it requires at least \$100,000 and at least two years of effort to generate the minimum experimental data on which the STCP curves and CF tables can be based for a new window shape with the high level of assurance demanded by service in manned applications.

Because of this large expense, experimental programs for development of new STCP curves and CF tables are rarely undertaken, even though the introduction of a new window configuration requires it. Instead, an attempt is generally made to discover structural similarities between the new and old proven window configurations that would allow the use of existing STCP curves and CF tables in design of new window configurations. Such is the case with plane disk windows with twin conical bearing surfaces. This paper is the summary of analytical and experimental studies that led the ANSI/ASME PVHO-1 Safety Standards Committee to the adaption of STCP curves and CF tables for disk with a single conical surface to the design of disks with twin conical bearing surfaces.

Background

Structural Considerations. Pressure vessels which are designed for both internal and external pressure services require viewports that are capable of withstanding and sealing off pressure applied in either face of the window. This imposes a special requirement upon the design of the viewport. To date, three types of viewports have been developed for manned service in pressure vessels that are subjected to both external and internal pressure service (Fig. 1). All of them have been found to be acceptable from structural and operational viewpoints.

The three designs differ significantly in fabrication cost, maintenance requirements, bulk, and weight, characteristics which are of great interest to operators of diving bells, personnel transfer capsules, and submersibles with diver lockout capability. Of the three designs the costliest, bulkiest, and heaviest viewport assembly is the one utilizing two plane disks with single conical bearing surfaces placed back to back in the mounting flange. The least expensive, but medium in bulk and weight design, is the one utilizing the single plane disk with plane bearing surfaces. The lightest and least bulky, but of medium cost design, utilizes the plane disk with twin conical bearing surface.

The most obvious approach of the three is to place two conical frustrum windows back to back and thus solve the problem but this approach has several disadvantages. The chief disadvantage is that two metal supporting frames must be used, each thicker than the two lenses. The additional cost of the lenses and frames is significant and the additional weight can be even more important. When the objective is to have a positively buoyant bell, each pound of bell weight above

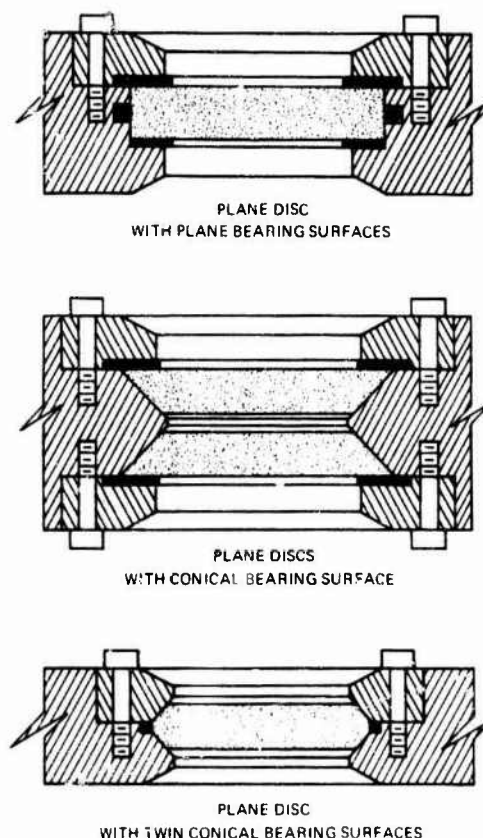


Fig. 1 Proven design concepts for viewports in pressure hulls subjected during their operational life to both internal and external pressures

a set amount must be offset by external flotation. Since existing syntactic foams are about half the specific gravity of water, one pound is added to the dry weight of the bell for each pound of buoyancy. This additional dry weight must then be accounted for when considering the dynamic loading on the padeyes, lift wire, winch and bell launching and recovering equipment on deck of the boat or platform.

Another problem with back to back lenses is that water invariably manages to get between the lenses causing fogging and corrosion that in a short time can decrease the visibility through the viewport to the point where it loses any value as an observation window.

At first glance it would appear that it might be a toss-up then between the two viewport designs utilizing only a single disk window. The weight disadvantage could be reduced and the fogging problem solved when only one piece of acrylic with supporting frames designed to seal in both directions was used. Plane acrylic disks with plane bearing surfaces were used in early designs for relatively shallow depths, but because of the presence of high tensile stresses in service and the subsequent thickness of acrylic required to decrease them, the weight saving was minimal. Sealing problems also occurred due to the requirement for hard gaskets on both sealing surfaces. What has finally given the third design, the plane disk with twin conical bearing surfaces, its definite advantage is its superior structural performance and positive sealing capability.

This structural superiority over the competing window with plane bearing surfaces is derived from its twin conical bearing surfaces that superimpose radial compression on the pressure generated flexure moment in the disk. As a result of this arrangement, radial compressive stress is superimposed upon the tensile component of the flexure stress. Because of this fortuitous superposition of stresses, the magnitude of principal tensile stress in the center of the low pressure face on the twin beveled disk is always lower than in a disk with plane

bearing surfaces. As one increases the t/D_i ratio of twin beveled plane disks, the magnitude of tensile stress decreases until in twin beveled disks with $t/D_i \geq 0.5$ the tensile stress disappears completely. This is not the case in plane disk with plane bearing surfaces, where one cannot eliminate tensile principal stresses on the low pressure face by increasing the magnitude of t/D_i ratio.

The fact that the tensile stress in a twin bevel plane disk is always less than in a disk with plane bearing surfaces has significant structural value since the lower tensile stresses make the twin bevel plane disk windows more resistant to point impact and dynamic pressure loading than the disk with plane bearing surfaces. In this respect the viewport with a twin bevel plane disk window behaves like the viewport with twin single bevel windows, except at one-half the cost, weight, and bulk. It is this advantageous combination of low cost, low weight, low bulk, and decreased magnitude (or total absence in $t/D_i \geq 0.5$) of tensile stresses that makes the viewports with twin bevel plane disk windows so attractive to designers, fabricators, and operators of pressure vessels for internal/external pressure service.

Sealing Considerations. Since the twin bevel plane disks have to seal securely against pressures applied to either face, considerable thought has been given to their design. To date, four approaches to seal design have been experimentally evaluated (Figs. 2-5). Of these three designs, the one containing O-ring grooves in the conical bearing surfaces of the window is the most reliable (Fig. 2), but the O-ring grooves in the bearing surfaces represent unacceptable stress concentrations that initiate fatigue cracks in the window's bearing surfaces after only a few pressure cycles (Fig. 6). Designs shown in Figs. 3-5 have comparable sealing ability, but the one with the O-ring groove in the cylindrical surface of the disk is considered less structurally desirable than the one where the O-ring groove is located in the cylindrical surface of the seat in the flange (Figs. 4 and 5).

Of the two design approaches for location of O-rings in the cylindrical surface of the steel seat, the one shown in Fig. 5 is considered more desirable as it is more economical to fabricate, easier to assemble, and more positive in sealing ability.

To insure leakproof performance, however, the outside diameter of the twin bevel plane disk must be only 0.010-0.020 in. less than the

diameter of the seat at minimum predicted operational temperature. If the lowest operational temperature cannot be predicted with certainty, 32°F should be used in its place. Since installation of windows is generally performed at room temperature, the windows and O-rings should be precooled to 32°F prior to placement in the mounting. Once they are installed at room temperature they will expand until there is a solid contact between them and the seat all around their circumference.

In 1969, Herb Newbury and the Sub Sea International design staff

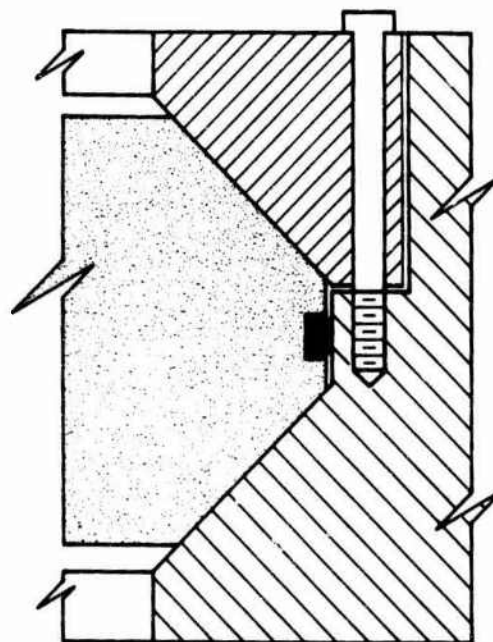


Fig. 3 Sealing arrangement for twin bevel disks utilizing a radially compressed O-ring located in the nonbearing surface of the window. This design is acceptable because the O-ring groove does not decrease the fatigue life of the window significantly

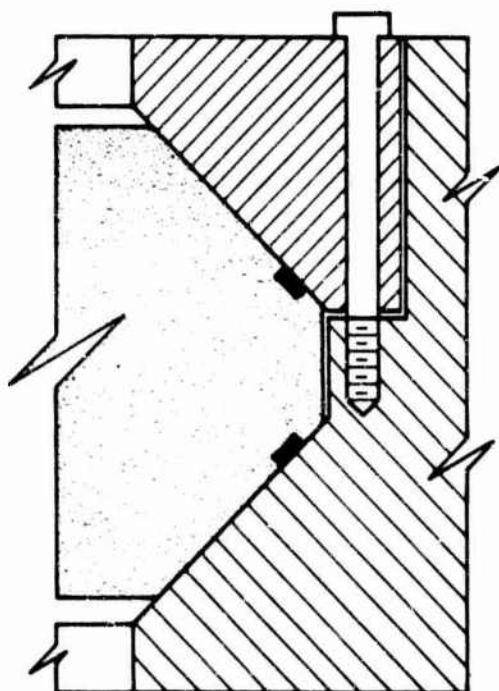


Fig. 2 Sealing arrangement for twin bevel disks utilizing axially compressed O-rings located in the bearing surfaces of the window. It is not a recommended design as the O-ring grooves in the bearing surfaces decrease significantly the fatigue life of the window

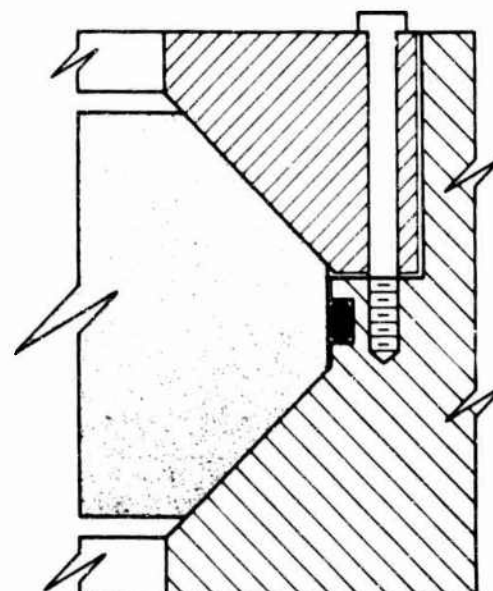


Fig. 4 Sealing arrangement for twin bevel disks utilizing a radially compressed O-ring located in the cylindrical surface of the mounting. This design is acceptable because the O-ring groove does not decrease the fatigue life of the window at all

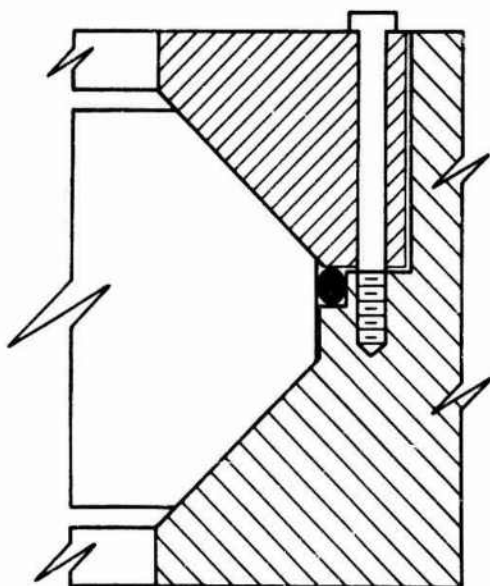


Fig. 5 Sealing arrangement for twin bevel disks utilizing a radially and axially compressed O-ring located in the cylindrical surface of the mounting. This design is recommended as it provides very positive sealing without decreasing the fatigue life of the window

introduced the double bevel lens into the commercial diving industry. The bell was designed for use in offshore exploration where observation dives were often made either by themselves or as part of a lock-out dive. To provide almost complete visibility, 13 viewports were used and the most efficient window design was a necessity. The twin bevel lens, which consists of one piece of acrylic with twin conical bearing surfaces, appeared to combine the strength of two conical frustrums with the weight of a single lens.

The basic considerations in this design were the placement of the O-ring, or low pressure seal, and the method of securing the retaining ring. The one disadvantage of the twin bevel window is that the initial fit is more critical than in other designs and tolerances must be carefully watched during design, fabrication, and assembly.

The Suh Sea International design, similar to that shown in Fig. 5, employs an O-ring seal on the flat surface or "land" between the conical bearing surfaces. Placing the O-ring in the sealing or bearing surfaces of the lens itself was considered; however, either of these designs would induce local stresses and shorten the life of the lens. The threaded retainer ring was selected on the basis of weight and simplicity. A study showed that the threaded ring design is approximately one-third lighter than bolted ring designs. In addition, it presents a smooth surface on the interior of the bell which adds to the diver safety and comfort.

Preliminary test showed the short term critical pressure to be satisfactory and the design has since been used in over 20 diving bells similar to the one shown in Fig. 7.

The diving bell undergoes the most severe usage of any pressure vessel designed for human occupancy. The constant exposure to sea air and salt water makes it a prime target for corrosion and periodic maintenance is a must. Experience in the field over the last seven years has shown the twin bevel window to be no more of a maintenance problem than other designs.

The overall effectiveness of the design has been proven by hydrostatic tests and field usage and the extra expense, if any, is more than offset by the operational advantages of handling a lighter bell.

Structural Evaluation

Because of the demand by the ocean engineering community for plane disks with twin bevel bearing surfaces, a structural evaluation of these windows had to be undertaken so that safe criteria for their design could be established. As a result of the twin bevel plane disk's

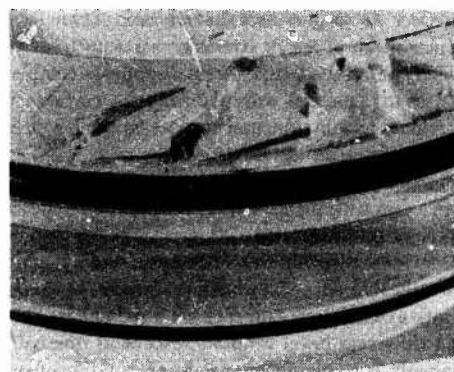


Fig. 6 Plane disk with twin bevel bearing surfaces showing fractures initiated by the O-ring grooves in the bearing surfaces



Fig. 7 Typical diving bell with twin bevel plane disk windows fabricated by Southwest Research Institute for the Suh Sea International. Note the small bulk of mountings for 8-in. dia. viewports

bearing surface similarity to the bearing surface of the single bevel plane disk, it was postulated that the structural performance of both configurations is probably similar enough where it could be considered identical for engineering purposes. This postulate was based on the fact that since both window configurations had conical bearing surfaces, both would have the same superposition of radial compression on membrane flexure moment. The only aspect that was significantly different between the two configurations was the difference in bearing surface areas (Fig. 8). This large difference in bearing surface areas could, but did not have to, cause significant dissimilarities in stress magnitude and distribution. If the structural similarity postulate could be proven with little expense, then the already validated design criteria for single bevel plane disks [2] could also be applied to design of twin bevel plane disks instead of proceeding with the expensive development of new criteria just for this purpose.

To prove structural similarity between the single and twin bevel

plane disks, both experimental and analytical approaches were chosen. The objective common to both approaches was to show that from a practical engineer's viewpoint both window configurations respond structurally to hydrostatic loading in the same manner. Since the experimental approach lends itself better than the analytical approach for determining the short term critical pressures and cyclic fatigue life, it was chosen for that purpose. On the other hand, because the analytical approach can determine, at less cost than the experimental approach, the magnitudes and distribution of stresses in the elastic range of window deformation, it was selected instead for that purpose.

Experimental Approach. The goals of the experimental approach were twofold, to show that (1) the modes of failure and short term critical pressures are approximately the same for both the twin and single bevel plane disks and that (2) the cyclic fatigue lives of both the twin and single bevel plane disks are of approximately the same length. If both goals could be proven with reasonable confidence, they would form the experimental basis for the postulate that the structural response of twin bevel plane disk windows is the same as of single bevel plane disk windows.

There was no difficulty in defining the experimental approach to reaching these two goals. The real difficulty was how to achieve this with a minimum of expenditure and time. The test program developed for this purpose reflected this philosophy (Tables 1 and 2). The basic feature of the test program was to select many included angles and t/D_1 ratios for defining the short term critical pressures and modes of failures and only a single cyclic pressure loading for establishing the cyclic fatigue life. The testing of many windows with widely differing critical pressures was deemed necessary to establish beyond any doubt the fact that the similarity of behavior between twin and single bevel plane disks under short term loading extends from thin to thick and small to large angle windows.

Once this was established, the similarity in cyclic fatigue lives could be reasonably substantiated with cyclic tests conducted only at a single pressure loading level. But even in this case there had to be several test specimens representing 60, 90, and 120 deg bevel angles with two different t/D_1 ratios. The data from specimens with different angles would show that the findings are applicable to the whole range of practical bevel angles while the two chosen t/D_1 ratios would hopefully bracket the desirable 1000 cycle crack-free fatigue life.

The lower t/D_1 ratio was selected on the basis of short term critical

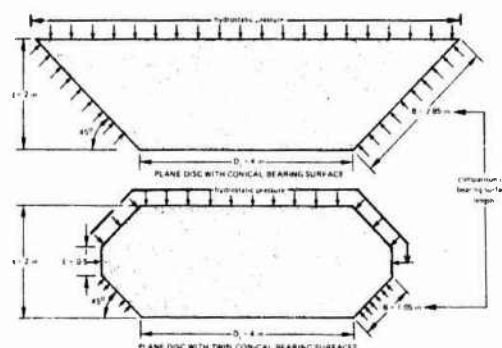


Fig. 8 Comparison of two windows with $t/D_1 = 0.5$. Note that the bearing surface of the twin bevel window is less than 50 percent of the single bevel window

pressure curves and $CF = 6$, the design approach recommended by ANSI/ASME PVHO-1 for single bevel plane disks serving at 75°F ambient temperature. The higher t/D_1 ratio was chosen, on the other hand, on the basis of $CF = 12$, a value thought to be so conservative that even if the fatigue life of specimen with $CF = 6$ were found to be inadequate the fatigue life of specimens with $CF = 12$ would definitely exceed it. If, by chance, the fatigue life of specimen with $CF = 12$ were found to be less than 1000 cycles, the fatigue life testing would be repeated with twin bevel plane disk specimens that have still a higher CF ratio, possibly 15. It was hoped of course that $CF = 6$ would be found adequate and thus serve as further proof that the fatigue life of both twin and single bevel plane disks is the same. As test condition for the cyclic pressure fatigue tests served 500 psi at 75°F ambient temperature. This value was chosen because it represented the middle of operational range for which twin bevel plane disk windows appear to be particularly suitable in the manned pressure vessels for both interior and exterior pressure service.

Short term and cyclic hydrostatic testing was conducted with the windows mounted in test flanges that simulated the rigidity of mountings in the pressure hull. For short term pressure testing to implosion, the hydrostatic pressure was applied to one face of the

Table 1 Experimental evaluation of twin bevel plane disk windows under cyclic pressure loading at ambient room temperature

90° included angle	Specimen #1	Specimen #2	Specimen #3	Specimen #4
	$D_0 = 3.520$ inches $t/D_1 = 0.23$ $l/t = 0.25$ $P_{cr} = 3000$ psi $DP = 500$ psi $P_{cr}/DP = CF = 6$	$D_0 = 3.720$ inches $t/D_1 = 0.32$ $l/t = 0.25$ $P_{cr} = 6000$ psi $DP = 500$ psi $P_{cr}/DP = CF = 12$	$D_0 = 2.737$ inches $t/D_1 = 0.308$ $l/t = 0.116$ $P_{cr} = 5500$ psi $DP = 500$ psi $P_{cr}/DP = CF = 11$	$D_0 = 3.616$ inches $t/D_1 = 0.308$ $l/t = 0.25$ $P_{cr} = 5500$ psi $DP = 500$ psi $P_{cr}/DP = CF = 11$
60° included angle	Specimen #5	Specimen #6	Description of Pressure Cycling Program Total number of pressure cycles = 1000	
	$D_0 = 3.337$ inches $t/D_1 = 0.26$ $l/t = 0.25$ $P_{cr} = 3000$ psi $DP = 500$ psi $P_{cr}/DP = CF = 6$	$D_0 = 3.461$ inches $t/D_1 = 0.355$ $l/t = 0.25$ $P_{cr} = 6000$ psi $DP = 500$ psi $P_{cr}/DP = CF = 12$		
120° included angle	Specimen #7	Specimen #8	NOTES: D_0 = major diameter, inches t = overall thickness, inches D_1 = minor diameter, inches l = width of cylindrical surface, inches P_{cr} = short term critical pressure, calculated on the basis of ANSI/ASME PVHO-1, psi DP = design pressure, psi Material = Plexiglas G satisfying requirements of ANSI/ASME PVHO-1	
	$D_0 = 3.320$ inches $t/D_1 = 0.25$ $l/t = 0.25$ $P_{cr} = 3000$ psi $DP = 500$ psi $P_{cr}/DP = CF = 6$	$D_0 = 4.130$ inches $t/D_1 = 0.29$ $l/t = 0.25$ $P_{cr} = 5000$ psi $DP = 500$ psi $P_{cr}/DP = CF = 12$		

Table 2 Experimental evaluation at twin bevel plane disk windows under short term pressure loading at ambient room temperature

Specimen #9 $D_o = 3.520$ inches $t/D_i = 0.23$ $l/t = 0.25$ $\alpha = 90^\circ$ $P_{cf} = 5000$ psi $STCP = 5640$ psi $STCP/P_{cf} = 1.128$ $T = 70^\circ F$	Specimen #10 $D_o = 3.720$ inches $t/D_i = 0.32$ $l/t = 0.25$ $\alpha = 90^\circ$ $P_{cf} = 9000$ psi $STCP = 10,640$ psi $STCP/P_{cf} = 1.18$ $T = 69.5^\circ F$	Specimen #11 $D_o = 4.020$ inches $t/D_i = 0.317$ $l/t = 0.120$ $\alpha = 90^\circ$ $P_{cf} = 9000$ psi $STCP = 9300$ psi $STCP/P_{cf} = 1.03$ $T = 72^\circ F$	Specimen #12 $D_o = 3.250$ inches $t/D_i = 0.423$ $l/t = 0.120$ $\alpha = 90^\circ$ $P_{cf} = 13,600$ psi $STCP = 13,780$ psi $STCP/P_{cf} = 1.01$ $T = 74^\circ F$	Specimens #13-18 $D_o = 10.310$ inches $t/D_i = 0.308$ $l/t = 0.116$ $\alpha = 90^\circ$ $P_{cf} = 8800$ psi $STCP = 9400$ psi (avg.) $STCP/P_{cf} = 1.07$ $T = 72^\circ F$ (avg.)
Specimen #19 $D_o = 3.820$ inches $t/D_i = 0.21$ $l/t = 0.25$ $\alpha = 120^\circ$ $P_{cf} = 3000$ psi $STCP = 4605$ psi $STCP/P_{cf} = 1.535$ $T = 69^\circ F$	Specimen #20 $D_o = 4.130$ inches $t/D_i = 0.29$ $l/t = 0.25$ $\alpha = 120^\circ$ $P_{cf} = 7000$ psi $STCP = 9455$ psi $STCP/P_{cf} = 1.350$ $T = 70^\circ F$	Specimen #21 $D_o = 3.337$ inches $t/D_i = 0.26$ $l/t = 0.25$ $\alpha = 60^\circ$ $P_{cf} = 5000$ psi $STCP = 6540$ psi $STCP/P_{cf} = 1.308$ $T = 69^\circ F$	Specimen #22 $D_o = 3.461$ inches $t/D_i = 0.355$ $l/t = 0.25$ $\alpha = 60^\circ$ $P_{cf} = 8000$ psi $STCP = 9455$ psi $STCP/P_{cf} = 1.18$ $T = 69^\circ F$	Specimens #23-27 $D_o = 10.500$ inches $t/D_i = 0.363$ $l/t = 0.25$ $\alpha = 90^\circ$ $P_{cf} = 10,500$ psi $STCP = >10,000$ psi (avg.) $STCP/P_{cf} = 1.0$ $T = 74^\circ F$

NOTES:

D_o = major diameter, inches
 t = overall thickness, inches
 l = width of cylindrical surface, inches
 D_i = minor diameter, inches
 α = included cone angle, degrees
 T = ambient test temperature, $^\circ F$

Material: Plexiglas G satisfying requirements of ANSI/ASME PVHO-1

P_{cf} = experimentally determined catastrophic failure pressure of an equivalent window with a single bevel and identical t/D_i and α , psi
 $STCP$ = experimentally determined short term critical pressure of the test specimen with twin bevels, psi

$STCP/P_{cf}$ = relationship between experimentally established short term critical pressure of test specimen with twin bevels and the catastrophic failure pressure of equivalent windows with twin bevels

window while the other one was open to atmospheric pressure through an opening in the pressure vessel. Upon implosion, fragments of the window were ejected to the atmosphere. For cyclic pressure loading special test flanges were designed that held simultaneously two windows with different t/D ratios. In this arrangement one face of the windows was subjected to hydrostatic pressure while the other one was exposed to atmospheric pressure trapped between the two windows in the flange (Fig. 9).

Short term pressurizations were conducted at Southwest Research Institute, San Antonio, Texas, and at the Civil Engineering Laboratory, Port Hueneme, California, where facilities exist for generating high pressures needed for implosion of the thicker windows. During the implosion testing of individual windows only the implosion pressures and temperatures were recorded, and modes of failure photographed. The cyclic fatigue tests were conducted at Stachiw Associates test facility, El Cajon, California. All windows were pressure cycled simultaneously in the same pressure vessel to shorten the pressure cycling program and to insure that all windows would be subjected to identical test conditions. This was accomplished by stacking the test assemblies upon each other in the pressure vessel until the small pressure vessel was fully loaded and only a 1-in. annular space remained full of water. Only pressures and temperatures at beginning and end of each pressure phase and duration of all pressure and relaxation phases were recorded. To make the pressure cycling more realistic (1) random length cycles, (2) random pressure deviations from 500 psi, and (3) random temperature deviations from 75° were allowed. Every 100 cycles the windows were removed from the test flanges and inspected for presence of fatigue cracks.

Experimental Findings. Short term critical pressures of twin bevel plane disk windows tested to destruction were found to be the same as of single bevel plane disk windows with the same t/D ratio and included angle α tested in previous experimental programs (Table 2 and Fig. 10), [3]. This serves as reasonable evidence that the structural response of all twin bevel plane disk windows under short term loading to destruction is the same as for single bevel plane disk windows with the same t/D_i ratio and included angle.

Short term mode of failure of twin bevel plane disk windows under short term loading appeared to be the same as single bevel plane disk windows. The fracture surface observed on the low pressure face of

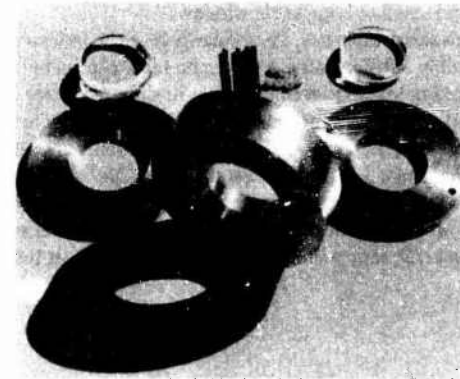


Fig. 9 Mountings used for pressure cycling of twin bevel plane disks. Note that the mounting holds two windows separated by a 1-in. wide air space

the disk was a typical conical shear cone whose apex penetrated the high pressure face at its center (Fig. 11). In thin windows this shear fracture cone was initiated at the center of low pressure face by the tensile component of the flexure stress whose maximum value was found at the center of the low pressure face. In thick windows the shear fracture cone was initiated by a combination of compressive radial, hoop, and longitudinal stresses whose maximum values were found in the transition zone between the plane disk surface and conical bevel surface.

Cyclic fatigue life of twin bevel plane disk windows tested in the program was found to be approximately the same as for single bevel plane disk windows with the same t/D_i ratios and included angles. This finding is based on the observation that the twin bevel plane disk windows designed with conversion factor of 6 ($CF = 6$ is the conversion factor for single bevel plane disk windows at ambient temperature of $75^\circ F$ designed on the basis of short term critical pressure curves specified by ANSI/ASME PVHO-1) did not have any fatigue cracks after 1000 pressure cycles at maximum design temperature and pressure. The absence of any fatigue cracks or crazing at 1000 pressure

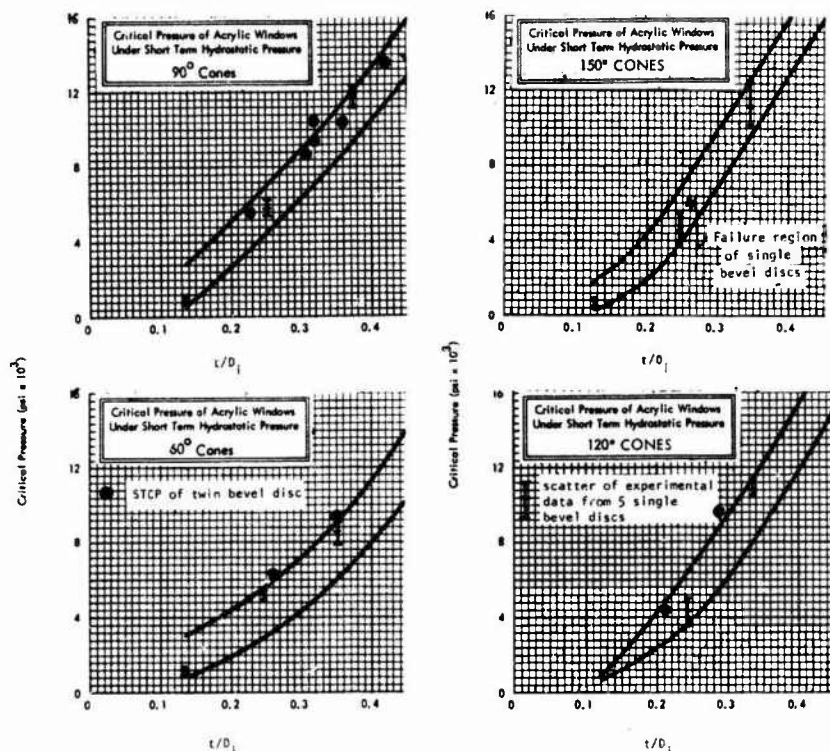


Fig. 10 Comparison of critical pressures for single and twin bevel plane disks. The curves have been previously established experimentally with 1-in. dia. single bevel disks (reference [3]) and the STCPs of twin bevel disks superimposed on them

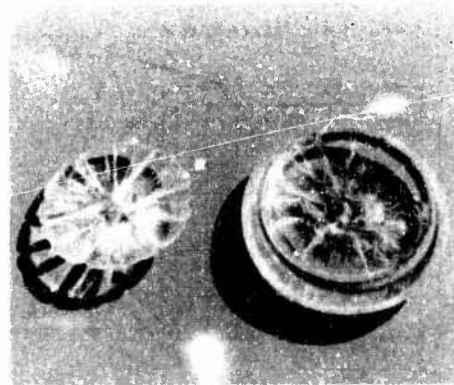


Fig. 11 Fracture surface on a twin bevel plane disk after short term hydrostatic loading to fracture initiation; $t/D_1 = 0.32$, $D_o = 4$ in., test pressure = 9300 psi, $\alpha = 90$ deg

cycles guarantees that these windows will not fail catastrophically in less than 10,000 pressure cycles (i.e., the minimum fatigue life specified by ANSI/ASME PVHO-1 for windows in manned service).

Experimental Conclusions. On the basis of experimental findings on twin bevel plane disk windows that were tested under short term and cyclic pressure loadings, it can be concluded with reasonable confidence that both the short term and cyclic fatigue strengths of all twin bevel plane disk windows are the same as of single bevel plane disk windows with the same t/D_1 ratios and included angles. Although the conclusion is based only on experimental data generated by 27

twin bevel plane disk test specimens, each with a different t/D_1 ratio and 60, 90, or 120 deg included angles, the excellent correlation between the experimental data and published results from other programs [4-8] on single bevel plane disk make the extrapolation of data from a limited number of t/D_1 ratios and angles to all t/D_1 ratios and included angles reasonable.

Analytical Approach. The principal purpose of the analytical investigation was to demonstrate that acrylic windows with both twin and single conical bearing surfaces exhibit similar structural behavior under short-term hydrostatic loadings. A secondary goal of the analysis was to show the effect of varying the t/D_1 ratio on the elastic stress distribution in a twin bevel conical window with a given diameter D_1 .

The analysis was conducted using the finite element method. Axisymmetric finite element models were made for different t/D_1 ratios ($t/D_1 = 0.23, 0.46, 1.00$), $\alpha = 90$ deg, and $l = 0.25t$. The ratio $t/D_1 = 0.46$ was selected (Fig. 12) to allow a direct comparison with a previous analysis conducted by Snoey and Crawford for a window with a single conical bearing surface and $t/D_1 = 0.46$. Using this t/D_1 ratio would allow direct comparison of results between the previous work and this investigation. The other t/D_1 ratios were selected because they represent geometries of approximately one-half or twice the window thickness of $t/D_1 = 0.46$. These ratios would serve as lower and upper bounds on the thicknesses under investigation, and the results would indicate what effect various t/D_1 's have on the nature of the stress intensity and distribution.

Figs. 13 and 14 show the axisymmetric model for $t/D_1 = 0.46$. This model is similar to that used by Snoey and Crawford except along the window flange interface. Whereas the previous investigation used a reduced mesh in this region, the present analysis used isoparametric quadrilateral elements with midside nodes. The geometry along this boundary was also the same for the other two t/D_1 ratios. The com-

puter program ANSYS, available from Swanson Analysis Systems, Inc., Elizabeth, Pennsylvania, was used for the analysis.

Two sets of boundary conditions were considered for each t/D_i ratio. Case I represented complete fixity of the window flange interface, while the window was free to slide along the flange in Case II. Since the coefficients of friction existing between the window and flange have not been quantitatively defined for different bearing stresses, these two conditions serve to bracket the true solution.

All nodes along the window's center ($\bar{X} = 0$) were free to move in the axial (\bar{Y} -direction) but constrained from moving in the radial (\bar{X} -direction). The finite element models were loaded by applying a 1000 psi pressure to top face of the window including the conical bevel surface and a portion of the outside cylindrical surface adjacent to the O-ring (Fig. 15).

Analytical Findings. For the $t/D_i = 0.46$ ratio, the results of the present investigation compare favorably with those of Snoey and Crawford on plane disks with a single conical bearing surface. For example, the maximum axial displacements along the center line are:

	Disks with single bevel (Snoey and Crawford)	Disks with twin bevels (Present Work)
Fixed	0.015 in.	0.0185 in.
Free sliding	0.019 in.	0.0196 in.

For comparison of stress distribution in the body, contour plots of radial (σ_r), axial (σ_x), and hoop (σ_{hoop}) were selected for output. These

plots can be directly compared with those given by Snoey and Crawford for single bevel disks with $t/D_i = 0.46$ (Figs. 16-18).

Figs. 19-21 show that the overall stress contour plots for single bevel disk compare quite favorably with twin bevel disk in terms of the general pattern and magnitudes of stress for a t/D_i ratio of 0.46. At the window-flange interface on the low pressure side of the window, a direct comparison of stresses is difficult because the finite element meshes are different in this region for the two studies. Nevertheless, the two analyses show that for this particular t/D_i ratio with the fixed boundary condition along the flange (Case I), the bending stresses increase in the window. For all t/D_i ratios the contour plots show that

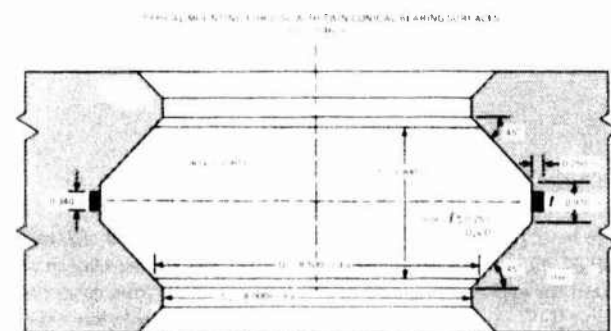


Fig. 12 Viewport with twin bevel plane disk window for 1600 psi service in the 0-120°F temperature range. Note the seat overhang on the mounting flange to provide support to the axially displacing window

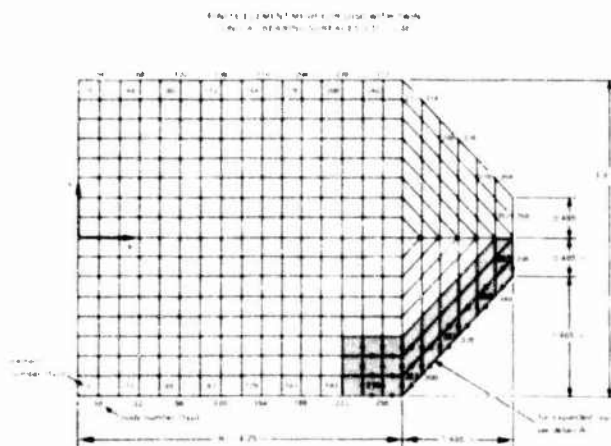


Fig. 13 Finite element mesh used in the stress analysis of a $t/D_i = 0.46$ disk with twin conical bearing surfaces

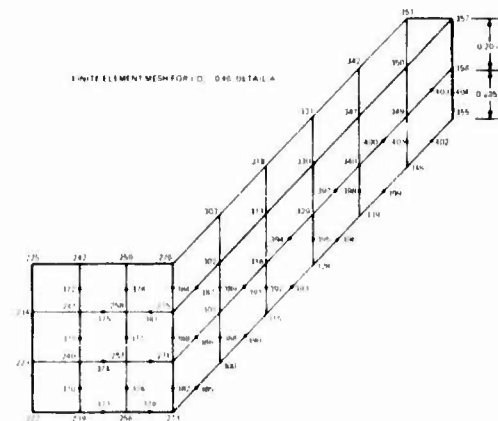


Fig. 14 Fine finite element mesh used at the edges of the $t/D_i = 0.46$ disk with twin conical bearing surfaces

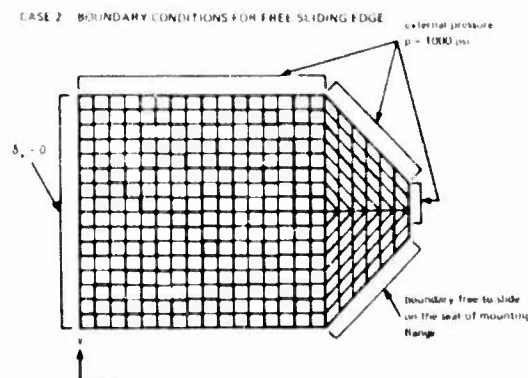
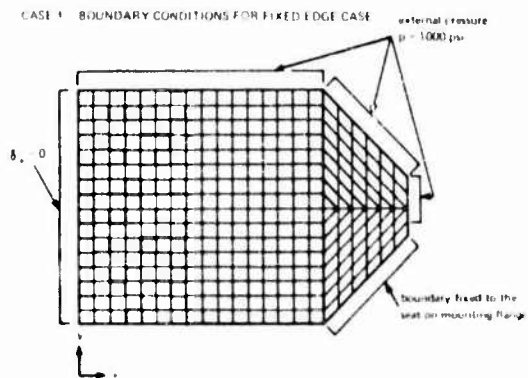


Fig. 15 Boundary conditions used in the finite element stress analysis of plane disks with twin conical bearing surfaces

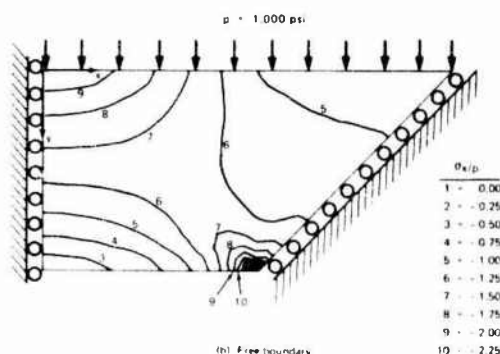
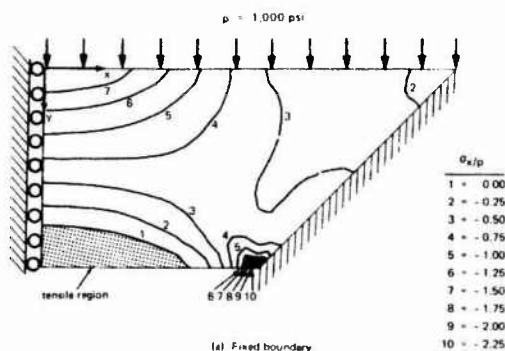


Fig. 16 Plot of σ_x stress contours in a $U/D_t = 0.46$ plane disk with single conical bearing surface

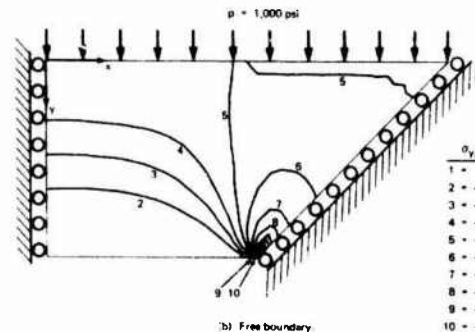
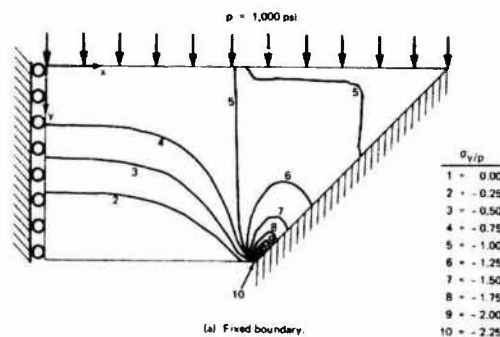


Fig. 17 Plot of σ_y stress contours in a $U/D_t = 0.46$ plane disk with single conical bearing surface

the largest stress gradient in twin bevel disks occur in the same location as for the single bevel disk windows.

Table 3 summarizes maximum element centroidal stresses for the three twin bevel disk models with 0.23, 0.46 and 1.0 t/D_t ratios. The table indicates that the stress level increases as t/D_t decreases. In fact, the magnitude of the maximum (highest compressive) stresses is almost doubled as t/D_t is decreased by 50 percent from 0.46 to 0.23. Increasing the t/D_t ratio by 117 percent from 0.46 to 1.0 does not decrease, however, the maximum stress by 50 percent. This would seem to indicate that peak compressive stresses along the edge of low pressure face cannot be significantly decreased by increasing the t/D_t ratio. This phenomenon has also been previously observed in finite element stress contour plots for single bevel windows with high t/D_t ratios. Since acrylic plastic deforms viscoelastically first in regions of stress concentrations, the high elastic stresses calculated by finite element computer programs surpass by a large margin the actual values of stresses in these locations.

Increasing the t/D_t ratio appears to have the largest effect on the magnitude of radial (σ_r) and hoop (σ_{hoop}) stresses at the center of low and high pressure faces. While in the twin bevel disk with $t/D_t = 0.23$ there is approximately a 6000 psi gradient between the low and high pressure faces (Figs. 22-24), in the disk with $t/D_t = 0.46$ this gradient has been decreased to 2100 psi (Figs. 19-21), and in disk with $t/D_t = 1.0$ it became only 700 psi (Figs. 25-27). Thus, increasing the t/D_t ratio of twin bevel disks does increase their load carrying capacity even though the susceptibility for initiation of cracks on the bearing surface also increases with the t/D_t ratio. This phenomenon has been experimentally observed previously in studies on single bevel disks, further confirming the general observation that the structural response of twin bevel disks to hydrostatic loading is similar to that of single bevel disks.

Analytical Conclusion. The magnitude, character, and distribution of stress in twin bevel plane disks with 90 deg included bevel angle appear to be very similar to single bevel plane disk with the same t/D_t ratio and included angle. On the basis of this finding it is reasonable to assume that the structural response of twin bevel disks with

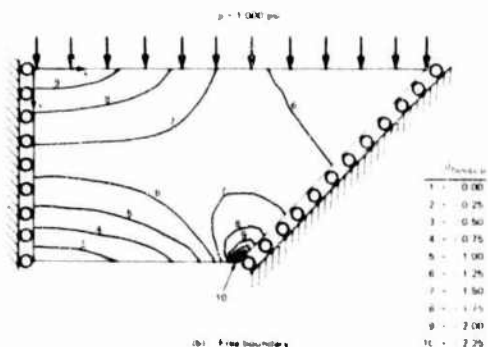
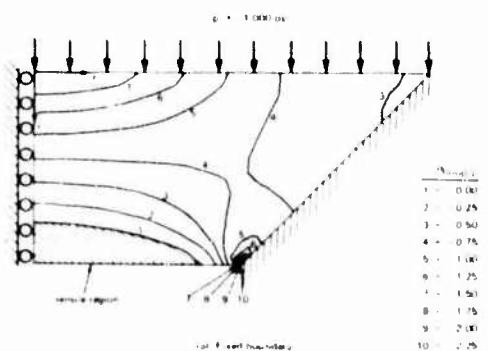


Fig. 18 Plot of σ_{hoop} stress contours in a $U/D_t = 0.46$ plane disk with single conical bearing surface

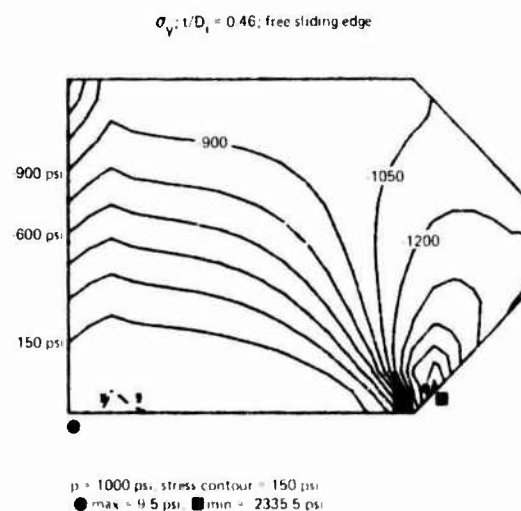
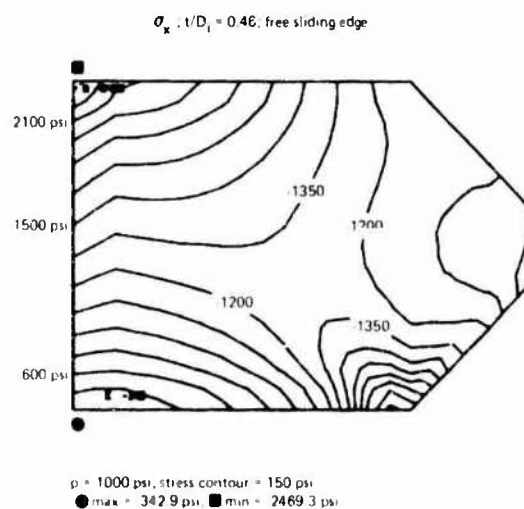
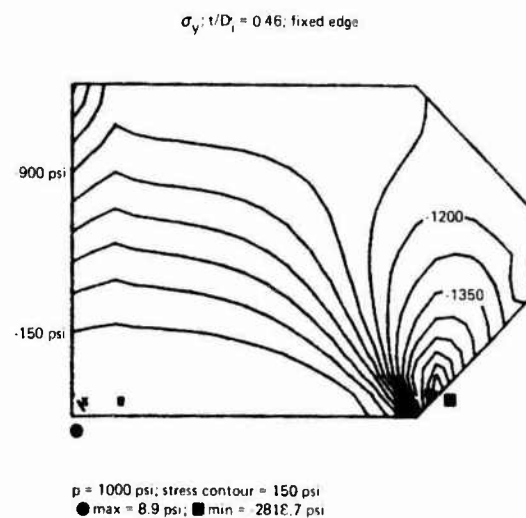
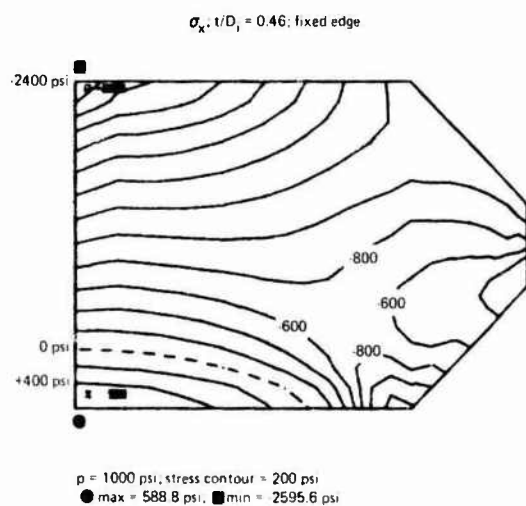


Fig. 19 Plot of σ_x stress contours in a $t/D_1 = 0.46$ plane disk with twin conical bearing surfaces

Fig. 20 Plot of σ_y stress contours in a $t/D_1 = 0.46$ plane disk with twin conical bearing surfaces

60 and 120 deg included bevel angle must be similar to single bevel disk with those included bevel angles.

Discussion

Both the experimental and analytical phases of the study have shown that there appears to be no significant difference in the structural responses of single and twin bevel plane disk windows even though the areas of their bearing surfaces differ significantly. Needless to say, the response is not identical, as the configuration of the windows is not identical. What the study has shown, however, is that the location and magnitude of maximum principal stresses is in both cases approximately the same. In a way this is amazing as the twin bevel plane disks have only about 30 percent of the bearing surface with which the single bevel plane disks are provided to carry bearing stresses.

The explanation for this apparent structural anomaly lies in the absence of any large stresses in the outer edge of the single bevel plane disk window. As a result of this fortuitous stress distribution, the outer edge of the single bevel plane disk can be machined off without significantly increasing the magnitude of maximum stresses which are generally found in the inner edge of the beveled disks. Comparison of principal stresses in the single and twin bevel plane disk with 90 deg included angle and $t/D_1 = 0.46$ certainly bears this out.

In general the conclusion can be formulated that the maximum value of principal stresses in plane disk windows with conical bearing surfaces appears to be more influenced by changes in t/D_1 ratio than in the area of bearing surfaces. Still, that does not mean that the bearing surface of plane disk with conical bevel can be decreased to nothing; at some point the lack of bearing surface will increase the magnitude of principal stresses significantly. How much the bearing surface on the conical bevel has to decrease before this happens is at the present time not known. However, because this critical point is not known at the present time, it is necessary for designers to stay within the limits of bearing surface area decrease experimentally evaluated in this study.

Thus, the findings of this study are considered to apply only to plane disks with twin conical bearing surfaces modified by a cylindrical seal surface with a width of $l/t \leq 0.25$. Cylindrical seal surfaces with $l/t > 0.25$ on plane disks with twin conical bevels may significantly increase the magnitude of principal stresses, and by the same token significantly decrease the window's short term critical, as well as safe maximum, operational pressures.

Although this study has focused primarily on plane disk with twin conical bearing surfaces, the findings of the study also apply to plane disks with a single conical bearing surface modified by a cylindrical seal surface since in this window configuration the conical bearing

surface has also been significantly decreased. Extrapolation of the findings from this study indicates that the cylindrical seal surface on a plane disk with a single conical bearing surface may be extended to $l/t \leq 0.5$ without significantly changing the critical pressure or safe maximum operational pressure of such a window. The validity of this postulate is also supported by some limited experimental data (Table 4).

Conclusion

The maximum safe operational pressure of acrylic plastic plane disk windows with twin conical bearing surfaces and a cylindrical sealing surface with a width of $l/t \leq 0.25$ can be specified on the basis of design criteria already developed in the ANSI/ASME PVHO-1 Safety Standard for plane disk windows with a single conical bearing surface. The same criteria can also be applied to the design of plane disk windows with a single conical bearing surface modified by the presence of a cylindrical sealing surface with a width of $l/t \leq 0.5$.

Design Recommendations

More thought and care must be given to the design of plane disk windows with twin bevel conical bearing surfaces than is generally given to the design of plane disks with a single conical bearing surface.

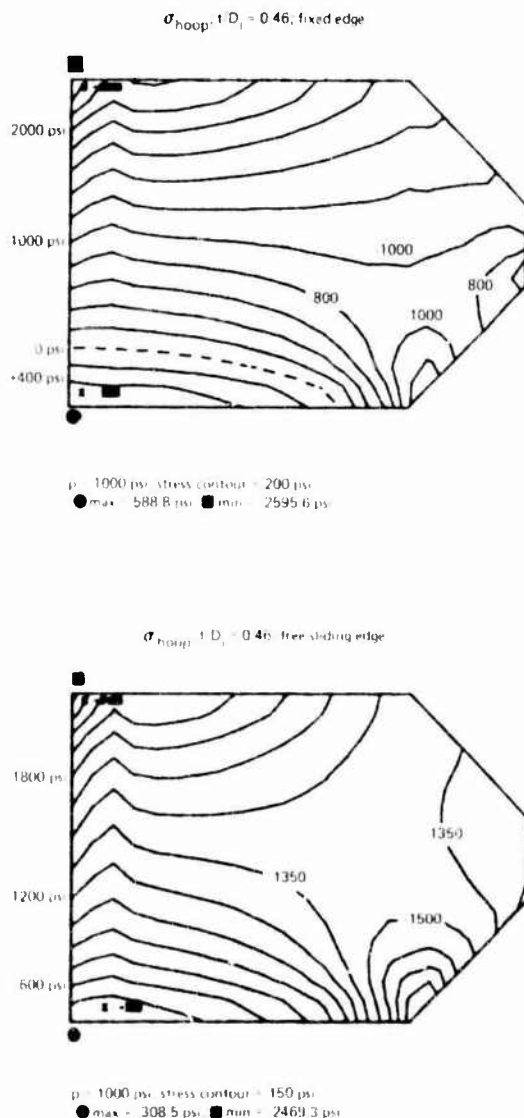


Fig. 21 Plot of σ_{hoop} stress contours in a $t/D_i = 0.46$ plane disk with twin conical bearing surfaces

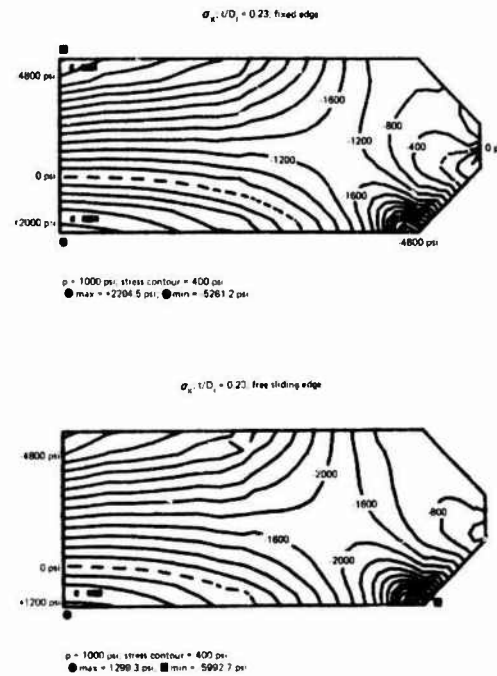


Fig. 22 Plot of σ_x stress contours in a $t/D_i = 0.23$ plane disk with twin conical bearing surfaces

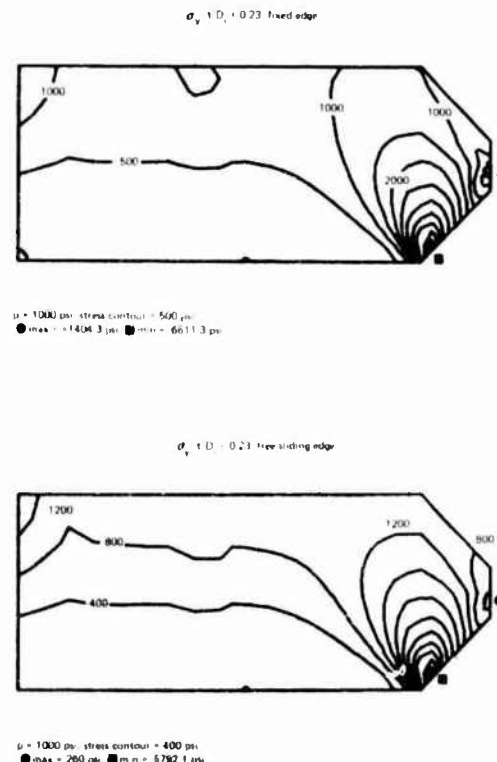


Fig. 23 Plot of σ_y stress contours in a $t/D_i = 0.23$ plane disk with twin conical bearing surfaces

The reason for it is that plane disks with twin bevels must be able to seal and withstand pressures acting upon either face of the disk, while plane disks with a single bevel have to seal and withstand pressure acting only upon one face of the disk.

Window Design. The t/D_i ratio of the plane disk window with twin bevel conical bearing surfaces depends on the magnitude of specified design pressure (safe maximum operational pressure), design temperature, and included conical angle. Depending on the value of design temperature, different conversion factors (CF) must be selected

for calculating the required short term critical pressure (STCP) of the window. For this purpose Table B-2 in Appendix A of the ANSI/ASME PVHO-1 Safety Standard is utilized. For example, 500 psi design pressure at 75°F calls for $CF = 6$ resulting in a specified STCP of 3000 psi ($500 \text{ psi} \times 6 = 3000 \text{ psi}$). Once the short term critical pressure has been calculated the minimum t/D_i ratio needed to meet this short term critical pressure requirement can be determined by using the design curves on Figure B-3 and B-4 in Appendix A of the same ANSI/ASME PVHO-1 Safety Standard. In the case of our example the t/D_i of a twin bevel plane disk with 90 deg included angle and STCP for 3000 psi is found to be equal to 0.23.

Seal Design. The recommended seal for plane disk windows with twin conical bevel bearing surfaces is a single radially compressed O-ring located on a ledge in the mounting flange (Fig. 5). To provide a nonbearing surface on the window which would contact the seal, a cylindrical surface is incorporated into the window design midway between the plane surfaces. The width of the cylindrical bearing surface must be wider than the O-ring groove, but less than 25 percent of window thickness.

Mounting Design: The mounting must be designed in such a manner that it provides adequate support to the twin bevel disk regardless of from which side the pressure may be applied. For this reason the conical seats on the mounting must be wider than the conical bearing surface on the window so that the window receives radial and vertical support even when it has displaced axially under the action of hydrostatic loading. The magnitude of seat overhang, defined by D_i/D_f ratio, varies with the included conical angle and the magnitude of design pressure. The values of seat overhang are found in Fig. C-2, Appendix A of ANSI/ASME PVHO-1 Safety Standard. For our example the value of D_i/D_f is 1.03.

To insure positive contact between the conical bearing surfaces on the disk and the conical seats in the mounting it is necessary to make the width of the cylindrical seat in the mounting less than the width of the conical sealing surface on the window (Figs. 4 and 5). In this manner there is insured a positive contact between bearing surfaces on the acrylic and/or the seating surfaces on the steel mounting. During pressurization of the disk the contact ceases on one side of the disk as the disk displaces axially, but upon depressurization the disk returns to its original position and re-establishes the contact with the seat on the side from which it was pressurized.

Dimensional Tolerances. Since the radially compressed O-ring serves as the primary seal in the viewport assembly, steps must be

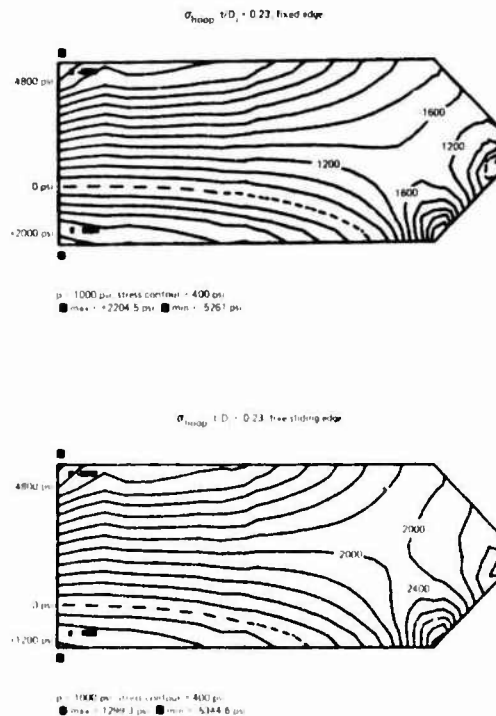


Fig. 24 Plot of σ_{hoop} stress contours in a $t/D_i = 0.23$ plane disk with twin conical bearing surfaces

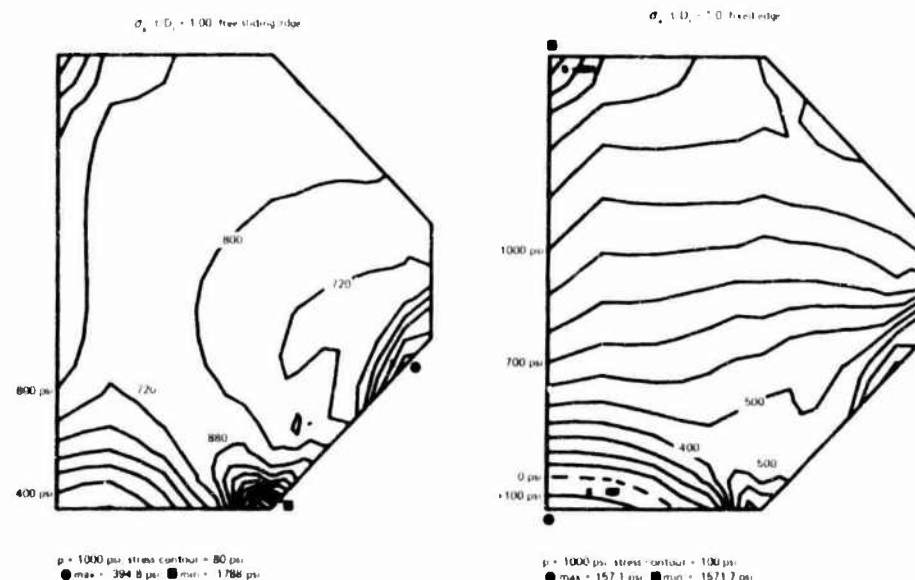


Fig. 25 Plot of σ_r stress contours in a $t/D_i = 1.0$ plane disk with twin conical bearing surfaces

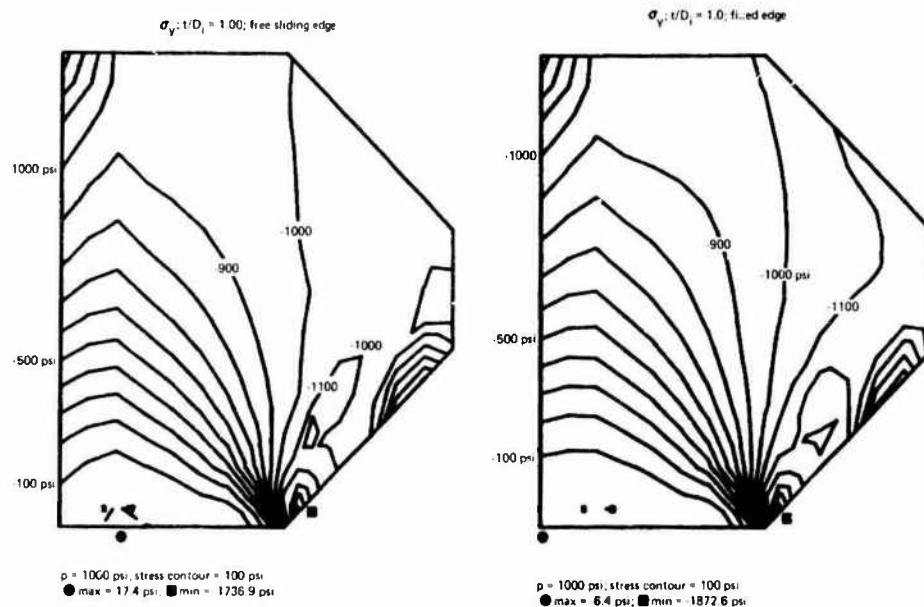


Fig. 26 Plot of σ_r stress contours in a $t/D_i = 1.0$ plane disk with twin conical bearing surfaces

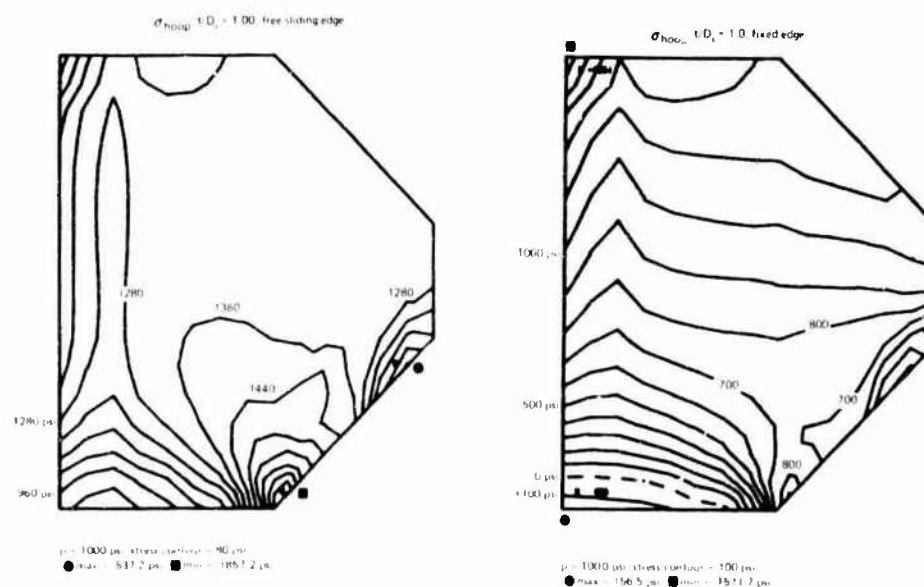


Fig. 27 Plot of σ_{hoop} stress contours in a $t/D_i = 1.0$ plane disk with twin conical bearing surfaces

taken to contain only minimum radial clearance between the cylindrical surface on the window and the cylindrical seat in the mounting even at lowest expected operational temperature. Since the ambient temperature during machining and installation of windows in the mounting is generally 30–40°F higher than the lowest predicted operational temperature in the ocean, the windows should be machined oversize and shrunk by precooling for installation. Failure to do so results in leakage around the window during a dive in cold ocean water when the pressure inside the chamber has been equalized to the ambient ocean pressure during lock-out procedure.

Angular tolerance on conical bearing surfaces should be kept within ± 15 min of the specified included conical angle. In this manner the maximum angular mismatch between contacting conical bearing surfaces will not exceed 0.5 deg, a mismatch value that has been found to be acceptable from the structural viewpoint.

References

- 1 Stachiw, J. D., "Transparent Structural Materials for Underwater Research and Exploration," *Industries Atomiques & Spatiales*, Vol. 3, 1974.
- 2 ANSI/ASME PVHO-1 Safety Standard for Pressure Vessels for Human Occupancy, June 1977.
- 3 Stachiw, J. D., "Critical Pressure of Conical Acrylic Windows Under Short Term Hydrostatic Loading," *JOURNAL OF ENGINEERING FOR INDUSTRY*, TRANS. ASME, Series B, Vol. 89, No. 3, 1967.
- 4 Stachiw, J. D., "Conical Acrylic Windows Under Long-Term Hydrostatic Pressure of 20,000 psi," *JOURNAL OF ENGINEERING FOR INDUSTRY*, TRANS. ASME, Series B, Vol. 92, No. 1, 1970.
- 5 Stachiw, J. D., "Conical Acrylic Windows Under Long-Term Hydrostatic Pressure of 10,000 psi," *JOURNAL OF ENGINEERING FOR INDUSTRY*, TRANS. ASME, Series B, Vol. 94, No. 4, 1972.
- 6 Stachiw, J. D., "Effect of Temperature and Flange Support on Critical Pressure of Conical Acrylic Windows Under Short Term Pressure Loading," *JOURNAL OF ENGINEERING FOR INDUSTRY*, TRANS. ASME, Series B, Vol. 94, Dec. 1972.

Table 3 Peak stresses and displacement calculated for typical acrylic plastic disks with twin conical bearing surfaces under short term hydrostatic loading of 1000 psi

α	t/D_1	Boundary Condition		σ_x (psi)	σ_y (psi)	σ_{Hoop} (psi)	Axial Displacement (inches)
90°	0.23	Fixed Edge	σ , Maximum σ , Minimum Displacement, Max.	2204.5 -5261.2	1404.3 -6611.3	2204.5 -5261.2	0.0534
		Free Sliding Edge	σ , Maximum σ , Minimum Displacement, Max.	1299.3 -5992.7	260.0 -5792.1	1299.3 -5344.6	0.0512
90°	0.46	Fixed Edge	σ , Maximum σ , Minimum Displacement, Max.	588.8 -2595.6	8.9 -2818.7	588.8 -2595.6	0.0185
		Free Sliding Edge	σ , Maximum σ , Minimum Displacement, Max.	-342.9 -2469.3	9.5 -2335.5	-308.5 -2469.3	0.0196
90°	1.00	Fixed Edge	σ , Maximum σ , Minimum Displacement, Max.	157.1 -1571.7	-6.4 -1872.6	156.5 -1571.7	0.0109
		Free Sliding Edge	σ , Maximum σ , Minimum Displacement, Max.	-394.8 -1788.0	17.4 -1736.9	-537.2 -1857.2	0.0142

NOTE: 1. Hydrostatic pressure is applied only to one face of the window.
2. All calculated values are valid only for short term pressurization at 75°F .
3. Physical constants for acrylic plastic are: $E = 444,000$ psi, Poisson's Ratio = 0.4.

Table 4 Experimental evaluation of single bevel disk windows with cylindrical sealing surface under short term pressure loading at ambient room temperature

Specimens 28-32	Specimens 33-37
$D_0 = 10.495$ in.	$D_0 = 11.500$ in.
$t/D_1 = 0.25$	$t/D_1 = 0.305$
$l/t = 0.375$	$l/t = 0.337$
$\alpha = 90^\circ$	$\alpha = 90^\circ$
$P_{cf} = 5900$ psi	$P_{cf} = 9200$ psi
STCP = 6020 avg.	STCP = 10,000 avg.
STCP/ $P_{cf} = 1.02$	STCP/ $P_{cf} = 1.08$
$T = 73^\circ\text{F}$	$T = 73^\circ\text{F}$

Notes

- D_0 = major diameter, inches
- t = overall thickness, inches
- l = width of cylindrical surface, inches
- D_1 = minor diameter, inches
- α = included cone angle, degrees
- T = ambient test temperature, $^\circ\text{F}$
- P_{cf} = experimentally determined catastrophic failure pressure of an equivalent window with a single bevel and identical t/D_1 and α , psi
- STCP = experimentally determined short term critical pressure of the test specimen with a single bevel modified by a cylindrical sealing surface, psi

7 Stachiw, J. D., "Conical Acrylic Windows Under Long-Term Hydrostatic Pressure of 5000 psi," JOURNAL OF ENGINEERING FOR INDUSTRY, TRANS. ASME, Series B, Vol. 4, No. 3, 1972.

8 Stachiw, J. D., et al., "Procurement of Safe Viewports for Hyperbaric Chambers," JOURNAL OF ENGINEERING FOR INDUSTRY, TRANS. ASME, Series B, Vol. 93, No. 4, 1971.

9 Snoey, M. R., and Crawford, J. E., "Stress Analysis of a Conical Acrylic Viewport," Technical Report R-675, Naval Civil Engineering Laboratory, Port Hueneme, Calif., April 1970.

APPENDIX

Definitions

- Acrylic** = methyl methacrylate plastic possessing physical and mechanical properties shown in Tables A-1 and A-2 of the ANSI/ASME PVHO-1.
- Conversion Factor** = an empirical ratio of short term critical pressure to design pressure specified on the basis of long experience as the safe relationship between the two variables for a given temperature.
- Critical Pressure** = hydrostatic pressure that, acting on one side of the window, causes it to lose structural integrity and ability to remain impermeable to water.
- Window, or Lens** = transparent, impermeable, and pressure-resistant insert in the viewport assembly.
- Viewport** = penetration in the pressure hull equipped with an impermeable and pressure-resistant transparent window that is seated in a mounting and held in place by a bolted-on or screwed on retaining ring.
- psi** = pounds per square in., equals 0.0702 kg/cm^2 .
- in.** = 2.54 cm
- BAR** = 14.5 psi
- MPa** = megapascal = 145 psi

J. D. Stachiw

Naval Ocean Systems Center,
Ocean Technology Department,
San Diego, Calif. 92152
Mem. ASME

Hyperhemispherical Viewports for Undersea Applications

Hyperhemispherical windows with included spherical angles in the 260–270 degree range have been fabricated from acrylic plastic and glass for a variety of undersea applications. When seated in NOSC rigid metallic mountings with conical seats they withstood cyclic design working pressures without failure, or cracking providing that a thin elastomeric gasket was interposed between the mating conical bearing surfaces, and two elastomeric O-rings served as compliant bushings between the spherical surfaces of the window and the retaining surfaces of the mounting.

Tests have shown that (1) critical pressures of acrylic plastic hyperhemispheres can be predicted with acceptable accuracy by analytical and empirical relationships developed previously for acrylic plastic hemispheres and spheres, (2) the mounting retains and seals plastic or glass windows in -40 to 120°F ambient temperature range even when subjected to lateral dynamic loading of 17G magnitude, and (3) dimensionally identical hyperhemispheres fabricated from glass and seated in the same mounting do not fail under a single pressurization at twice the critical pressure of acrylic windows.

Introduction

Because of extensive research conducted over the years at U. S. Navy Laboratories, a plethora of window designs have been developed for undersea applications (Fig. 1). These shapes are: plane disc with plane bearing surface, plane disc with a single conical bearing surface, plane disc with twin conical bearing surfaces, spherical sector with conical bearing surface, hemisphere with and without flanges, sphere with penetrations, and cylinder.

There was one application, however, for which an optimum window shape was lacking. This application was a window with panoramic visibility for periscopes, conning towers, and personnel hatches on submersibles. Such a window, when mounted to a pressure resistant hull, would allow the crew to (1) avoid surface craft while cruising just below the ocean's surface, (2) study ocean floor while cruising several feet above it, and (3) monitor the hull's exterior for any entanglements with submerged cables or lines (Fig. 2).

The window shape which would allow the crew to perform all of these functions is the hyperhemisphere. When fastened securely around the perimeter of its opening to the pressure hull of a submersible it can withstand not only hydrostatic, but also hydrodynamic forces generated by wave slap and drag. Depending on the size of the

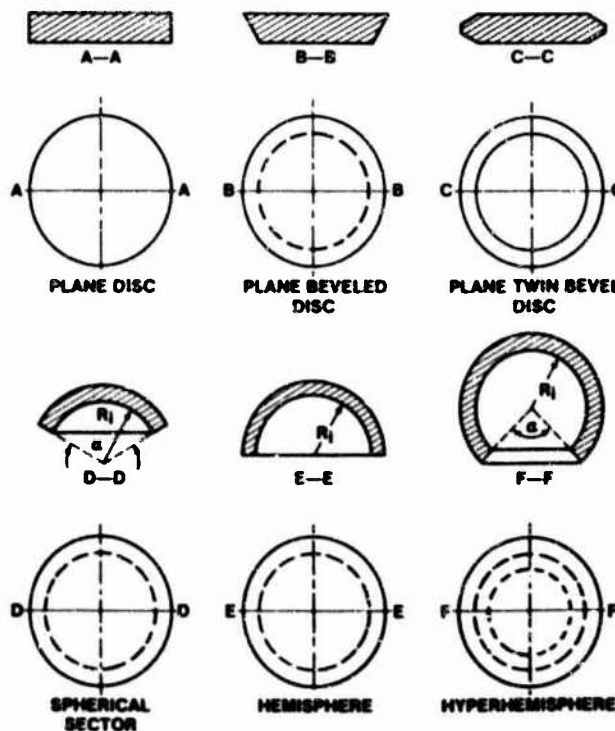


Fig. 1 Typical shapes of windows for diving systems.

Contributed by the Ocean Engineering Division and presented at the Winter Annual Meeting, San Francisco, Calif., December 10–15, 1978 of THE AMERICAN SOCIETY OF MECHANICAL ENGINEERS. Manuscript received at ASME headquarters July 1, 1978. Paper No. 78-WA/OCE-2.

were developed and hardware fabricated that served not only as scale test specimens of man-sized viewports, but also as full scale viewport assemblies for optical or electro-optical systems (Table 1 and Fig. 6). In this manner an experimentally validated design could be used immediately for applications requiring transparent housings for television cameras mounted externally on submersibles, while at the same time the same design could be scaled up to any desirable size to enclose the head or the whole body of an observer. To make the design even more versatile, its dimensions were chosen to serve two operational depth ranges often specified for submersibles. The two operational depth ranges selected for the design were 0-2500 and 0-12,000 ft. The first depth range covered the continental shelf while the other one covered the abyssal plains. To cover both depth ranges with the same design of the hyperhemispherical viewport assembly acrylic plastic was paired with 6061-T6 aluminum alloy and borosilicate glass with Ti-6-Al4V titanium alloy. The reason for choosing aluminum and titanium as mounting materials was their resistance to corrosion and high strength-to-weight ratios. If for some reason the aluminum mounting could not be used on the submersible, because of galvanic reaction the more expensive titanium mounting could be substituted for it without decreasing the depth rating of the acrylic window.

Windows. The t/R_o ratio of the hyperhemispherical window was chosen on the basis of nominal compressive stresses calculated with the aid of Lamé's equation for thick spheres:

$$S_1 = S_2 = -p \frac{R_o^3(R_i^3 + 2r^3)}{2r^3(R_o^3 - R_i^3)} \quad (1)$$

$$S_3 = p \frac{R_o^3(r^3 - R_i^3)}{r^3(R_o^3 - R_i^3)}$$

where

- S_1 = meridional membrane stress, psi
- S_2 = hoop membrane stress, psi
- S_3 = radial wall stress, psi
- p = external hydrostatic pressure, psi
- R_o = external radius of curvature, in.
- R_i = internal radius of curvature, in.
- r = radius to point where stress is being calculated, in.
(maximum S_1 and S_2 are located at $r = R_i$, while maximum S_3 is found at $r = R_o$)

Since it was known from past studies with spherical acrylic hulls that the meridional stresses on the concave surface of the sphere near the metallic hatches are approximately 100 percent higher than the nominal membrane stress at the apex, the magnitude of nominal membrane stress calculated by equation (1) had to be multiplied by a factor of two to take this fact into account. For this reason—4500 psi and -26,000 psi were chosen as maximum nominal membrane working stresses for acrylic plastic, and glass, respectively. These values of maximum nominal membrane working stresses, when multiplied by the stress concentration factor of two would still fall within the allowable range of working stresses for these materials in areas of local stress risers.

In addition to stresses short term catastrophic failures initiated by buckling were also calculated. This was accomplished with the classical Zoelly equation empirically modified by Krenzel and Stachiw:

$$P_{cr} = \frac{0.8\sqrt{E_t E_s (t/R_o)^2}}{\sqrt{1-\mu^2}} \quad (2)$$

where

- P_{cr} = critical pressure, psi
- E_t = tangent modulus of elasticity, psi
- E_s = secant modulus of elasticity, psi
- t = shell thickness, inches
- μ = Poisson's ratio
- R_o = external radius

Utilizing equation (2) the short term critical pressures of hyperhemispherical windows were calculated to be 4500 psi for acrylic

plastic¹ and 120,000 for glass. Since both values exceed by at least a factor of four the specified operational depths of 2500 and 12,000 ft for plastic and glass hyperhemispheres the t/R_o ratio of the windows selected on the basis of stress calculations is considered to be adequate as it provides the windows also with sufficient elastic stability.

Mountings. Although the conical seat may be incorporated into a hatch cover, or pressure hull equipped with integral penetration reinforcing flanges, experience has shown that it is more advantageous to mount the hyperhemispherical window in a flange which is structurally independent of the hull to which it is bolted. This approach not only facilitates the calculation of stresses in the mounting during design, but also makes the viewport assembly design more universal since it can be now bolted without any modifications to different submersibles (Fig. 6).

Because of these considerations the mountings for the test program were designed to be independent of the structure on which they would be mounted in service. The only requirement imposed on the penetration in the hull structure to which the mounting is bolted, was that it be reinforced and provided with a plane smooth surface against which the O-ring in the bottom of the mounting may seal. Since the radial contraction of the penetration in the hull may differ substantially from that of the window mounting, oversize holes must be provided in the mounting for bolts with which the mounting is attached to the hull. In this manner, differential movement between the mounting and the hull may take place by sliding without straining of bolts.

In the design of the window mountings -15,000 psi and -50,000 psi were considered to be acceptable maximum nominal working hoop stress values for 6061-T6 aluminum and Ti6Al4V titanium alloys, respectively. These nominal working stress values in the mounting represent less than 50 percent of the material's yield strength, thus providing a comfortable margin of safety for (1) unknown stress concentrations in the mounting, and (2) static and dynamic overpressurizations which the window assembly may encounter prior to, and during service.

Retainers. In order to arrive at a functional, but compliant retainer for the hyperhemisphere a tradeoff had to be performed between the compression of the O-rings required to secure the window against external vertical and horizontal forces, and the magnitude of stresses generated in the window by the static compression of O-rings. If the O-rings were not sufficiently compressed, the window would break loose under intense wave slap, hydrodynamic drag, or minor pressurization of the submersible's interior. On the other hand, excessive compression of the internal O-ring would generate such high tensile stresses in the window during tightening of the retaining ring bolts that a tensile crack could be initiated at the edge of the window. The possibility of this occurring was very slim for acrylic windows with their low modulus of elasticity and high tensile strength. A different case presented itself however if the windows were fabricated from brittle material with high modulus of elasticity and low tensile strength like glass, quartz, ceramic, or germanium.

Based on this tradeoff the mounting was designed to allow for extensive deformation of the O-rings' circular cross-section but to stop short of volumetric compression of the material.

Experimental Evaluation

Instrumentation. All of the viewport assemblies were instrumented with electric resistance strain gages. The majority of the gages were mounted on external and internal surfaces of windows. Only one gage was placed on the interior surface of the mounting 0.650 in. below its top surface, where maximum hoop stresses were expected to occur.

The gages mounted on the windows were intended to measure not only the membrane compressive stresses but also flexure stresses

¹ This equation is difficult to solve for acrylic plastic as it must be solved simultaneously with equation (1) utilizing E_t and E_s from (8). A graphical solution to equation (2) has been, however already prepared and can be found in ANSI/ASME PVHO-1, Appendix A, Figure B-12 Reference [13].

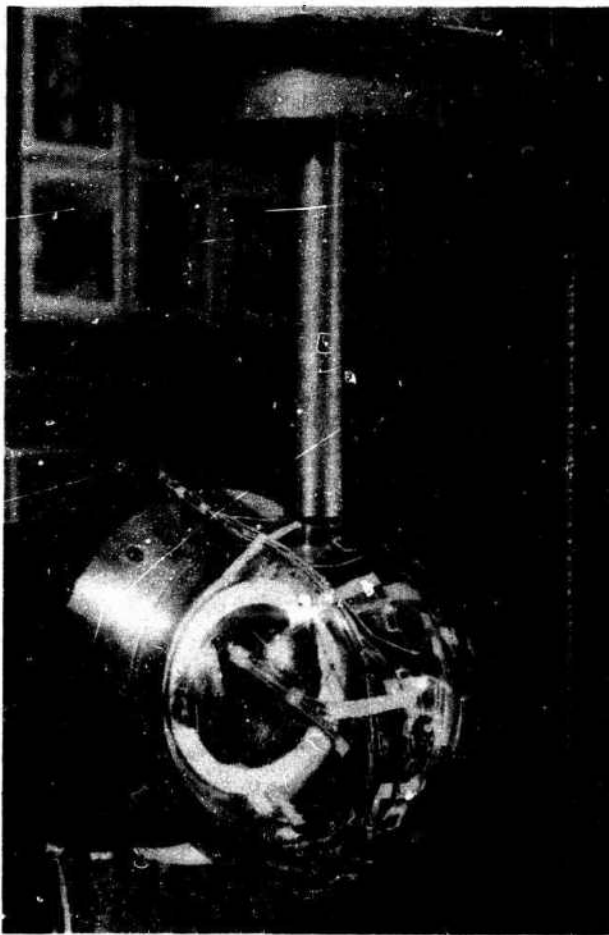


Fig. 7 Test setup for applying lateral point load (simulating hydrodynamic drag) to the viewport assembly

generated by the mounting and elastomeric restraint. Since it was not physically feasible to place the centers of gages at the very edge of the window where maximum stresses are found, the maximum values can only be estimated on the basis of measured values.

Test Procedure

Tightening of retaining ring was accomplished by uniformly tightening all the bolts in the retainer ring until a torque reading of 14 in./lbs was achieved. Strains were read in the window at that time.

Hydrodynamic drag was simulated by applying a hydraulically actuated plunger against the equator of the window while the window was held in the mounting rigidly bolted to the frame of the hydraulic press (Fig. 7). Strain readings were taken at simulated drag force of 600 lbs.

Wave slap was simulated by dropping the viewport assembly from different elevations into a water tank. At moment of impact the window's axis of revolution was always parallel to the water surface. The maximum velocity measured during the drops was 44 ft/sec.

Vibration test was performed by placing a viewport assembly on a shaker and subjecting it to sinusoidal vibration in horizontal plane while the frequency, amplitude and ambient temperature were varied. The maximum lateral acceleration applied to the window was 17Gs. Accelerations of this magnitude were applied for 150 min while the ambient temperature varied from -40° to $+120^{\circ}$ F. While the viewport assembly was subjected to lateral vibration of 17G magnitude, the air-leakage rate across O-ring seals was monitored.

Internal pressure test was accomplished by bolting the viewport assembly on a rigid bulkhead and pressurizing the interior of the assembly with water to a maximum pressure of 100 psi. Strains and axial window displacements were read at 10 psi intervals.

External pressure test was performed by bolting the viewport assembly to a flat aluminum bulkhead, immersing it in a pressure vessel full of water and pressurizing the interior of the vessel at 100 psi/min rate. The magnitudes of external hydrostatic pressure applied to the viewport assemblies varied from one test to another depending on the test objective. Strains were read at 200 psi intervals.

Test Results

a. Acrylic windows

- 1 Tightening of 22 retaining bolts to 14-in./lbs torque generated

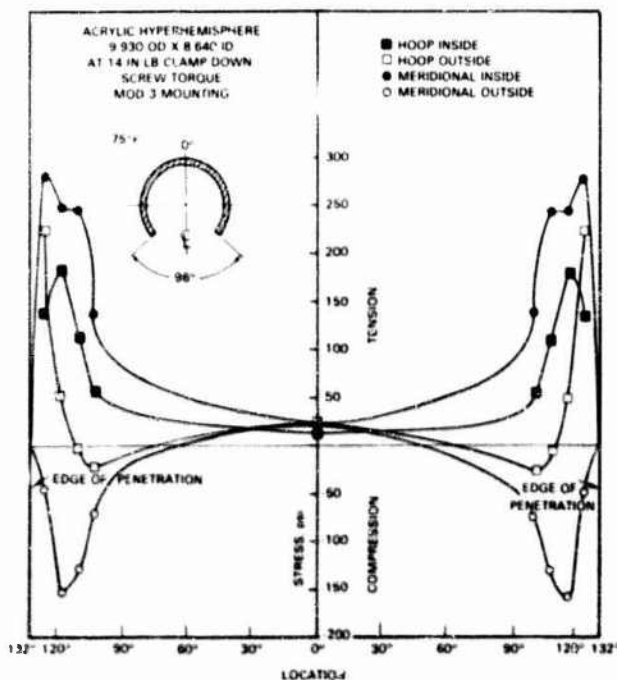


Fig. 8 Stresses in acrylic window generated by tightening of retaining screws shown in Figure 3

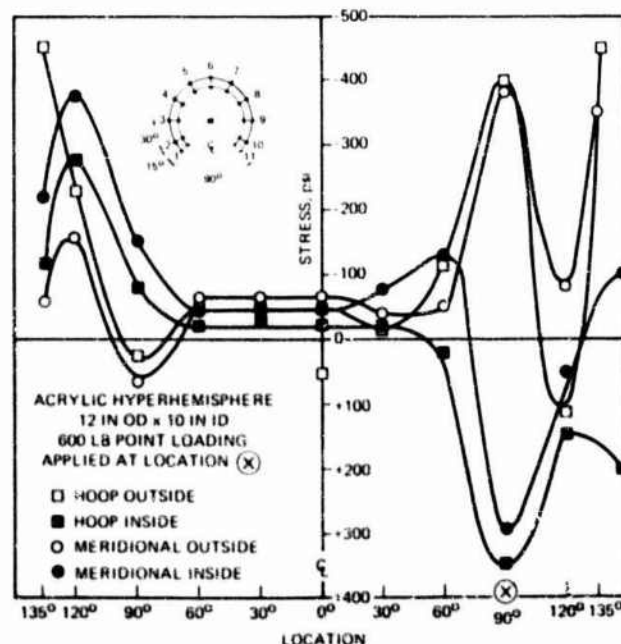


Fig. 9 Stresses in acrylic window under point loading applied to its equator

in the window a maximum stress of approximately 275 psi. The recorded maximum stress was tensile in character, oriented meridionally, and located on the concave surface approximately 0.1 rad away from the window's edge (Fig. 8).

2 *Simulated hydrodynamic drag* of 600 lb magnitude generated in the window maximum stress of -450 psi which was compressive in character, oriented circumferentially, and located on the convex surface at the very edge of the window (Fig. 9).

3 *Internal pressurization* generated a maximum normalized stress of 14 which was tensile in character, oriented meridionally, and located on the concave surface approximately 0.1 rad away from the window's edge (Fig. 10). Axial displacement was found to be 0.060 in. at 100 psi internal pressure (Fig. 11).

4 *External pressurization* generated a maximum stress which was compressive in nature, oriented meridionally, and located on the concave surface at the edge of the window. The magnitude of the

measured peak compressive stress was approximately 50 percent higher than the membrane stress measured on the concave surface at the apex of the window. The normalized membrane stress on the concave surface at the apex was found to be in the 4.3 to 4.4 range for windows with $t/R_o = 0.13$, and 3.5 to 3.6 range for windows with $t/R_o = 0.166$ (Fig. 12).

When pressurized to destruction the acrylic hyperhemisphere with $t/R_o = 0.13$ imploded under short term loading at 4400 psi. The experimental implosion pressure differs only by 50 psi from the critical pressure predicted for this t/R_o ratio. That prediction was based on empirically derived graph of Fig. B-12 developed by the author on the basis of experimental data for ANSI/ASME PVHO-1 Safety Standard ([13] and Fig. 13).

b. Glass windows

The glass hyperhemisphere with $t/R_o = 0.13$ did not fail or develop any cracks when pressurized to 10,000 psi. Inspection after the test

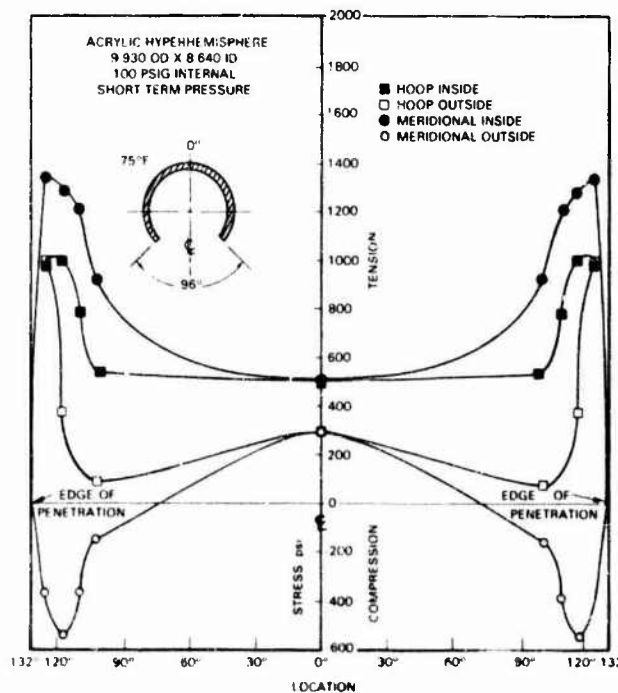


Fig. 10 Stresses in acrylic window under internal pressure

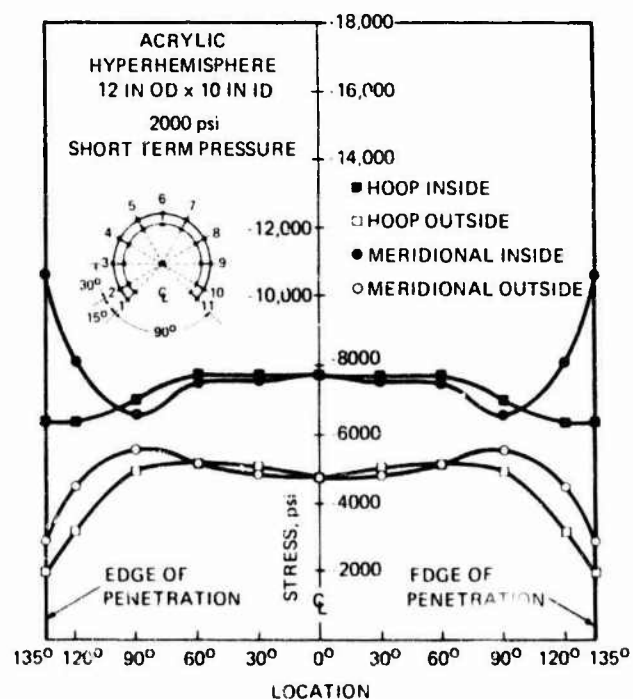


Fig. 12 Stresses in acrylic window under external pressure

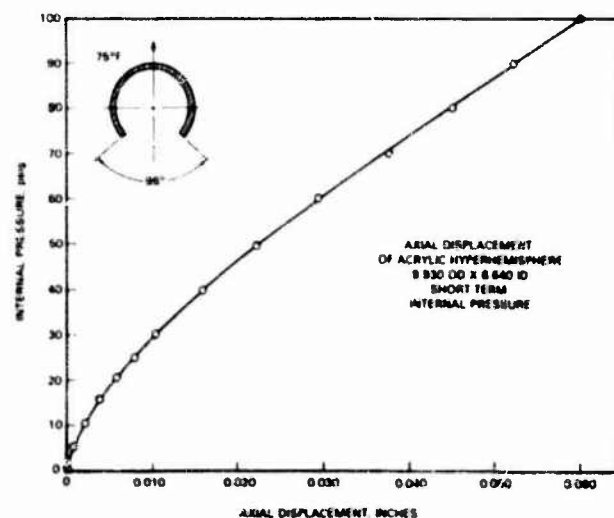


Fig. 11 Axial displacement of acrylic window under internal pressure



Fig. 13 Acrylic plastic viewport assembly after implosion at 4400 psi. Note the twisted split retaining ring and ripped out hold-down screws.

of the nylon reinforced neoprene bearing gasket failed to discover any sign of wear.

Findings

1 Acrylic hyperhemispheres with included spherical angle of ≥ 260 deg designed on the basis of nominal membrane work stress ≤ 4500 psi and equation (1) perform satisfactorily in simulated operational environment provided that:

- (a) the mounting is equipped with a conical seat,
- (b) the conical bearing surface of the window is protected by a 0.020 in. thick nylon reinforced neoprene gasket bonded to the acrylic with contact cement,
- (c) the retaining arrangement consists of internal and external O-rings wedged between the faces of the hyperhemisphere, a split retaining ring, and mounting,
- (d) the circumferential strains on the seat in the mounting under hydrostatic loading are equal to, or less than on the edge of the window,
- (e) the short term critical pressure of the window predicted on the basis of equation (2), or Fig. B-12 in ANSI/ASME PVHO-1 exceeds the working pressure by ≥ 300 percent.

2 Glass hyperhemispheres with included spherical angle of ≥ 260 deg designed on the basis of nominal membrane working stress $\leq 26,000$ psi and equation (1) perform satisfactorily in simulated operational environment provided that:

- (a) The design of the mounting seat and retainer arrangement, is identical, or at least similar to the one described in this paper,
- (b) the circumferential strains on the seat in the mounting under hydrostatic loading are equal to, or larger than on the edge of the window,
- (c) all metallic components of the assembly are fabricated from titanium with yield strength $\geq 120,000$ psi,
- (d) the short term critical pressure of the window predicted on the basis of equation (2) exceeds the working pressure by ≥ 300 percent.

Conclusion

1 A successful mounting has been developed that performs equally well with acrylic or glass hyperhemispheres subjected to typical marine environment in -40 to 120°F ambient temperature range. The model scale viewport assemblies developed in this study performed satisfactorily in the 0 to 12,000 ft depth range.

2 Since the performance of hyperhemispherical acrylic plastic windows can be predicted accurately on the basis of existing extensive experimental data for spherical NEMO hulls, the acrylic hyperhemispheres are considered acceptable for manned service provided that their t/R_s ratio is based on design criteria of ANSI/ASME PVHO-1.

References

- 1 Stachiw, J. D., "Critical Pressure of Conical Acrylic Windows Under Short-Term Hydrostatic Loading," ASME JOURNAL OF ENGINEERING FOR INDUSTRY, Vol. 89, No. 3, 1967.
- 2 Stachiw, J. D., "Conical Acrylic Windows Under Long-Term Hydrostatic Pressure of 5000 psi," ASME Paper No. 71-Unt-A, 1971.
- 3 Stachiw, J. D., "Conical Acrylic Windows Under Long-Term Hydrostatic Pressure of 10,000 psi," ASME Paper No. 71-WA/Unt-3, 1971.
- 4 Stachiw, J. D., "Conical Acrylic Windows Under Long-Term Hydrostatic Pressure of 20,000 psi," ASME JOURNAL OF ENGINEERING FOR INDUSTRY, Vol. 92, No. 1, 1970.
- 5 Stachiw, J. D., "Effect of Temperature and Flange Support on Critical Pressure of Conical Acrylic Windows Under Short-Term Pressure Loading," ASME Paper No. 72-OT-A, 1972, ASME JOURNAL OF ENGINEERING FOR INDUSTRY, Vol. 94, Dec. 1972.
- 6 Stachiw, J. D., "Critical Pressure of Flat Acrylic Windows Under Short-Term Hydrostatic Loading," ASME Paper No. 67-WA/Unt-1, 1967.
- 7 Stachiw, J. D., "Critical Pressure of Spherical Shell Acrylic Windows Under Short-Term Pressure Loading," ASME JOURNAL OF ENGINEERING FOR INDUSTRY, Vol. 91, No. 3, 1969.
- 8 Stachiw, J. D., "Spherical Acrylic Pressure Hulls for Undersea Exploration," ASME JOURNAL OF ENGINEERING FOR INDUSTRY, Vol. 93, No. 2, 1971.

- 9 Stachiw, J. D., and Maison, J., "Flanged Acrylic Plastic Hemispherical Shells for Undersea Applications," ASME Paper 73-Oct-A, 1973.
- 10 Stachiw, J. D., and Sletten, K., "Flanged Acrylic Plastic Hemispherical Shells for Undersea Systems—Part II—Static and Cyclic Fatigue Life Under Hydrostatic Loading," ASME JOURNAL OF ENGINEERING FOR INDUSTRY, Vol. 100, No. 2, pp. 249-260.
- 11 Stachiw, J. D., Smith, N. E., and Burnside, O. H., "Structural Performance of Acrylic Plastic Plane Disc Windows with Twin Conical Bearing Surfaces," ASME JOURNAL OF ENGINEERING FOR INDUSTRY, Vol. 100, No. 2, pp. 273-286.
- 12 Stachiw, J. D., and Dolan, R. B., "Spherical Acrylic Pressure Hulls With Multiple Penetrations," ASME JOURNAL OF ENGINEERING FOR INDUSTRY, Vol. 100, No. 2, pp. 261-272.
- 13 ANSI/ASME PVHO-1 Safety Standard, "Pressure Vessels For Human Occupancy," 1977.
- 14 Stachiw, J. D., and Burnside, O. H., "Acrylic Plastic Spherical Shell Windows Under Point Impact Loading," ASME Paper 75-WA/Oct-6, Winter Annual Conference, 1-5 Dec. 1975, Houston, Texas.
- 15 Stachiw, J. D., "Spherical Acrylic Plastic Hulls Under External Explosive Loadup," ASME JOURNAL OF ENGINEERING FOR INDUSTRY, Vol. 99, No. 2, 1977.

APPENDIX

Definition of Technical Terms

Window, or Lens = transparent, impermeable, and pressure-resistant insert in the viewport assembly.

Viewport = penetration in the pressure hull equipped with an impermeable and pressure-resistant transparent window that is seated in a mounting and held in place by a bolted-on or screwed-on retaining ring.

Acrylic = methyl methacrylate plastic possessing physical and mechanical properties shown in Tables A-1 and A-2 of the ANSI/ASME PVHO-1.

Short term loading = increasing the hydrostatic pressure at 650 psi/min rate.

Short term critical pressure = pressure at which catastrophic failure of the window occurs when subjected to short term hydrostatic loading at 75°F ambient temperature.

Long term loading = pressurizing the window to specified pressure at 650 psi/min rate and maintaining the pressure for specified number of hours.

Cyclic loading = pressurizing the window repeatedly to specified pressure at 650 psi/min rate, maintaining this pressure for a specified number of hours, depressurizing at 650 psi per min to 0 psi, and allowing the window to relax for a specified number of hours before repeating the procedure.

Strain = unit deformation, in./in. of original length.

Relaxation = time dependent restoration of material to its original dimensions under absence of external loading; in./in. of original length.

Creep = time dependent deformation of material under sustained loading of constant magnitude; in./in. of original length.

Hoop orientation of strains or stresses = direction parallel to the edge of spherical sector window.

Meridional orientation of strains or stresses = direction at right angle to the hoop direction.

Total strain = total deformation of material, includes both the short term and creep components of strain, in./in. of original length.

Short term strain = deformation of material under short term loading, in./in. of original length.

Radial displacement = displacement of the interior surface at the apex of the hemisphere.

Normalized strain = strain per unit increase of pressure under short term loading, (in./in.)/psi.

Normalized stress = stress per unit increase of pressure under short term loading.

Conversion factors = psi = 0.00689 megapascals, in. = 2.54 centimeters, MPa = megapascal = 145 psi.

DISCUSSION

J. L. Atkerson¹

Introduction

The author needs to be commended for a very timely paper on hyperhemispherical viewports. The paper presents valuable design information not only on acrylic viewports that serve as pressure-resistant conning towers with panoramic visibility for manned submersibles, but also on glass viewports that serve as pressure housings with panoramic visibility for television cameras mounted on top, below, or in the rear of the submersibles. Either way, the hyperhemispherical windows described in this paper complement the forward visibility provided to the crews of modern submersibles by the spherical sector bow windows (developed by Dr. Stachiw in 1968). The data described in this paper have already been utilized in the design of a hyperhemispherical conning tower for Mermaid VI submersible.

Discussion

Although the author covered the technical subject adequately, the physical constraints imposed by the length of the paper forced him to omit experimental data that are of great potential value to the researcher into the effect of penetrations on the distributions of strains and stresses in spheres of viscoelastic material. Thus, to complement the paper the omitted experimental data have been reviewed and are presented here in the form of a brief summary.

Penetrations as Stress Raisers in Plastic. Circular penetrations in spherical shells serve as sources of serious stress concentrations when the reinforcement around the penetration is significantly stiffer than the material of the shell that it replaces. This is particularly the case with acrylic plastic spherical shells under external pressure where the opening has been reinforced with a metallic flange that is significantly stiffer than the acrylic plastic which it replaces.

If the acrylic plastic was a perfectly elastic material with linear strain response, the magnitude of meridional stress on the interior surface of the shell in contact with the metallic flange would be 4 to 5 times higher than the nominal membrane stress measured on the interior apex of the sphere (Reference 8). Fortunately the response of acrylic plastic to biaxial compressive stresses is only linear in the 0 to 10,000 microinches/inch range under short term loading, and 0 to 5000 microinches/inch range under long term sustained loading (Reference 8). At higher strain levels the response of acrylic plastic to compressive biaxial stress becomes markedly non-linear, both with respect to imposed stress, and duration of loading.

As a result of this non-linear and viscoelastic behavior, the inner edge of the conical penetration in acrylic shell deforms at a non-linear rate without generating excessive stresses in acrylic plastic around the penetration. Figs. 13 and 14 show the results of this response to overstressing at the edge of penetration under short term loading. Thus, while the stresses on the interior surface of the sphere at the apex increase linearly with pressure under short term loading those near the penetration do not. If the graph of the meridional stress at interior edge of penetration was to be extrapolated along the slope seen at the beginning of pressurization, the maximum stress at 1000 psi pressure would have been 20,000 psi (stress concentration of approximately 5) instead of 4500 psi (stress concentration of approximately 2.25). It is only because of local deformation of the penetration's inner edge that the magnitude of stresses in acrylic plastic near the edge remains within acceptable limits.

The amelioration of peak stress near the edge of penetration is further extended under sustained long term loading. Comparison of

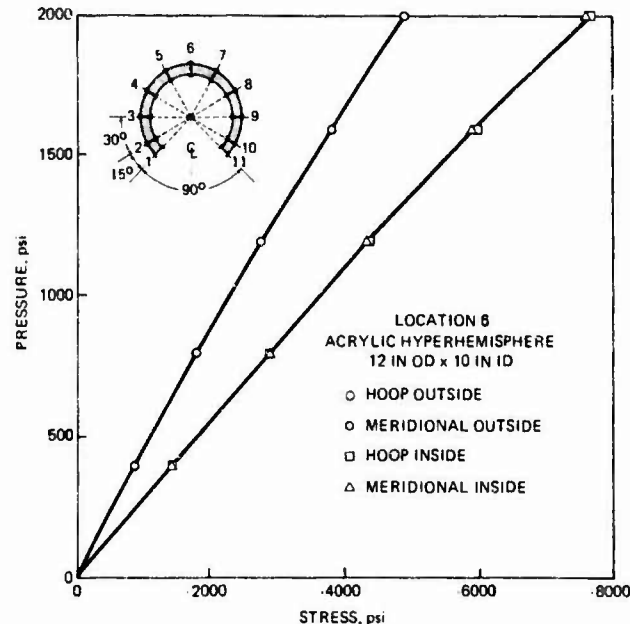


Fig. 13 Membrane stresses at the apex of the acrylic hyper-hemisphere under short term hydrostatic loading. Note the linearity of stress on both exterior and interior surfaces.

Figs. 15 and 16 shows clearly that while the hoop and meridional strains on the interior surface of the sphere at the apex shows only a small amount of creep, the meridional strain near the edge shows a very significant amount of creep, while the hoop strain shows none. This is as it should be, since the rotation of the sphere's edge in contact with the metallic flange generates very high forces along meridional axis and none in the hoop direction.

Although the high modulus of elasticity commonly found in transparent brittle materials (glass, sapphire, quartz, etc.) makes it easier to match the membrane strains in the window with the hoop strains in the metallic mounting extreme care must be taken that this match is perfect, or if this is not feasible, that the hoop strains in the mounting are higher than the membrane strains in the hyperhemispherical window. If this is not done, the meridional compressive stress on the interior surface of these perfectly elastic and brittle windows at the edge of penetration will be 4 to 5 higher than the membrane stress. As a result of this high stress concentration the safe operational

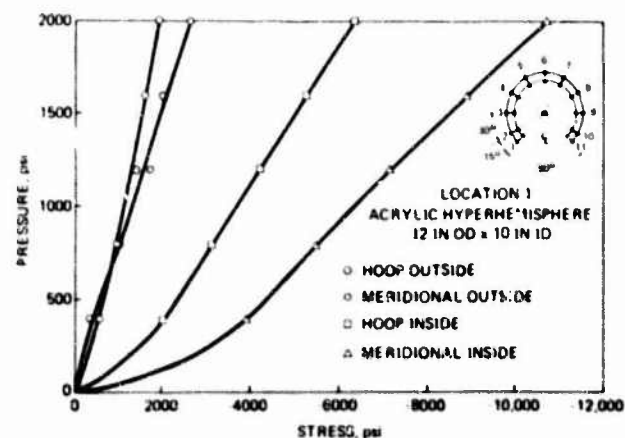


Fig. 14 Combined stresses at the edge of penetration in acrylic hyper-hemisphere under short term hydrostatic loading. Note the nonlinearity of stresses on the interior surface, indicating local, nonlinear, elastic deformation at the inner edge due to large bending movement.

¹P.O. Box 2343, El Cajon, CA 92021.

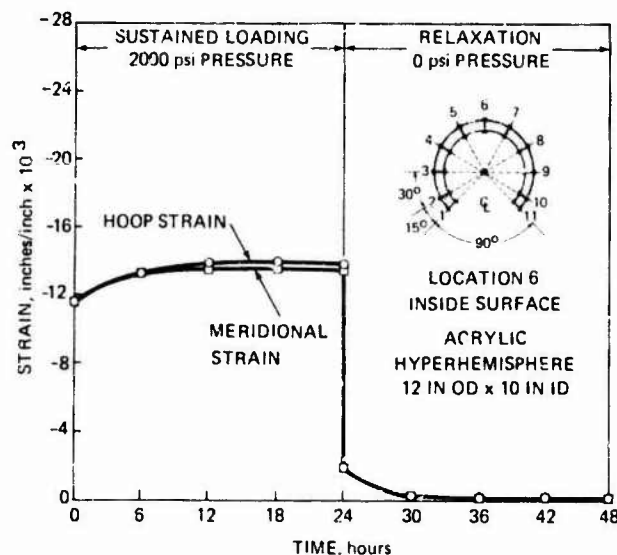


Fig. 15 Membrane strains at the apex of the acrylic hyperhemisphere under long term hydrostatic loading. Note that there is very little creep at this location, and that it is of the same magnitude in both meridional and hoop directions.

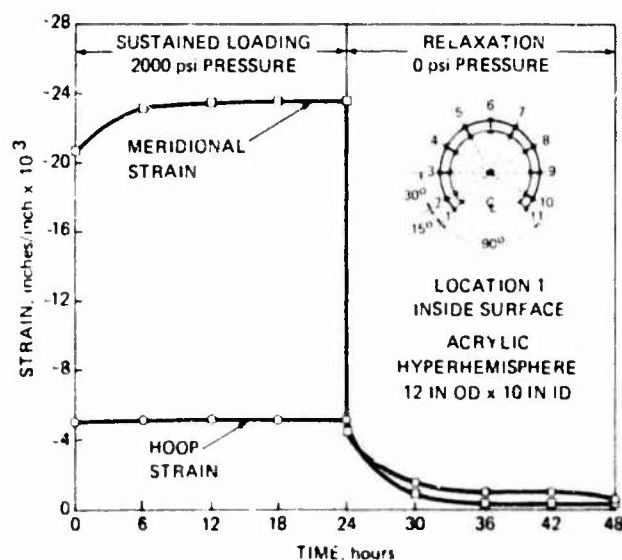


Fig. 16 Combined stresses at the edge of penetration in acrylic hyperhemisphere under long term loading. Note the large elastic creep in meridional direction and the total absence of creep in hoop direction indicating local elastic creep of the inner edge due to large bending moment.

depth of the glass window would not be significantly higher than of an acrylic window with identical dimensions even though the compressive strength of glass is an order of magnitude higher than of acrylic plastic.

It is only because the titanium mounting, shown in Figs. 3 and 4, had a higher circumferential strain than the membrane strain in a glass hyperhemisphere that Dr. Stachiw was able to reach 10,000 psi pressure without failure or initiation of cracks. If steel (which has a modulus of elasticity twice as large as titanium) is substituted for titanium in that mounting implosion of the window would occur below 10,000 psi. If a material with modulus of elasticity in the 30×10^6 to 50×10^6 psi range (i.e., sapphire) was substituted for glass in the hyperhemisphere a steel mounting would probably be found to be just right.

Conclusion

Acrylic plastic is well suited for construction of hyperhemispherical windows in manned submersibles as the nonlinear, but still elastic, response of acrylic plastic to compressive stresses allows the use of metallic mountings, which are significantly stiffer than acrylic plastic hyperhemispherical windows because the peak compressive stress in the acrylic plastic at the edge of penetration rises only about 100 percent above the membrane stress on the interior of the window at its apex.

The use of mountings that are significantly stiffer than the windows provides the designer of the submersible with more design options, and requires simpler calculations than mountings whose stiffness has to match the stiffness of the window exactly. This reason, in addition to the lower cost of acrylic plastic, make the acrylic plastic rather than glass hyperhemispheres a cost-effective solution to applications where a pressure-resistant dome of transparent material is required for depths less than 1000 meters (3280 feet).

Author's Closure

The discussion presented by J. L. Atkerson is a very valuable contribution to the paper as it highlights the difference in responses of acrylic and glass hyperhemispheres to penetrations supported by rigid mountings with conical seats. The discussion reinforces well the main point of the paper: the radial displacement of the mounting for acrylic hyperhemisphere must be equal to or less than that of the plastic that it replaces, while the displacement of the mounting for a hyperhemisphere made of brittle material (i.e., glass, quartz, sapphire, germanium etc.) must be equal to or larger than that of brittle material that it replaces. Since it is easier and less expensive to design and fabricate such mountings for acrylic plastic hyperhemispheres the use of acrylic plastic for hyperhemispheres with maximum design depth of less than 3280 feet (1000 meters) is a more cost effective solution than the application of brittle material like glass.

The author deeply appreciates the time and effort expended by J. L. Atkerson in preparation of this excellent discussion.



380 E. 47 St., New York, N.Y. 10017

The Society shall not be responsible for statements or opinions advanced in papers or in discussion at meetings of the Society or of its Divisions or Sections, or printed in its publications. Disposition is printed only if the paper is published in an ASME Journal. Papers are available from ASME for fifteen months after the meeting.

Printed in USA

The Origins of Acrylic Plastic Submersibles

JERRY D. STACHIW, Fellow ASME

Ocean Engineering Division

Naval Ocean Systems Center

San Diego, CA 92152-5000

ABSTRACT

The research submersible NEMO, launched and certified in 1970 by the U.S. Navy, represents the first seaworthy, deep diving, one atmosphere environment, diving system which utilizes a pressure hull fabricated from transparent acrylic (polymethyl methacrylate) plastic. Its pressure hull is the culmination of (1) research into the structural performance of acrylic plastic spherical shells under long term cyclic external pressure loading, (2) development of economical fabrication techniques for acrylic plastic spheres with uniform curvature and thickness. Since the launching of NEMO many other submersibles with acrylic plastic pressure hulls have been built and successfully operated in the 0 to 3270 feet (0 to 1000 meter) depth range.

INTRODUCTION

Although men have been diving in the oceans since time immemorial, they were doing it either for food, pearls, sponges, or shipwrecked treasures. It is only recently however, that a concerted effort has been made to explore the ocean and exploit its riches by having scientists and engineers descend into hydrospace, protected from the hostile environment by one atmosphere enclosures with life supporting environment.

The fearless explorers that pioneered in this area were William Beebe (Reference 1), Otis Barton (Reference 2) and Auguste Piccard (Reference 3). At great personal risk and expense they developed in the short time span between 1930 to 1950 bathyspheres and bathyscaphs that allowed them to descend several thousand feet into the ocean and observe salt water animals never described before (Figure 1). Their observations were, however, limited by the small size of

viewports incorporated into pressure resistant opaque metallic hulls of their bathyspheres and bathyscaphs (three viewports with 6 inches inside diameter in Barton's Bathysphere, and a single 4 inches inside diameter viewport in Piccard's Bathyscaph TRIESTE).

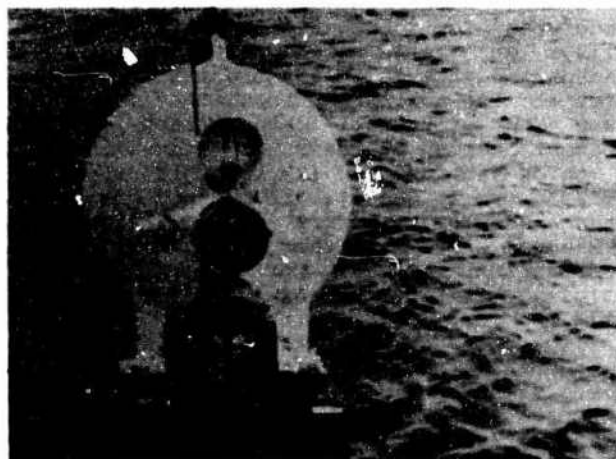


Figure 01 Otis Barton's Bathyscope with two 6 in. inside diameter fused quartz viewports in which he successfully dove to 4500 feet depth offshore California during 1949.

The explorers who followed in the pioneers footsteps had at their disposal submersibles that were significantly more agile, and comfortable. Furthermore, they were equipped with manipulators that scientists could use to collect mineral and live specimen for further study in their shipboard laboratories. Still, the size of the viewports had remained approximately the same from 1950 to 1970, as the shape of

viewports and materials used in their construction remained unchanged since the days of Beebe, Barton and Piccard. This bottleneck in pressure hull design for diving systems had to be eliminated if exploration of hydrospace had to proceed beyond the operational constraint set by individual viewports with less than 90 degree field of vision for a single observer.

Attempts were made to overcome this limitation by brute force approach: the number of viewports in pressure hulls proliferated, each covering a small field of view around the bow of the submersible. Unfortunately, this did not resolve the problem, as the scientist's field of view through his viewport did not overlap the pilot's field of view through the pilot's viewport, or vice versa. Ultimately it dawned upon the vehicle designers that this problem could be resolved satisfactorily only by making either a large section, or the complete pressure hull from a transparent material. In a pressure hull fabricated totally, or partially, from a transparent material both the pilot and the scientist, or several scientists would be viewing together the same panorama outside the vehicle, and direct the pilot from the comfort of their contoured seats to gather specimens outside the hull.

A practical solution to this problem required the availability of (1) inexpensive, transparent material with reliable engineering properties, (2) proven designs of entire pressure hulls, or their components from a transparent material with predictable structural performance, and (3) economical procedures for fabrication of entire pressure hulls, or large sections thereof from transparent material. In the search for such material the attention immediately focused on glass and polymethyl methacrylate (acrylic plastic) because of their (1) optical clarity in thick sections and (2) low intrinsic cost (References 4 and 5). It did not take very long, however, before massive glass was eliminated from further consideration as construction material for large, panoramic visibility viewports, or complete pressure hulls.

The reason for it were both of engineering and economic nature. Massive glass was found to be very sensitive to internal flaws and surface imperfections, making it very expensive to devise a quality assurance program that would qualify it for service as structural components in pressure hulls of diving bells, habitats or submersibles. Furthermore, the cost of fabricating large, high quality massive glass components with optical surface finish was found to be beyond the reach of individual entrepreneurs or oceanographic research institutions with meager budgets. And thus, unless the U. S. Congress was willing to create a new agency for exploration of hydrospace with a budget matching that of NASA, massive glass for undersea structures would remain forever a desirable wonder material, outside the scope of consideration for designers of manned submersibles.

By the middle of nineteen sixties it became apparent that the US Congress was not favorably disposed to creation of such an agency and that the required funding would not be forthcoming from other potential sources (i.e. U. S. Navy, or large glass companies like Corning Glass etc). Based upon the above realistic evaluation of the situation private entrepreneurs, oceanographic research institutions and Navy laboratories directed their attention to clear acrylic plastic as the potential structural material for undersea vehicles with panoramic visibility.

With the shift in focus from glass to acrylic plastic as the potential structural material came also a change in the projected operational scope for the undersea vehicles. Instead of concentrating on the scientific exploration of abyssal depths and establishing dive records the objective shifted to exploitation of the continental shelves for economic, or defense purposes. The scene was now set for the appearance of a new generation of submersibles that would extensively utilize acrylic plastic in their construction, so that the crews would utilize fully their sense of vision in the performance of scientific and engineering tasks.

EARLY EXPERIMENTS WITH ACRYLIC STRUCTURES

When the attention of ocean engineers began to focus on acrylic plastic as the potential structural material for undersea vehicles with panoramic visibility the state of technology encompassing massive acrylic plastic was in its infancy.

Supply of massive acrylic plastic was limited to 4 inches thick x 48 x 60 sheets cast from monomer resin between glass plates, and there was very little hope for the availability of thicker, or larger sheets as the duration of monomer resin polymerization process rapidly became uneconomical for thicker sheets.

The strength of massive acrylic plastic under cyclic and long term compressive loading was not defined in terms of allowable design stresses, as up to this time massive acrylic plastic has not been utilized in structures under cyclic compressive loading.

The structural performance of spherical pressure hulls made from massive acrylic plastic was not understood, particularly the (1) effect of creep upon elastic stability of shell structures and the (2) recuperation of the material after removal of the hydrostatic pressure from the shell.

The fabrication of spherical shells was limited to free forming of small hemispheres with compressed air from thin acrylic sheets. The small sizes of available sheets in thickness over 2 inches, and uneven reduction in thickness during the free forming process limited the maximum size of spheres to less than 60 inches, and actual wall thickness to less than one inch.

The early acrylic pressure hulls for diving systems were severely restricted in size and depth because of the immature state of massive acrylic plastic technology. And

yet, even with all their structural and operational limitations the first acrylic spheres built for diving systems displayed to the ocean engineering community the advantages of panoramic vision from one atmosphere pressure hulls for diving systems.

For the first time in the history of ocean exploration the occupants of one atmosphere diving systems could utilize their sense of vision unhampered by opaque enclosures and thus maximize the operational value of the dive duration. The diving systems with the all-acrylic pressure hulls, which demonstrated to the ocean engineering community the potential of panoramic visibility were HIKINO, KUMUKAHI, and NUCOTE.

HIKINO was conceived in 1962 by the late Dr. W. McLean and engineered by D. K. Moore of Naval Ordnance Test Station, China Lake, CA. The two-person vehicle had the shape of a catamaran with the acrylic sphere suspended between the two hulls (Figure 2). Flooding of ballast tanks in the catamaran hulls controlled the buoyancy of the vehicle. Cycloidal propellers mounted on the catamaran hulls provided the vehicle with mobility along three axis of travel. The acrylic sphere itself was assembled from two hemispheres mated at the equator to a metallic joint ring. A clamshell arrangement allowed ingress and egress from the sphere by its crew.

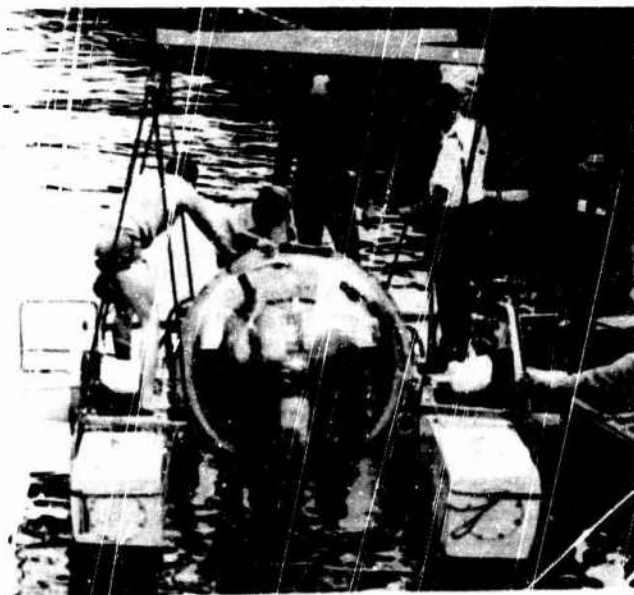


Figure 02. Dr. W. McLean's HIKINO, the first concept of a submersible with panoramic visibility undergoing pierside testing during 1965.

The vehicle demonstrated successfully the design concept of panoramic visibility and triaxial mobility. However, because of thin spots in the free formed acrylic hemispheres their design depth was less than 20 feet, and because of it the operation of the vehicle was restricted to reservoirs and lakes with less

than 20 feet depth. As a result of its severe operational depth limitation HIKINO was subsequently used only as a concept demonstrator. It was never certified by the Navy and finished its career as a museum display.

KUMUKAHI was conceived in 1967 by T.A. Prior, engineered by W. R. Forman, fabricated by Fortin Plastics, and delivered to Oceanic Institute of Hawaii in September 1969 (Reference 6). The 3700lb submersible was configured as a self propelled diving bell with the batteries and a variable displacement tank contained in a pod suspended directly under the sphere (Figure 3). The 56 inch OD acrylic pressure hull was fabricated by thermoforming 1.25 inch thick acrylic sheets into flanged spherical quadrants inside a female/male mold assembly. The use of a clamped mold assembly resulted in a thickness reduction of only 8 percent at the center of each sector. The quadrants were subsequently bonded together with acrylic adhesive, an opening was cut out at the top of the sphere, and the edge of the opening was reinforced with adhesive impregnated glass fiber tape. An acrylic spherical hatch cover, whose edges were also reinforced with adhesive impregnated glass fiber tape completed the spherical hull. Six electric motor driven propellers provided the vehicle with triaxial mobility at approximately 1 knot.



Figure 03. KUMUKAHI the first acrylic plastic submersible to perform open sea dives in 1967.

KUMUKAHI experienced extensive manned operational evaluation at snorkel diver depth, and unmanned structural testing to 350 and 450 feet depths in the open sea off Poka Bay on Oahu Island. The recorded strains indicated that there was no permanent deformation in the 0 to 350 feet depth range during 10 successive 30 minutes long dives, and therefore the pressure hull appeared to be safe for manned dives to 300 feet. Unfortunately, at the completion of the 6 hour long unmanned proof

test dive to 450 feet the submersible was smashed against the support ship and the acrylic pressure hull damaged. After repair to the pressure hull the submersible saw some limited service to 90 feet, however it was never certified by the Navy, or American Bureau of Shipping for commercial use.

NUCOTE was conceived in 1969 by E. Rosenberg and engineered by Mike Cook and Ron Reich at the Naval Undersea Center, San Diego, CA. The diving system consisted of a ballasted acrylic sphere suspended by cable from an overhead winch on the NUC offshore tower (Figure 4). Air was supplied to the sphere by a flexible tube from the tower. The vertical movement of the undersea elevator was controlled from the interior of the sphere by its occupants. The two man capsule was assembled from two acrylic hemispheres fastened to metallic equatorial rings that served as a mechanical equatorial joint (Reference 7). The 54 inch OD flanged hemispheres were freeformed by Fortin Plastics from 2 inch thick sheets that thinned out to 0.91 inches at the poles of hemispheres. The hemispheres were fastened to equatorial steel rings by clamping the acrylic flanges of the hemispheres between the steel equatorial rings and the steel retaining rings bolted to them. The pressure hull saw extensive hydrostatic testing to 100 psi pressure at Southwest Research Institute before it was placed in operation at the NUC offshore tower to a depth of 56 feet in 1973. After two years of operation it was taken out of service and placed in storage.



Figure 04. NUCOTE, underwater acrylic plastic elevator installed in the Naval Ocean System's offshore tower at La Jolla, California during 1971.

The first generation of diving systems with acrylic pressure hulls, like flowers in the spring, had a very short operational life, but it alerted the ocean engineering community to (1) the potential of acrylic plastic as an

optically clear structural material and (2) to the operational advantages of panoramic visibility for operators of one atmosphere diving system. The pioneers who conceived these diving systems and personally piloted them during seatrials deserve the thanks of the ocean engineering community as their example widened the operational and engineering horizons for all ocean engineers.

Still, successful as the individual acrylic plastic hulls may been in their application, they were not copied and applied to the following diving systems by other designers. The major reasons for it were (1) shallow design depths and small sizes, resulting from the inability of the chosen fabrication processes to produce larger, thicker spherical shells, (2) absence of published design and test data applicable to larger acrylic spheres and greater depth, and (3) lack of approval for acrylic plastic pressure hulls by the U. S. Navy, American Bureau of Shipping, Lloyd's Register of Shipping, or Det Norske Veritas.

Clearly with this stagnant state of affairs the pioneering momentum of HIKINO, KUMUKAHI, and NUCOTE appeared to have been lost, a flash in the pan, to be followed by years and probably decades of inactivity in the area of acrylic plastic pressure hulls. It remained for DSV NEMO to generate the needed additional momentum that would put acrylic plastic pressure hulls over the top of acceptance barrier in the mind of ocean engineers, and to place acrylic plastic among other, already proven pressure hull materials like steel, aluminum, or titanium.

THE CONCEPT OF NEMO

NEMO (Naval Edreobenthic Manned Observatory) had its origin at the Naval Missile Center, Point Mugu, CA. It is there that Richard G. McCarty and James G. Moldenhauer conceived in 1964 NEMO, a self propelled underwater observatory capable at will to move about in hydrospace until a desirable location was found for detailed study. At that time NEMO would deploy a gravity anchor and by winching itself up or down along the tether it would function as a powered underwater elevator (Figure 5). By maintaining a fixed position with respect to its anchor location, and at the same time being able to traverse vertically the water column above the anchor made NEMO an ideal vantage point for the study of marine animals that periodically migrate upwards or downwards in response to water temperature, phase of the moon, location of the sun, or other environmental factors. Since the quality and quantity of data collected by such an observatory would depend primarily on the ability of the investigators to observe unhindered the hydrospace around the observatory a transparent enclosure would be the ideal solution to this operational requirement.

When the inventors of this concept contacted Corning Glass and Rohm and Haas, leaders in their respective fields, about the feasibility of fabricating a glass or plastic spherical pressure hull capable of

transporting two men to a depth of 1000 feet they were told that such a structure was outside the scope of existing massive glass and acrylic plastic technologies. Only if the Navy was willing to sponsor a multimillion dollar program spanning many years would they promise to deliver such a structure. Since the Navy was not interested in sponsoring a program of such a magnitude the inventors had to regroup and consider other, preferably low cost approaches to fabrication of the 120 inch large transparent spherical pressure hull for their underwater observatory.

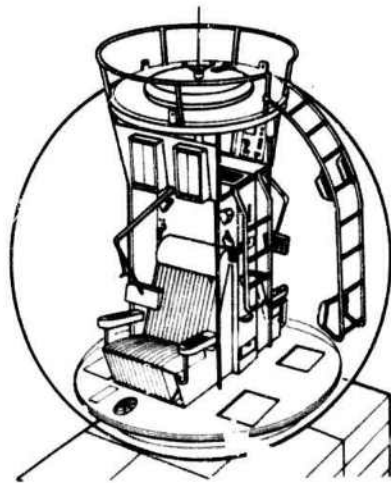


Figure 05. Jim Moldenhauer's concept of NEMO, a 120 inch diameter underwater observatory with panoramic visibility, proposed in 1964.

While researching the problem Moldenhauer ran across two Ordnance Research Laboratory Technical reports published in 1964 by the Pennsylvania State University (Refs. 8,9). In these publications a young structural materials investigator Dr. Jerry D. Stachiw had experimentally shown that (1) acrylic plastic is a suitable engineering material for external pressure hulls, (2) large acrylic pressure hulls can be assembled from small structural modules, (3) the implosion pressure of such hulls did not depend upon the strength of the adhesive bonded joints, provided that the compressive stresses were transferred at right angles across the mating surfaces of the joint, (4) the short term implosion pressure of acrylic hulls can be calculated with classical analytical formulas for buckling of shells if the magnitude of tangential modulus of elasticity is considered to be a function of compressive stress in the shell, and the (5) ideal shapes of structural modules for construction of spherical shells are the equilateral spherical triangle and the spherical pentagon (Figure 6).

Intrigued by these findings the inventors of NEMO tried to contact the author of these reports for further details. To their great surprise he was found nearby at

the Naval Civil Engineering Laboratory in Port Hueneme Co., where he had accepted employment in 1964 after graduation from the Pennsylvania State University. Since Port Hueneme was practically next door to Pt. Mugu a personal meeting was arranged between Moldenhauer, a physicist turned oceanographer and Stachiw, an engineering mechanics graduate turned ocean engineer, that laid the foundation for the engineering development of the NEMO concept. They were soon joined by Kiyoshi Tsuji and Dan T. Stowell, engineers, also employed at the Pacific Missile range. Due to the combined efforts of these individuals the NEMO concept began to be transformed from an idea into engineering design.

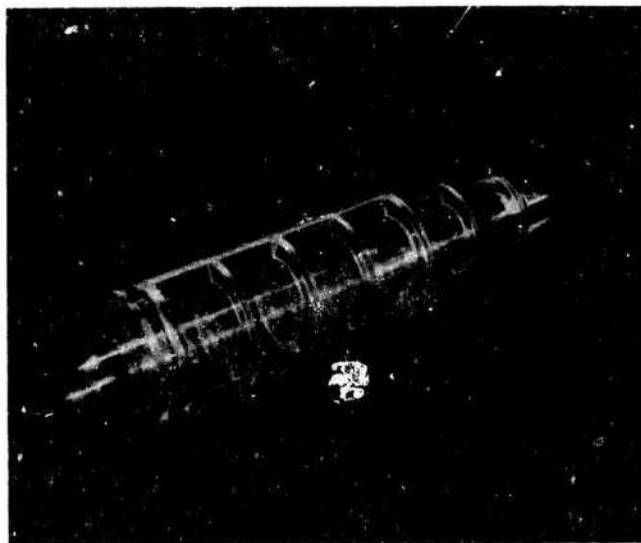


Figure 06. Acrylic plastic housing for oceanographic instrumentation designed for 1000 feet depth by Dr. Stachiw in 1961 while at the Pennsylvania State University. The cylinder is made up of two rib stiffened halfshells sealed by an axial mechanical joint.

Several important problems had to be resolved before NEMO could be launched with a crew in the ocean:

1. A reliable, but economical fabrication technique had to be developed that performed well not only for the construction of scale models, but also for full scale spherical hulls.
2. A proven design for the hull assembly had to be formulated which incorporated into the plastic sphere a metallic hatch for ingress and egress of the crew, and a metallic bulkhead for feedthrough of electrical cables, hydraulic piping and compressed air tubes.
3. The acrylic plastic sphere had to be qualified for manned service to the satisfaction of the Naval Ship Systems Command; the Navy

authorized safety inspector for certification of non-combatant submersibles.

4. Life support, and a propulsion system had to be selected, and mated with the acrylic hull assembly without imposing additional stresses in the acrylic hull.

To facilitate the solution of above problems they were parcelled out to different investigators. Tsuji and Stowell worked on the development of fabrication processes, sizing of life support components and selection of propulsion components. Stachiw devoted his efforts to the design and subsequent evaluation of the model scale and full scale acrylic hull assemblies, and Moldenhauer concentrated his endeavors on the definition of scientific mission objectives for the NEMO.

Each of the components being considered for incorporation into NEMO presented an engineering challenge. The acrylic hull assembly however, posed the toughest challenge of all. Unless the design, fabrication process and structural performance met the U. S. Navy Material Certification Procedures and Criteria Manual for Manned Non-Combatant Submersibles NEMO would never see service in support of Navy missions. Since the Navy had never certified before a diving system with a non-metallic pressure hull the qualification of acrylic plastic as an approved structural material for NEMO would constitute a landmark in the development of Navy's manned non-combatant submersibles. Because the certification of the acrylic hull assembly constituted such a critical element in the realization of the NEMO concept the bulk of available funding during the 1964 - 1969 period was budgeted for the design, fabrication and testing of acrylic hull components.

NEMO PRESSURE HULL DESIGN VALIDATION

As a result of the intensive engineering effort at both NEMO and NCEL a successful hull design was formulated in September 1964, and the first 15 inch OD model scale hull assembly fabricated in January 1965 (Fig. 7). The structural scale model consisted of 12 spherical sectors thermoformed in a female vacuum mold from 0.5 inch thick acrylic discs and subsequently machined into spherical pentagons. Two of the pentagons had beveled openings machined in their center to receive stainless steel hatch and bulkhead assemblies with matching beveled edges. The spherical pentagons, were placed subsequently into an alignment fixture and bonded with solvent injected into the joints with a hypodermic needle. When tested at the NCEL's Deep Ocean Test Facility the 15 x 14 inch spherical hull (1) displayed no permanent deformation after a simulated dive of 5 days duration to 420 feet depth (Figure 8) and (2) it imploded during a simulated dive only after attaining a depth of 3650 feet, predicted by prior analytical calculation of plastic instability.

Encouraged by these results additional twenty 15 x 14 inch scale models were built and tested to destruction under short term, cyclic, and sustained pressure loadings.

These models were identical to the first one except in order to improve the joint quality the gap width between spherical pentagons was increased to 0.125 inches. This gap was subsequently covered with adhesive backed aluminum tape, and filled by gravity through a funnel with self polymerizing adhesive cement (Reference 10).

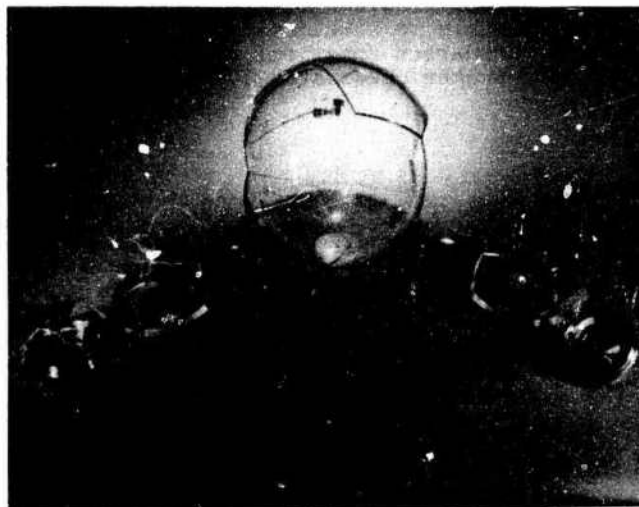


Figure 07. Components of the 15 x 14 inch structural scale model of acrylic plastic pressure hull for NEMO designed by Dr. J. D. Stachiw at the Naval Civil Engineering Laboratory, and fabricated under the supervision of K. Tsuji at the Naval Missile Center, Pt. Mugu, CA in 1964.

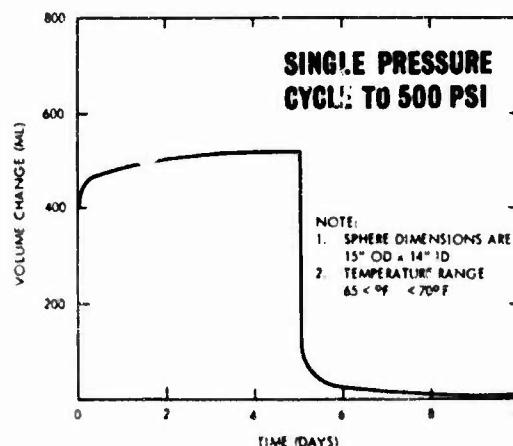


Figure 08. Volume displacement plot generated during the hydrostatic testing of NEMO scale model. Note that the pressure hull returns to its original shape following depressurization and relaxation.

After two years of pressure testing twenty spherical 15 x 14 inch scale models that required 3000 hours of pressure vessel time the NEMO type design of acrylic plastic spheres was considered to be ready for transitioning to full scale construction. The experimental data showed that the structural behavior of acrylic spheres with less than 0.5 percent spherical deviation and 3 percent local thinning out due to thermoforming was repeatable. The major findings were:

- a. The short term implosion depth can be predicted in advance on the basis of analytical calculations.
- b. The time dependent implosion at any dive depth can be predicted far in advance on the basis of an empirically generated linear plot on log-log coordinates of implosion pressure versus duration of loading.
- c. The crack free cyclic fatigue life is in excess of 1000 dives if the maximum dive depth is less than 33 percent of the short term implosion depth and the relaxation periods between individual dives equal, or surpass the duration of individual dives.
- d. The effect of temperature on implosion depth can be predicted from empirically generated graphic plot relating temperature to implosion pressures.

The fabrication of the full scale NEMO, hull was initiated in 1967 and completed in 1968 at NMC Point Mugu, CA. The outside diameter of the sphere was 66 inches, the largest size that could be achieved assembling 12 pentagons formed and machined from standard 48 x 60 inch acrylic sheets with 2.5 inch nominal thickness (Fig. 9). The design of the full scale hull assembly and the fabrication procedures were the same as in the scale model hulls to insure reproducibility of structural performance (Ref. 11).

The quality assurance procedures instituted during the fabrication produced a hull whose sphericity and uniformity of thickness matched that of the 15 inch scale models (Fig. 10). The thinning out due to thermal forming was less than 2 percent and the deviation in sphericity less than 0.5 percent at the center of each pentagon. The completed sphere deviated less than 0.5 percent from the ideal 33 inch radius of sphericity. The fit between the machined metallic components and the acrylic hull was very good; the mismatch between the bevel angle on the hatch and the opening in the hull was less than 0.5 degree. The resulting 66 inch hull assembly was in all respects a scaled up copy of the 15 inch model (Figure 9), and its structural performance, provided there was no material scaling factor involved, (like for example in glass), would be identical to that of the scale models. If the test results supported this hypothesis the last obstacle in the mind of the safety review members would be removed to the utilization of acrylic plastic in the construction of pressure hulls for manned diving systems.

After being pressure cycled 104 times in the 500 to 1140 psi range the 66 inch NEMO was imploded at 1850 psi during a simulated rapid descent at 220 feet/second rate. This test confirmed the basic postulate of the material qualification program:

Experimental data generated with 15 inch scale model spheres is directly applicable to 66 inch full scale spheres (i.e. large thick acrylic spheres behave identically like small, thin acrylic spheres with the same t/Do ratio).



Figure 09.

Full size 66 x 51 inch NEMO hull fabricated by the Naval Missile Center in 1967 and tested to implosion at the Naval Civil Engineering Laboratory in 1969 under the supervision of Dr. Stachiw.

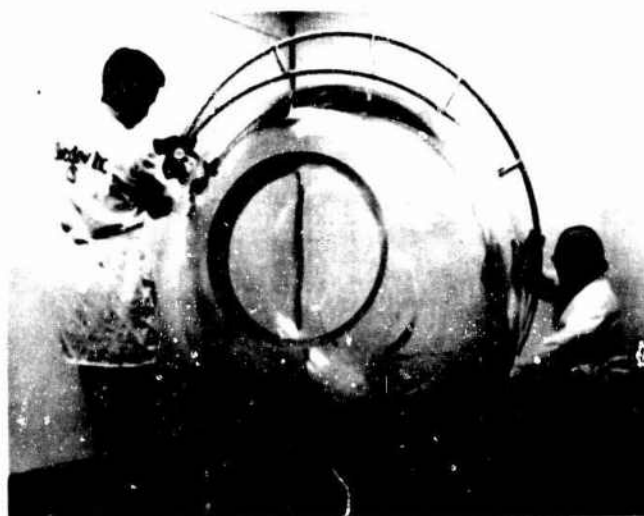


Figure 10.

Checking the dimensions of a finished 66 inch diameter NEMO hull.

NEMO DIVING SYSTEM

As soon as the pressure testing of the first full scale NEMO pressure hull was completed a patent disclosure was filed (Fig. 11) and proposals were submitted to various Navy Bureaus (present name: Commands) for funding of the NEMO diving system. Only the U.S. Navy Bureau of Yards and Docks (present name NAVFAC; Naval Facilities Engineering Command) promised financial support, provided that (1) the diving system is modified to serve as a diving superintendent's office on underwater construction sites employing divers (Figure 12) and (2) the pressure hull assembly is standardized to serve as a self contained multipurpose one atmosphere cockpit for a variety of underwater construction equipments (Figures 13).

The contract for the construction of one NEMO system for NAVFAC was awarded in 1969 to the Southwest Research Institute, and a separate contract for fabrication of three 66 x 51 inch acrylic pressure hulls to Swedlow Inc. One of those hulls was slated for incorporation into NEMO system, one for cyclic pressure testing at NCEL, and one was to be delivered to Naval Undersea Center (present name NOSC; Naval Ocean Systems Center) for incorporation into the submersible MAKAKAI, the successor to HIKINO (References 12,13,14,15,16).

United States Patent

111 3,527,184

[72] Inventor: Richard G. McCarty
Staten Falls, South Dakota;
James C. Hollenhorst, Staten Falls, South
Dakota; Jerry D. Buckle, Chasard,
California
[21] Appl. No. 866,894
[22] Filed July 28, 1966
[43] Patented Sept. 8, 1970
[73] Assignee: The United States of America as represented
by the Secretary of the Navy

[56] References Cited
UNITED STATES PATENTS
700,759 5/1902 Masur 114/16UX
2,291,940 8/1942 Bobrobs 114/16
2,294,296 8/1942 Hansen 114/14R
Primary Examiner - Benjamin A. Borchelt
Assistant Examiner - Thomas M. Webb
Attorneys - O. Baxter Warner, George J. Ruben and C. E.
Vautour, Jr.

[54] SUBSEQUENTLY MANAGED OBSERVATORY
FOR UNDERSEA RESEARCH
14 Claims, 14 Drawing Figs.

[52] U.S. Cl. 114/16, 114/18, 114/19
[51] Int. Cl. B63J 11/34, B63J 11/00, B63J 11/11
[50] Field of Invention 114/16, 114/18, 114/19, 114/20, 114/21, 114/22, 114/23, 114/24, 114/25, 114/26, 114/27, 114/28, 114/29, 114/30, 114/31, 114/32, 114/33, 114/34, 114/35, 114/36, 114/37, 114/38, 114/39, 114/40, 114/41, 114/42, 114/43, 114/44, 114/45, 114/46, 114/47, 114/48, 114/49, 114/50, 114/51, 114/52, 114/53, 114/54, 114/55, 114/56, 114/57, 114/58, 114/59, 114/60, 114/61, 114/62, 114/63, 114/64, 114/65, 114/66, 114/67, 114/68, 114/69, 114/70, 114/71, 114/72, 114/73, 114/74, 114/75, 114/76, 114/77, 114/78, 114/79, 114/80, 114/81, 114/82, 114/83, 114/84, 114/85, 114/86, 114/87, 114/88, 114/89, 114/90, 114/91, 114/92, 114/93, 114/94, 114/95, 114/96, 114/97, 114/98, 114/99, 114/100, 114/101, 114/102, 114/103, 114/104, 114/105, 114/106, 114/107, 114/108, 114/109, 114/110, 114/111, 114/112, 114/113, 114/114, 114/115, 114/116, 114/117, 114/118, 114/119, 114/120, 114/121, 114/122, 114/123, 114/124, 114/125, 114/126, 114/127, 114/128, 114/129, 114/130, 114/131, 114/132, 114/133, 114/134, 114/135, 114/136, 114/137, 114/138, 114/139, 114/140, 114/141, 114/142, 114/143, 114/144, 114/145, 114/146, 114/147, 114/148, 114/149, 114/150, 114/151, 114/152, 114/153, 114/154, 114/155, 114/156, 114/157, 114/158, 114/159, 114/160, 114/161, 114/162, 114/163, 114/164, 114/165, 114/166, 114/167, 114/168, 114/169, 114/170, 114/171, 114/172, 114/173, 114/174, 114/175, 114/176, 114/177, 114/178, 114/179, 114/180, 114/181, 114/182, 114/183, 114/184, 114/185, 114/186, 114/187, 114/188, 114/189, 114/190, 114/191, 114/192, 114/193, 114/194, 114/195, 114/196, 114/197, 114/198, 114/199, 114/200, 114/201, 114/202, 114/203, 114/204, 114/205, 114/206, 114/207, 114/208, 114/209, 114/210, 114/211, 114/212, 114/213, 114/214, 114/215, 114/216, 114/217, 114/218, 114/219, 114/220, 114/221, 114/222, 114/223, 114/224, 114/225, 114/226, 114/227, 114/228, 114/229, 114/230, 114/231, 114/232, 114/233, 114/234, 114/235, 114/236, 114/237, 114/238, 114/239, 114/240, 114/241, 114/242, 114/243, 114/244, 114/245, 114/246, 114/247, 114/248, 114/249, 114/250, 114/251, 114/252, 114/253, 114/254, 114/255, 114/256, 114/257, 114/258, 114/259, 114/260, 114/261, 114/262, 114/263, 114/264, 114/265, 114/266, 114/267, 114/268, 114/269, 114/270, 114/271, 114/272, 114/273, 114/274, 114/275, 114/276, 114/277, 114/278, 114/279, 114/280, 114/281, 114/282, 114/283, 114/284, 114/285, 114/286, 114/287, 114/288, 114/289, 114/290, 114/291, 114/292, 114/293, 114/294, 114/295, 114/296, 114/297, 114/298, 114/299, 114/300, 114/301, 114/302, 114/303, 114/304, 114/305, 114/306, 114/307, 114/308, 114/309, 114/310, 114/311, 114/312, 114/313, 114/314, 114/315, 114/316, 114/317, 114/318, 114/319, 114/320, 114/321, 114/322, 114/323, 114/324, 114/325, 114/326, 114/327, 114/328, 114/329, 114/330, 114/331, 114/332, 114/333, 114/334, 114/335, 114/336, 114/337, 114/338, 114/339, 114/340, 114/341, 114/342, 114/343, 114/344, 114/345, 114/346, 114/347, 114/348, 114/349, 114/350, 114/351, 114/352, 114/353, 114/354, 114/355, 114/356, 114/357, 114/358, 114/359, 114/360, 114/361, 114/362, 114/363, 114/364, 114/365, 114/366, 114/367, 114/368, 114/369, 114/370, 114/371, 114/372, 114/373, 114/374, 114/375, 114/376, 114/377, 114/378, 114/379, 114/380, 114/381, 114/382, 114/383, 114/384, 114/385, 114/386, 114/387, 114/388, 114/389, 114/390, 114/391, 114/392, 114/393, 114/394, 114/395, 114/396, 114/397, 114/398, 114/399, 114/400, 114/401, 114/402, 114/403, 114/404, 114/405, 114/406, 114/407, 114/408, 114/409, 114/410, 114/411, 114/412, 114/413, 114/414, 114/415, 114/416, 114/417, 114/418, 114/419, 114/420, 114/421, 114/422, 114/423, 114/424, 114/425, 114/426, 114/427, 114/428, 114/429, 114/430, 114/431, 114/432, 114/433, 114/434, 114/435, 114/436, 114/437, 114/438, 114/439, 114/440, 114/441, 114/442, 114/443, 114/444, 114/445, 114/446, 114/447, 114/448, 114/449, 114/450, 114/451, 114/452, 114/453, 114/454, 114/455, 114/456, 114/457, 114/458, 114/459, 114/460, 114/461, 114/462, 114/463, 114/464, 114/465, 114/466, 114/467, 114/468, 114/469, 114/470, 114/471, 114/472, 114/473, 114/474, 114/475, 114/476, 114/477, 114/478, 114/479, 114/480, 114/481, 114/482, 114/483, 114/484, 114/485, 114/486, 114/487, 114/488, 114/489, 114/490, 114/491, 114/492, 114/493, 114/494, 114/495, 114/496, 114/497, 114/498, 114/499, 114/500, 114/501, 114/502, 114/503, 114/504, 114/505, 114/506, 114/507, 114/508, 114/509, 114/510, 114/511, 114/512, 114/513, 114/514, 114/515, 114/516, 114/517, 114/518, 114/519, 114/520, 114/521, 114/522, 114/523, 114/524, 114/525, 114/526, 114/527, 114/528, 114/529, 114/530, 114/531, 114/532, 114/533, 114/534, 114/535, 114/536, 114/537, 114/538, 114/539, 114/540, 114/541, 114/542, 114/543, 114/544, 114/545, 114/546, 114/547, 114/548, 114/549, 114/550, 114/551, 114/552, 114/553, 114/554, 114/555, 114/556, 114/557, 114/558, 114/559, 114/560, 114/561, 114/562, 114/563, 114/564, 114/565, 114/566, 114/567, 114/568, 114/569, 114/570, 114/571, 114/572, 114/573, 114/574, 114/575, 114/576, 114/577, 114/578, 114/579, 114/580, 114/581, 114/582, 114/583, 114/584, 114/585, 114/586, 114/587, 114/588, 114/589, 114/590, 114/591, 114/592, 114/593, 114/594, 114/595, 114/596, 114/597, 114/598, 114/599, 114/600, 114/601, 114/602, 114/603, 114/604, 114/605, 114/606, 114/607, 114/608, 114/609, 114/610, 114/611, 114/612, 114/613, 114/614, 114/615, 114/616, 114/617, 114/618, 114/619, 114/620, 114/621, 114/622, 114/623, 114/624, 114/625, 114/626, 114/627, 114/628, 114/629, 114/630, 114/631, 114/632, 114/633, 114/634, 114/635, 114/636, 114/637, 114/638, 114/639, 114/640, 114/641, 114/642, 114/643, 114/644, 114/645, 114/646, 114/647, 114/648, 114/649, 114/650, 114/651, 114/652, 114/653, 114/654, 114/655, 114/656, 114/657, 114/658, 114/659, 114/660, 114/661, 114/662, 114/663, 114/664, 114/665, 114/666, 114/667, 114/668, 114/669, 114/670, 114/671, 114/672, 114/673, 114/674, 114/675, 114/676, 114/677, 114/678, 114/679, 114/680, 114/681, 114/682, 114/683, 114/684, 114/685, 114/686, 114/687, 114/688, 114/689, 114/690, 114/691, 114/692, 114/693, 114/694, 114/695, 114/696, 114/697, 114/698, 114/699, 114/700, 114/701, 114/702, 114/703, 114/704, 114/705, 114/706, 114/707, 114/708, 114/709, 114/710, 114/711, 114/712, 114/713, 114/714, 114/715, 114/716, 114/717, 114/718, 114/719, 114/720, 114/721, 114/722, 114/723, 114/724, 114/725, 114/726, 114/727, 114/728, 114/729, 114/730, 114/731, 114/732, 114/733, 114/734, 114/735, 114/736, 114/737, 114/738, 114/739, 114/740, 114/741, 114/742, 114/743, 114/744, 114/745, 114/746, 114/747, 114/748, 114/749, 114/750, 114/751, 114/752, 114/753, 114/754, 114/755, 114/756, 114/757, 114/758, 114/759, 114/760, 114/761, 114/762, 114/763, 114/764, 114/765, 114/766, 114/767, 114/768, 114/769, 114/770, 114/771, 114/772, 114/773, 114/774, 114/775, 114/776, 114/777, 114/778, 114/779, 114/780, 114/781, 114/782, 114/783, 114/784, 114/785, 114/786, 114/787, 114/788, 114/789, 114/790, 114/791, 114/792, 114/793, 114/794, 114/795, 114/796, 114/797, 114/798, 114/799, 114/800, 114/801, 114/802, 114/803, 114/804, 114/805, 114/806, 114/807, 114/808, 114/809, 114/810, 114/811, 114/812, 114/813, 114/814, 114/815, 114/816, 114/817, 114/818, 114/819, 114/820, 114/821, 114/822, 114/823, 114/824, 114/825, 114/826, 114/827, 114/828, 114/829, 114/830, 114/831, 114/832, 114/833, 114/834, 114/835, 114/836, 114/837, 114/838, 114/839, 114/840, 114/841, 114/842, 114/843, 114/844, 114/845, 114/846, 114/847, 114/848, 114/849, 114/850, 114/851, 114/852, 114/853, 114/854, 114/855, 114/856, 114/857, 114/858, 114/859, 114/860, 114/861, 114/862, 114/863, 114/864, 114/865, 114/866, 114/867, 114/868, 114/869, 114/870, 114/871, 114/872, 114/873, 114/874, 114/875, 114/876, 114/877, 114/878, 114/879, 114/880, 114/881, 114/882, 114/883, 114/884, 114/885, 114/886, 114/887, 114/888, 114/889, 114/890, 114/891, 114/892, 114/893, 114/894, 114/895, 114/896, 114/897, 114/898, 114/899, 114/900, 114/901, 114/902, 114/903, 114/904, 114/905, 114/906, 114/907, 114/908, 114/909, 114/910, 114/911, 114/912, 114/913, 114/914, 114/915, 114/916, 114/917, 114/918, 114/919, 114/920, 114/921, 114/922, 114/923, 114/924, 114/925, 114/926, 114/927, 114/928, 114/929, 114/930, 114/931, 114/932, 114/933, 114/934, 114/935, 114/936, 114/937, 114/938, 114/939, 114/940, 114/941, 114/942, 114/943, 114/944, 114/945, 114/946, 114/947, 114/948, 114/949, 114/950, 114/951, 114/952, 114/953, 114/954, 114/955, 114/956, 114/957, 114/958, 114/959, 114/960, 114/961, 114/962, 114/963, 114/964, 114/965, 114/966, 114/967, 114/968, 114/969, 114/970, 114/971, 114/972, 114/973, 114/974, 114/975, 114/976, 114/977, 114/978, 114/979, 114/980, 114/981, 114/982, 114/983, 114/984, 114/985, 114/986, 114/987, 114/988, 114/989, 114/990, 114/991, 114/992, 114/993, 114/994, 114/995, 114/996, 114/997, 114/998, 114/999, 114/1000, 114/1001, 114/1002, 114/1003, 114/1004, 114/1005, 114/1006, 114/1007, 114/1008, 114/1009, 114/1010, 114/1011, 114/1012, 114/1013, 114/1014, 114/1015, 114/1016, 114/1017, 114/1018, 114/1019, 114/1020, 114/1021, 114/1022, 114/1023, 114/1024, 114/1025, 114/1026, 114/1027, 114/1028, 114/1029, 114/1030, 114/1031, 114/1032, 114/1033, 114/1034, 114/1035, 114/1036, 114/1037, 114/1038, 114/1039, 114/1040, 114/1041, 114/1042, 114/1043, 114/1044, 114/1045, 114/1046, 114/1047, 114/1048, 114/1049, 114/1050, 114/1051, 114/1052, 114/1053, 114/1054, 114/1055, 114/1056, 114/1057, 114/1058, 114/1059, 114/1060, 114/1061, 114/1062, 114/1063, 114/1064, 114/1065, 114/1066, 114/1067, 114/1068, 114/1069, 114/1070, 114/1071, 114/1072, 114/1073, 114/1074, 114/1075, 114/1076, 114/1077, 114/1078, 114/1079, 114/1080, 114/1081, 114/1082, 114/1083, 114/1084, 114/1085, 114/1086, 114/1087, 114/1088, 114/1089, 114/1090, 114/1091, 114/1092, 114/1093, 114/1094, 114/1095, 114/1096, 114/1097, 114/1098, 114/1099, 114/1100, 114/1101, 114/1102, 114/1103, 114/1104, 114/1105, 114/1106, 114/1107, 114/1108, 114/1109, 114/1110, 114/1111, 114/1112, 114/1113, 114/1114, 114/1115, 114/1116, 114/1117, 114/1118, 114/1119, 114/1120, 114/1121, 114/1122, 114/1123, 114/1124, 114/1125, 114/1126, 114/1127, 114/1128, 114/1129, 114/1130, 114/1131, 114/1132, 114/1133, 114/1134, 114/1135, 114/1136, 114/1137, 114/1138, 114/1139, 114/1140, 114/1141, 114/1142, 114/1143, 114/1144, 114/1145, 114/1146, 114/1147, 114/1148, 114/1149, 114/1150, 114/1151, 114/1152, 114/1153, 114/1154, 114/1155, 114/1156, 114/1157, 114/1158, 114/1159, 114/1160, 114/1161, 114/1162, 114/1163, 114/1164, 114/1165, 114/1166, 114/1167, 114/1168, 114/1169, 114/1170, 114/1171, 114/1172, 114/1173, 114/1174, 114/1175, 114/1176, 114/1177, 114/1178, 114/1179, 114/1180, 114/1181, 114/1182, 114/1183, 114/1184, 114/1185, 114/1186, 114/1187, 114/1188, 114/1189, 114/1190, 114/1191, 114/1192, 114/1193, 114/1194, 114/1195, 114/1196, 114/1197, 114/1198, 114/1199, 114/1200, 114/1201, 114/1202, 114/1203, 114/1204, 114/1205, 114/1206, 114/1207, 114/1208, 114/1209, 114/1210, 114/1211, 114/1212, 114/1213, 114/1214, 114/1215, 114/1216, 114/1217, 114/1218, 114/1219, 114/1220, 114/1221, 114/1222, 114/1223, 114/1224, 114/1225, 114/1226, 114/1227, 114/1228, 114/1229, 114/1230, 114/1231, 114/1232, 114/1233, 114/1234, 114/1235, 114/1236, 114/1237, 114/1238, 114/1239, 114/1240, 114/1241, 114/1242, 114/1243, 114/1244, 114/1245, 114/1246, 114/1247, 114/1248, 114/1249, 114/1250, 114/1251, 114/1252, 114/1253, 114/1254, 114/1255, 114/1256, 114/1257, 114/1

There were only three major departures in NAFVAC NEMO from the original NEMO concept proposed by the Naval Missile Center in 1965 (Ref. 10). The diameter was 66 instead of 120 inches, and as a result of the reduced diameter the two occupants had to sit side by side, instead of back to back. The life support duration was shortened from 100 to 32 hours as the function of the diving system shifted from a long term in situ oceanographic observatory to a short term diving supervisors observatory. Finally, the diving system was equipped with external hydraulic and electrical connectors for powering of diver operated power tools at the work site in the vicinity of NEMO (Figure 15).

The NAFVAC NEMO was officially launched in May 1970 by Rear Admiral Johnson amid great ceremonies attended by representatives of U.S. ocean engineering community at Freeport, Bahamas. After several preliminary dives NEMO reached 600 ft. depth piloted by E. Briggs and L. Poirer of Southwest Research Institute.



Figure 12. The NEMO concept funded for construction by the Naval Facilities Engineering Command

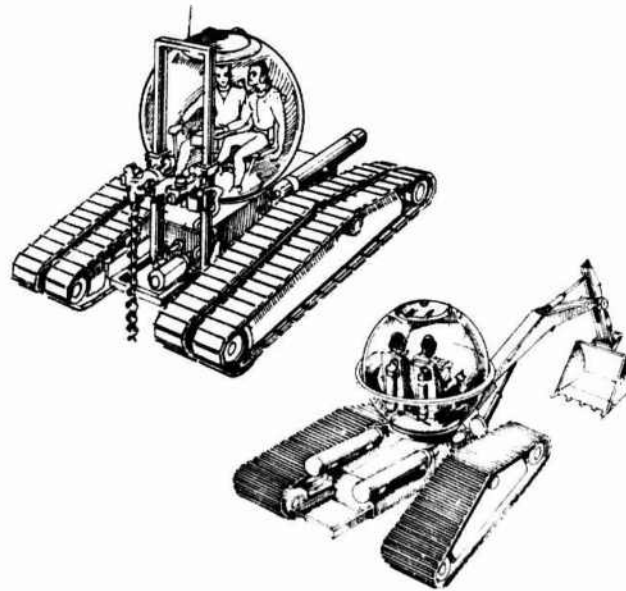


Figure 13. The concept of standardized 66 inch diameter one atmosphere acrylic plastic cockpit integrated with proposed undersea earth moving equipment.



Figure 14. Naval Civil Engineering Laboratory's NEMONAUTS; Lt. R. E. Elliott, R. F. Crowe Jr., P. R. Rockwell, and M. R. Snoey (from left to right).

During the remainder of the two week long seatrials NEMO dove repeatedly to 600 feet under the charge of four NCEL trained NEMONAUTS without any mishap. The diving operations were supervised by CDR Noel Brady, assisted by LCDR Donald Black and Lt. Ross Saxon from SUBDEVGRU ONE, San Diego.

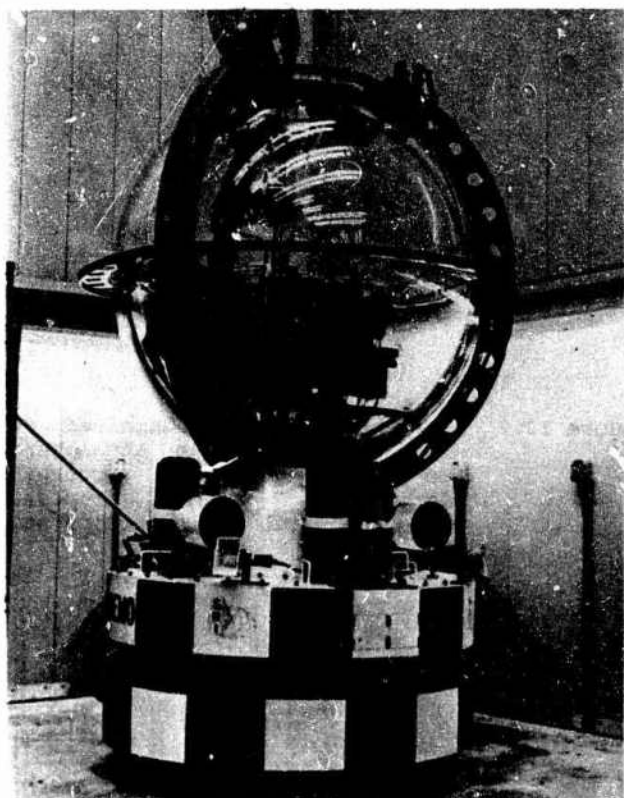


Figure 15 The 66x51 inch acrylic plastic hull installed in the NEMO submersible fabricated at SWRI under supervision of E. Briggs.

The sea trials off Freeport, Bahamas were followed in July 1970 by material certification dives off Port Hueneme, CA. As a result of the extensive test and evaluation program the U.S. Navy Ship Systems Command certified on 12/15/1970 DSV (Deep submergence Vehicle) NEMO as materially adequate for Navy service to 600 ft. depth. The certification was renewed thereafter annually (Figure 16). DSV NEMO saw extensive diving service from 1970 to 1980 during which it experienced 671 dives in the 50 to 600 foot range without any visible sign of material fatigue in the acrylic pressure hull assembly.

The other NEMO hull, which was incorporated by Doug Murphy into the MAKAKAI submersible at NUC Hawaii Laboratory was also certified by the U.S. Navy for 600 feet depth service in 1971. It saw extensive service in support of the sea animal research and training program at the NUC Hawaii Laboratory (Figure 17). It was removed from service in 1976 and placed on permanent display at Sea World, San Diego.

After 10 years of service NEMO was decommissioned in 1980 as part of an economy measure from Navy service and placed on display at the Naval Ocean Systems Center. Specimens taken from the acrylic hull after its decommissioning showed that after 10 years of service in marine environment the photochemical deterioration in the acrylic material had penetrated less than 0.040 inches deep (Reference 18). Since the thick hull material sees mostly only membrane compressive stresses during a typical dive the deterioration of a thin layer on its outside surface would not affect its safe maximum operational depth, particularly in view of the safety factor of 7 used by NAVSHIPS in

U.S. NAVY SAFETY CERTIFICATION FOR NON-COMBATANT SUBMERSIBLES		
1. NAME OF SUBMERSIBLE NEMO	2. BUILDING South West Research Institute	3. TYPE Oceanographic Research Vehicle
4. DISPLACEMENT 7850	5. REGISTRATION NO. N/A	6. AUTHORIZED DEPTH 600 FT.
7. AUTHORITY AND BASIS FOR ISSUANCE: This certificate is issued pursuant to the current EECNAVIST 9200-1 and certifies that, as of date of issuance, the submersible to which issued, has been inspected and found to be materially adequate as described in the MATERIAL CERTIFICATION PROCEDURES AND CRITERIA MANUAL FOR MANNED, NON-COMBATANT SUBMERSIBLES.		
8. TERMS AND CONDITIONS: Unless sooner surrendered, suspended, revoked, or a termination date is otherwise established by the Naval Ship Systems Command, Washington, D.C., this certification is effective until it expires (see date below), as long as the submersible operates within the authorized depths noted in item 6 above, and preventive maintenance and alterations are performed in accordance with the MATERIAL CERTIFICATION PROCEDURES AND CRITERIA MANUAL FOR MANNED, NON-COMBATANT SUBMERSIBLES.		
DATE CERTIFICATE ISSUED 13 February 1973 BY AUTHORITY OF NAVSHIPS/SCOM <i>R. S. Wilson</i>	DATE CERTIFICATE EXPIRES 60,000 13 Feb 1974 or dive-ft. (Signature & Title) <i>R. S. Wilson</i>	NAVSHIPS LTR. FILE REF. Ser 665-425 NAVSHIPS LTR. DATE 27 Feb 1973
NAVSHIPS 9200-1 (10-67) NOTE: VOID IF ALTERED, DEFACED OR EXPIRED		

Figure 16. U. S. Navy Certification For DSV NEMO, awarded originally on December 1970 and renewed thereafter on an annual basis to 1980.

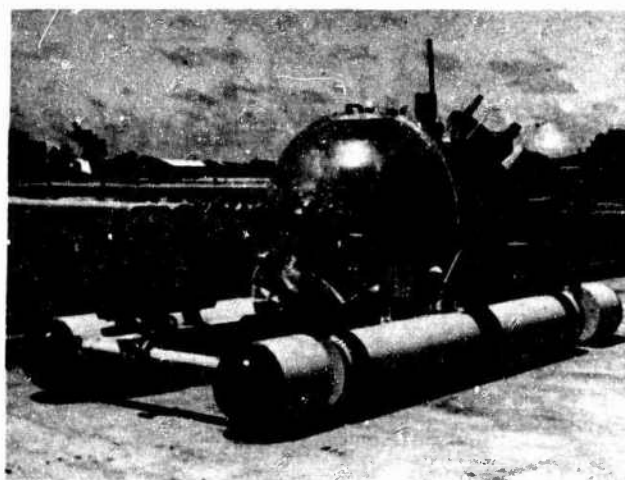


Figure 17. The 66 x 61 inch acrylic plastic hull after installation in the MAKAKAI submersible fabricated under the supervision of D. Murphy in 1971 at the Hawaii Laboratory of the Naval Undersea Center.

establishing the overly conservative safe design depth of 600 feet. One of the valuable side benefits of the 10 years of NEMO's satisfactory service was the change in Navy's thinking about the magnitude of safety factors; a safety factor of 4 is considered now to be totally adequate for acrylic pressure hulls.

The decommissioning of NEMO in 1980 signaled the closing of the pioneering, and the beginning of the application epochs for acrylic submersibles. Prior to NEMO acrylic submersibles were considered on par with hot air balloons at county fairs; thrilling for the pilots, but of no commercial value to the industry. In the short time span between NEMO certification in 1970 and its decommissioning in 1980 the stature of acrylic submersibles grew from interesting, but nevertheless exotic freaks to accepted work horses of the ocean engineering community.

IN THE FOOTSTEPS OF NEMO

NEMO was followed by the Johnson Sea Link I, a unique submersible designed by Mr. E. Link for the Smithsonian Institution (Figure 18). It combined the advantages of panoramic visibility, provided by the acrylic spherical hull, with the lockout capability, provided by the aluminum cylindrical hull. The acrylic spherical hull, also engineered by Stachiw, was of the same size, design (Figures 19 and 20) as NEMO hull, except that aluminum was used in hatches, a polycarbonate gasket was placed between the metallic components and the acrylic hull and the wall thickness was increased to 4 inches, giving the Johnson Sea Link I a design depth of 3000 feet (References 19 and 20).



Figure 18. The 66 x 58 inch acrylic plastic hull after installation in the Johnson-Sea-Link # 1 submersible designed by E. Link and fabricated in 1971 under the supervision of R. Dolan at the Harbor Branch Foundation.

To facilitate the certification of this submersible the Naval Undersea Center conducted a testing program on one full scale and four 15 x 13 inch scale models fabricated by Swedlow Inc. in the same manner as the full scale hull. The test results validated the 3000 design depth of the acrylic hull. The 66 x 58 inch acrylic hull withstood 24 hour long pressure cycles to 2000, 3000, and 4000 feet without any permanent deformation in the acrylic or metallic components. One of the 15 x 13 inch scale models was imploded at 10,000 feet depth, while the remainder of the 15 x 13 inch spheres withstood 1000 typical simulated dives to 3000 feet depth without initiation of any cracks in the hull (References 21). The testing program was concluded by imploding the scale models under dynamic pressure loading generated by underwater explosions (References 22).

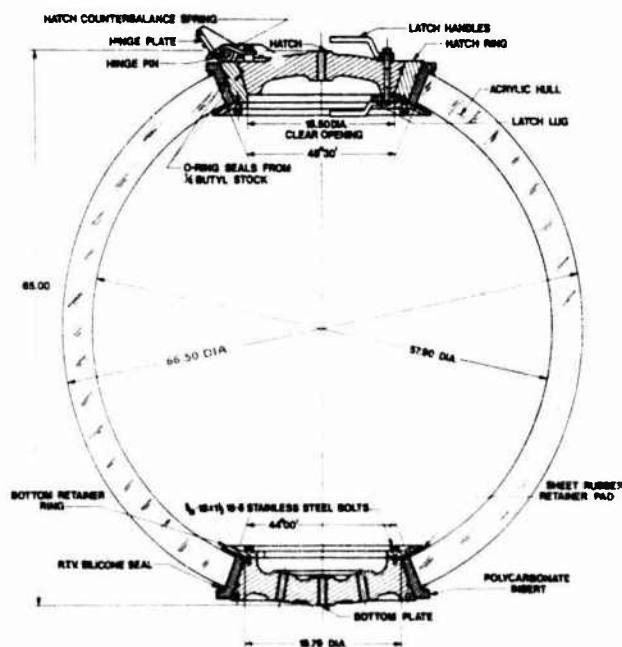


Figure 19. Typical features of the NEMO type acrylic plastic hull design. The dimensions shown are for the 66 x 58 inch hull with 3000 feet design depth.

The submersible was certified by the American Bureau of Shipping to 1000 feet depth in 1971 and to 2640 feet depth in 1983. The submersible is still in service, a veteran of more than 1000 dives in the ocean.

Even though the construction of Johnson Sea Link I conclusively showed that the fabrication technique developed for the 2.5 inch thick 66 inch diameter NEMO hull was also applicable to the 4 inch thick 66 inch diameter JSLI hull it also showed that this construction technique was severely circumscribed by several limitations characteristic to this type of construction technique.

1. Thermal forming of spherical pentagons with t/R_0 ratios in excess of 0.15 introduced into the external surface of pentagons unacceptably high residual tensile stresses that with time initiated crazing of the surface.
2. The size of the spheres was limited to 66 inches, the largest size that could be assembled by thermoforming of pentagons cut out of largest available 4 inch thick sheets cast from monomer resin.

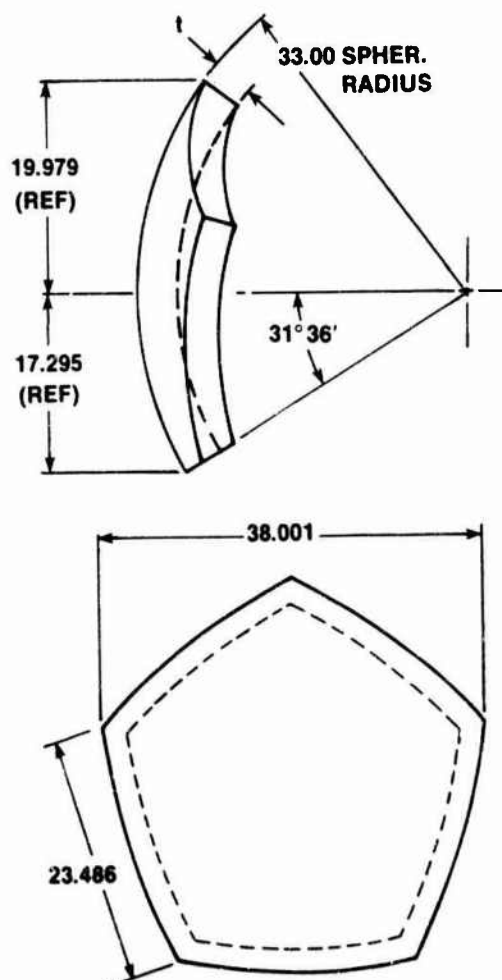


Figure 20. Typical dimensions of spherical pentagons used in the assembly of 66 inch diameter NEMO type acrylic plastic hulls.

The effect of these limitations was that for acrylic plastic spherical hulls with 66 inch outside diameter, fabricated by bonding of 12 spherical pentagons, the 3000 foot design depth was probably the maximum design depth attainable in that size. This technological barrier to the orderly development of large and deeper diving acrylic plastic spherical hulls was early recognized by Stachiw and

brought to the attention of Dr. W. McLean, Technical Director of Naval Undersea Center (NUC) and E. Link, Director of the Harbor Branch Foundation (HBF), both enthusiastic supporters of the transparent hull technology (Figure 21)



Figure 21. Dr. W. B. McLean, Technical Director of the Naval Undersea Center, and E. A. Link, Vice President of the Harbor Branch Foundation reviewing in 1973 with Bruce Beasley, owner of Polymer Products, the potential of his slush casting process for casting of large hemispheres

The solution to this problem was suggested by Bruce Beasley, a noted sculptor who specialized in massive monolithic acrylic sculptures cast in his own studio in Oakland, CA. He proposed in 1969 that the acrylic spheres be fabricated by casting of monolithic spherical shells, or if this was too expensive, by joining of hemispherical shells cast inside permanent metallic molds in his own shop. His suggestion was accepted and with funding provided jointly by NOSC and HBF he developed a technique for casting of hemispheres in permanent steel molds from a carefully compounded mixture of methyl methacrylate monomer resin and polymerized methyl methacrylate powder.

The pre-polymerized methyl methacrylate powder dissolved in the monomer resin minimized shrinkage and exothermic reaction during the polymerization cycle. The addition of polymerized powder to the monomer resin gave it the consistency of slush ice and as a result of it this type of casting technique was referred to as slush casting. This mixture turned after several hours at room temperature into a firm jelly which after application of heat in a pressurized autoclave became crystal clear, hard acrylic plastic. The application of pressure in the autoclave served to suppress the formation of gas bubbles inside the jelly like mixture during exothermic reaction.

There appeared to be no physical limit on the thickness of the sphere cast by this process, and the only limit on the size of the sphere was the size of available autoclaves in which the molds with the casting mixture had to be placed for polymerization. The required validation of slush casting technique was performed in 1974 on 18 inch OD x 10 inch ID hemispheres which were subsequently bonded together by Stachiw into spheres and subjected to hydrostatic testing. The results of the tests performed at the Southwest Research Test Institute were satisfactory (Reference 23), and Beasley was given authorization to proceed with the casting of several 66 inch x 58 inch NEMO spheres (Figure 22). Two of these spheres were delivered to HBF for incorporation into submersibles and one was delivered to NUC for test and evaluation under hydrostatic loading (Reference 24).

The results of hydrostatic test performed in 1975 on the cast 66 x 58 inch sphere at the Southwest Research Institute were satisfactory. The pressure hull successfully withstood 24 hours long simulated dives to 2000, 3000 and 4000 feet without permanent deformation after 24 hours long relaxation periods following each dive. It imploded only after 13 minutes of sustained pressurization during a simulated dive to 9000 feet. The testing of the full scale hull proved conclusively that (1) the structural performance of slush cast spherical hulls is identical to thermoformed spherical hulls, and similarly that (2) the structural performance of full scale slush cast spherical hulls is identical to that of scale models.

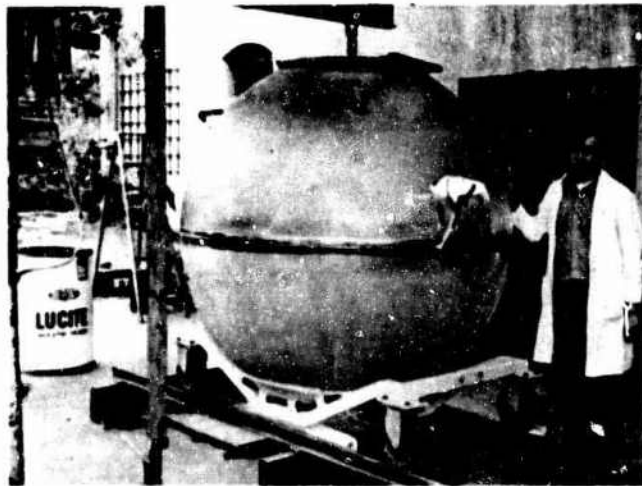


Figure 22. The first successful pair of 66 x 58 inch hemispheres slush cast by Bruce Beasley for the Naval Undersea Center in 1974. Mike Stachiw is assisting Beasley during the critical bonding of the equatorial joint.

Now there was no further doubt that the slush casting process produces acrylic plastic pressure hulls with the same structural performance as thermoformed hulls, and therefore all the design criteria generated with thermoformed spheres during the developments of NEMO design apply also to the spheres fabricated by slush casting. The slush casting technique made it now feasible for the first time in ocean engineering history to fabricate economically spherical pressure hulls of any desirable thickness or size, the only limitations being the imagination of the designer and the pocketbook of the customer.

Since the slush casting technique lends itself also to casting of acrylic plastic shells of any shape, pressure hulls can be now cast in any imaginable configuration. To date the slush casting technique has been already employed to cast cylinders and paraboloids of revolution. There is no doubt it will be used in the future to cast ellipsoidal and toroidal pressure hulls; shapes that previously could never be thermoformed successfully (Reference 25).

ACCEPTANCE OF ACRYLIC PLASTIC FOR CONSTRUCTION OF DIVING SYSTEMS

As a result of NEMO's certification by the U. S. Navy in 1970 the American Bureau of Shipping and Det Norske Veritas (U.S. and Norwegian based ship classification societies) took administrative steps to incorporate acrylic plastic into their rules for construction and classification of underwater systems and vehicles. The American Society of Mechanical Engineers, Pressure Technology, Codes and Standards under the leadership of M. R. Green recognized immediately the emergence of acrylic plastic technology for construction of pressure hull components and formulated in 1971 the Safety Code Committee on Pressure Vessels for Human Occupancy (PVHO) to formulate design rules for its use in manned diving systems.

In 1977 ASME published ANSI/ASME PVHO-1 Safety Standard for Pressure Vessels for Human Occupancy which includes a section on the application of acrylic plastic to pressure vessel construction. The Coast Guard, U. S. Department of Transportation referenced ANSI/ASME PVHO-1 in its 1978 Rules and Regulations for Commercial Diving Operations, immediately followed by the American Bureau of Shipping which also referenced ANSI/ASME PVHO-1 in their 1979 Rules for Building and Classing of Underwater Systems and Vehicles. Foreign classing societies also included acrylic plastic in their Rules of Construction of Diving Systems so that by 1980 the acceptance of acrylic plastic pressure hulls and pressure hull components was complete. Thus, in one short decade from 1970 to 1980 the acrylic plastic pressure hull technology incorporated in NEMO transitioned from the experimental to the proven state of pressure hull construction. From that period on there were no further administrative obstacles in the path of acrylic pressure hull development and utilization in underwater vehicles and diving systems.

THE LEGACY OF NEMO PROGRAM

Twenty years have passed since the initiation of NEMO program by the U. S. Navy at the Naval Civil Engineering Laboratory Port Hueneme, CA and the Naval Missile Center, Point Mugu, CA. The program achieved at a very modest cost its original objective; the design, fabrication, and operation of a manned, one atmosphere underwater vehicle/observatory with panoramic visibility for 600 feet depth. In addition, it not only qualified acrylic plastic for construction of external pressure hulls, but also developed a novel fabrication process that allows the casting of acrylic plastic structural components of any size, thickness, or shape.

The number of acrylic plastic submersibles operating today is fairly modest (i.e. Johnson Sea Link #1, Johnson Sea Link #2 Checkmate and Deep Rover). The primary reason for their modest number is the depressed state of offshore oil production industry. But even so the operational depth reached by acrylic plastic submersibles (Figures 23, 24) has progressed steadily from the historic dive to 600 feet in 1970 by NEMO to the 3000 feet dive in 1986 by Deep Rover (Reference 26). There is no doubt that the depth capability and size of acrylic pressure hulls will expand further, a spherical pressure hull with 108 inch diameter has been already designed for 8000 feet depth, scale models of that hull have been built, and a hydrostatic pressure cycling program has been initiated at the Harbor Branch Foundation at Link Port, Florida (Reference 27).



Figure 23. One man minisub Deep Rover designed by Graham Hawkes and fabricated by Deep Ocean Engineering Inc., in 1984. The 63 x 53 inch slush cast acrylic plastic hull provides the 6800 lb. submersible with 3280 feet operational depth capability.

At what depth the development of spherical acrylic plastic hulls will stop is

hard to predict, but in all likelihood it will reach a limit at 10,000 feet, as beyond this depth the weight to displacement ratio and optical effects of the very thick hulls will make the acrylic plastic hull operationally unacceptable (References 28,29,30,31).

For depths beyond 10,000 feet the spherical hulls will have to be fabricated from glass or transparent ceramic possessing compressive strength in excess of 100,000 psi. To qualify those materials for construction of manned diving systems calls for initiation of a second NEMO program. But this is yet another story to be written in the future by ocean engineers dedicated to exploration of hydrospace for scientific knowledge and economic benefits to the nation.



Figure 24. Slush cast hemisphere used by Mark Stachiw in 1984 for assembling a 18 x 12.85 inch scale model of acrylic plastic hull with 8000 feet design depth for the Harbor Branch Foundation.

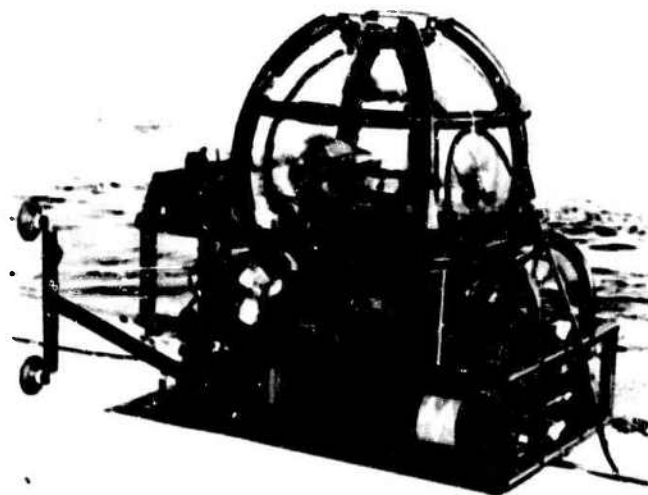


Figure 25 Tethered submersible CHECKMATE with 81 x 74.8 inch acrylic plastic hull for 1600 feet depth. Launched in 1979 off Norway by Mollerodden A.S.

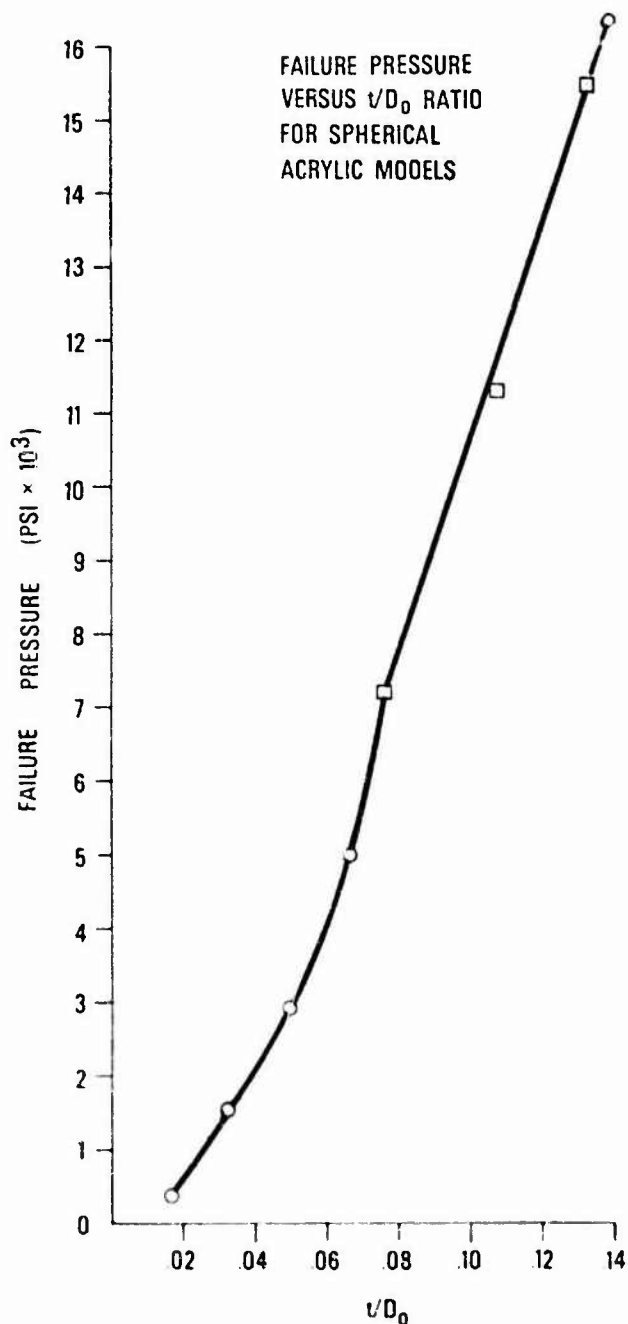


Figure 26

Critical pressure of acrylic plastic spheres pressurized to implosion at 100 psi minute rate in 75 degree Fahrenheit ambient environment. Spheres with $t/D = 0.22$ have been pressurized to 20,000 psi, the maximum available pressure, without imploding. Applying the conversion factor of 4 recommended by ASME PVHO it appears feasible to reach 10,000 feet depth in a submersible equipped with acrylic plastic spherical pressure hulls.



Figure 27 Typical arrangement for hydrostatic testing of acrylic plastic spherical hull scale models. The spherical hulls are suspended from the pressure vessel end closure by means of a pipe open at one end to the interior of the hull and on the other end to the exterior of the vessel. This tube served as pressure resistant conduit for instrumentation wires and relief for internal pressure buildup in the sphere.

The specimen shown here is a 18x12.85 inches acrylic plastic sphere being tested by Mark Stachiw and Karl Hilton at NCEL's Deep Ocean Test Facility. The sphere imploded at 16,000 psi under short term pressurization in 65 degree F water, indicating that cyclic fatigue life will probably exceed 1000 pressurizations to 4000 psi.

CONVERSIONS

psi = 2.247 feet seawater depth
psi = 0.6849 meters of seawater depth
psi = 6.895 kPa
psi = 0.07031 kg/square centimeter
inch = 2.54 centimeters
pound = 0.454 kilograms

REFERENCES

1. BEEBE, William, "Half Mile Down," Harcourt Brace and Company, New York, 1934.
2. Barton, O., "The World Beneath The Sea," Thomas Y. Crowell Co., New York, 1953.
3. PICCARD, Auguste, "Earth, Sky and Sea," Oxford University Press, New York, 1956.
4. Lang T. G. and Scholz "A Two Man Plexiglass Submarine for Oceanic Research," Undersea Technology, April 1963.
5. Perry H. A. "The Argument For Glass Submersibles", Undersea Technology, September 1964.
6. Forman W. R., "Kumukahi," ASME Paper No. 70-WA/Unt-11.
7. Stachiw, J. D., "Acrylic Hemispheres for NUC Undersea Elevator," ASME Paper 72-WA/Oct-4, 1972.

8. Stachiw, J. D., "General Instability of Circumferentially Stiffened Sandwich Shells Subjected to Uniform External Pressure", Pennsylvania State University, Institute For Science and Engineering, Technical Report NORD 16597-91, Dec 1962
9. Stachiw, J. D., "Solid Glass and Ceramic External Pressure Vessels," Pennsylvania State University, Institute For Science and Engineering, Technical Report NOW 63-0209-C-2, January 1964.
10. Moldenhauer, J. G., Stachiw, J. D., Tsuji, K., and Stowell, D. T., "The Design, Fabrication and Testing of Acrylic Pressure Hulls For Manned Vehicles," ASME Paper No. 65-WA/UNT-10.
11. Stachiw, J. D., "Spherical Acrylic Pressure Hulls for Undersea Exploration," ASME Transactions/Journal of Engineering for Industry, Vol. 93, No. 2, 1971.
12. Tsuji, K. and Shelton, R., "Fabrication of NEMO-Type Spherical Acrylic Capsules for Underwater Vehicles," ASME Paper 70 WA/UNT-4, 1970.
13. Stachiw, J. D., "Acrylic Pressure Hull for Submersible NEMO," ASME Paper 71 Unt-2, 1971.
14. Trowbridge, T., "Optical Properties of a Spherical Plastic Underwater Observatory, NEMO," ASME Paper 70-Unt-A, 1970.
15. Snoey, M. R. and Katona, M. G., "Stress Analysis of a Spherical Acrylic Pressure Hull," ASME Paper 70-Unt-B, 1970.
16. Snoey, M. R. and Briggs, E. M., "The NEMO Submersible," ASME Paper 70-Unt-C, 1970.
17. Murphy, D. and Mazzone, W., "Transparent Hull Submersible MAKAKAI," ASME Paper 72-WA/Oct-8
18. Stachiw, J. D. and Dolan, R. B., "Effects of Weather, Age, and Cyclic Pressurizations on Structural Performance of Acrylic Plastic Spherical Shells Under External Pressure Loading," ASME Transactions/Journal of Engineering for Industry, Vol. 104, No. 2, 1982.
19. Kelsey, R. A. and Dolan, R. B. "Johnson-Sea-Link, the First Deep Diving Welded Aluminum Submersible," ASME Paper 70-WA/Unt-6, 1970.
20. Maison, J. R. and Stachiw, J. D., "Acrylic Pressure Hull for Johnson-Sea-Link Submersible," ASME Paper No. 71-WA/Unt-6, 1971.
21. Stachiw, J. D., "NEMO Type Acrylic Plastic Spherical Hull for Manned Operation to 3000 feet Depth," ASME Transactions/Journal of Engineering for Industry, Vol. 98, No. 2, 1976.
22. Stachiw, J. D. "Spherical Plastic Hulls Under External Explosive Loading," ASME Transactions/Journal of Engineering for Industry, Vol. 99, No. 2, 1977.
23. Stachiw, J. D. and Beasley, B., "Precision Casting Process for Acrylic Plastic Spherical Windows in High Pressure Service," ASME Paper 74-WA/Oct-70,
24. Stachiw, J. D. and Lones J. J., "Development of Economical Casting Process for NEMO Type Acrylic Submersible Hulls," ASME Transactions/Journal of Engineering for Industry, Vol. 99, No. 2, 1977.
25. Stachiw, J. D., "Hyperhemispherical Viewports for Undersea Applications," ASME Transactions/Journal of Engineering for Industry, Vol. 101, No. 3, 1979.
26. Stachiw, J. D., Clark A., and Brenn, C. B., "Acrylic Plastic Spherical Pressure Hull For 8000 feet Design Depth: Phase I," The Ninth Annual Energy Sources Technology Conference and Exhibition, New Orleans, LA February 23, 1986, ASME Ocean Engineering Division Volume II.
27. Hawkes, G. S., "The Future of Atmospheric Diving Systems and Associated Manipulator Technology, with Special Reference to a New Microsubmersible, DEEP ROVER," Marine Technology Society Journal, Vol. 17-No.3, 1983.
28. Stachiw, J. D. and Dolan, R. B., "Spherical Acrylic Pressure Hulls With Multiple Penetrations," ASME Transactions/Journal of Engineering for Industry, Vol. 100, No. 2, 1978.
29. Stachiw, J. D., Dolan, R. B., and Clayton, D. L., "Polycarbonate Plastic Inserts for Spherical Acrylic Plastic Shells Under Hydrostatic Loading," ASME Transactions/Journal of Engineering for Industry, Vol. 103, No. 1, 1981.
30. Stachiw, J. D., "Critical Pressure of Spherical Shell Acrylic Windows Under Short-Term Pressure Loading," ASME Transaction/Journal of Engineering for Industry, Vol. 91, No. 3, 1969.
31. Stachiw, J. D., "Acrylic Plastic Spherical Shell Windows Under Point Impact Loading," ASME Transactions/Journal of Engineering for Industry, Vol. 98, No. 2, 1976.
32. Stachiw, J. D., "Failure Modes of Spherical Acrylic Shells Under External Hydrostatic Loading, Hydrodynamically Loaded Shells-Part 1, Edited by R. Szilard, The University Press of Hawaii, 1973.
33. Stachiw, J. L., and Stachiw, J. D., "Effect of Weathering And Submersion in Seawater on the Mechanical Properties of Acrylic Plastic," ASME Paper 77-WA/OCE-5.
34. Stachiw, J. D. and Maison, J., "Flanged Acrylic Plastic Hemispherical Shells for Undersea Applications," ASME Paper 73-Oct-A, 1973.
35. Stachiw, J. D. and R. Sletten, "Flanged Acrylic Hemispherical Shells for Undersea Systems Part II-Static and Cyclic Fatigue Life Under Hydrostatic Loading," ASME Transactions/Journal of Engineering for Industry, Vol. 100, No. 2, 1978.
36. Stachiw, J. D., "Spherical Sector Windows with Restrained Edges for Undersea Applications," ASME Transactions/Journal of Engineering for Industry, Vol. 99, No. 2, 1977.

462-364